Ways to Novel Inorganic-Organic Hybrid Materials Applying New B–C Bond Formation Strategies

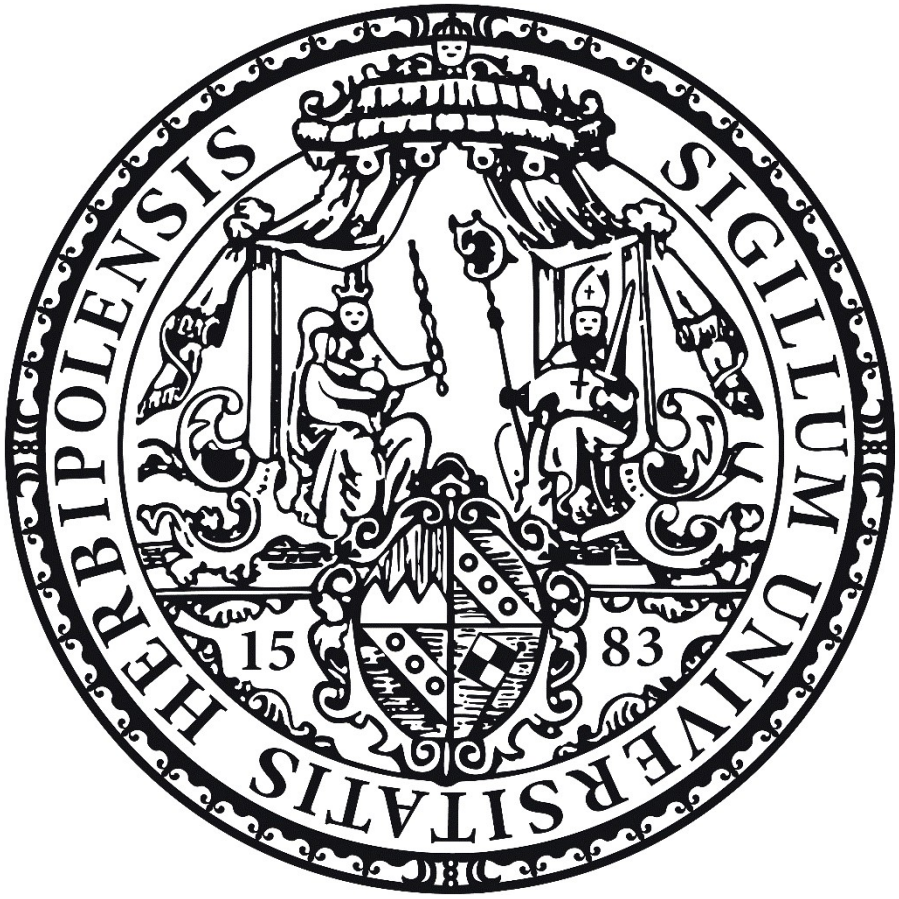

Dissertation zur Erlangung des naturwissenschaftlichen Doktorgrades der Julius-Maximilians-Universität Würzburg

vorgelegt von

Lars Fritze

aus Hilden

Würzburg, 2021

Eingereicht bei der Fakultät für Chemie und Pharmazie am

_____

Gutachter der schriftlichen Arbeit

1. Gutachter: Prof. Dr. Holger Helten
2. Gutachter: PD Dr. Crispin Lichtenberg

Prüfer des öffentlichen Promotionskolloquiums

1. Prüfer: Prof. Dr. Holger Helten
2. Prüfer: PD Dr. Crispin Lichtenberg
3. Prüfer: _____

Datum des öffentlichen Promotionskolloquiums

_____

Doktorurkunde ausgehändigt am

_____

meinen Eltern

gewidmet

Bad biscuits make the baker broke, bro.

– Jake the Dog

Acknowledgements

I want to thank all people, that made that work possible.

First of all, I would like to thank Prof. Dr. Holger Helten for giving me the opportunity to do my PhD research in his young research group, allowing me to work in this very interesting field of chemistry. Thank you for the personal and scientific growth I experienced over the last view years through your support, advice, and deed. Also, I am grateful that I was allowed to travel the world through various conferences and meet interesting people and places.

I would like to thank PD Dr. Crispin Lichtenberg for taking over the second report on my thesis.

Also, I would like to thank all present and past members of the Helten Group for always providing a great working experience. I thank Dr. Ozan Ayhan, Dr. Artur Lik and Dr. Thomas Lorenz for the heartwarming welcome in the group and passing on their scientific experience and topics to us. I was lucky to always work amongst friends. I especially thank Nicolas Riensch and Merian Crumbach to go this winding and stony road together with me, always providing support and fun in- and outside of the lab and becoming close friends. Additionally, I want to thank Matthias Maier for the many fun moments during and after working hours.

In my PhD research, several talented youngsters helped me to overcome scientific hurdles by carrying out reactions, so I didn't have to. I thank Felix Garg, Marina Chuchmareva, Felix Herter, Florian Seebauer and Ann-Sophie Mack for doing that.

I would like to thank the staff of both inorganic institutes, RWTH and JMU, for helping me along the way, scientifically or otherwise. In Aachen, Dr. Klaus Beckerle, Toni Gossen, Rachida Bohmarat, Dr. Gerhard Fink, Brigitte Pütz, Barbara Bailly-Kaminski and Manuela Lumbardu-Böhme. In Würzburg, Alfred Schertzer, Gertrud Wunderling, Sabine Timmroth, Liselotte Michels, Marie-Luise Schäfer, Dr. Rüdiger Bertermann, Dr. Ivo Krummenacher, Bernhard Werner, Dr. Alexandra Friedrich, Sabine Lorenzen, Christoph Mahler and Manfred Reinhart. Special thanks to Dr. Krzysztof Radacki, for helpful advice, IT support and for trying to teach me the ways of X-Ray structure analysis.

I thank Prof. Dr. Todd Marder and his group for providing a warm welcome in Würzburg, as well as access and introduction to their machines.

During my PhD research, I could always rely on my friends. I thank my closest friends from my hometown, Adnan Halilovic, Jan Koetsier and Stjepan Kunac. Also, my new companions from Aachen and Würzburg, who made my chemistry studies the best time of my life. Especially, I

want to thank Dr. Marcel Lach for becoming a great friend, many situations only some of us can remember, vacations, Football discussions, advice, and deed.

I also want to thank my family. My parents and my bother always had my back, whether emotional or financial. Thank you for never losing faith, inspiring me to keep going and keeping me grounded. This whole thing would not have been possible without you. I love you.

In the end, I thank Marina Chuchmareva. Thank you for the support through the good and the frustrating times, the move to Würzburg and my occasional grumpiness. Thank you for being my partner, my health advisor, and my light in the dark. I love and admire you.

List of Publications

The publications listed below are partly reproduced in this dissertation with permission from The Royal Society of Chemistry [1] and from Georg Thieme Verlag KG [2].

The table itemizes at which position in this work the paper has been reproduced.

Publication	Chapter
[1] N. A. Riensch, L. Fritze, T. Schindler, M. Kremer, H. Helten, *Dalton Trans.* **2018**, *47*, 10399.	2.1
[2] L. Fritze, N. A. Riensch, H. Helten, *Synthesis* **2019**, *51*, 399.	2.2

Further publications:

- R. Philipps, L. Fritze, N. Erdmann, D. Enders, *Synthesis* **2015**, *47*, 2377.
- C. A. Dannenberg, L. Fritze, F. Krauskopf, C. Bolm, *Org. Biomol. Chem.* **2017**, *15*, 1086.
- A. Lik, L. Fritze, L. Müller, H. Helten, *J. Am. Chem. Soc.* **2017**, *139*, 5692.
- A. Lik, S. Jenthra, L. Fritze, L. Müller, K.-N. Truong, H. Helten, *Chemistry* **2018**, *24*, 11961.
- N. A. Riensch, M. Fest, L. Fritze, A. Helbig, I. Krummenacher, H. Braunschweig, H. Helten, *New J. Chem.* **2020**, doi: 10.1039/c8dt01716f.
- M. Crumbach, O. Ayhan, L. Fritze, J. A. P. Sprenger, L. Zapf, M. Finze, H. Helten, *Chem. Commun.* **2021**, *57*, 2408.
- M. Crumbach, J. Bachmann, L. Fritze, A. Helbig, I. Krummenacher, H. Braunschweig, H. Helten, *Angew. Chem. Int. Ed.* **2021**, *60*, 9290.

List of Abbreviations

°C	degree celsius
Å	Angström
abs	absorbance
APCI	atmospheric pressure chemical ionization
aq	aqueous
Ar	aryl group
arom	aromatic
ASAP	atmospheric solid analysis probe
BBr_3	tribromoborane
BCl_3	trichloroborane
BX_2	dihaloboryl
BX_3	trihaloborane
$BF_3{\cdot}OEt_2$	trifluoroborane etherate
$B(OMe)_3$	trimethoxyborane
$B(OR^F)_3$	tris-2,2,2-trifluoroethoxyborane
br	broad
c	concentration
CaH_2	calcium hydride
CH_2Cl_2	dichloromethane
COSY	correlation spectroscopy
C_q	quaternary carbon atom
CV	cyclic voltammetry
D	deuterium
d	days
d	doublet
δ	chemical shift
Da	Dalton
DCB	dichlorobenzene
DCM	dichloromethane
DCM-d2	deuterated dichloromethane
dd	doublet of doublet
DMF	dimethylformamid
DP_n	average degree of polymerization

ε	extinction coefficient
$E_{1/2}$	half wave potential
EI	electron ionization
em	emission
equiv	equivalents
ESI	electrospray ionization
Et	ethyl group
et al.	and others
EtOH	ethanol
eV	electron Volt
EWG	electron-withdrawing group
ex	excitation
Φ_f	fluorescence quantum yield
^{F}Mes	2,4,6-tris(trifluoromethyl)phenyl group
Fur	furyl group
GPC	gel permeation chromatography
GRIM	Grignard metathesis
h	hour
HH	head to head
HCl	hydrogen chloride
HMBC	heteronuclear multiple quantum correlation
HOMO	highest occupied molecular orbital
HRMS	high resolution mass spectroscopy
HSQC	heteronuclear single quantum coherence
HT	head to tail
Hz	Hertz
ICT	intermolecular charge transfer
i-Pr	isopropyl group
IR	infrared
J	coupling constant
K	Kelvin
L	liter
λ	wavelength
λ_{em}^{max}	wavelength of the maximum fluorescence emmision
λ_{ex}^{max}	wavelength of the maximum extinction

LIFDI	liquid injection field desorption ionization
LED	light-emitting diode
LUMO	lowest unoccupied molecular orbital
m	multiplet
m.p.	melting point
m/z	mass per charge
max	maximum
mbar	millibar
Me	methyl group
Mes	mesityl/ 2,4,6-trimethylphenyl group
Mes*	supermesityl/ 2,4,6-tri(*tert*-butyl)phenyl group
Mes*BBr_2	dibromo-2,4,6-tri(*tert*-butyl)phenyl borane
Mes*BCl_2	dichloro-2,4,6-tri(*tert*-butyl)phenyl borane
Mes*Li	2,4,6-tri(*tert*-butyl)phenyl lithium
Mes*MgBr	2,4,6-tri(*tert*-butyl)phenylmagnesium bromide
mg	milligram
Mg	Magnesium
MHz	megahertz
min	minute
mL	milliliter
mmol	millimol
M_n	number-average molecular weight
MS	mass spectroscopy
mV	millivolt
M_v	viscosity-average molecular weight
M_w	weight-average molecular weight
M_z	Z average molecular weight
n-BuLi	*n*-Butyllithium
Na	sodium
nm	nanometer
NMR	nuclear magnetic resonance
norm.	normalized
NTf_2	triflimide/ bis(trifluoromethanesulfonyl)imide
o	ortho
o-DCB	ortho-dichlorobenzene

OFET	organic field-effect transistor
OLED	organic light-emitting diode
on	over night
p	para
P3AT	poly(3-alkylthiophene)
P3AF	poly(3-alkylfuran)
PIB	poly(iminoborane)
pin	pinacol
PPV	poly(*p*-phenylene vinylene)
QY	quantum yield
rt	room temperature
RI	refractive index
s	singlet
SIMS	secondary ion mass spectrometry
t	triplet
TT	tail to tail
t-Bu	*tert*-butyl group
t-BuLi	*tert*-butyllithium
TD DFT	time-dependent density functional theory
Thi	thienyl group
Tip	2,4,6-triisopropylphenyl group
TipLi	2,4,6-triisopropylphenyllithium
$TIPSNTf_2$	triisopropylsilyl triflimide
THF	tetrahydrofuran
TMS	trimethylsilyl group
$TMSNTf_2$	trimethylsilyl triflimide
TMSOMe	methoxytrimethylsilane
$TMSOR^F$	2,2,2-trifluoroethoxytrimethylsilane
TMSX	halotrimethylsilane
UV	vltra violet light
V	volt
Vis	visible light
vs	versus
VT	variable temperature
WCA	weakly coordinating anion

Table of Contents

1 Introduction

1.1 Semiconducting Organic Materials

In the recent past, (semi)conducting π-conjugated organic polymers have continued to attract enormous attention for both scientific and technological reasons, due to their application as an active component in electronic and optoelectronic devices such as (polymer-based) organic light-emitting diodes (OLEDs), field-effect transistors (OFETs), and photovoltaic cells (OPVs).[1] As a replacement for classical inorganic solid-state materials, organic polymers serve the purpose of reducing production costs due to their easy processability. In addition, soft organic materials have the advantage of being lightweight.

Polymers based on five-membered unsaturated heterocycles, such as polypyrrole,[2] polyfuran,[3] polythiophene,[4,5,6] polyselenophene,[7,8] polytellurophen,[9] and derivatives thereof, have emerged as important material classes, being extensively studied and applied. Substituted and unsubstituted α-oligo- and α-polythiophenes are currently the most important materials for the development of organic thin-film transistors and photovoltaics.[5,10] Synthetic routes with varying sidechains and sidechain densities, stereo- and regiochemistry have been reported over the last decades. The critical issue in these studies is the solubility of the resulting compounds. For example, the α-sexithiophene **1** was reported to be almost completely insoluble in common organic solvents (Figure 1.1.1).[11] To obtain polythiophene materials that are soluble in common organic solvents, flexible alkyl side chains need to be attached to form poly(3-alkylthiophene)s (P3ATs) **2**.[12]

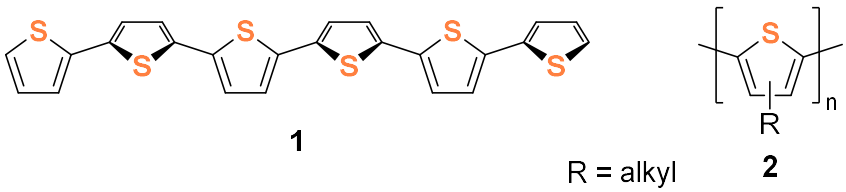

Figure 1.1.1: *Structures of sexithiophene **1** and P3AT **2**.*

Because of the asymmetric nature of the used monomer species to form P3ATs and the associated lack of structural integrity of the materials, investigation of electrical and optical properties has been difficult. Physical studies on polymers are particularly affected by solubility issues, which can lead to difficulties in data interpretation and inaccurate conclusions.[13]

If P3ATs are formed by C–C coupling reactions in a random fashion, the thiophene rings in P3ATs are connected in either head-to-head (HH), head-to-tail (HT), or tail-to-tail (TT) regiochemistry (Figure 1.1.2). In regioirregular configurations, the steric demand of the alkyl groups in HH and TT couplings can cause a twist of the thiophene rings, pushing them out of their coplanar conformation and preventing unhindered π-conjugation along the main chain,

which is needed for the P3AT to develop its full optoelectronic potential. The regioregular HT configuration is the most desirable because it provides the most space for the alkyl groups and therefore the least drive for twisting.

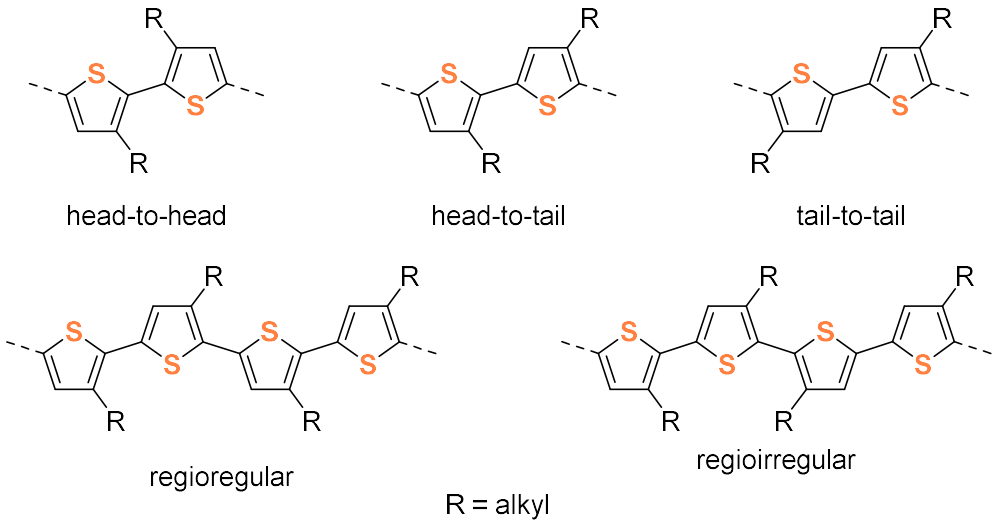

Figure 1.1.2: *Configuration possibilities of P3ATs.*

One of the earliest examples of the synthesis of P3ATs was given by Sugimoto and coworkers, where the coupling of the monomer was catalyzed by iron(III) chloride ($FeCl_3$),[14] and Morii and coworkers, using electrochemical polymerization conditions.[15] Later, McCullough and coworkers presented a polymerization strategy using Kumada-type coupling. They reported high regioregularity with HT coupling percentages of up to 91% (Scheme 1.1.1).[16] In a one-pot reaction, 2-bromo-3-alkylthiophenes **3** were used to generate species **4**, which were then polymerized through the Ni-catalyzed Kumada reaction to form P3ATs **5**. Interestingly, this Grignard metathesis (GRIM) polymerization reaction was later reported to be of a quasi-"living" nature.[17] Via this route[18] or different approaches that use Stille or Suzuki-Miyaura coupling reactions,[19] P3ATs with >99% HT were synthesized.

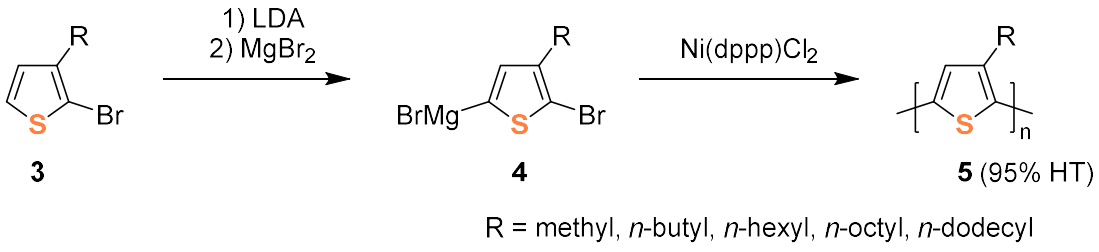

Scheme 1.1.1: *Early approaches to P3ATs with high regioregularity.*

However, compared to polythiophenes, their other group 16 analogues are significantly less well studied. Polyfurans, for example, have enjoyed far less attention. In the past, issues with their low stability, poor properties and difficulties in polymerization have been reported.[20] Still,

their molecular structure promises advantages: Whereas the sexithiophene **1** is planar in the solid state, oligo- and polythiophenes adopt twisted conformations in solution, which is evidenced by their normally broad and featureless absorption spectra.[21] On the other hand, α-oligo- and α-polyfuranes like **6** and **7** (R = octyl) have been reported to be planar, as supported by experiments and theoretical calculations (Figure 1.1.3).[22] This planarity leads to increases in conjugation, improved solubility, and better transport properties. Another benefit of furan-based chemicals is their derivability from biomass and their biodegradability.[23]

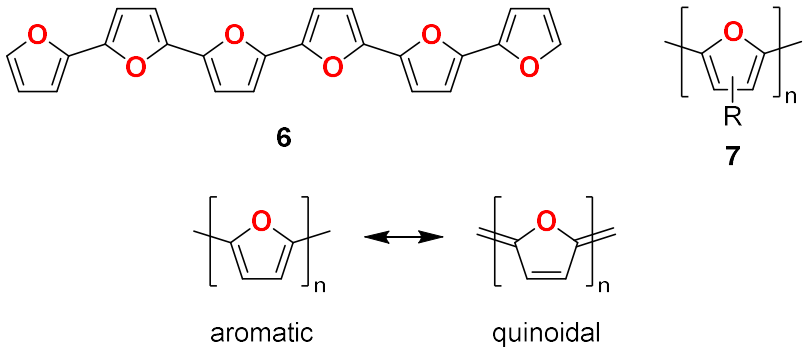

Figure 1.1.3: *Structures of sexifuran **6** and P3AF **7**.*

Additionally, furan possesses a lower aromaticity compared to thiophene[24] and the use of furan as a building block in polymer structures leads to an increase in the band gap of that system.[25] Furthermore, furan tends to a larger contribution from the quinoidal resonance structure in polyfurans (Figure 1.1.3),[26] resulting in much higher rigidity of the system, and it being more likely to adopt a planar conformation compared to the related thiophene analogues.

Curtis and coworkers presented the first synthesis of poly(3-alkylfuran)s (P3AFs), yielding compound **10** by subsequently forming **9** from 2,5-dibromo-3-alkylfuran **8** using Rieke zinc and performing a Ni-catalyzed polymerization (Scheme 1.1.2).[22]

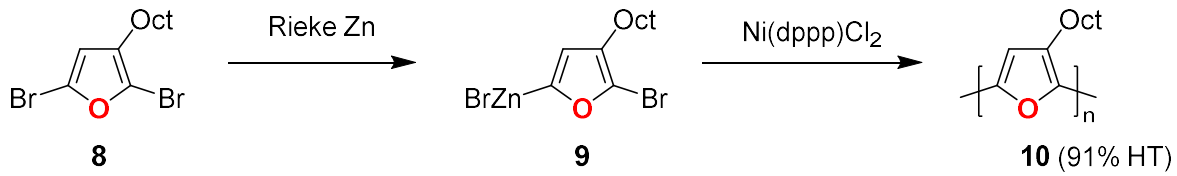

Scheme 1.1.2: *Early approaches to P3AFs with high regioregularity.*

Changing the heteroatom in the five-membered ring from sulfur and oxygen to selenium or tellurium has a great impact on the properties of the resulting polymers.[8] Because of their bigger atom size, selenium and tellurium are more easily polarized and can accommodate more charge upon doping. Other characteristics are the more pronounced interactions between heteroatoms when adjacent to each other, lower oxidation and reduction potentials, as well as lower band gaps, which can be beneficial for their optical and electronical properties.

1.2 Conjugated Inorganic–Organic Hybrid Polymers

By incorporating inorganic main group elements into the polymer structure, conjugated polymers can be provided with fascinating properties and functions specific for each incorporated element, which cannot be achieved with purely organic macromolecules.[12,27] The huge potential associated with this doping strategy has been recognized making it the subject of tremendous research activity in the last years.[2]

The incorporation of main group elements into polymers can happen through different strategies, resulting in different types of polymers: If the backbone of the polymer only consists of main group elements other than carbon, the polymer is titled as an *inorganic polymer* (Figure 1.2.1). That is independent of the nature of the side groups. Well-known examples are polysiloxanes and polysilazanes,[28] polyphosphazenes,[28] polyborazylenes,[29] polyaminoboranes,[30] and polythiazyl.[31] When both organic and inorganic building blocks form the backbone of a polymer, it is classified as an *inorganic–organic hybrid polymer*. If the main group element is only part of the side groups, the polymer is called an *organic–inorganic polymer*.[32]

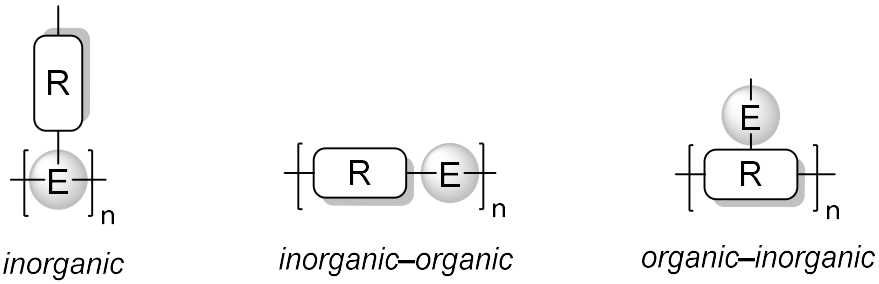

Figure 1.2.1: *Classes of polymers containing main group elements.*

Incorporation of trivalent, tricoordinate boron into extended π-systems results in an interaction of the vacant p orbital on boron with the π-electron system (Figure 1.2.2, left). Boron is more electropositive than carbon, and thereby a boryl group acts as an inductively σ-donating group.[33] B-doping produces electron-deficient, possibly n-type semiconducting materials with interesting properties, which makes it a viable strategy that can be used for various applications.[34] Moreover, a boryl group has a pronounced Lewis acidity, which opens up the ability to bind Lewis bases. Triarylboranes readily react with certain nucleophiles to produce the corresponding tetracoordinate borates. That allows these materials to be used as chemosensors, for example, for detection of certain anions or amines in combination with an optical or electric response.[35]

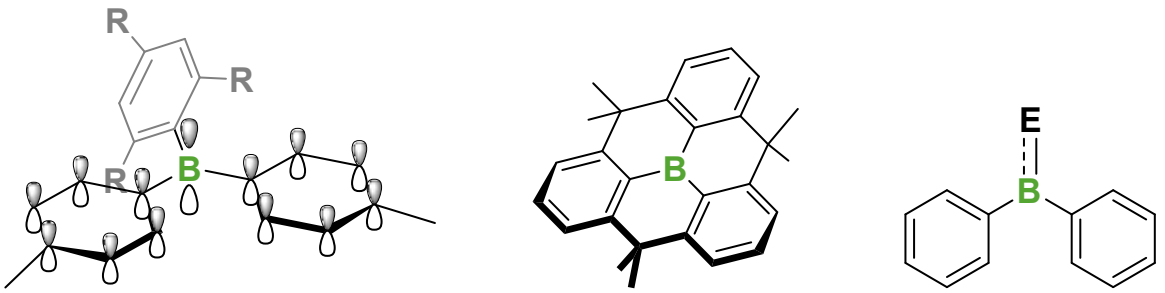

Figure 1.2.2: *Stabilization of a boron center in an extended π-system.*

An issue in designing organoboron materials is stabilizing the reactive Lewis acidic boron center against nucleophilic attacks, to ensure stability against air and moisture. A general strategy for kinetic stabilization of the boron moiety is steric protection (Figure 1.2.2, left). Most of the reported materials hold at least one bulky aryl group on the boron atom. However, their bulkiness sometimes gives rise to a detrimental effect on the solid-state properties that rely on the intermolecular interaction, such as charge carrier transporting properties. Different approaches are the stabilization based on structural constraint (Figure 1.2.2, center) or stabilization by electronic effects (Figure 1.2.2, right).[36] All options have been chosen in the last decades to produce a range of different organoborane compounds.

1.2.1 Synthesis Routes to Conjugated Organoborane Polymers

The strategies for synthesizing organoboron polymers mainly depend on the kind of bonds that are present in the polymer main chain. The outlined synthetic routes to polymers with tricoordinate boron in their main chain are divided into three categories: B–C coupling, C–C coupling, and B–E coupling (E denotes another main group element such as nitrogen or oxygen).

1.2.1.1 Polymerization via B–C coupling

Chujo and coworkers presented an early example of a polymerization procedure via B–C coupling (Scheme 1.2.1).[37] They synthesized poly-(vinylenearylenevinylene-borane)s **11a-c** by using hydroboration of 1-ethynyl-4-vinylbenzene with thexylborane. To achieve stability towards air and moisture, they also performed this polyaddition route using mesitylborane (Mes = 2,4,6-trimethylphenyl, mesityl) for **11b**[38] and $TipBH_2$ (Tip = 2,4,6-triisopropylphenyl) for **11c**,[39] which allowed them to determine the molecular weights by gel permeation chromatography (GPC) relative to polystyrene standards. These reactions take place in tetrahydrofuran (THF) at ambient temperature (rt).[39]

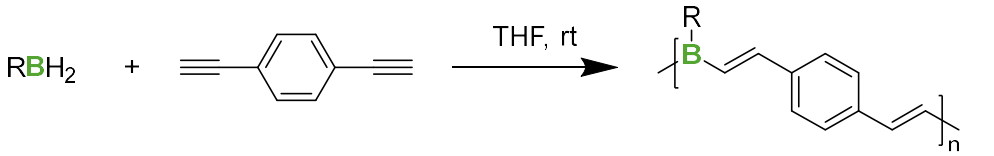

11a: R = 2,3-dimethylbutane
11b: R = Mes
11c: R = Tip

Scheme 1.2.1: *Hydroboration polymerization reaction by Chujo and coworkers.*

The UV-vis absorption and emission characteristics of the polymers indicated effective π-conjugation along their backbone, showing a contribution of the vacant p orbitals of the boron atoms.[39]

In a similar approach, Wagner, Holthausen, Jäkle, and coworkers introduced the organoborane 9,10-dihydro-9,10-diboraanthracene **12** as a building block for conjugated polymers, which should give several advantages like an already inherited π-conjugated electron system in the monomer, maximum π overlap between the boron atom and the aromatic substituents, and higher stability compared to the open chain derivatives (Scheme 1.2.2).[40] This stability is induced by the rigidity of the polycyclic structure. This organoborane **12** serves as an efficient precursor for the preparation of boron-doped π-conjugated polymers by hydroboration polymerization with a functionalized 1,4-diethynylbenzene.

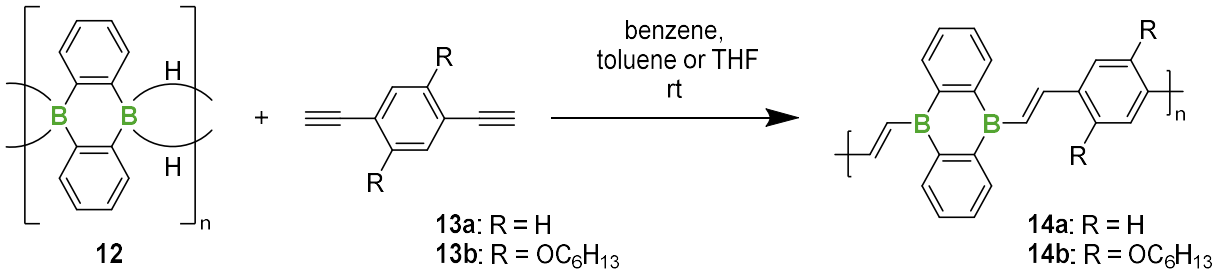

12

13a: R = H
13b: R = OC_6H_{13}

14a: R = H
14b: R = OC_6H_{13}

Scheme 1.2.2: *Hydroboration polymerization of 9,10-dihydro-9,10-diboraanthracene* ***2****.*

The reaction takes place in benzene (R = H), toluene and THF (R = OC_6H_{13}) at ambient temperature. A GPC analysis was not possible due to the polymers' high sensitivity towards air and moisture.[40]

While hydroboration polymerization has proven to be a potent strategy for the synthesis of conjugated organoborane polymers, the formation of B-aryl or B-alkynyl bonds in the backbone of the polymer chain is not feasible via this route. For this purpose, polycondensation protocols, for example, organometallic metathesis reactions of difunctional Grignard reagents[41] or dilithio compounds[42] with aryldihalo- or aryldialkoxyborane can be applied.

Jäkle and coworkers introduced the tin/boron exchange metathesis reaction to polymer chemistry, which provides facile and selective access to polymeric Lewis acids.[43] Distannylated bithiophene **15** substituted with solubilizing hexyl substituents serves as a versatile polymer precursor. Condensation polymerization was achieved under mild conditions by treatment with various bifunctional arylboron halides [$ArBBr_2$; Ar = 4-*i*PrPh, C_6F_5, ferrocenyl (Fc)] in CH_2Cl_2 (DCM) at ambient temperature to give **16a-c** (Scheme 1.2.3).[44]

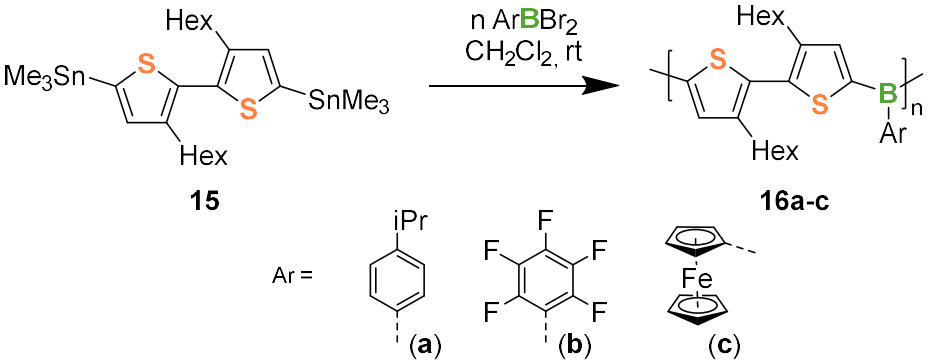

Scheme 1.2.3: *Synthesis of boron-modified polythiophenes* ***16a-c*** *via Sn/B exchange polycondensation.*

Subsequently, Jäkle and coworkers reported the synthesis of a poly(fluorenylborane) scaffold **19** from bis-stannyl fluorene **17** and bis(dibromoboryl) fluorene **18** (Scheme 1.2.4).[45] Both substrates could be derived from the same fluorene precursor. From this universal polymer scaffold, the triaryl borane polymers **20a,b** were obtained by reaction with the mild aryl transfer reagents 2,4,6-trimethylphenylcopper (MesCu) and 2,4,6-triisopropylphenylcopper (TipCu), respectively.

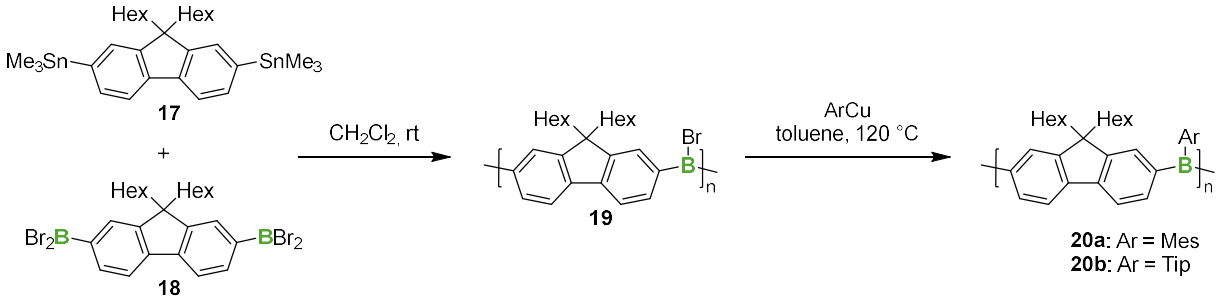

Scheme 1.2.4: *Modular synthesis of fluorenylborane polymers* ***20a-b****.*

The modification of the boron centers in the last reaction step is crucial to this route, making it possible to quickly generate different compounds and tailoring their properties.

Jäkle and coworkers applied the tin/boron exchange condensation protocol to gain access to various organoborane polymers and oligomers; for example, a poly(thienylborane) was obtained by a similar two step protocol to the one shown in Scheme 1.2.4.[44,46,47,48]

Very recently, Helten and coworkers developed an environmentally benign and broadly applicable method for the controlled synthesis of π-conjugated organoborane compounds via catalytic silicon/boron exchange and presented a synthesis of poly(thienylborane)s and poly(furylboranes)s (Scheme 1.2.5).[49] Their route avoids toxic organotin compounds used as substrates or formed as byproducts. To allow the B–C bond formation to proceed under mild conditions, they used an electrophilic silyl reagent, trimethylsilyl bistriflimide (Me_3SiNTf_2), to effectively catalyze the reaction.

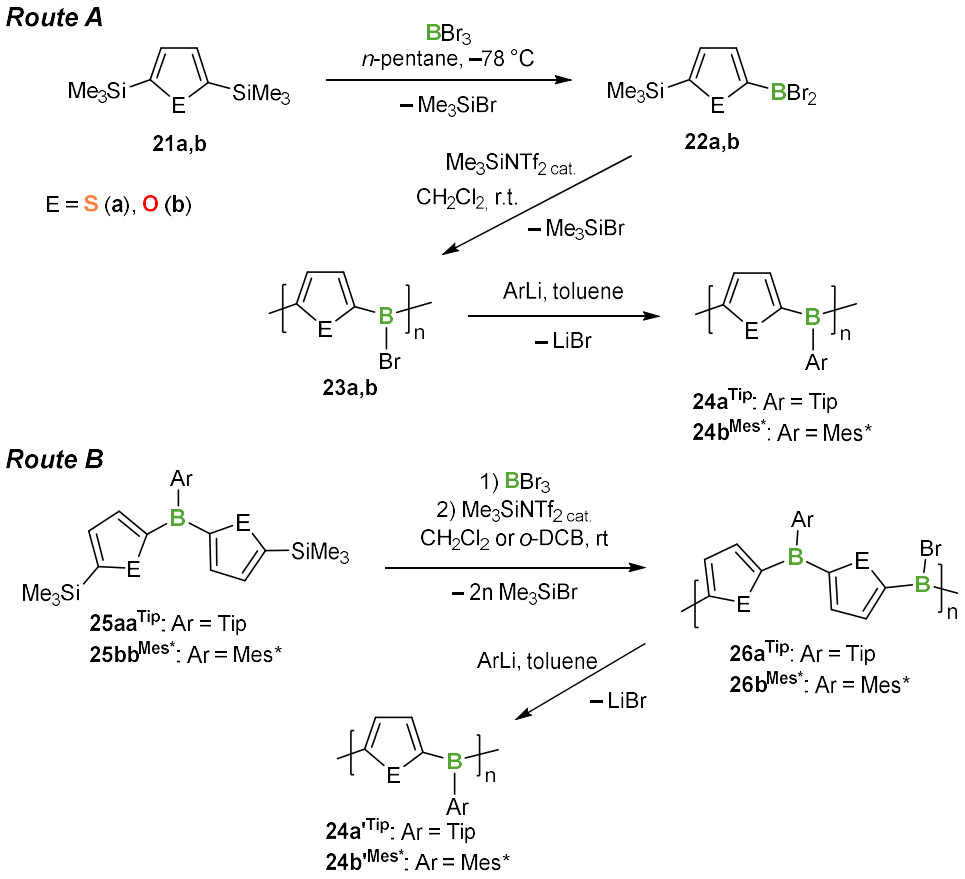

Scheme 1.2.5: *Synthesis of oligomers* ***24a-b*** *and* ***24a'-b'*** *via Si/B exchange polycondensation.*

The otherwise lower activity of the Si/B exchange reaction additionally allowed the selective synthesis of AB type monomers to form the oligomer scaffold **23a,b** (Scheme 1.2.5, Route A). Using such types of monomers has the great advantage over previous approaches that the reaction no longer depends on the exact stoichiometry of the monomers, because every monomer inherits both reactive sites, trimethylsilyl ($SiMe_3$) and BBr_2, in the needed ratio of 1:1. Postmodification with TipLi or Mes*Li (Mes* = 2,4,6-tertbutylphenyl, supermesityl) allowed the synthesis of thienyl- and furyl oligomers **24a,b**, which are stable against air and moisture. A second route was reported (Scheme 1.2.5, Route B), where substrate **25** was used. The solubility-enhancing aryl groups of **25** were introduced to enhance the solubility of the growing polymer chain **26**. That modification lead to improved molecular weights of resulted polymers

24a',b' compared to Route A. Helten and coworkers used the Si/B exchange protocol for the synthesis of various mixed organoboranes and oligomers.[50]

1.2.1.2 Polymerization via C–C coupling

C–C coupling polymerizations are usually performed with the use of transition metal catalyzed cross-coupling protocols, putting them in the class of polycondensation reactions. The reactants must already contain the boron centers, which need to be kinetically well stabilized, since the reaction conditions are oftentimes harsh.

Yamaguchi and coworkers reported the synthesis of rigid-rod oligomers and polymers comprising a recurring benzodiazaborole unit by palladium catalyzed Stille-type polycondensation (Scheme 1.2.6).[51] The expansion of the electron system through the B–C and B–N bonds of the oligomers was confirmed by UV-visible spectroscopy. The reaction was carried out at 90 °C in dimethylformamide (DMF) for 48 h.

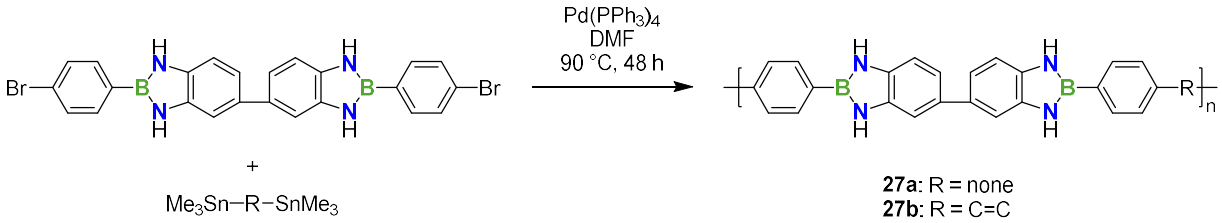

Scheme 1.2.6: *Synthesis of bisbenzodiazaborole oligomers **27** via Stille-type polycondensation.*

Marder, Jäkle and coworkers presented the synthesis of a conjugated copolymer by Suzuki-Miyaura cross-coupling. By reacting a 5,5'-diiododithienylborane **28a** and a diboronated fluorene derivative **29** they prepared oligomer **30** (Scheme 1.2.7).[52]

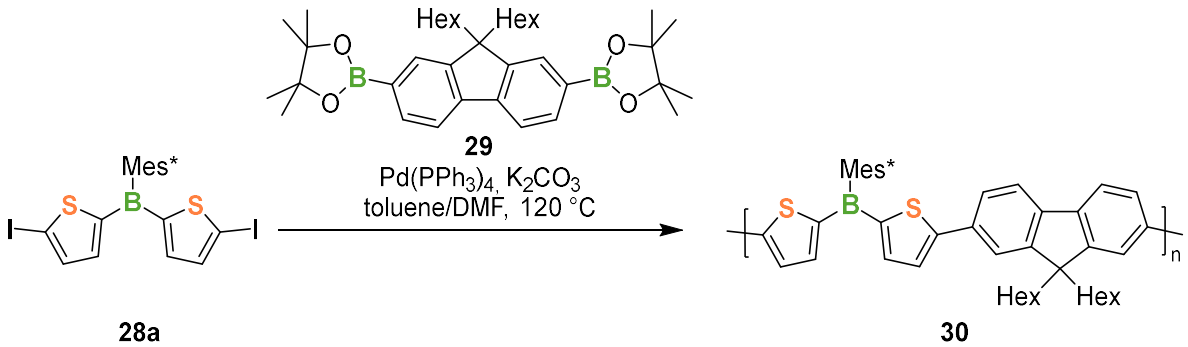

Scheme 1.2.7: *Synthesis of a conjugated oligomer **30** via Suzuki-Miyaura cross-coupling.*

The bulky Mes* groups on the boron centers greatly increase the stability, thus making the borane species inert to air, moisture, and even acids and bases.[52] They also presented the highly electron-deficient fluoromesityl- (2,4,6-tris(trifluoromethyl)phenyl, ^{F}Mes) substituted dithienylborane **28b**.

Using the same thienylborane building blocks **28a,b**, Jäkle and coworkers subsequently synthesized a series of different luminescent organoborane polymers with oligothiophene bridges between the boron centers consisting of m = 1 to 5 thiophene rings using stannylated thienyl and thienylborane monomers (Scheme 1.2.8).[48] Again, the properties of the electron-deficient fluoromesityl dithienylborane **28b** were examined.

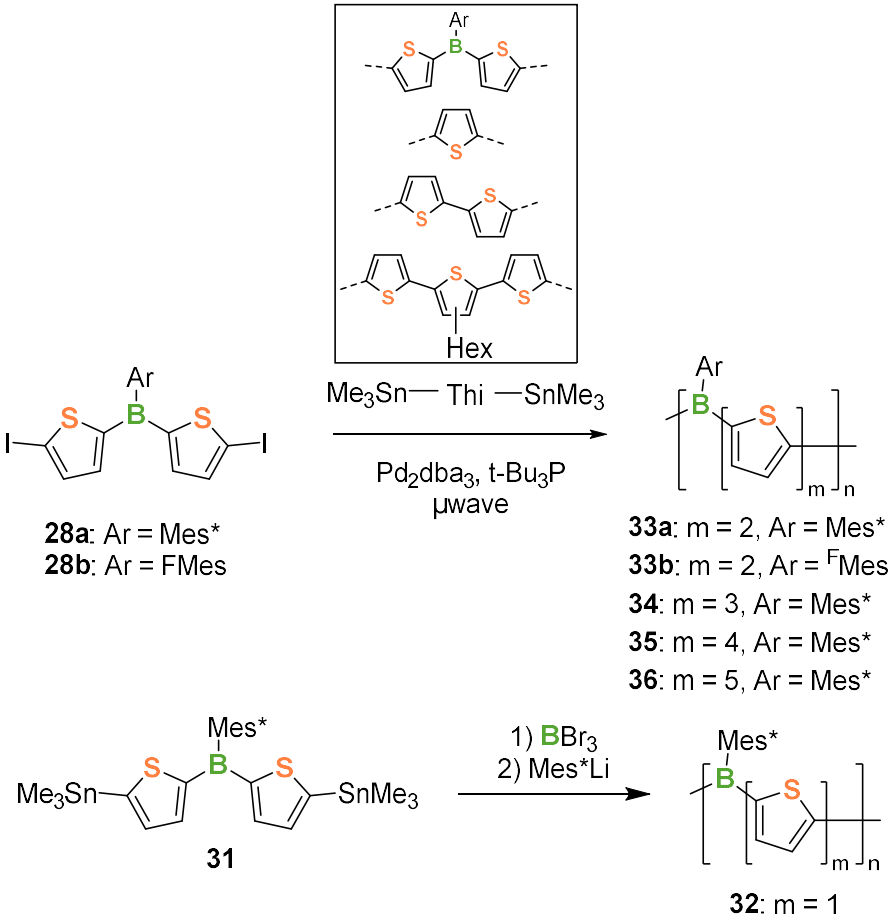

Scheme 1.2.8: *Synthesis of boron-containing polymers **32** to **36** with different lengths of the oligothiophene bridges.*

For m = 1, polymer **32**, they applied their Sn/B exchange polycondensation protocol. The other polymers m = 2 to 5, **33** to **36**, were synthesized via Pd-catalyzed Stille coupling. A hexyl group was introduced on the central thiophene ring of **36** to increase the solubility of the resulting polymer. The polymers exhibit excellent long-term chemical stability to air and moisture and remarkable thermal stability

Bonifácio and coworkers developed the synthesis of a boron-containing copolymer capable of producing a photoluminescence response towards anions (Scheme 1.2.9).[53] The random 9,9-dialkylfluorene/dibenzoborole copolymer **37** was synthesized in a Yamamoto-type aryl–aryl coupling using a 90:10 molar ratio of both comonomers.

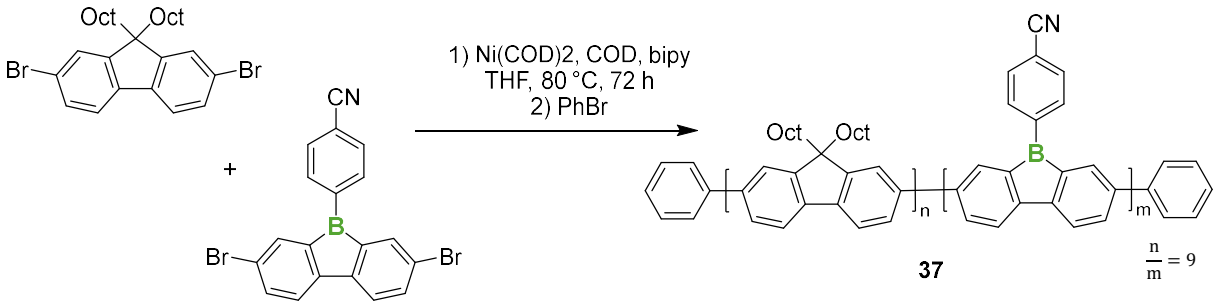

Scheme 1.2.9: *Synthesis of the random fluorene/dibenzoborole copolymer* ***37*** *via Yamamoto-type coupling.*

After the polymerization time of 3 days, bromobenzene (PhBr) was added for end capping. In their study, they found that the ‘‘unprotected’’ dibenzoborole that is electronically stabilized by a cyano group in the *para*-position of the 9-phenyl substituent exhibits good environmental stability. Photoluminescence quenching with sensitivity in the micromolar range was observed for fluoride, cyanide, and iodide.

Rupar and coworkers later prepared the first poly(9-borafluorene) homopolymer, a boron congener of polyfluorene, by Ni-catalyzed Yamamoto coupling of a Tip-substituted borafluorene.[54] The bulky Tip group on the boron center renders this polymer moderately air-stable in solution and indefinitely air-stable in the solid state. The polymer was reported as also capable of a photoluminescence response towards fluorine anions.

Liu, Jäkle and coworkers presented a regioregular synthesis of the first azaborine oligomers and a corresponding conjugated polymer, accomplished by Pd-catalyzed Suzuki-Miyaura polycondensation of an AB-type monomer **38** (Scheme 1.2.10).[55] An almost perfectly coplanar syn arrangement of the heterocycles was derived from an X-Ray crystal structure of the dimer model compound, which also revealed that N–H···π interactions play a key role.

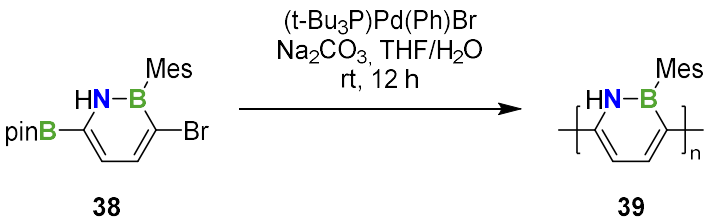

Scheme 1.2.10: *Synthesis of* ***39*** *via Suzuki-Miyaura polycondensation.*

The electronic structure of the longer azaborine oligomers and polymer resembles that of poly(cyclohexadiene) more than poly(*p*-phenylene), as supported by computational studies. Upon chain elongation, the oligomers and polymers undergo a strong bathochromic shift, suggesting highly effective extension of conjugation.

He and coworkers developed a versatile way to synthesize polymerizable 9,10-azaboraphenanthrene-containing monomers by aromaticity-driven ring expansion reactions between highly antiaromatic borafluorene and azides.[56] To show the versatility of monomer

40, it was used in Suzuki-Miyaura- and Stille-type polycondensation reactions (Scheme 1.2.11).

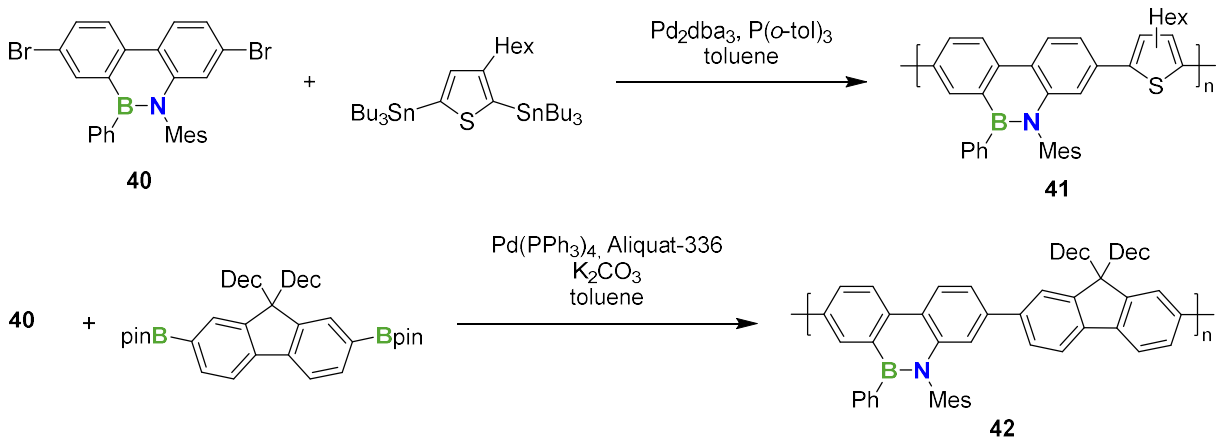

Scheme 1.2.11: *Synthesis of the polymers **41** by Stille cross-coupling and **42** by Suzuki-Miyaura cross-coupling.*

The conjugated polymers show good stability towards air and moisture and notable fluorescence properties. Addition of fluoride anions induced a rapid and fully reversible change in the emission color from blue to green and yellow, showing the sensing abilities of the system.

1.2.1.3 Polymerization via B–E coupling

Formation of new boron-element bonds in the backbone of a polymer has proven to be another viable strategy for their synthesis. To this end, Chujo and coworkers presented an alkoxyboration polymerization of diisocyanates with mesityldimethoxyborane, giving an example for a polyaddition reaction with formation of new B–N bonds.[57] Helten and coworkers recently demonstrated different approaches to a range of B–N containing polymers and oligomers.[58,59,60] They presented the first examples of a new class of inorganic-organic hybrid polymers **43**, which consist of alternating NBN and *p*-phenylene units. Polycondensation by B/Si exchange with B–N bond formation provided facile access to soluble materials under mild conditions (Scheme 1.2.12).[58] In that study, they provided evidence for π conjugation across the NBN units along the polymer backbone. After an endcapping procedure, cross-linking this polymer with $Zr(NMe_2)_4$ gave a highly cross-linked metallopolymer **44** with adjustable cross-linking density.

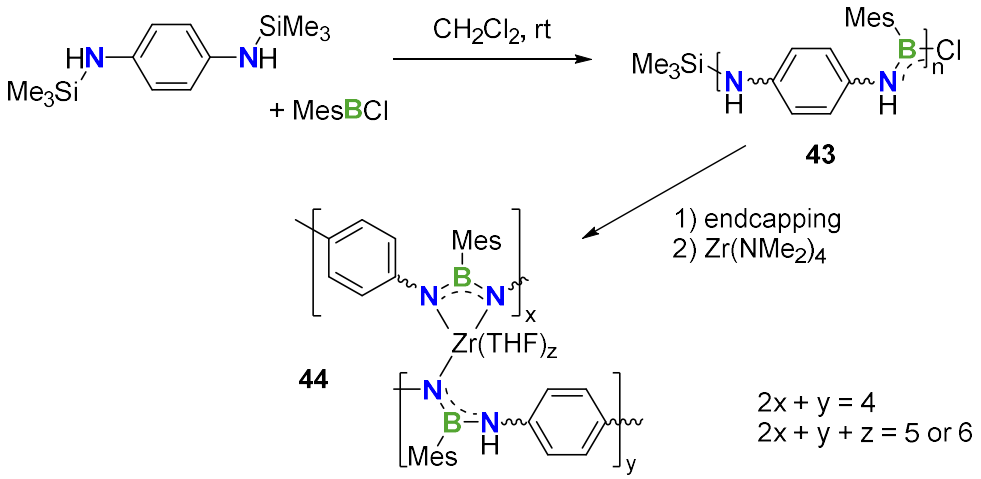

Scheme 1.2.12: *Synthesis of polymer **43** by Si/B exchange and subsequent cross-linking via Zr^{IV} to give **44**.*

With the synthesis of a BN-analogue of poly(*p*-phenylene vinylene) (PPV), they provided the first example of a poly(*p*-phenylene iminoborane).[61] Using a similar polycondensation procedure, they performed B–N bond formation through B/Si exchange and showed that effective π-conjugation across the BN units occurs along the polymer backbone.

Subsequently, they demonstrated the synthesis of an inorganic polymer, a polymer that exclusively consists of elements other than carbon, by giving the first example of a poly(iminoborane) (PIB) **46**.[59] By linking the adjacent nitrogen centers in the monomer, they avoided the formation of borazine during the polymerization process. The polymerization can be achieved via different routes: Si/B exchange, Sn/B exchange, and, as a novel approach, the polymerization of a dormant A-B type monomer **45** initiated by a Brønsted acid (Scheme **1.2.13**).

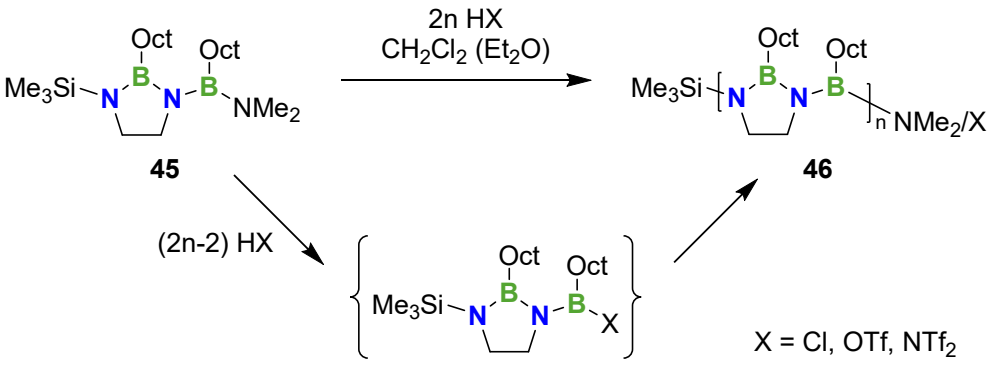

Scheme 1.2.13: *Polymerization of dormant monomer **45** initiated by Brønsted acids.*

Lavigne and coworkers reported an example for a polymerization by B–O bond formation by presenting a synthesis of borole-linked polymers that have been self-assembled based on boronate ester formation between a fluorene-2,7-diboronic acid and 1,2,4,5-tetrahydroxybenzene.[62]

1.3 Organic Macrocycles

Fully π-conjugated and shape persistent macrocycles represent a structure motif, which attracted great interest in the last decades. In comparison with their linear congeners, these systems have the benefit to combine the advantages of a defect free π-conjugated chain of an idealized polymer with the advantages of a structurally well-defined oligomer. The absence of end groups additionally excludes disruptive end effects.[63] Additional properties and behaviors like aggregation, host-guest interaction, and self-assembly at interfaces, make π-conjugated macrocycles especially interesting for applications in organic and molecular electronics.[6][64]

Thiophene-based macrocycles like the ones shown in Figure 1.3.1 have special significance in research. The smallest rings, cyclo[2]thiophenes **47**, were presented by Shepherd and coworkers and showing evidence of effective electronic interaction between the two thiophene units.[65] Subsequently, Bendikow and coworkers presented their Ni-catalyzed cyclotrimerization reaction to cyclo[3]thiophenes **48a**, which were reported as practically planar.[66] The [*b*]-fused analogue **48b** was presented by Korte and coworkers.[67] The larger cyclo[6]thiophene **49** was reported by Kauffmann and coworkers to be heavily distorted with strongly twisted thiophene rings [68]

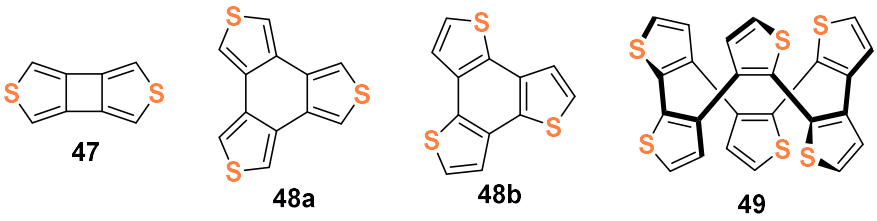

Figure 1.3.1: *Examples of small cyclothiophenes* ***47-49****.*

Tol performed theoretical investigations on fully α-conjugated cyclothiophenes, which revealed that an all-*syn* conformation of α-bonded thiophenes resulted in a nearly unstrained and coplanar structure.[69] Since then, Bäuerle and coworkers have made significant progress in the synthesis of these systems. They presented the synthesis of the first fully α-conjugated cyclothiophenes **50**, performing the ring synthesis under pseudo high-dilution (Scheme 1.3.1).[70]

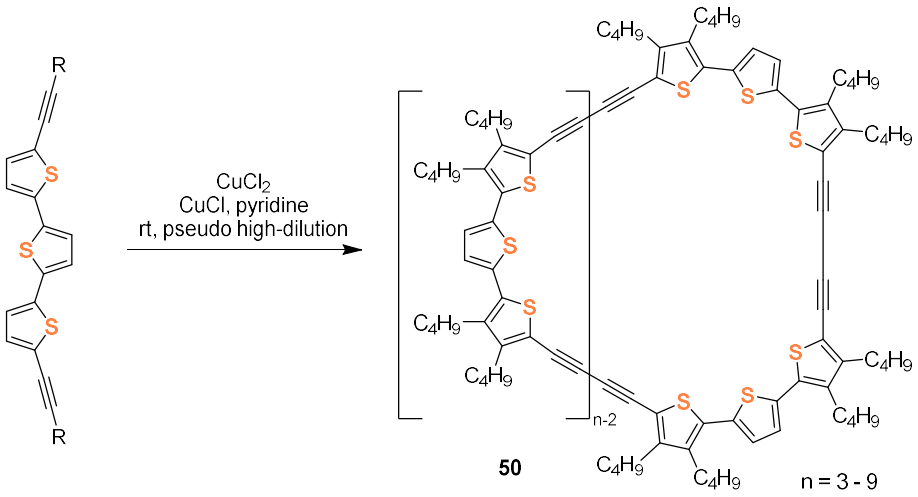

Scheme 1.3.1: *Synthesis of first fully α-conjugated cyclothiophene* ***50****.*

Among thiophene-based macrocycles, bridged heterocyclic analogues of [18]annulene, have special significance. Vogel and coworkers synthesized the first tetrathiaporphyrin dication **51** and its furan **52** and selenophene **53** congeners (Scheme 1.3.2).[71] According to Hückel's rule, the neutral precursor of **51** is an antiaromatic system and therefore unstable. Compound **51** on the other hand was reported to have an aromatic and fully conjugated π-system, comparable to that of [18]annulene. X-Ray analysis of **51** revealed a twist of the thiophene rings of 3.7 ° and 23 °, which was reported to be too small to significantly hinder aromaticity.

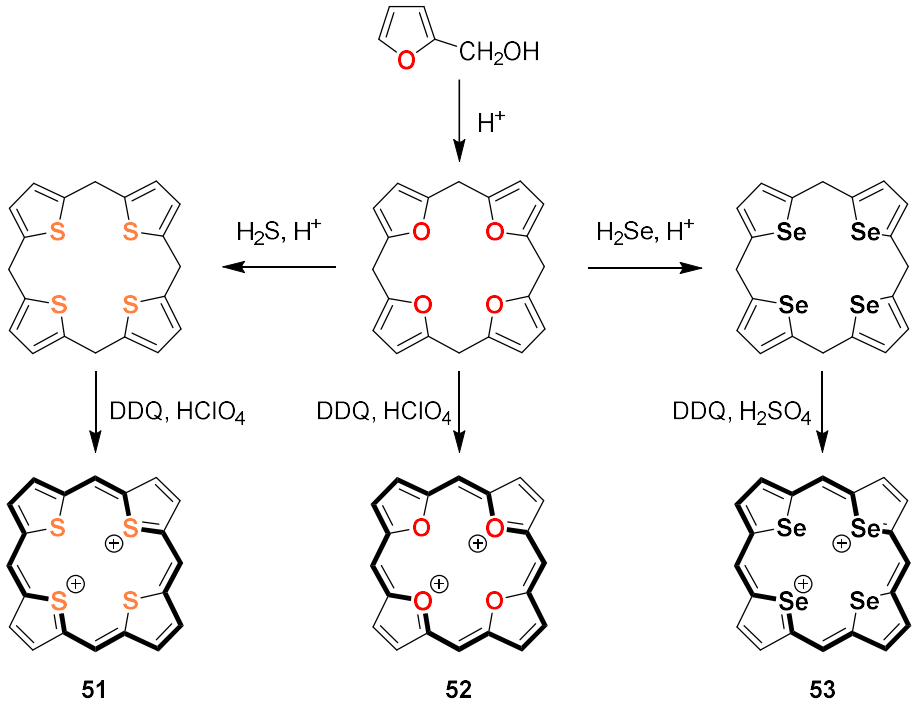

Scheme 1.3.2: *Synthesis of the first heterocyclic porphyrins and their dications* ***51-53****.*

1.4 Inorganic–Organic Macrocycles

Introducing heteroatoms into the conjugated macrocycles can lead to additional functionality and enable new applications.[72] However, examples of tricoordinate boron-embedded macrocycles are still rare, partly because unprotected tricoordinate boron species are generally unstable and difficult to handle in air.[73]

While Tanaka and coworkers presented an early example of a doped cyclophane **54** (Figure 1.4.1),[74] Jäkle and coworkers have replaced the implemented nitrogen atoms with boron in the synthesis of **55** and **56**, and particularly highlighted the differences of those systems to the corresponding linear compounds. Macrocycle **55** inherits both electron-acceptor (boron) and electron-donor groups (nitrogen) together in the ring structure, which leads to enhanced π-conjugation.[75] Subsequently, they presented **57**, where dimethylfluoryl-linker were placed between the boron centers, reducing the ring strain.[47] All these moieties captivate through their optical properties, especially in contrast to their linear analogues, and show distinct anion binding capabilities. One of their latest macrocycles **58** presents a new class of element-hybrid conjugated systems, reported to show intramolecular photo energy transfer between the germanium and boron building blocks.[73]

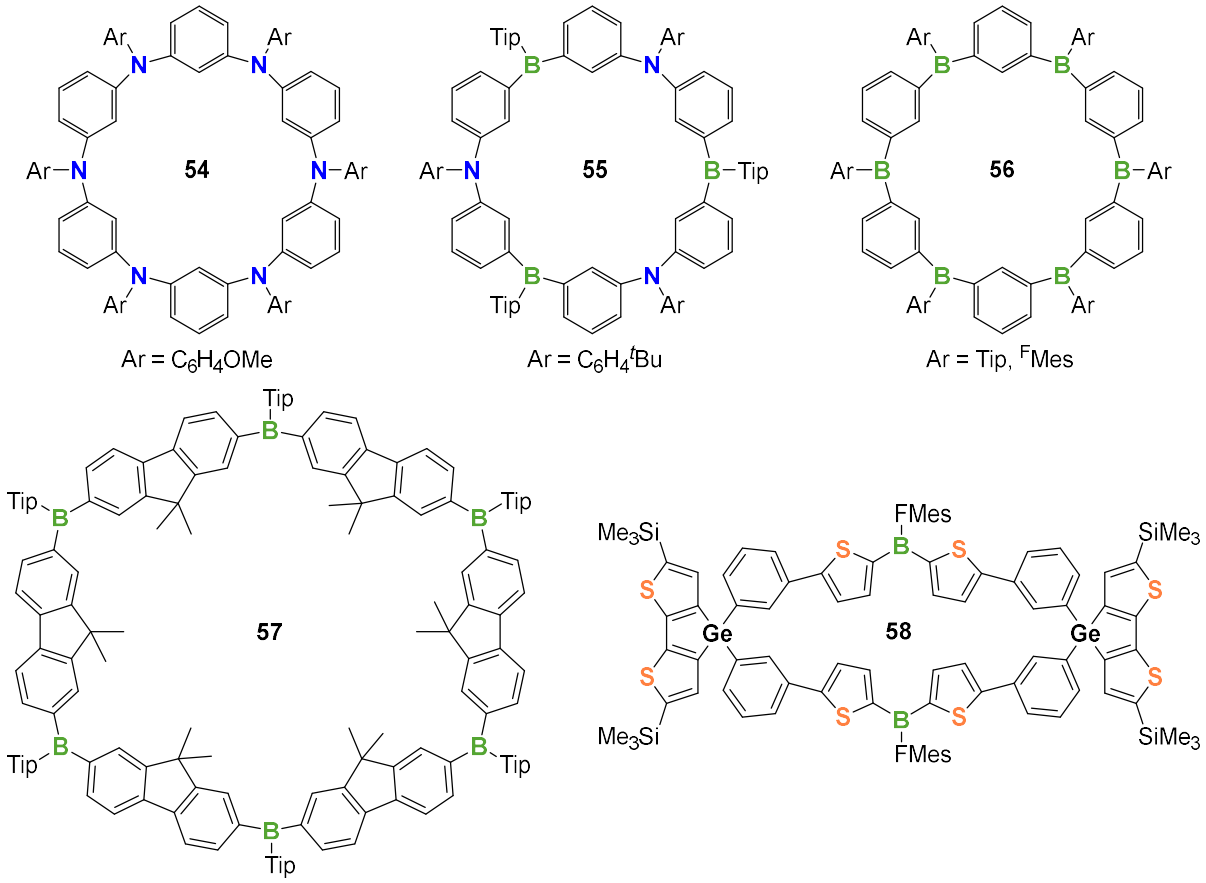

Figure 1.4.1: *Different boron-containing macrocycles.*

König and coworkers investigated incorporation of heteroatoms in the tetrameric methine-bridged oligothiophenes, forming silicon-, tin- and phosphorous-bridged tetrathiaporphyrins.[76] For their boron-bridged analogue, the first example was given by Siebert, Corriu and coworkers, which was synthesized via [2+2]-cycloaddition reaction route (Figure 1.4.2, top route).[77] X-Ray structure determination reported this macrocycle as non-planar, with heavily twisted thiophene rings, which prevents effective π-conjugation along the ring structure. Later, they presented a [3+1]-cyclisation approach to access tetraboratetrathiabora-porphyrinogen **60** and tetraboradithiaporphyrinogen **61** (Figure 1.4.2, bottom route), again featuring heavily twisted heterocycles in the ring.

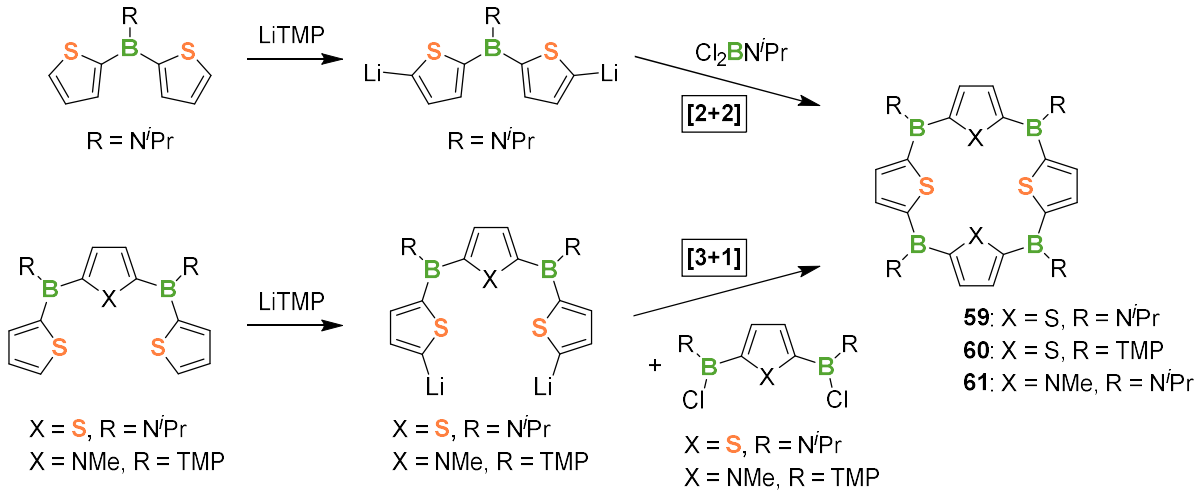

Figure 1.4.2: *Routes to boron-bridged tetrathiaporphyrins* ***59-61****.*

1.5 References

[1] a) T. M. Swager, *Macromolecules* **2017**, *50*, 4867; b) C. Wang, H. Dong, W. Hu, Y. Liu, D. Zhu, *Chem. Rev.* **2012**, *112*, 2208; c) C. Li, M. Liu, N. G. Pschirer, M. Baumgarten, K. Müllen, *Chem. Rev.* **2010**, *110*, 6817; d) A. C. Grimsdale, K. L. Chan, R. E. Martin, P. G. Jokisz, A. B. Holmes, *Chem. Rev.* **2009**, *109*, 897.

[2] a) R. McNeill, R. Siudak, J. H. Wardlaw, de Weiss, *Aust. J. Chem.* **1963**, *16*, 1056; b) S. J. Higgins, *Chem. Soc. Rev.* **1997**, *26*, 247; c) G. Sabouraud, S. Sadki, N. Brodie, *Chem. Soc. Rev.* **2000**, *29*, 283.

[3] a) O. Gidron, Y. Diskin-Posner, M. Bendikov, *J. Am. Chem. Soc.* **2010**, *132*, 2148; b) X.-H. Jin, D. Sheberla, L. J. W. Shimon, M. Bendikov, *J. Am. Chem. Soc.* **2014**, *136*, 2592; c) D. Sheberla, S. Patra, Y. H. Wijsboom, S. Sharma, Y. Sheynin, A.-E. Haj-Yahia, A. H. Barak, O. Gidron, M. Bendikov, *Chem. Sci.* **2015**, *6*, 360; d) S. Sharma, N. Zamoshchik, M. Bendikov, *Isr. J. Chem.* **2014**, *54*, 712; e) U. H. F. Bunz, *Angew. Chem. Int. Ed.* **2010**, *49*, 5037.

[4] a) S. Wood, J. B. Franklin, P. N. Stavrinou, M. A. McLachlan, J.-S. Kim, *Appl. Phys. Lett.* **2013**, *103*, 153304; b) I. Osaka, R. D. McCullough, *Acc. Chem. Res.* **2008**, *41*, 1202; c) R. D. McCullough, P. C. Ewbank, R. S. Loewe, *J. Am. Chem. Soc.* **1997**, *119*, 633.

[5] J. Roncali, *Chem. Rev.* **1992**, *92*, 711.

[6] A. Mishra, C.-Q. Ma, P. Bäuerle, *Chem. Rev.* **2009**, *109*, 1141.

[7] a) M. Heeney, W. Zhang, D. J. Crouch, M. L. Chabinyc, S. Gordeyev, R. Hamilton, S. J. Higgins, I. McCulloch, P. J. Skabara, D. Sparrowe et al., *Chem. Commun.* **2007**, 5061; b) L. Li, J. Hollinger, A. A. Jahnke, S. Petrov, D. S. Seferos, *Chem. Sci.* **2011**, *2*, 2306.

[8] A. Patra, M. Bendikov, *J. Mater. Chem.* **2010**, *20*, 422.

[9] a) J. Razzell-Hollis, F. Fleischli, A. A. Jahnke, N. Stingelin, D. S. Seferos, J.-S. Kim, *J. Phys. Chem. C* **2017**, *121*, 2088; b) A. A. Jahnke, B. Djukic, T. M. McCormick, E. Buchaca Domingo, C. Hellmann, Y. Lee, D. S. Seferos, *J. Am. Chem. Soc.* **2013**, *135*, 951.

[10] M. Jeffries-EL, G. Sauvé, R. D. McCullough, *Macromolecules* **2005**, *38*, 10346.

[11] Y. Miyata, T. Nishinaga, K. Komatsu, *J. Org. Chem.* **2005**, *70*, 1147.

[12] H. Helten in *Encyclopedia of Inorganic and Bioinorganic Chemistry* (Ed.: R. A. Scott), John Wiley & Sons, Ltd, Chichester, UK, **2011**, pp. 1–27.

[13] R. D. McCullough, S. Tristram-Nagle, S. P. Williams, R. D. Lowe, M. Jayaraman, *J. Am. Chem. Soc.* **1993**, *115*, 4910.

[14] a) K. Yoshino, K. Nakao, R.-i. Sugimoto, *Jpn. J. Appl. Phys.* **1989**, *28*, L490-L492; b) R. Sugimoto, S. Takeda, H. B. Gu, K. Yushino, *Chem. Express* **1989**, *1*, 635.

[15] M. Sato, H. Morii, *Macromolecules* **1991**, *24*, 1196.

[16] R. D. McCullough, R. D. Lowe, *J. Chem. Soc., Chem. Commun.* **1992**, 70.

[17] a) R. S. Loewe, P. C. Ewbank, J. Liu, L. Zhai, R. D. McCullough, *Macromolecules* **2001**, *34*, 4324; b) R. S. Loewe, S. M. Khersonsky, R. D. McCullough, *Adv. Mater.* **1999**, *11*, 250; c) A. Yokoyama, R. Miyakoshi, T. Yokozawa, *Macromolecules* **2004**, *37*, 1169; d) M. C. Iovu, E. E. Sheina, R. R. Gil, R. D. McCullough, *Macromolecules* **2005**, *38*, 8649; e) M. C. Iovu, M. Jeffries-EL, E. E. Sheina, J. R. Cooper, R. D. McCullough, *Polymer* **2005**, *46*, 8582.

[18] a) R. Miyakoshi, A. Yokoyama, T. Yokozawa, *J. Am. Chem. Soc.* **2005**, *127*, 17542; b) M. P. Bhatt, H. D. Magurudeniya, P. Sista, E. E. Sheina, M. Jeffries-EL, B. G. Janesko, R. D. McCullough, M. C. Stefan, *J. Mater. Chem. A* **2013**, *1*, 12841.

[19] a) A. Iraqi, G. W. Barker, *J. Mater. Chem.* **1998**, *8*, 25; b) S. D. Pike, F. M. Chadwick, N. H. Rees, M. P. Scott, A. S. Weller, T. Krämer, S. A. Macgregor, *J. Am. Chem. Soc.* **2015**, *137*, 820.

[20] M. J. González-Tejera, E. S. de La Blanca, I. Carrillo, *Synth. Met.* **2008**, *158*, 165.

[21] a) S. Hotta, S. D. D. V. Rughooputh, A. J. Heeger, F. Wudl, *Macromolecules* **1987**, *20*, 212; b) S. S. Zade, M. Bendikov, *Chem. Eur. J.* **2007**, *13*, 3688; c) P. Bäuerle, T. Fischer, B. Bidlingmeier, J. P. Rabe, A. Stabel, *Angew. Chem. Int. Ed.* **1995**, *34*, 303.

[22] J. K. Politis, J. C. Nemes, M. D. Curtis, *J. Am. Chem. Soc.* **2001**, *123*, 2537.

[23] H. Cao, P. A. Rupar, *Chem. Eur. J.* **2017**, *23*, 14670-14678.

[24] K. E. Horner, P. B. Karadakov, *J. Org. Chem.* **2013**, *78*, 8037.

[25] S. Glenis, M. Benz, E. LeGoff, J. L. Schindler, C. R. Kannewurf, M. G. Kanatzidis, *J. Am. Chem. Soc.* **1993**, *115*, 12519.

[26] a) O. Gidron in *Organic Redox Systems* (Ed.: T. Nishinaga), John Wiley & Sons, Inc, Hoboken, NJ, **2016**, pp. 445–462; b) O. Gidron, M. Bendikov, *Angew. Chem. Int. Ed.* **2014**, 2546; c) M. Jeffries-EL, B. M. Kobilka, B. J. Hale, *Macromolecules* **2014**, *47*, 7253.

[27] a) I. Manners, *Angew. Chem. Int. Ed.* **1996**, *35*, 1602; b) D. A. Resendiz-Lara, N. E. Stubbs, M. I. Arz, N. E. Pridmore, H. A. Sparkes, I. Manners, *Chem. Commun.* **2017**, *53*, 11701; c) X. He, T. Baumgartner, *RSC Adv.* **2013**, *3*, 11334; d) A. M. Priegert, B. W. Rawe, S. C. Serin, D. P. Gates, *Chem. Soc. Rev.* **2016**, *45*, 922; e) F. Vidal, F. Jäkle, *Angew. Chem.* **2019**, *131*, 5904.

[28] J. E. Mark, H. R. Allcock, R. West, *Inorganic polymers*, Prentice Hall, Englewood Cliffs, New Jersey, **1992**.

[29] S. Bernard, C. Salameh, P. Miele, *Dalton Trans* **2016**, *45*, 861.

[30] a) E. M. Leitao, T. Jurca, I. Manners, *Nat. Chem.* **2013**, *5*, 817; b) H. C. Johnson, T. N. Hooper, A. S. Weller in *Topics in Organometallic Chemistry* (Eds.: E. Fernández, A. Whiting), Springer International Publishing, Cham, **2015**, pp. 153–220.

[31] M. M. Labes, P. Love, L. F. Nichols, *Chem. Rev.* **1979**, *79*, 1.

[32] H. Helten, *Chem. Asian J.* **2019**, *14*, 919.

[33] S. Yamaguchi in *Chemical Science of π-Electron Systems* (Eds.: T. Akasaka, A. Osuka, S. Fukuzumi, H. Kandori, Y. Aso), Springer Japan, Tokyo, **2015**, pp. 363–377.

[34] a) C. D. Entwistle, T. B. Marder, *Angew. Chem. Int. Ed.* **2002**, *41*, 2927; b) C. D. Entwistle, T. B. Marder, *Chem. Mater.* **2004**, *16*, 4574; c) N. Matsumi, Y. Chujo, *Polym J* **2008**, *40*, 77; d) K. Tanaka, Y. Chujo, *Macromol. Rapid Commun.* **2012**, *33*, 1229; e) M. M. Morgan, E. A. Patrick, J. M. Rautiainen, H. M. Tuononen, W. E. Piers, D. M. Spasyuk, *Organometallics* **2017**; f) F. P. Gabbaï, *Angew. Chem. Int. Ed.* **2012**, *51*, 6316; g) C. R. Wade, A. E. J. Broomsgrove, S. Aldridge, F. P. Gabbaï, *Chem. Rev.* **2010**, *110*, 3958; h) H. Zhao, L. A. Leamer, F. P. Gabbaï, *Dalton Trans.* **2013**, *42*, 8164; i) S. Solé, F. P. Gabbaï, *Chem. Commun.* **2004**, 1284; j) A. Wakamiya, S. Yamaguchi, *BCSJ* **2015**, *88*, 1357; k) S. Yamaguchi, S. Akiyama, K. Tamao, *J. Am. Chem. Soc.* **2001**, *123*, 11372; l) N. Ando, H. Soutome, S. Yamaguchi, *Chem. Sci.* **2019**, *10*, 7816; m) L. Ji, S. Griesbeck, T. B. Marder, *Chem. Sci.* **2017**, *8*, 846; n) S. Griesbeck, E. Michail, C. Wang, H. Ogasawara, S. Lorenzen, L. Gerstner, T. Zang, J. Nitsch, Y. Sato, R. Bertermann et al., *Chem. Sci.* **2019**, *10*, 5405; o) G. Bélanger-Chabot, H. Braunschweig, D. K. Roy, *Eur. J. Inorg. Chem.* **2017**, *38*, 4353; p) C. Reus, M. Wagner, *Nat. Chem.* **2014**, *6*, 466; q) Z. X. Giustra, S.-Y. Liu, *J. Am. Chem. Soc.* **2018**, *140*, 1184.

[35] S. W. Thomas, G. D. Joly, T. M. Swager, *Chem. Rev.* **2007**, *107*, 1339.

[36] a) Z. Zhou, A. Wakamiya, T. Kushida, S. Yamaguchi, *J. Am. Chem. Soc.* **2012**, *134*, 4529; b) S. Saito, K. Matsuo, S. Yamaguchi, *J. Am. Chem. Soc.* **2012**, *134*, 9130; c) von Grotthuss, E.; John, A.; Kaese, T.; Wagner, M. *Asian J. Org. Chem.* **2018**, *7*, 37–53.

[37] Y. Chujo, I. Tomita, Y Hashiguchi, T. Saegusa, *Macromolecules* **1992**, *25*.

[38] N. Matsumi, Y. Chujo, *Polym. Bull.* **1997**, *38*, 531.

[39] A. Nagai, T. Murakami, Y. Nagata, K. Kokado, Y. Chujo, *Macromolecules* **2009**, *42*, 7217.

[40] A. Lorbach, M. Bolte, H. Li, H.-W. Lerner, M. C. Holthausen, F. Jäkle, M. Wagner, *Angew. Chem. Int. Ed.* **2009**, *48*, 4584.

[41] N. Matsumi, K. Naka, Y. Chujo, *J. Am. Chem. Soc.* **1998**, *120*, 10776.

[42] N. Matsumi, T. Umeyama, Y. Chujo, *Polym. Bull.* **2000**, *44*, 431.

[43] a) Y. Qin, G. Cheng, A. Sundararaman, F. Jäkle, *J. Am. Chem. Soc.* **2002**, *124*, 12672; b) Y. Qin, G. Cheng, O. Achara, K. Parab, F. Jäkle, *Macromolecules* **2004**, *37*, 7123.

[44] A. Sundararaman, M. Victor, R. Varughese, F. Jäkle, *J. Am. Chem. Soc.* **2005**, *127*, 13748.

[45] H. Li, F. Jäkle, *Angew. Chem. Int. Ed.* **2009**, *48*, 2313.

[46] a) P. Chen, R. A. Lalancette, F. Jäkle, *J. Am. Chem. Soc.* **2011**, *133*, 8802; b) P. Chen, X. Yin, N. Baser-Kirazli, F. Jäkle, *Angew. Chem. Int. Ed.* **2015**, *54*, 10768.

[47] P. Chen, F. Jäkle, *J. Am. Chem. Soc.* **2011**, *133*, 20142.

[48] X. Yin, F. Guo, R. A. Lalancette, F. Jäkle, *Macromolecules* **2016**, *49*, 537.

[49] A. Lik, L. Fritze, L. Müller, H. Helten, *J. Am. Chem. Soc.* **2017**, *139*, 5692.

[50] a) L. Fritze, N. A. Riensch, H. Helten, *Synthesis* **2019**, *51*, 399; b) A. Lik, S. Jenthra, L. Fritze, L. Müller, K.-N. Truong, H. Helten, *Chem. Eur. J.* **2018**, *24*, 11961; c) N. A. Riensch, L. Fritze, T. Schindler, M. Kremer, H. Helten, *Dalton Trans.* **2018**, *47*, 10399; d) N. A. Riensch, M. Fest, L. Fritze, A. Helbig, I. Krummenacher, H. Braunschweig, H. Helten, *New J. Chem.*, doi: 10.1039/D0NJ04297H.

[51] I. Yamaguchi, T. Tominaga, M. Sato, *Polym. Int.* **2009**, *58*, 17.

[52] X. Yin, J. Chen, R. A. Lalancette, T. B. Marder, F. Jäkle, *Angew. Chem. Int. Ed.* **2014**, *53*, 9761.

[53] V. D. B. Bonifácio, J. Morgado, U. Scherf, *J. Polym. Sci. A Polym. Chem.* **2008**, *46*, 2878.

[54] I. A. Adams, P. A. Rupar, *Macromol. Rapid Commun.* **2015**, *36*, 1336.

[55] A. W. Baggett, F. Guo, B. Li, S.-Y. Liu, F. Jäkle, *Angew. Chem. Int. Ed.* **2015**, *54*, 11191.

[56] W. Zhang, G. Li, L. Xu, Y. Zhuo, W. Wan, N. Yan, G. He, *Chem. Sci.* **2018**, *9*, 4444.

[57] N. Matsumi, Y. Chujo, *Macromolecules* **1998**, *31*, 3802.

[58] T. Lorenz, A. Lik, F. A. Plamper, H. Helten, *Angew. Chem. Int. Ed.* **2016**, *55*, 7236.

[59] O. Ayhan, T. Eckert, F. A. Plamper, H. Helten, *Angew. Chem. Int. Ed.* **2016**, *55*, 13321.

[60] a) O. Ayhan, N. A. Riensch, C. Glasmacher, H. Helten, *Chem. Eur. J.* **2018**, *24*, 5883; b) T. Lorenz, M. Crumbach, T. Eckert, A. Lik, H. Helten, *Angew. Chem. Int. Ed.* **2017**, *56*, 2780.

[61] T. Lorenz, M. Crumbach, T. Eckert, A. Lik, H. Helten, *Angew. Chem.* **2017**, *129*, 2824.

[62] W. Niu, M. D. Smith, J. J. Lavigne, *J. Am. Chem. Soc.* **2006**, *128*, 16466.

[63] P. Bäuerle, J. Becher, J. Lau, P. Mark in *Electronic Materials: The Oligomer Approach* (Eds.: K. Müllen, G. Wegner), Wiley-VCH Verlag GmbH, Weinheim, Germany, **1998**, pp. 105–233.

[64] a) M. Ball, Y. Zhong, B. Fowler, B. Zhang, P. Li, G. Etkin, D. W. Paley, J. Decatur, A. K. Dalsania, H. Li et al., *J. Am. Chem. Soc.* **2016**, *138*, 12861; b) M. Ball, C. Nuckolls, *ACS Cent. Sci.* **2015**, *1*, 416; c) B. Zhang, M. T. Trinh, B. Fowler, M. Ball, Q. Xu, F. Ng, M. L. Steigerwald, X.-Y. Zhu, C. Nuckolls, Y. Zhong, *J. Am. Chem. Soc.* **2016**, *138*, 16426.

[65] M. K. Shepherd, *J. Chem. Soc., Chem. Commun.* **1985**, 880.

[66] A. Patra, Y. H. Wijsboom, L. J. W. Shimon, M. Bendikov, *Angew. Chem. Int. Ed.* **2007**, *46*, 8814.

[67] R. Proetzsch, D. Bieniek, F. Korte, *Tetrahedron Letters* **1972**, *13*, 543.

[68] a) T. Kauffmann, B. Greving, J. König, A. Mitschker, A. Woltermann, *Angew. Chem. Int. Ed.* **1975**, *14*, 713; b) H. Irngartinger, U. Huber-Patz, H. Rodewald, *Acta Cryst. C* **1985**, *41*, 1088.

[69] A.J.W. Tol, *Synthetic Metals* **1995**, *74*, 95.

[70] J. Krömer, I. Rios-Carreras, G. Fuhrmann, C. Musch, M. Wunderlin, T. Debaerdemaeker, E. Mena-Osteritz, P. Bäuerle, *Angew. Chem. Int. Ed.* **2000**, *39*, 3481.

[71] a) E. Vogel, M. Pohl, A. Herrmann, T. Wiss, C. König, J. Lex, M. Gross, J. P. Gisselbrecht, *Angew. Chem. Int. Ed.* **1996**, *35*, 1520; b) E. Vogel, P. Röhrig, M. Sicken, B. Knipp, A. Herrmann, M. Pohl, H. Schmickler, J. Lex, *Angew. Chem. Int. Ed.* **1989**, *28*, 1651.

[72] a) W. Zhang, D. Yu, Z. Wang, B. Zhang, L. Xu, G. Li, N. Yan, E. Rivard, G. He, *Org. Lett.* **2019**, *21*, 109; b) M. Yousaf, X. Zarate, E. Schott, A. J. Lough, B. D. Koivisto, *RSC Adv.* **2018**, *8*, 28533; c) M.-X. Wang, *Acc. Chem. Res.* **2012**, *45*, 182; d) F. Schlütter, F. Rossel, M. Kivala, V. Enkelmann, J.-P. Gisselbrecht, P. Ruffieux, R. Fasel, K. Müllen, *J. Am. Chem. Soc.* **2013**, *135*, 4550; e) M. Iyoda, J. Yamakawa, M. J. Rahman, *Angew. Chem. Int. Ed.* **2011**, *50*, 10522; f) A. Ito, *J. Mater. Chem. C* **2016**, *4*, 4614; g) B. König, M. H. Fonseca, *Eur. J. Inorg. Chem.* **2000**, *2000*, 2303; h) Y. Qin, X. Liu, P.-P. Jia, L. Xu, H.-B. Yang, *Chem. Soc. Rev.* **2020**.

[73] Y. Adachi, T. Nabeya, K. Kawakami, K. Yamaji, F. Jäkle, J. Ohshita, *Chemistry* **2020**.

[74] a) A. Ito, Y. Yokoyama, R. Aihara, K. Fukui, S. Eguchi, K. Shizu, T. Sato, K. Tanaka, *Angew. Chem. Int. Ed.* **2010**, *49*, 8205; b) D. Sakamaki, A. Ito, K. Furukawa, T. Kato, K. Tanaka, *J. Org. Chem.* **2013**, *78*, 2947.

[75] a) P. Chen, R. A. Lalancette, F. Jäkle, *Angew. Chem. Int. Ed.* **2012**, *51*, 7994; b) P. Chen, X. Yin, N. Baser-Kirazli, F. Jäkle, *Angew. Chem. Int. Ed.* **2015**, *54*, 10768; c) N. Baser-Kirazli, R. A. Lalancette, F. Jäkle, *Angew. Chem. Int. Ed.* **2020**, *59*, 8689.

[76] a) B. König, M. Roedel, P. Bubenitschek, P. G. Jones, I. Thondorf, *J. Org. Chem.* **1995**, *60*, 7406; b) B. König, M. Rödel, P. Bubenitschek, P. G. Jones, *Angew. Chem. Int. Ed.* **1995**, *34*, 661.

[77] F. H. Carré, R. J.-P. Corriu, T. Deforth, W. E. Douglas, W. S. Siebert, W. Weinmann, *Angew. Chem. Int. Ed.* **1998**, *37*, 652.

2 Results and Discussion

2.1 Difuryl(supermesityl)borane: A Versatile Building Block for Extended π-conjugated Materials

The following section is slightly modified and reproduced from published article[§] with permission from The Royal Society of Chemistry.

π-Conjugated organic materials have aroused tremendous research interest in the last few decades due to their applications in (opto)electronic devices (OLEDs, OFETs, OPVs, *etc.*) and for sensory and imaging purposes.[1] While thiophene is one of the most popular electron-rich building blocks of organic electronic materials,[2] the use of its lighter congener, furan, as a conceivable alternative for this purpose, has been limited until quite recently.[3] This has been associated with the reduced stability of furan moieties in the presence of oxygen and incident light.[3a,d,h] However, furan rings have some favorable characteristics; significantly, they are biodegradable and can be obtained from entirely renewable resources. Consequentially, the interest in furan-based materials has considerably increased recently.[3] A number of possible ways to stabilize furan against oxygen and light-driven degradation have been identified, one of which being the combination with a strong electron-withdrawing component. This causes lowering of the HOMO energy and, hence, improved oxidation resistance.[3]

In recent years, triorganoboranes have emerged as potent electron-acceptor building blocks in organic electronics,[4–7] thus, making the development of boron-containing π-conjugated materials a very active field of current research. The incorporation of the vacant p_π orbital on boron into extended π-systems imparts intriguing properties and special features to the resulting materials. Of particular interest has been the combination of borane with thiophene moieties, resulting in valuable donor–acceptor arrays.[4b,6,7] Jäkle and Marder *et al*. demonstrated the use of very robust dithienylboranes that are kinetically stabilized by bulky 2,4,6-tri-*tert*-butylphenyl (Mes*, supermesityl) or 2,4,6-tris(trifluoromethyl)phenyl (^{F}Mes, fluoromesityl) groups as building blocks for extended π-conjugated materials (Figure 2.1.1).[7a] Jäkle and co-workers subsequently extended the application thereof to combinations with further π systems of varying electronic demands.[7b–e] One finding from their studies was that the change from mono- to bithiophene moieties attached to boron leads to enhanced luminescence properties of such materials.[7b]

[§] Riensch, N. A.; Fritze, L.; Schindler, T.; Kremer, M.; Helten, H. *Dalton Trans.* **2018**, *47*, 10399–10403.

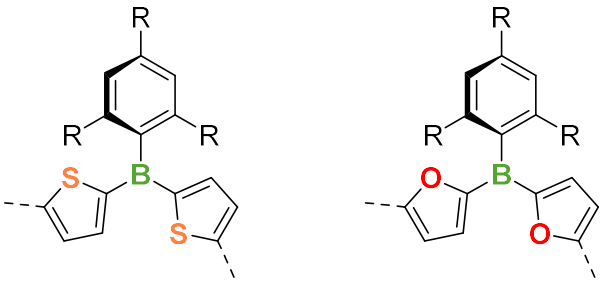

R = ^{i}Pr (i.e., *B*-Tip), ^{t}Bu (i.e., *B*-Mes*), or CF3 (i.e., *B*-^{F}Mes)

Figure 2.1.1: *Kinetically stabilized π-conjugated dithienyl- and difurylborane building blocks.*

The combination of borane with furan moieties has only been scarcely explored thus far.[8,9] We recently developed a novel catalytic B–C coupling method, which we applied to access a series of thienylboranes and the first furylborane oligomers and polymers along with some mixed thienyl-/furylborane species.[9,10] We found that *B*-Mes* substituted furylboranes were perfectly stable in air and moisture as well, and, moreover, they showed significantly stronger luminescence than their thiophene congeners;[9] in mixed derivatives, emission intensities increased with the increasing ratio of furan rings.[9b] Herein, we demonstrate the extension of the conjugated π-system in a difurylborane *via* direct functionalization and Suzuki–Miyaura cross-coupling. The resulting biaryl-substituted, kinetically stabilized boranes are highly fluorescent, very robust, and exhibit narrowed band gaps. By quantum chemical calculations we elucidate the effect of B-doping in oligo(heteroarene)s.

The reaction of difuryl(supermesityl)borane (**1**)[9a] with 2 equivalents of *t*-BuLi in diethyl ether at −78 °C led to selective dilithiation in the α-position of the furyl groups (Scheme 2.1.1). The subsequent reaction with elemental bromine and iodine afforded the functionalized difurylboranes **2a** and **2b**, respectively, which were isolated in good yields (77 and 80%). Compounds **2a** and **2b** were then employed in the Suzuki–Miyaura cross-coupling reactions with 2-thienyl- and 2-furyl-Bpin (pin = pinacolato), to give the biaryl-substituted boranes **3** and **4**, respectively, which proved to be perfectly stable in air for at least two weeks.

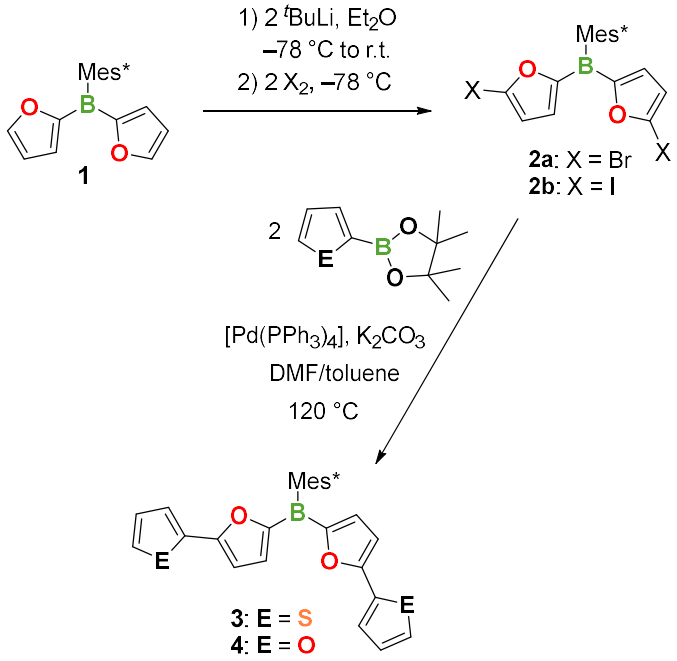

Scheme 2.1.1: *Synthesis of π-conjugated organoboranes **3** and **4**.*

The constitutions of **2a,b**, **3**, and **4** were unambiguously ascertained by multinuclear NMR spectroscopy and mass spectrometry. The $^{11}B\{^1H\}$ NMR spectra of each compound displayed a resonance at about 46 to 47 ppm, confirming the presence of three-coordinate boron. The ^1H and $^{13}C\{^1H\}$ NMR spectra showed all the expected resonances for the proposed constitution of the products. What is noteworthy is that the protons at C^3 of the B-bound furyl groups gave rise to a significantly broadened ^1H signal. This points to hindered rotation about the B–C(furyl) bonds.

The molecular structures of **2a**, **2b**, and **3** in the solid state were additionally determined by single-crystal X-Ray diffractometry (Figure 2.1.2). This showed that the boron atoms are trigonal-planar coordinated (sum of the bond angles around boron, $\Sigma(BC_3)$, 359.8 to 360.0°), and the Mes* substituents are nearly perpendicular oriented to the respective BC_3 plane (torsion angles ≥84°). The B–C(furyl) bond lengths are in a similar range (1.531–1.543 Å) to those of other furylborane species reported by us previously[9] but significantly shorter than the B–C(thienyl) bonds in Mes*B(2-thienyl)$_2$ (1.589(6) and 1.568(4) Å).[7a] In each compound, the B-bound furan rings adopt an *anti* arrangement (*i.e.*, with respect to the relative orientation of the O atoms) and form quasiplanar structures which also involve the coordination environments of the boron atoms. The twist angles between the furan ring planes are only 7.1(1)° in **2a**, and 10.1(2), 6.9(2), and 17.1(2)° for the three independent molecules in the asymmetric unit of **2b**. Compound **3** shows a slight rotational disorder about the B1–C1 bond which, however, does not invert the *anti* conformation of the two furan rings. The furan–furan twist angles are 1.5(1) and 13.6(3)° for the two rotational isomers. The terminal thiophene rings are also largely coplanar with their adjacent furan moieties. The rings that involve the atoms

O1 and S1 are *anti*-arranged and have twist angles of 24.7(2) and 25.6(3)° for the two rotamers. The thiophene moiety involving the S2 atom shows another rotational disorder, which leads to *syn*/*anti*-isomeric conformations at this part of the molecule with the twist angles of 5.6(4) and 6.5(5)°. Overall, the largely quasiplanar structures observed in the solid state form an ideal prerequisite for effective π conjugation over the hetarene rings and the boron centers.

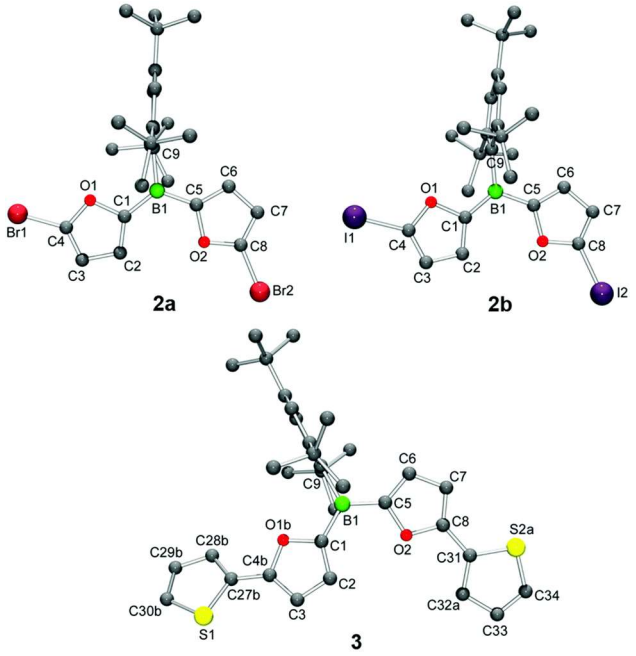

Figure 2.1.2: *Molecular structures of* ***2a***, ***2b***, *and* ***3*** *in the solid-state (H atoms omitted for clarity; for* ***2b****, only one of three independent molecules of the asymmetric unit with similar structural data is shown; compound* ***3*** *shows rotational disorder at the thiophene ring at C31 and the furan–thiophene moiety at C1, and only one conformer is shown).*

The photophysical characteristics of **2a**, **2b**, **3**, and **4** were investigated by UV–vis and fluorescence spectroscopy. The absorption bands assigned to π–π* transitions in the UV–vis spectra of **2a,b** are slightly red-shifted with respect to that of unsubstituted **1** (Figure 2.1.3, left); the wavelengths of the maxima increase in the order: **1** ($\lambda_{abs,max}$ = 315 nm)[9] < **2a** ($\lambda_{abs,max}$ = 332 nm) < **2b** ($\lambda_{abs,max}$ = 341 nm). The spectra of **3** and **4** each display a strong absorption band at significantly longer wavelengths (**3**: $\lambda_{abs,max}$ = 400 nm; **4**: $\lambda_{abs,max}$ = 394 nm) and a weaker band at higher energies (**3**: $\lambda_{abs,max}$ = 329 nm; **4**: $\lambda_{abs,max}$ = 336 nm). While **2a,b** were virtually non-fluorescent, compounds **3** and **4** showed strong blue fluorescence emission with relatively small Stokes shifts (**3**: $\lambda_{em,max}$ = 433 nm; **4**: $\lambda_{abs,max}$ = 427 nm) and quantum yields of Φ_F = 87 (**3**) and Φ_F = 67% (**4**). These values are considerably larger than, for instance, that of the difurylborane **1** (Φ_F = 24%).[9] The thiophene congener of the latter was reported to be essentially non-emissive in THF,[7a] while π-extended derivatives thereof comprising bithiophene units showed quantum yields of up to Φ_F = 38%.[7b] This points to an effective

extension of the conjugated π system through the extra thienyl and furyl groups in **3** and **4**, respectively. Cyclic voltammetry (CV) measurements revealed a reversible reduction wave for **4** with a half-wave potential of $E_{1/2}$ = −2.53 V (Figure 2.1.3, right) and a quasi-reversible reduction wave for **3** ($E_{1/2}$ = −2.48 V; see Appendix, Figure S5.1.30), which is somewhat anodic shifted with respect to the reduction wave for **1** ($E_{1/2}$ = −2.83 V).[9b]

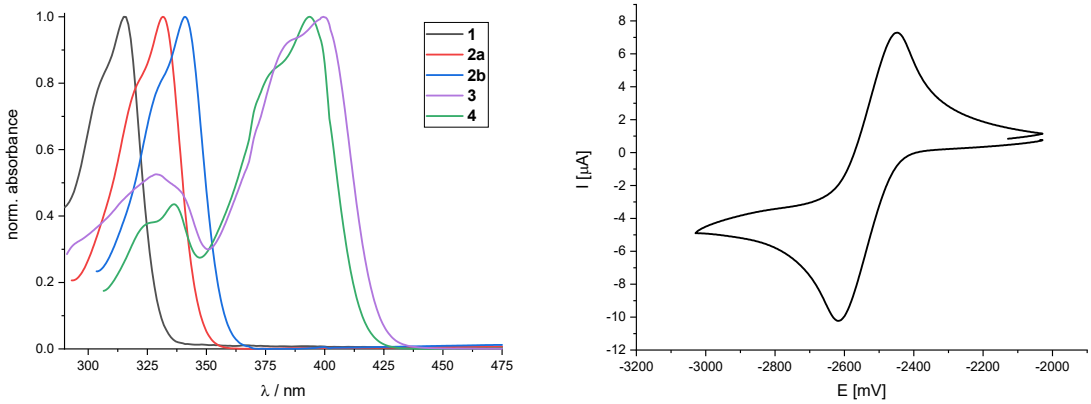

Figure 2.1.3: *Left: UV–vis absorption spectra of **1**, **2a,b**, **3**, and **4** (in THF). Right: Cyclic voltammogram of **4** (1 × 10^{-3} M in THF; vs. Fc^{+}/Fc; scan rate: 100 mV s^{-1}).*

To gain deeper insight into the electronic structures of the new compounds, we carried out a series of time-dependent DFT (TD-DFT) calculations on the B3LYP-D3(BJ)/def2-SV(P) level. For computational convenience, we slightly truncated the molecules by using mesityl substituents instead of supermesityl substituents (*i.e.*, model systems **1′**,[9b] **2a**,**b′**, **3′**, and **4′**). Our calculations revealed that the maximum absorption band observed in the UV–vis spectrum of each compound can be assigned to the excitation from an extended π orbital, fully delocalized over the hetarene rings, to the LUMO, which is an extended π orbital as well but has a considerable contribution from the boron atom (Figure 2.1.4 and Appendix, Figures S5.3.32–S5.3.37 and Table S2.1.2). Accordingly, this process is characterized as a π–π* transition associated with some intramolecular charge transfer (ICT) to the boron center.

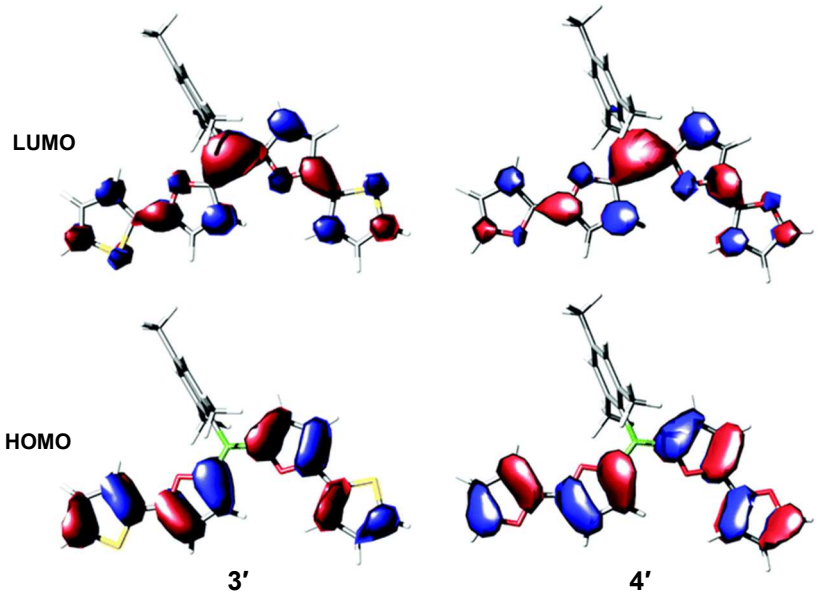

Figure 2.1.4: *Calculated frontier orbitals of **3′** and **4′** (isovalue 0.03 a.u.).*

The experimentally observed trend of decreasing excitation energies in the order **1** > **2a** > **2b** is well reproduced by the calculations (Figure 2.1.5). The introduction of bromo or iodo substituents leads to a reduced energy gap between the frontier π MOs. According to our calculations, this is due to both an increase in the energy of the occupied π orbital and a decrease in the energy of the LUMO. It should be noted that, in this series, the energetic order of the highest occupied MOs undergoes an inversion. While in **1′**, the π orbital involved in these transitions constitutes the HOMO−2, in **2a′** and **2b′**, it is the HOMO−1. The HOMO (and the HOMO−1 in **1′**) is localized on the mesityl ring, and, hence, the HOMO-to-LUMO transition – as it involves nearly orthogonal π orbitals – is of negligible probability.

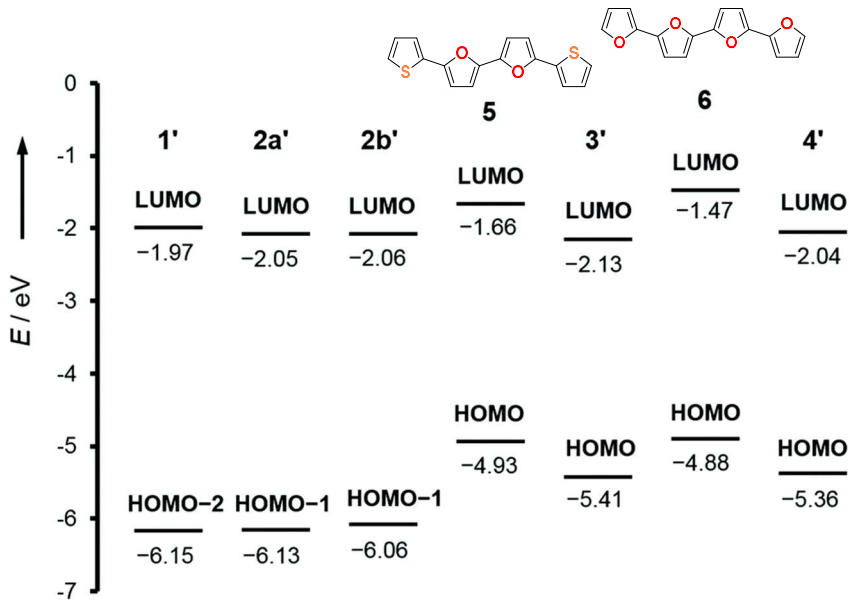

Figure 2.1.5: *Calculated frontier π orbital energy levels (B3LYP-D3/def2-SV(P); values in eV).*

The major effect of the extension of the conjugated π system when moving to **3′** and **4′** is that the energy of the highest occupied π orbital, which is in this case the HOMO, is significantly elevated. This is the main reason for the observed dramatic red-shift of the π–π* absorption band in these species. The additional minor decrease in the LUMO energy is consistent with the observation of an anodic shift in the electrochemical reduction wave (*vide supra*). Our calculations further revealed that the high-energy band observed in the spectra of **3** and **4** is assigned to a second π–π* transition involving the HOMO and the LUMO+1. The latter has a vertical nodal plane through the boron atom.

With a view to learn more about the effect of the borane group on the electronic structure of the extended π systems in **3** and **4**, we additionally calculated the oligo(hetarene)s **5** and **6** which have the same sequence of hetarene rings as **3** and **4** but lack the borane moiety[11] (see Figure 2.1.5 for their structures). This revealed that the introduction of boron results in a significant decrease of both the HOMO and the LUMO energies. A slightly larger influence on the LUMO causes somewhat lower excitation energies for **3′** and **4′** compared to **5** and **6**.

In conclusion, we demonstrated the use of difuryl(supermesityl)borane (**1**) as a valuable building block for extended π-conjugated materials. Facile direct functionalization of **1** and the subsequent Suzuki–Miyaura cross-coupling using **2a,b** led to highly fluorescent organoboron hybrid compounds **3** and **4**. The increased hetarene content in these species causes a strong elevation of the HOMO levels, resulting in dramatic bathochromic shifts and intensification of the absorption and emission properties. According to our DFT calculations, the B-doping of oligo(heteroarene)s such as **5** and **6** causes a significant lowering of both the HOMO and LUMO energy levels. The former effect leads to an improved oxidative stability of such materials, while the latter results in enhanced electron-acceptor properties, which is of interest for the development of effective electron-transporting organic materials.[12]

2.1.1 Experimental Section

General procedures. All manipulations were performed under an atmosphere of dry argon using standard Schlenk techniques or in an MBraun glove box. Solvents (dichloromethane, *n*-pentane, diethylether, toluene, and tetrahydrofuran) were dried and degassed by means of an MBraun SPS-800 solvent purification system. *N,N′*-Dimethylformamide was dried over $mgSO_4$ and distilled prior to use. Deuterated solvents for NMR spectroscopy were dried and degassed at reflux over Na (C_6D_6) or CaH_2 ($CDCl_3$ and CD_2Cl_2) and freshly distilled prior to use. *n*-Hexane for aqueous work-up, tribromoborane, bromobenzene, thiophene, magnesium turnings, iodine, bromine, and $Pd(PPh_3)_4$ were purchased from commercial sources and used as received. Solutions of *n*-butyllithium (1.6 M and 2.5 M in hexane, respectively) and *tert*-butyllithium (1.7 M in pentane) were purchased from Sigma Aldrich and

used as received as well. Furan and 2-isopropoxy-4,4,5,5-tetramethyl-1,3,2-dioxaborolane were commercially purchased and freshly distilled prior to use. Compound **1**,[13a] 4,4,5,5-tetramethyl-2-(2-thienyl)-1,3,2-dioxaborolane,[13b] and 4,4,5,5-tetramethyl-2-(2-furyl)-1,3,2-dioxaborolane[13c] were prepared according to methods described in the literature. NMR spectra were recorded at 25 °C on a Bruker Avance II-400 spectrometer or on a Bruker Avance III HD spectrometer operating at 400 MHz. Chemical shifts were referenced to residual protic impurities in the solvent (^{1}H) or the deuterio solvent itself (^{13}C) and reported relative to external $SiMe_4$ (^{1}H, ^{13}C) or $BF_3{\cdot}OEt_2$ (^{11}B) standards. Mass spectra were obtained with the use of a Finnigan MAT95 spectrometer employing electron ionization (EI) using a 70 eV electron impact ionization source. Elemental analysis was performed with a CHN-O-Rapid VarioEL by Heraeus. UV–vis spectra were obtained using a Jasco V-630 spectrophotometer. Fluorescence spectra were obtained with a Jasco FP-6600 spectrofluorometer. Fluorescence quantum yields were determined against perylene as the standard. Melting points (uncorrected) were obtained using a SMP3 melting point apparatus by Stuart in 0.5 mm (o.d.) glass capillaries. Cyclic voltammetry (CV) experiments were carried out on a PGSTAT101 analyzer from Metrohm. The three-electrode system consisted of a Pt disk as working electrode, a Pt wire as counter electrode, and an Ag wire as the reference electrode. The voltammograms were recorded with ca. 10^{-3} M solutions in THF containing $[Bu_4N][PF_6]$ (0.1 M) as the supporting electrolyte. The scans were referenced after the addition of a small amount of ferrocene as internal standard. The potentials are reported relative to the ferrocene/ferrocenium couple.

Synthesis of 2a. To a solution of **1** (468.4 mg, 1.20 mmol) in Et_2O (9.0 mL) was added *tert*-butyllithium (1.7 M, 1.45 mL, 2.46 mmol) at −78 °C. Subsequently, the mixture was warmed to room temperature and stirred at for further 3 h. Then, bromine (479.4 mg, 3.00 mmol) was added at −78 °C. The reaction mixture was allowed to warm up to room temperature overnight. All volatiles were removed *in vacuo*, and the brownish crude product was subjected to column chromatography (AlOx; *n*-hexane) to give **2a** as a colorless solid (m.p. 179.4 °C). Yield: 505.7 mg (0.92 mmol, 77 %); ^{1}H NMR (400 MHz, $CDCl_3$): δ = 7.42 (s, 2H, Mes*-C*H*), 7.30–6.95 (br, 2H, Fur-*H*), 6.44 (d, $^{3}J_{HH}$ = 3.4 Hz, 2H, Fur-*H*), 1.39 (s, 9H, *p*-^{t}Bu-CH_3), 1.19 (s, 18H, *o*-^{t}Bu-CH_3); ^{11}B{^{1}H} NMR (128 MHz, $CDCl_3$): δ = 46.1 (s); ^{13}C{^{1}H} NMR (101 MHz, $CDCl_3$): δ = 166.8 (Fur-*C*-B), 152.7 (Mes*-*C*–*o*-^{t}Bu), 148.9 (Mes*-*C*–*p*-^{t}Bu), 130.7 (Mes*-*C*-B, Fur-*C*H), 129.7 (Fur-*C*Br), 122.1 (Mes*-*C*H), 113.7 (Fur-*C*H), 38.4 (*o*-^{t}Bu-*C*), 34.9 (*p*-^{t}Bu-*C*), 34.4 (*o*-^{t}Bu-*C*H_3), 31.6 (*p*-^{t}Bu-*C*H_3); MS (EI, 70 eV): *m/z* (%) = 548.1 ([M]$^{+}$, 45), 231.2 (C_6H_2-^{i}Pr-(^{t}Bu)$_2$]$^{+}$, 72), 151.1 ([$C_{10}H_4BO$]$^{+\bullet}$, 51), 77.1 ([Ph]$^{+}$, 100); elem. anal. calcd (%) for $C_{26}H_{33}BBr_2O_2$: C 56.

97, H 6.07, found: C 57.26, H 6.08; UV–vis (THF): $\lambda_{abs,max}$ = 331.5 nm (ε = 26967 L mol^{-1} cm^{-1}); fluorescence (THF): non-emissive.

Synthesis of 2b. To a solution of **1** (780.7 mg, 2.00 mmol) in Et_2O (15 mL) was added *tert*-butyllithium (1.7 M, 2.41 mL, 4.10 mmol) at −78 °C. Subsequently, the mixture was warmed to room temperature and stirred at for further 3 h. Then, a solution of iodine (1.27 g, 5.00 mmol) in THF (2.5 mL) was added at −78 °C. The reaction mixture was allowed to warm up to room temperature overnight. All volatiles were removed *in vacuo*, and the brownish crude product was subjected to column chromatography (silica; *n*-hexane) and sublimation to remove residual iodine to give **2b** as a colorless solid (m.p. 204.5 °C). Yield: 1.03 g (1.60 mmol, 80 %); ^{1}H NMR (400 MHz, $CDCl_3$): δ = 7.41 (s, 2H, Mes*-C*H*), 7.20–6.90 (br, 2H, Fur-*H*), 6.66 (d, $^3J_{HH}$ = 3.4 Hz, 2H, Fur-*H*), 1.38 (s, 9H, *p*-^{t}Bu-CH_3), 1.17 (s, 18H, *o*-^{t}Bu-CH_3); ^{11}B{^{1}H} NMR (128 MHz, $CDCl_3$): δ = 45.9 (s); ^{13}C{^{1}H} NMR (101 MHz, $CDCl_3$): δ = 170.5 (Fur-*C*-B), 152.7 (Mes*-*C*–*o*-^{t}Bu), 148.8 (Mes*-*C*–*p*-^{t}Bu), 130.8 (Mes*-*C*-B, Fur-*C*H), 122.3 (Fur-*C*H), 122.0 (Mes*-*C*H), 97.4 (Fur-*C*H), 38.4 (*o*-^{t}Bu-*C*), 34.9 (*p*-^{t}Bu-*C*), 34.4 (*o*-^{t}Bu-*C*H$_3$), 31.6 (*p*-^{t}Bu-*C*H$_3$); MS (EI, 70 eV): *m/z* (%) = 642.1 ([M]$^+$, 4), 246.3 ([BH$_2$Mes*]$^+$), 69), 232.4 ([C$_6$H$_3$-^{i}Pr-(^{t}Bu)$_2$]$^+$), 100); elem. anal. calcd (%) for $C_{26}H_{33}BI_2O_2$: C 48.63, H 5.18, found: C 49.89, H 5.25; UV–vis (THF): $\lambda_{abs,max}$ = 341 nm (ε = 31466 L mol^{-1} cm^{-1}); fluorescence (THF): non-emissive.

Synthesis of 3. Compound **2a** (109.6 mg, 0.20 mmol) and 4,4,5,5-tetramethyl-2-(2-thienyl)-1,3,2-dioxaborolane (85.1 mg, 0.405 mmol) were charged into a Schlenk flask. Subsequently, dry DMF (3 mL) and toluene (3 mL) were added and the mixture was degassed by freeze-pump-thaw cycles. Then, $Pd(PPh_3)_4$ (15 mol%) followed by K_2CO_3 (164.4 mg, 1.190 mmol) were added under nitrogen. The reaction mixture was heated at 120 °C for 18 hours with vigorous stirring. Then, the mixture was cooled to ambient temperature and diluted with DCM (10 mL). After filtration, all volatiles were removed *in vacuo*, and the product was purified by column chromatography with gradient (hexane:DCM 100:0 -> 80:20). Compound **3** was obtained as a yellow solid (m.p. 184.9 °C). Yield: 62 mg (0.11 mmol, 56 %); ^{1}H NMR (400 MHz, $CDCl_3$): δ = 7.37 (s, 2H, Mes*-C*H*), 7.34 (br d, $^3J_{HH}$ = 2.8 Hz, 2H, Thi-*H*), 7.20 (d, $^3J_{HH}$ = 5.0 Hz, 2H, Thi-*H*), 6.96–6.94 (dd, $^3J_{HH}$ = 3.5 Hz, $^4J_{HH}$ = 1.8 Hz, 2H, Thi-*H*), 6.54 (d, $^3J_{HH}$ = 3.0 Hz, 2H, Fur-*H*), 1.34 (s, 9H, *p*-Mes*-CH_3), 1.17 (s, 18H, *o*-Mes*-CH_3); ^{11}B{^{1}H} NMR (128 MHz, $CDCl_3$): δ = 47.2 (s); ^{13}C{^{1}H} NMR (101 MHz, $CDCl_3$): δ = 163.7 (Fur-*C*-B), 154.3 (Fur-*C*-C$_{Thi}$), 152.3 (Mes*-*C*–*o*-^{t}Bu), 148.1 (Mes*-*C*–*p*-^{t}Bu), 133.7 (Thi-*C*-C$_{Fur}$), 132.2 (Mes*-*C*-B), 130.1 (Fur-*C*H), 127.7 (Thi-*C*H), 125.3 (Thi-*C*H), 124.0 (Thi-*C*), 121.5 (Mes*-*C*H), 107.0 (Fur-*C*), 38.3 (*o*-^{t}Bu-*C*), 34.3 (*p*-^{t}Bu-*C*), 31.5 (*o*-^{t}Bu-*C*H$_3$), 31.3 (*p*-^{t}Bu-*C*H$_3$); MS (EI, 70 eV): *m/z* (%) = 553.7 ([M]$^+$, 3), 471.7 ([Mes*BFur$_2$Thi]$^+$, 3), 256.9 ([Mes*B]$^+$, 70), 230.9 (C$_6$H$_2$-^{i}Pr-(^{t}Bu)$_2$]$^+$), 100); UV–vis

(THF): $\lambda_{abs,max}$ = 329 nm (ε = 60467 L mol^{-1} cm^{-1}), 400 nm (ε = 115763 L mol^{-1} cm^{-1}); fluorescence (THF): $\lambda_{em,max}$ (λ_{ex}=400 nm) = 433 nm (Φ_f = 87.2 %).

Synthesis of 4. Compound **2b** (128.4 mg, 0.20 mmol) and 4,4,5,5-tetramethyl-2-(2-furyl)-1,3,2-dioxaborolane (78.6 mg, 0.405 mmol) were charged into a Schlenk flask. Subsequently, dry DMF (3 mL) and toluene (3 mL) were added and the mixture was degassed by freeze-pump-thaw cycles. Then, $Pd(PPh_3)_4$ (15 mol%) followed by K_2CO_3 (164.4 mg, 1.190 mmol) were added under nitrogen. The reaction mixture was heated at 120 °C for 18 hours with vigorous stirring. Then, the mixture was cooled to ambient temperature and diluted with DCM (10 mL). After filtration, all volatiles were removed *in vacuo*, and the product was purified by column chromatography with gradient (hexane:DCM 100:0 -> 80:20). Compound **4** was obtained as a brownish solid (m.p. 125 °C). Yield: 34 mg (0.065 mmol, 33 %); ^{1}H NMR (400 MHz, $CDCl_3$): δ = 7.47 (d, $^3J_{HH}$ = 1.7 Hz, 2H, Fur-*H*), 7.43 (s, 2H, Mes*-C*H*), 7.39–7.06 (br, 2H, Fur-*H*), 6.74 (d, $^3J_{HH}$ = 3.4 Hz, 2H, Fur-*H*), 6.70 (d, $^3J_{HH}$ = 3.5 Hz, 2H, Fur-*H)*, 6.50 (dd, $^3J_{HH}$ = 3.5, $^4J_{HH}$ = 1.8 Hz, 2H, Fur-*H*), 1.40 (s, 9H, *p*-Mes*-CH_3), 1.22 (s, 18H, *o*-Mes*-CH_3); ^{11}B{^{1}H} NMR (128 MHz, $CDCl_3$): δ = 46.9 (s); ^{13}C{^{1}H} NMR (101 MHz, $CDCl_3$): δ = 164.3 (Fur-*C*-B), 152.9 (Mes*-*C*–*o*-^{t}Bu), 151.7 (Fur-*C*-C_{Fur}), 148.8 (Mes*-*C*–*p*-^{t}Bu), 147.2 (Fur-*C*-C_{Fur}), 143.1 (Fur-*C*H), 132.8 (Mes*-*C*-B), 130.4 (Fur-*C*H), 122.1 (Mes*-*C*H), 112.2 (Fur-*C*H), 107.7 (Fur-*C*H), 107.6 (Fur-*C*H), 38.8 (*o*-^{t}Bu-*C*), 35.2 (*p*-^{t}Bu-*C*), 34.8 (*o*-^{t}Bu-*C*H_3), 31.9 (*p*-^{t}Bu-*C*H_3); MS (EI, 70 eV): *m/z* (%) = 521.7 ([M]$^+$, 37), 481.1 ([Ph-*p*-CH_3-o-(^{t}Bu)$_2$)$^+$], 63), 230.9 ([C_6H_2-^{i}Pr-(^{t}Bu)$_2$]$^+$), 100); UV–vis (THF): $\lambda_{abs,max}$ = 336 nm (ε = 45808 L mol^{-1} cm^{-1}), 394 nm (ε = 107771 L mol^{-1} cm^{-1}); fluorescence (THF): $\lambda_{em,max}$ (λ_{ex}= 394 nm) = 427 nm (Φ_f = 67.0 %).

X-Ray crystallographic analysis

Suitable single crystals of **2a** and **2b** were obtained by slow evaporation of dichloromethane at 4 °C. **3** was obtained by slow evaporation of hexane at −40 °C. Data were collected on a Bruker SMART APEX CCD detector on a D8 goniometer equipped with an Oxford Cryostream 700 temperature controller at 100(2) K using graphite monochromated Mo-K_α radiation (λ = 0.71073 Å). An absorption correction was carried out semi-empirically using SADABS[14]. The structures were solved with Olex2[15] using Direct Methods (ShelXS[16a]) and refined with the ShelXL[16b] refinement package by full-matrix least squares on F^2. All non-hydrogen atoms were refined anisotropically. In the structure of **3**, atom C4a was refined isotropic to yield a stable structure. The hydrogen atoms were included isotropically and treated as riding. The structure of **2b** displays three independent molecules within the asymmetric unit.

Table S2.1.1: *Crystal structure and refinement data for* ***2a****,* ***2b*** *and* ***3****.*

No.	**2a**	**2b**	**3**
Color, habit	colorless plate	colorless block	colorless block
Empirical Formula	$C_{26}H_{33}BBr_2O_2$	$C_{26}H_{33}BI_2O_2$	$C_{34}H_{39}BO_2S_2$
M	548.15	642.17	554.61
Crystal system	triclinic	triclinic	triclinic
Space group	P-1	P-1	P-1
a/Å	9.0914(12)	10.7568(12)	9.299(3)
b/Å	10.6006(14)	17.0259(18)	13.239(5)
c/Å	14.3655(18)	22.758(2)	13.676(5)
α/°	71.643(2)	94.956(2)	97.674(8)
β/°	86.345(2)	94.394(2)	101.180(7)
γ/°	78.848(2)	103.556(2)	107.537(7)
V/Å^3	1289.2(3)	4016.5(7)	1541.5(10)
Z	2	8	2
μ/mm^{-1}	3.163	2.368	0.201
T/K	100	100	100
$\theta_{min,max}$	2.28, 28.66	2.30, 25.32	2.37, 21.82
Completeness	0.90 to θ = 31.2	0.99 to θ = 25.6	0.99 to θ = 26.1
Reflections: total/independent	20064/7513	45558/15014	18294/6097
R_{int}	0.0463	0.0386	0.0794
Final *R*1 and *wR*2	0.0393, 0.0644	0.0351, 0.0464	0.0661, 0.0611
Largest peak, hole/eÅ^{-3}	0.967/−0.715	1.579, −0.719	0.306, −0.401
ρ_{calc}/g cm^{-3}	1.412	1.593	1.195

Computational methods

DFT calculations were carried out with the TURBOMOLE V7.0.1 program package.[17] Optimizations were performed with Becke's three parameter exchangecorrelation hybrid functional B3LYP[18] in combination with the valence-double-ζ basis set def2- SV(P).[19] The empirical dispersion correction DFT-D3 by Grimme was used including the threebody term and with Becke-Johnson (BJ) damping.[20] The stationary points were characterized as minima by analytical vibrational frequency calculations.[21] Vertical singlet excitations were calculated by means of time-dependent DFT[22] using the same density functional–basis set combination as specified above.

Table S2.1.2: *Results from TD-DFT calculations (π–π* excitation marked in bold).*

Compound	No.	λ / nm	Oscillator strength *f*	Orbital contributions	$\|c\|^2$ / %
2a	1	382.6	0.0108	HOMO → LUMO	99.3
	2	355.5	0.0031	HOMO−2 → LUMO	93.7
	3	**330.6**	**0.5918**	**HOMO−1 → LUMO**	**93.1**
2b	1	384.3	0.0126	HOMO → LUMO	95.7
	2	356.9	0.0063	HOMO−2 → LUMO	95.1
	3	**339.6**	**0.6164**	**HOMO−1 → LUMO**	**91.1**
5	**1**	**404.8**	**1.2140**	**HOMO → LUMO**	**99.4**
3	**1**	**418.1**	**0.9106**	**HOMO → LUMO**	**99.4**
	2	397.3	0.0201	HOMO−1 → LUMO	81.0
				HOMO−2 → LUMO	17.3
	3	367.7	0.0015	HOMO−3 → LUMO	97.1
6	**1**	**384.6**	**1.2270**	**HOMO → LUMO**	**99.5**
4	**1**	**410.6**	**0.8855**	**HOMO → LUMO**	**99.4**
	2	390.9	0.0176	HOMO−1 → LUMO	61.6
				HOMO−2 → LUMO	37.2
	3	361.5	0.0014	HOMO−3 → LUMO	98.7

2.1.2 References

[1] (*a*) T. M. Swager, *Macromolecules*, 2017, **50**, 4867 ; (*b*) J. Mei, Y. Diao, A. L. Appleton, L. Fang and Z. Bao, *J. Am. Chem. Soc.*, 2013, **135**, 6724; (*c*) S. Allard, M. Forster, B. Souharce, H. Thiem and U. Scherf, *Angew. Chem., Int. Ed.*, 2008, **47**, 4070.

[2] (*a*) S. C. Rasmussen, S. J. Evenson and C. B. McCausland, *Chem. Commun.*, 2015, **51**, 4528; (*b*) A. Mishra, C.-Q. Ma and P. Bäuerle, *Chem. Rev.*, 2009, **109**, 1141.

[3] (*a*) O. Gidron, Y. Diskin-Posner and M. Bendikov, *J. Am. Chem. Soc.*, 2010, **132**, 2148; (*b*) U. H. F. Bunz, *Angew. Chem., Int. Ed.*, 2010, **49**, 5037; (*c*) C. H. Woo, P. M. Beaujuge, T. W. Holcombe, O. P. Lee and J. M. J. Fréchet, *J. Am. Chem. Soc.*, 2010, **132**, 15547; (*d*) O. Gidron and M. Bendikov, *Angew. Chem., Int. Ed.*, 2014, **53**, 2546; (*e*) A. Luzio, D. Fazzi, F. Nübling, R. Matsidik, A. Straub, H. Komber, E. Giussani, S. E. Watkins, M. Barbatti, W. Thiel, E. Gann, L. Thomsen, C. R. McNeill, M. Caironi and M. Sommer, *Chem. Mater.*, 2014, **26**, 6233; (*f*) C.-H. Tsai, A. Fortney, Y. Qiu, R. R. Gil, D. Yaron, T. Kowalewski and K. J. T. Noonan, *J. Am. Chem. Soc.*, 2016, **138**, 6798; (*g*) H. Cao, I. A. Brettell-Adams, F. Qu and P. A. Rupar, *Organometallics*, 2017, **36**, 2565; (*h*) H. Cao and P. A. Rupar, *Chem. – Eur. J.*, 2017, **23**, 14670.

[4] (*a*) L. Ji, S. Griesbeck and T. B. Marder, *Chem. Sci.*, 2017, **8**, 846; (*b*) Y. Ren and F. Jäkle, *Dalton Trans.*, 2016, **45**, 13996.

[5] (*a*) A. John, M. Bolte, H.-W. Lerner and M. Wagner, *Angew. Chem., Int. Ed.*, 2017, **56**, 5588; (*b*) K. Schickedanz, J. Radtke, M. Bolte, H.-W. Lerner and M. Wagner, *J. Am. Chem. Soc.*, 2017, **139**, 2842; (*c*) D. L. Crossley, R. J. Kahan, S. Endres, A. J. Warner, R. A. Smith, J. Cid, J. J. Dunsford, J. E. Jones, I. Vitorica-Yrezabal and M. J. Ingleson, *Chem. Sci.*, 2017, **8**, 7969; (*d*) D. Marinelli, F. Fasano, B. Najjari, N. Demitri and D. Bonifazi, *J. Am. Chem. Soc.*, 2017, **139**, 5503; (*e*) K. Matsuo, S. Saito and S. Yamaguchi, *Angew. Chem., Int. Ed.*, 2016, **55**, 11984; (*f*) S. Osumi, S. Saito, C. Dou, K. Matsuo, K. Kume, H. Yoshikawa, K. Awaga and S. Yamaguchi, *Chem. Sci.*, 2016, **7**, 219; (*g*) S. Wang, D.-T. Yang, J. Lu, H. Shimogawa, S. Gong, X. Wang, S. K. Mellerup, A. Wakamiya, Y.-L. Chang, C. Yang and Z.-H. Lu, *Angew. Chem., Int. Ed.*, 2015, **54**, 15074; (*h*) X.-Y. Wang, A. Narita, X. Feng and K. Müllen, *J. Am. Chem. Soc.*, 2015, **137**, 7668; (*i*) L. Ji, R. M. Edkins, A. Lorbach, I. Krummenacher, C. Bruckner, A. Eichhorn, H. Braunschweig, B. Engels, P. J. Low and T. B. Marder, *J. Am. Chem. Soc.*, 2015, **137**, 6750; (*j*) M. Krieg, F. Reicherter, P. Haiss, M. Ströbele, K. Eichele, M.-J. Treanor, R. Schaub and H. F. Bettinger, *Angew. Chem., Int. Ed.*, 2015, **54**, 8284; (*k*) A. W. Baggett, F. Guo, B. Li, S.-Y. Liu and F. Jäkle, *Angew. Chem., Int. Ed.*, 2015, **54**, 11191; (*l*) V. M. Hertz, M. Bolte, H.-W. Lerner and M. Wagner, *Angew. Chem., Int. Ed.*, 2015, **54**, 8800; (*m*) H. Hirai, K. Nakajima, S. Nakatsuka, K. Shiren, J. Ni, S. Nomura,

T. Ikuta and T. Hatakeyama, *Angew. Chem., Int. Ed.*, 2015, **54**, 13581; (*n*) B. Neue, J. F. Araneda, W. E. Piers and M. Parvez, *Angew. Chem., Int. Ed.*, 2013, **52**, 9966; (*o*) A. J. V. Marwitz, A. N. Lamm, L. N. Zakharov, M. Vasiliu, D. A. Dixon and S.-Y. Liu, *Chem. Sci.*, 2012, **3**, 825; (*p*) Y. Kim, H.-S. Huh, M. H. Lee, I. L. Lenov, H. Zhao and F. P. Gabbaï, *Chem. – Eur. J.*, 2011, **17**, 2057.

[6] (*a*) Y. Adachi and J. Ohshita, *Organometallics*, 2018, **37**, 869; (*b*) H. Shimogawa, O. Yoshikawa, Y. Aramaki, M. Murata, A. Wakamiya and Y. Murata, *Chem. – Eur. J.*, 2017, **23**, 3784; (*c*) S. K. Sarkar, G. R. Kumar and P. Thilagar, *Chem. Commun.*, 2016, **52**, 4175; (*d*) Z. Zhang, R. M. Edkins, J. Nitsch, K. Fucke, A. Eichhorn, A. Steffen, Y. Wang and T. B. Marder, *Chem. – Eur. J.*, 2015, **21**, 177; (*e*) X.-Y. Wang, F.-D. Zhuang, R.-B. Wang, X.-C. Wang, X.-Y. Cao, J.-Y. Wang and J. Pei, *J. Am. Chem. Soc.*, 2014, **136**, 3764; (*f*) D. R. Levine, M. A. Siegler and J. D. Tovar, *J. Am. Chem. Soc.*, 2014, **136**, 7132; (*g*) L. G. Mercier, W. E. Piers, R. W. Harrington and W. Clegg, *Organometallics*, 2013, **32**, 6820; (*h*) H. Braunschweig, V. Dyakonov, B. Engels, Z. Falk, C. Hörl, J. H. Klein, T. Kramer, H. Kraus, I. Krummenacher, C. Lambert and C. Walter, *Angew. Chem., Int. Ed.*, 2013, **52**, 12852; (*i*) H. Braunschweig, A. Damme, J. O. C. Jimenez-Halla, C. Hörl, I. Krummenacher, T. Kupfer, L. Mailänder and K. Radacki, *J. Am. Chem. Soc.*, 2012, **134**, 20169; (*j*) C.-T. Poon, W. H. Lam and V. W.-W. Yam, *J. Am. Chem. Soc.*, 2011, **133**, 19622; (*k*) A. Iida and S. Yamaguchi, *J. Am. Chem. Soc.*, 2011, **133**, 6952; (*l*) A. Wakamiya, K. Mori, T. Araki and S. Yamaguchi, *J. Am. Chem. Soc.*, 2009, **131**, 10850; (*m*) S. Miyasaka, J. Kobayashi and T. Kawashima, *Tetrahedron Lett.*, 2009, **50**, 3467; (*n*) A. Sundararaman, M. Victor, R. Varughese and F. Jäkle, *J. Am. Chem. Soc.*, 2005, **127**, 13748.

[7] (*a*) X. Yin, J. Chen, R. A. Lalancette, T. B. Marder and F. Jäkle, *Angew. Chem., Int. Ed.*, 2014, **53**, 9761; (*b*) X. Yin, F. Guo, R. A. Lalancette and F. Jäkle, *Macromolecules*, 2016, **49**, 537; (*c*) X. Yin, K. Liu, Y. Ren, R. A. Lalancette, Y.-L. Loo and F. Jäkle, *Chem. Sci.*, 2017, **8**, 5497; (*d*) B. Meng, Y. Ren, J. Liu, F. Jäkle and L. Wang, *Angew. Chem., Int. Ed.*, 2018, **57**, 2183; (*e*) Y. Adachi, Y. Ooyama, Y. Ren, X. Yin, F. Jäkle and J. Ohshita, *Polym. Chem.*, 2018, **9**, 291.

[8] (*a*) B. Wrackmeyer and H. Nöth, *Chem. Ber.*, 1976, **109**, 1075; (*b*) T. Köhler, J. Faderl, H. Pritzkow and W. Siebert, *Eur. J. Inorg. Chem.*, 2002, 2942; (*c*) H. Braunschweig, R. D. Dewhurst, C. Hörl, A. K. Phukan, F. Pinzner and S. Ullrich, *Angew. Chem., Int. Ed.*, 2014, **53**, 3241; (*d*) B. Wrackmeyer, *Z. Naturforsch., B: Chem. Sci.*, 2015, **70**, 421; (*e*) H. Braunschweig, R. D. Dewhurst and T. Kramer, *Inorg. Chem.*, 2015, **54**, 3619; (*f*) B. Chen, H. Nie, R. Hu, A. Qin, Z. Zhao and B.-Z. Tang, *Sci. China: Chem.*, 2016, **59**, 699.

[9] (*a*) A. Lik, L. Fritze, L. Müller and H. Helten, *J. Am. Chem. Soc.*, 2017, **139**, 5692; (*b*) A. Lik, S. Jenthra, L. Fritze, L. Müller, K.-N. Truong and H. Helten, *Chem. – Eur. J.*, 2018, **24** DOI:10.1002/chem.201706124.

[10] In this case, we achieved B–C coupling by a catalytic Si/B exchange approach. We also demonstrated B–N coupling via Si/B exchange condensation as a route to BCN hybrid polymers and oligomers; see (*a*) T. Lorenz, A. Lik, F. A. Plamper and H. Helten, *Angew. Chem., Int. Ed.*, 2016, **55**, 7236; (*b*) O. Ayhan, T. Eckert, F. A. Plamper and H. Helten, *Angew. Chem., Int. Ed.*, 2016, **55**, 13321; (*c*) H. Helten, *Chem. – Eur. J.*, 2016, **22**, 12972; (*d*) T. Lorenz, M. Crumbach, T. Eckert, A. Lik and H. Helten, *Angew. Chem., Int. Ed.*, 2017, **56**, 2780; (*e*) N. A. Riensch, A. Deniz, S. Kühl, L. Müller, A. Adams, A. Pich and H. Helten, *Polym. Chem.*, 2017, **8**, 5264; (*f*) O. Ayhan, N. A. Riensch, C. Glasmacher and H. Helten, *Chem. – Eur. J.*, 2018, **24**, 5883.

[11] This approach was also recently applied by Liu and Jäkle.[7d]

[12] (*a*) J. Dhar, U. Salzner and S. Patil, *J. Mater. Chem. C*, 2017, **5**, 7404; (*b*) M. Stolar and T. Baumgartner, *Phys. Chem. Chem. Phys.*, 2013, **15**, 9007.

[13] (a) A. Lik, L. Fritze, L. Müller and H. Helten, *J. Am. Chem. Soc.* 2017, **139**, 5692. b) Y. Dienes, S. Durben, T. Karpati, T. Neumann, U. Englert, L. Nyulaszi and T. Baumgartner, *Chem. Eur. J.* 2007, **13**, 7487. c) D. C. Ebner, J. T. Bagdanoff, E. M. Ferreira, R. M. McFadden, D. D. Caspi, R. M. Trend and B. M. Stoltz, *Chem. Eur. J.* 2009, **15**, 12978.

[14] SADABS: Area-Detector Absorption Correction; Siemens Industrial Automation, Inc.: Madison, WI, 1996.

[15] O. V. Dolomanov, L. J. Bourhis, R. J. Gildea, J. A. K. Howard, and H. J. Puschmann, *J. Appl. Cryst.* 2009, **42**, 339.

[16] a) G. M. Sheldrick, *Acta Crystallogr., Sect. A* 2008, **64**, 112; b) G. M. Sheldrick, *Acta Crystallogr., Sect. C* 2015, **71**, 3.

[17] Turbomole: R. Ahlrichs, M. Bär, M. Häser, H. Horn and C. Kölmel, *Chem. Phys. Lett.* 1989, **162**, 165–169.

[18] a) P. A. M. Dirac, *Proc. R. Soc. London, Ser. A* 1929, **123**, 714–733; b) J. C. Slater, *Phys. Rev.* 1951, **81**, 385–390; c) A. D. Becke, *Phys. Rev. A.* 1988, **38**, 3098–3100; d) C. Lee, W. Yang, R. G. Parr, *Phys. Rev. B* 1988, **37**, 785–789; e) A. D. Becke, *J. Chem. Phys.* 1993, **98**, 5648–5652.

[19] A. Schäfer, H. Horn and R. Ahlrichs, *J. Chem. Phys.* 1992, **97**, 2571–2577.

[20] a) S. Grimme, J. Antony, S. Ehrlich and H. Krieg, *J. Chem. Phys.* 2010, **132**, 154104; b) S. Grimme, S. Ehrlich and L. Goerigk, *J. Comput. Chem.* 2011, **32**, 1456–1465.

[21] P. Deglmann, F. Furche and R. Ahlrichs, *Chem. Phys. Lett.* 2002, **362**, 511–518; b) P. Deglmann and F. Furche, *J. Chem. Phys.* 2002, **117**, 9535–9538.

[22] a) R. Bauernschmitt and R. Ahlrichs, *Chem. Phys. Lett.* 1996, **256**, 454–464; b) R. Bauernschmitt and R. Ahlrichs, *J. Chem. Phys.* 1996, **104**, 9047–9052; c) F. Furche and D. Rappoport, in *Density functional methods for excited states: equilibrium structure and electronic spectra*, ed. M. Olivucci, Elsevier, Amsterdam, 2005.

2.2 Catalytic Si/B Exchange Condensation: A Green B–C Coupling Method That Provides Access to Monodisperse (Het)arylborane 'Trimers'

The following section is slightly modified and reproduced from published article‡ with permission from Georg Thieme Verlag KG.

π-Conjugated organoboranes and organoborane oligomers and polymers have attracted considerable attention in recent years because of the intriguing optical and electronic properties such materials can have, resulting from the interaction of the vacant pπ orbital of trivalent boron with an adjacent π system (*p*–π conjugation).[2-14] This has enabled applications thereof in organic (opto)electronics, for anion or amine sensing, as well as bio-imaging.[2] For the preparation of organoborane compounds in general, B–C bond-forming reactions must be accomplished at one stage, and these are often the crucial steps in the synthesis. The development of efficient B–C coupling processes is therefore a highly active field of current research.[15]

For the synthesis of compounds with recurrent (het)arylborane moieties, i.e. polymers and oligomers, in particular, a number of strategies have been explored.[2] One approach is to assemble the triorganoborane building blocks first and build up the extended structure in a subsequent step via C–C coupling reactions.[8-10] For this, Stille-type cross-coupling reactions were found to be particularly useful,[8] but also Suzuki–Miyaura,[9] Sonogashira,[9a] and Yamamoto[10]-type coupling reactions have been successfully applied in some cases. It should be noted that the boron center needs to be kinetically well protected to survive under the cross-coupling conditions applied. An alternative approach makes use of B–C bond formation reactions to construct the extended π-conjugated framework.[7][11][12] With regard to the synthesis of (cyclo)linear polymers and oligomers, this latter method has the advantage that after the B–C coupling process the boron centers may still carry one further leaving group (e.g., Br), which can be replaced by appropriate organic substituents at the post-polymerization stage. This offers the opportunity to generate various materials with tailored properties through 'side-group engineering' from a single common precursor.[11b,d,e,][12] In this vein, one very efficient B–C coupling polymerization method involves the Sn/B exchange reaction, as demonstrated mainly by Jäkle and colleagues.[8d][11] The major drawback of this method, however, is the use of highly toxic and environmentally harmful organotin compounds (which are also employed in the very popular Stille reaction).

We recently developed a highly efficient and environmentally benign organocatalytic B–C coupling method that uses organosilicon compounds instead (Scheme 2.2.1).[12][14] The

‡ Fritze, L.;[1] Riensch, N. A.;[1] Helten, H. *Synthesis* **2019**, *51*, 399–406.

uncatalyzed coupling of an aryl(trimethyl)silane with an aryl(dibromo)borane to form a second B–C_{aryl} bond proceeds generally too slowly to be of practical use. However, we found that such reactions can be effectively accelerated by the addition of the electrophilic silyl reagent Me_3SiNTf_2 (Tf = CF_3SO_2) in substoichiometric amounts.[12]

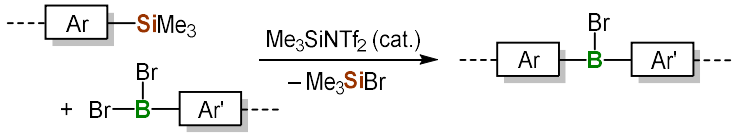

Scheme 2.2.1: *General scheme of B–C coupling by catalytic Si/B exchange condensation.*

We demonstrated the application of this catalytic approach for the synthesis of a series of (het)arylborane molecules, oligomers, and polymers.[12] While the combination of borane and thiophene moieties has evolved into an attractive and highly valued motif of electronic materials,[4][5] and poly(thienylborane)s had been previously known,[8d,11a] the combination of trivalent boron with furan moieties had been largely unexplored, although the potential of the resulting materials has been recently recognized.[6,16] Our new synthesis method allowed the preparation of the first oligo- and poly(furylborane)s as well as mixed thienyl-/furyl-borane species.[12] We found that the properties of the obtained materials are effectively tuned by the ratio of the aromatic rings.[12b] With the synthesis of Ph_2BMes^*, we also incorporated benzene rings into a π-extended borane. In the latter case, the Si/B exchange reaction proceeded significantly slower and required increased catalyst loadings; however, it also afforded the desired product fully selectively.[12] Therefore, the incorporation of benzene rings into longer oligomers has not been further explored as yet.

The longest truly monodisperse hetarylborane oligomers that we prepared so far are one thienylborane trimer and one mixed derivative with a chain composed of three thiophene moieties and one furan ring.[12][17] Herein, we present the synthesis of four new (het)arylborane ‘trimers’, two of which comprise two furan rings; we also succeeded in the incorporation of benzene moieties into such extended π-conjugated scaffolds.

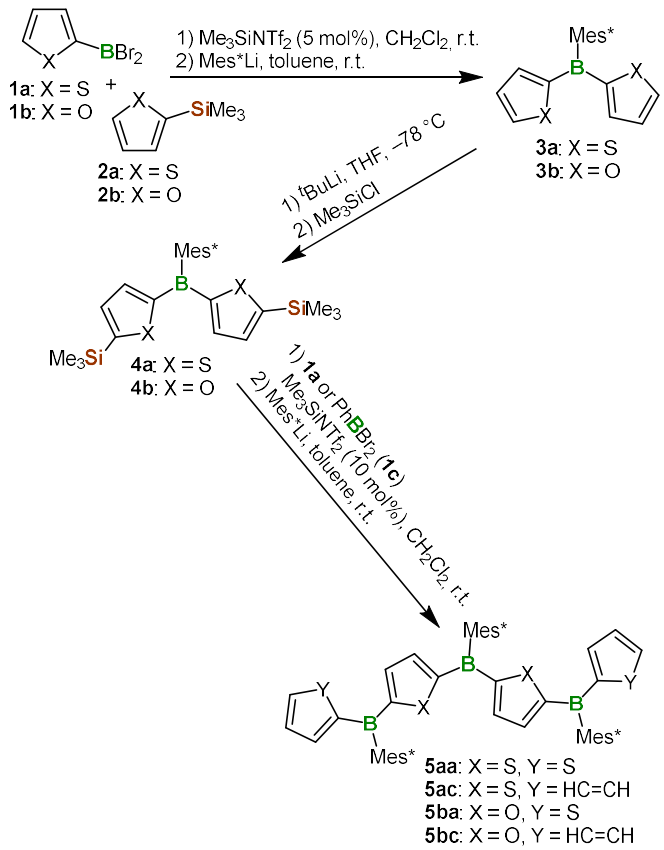

Scheme 2.2.2: *Synthesis of cyclolinear (het)arylborane 'trimers' **5**.*

In the first step of the synthesis, we prepared the dithienyl- and difurylboranes **3a** and **3b** using our catalytic Si/B exchange approach from **1a** and **2a** or **1b** [18] and **2b**, respectively (Scheme 2.2.2). Compound **3b** had been recently reported by us.[12] Here, we used an analogous procedure to synthesize **3a**; the latter of which had been previously reported by Jäkle and Marder, but was in this case prepared via a Sn/B exchange condensation reaction.[9b] We chose 2,4,6-tri-*tert*-butylphenyl (Mes*, supermesityl) as the third, pending substituent on boron, as this group is known to impart effective kinetic stabilization, thus, potentially leading to highly robust materials.[3a,d][8d][9b][12] Compounds **3a**,**b** were transformed into **4a**,**b** via dilithiation and subsequent twofold silylation, as we recently described for **4b**.[12a] The syntheses of the (het)arylborane 'trimers' **5aa**, **5ac**, **5ba**, and **5bc** were achieved by catalytic silicon/boron exchange reactions between **4a**,**b** and dibromo(2-thienyl)borane (**1a**) or $PhBBr_2$ (**1c**)[19] in the presence of 10 mol% Me_3SiNTf_2 with respect to **4a**,**b** (i.e., 5 mol% for each site), followed by postmodification with Mes*Li.

Compounds **5aa**, **5ac**, **5ba**, and **5bc** were purified by column chromatography on alumina and isolated in moderate yields (17–47%). Their constitution was unambiguously ascertained by ^{1}H, ^{11}B, and ^{13}C NMR spectroscopy and mass spectrometry; elemental analyses also yielded satisfactory results. In their $^{11}B\{^{1}H\}$ NMR spectra, each oligomer gave rise to only one broad peak at about δ = 52–63 ppm, which is in a range typical for triarylboranes.[3][5][6] The ^{1}H NMR spectra of each compound recorded at room temperature showed significantly

broadened signals for the aromatic protons of the (het)arene rings of the oligomer chain. This effect can be ascribed to hindered rotation about the B–$C_{(het)arene}$ bonds, caused by the presence of the bulky Mes* substituents, which is slow on the NMR time scale in that temperature regime.

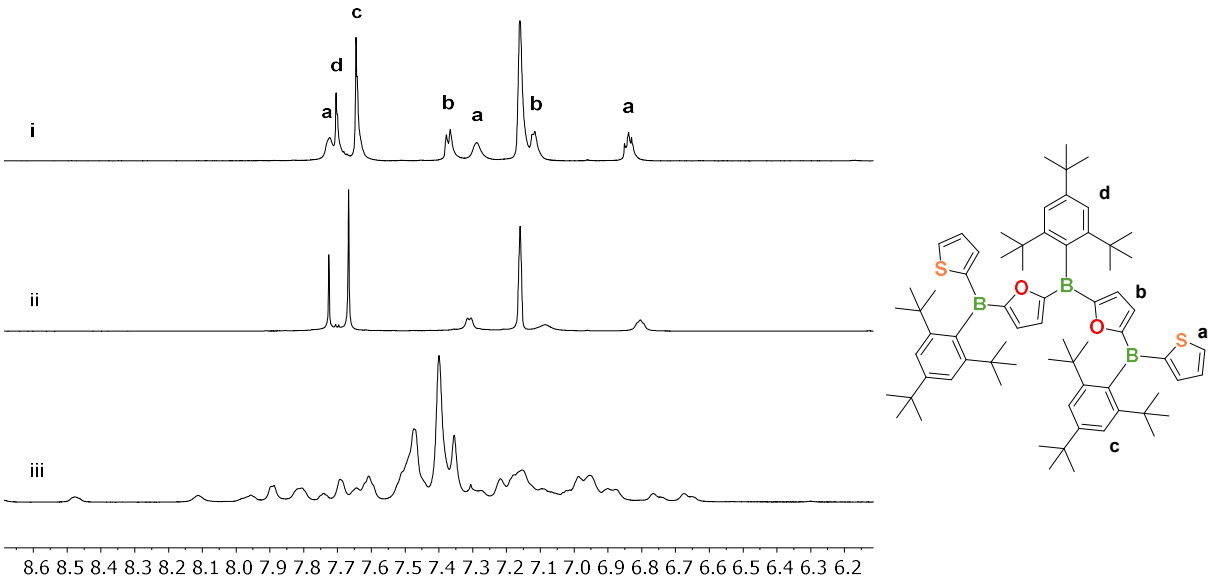

Figure 2.2.1: *Aromatic region of the ^{1}H NMR spectrum of **5ba** (i) at 70 °C (C_6D_6), (ii) at 25 °C (C_6D_6), and (iii) at –80 °C (CD_2Cl_2).*

This was confirmed by ^{1}H NMR experiments at variable temperature (VT NMR) for compound **5ba** as a good case in point. At 25 °C in C_6D_6 only three broad, featureless peaks were observed for all hetarene protons (Figure 2.2.1, ii). At elevated temperatures (70 °C, Figure 2.2.1, i) free rotation about the B–$C_{hetarene}$ bonds was enhanced, resulting in significant line sharpening associated with separation of the five expected heteroaromatic proton resonances in the correct ratio. At low temperatures (–80 °C in CD_2Cl_2, Figure 2.2.1, iii) the rotational processes were frozen, giving rise to a huge number of peaks in the spectrum. Assuming different relative orientations of the hetarene rings (*syn*/*anti* conformers) and, additionally, different relative orientations of the three Mes* groups along the chain, the presence of up to ca. 40 distinct conformers of **5ba** is conceivable.

The UV/Vis absorption spectra of the trimers in tetrahydrofuran (THF) (Figure 2.2.2 and Table 2.2.1) show each an intense band at $\lambda_{abs,max}$ = 371–378 nm and a further band at higher energies ($\lambda_{abs,max}$ = 275–288 nm). Referring to our previous theoretical investigations, both of them originate from π–π* transitions. The significant bathochromic shifts of the major band of **5** with respect to that of the respective monomers **3a** [9b] and **3b**,[12a] and their silylated derivatives **4a**,**b** [12] confirms an effective extension of the π-conjugated system through chain elongation in the trimers. This effect is somewhat more pronounced for the thienyl-flanked

species **5aa** and **5ba**, pointing to superior conjugation over the thienyl than over the phenyl rings in these systems. As an aside, a comparison of the UV/Vis data for **3a**,**b** and **4a**,**b** reveals a slight redshift of the π–π* absorption upon silylation at the heterocycles.

Table 2.2.1: *Photophysical Data of Triarylboranes **3**, **4** and Trimeric Species **5** in THF.*

Compd.	$\lambda_{abs,max}$ (nm)	$\lambda_{em,max}$ (nm)
3a [9b]	325	–
3b [12a]	315	400
4a	334	–
4b [12a]	331	–
5aa	377	–
5ac	371	–
5ba	378	404
5bc	371	–

Notable blue fluorescence was only observed for **5ba**. This is consistent with the findings of our previous studies, which revealed enhanced fluorescence intensities with increasing ratio of furan rings in related oligomers and polymers.[12]

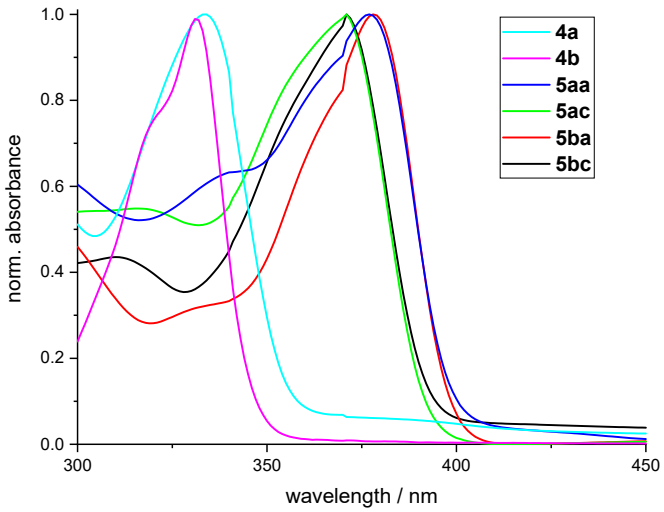

Figure 2.2.2: *UV/Vis absorption spectra of trimeric species **5** and their precursors **4a** and **4b** [12a] in THF (high-energy bands omitted for clarity).*

Cyclic voltammetry (CV) investigations gave for all four trimers two quasi reversible reduction waves, **5aa**: $E_{1/2}$ = −1.96 V, −2.53 V; **5ac**: $E_{1/2}$ = −1.97 V, −2.56 V; **5ba**: $E_{1/2}$ = −2.10 V, −2.75 V; **5bc**: $E_{1/2}$ = −2.11 V, −2.78 V (Figure 2.2.3), consistent with a stepwise reduction of the individual borane moieties in the molecules. A comparison with the corresponding mono-borane **3a** and the dimer analogue by Jäkle and Marder et al.[9b] provides interesting insights.

These compounds show one and two reduction waves, respectively, corresponding to the number of boron atoms per molecule. In the trimers **5**, the putative third reduction process is presumably outside the accessible potential range, which is limited by the solvent. It is plausible to assume that the two reductions of **5** occur at the outer two boron centers, due to Coulombic repulsion of the negative charges in the generated dianion. Within the series of the thienylboranes, the first reduction wave shifts to less negative potentials with increasing chain length in the order: monomer (**3a**, $E_{1/2}$ = −2.58 V[9b]) < dimer ($E_{1/2}$ = −2.14 V[9b]) < trimer (**5aa**, $E_{1/2}$ = −1.96 V). This demonstrates a decrease of the LUMO energy and, hence, an enhancement of the electron-accepting abilities with chain elongation.

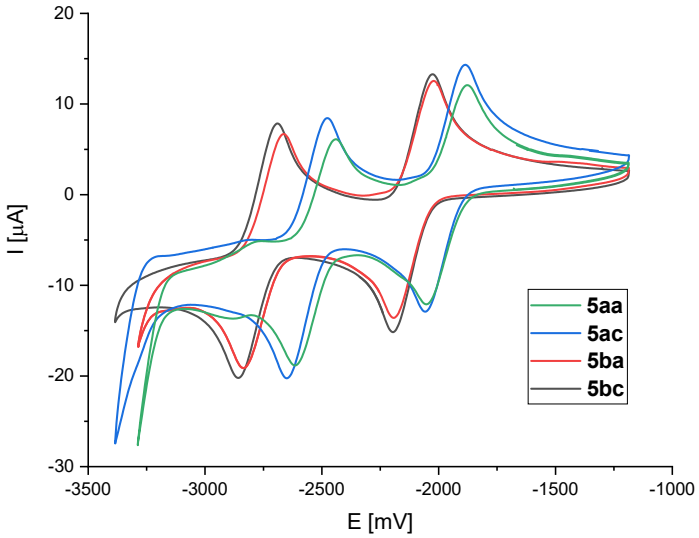

Figure 2.2.3: *Cyclic voltammograms of oligomers **5** in THF/0.1 M [n-Bu$_4$N][PF$_6$] (vs. [Cp$_2$Fe]$^{0/+}$, scan rate: 100 mVs^{-1})*

The large separation between the first and the second reduction waves in **5aa**, **5ac**, **5ba**, and **5bc** evidences strong electronic communication over the heterocycles and the boron center. The slightly smaller separation for **5aa** ($\Delta E_{1/2}$ = 570 mV) compared with that for the corresponding dimer ($\Delta E_{1/2}$ = 700 mV[9b]) is in accordance with the hypothesis that in **5aa** $^{2-}$ the two added electrons on average reside in more distant positions. Comparison of the voltammograms for the four different 'trimers' reveals that the reduction waves of the derivatives featuring furan rings in their center positions, i.e., **5ba** and **5bc**, are cathodically shifted from those of **5aa** and **5ac**. This correlates with the more electron-rich nature of furan compared with thiophene. It is furthermore noteworthy that the redox waves of **5ba** and **5bc** show a slightly larger spacing ($\Delta E_{1/2}$ = 650–670 mV) than those of **5aa** and **5ac** ($\Delta E_{1/2}$ = 570–590 mV). This points to a slightly stronger electronic communication within the furylborane derivatives. The nature of the terminal aryl substituent (i.e., thienyl vs. phenyl) has a negligible effect on the reduction potentials of the compounds.

In summary, we have demonstrated the use of our catalytic Si/B exchange condensation method for the synthesis of four new monodisperse oligomers comprising a cyclolinear chain of four (het)arenes and three boron centers, i.e., **5aa**, **5ac**, **5ba**, and **5bc**. We showed that the incorporation of benzene moieties into such (het)arylborane 'trimers' is indeed possible, and we succeeded in incorporating two furan rings, thus, leading to materials with enhanced luminescence properties and strong electronic communication between the boron centers along the chain.

2.2.1 Experimental Section

Manipulations involving air- and/or moisture-sensitive compounds were performed under an atmosphere of dry argon using standard Schlenk techniques or in an MBraun glove box. Solvents (dichloromethane, *n*-pentane, diethyl ether, toluene, and tetrahydrofuran) were dried and degassed with an MBraun SPS-800 solvent purification system. Deuterated solvents for NMR spectroscopy were dried and degassed at reflux over Na (C_6D_6) or CaH_2 ($CDCl_3$ and CD_2Cl_2) and freshly distilled prior to use. Solvents for aqueous work up (*n*-hexane, *n*-pentane, dichloromethane, ethanol, diethyl ether), sulfuric acid, tribromoborane, bromobenzene, thiophene, 2-bromothiophene, bromine, 2-bromo-1,3,5-triisopropylbenzene, 1,3,5-tri-*tert*-butylbenzene, 1,3,5-tris(trifluoromethyl)benzene, and lithium bis(trifluoromethylsulfonyl)imide were purchased from commercial sources and used as received. Solutions of *n*-butyllithium (1.6 M and 2.5 M in hexane, respectively) and *tert*-butyllithium (1.7 M in pentane) were purchased from Sigma Aldrich and used as received. Furan and trimethylsilylchloride were commercially purchased and freshly distilled prior to use. 2,4,6-Triisopropylphenyllithium,[20] trimethylsilylbis(trifluoromethylsulfonyl)imide,[21] 2-bromo-1,3,5-tri-*tert*-butylbenzene,[22] and 2,4,6-tri-*tert*-butylphenyllithium[9b] were prepared according to described methods. Compound **3b** was prepared according to a procedure previously described by our group.[12] NMR spectra were recorded at 25 °C with a Bruker Avance II-400 spectrometer or with a Bruker Avance III HD spectrometer operating at 400 MHz. Chemical shifts were referenced to residual protic impurities in the solvent (^1H) or the deuterio solvent itself (^{13}C) and reported relative to external $SiMe_4$ (^1H, ^{13}C) or $BF_3{\cdot}OEt_2$ (^{11}B) standards. Mass spectra were obtained with a Finnigan MAT95 spectrometer employing electron ionization (EI) or secondary ionization (SIMS) using a 70 eV electron impact ionization source. Elemental analysis was performed with a CHN-O-Rapid VarioEL by Heraeus. UV/Vis spectra were obtained with a Jasco V-630 spectrophotometer. Fluorescence spectra were obtained with a Jasco FP-6600 spectrofluorometer. Fluorescence quantum yields were determined against perylene as the standard. Melting points (uncorrected) were obtained with an SMP3 melting-point apparatus (Stuart) in 0.5 mm (o.d.) glass capillaries. Cyclic voltammetry (CV) experiments were carried out with a BioLogic SP-50 potentiostat. The three-electrode system consisted of a glassy-

carbon disk as working electrode, a Pt wire as counter electrode, and an $Ag/AgNO_3$ electrode as the reference electrode. The voltammograms were recorded with ca. 10^{-3} M solutions in THF containing [*n*-Bu_4N][PF_6] (0.1 M) as the supporting electrolyte. The scans were referenced after the addition of a small amount of ferrocene as internal standard. The potentials are reported relative to the ferrocene/ferrocenium couple.

Bis(thien-2-yl)(2,4,6-tri-*tert*-butylphenyl)borane (**3a**)

A solution of **1a** (1.25 g, 5.0 mmol) in dichloromethane (2.5 mL) was added to a solution of **2a** (781.6 mg, 5.0 mmol) and TMS-NTf_2 (176.8 mg, 0.5 mmol, 10 mol%) in dichloromethane (2.5 mL) at ambient temperatures and the mixture was stirred overnight. Subsequently, the solvent was removed in vacuo, and the solid residue was redispersed in toluene (15 mL). The solution was added dropwise to a suspension of freshly prepared Mes*Li (from Mes*Br, 8 mmol) in toluene (15 mL) at –78 °C and the reaction mixture was allowed to warm to r.t. overnight. The resulting suspension was diluted with pentane (40 mL) and the reaction was quenched by the addition of water (50 mL). The organic phase was washed with water (50 mL) and brine (2 × 50 mL), dried over mgSO_4, and the solvent was removed under reduced pressure. The crude product was further purified by column chromatography (Al_2O_3) using PE.

Yield: 854 mg (2.0 mmol, 40%); colorless solid.

The analytical data obtained agree well with those reported for **3a**.[9b]

Bis(5-trimethylsilyl-thien-2-yl)(2,4,6-tri-*tert*-butylphenyl)borane (**4a**)

To a solution of **3a** (1.27 g, 3.0 mmol) dissolved in Et_2O (30.0 mL) was added *t*-butyllithium (3.72 mL, 6.3 mmol) at –78 °C. The resulting mixture was stirred for 3 h at –78 °C and then allowed to warm to 0 °C and stirred for 30 minutes. Subsequently, the reaction mixture was cooled to –78 °C again, and trimethylsilylchloride (0.72 g, 6.60 mmol) was added dropwise. The reaction mixture was allowed to warm to r.t. overnight. After aqueous work-up, all volatiles were removed in vacuo and the resulting greenish residue was further purified by column chromatograph (silica; *n*-hexane). The product was obtained as a colorless solid (500 mg, 0.89 mmol, 37%).

^{1}H NMR (400 MHz, $CDCl_3$): δ = 7.68 (d, $^3J_{H–H}$ = 3.4 Hz, 2 H, Thi-*H*), 7.42 (s, 2 H, Mes*-C*H*), 7.28 (d, $^3J_{H–H}$ = 3.4 Hz, 2 H, Thi-*H*), 1.39 (s, 9 H, *p*-*t*Bu-CH_3), 1.14 (s, 18 H, *o*-*t*Bu-CH_3), 0.36 (s, 18 H, *o*-*t*Bu-CH_3).

^{11}B{^{1}H} NMR (128 MHz, $CDCl_3$): δ = 51.5.

^{13}C{^{1}H} NMR (101 MHz, $CDCl_3$): δ = 153.6 (Thi-*C*-B), 151.9 (Thi-*C*-(Si-(*C*H_3)$_3$)), 151.5 (Mes*-*C*-*o*-*t*Bu), 148.2 (Mes*-*C*-*p*-*t*Bu), 142.3 (Thi-*C*H), 135.6 (Mes*-*C*-B), 134.9 (Thi-*C*H), 122.5

(Mes*-*C*H), 38.5 (*o*-*t*Bu-*C*(CH_3)$_3$), 34.9 (*o*-*t*Bu-C(*C*H_3)$_3$), 34.6 (*p*-*t*Bu-*C*(*C*H_3)$_3$), 31.4 (*p*-*t*Bu-C(*C*H_3)$_3$), 0.0 (Si-(*C*H_3)$_3$).

MS (EI, 70 eV): *m*/*z* (%) = 566.6 (65) $[M]^+$, 395.5 (65) $[C_{20}H_{24}BS_2Si_2]^+$, 231.2 (30) $[C_{17}H_{27}]^+$, 147.2 (100) $[C_{11}H_{15}]^+$.

Anal. Calcd (%) for $C_{32}H_{51}BS_2Si_2$: C, 67.80; H, 9.07. Found: C, 68.20; H, 9.04.

UV/Vis (THF): $\lambda_{abs,max}$ = 281 nm (ε = 16664 L mol^{-1} cm^{-1}), 334 (ε = 20893 L mol^{-1} cm^{-1}).

Synthesis of Oligomers **5aa** and **5ac**; General Procedure

To a solution of **4a** (0.48 mmol) in dichloromethane (1 mL) was added TMS-NTf_2 (10 mol%) and the respective diborylated compound **1a** or **1c** (1.0 mmol) in dichloromethane (1 mL) at r.t. The reaction mixture was stirred for 72 hours. After removal of the solvent in vacuo, the residue was redissolved in toluene (1 mL) and added dropwise to a suspension of freshly prepared Mes*Li (from Mes*Br, 1.6 mmol) in toluene (1 mL) at –78 °C. The mixture was stirred for 7 days at r.t., then the solvent was removed in vacuo and the residue was extracted with pentane. The organic phase was washed with brine, dried over $mgSO_4$, and the solvent was removed in vacuo. The crude product was purified by column chromatography (AlOx) using PE.

5,5′-Bis[(thien-2-yl)(2,4,6-tri-*tert*-butylphenyl)boryl]bis(2-thien-5-yl)(2,4,6-tri-*tert*-butyphenyl)borane (**5aa**)

Yield: 128 mg (0.12 mmol, 23%); yellow powder; mp 154 °C; R_f = 0.16 (PE).

^{1}H NMR (400 MHz, $CDCl_3$): δ = 7.85 (d, $^3J_{H–H}$ = 4.7 Hz, 2 H, Thi-*H*), 7.83–7.77 (br, 4 H, Thi- *H*), 7.78–7.74 (br, 2 H, Thi-*H*), 7.43 (s, 4 H, Mes*-*H*), 7.41 (s, 2 H, Mes*-*H*), 7.22 (dd, $J_{H–H}$ = 4.7, 3.5 Hz, 2 H, Thi-*H*), 1.39 (s, 18 H, *p*-*t*Bu-CH_3), 1.38 (s, 9 H, *p*-*t*Bu-CH_3), 1.18 (s, 54 H, *o*-*t*Bu-CH_3).

^{11}B{^{1}H} NMR (128 MHz, $CDCl_3$): δ = 55.8 (br).

^{13}C{^{1}H} NMR (101 MHz, $CDCl_3$): δ = 158.4 (Thi-*C*-B), 158.0 (Thi-*C*-B), 152.0 (Mes*-*C*-*o*-*t*Bu), 151.9 (Mes*-*C*-*o*-*t*Bu), 148.8 (Mes*-*C*-*p*-*t*Bu), 148.8 (Mes*-*C*-*p*-*t*Bu), 148.5 (Thi-*C*-B), 142.0 (Thi-*C*H), 141.9 (Thi-*C*H), 141.6 (Thi-*C*H), 136.1 (Thi-*C*H), 135.4 (Mes*-*C*-B), 135.4 (Mes*-*C*-B), 128.7 (Thi-*C*H), 122.7 (Mes*-*C*H), 122.6 (Mes*-*C*H), 38.7 (*o*-*t*Bu-C(*C*H_3)$_3$), 38.7 (*o*-*t*Bu-*C*(CH_3)$_3$), 35.2 (*o*-*t*Bu-*C*(CH_3)$_3$), 35.1 (*o*-*t*Bu-C(*C*H_3)$_3$), 34.9 (*p*-*t*Bu-*C*(CH_3)$_3$ and *p*-*t*Bu-C(*C*H_3)$_3$), 31.6 (*p*-*t*Bu-C(*C*H_3)$_3$), 31.6 (*p*-*t*Bu-*C*(CH_3)$_3$).

MS (SIMS, 70 eV): *m*/*z* (%) = 1098.7 (3) $[M]^+$, 853.5 (3) $[C_{52}H_{68}B_3S_4]^+$, 677.5 (3) $[C_{44}H_{63}B_2S_2]^+$, 339.3 (13) $[C_{22}H_{32}BS]^+$, 255.3 (65) [Mes*-B]$^+$, 181.2 (18) $[C_{11}H_5BS]^+$, 151.2 (100) $[C_{11}H_8B]^+$.

Anal. Calcd (%) for $C_{70}H_{97}B_3S_4$: C, 76.49; H, 8.90; found: C, 76.63; H, 8.76.

UV/Vis (THF): $\lambda_{abs,max}$ = 288 nm (ε = 19557 L mol^{-1} cm^{-1}), 377 (ε = 30347 L mol^{-1} cm^{-1}).

CV (THF/0.1 M [*n*-Bu$_4$N][PF$_6$], vs. [Cp$_2$Fe]$^{0/+}$, scan rate: 100 mVs^{-1}): $E_{1/2}$ = –1.96 V, –2.53 V.

5,5′-Bis[phenyl(2,4,6-tri-*tert*-butylphenyl)boryl]bis(2-thien-5-yl)(2,4,6-tri-*tert*-butyphenyl)borane (**5ac**)

Yield: 241 mg (0.22 mmol, 47%); colorless powder; mp 139 °C; R_f = 0.34 (PE).

^{1}H NMR (400 MHz, CDCl$_3$): δ = 8.13 (d, $^3J_{H–H}$ = 6.9 Hz, 4 H, Ph-*H*), 7.80–7.74 (br, 2 H, Thi-*H*), 7.60 (d, $^3J_{H–H}$ = 3.6 Hz, 2 H, Thi-*H*), 7.50–7.38 (m, 6 H, Ph-*H*), 7.42 (s, 4 H, Mes*-*H*), 7.40 (s, 2 H, Mes*-*H*), 1.38 (s, 18 H, *p*-*t*Bu-C*H*$_3$), 1.37 (s, 9 H, *p*-*t*Bu-C*H*$_3$), 1.16 (s, 18 H, *o*-*t*Bu-C*H*$_3$), 1.12 (s, 36 H, *o*-*t*Bu-C*H*$_3$).

^{11}B{^{1}H} NMR (128 MHz, CDCl$_3$): δ = 63.4 (br).

^{13}C{^{1}H} NMR (101 MHz, CDCl$_3$): δ = 158.1 (br, 2 × Thi-*C*-B), 151.9 (Mes*-*C*-*o*-*t*Bu), 151.7 (Mes*-*C*-*o*-*t*Bu), 148.8 (Mes*-*C*-*p*-*t*Bu), 148.8 (Mes*-*C*-*p*-*t*Bu), 143.8 (Ph-*C*-B), 142.8 (Thi-*C*-H), 141.7 (Thi-*C*-H), 138.4 (Ph-*C*H), 136.4 (Mes*-*C*-B), 135.4 (Mes*-*C*-B), 131.2 (Ph-*C*H), 127.8 (Ph-*C*H), 122.6 (Mes*-*C*H), 122.4 (Mes*-*C*H), 38.7 (*o*-*t*Bu-*C*(CH$_3$)$_3$), 38.5 (*o*-*t*Bu-C(*C*H$_3$)$_3$), 35.2 (*o*-*t*Bu-*C*(CH$_3$)$_3$), 35.2 (*o*-*t*Bu-C(*C*H$_3$)$_3$), 34.9 (*p*-*t*Bu-C(*C*H$_3$)$_3$), 34.9 (*p*-*t*Bu-*C*(CH$_3$)$_3$), 31.6 (*p*-*t*Bu-C(*C*H$_3$)$_3$), 31.6 (*p*-*t*Bu-*C*(CH$_3$)$_3$).

MS (SIMS, 70 eV): *m*/*z* (%) = 1086.8 (3) [M]$^+$, 841.6 (3) [C$_{56}$H$_{72}$B$_3$S$_2$]$^+$, 671.6 (3) [C$_{46}$H$_{65}$B$_2$S]$^+$, 333.3 (9) [Mes*-B-Ph]$^+$, 255.3 (28) [Mes*-B]$^+$, 199.2 (11) [C$_{14}$H$_{20}$B]$^+$, 151.2 (100) [C$_{11}$H$_8$B]$^+$.

Anal. Calcd (%) for C$_{74}$H$_{101}$B$_3$S$_2$: C, 81.75; H, 9.36; found: C, 81.60; H, 9.28.

UV/Vis (THF): $\lambda_{abs,max}$ = 278 nm (ε = 25022 L mol^{-1} cm^{-1}), 316 nm (ε = 21339 L mol^{-1} cm^{-1}), 371 nm (ε = 41004 L mol^{-1} cm^{-1}).

CV (THF/0.1 M [*n*-Bu$_4$N][PF$_6$], vs. [Cp$_2$Fe]$^{0/+}$, scan rate: 100 mVs^{-1}): $E_{1/2}$ = –1.97 V, –2.56 V.

Synthesis of Oligomers **5ba** and **5bc**; General Procedure

To a solution of **4b** (256.7 mg, 0.48 mmol) in dichloromethane (1 mL) was added TMS-NTf$_2$ (10 mol%) and the respective diborylated compound **1a** or **1c** (1.0 mmol) in dichloromethane (1 mL) at r.t. The reaction mixture was stirred for 72 hours. After removal of the solvent in vacuo, the residue was redissolved in toluene (1 mL) and added dropwise to a suspension of freshly prepared Mes*Li (from Mes*Br, 1.6 mmol) in toluene (1 mL) at r.t. The reaction was stirred for 7 days at r.t., then the solvent was removed in vacuo and the residue was extracted with pentane. The organic phase was washed with brine, dried over mgSO$_4$, and the solvent was removed in vacuo. The crude product was purified by column chromatography (AlOx) using PE, followed by a reprecipitation from CH$_2$Cl$_2$/EtOH.

5,5′-Bis[(thien-2-yl)(2,4,6-tri-*tert*-butylphenyl)boryl]bis(2-fur-5-yl)(2,4,6-tri-*tert*-butyphenyl)borane (**5ba**)

Yield: 94 mg (0.08 mmol, 17%); colorless powder; mp 224 °C; R_f = 0.29 (PE).

^{1}H NMR (400 MHz, C_6D_6, 70 °C): δ = 7.75–7.70 (br, 2 H, Thi-*H*), 7.70 (s, 2 H, Mes*-*H*), 7.65 (s, 4 H, Mes*-*H*), 7.38 (d, $^3J_{H–H}$ = 4.7 Hz, 2 H, Thi-*H*), 7.32–7.26 (br, 2 H, Fur-*H*), 7.14–7.07 (m, 2 H, Fur-*H*), 6.87–6.77 (m, 2 H, Thi-*H*), 1.50 (s, 9 H, *p*-*t*Bu-C*H*$_3$), 1.41 (s, 18 H, *p*-*t*Bu-C*H*$_3$), 1.37 (s, 18 H, *o*-*t*Bu-C*H*$_3$), 1.31 (s, 36 H, *o*-*t*Bu-C*H*$_3$).

^{11}B{^{1}H} NMR (128 MHz, C_6D_6, 70 °C): δ = 51.5 (br).

^{13}C{^{1}H} NMR (101 MHz, C_6D_6, 70 °C): δ = 170.6 (br, Fur-*C*-B), 169.2 (br, Fur-*C*-B), 152.8 (Mes*-*C*-*o*-*t*Bu), 152.6 (Mes*-*C*-*o*-*t*Bu), 149.1 (Mes*-*C*-*p*-*t*Bu), 149.1 (Mes*-*C*-*p*-*t*Bu), 147.3 (br, Thi-*C*-B), 142.3 (br, Thi-*C*H), 136.9 (Thi-*C*H), 134.6 (Mes*-*C*-B), 133.5 (Mes*-*C*-B), 128.7 (Thi-*C*H), 128.0 (Fur-*C*H),[23] 127.9 (Fur-*C*H),[23] 122.9 (Mes*-*C*H), 122.3 (Mes*-*C*H), 38.9 (*o*-*t*Bu-C(*C*H$_3$)$_3$), 38.7 (*o*-*t*Bu-*C*(CH$_3$)$_3$), 35.2 (*o*-*t*Bu-C(*C*H$_3$)$_3$), 35.0 (*p*-*t*Bu-C(*C*H$_3$)$_3$), 34.9 (*o*-*t*Bu-*C*(CH$_3$)$_3$), 34.7 (*p*-*t*Bu-*C*(CH$_3$)$_3$), 31.8 (*p*-*t*Bu-*C*(CH$_3$)$_3$), 31.7 (*p*-*t*Bu-C(*C*H$_3$)$_3$).

MS (EI, 70 eV): *m*/*z* (%) = 1066.8 (8) [M]$^+$, 645.5 (4) [$C_{44}H_{62}B_2O_2$]$^+$, 415.3 (8) [$C_{26}H_{34}B_2OS$]$^+$, 339.3 (30) [$C_{22}H_{32}BS$]$^+$, 323.3 (29) [$C_{22}H_{31}BO$]$^+$, 283.2 (35) [$C_{18}H_{24}BS$]$^+$, 255.3 (100) [Mes*-B]$^+$, 231.3 (63) [$C_{17}H_{27}$]$^+$, 199.2 (46) [$C_{14}H_{20}B$]$^+$, 133.0 (65) [$C_{10}H_{11}$]$^+$.

Anal. Calcd (%) for $C_{70}H_{97}B_3O_2S_2$: C 78.79, H 9.16. Found: C 77.46, H 9.05.

UV/Vis (THF): $\lambda_{abs,max}$ = 286 nm (ε = 19866 L mol^{-1} cm^{-1}), 378 nm (ε = 39432 L mol^{-1} cm^{-1}).

Fluorescence (THF): $\lambda_{em,max}$ (λ_{ex} = 378 nm) = 404 nm (Φ_f = 4.3%).

CV (THF/0.1 M [*n*-Bu$_4$N][PF$_6$], vs. [Cp$_2$Fe]$^{0/+}$, scan rate: 100 mVs^{-1}): $E_{1/2}$ = –2.10 V, –2.75 V.

5,5′-Bis[phenyl(2,4,6-tri-*tert*-butylphenyl)boryl]bis(2-fur-5-yl)(2,4,6-tri-*tert*-butyphenyl)borane (**5bc**)

Yield: 181 mg (0.17 mmol, 36%); colorless powder; mp 244 °C; R_f = 0.21 (PE).

^{1}H NMR (400 MHz, $CDCl_3$): δ = 8.25–7.90 (br, 4 H, Ph-*H*), 7.49 (s, 2 H, Mes*-*H*), 7.43 (s, 4 H, Mes*-*H*), 7.40–7.35 (m, 2 H, Ph-*H*), 7.33–7.20 (br, 4 H, Ph-*H*), 7.19–7.08 (br, 2 H, Fur-*H*), 7.08–6.95 (br, 2 H, Fur-*H*), 1.47 (s, 9 H, *p*-*t*Bu-C*H*$_3$), 1.39 (s, 18 H, *o*-*t*Bu-C*H*$_3$), 1.15 (s, 18 H, *p*-*t*Bu-C*H*$_3$), 1.09 (s, 36 H, *o*-*t*Bu-C*H*$_3$).

^{11}B{^{1}H} NMR (128 MHz, C_6D_6): δ = 55.3 (br).

^{13}C{^{1}H} NMR (101 MHz, $CDCl_3$): δ = 170.2 (br, Fur-*C*-B), 168.9 (br, Fur-*C*-B), 152.3 (Mes*-*C*-*o*-*t*Bu), 151.9 (Mes*-*C*-*o*-*t*Bu), 148.6 (Mes*-*C*-*p*-*t*Bu), 148.5 (Mes*-*C*-*p*-*t*Bu), 143.1 (Ph-*C*-B), 138.4 (br, Ph-*C*H), 135.0 (Mes*-*C*-B), 132.5 (Mes*-*C*-B), 131.2 (Ph-*C*-H), 128.8 (br, Fur-*C*H), 127.7 (Ph-*C*H), 127.6 (br, Fur-*C*H), 122.3 (Mes*-*C*H), 121.9 (Mes*-*C*H), 38.5 (*o*-*t*Bu-C(*C*H$_3$)$_3$),

38.4 (*o*-*t*Bu-*C*(CH_3)$_3$), 35.0 (*p*-*t*Bu-C(*C*H_3)$_3$), 34.9 (*o*-*t*Bu-C(*C*H_3)$_3$), 34.8 (*p*-*t*Bu-*C*(CH_3)$_3$), 34.6 (*o*-*t*Bu-*C*(CH_3)$_3$), 31.8 (*p*-*t*Bu-*C*(CH_3)$_3$), 31.6 (*p*-*t*Bu-C(*C*H_3)$_3$).

MS (EI, 70 eV): *m*/*z* (%) = 1054.9 (26) $[M]^+$, 732.6 (26) $[C_{50}H_{67}B_3O_2]^+$, 722.6 (15) $[C_{50}H_{67}B_2O_2]^+$, 527.5 (5) $[C_{37}H_{45}B_2O]^+$, 400.4 (23) $[C_{28}H_{37}BO]^+$, 317.3 (27) $[C_{22}H_{31}BO]^+$, 231.3 (100) $[C_6H_2$-^{i}Pr-(^{t}Bu)$_2]^+$.

Anal. Calcd (%) for $C_{74}H_{101}B_3O_2$: C, 84.24; H, 9.65. Found: C, 83.53; H, 9.68.

UV/Vis (THF): $\lambda_{abs,max}$ = 275 nm (ε = 50735 L mol^{-1} cm^{-1}), 310 nm (ε = 23040 L mol^{-1} cm^{-1}), 371 nm (ε = 36274 L mol^{-1} cm^{-1}).

CV (THF/0.1 M [*n*-Bu_4N][PF_6], vs. $[Cp_2Fe]^{0/+}$, scan rate: 100 mVs^{-1}): $E_{1/2}$ = –2.11 V, –2.78 V.

2.2.2 References

[1] These authors contributed equally to this work.

[2] Reviews: (a) Wade, C. R.; Broomsgrove, A. E. J.; Aldridge, S.; Gabbai, F. P. *Chem. Rev.* **2010**, *110*, 3958. (b) Jäkle, F. *Chem. Rev.* **2010**, *110*, 3985. (c) Hudson, Z. M.; Wang, S. *Dalton Trans.* **2011**, 7805. (d) Tanaka, K.; Chujo, Y. *Macromol. Rapid Commun.* **2012**, *33*, 1235. (e) Zhao, H.; Leamer, L. A.; Gabbai, F. P. *Dalton Trans*. **2013**, 8164. (f) He, X.; Baumgartner, T. *RSC Adv.* **2013**, *3*, 11334. (g) Wakamiya, A.; Yamaguchi, S. *Bull. Chem. Soc. Jpn.* **2015**, *88*, 1357. (h) Ji, L.; Griesbeck, S.; Marder, T. B. *Chem. Sci.* **2017**, *8*, 846. (i) Helten, H. *In Encyclopedia of Inorganic and Bioinorganic Chemistry; Scott,* R. A., Ed.; Wiley: Chichester, **2017**, DOI: https://doi.org/10.1002/9781119951438.eibc2496.

[3] Selected examples: (a) Wakamiya, A.; Mishima, K.; Ekawa, K.; Yamaguchi, S. *Chem. Commun.* **2008**, 579. (b) Kim, Y.; Huh, H.-S.; Lee, M. H.; Lenov, I. L.; Zhao, H.; Gabbaï, F. P*. Chem. Eur. J*. **2011**, *17*, 2057. (c) Marwitz, A. J. V.; Lamm, A. N.; Zakharov, L. N.; Vasiliu, M.; Dixon, D. A.; Liu, S.-Y. *Chem. Sci.* **2012**, *3*, 825. (d) Levine, D. R.; Caruso, A.; Siegler, M. A.; Tovar, J. D. *Chem. Commun.* **2012**, 6256. (e) Neue, B.; Araneda, J. F.; Piers, W. E.; Parvez, M. *Angew. Chem. Int. Ed.* **2013**, *52*, 9966. (f) Hirai, H.; Nakajima, K.; Nakatsuka, S.; Shiren, K.; Ni, J.; Nomura, S.; Ikuta, T.; Hatakeyama, T. *Angew. Chem. Int. Ed.* **2015**, *54*, 13581. (g) Hertz, V. M.; Bolte, M.; Lerner, H.-W.; Wagner, M. *Angew. Chem. Int. Ed.* **2015**, *54*, 8800. (h) Krieg, M.; Reicherter, F.; Haiss, P.; Ströbele, M.; Eichele, K.; Treanor, M.-J.; Schaub, R.; Bettinger, H. F*. Angew. Chem. Int. Ed.* **2015**, *54*, 8284. (i) Ji, L.; Edkins, R. M.; Lorbach, A.; Krummenacher, I.; Bruckner, C.; Eichhorn, A.; Braunschweig, H.; Engels, B.; Low, P. J.; Marder, T. B. *J. Am. Chem. Soc.* **2015**, *137*, 6750. (j) Wang, X.-Y.; Narita, A.; Feng, X.; Müllen, K. *J. Am. Chem. Soc.* **2015**, *137*, 7668. (k) Wang, S.; Yang, D.-T.; Lu, J.; Shimogawa, H.; Gong, S.; Wang, X.; Mellerup, S. K.; Wakamiya, A.; Chang, Y.-L.; Yang, C.; Lu, Z. H. *Angew. Chem. Int. Ed.* **2015**, *54*, 15074. (l) Osumi, S.; Saito, S.; Dou, C.; Matsuo, K.; Kume, K.; Yoshikawa, H.; Awaga, K.; Yamaguchi, S. *Chem. Sci.* **2016**, *7*, 219. (m) Matsuo, K.; Saito, S.; Yamaguchi, S. *Angew. Chem. Int. Ed.* **2016**, *55*, 11984. (n) Crossley, D. L.; Kahan, R. J.; Endres, S.; Warner, A. J.; Smith, R. A.; Cid, J.; Dunsford, J. J.; Jones, J. E.; Vitorica-Yrezabal, I.; Ingleson, M. *J. Chem. Sci.* **2017**, *8*, 7969. (o) Schickedanz, K.; Radtke, J.; Bolte, M.; Lerner, H.-W.; Wagner, M. *J. Am. Chem. Soc.* **2017**, *139*, 2842. (p) John, A.; Bolte, M.; Lerner, H.-W.; Wagner, M. *Angew. Chem. Int. Ed.* **2017**, *56*, 5588.

[4] Ren, Y.; Jäkle, F. *Dalton Trans.* **2016**, 13996.

[5] For examples of thiophene–borane-based materials, see: (a) Wakamiya, A.; Mori, K.; Araki, T.; Yamaguchi, S. *J. Am. Chem. Soc.* **2009**, *131*, 10850. (b) Iida, A.; Yamaguchi, S. *J. Am. Chem. Soc.* **2011**, *133*, 6952. (c) Poon, C.-T.; Lam, W. H.; Yam, V. W.-W. *J. Am. Chem. Soc.* **2011**, *133*, 19622. (d) Braunschweig, H.; Damme, A.; Jimenez-Halla, J. O. C.; Hörl, C.; Krummenacher, I.; Kupfer, T.; Mailänder, L.; Radacki, K. *J. Am. Chem. Soc.* **2012**, *134*, 20169. (e) Braunschweig, H.; Dyakonov, V.; Engels, B.; Falk, Z.; Hörl, C.; Klein, J. H.; Kramer, T.; Kraus, H.; Krummenacher, I.; Lambert, C.; Walter, C. *Angew. Chem. Int. Ed.* **2013**, *52*, 12852. (f) Mercier, L. G.; Piers, W. E.; Harrington, R. W.; Clegg, W. *Organometallics* **2013**, *32*, 6820. (g) Levine, D. R.; Siegler, M. A.; Tovar, J. D. *J. Am. Chem. Soc*. **2014**, *136*, 7132. (h) Wang, X.-Y.; Zhuang, F.-D.; Wang, R.-B.; Wang, X.-C.; Cao, X.-Y.; Wang, J.-Y.; Pei, J. *J. Am. Chem. Soc.* **2014**, *136*, 3764. (i) Zhang, Z.; Edkins, R. M.; Nitsch, J.; Fucke, K.; Eichhorn, A.; Steffen, A.; Wang, Y.; Marder, T. B. *Chem. Eur. J.* **2015**, *21*, 177. (j) Sarkar, S. K.; Kumar, G. R.; Thilagar, P. *Chem. Commun.* **2016**, 4175. (k) Shimogawa, H.; Yoshikawa, O.; Aramaki, Y.; Murata, M.; Wakamiya, A.; Murata, Y. *Chem. Eur. J.* **2017**, *23*, 3784. (l) Adachi, Y.; Ohshita, J. *Organometallics* **2018**, *37*, 869.

[6] For furan–borane-based materials, see: (a) Wrackmeyer, B.; Nöth, H. *Chem. Ber.* **1976**, *109,* 1075. (b) Köhler, T.; Faderl, J.; Pritzkow, H.; Siebert, W. Eur. *J. Inorg. Chem.* **2002**, 2942. (c) Braunschweig, H.; Dewhurst, R. D.; Hörl, C.; Phukan, A. K.; Pinzner, F.; Ullrich, S. *Angew. Chem. Int. Ed.* **2014**, *53*, 3241. (d) Braunschweig, H.; Dewhurst, R. D.; Kramer, T. *Inorg. Chem*. **2015**, *54*, 3619. (e) Chen, B.; Nie, H.; Hu, R.; Qin, A.; Zhao, Z.; Tang, B.-Z. *Sci. China Chem.* **2016**, *59*, 699.

[7] (a) Matsumi, N.; Naka, K.; Chujo, Y. *J. Am. Chem. Soc.* **1998**, *120*, 10776. (b) Heilmann, J. B.; Scheibitz, M.; Qin, Y.; Sundararaman, A.; Jäkle, F.; Kretz, T.; Bolte, M.; Lerner, H.-W.; Holthausen, M. C.; Wagner, M. *Angew. Chem. Int. Ed.* **2006**, *45*, 920. (c) Nagai, A.; Murakami, T.; Nagata, Y.; Kokado, K.; Chujo, Y. *Macromolecules* **2009**, *42*, 7217. (d) Lorbach, A.; Bolte, M.; Li, H.; Lerner, H.-W.; Holthausen, M. C.; Jäkle, F.; Wagner, M. *Angew. Chem. Int. Ed.* **2009**, *48*, 4584.

[8] (a) Yamaguchi, I.; Tominaga, T.; Sato, M. *Polym. Int.* **2009**, *58*, 17. (b) Reus, C.; Guo, F.; John, A.; Winhold, M.; Lerner, H.-W.; Jäkle, F.; Wagner, M. *Macromolecules* **2014**, *47*, 3727. (c) Wang, X.-Y.; Zhuang, F.-D.; Wang, J.-Y.; Pei, *J. Chem. Commun.* **2015**, 17532. (d) Yin, X.; Guo, F.; Lalancette, R. A.; Jäkle, F. *Macromolecules* **2016**, *49*, 537. (e) Yin, X.; Liu, K.; Ren, Y.; Lalancette, R. A.; Loo, Y.-L.; Jäkle, F. *Chem. Sci.* **2017**, *8*, 5497. (f) Adachi, Y.; Ooyama, Y.; Ren, Y.; Yin, X.; Jäkle, F.; Ohshita, *J. Polym. Chem.* **2018**, *9*, 291. (g) Meng, B.; Ren, Y.; Liu, J.; Jäkle, F.; Wang, L. *Angew. Chem. Int. Ed.* **2018**, *57*, 2183.

[9] (a) Zhao, W.; Zhuang, X.; Wu, D.; Zhang, F.; Gehrig, D.; Laquai, F.; Feng, X. *J. Mater. Chem. A* **2013**, *1*, 13878. (b) Yin, X.; Chen, J.; Lalancette, R. A.; Marder, T. B.; Jäkle, F. *Angew. Chem. Int. Ed.* **2014**, *53*, 9761. (c) Baggett, A. W.; Guo, F.; Li, B.; Liu, S.-Y.; Jäkle, F. *Angew. Chem. Int. Ed.* **2015**, *54*, 11191.

[10] (a) Bonifácio, V. D. B.; Morgado, J.; Scherf, U. *J. Polym. Sci., Part A: Polym. Chem.* **2008**, *46*, 2878. (b) Adams, I. A.; Rupar, P. A. *Macromol. Rapid Commun.* **2015**, *36*, 1336.

[11] (a) Sundararaman, A.; Victor, M.; Varughese, R.; Jäkle, F. *J. Am. Chem. Soc.* **2005**, *127*, 13748. (b) Li, H.; Jäkle, F. *Angew. Chem. Int. Ed.* **2009**, *48*, 2313. (c) Chai, J.; Wang, C.; Jia, L.; Pang, Y.; Graham, M.; Cheng, S. Z. D. *Synth. Met.* **2009**, *159*, 1443. (d) Li, H.; Jäkle, F. *Macromol. Rapid Commun.* **2010**, *31*, 915. (e) Chen, P.; Lalancette, R. A.; Jäkle, F. *J. Am. Chem. Soc.* **2011**, *133*, 8802

[12] (a) Lik, A.; Fritze, L.; Müller, L.; Helten, H. *J. Am. Chem. Soc.* **2017**, *139*, 5692. (b) Lik, A.; Jenthra, S.; Fritze, L.; Müller, L.; Truong, K.-N.; Helten, H. *Chem. Eur. J.* **2018**, *24*, 11961.

[13] Riensch, N. A.; Fritze, L.; Schindler, T.; Kremer, M.; Helten, H. *Dalton Trans*. **2018**, 10399.

[14] We also demonstrated B–N coupling via Si/B exchange condensation as a route to BCN hybrid polymers and oligomers; see: (a) Lorenz, T.; Lik, A.; Plamper, F. A.; Helten, H. *Angew. Chem. Int. Ed.* **2016**, *55*, 7236. (b) Ayhan, O.; Eckert, T.; Plamper, F. A.; Helten, H. *Angew. Chem. Int. Ed.* **2016**, *55*, 13321. (c) Helten, H. *Chem. Eur. J.* **2016**, *22*, 12972. (d) Lorenz, T.; Crumbach, M.; Eckert, T.; Lik, A.; Helten, H. *Angew. Chem. Int. Ed.* **2017**, *56*, 2780. (e) Riensch, N. A.; Deniz, A.; Kühl, S.; Müller, L.; Adams, A.; Pich, A.; Helten, H. *Polym. Chem.* **2017**, *8*, 5264. (f) Ayhan, O.; Riensch, N. A.; Glasmacher, C.; Helten, H. *Chem. Eur. J.* **2018**, *24*, 5883.

[15] (a) Mkhalid, I. A. I.; Barnard, J. H.; Marder, T. B.; Murphy, J. M.; Hartwig, J. F. *Chem. Rev.* **2010**, *110*, 890. (b) Dudnik, A. S.; Fu, G. C. *J. Am. Chem. Soc.* **2012**, *134*, 10693. (c) Bagutski, V.; Del Grosso, A.; Carrillo, J. A.; Cade, I. A.; Helm, M. D.; Lawson, J. R.; Singleton, P. J.; Solomon, S. A.; Marcelli, T.; Ingleson, M. J. *J. Am. Chem. Soc.* **2013**, *135*, 474. (d) Moon, P. J.; Halperin, H. M.; Lundgren, R. *J. Angew. Chem. Int. Ed.* **2016**, *55*, 1894. (e) Zhao, D.; Xie, Z. *Angew. Chem. Int. Ed.* **2016**, *55*, 3166.

[16] Cao, H.; Rupar, P. A. *Chem. Eur. J.* **2017**, *23*, 14670.

[17] A trimer with three furan rings could only be detected by mass spectrometry, see ref. 12b.

[18] Compound **1b** was generated and reacted in situ.

[19] Reactions of **1b** with **4a,b** did not yield conclusive results, presumably because of the poor stability of **1b**.

[20] Ruhlandt-Senge, K.; Ellison, J. J.; Wehmschulte, R. J.; Pauer, F.; Power, P. P. *J. Am. Chem. Soc.* **1993**, *115*, 11353.

[21] Mathieu, B.; Ghosez, L. *Tetrahedron* **2002**, *58*, 8219.

[22] Pearson, D. E.; Frazer, M. G.; Frazer, V. S.; Washburn, L. C. *Synthesis* **1976**, 621.

[23] Determined by HSQC (see the Appendix, Figure S5.2.20).

2.3 Boron-Doped α-Oligo- and Polyfurans: Highly Luminescent Hybrid Materials, Color-Tunable through the Doping Density

The following section was written with support of the following collaborators: M. Fest (syntheses and spectrochemical measurements), A. Helbig (DFT calculations), T. Bischof (X-Ray measurements), Dr. I. Krummenacher (CV measurements), and Dr. J. A. P. Sprenger (TG measurements).

2.3.1 Introduction

π-Conjugated organic polymers and oligomers continue to attract tremendous attention[1] due to their use in organic electronic and optoelectronic devices, such as (polymer-based) organic light-emitting diodes (OLEDs/PLEDs),[2] organic field-effect transistors (OFETs),[3] and photovoltaic cells (OPVs),[4,3b] as well as for sensory[5] and imaging purposes.[6] α-Thiophene-based compounds are among the best-studied classes of electron-rich components for organic electronic applications.[7] In recent years, materials that comprise the five-membered hetarene rings of the other group 16 elements have become of increasing interest in this field as well.[8-10] Selenophene- and tellurophene-containing species have been particularly noted for their element-specific features.[8-10] Furan-based materials, on the other hand, have received relatively little consideration in the past.[8,11-14] A likely reason for that is the reduced stability of furan moieties when exposed to air and incident light.[11] However, such compounds have several notable features, and they are in many ways complementary to their heavier-element congeners.[8,11-14] While α-oligothiophenes in solution usually adopt slightly twisted conformations along the backbone, which has been attributed to steric repulsion between the sulfur atoms and the 3'-hydrogens of the adjacent rings, α-oligofurans are much more rigid, favoring highly planar structures. This, together with the lower aromaticity of the furan system compared to thiophene, provides ideal conditions for effective π-electron delocalization along the backbone. In addition, α-oligofurans generally show enhanced solubility in organic media compared to their heavier relatives. It is furthermore noteworthy that furan rings are biodegradable, and they can be derived from biomass.[11,14] In light of these favorable features, furan-based materials have recently gained increasing interest.[8,11-14]

An important recent finding in this regard was that the combination of furan rings with strongly electron-withdrawing groups substantially improves their resistance to oxidative degradation by lowering the compound's HOMO energy and therefore enhancing its overall stability.[11e,13] The doping of conjugated π systems with trivalent boron atoms has emerged as an effective strategy to produce novel compounds with intriguing properties and functions.[15-27] The vacant p orbital of boron incorporated therein acts as a strong π acceptor. In this respect, too, thiophene-based materials[15,16b,k,17-26] have been much more extensively investigated than their

furylborane congeners.[18f,27] Jäkle and co-workers have explored dithienylboranes that are kinetically stabilized with bulky aryl groups as the third *B*-substituent, such as supermesityl (Mes*, 2,4,6-tri-*tert*-butylphenyl) or fluoromesityl (^{F}Mes, 2,4,6-tris(trifluoromethyl)phenyl), as building blocks for various conjugated polymers[19,20] and π-extended molecules.[21] Recently, they presented a series of fluorescent poly(oligothiophene boranes) (**A**, Figure 2.3.1), the emsission color of which varied with the length of the conjugated oligothiophene linker.[20] Oligomers **B** served as molecular model compounds for the dithiophene-bridged polymer **A** with *m* = 2. Our group recently developed a novel organocatalytic Si/B exchange condensation procedure for B–C coupling.[22–26] This method proved to be a highly effective means for the synthesis of organoborane polymers with B–C(aryl) linkages, including poly(thienylboranes) **A** (*m* = 1) and the first poly(furylboranes) **C**.[22] Especially the latter are characterized by exceptionally intense fluorescence emission (quantum yields, Φ_f > 70%).[28] We found that the luminescence of furylborane compounds generally exceeds that of their thienylborane congeners.[22] In mixed polymers and oligomers such as **D**[23] emission intensities increased with the ratio of incorporated furan rings.[22,23] Recently, we added a series of molecular compounds of types **E**[24] and **F**,[25,29] which feature one or two boron centers, respectively, in combination with dihetarene moieties. These species generally show particularly strong luminescence.

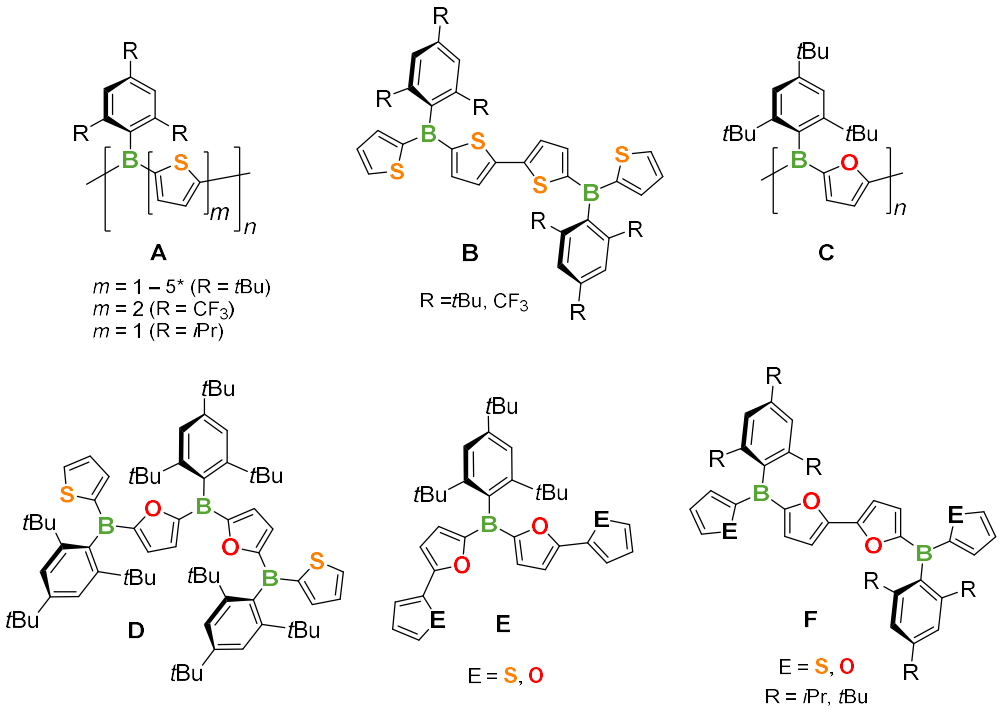

Figure 2.3.1: *Kinetically stabilized thienyl- and furylborane oligomers and polymers and some mixed derivatives. *The derivative of **A** with m = 5 carries a solubilizing hexyl group at the central thiophene ring of the repeat unit, which is omitted here for clarity.*

Taken together, these findings motivated us to investigate poly(oligofuran boranes) with varying lengths of the oligofuran linker (i.e., varying levels of *B*-doping) as well as a series of

oligofuran-bridged bisboranes as molecular model systems for the polymers. Our studies, as presented herein, reveal that these new materials are highly luminescent, and their emission colors are effectively tuned by the doping density.

2.3.2 Results and Discussion

Synthesis of Bisboranes BB*m*F. We started our investigations with the synthesis of bisboranes **BB*m*F**, which feature $m = 1 – 5$ furan moieties bridging the boron centers (Scheme 2.3.1). The synthesis of compound **BB1F**, previously described by us,[22b] was repeated for the current study in order to acquire all analytical data required for the comparison with the longer-chain bisboranes. **BB1F** was obtained via our catalytic Si/B-exchange condensation procedure[22] applied to dibromoborane **1** and 2,5-bis(trimethylsilyl)furan (**2**) (2 : 1 equiv.) using Me_3SiNTf_2 (Tf = SO_2CF_3; 10 mol%) as the catalyst, followed by substitution of the remaining B–Br bonds with Mes*Li. For the synthesis of compound **BB2F**, difuryl(supermesityl)borane (**3**),[22] which has been obtained by a Si/B exchange condensation process as well, was selectively monolithiated and subsequently reacted with I_2 or Me_3SnCl to give **4** and **5**, respectively. The solid-state structure of **5** was determined by single-crystal X-Ray diffractometry (see Appendix, Figure S5.3.107). Compound **BB2F** was obtained via Pd-catalyzed Stille coupling of **4** with **5**. By using microwave radiation the reaction time shortened to just 40 minutes. The longer-chain bisboranes **BB3F** – **BB5F** were likewise prepared by microwave-assisted Stille cross-coupling of **4** (2 equiv.) with 5,5'-bis(trimethylstannyl)-mono-, -di-, and -trifuran (**6a-c**), respectively.

The new compounds, **BB2F** – **BB5F**, were isolated as yellow solids after column chromatography in yields of 66 (**BB2F**), 42 (**BB3F**), 71 (**BB4F**), and 75 % (**BB5F**). Their constitution was unambiguously ascertained by multinuclear NMR spectroscopy and high-resolution mass spectrometry (HRMS). Their $^{11}B\{^1H\}$ NMR spectra display a single broad resonance at around $\delta = 49$ ppm, which is in the expected range for boranes carrying one supermesityl and two furyl or thienyl substituents, as is the case also for the boron centers in **A–F**.[20,22–25] The ^1H and $^{13}C\{^1H\}$ NMR spectra for **BB2F** – **BB5F** show all expected signals. The two resonances for the β-furyl protons in direct vicinity of the Mes* groups are significantly broadened, which is due to hindered rotation about the B–C_{Fur} bonds, caused by the steric demand of the Mes* substituent. This feature is often observed for Mes*-substituted oligo- and polyfurylboranes, but it is usually not observed for the related thienylborane species.[20,22–25] All bisboranes **BB*m*F** exhibited excellent stability towards air and moisture for a prolonged period, as well as pronounced thermal stability. Thermogravimetric analyses (TGA) indicated no sign of decomposition up to temperatures about 280 °C.

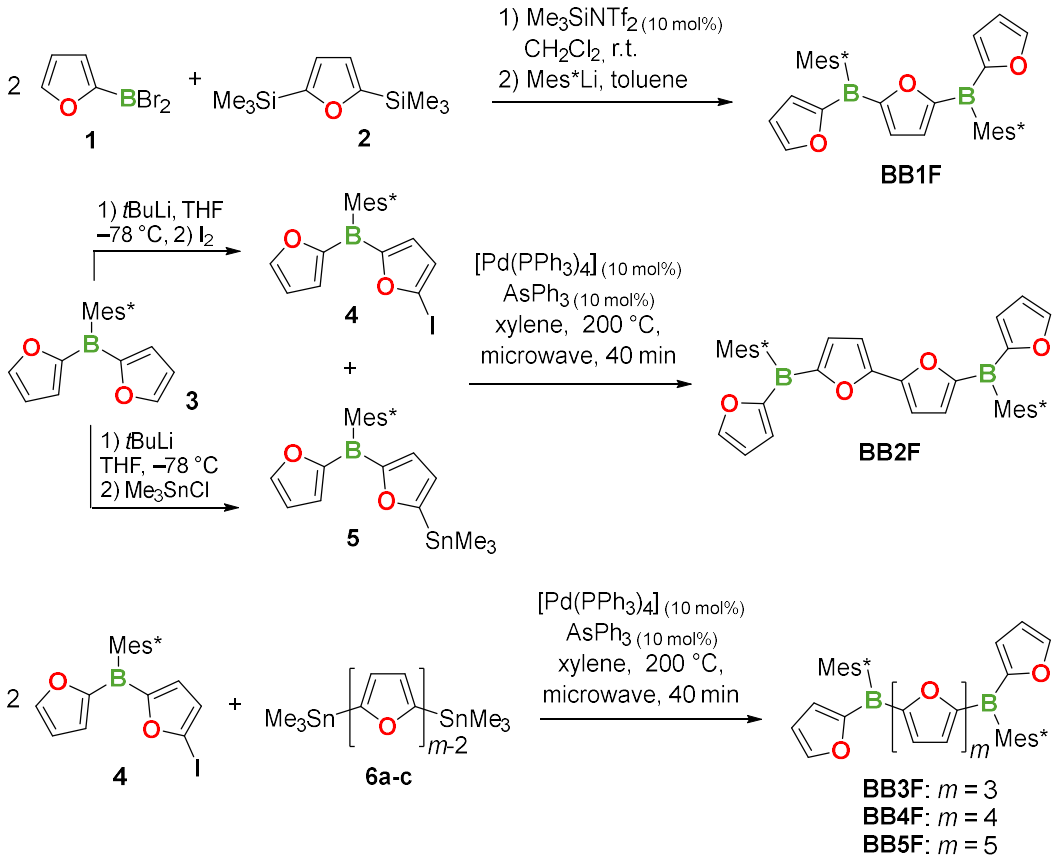

Scheme 2.3.1: *Synthesis of bisboranes* ***BBmF****.*

X-Ray Crystallographic Characterization. For all the bisboranes **BB1F** – **BB5F** we obtained single-crystals suitable for X-Ray diffraction studies (for the molecular structures of **BB2F** – **BB5F**, see Figure 2.3.2). The solid-state structure of **BB1F** was reported by us previously,[22b] but we have now obtained improved structural data for it from a higher-quality crystal (see Appendix, Figure S5.3.108). Each bisborane features a quasiplanar arrangement involving the furan rings and the trigonal-planar BC_3 units. This is a key prerequisite for effective π conjugation over the backbone of these oligomer-type species. In all structures the Mes* groups are nearly perpendicular oriented to the respective BC_3 planes (dihedral angles: > 81°). In compounds **BB1F** – **BB4F** the furan rings are almost perfectly coplanar, both within the oligofuran bridges as well as over the boron centers (mean twist angle: 5.5°). Their relative orientation corresponds to a strict all-*anti* conformation. For comparison, the dithiophene-bridged bisborane **B** (R = *t*Bu; Figure 2.3.1), crystallographically studied by Jäkle and co-workers,[20] showed a twist angle between the thiophene rings of 14.6°. In the crystal structures of **BB1F** – **BB4F** no evidence of significant intermolecular interactions such as π−π stacking or C–H···π or C–H···O interactions between the molecules was observed. Such interactions are probably prevented by the sterically demanding Mes* groups. This is different in the solid-state structure of compound **BB5F**. The pentafuran bridge therein is obviously long enough to allow for π−π stacking between the molecules (distance between

the central furyl rings: 3.42 Å), resulting in dimeric entities with the Mes* groups of both molecules pointing away from each other (Figure S5.3.112). This bisborane derivative also shows a certain twist in its oligofuran chain. The torsion angle between the furan rings around O3 and O4 amounts to 21.9°, which is most likely a result of the aforementioned intermolecular forces. Within each of the two parts of the molecule the interplanar angles between the furan rings are below 16.8°. In this derivative one of the terminal furyl rings is disordered by rotation about the B−C bond, with preference for the *anti* conformer (ratio 9/1).

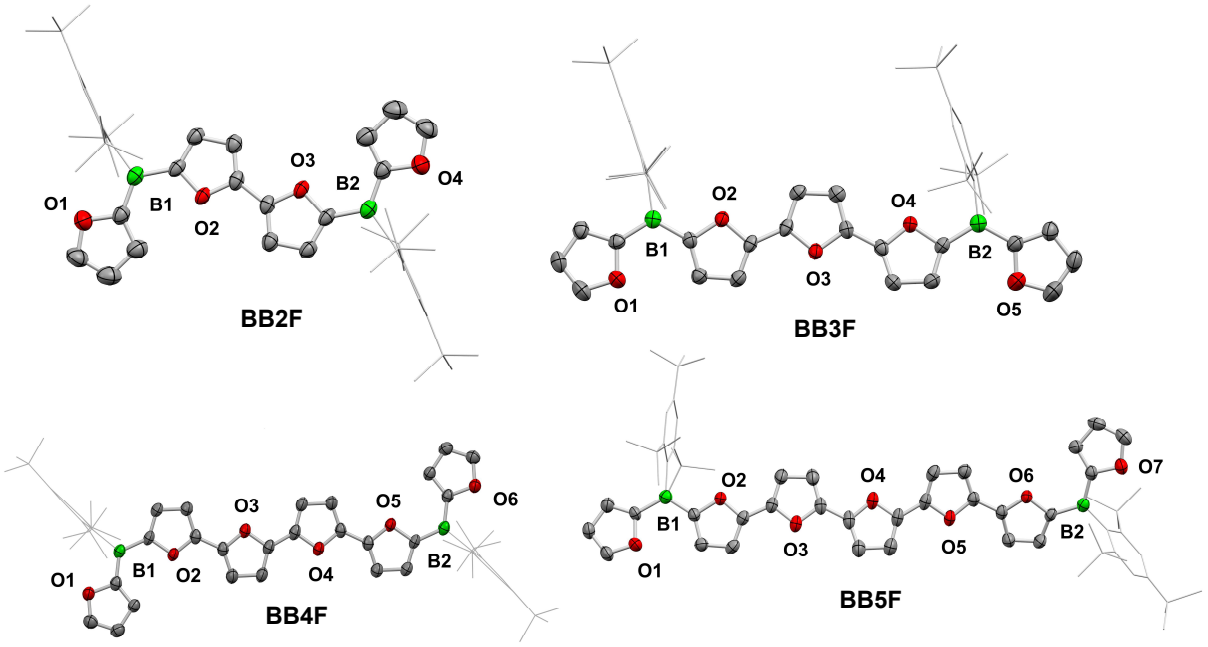

Figure 2.3.2: *Molecular structures of* ***BB2F*** *–* ***BB5F*** *by single-crystal X-Ray diffractometry (H atoms and disorders in the tBu groups of some of the Mes* substituents omitted for clarity).*

Synthesis of Poly(oligofuran boranes). Next, we synthesized a series of α-oligofuran borane polymers with varying length of the oligofuran moiety (Scheme 2.3.2). We additionally prepared **PB1F** for comparison, which features only one furan group per repeat unit, via our catalytic Si/B exchange condensation approach, as we have reported earlier.[22] For the synthesis of polymers **PB2F** to **PB5F^{Hex}** we applied Stille-type catalytic cross-coupling polycondensation reactions with microwave assistance to the appropriate difunctional co-monomers, similar to the procedure used for the synthesis of the bisboranes. The solubility of **PB2F** – **PB5F** in common organic solvents gradually decreased with increasing length of the oligofuran spacer. However, even the derivative with five furan rings bridging the boron centers, **PB5F**, was sufficiently soluble in THF and $CDCl_3$ to allow analysis thereof by gel permeation chromatography (GPC) and ^{1}H NMR spectroscopy. This is in marked contrast to the thiophene congeners by Jäkle et al.:[20] in the case of polymer **A** with *m* = 5 an additional solubilizing hexyl group was introduced at the pentathiophene spacer. This parallels the trend found for linear

oligofurans vs. oligothiophenes, where the fomer have significantly enhanced solubility.[11b-e,11] We nevertheless decided to prepare polymer **PB5F^{Hex}** as well, which has a hexyl group installed at the central furan ring of the repeat unit, to obtain a derivative of **PB5F** with improved solubility. In this case, we employed a monomer with tri-*n*-butyltin instead of trimethyltin groups as the leaving groups, **6c^{Hex}**, as this facilitated the workup of the monomer but had no noticeable detrimental effect on the polymerization process.

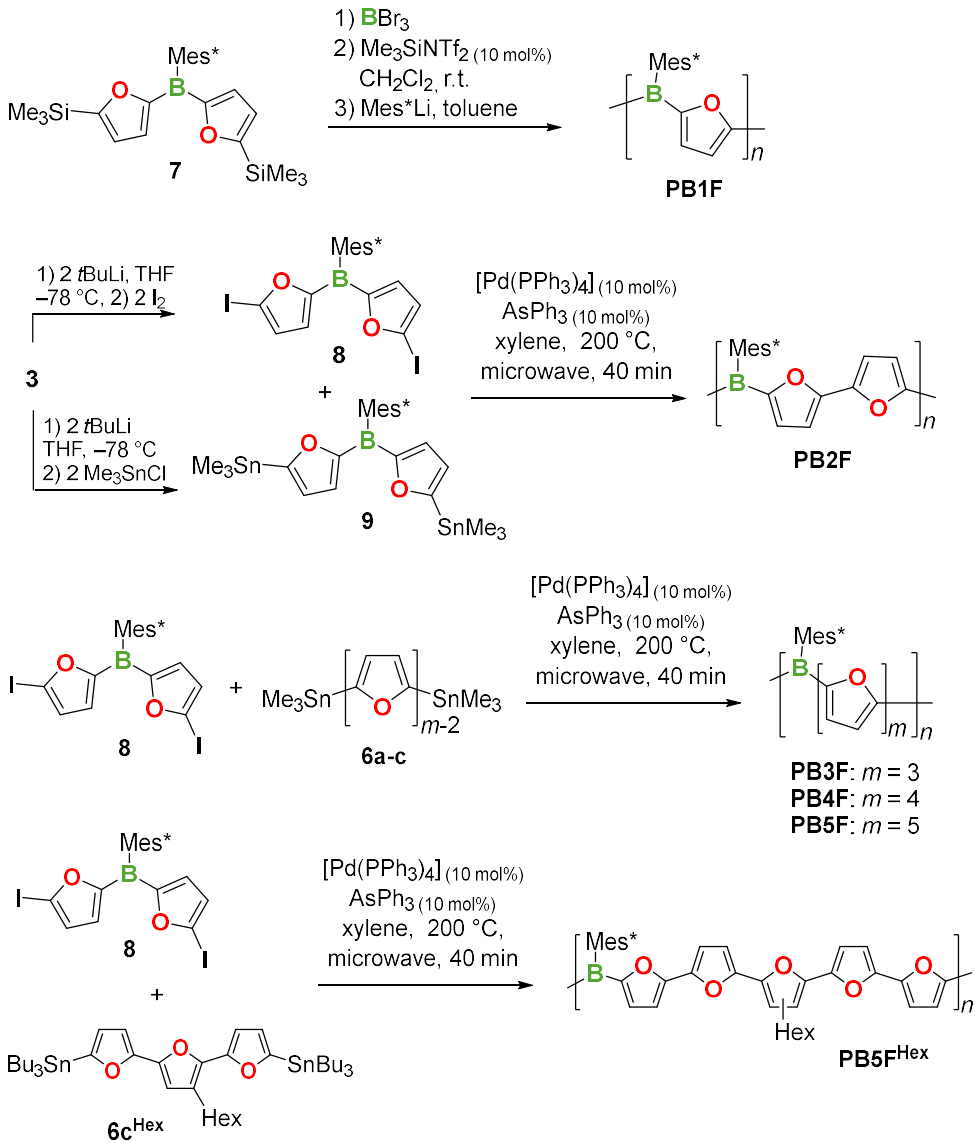

Scheme 2.3.2: *Synthesis of poly(oligofuran boranes)* ***PBmF****.*

The polymers **PB1F** – **PB5F^{Hex}** were isolated as light yellow to dark red solids after precipitation with methanol in yields of 35 (**PB2F**), 20 (**PB3F**), 18 (**PB4F**), 27 (**PB5F**), and 19 % (**PB5F^{Hex}**). Analysis via GPC (in THF, vs. polystyrene standards) suggested number average molecular weights of M_n = 4 – 7 kDa and relatively narrow polydispersities (Đ = 1.4, mean value; Table 2.3.2). The matrix-assisted laser desorption/ionization-time-of-flight (MALDI-TOF) mass

spectra of the new polymers showed successive peaks with a mass difference corresponding to their repeat unit (Figures S5.3.83 – S5.3.87). **PB1F** – **PB5F** proved to be stable towards air and moisture and showed excellent thermal stability, with decomposition temperatures of 285 – 300 °C (determined by TGA, Figure S5.3.100). For **PB5F^{Hex}** we observed 13 % mass loss at 170 °C, which matches the mass fraction of the hexyl groups. At 300 °C, the decomposition behavior of **PB5F^{Hex}** was analogous to that of the other polymers.

Optoelectronic Properties of BB*m*F and PB*m*F$^{(Hex)}$. The UV-vis absorption spectra of the bisboranes **BB*m*F** display each one low-energy band with vibronic fine structure with two maxima (Figure 2.3.3, top; Table 2.2.1). While the longest-wavelength maximum represents the highest peak in the spectra of **BB1F** and **BB2F**, this is reversed in those of **BB3F** to **BB5F**. With increasing length of the oligofuran bridge, this band experiences a continuous red-shift from 360 nm for **BB1F** to 457 nm for **BB5F** (referring to the respective longest-wavelength peak). The bisboranes **BB1F** – **BB5F** show blue to green fluorescence upon excitation, which is particularly intense in the cases of **BB2F** – **BB5F**. Their structured emission band appears at relatively small Stokes shifts (1061 – 3639 cm^{-1}), in the same relative order as the absorption bands, that is, with progressive bathochromic shifts upon elongation of the oligofuran bridge. Interestingly, while the fluorescence quantum yield for compound **BB1F** is only 7 %, and its excited state has a slightly longer lifetime (4.00 ns), the quantum yields for the longer-chain compounds **BB2F** – **BB5F** are nearly quantitative (97 to 89 %), accompanied with fluorescence lifetimes below 2.10 ns.

Table 2.3.1: *Photophysical data for bisboranes BBmF.*

compd	λ_{abs}[a] [nm]	λ_{em}[a] [nm]	Φ_f[b] [%]	τ[a,c] [ns]
BB1F[14]	346, **360**	382,**403**	7	< 1.00 (20 %), 4.40 (80 %)
BB2F	382, **403**	**421**, 443	97	< 1.00 (100%)
BB3F	**408**, 432	**455**, 477	94	1.43 (80 %), 1.96 (20 %)
BB4F	**424**, 448	**478**, 501	93	1.42 (64%), 2.09 (36%)
BB5F	**433**, 457	492, **514**	89	1.36 (65%), 1.96 (35%)

[a]In THF solution; absorption and emission maxima bold. [b]Determined by using an integration sphere. [c]Fluorescence lifetime.

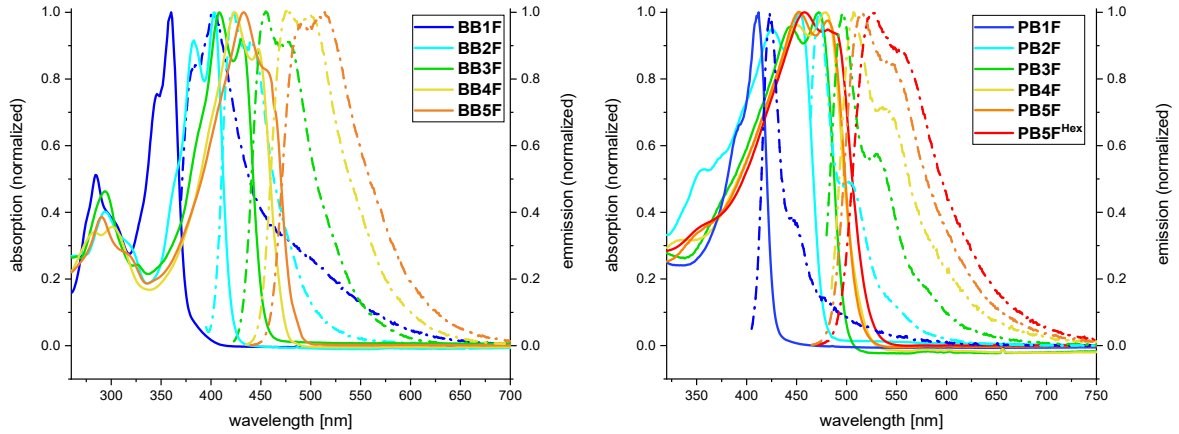

Figure 2.3.3: *UV-vis absorption (solid lines) and fluorescence (dashed lines) spectra for* ***BB1F*** *–* ***BB5F*** *(left) and* ***PB1F*** *–* ***PB5F^{Hex}*** *(right).*

In order to assess the origin of these bands and to gain deeper insight into the electronic structure of the new compounds, we performed time-dependent density functional theory (TD-DFT) calculations on model systems having mesityl (2,4,6-trimethylphenyl, Mes) instead of Mes* substituents on boron (**BB*m*F^{Mes}**, Figure 2.3.4 and Figures S5.3.113 – S5.3.117). The computed excitation wavelengths are in fairly good agreement with the experimentally determined values (Table S5.3.2). Our calculations revealed that the low-energy bands are unambiguously assigned as π−π* transitions, involving the HOMO and the LUMO in the oligofuran-bridged bisboranes **BB2F**[30] – **BB5F**. Both of them are characterized as π orbitals extended over all furan rings and including the p_π orbitals of the boron centers (Figure 2.3.4). The oligofuran bridge has a strong contribution to both frontier orbitals, while the contribution from the terminal furan rings is somewhat less pronounced. Furthermore, the LUMO shows a considerable contribution from the boron center, thus pointing to some degree of charge transfer to boron upon excitation.

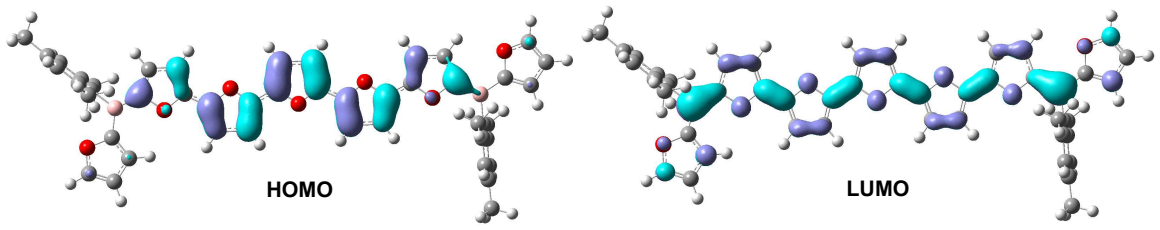

Figure 2.3.4: *Calculated frontier orbitals of* ***BB5F*** *(isovalue 0.03 a.u.).*

The UV-vis absorption spectra of the polymers **PB1F** – **PB5F^{Hex}** display each one structured low-energy band with two maxima as well (Figure 2.3.3, left; Table 2.3.2). This is in marked contrast to the poly(oligothiophene boranes) **A** (Figure 2.3.1), where the derivatives with $m \geq 3$ show no resolution of the vibronic structure under comparable conditions.[20] Compared to the corresponding bisboranes **BB1F** – **BB5F** having the same oligofuran bridge-length, the bands

of their polymeric analogues **PB1F** – **PB5F** are considerably red-shifted (by 29 – 52 nm). This evidences facile π-electron delocalization over the boron centers, and thus, effective conjugation along the polymer chain. Similar to the bisboranes, within the series **PB1F** to **PB5F** the visible absorption band undergoes progressive red-shifts with increasing number of furan moieties in the structural unit. Incorporation of a hexyl side chain at the oligofuran bridge, when going from **PB5F** to **PB5F^{Hex}**, leads to a further red-shift of the absorption. This is probably a result of the inductive effect of the alkyl group, which further enhances the electron-rich character of the bridge, thus increasing the HOMO energy.

As well as the bisboranes, the polymers proved to be highly emissive. The fluorescence spectra likewise showed progressive bathochromic shifts with increasing length of the oligofuran bridge. This results in emission colors from blue for **PB1F** to orange for **PB5F^{Hex}**. All polymers show considerably high fluorescence quantum yields – with the maximum being Φ_f = 87 % for **PB2F** – and relatively short fluorescence lifetimes.

The bisboranes **BB1F** – **BB5F** and polymers **PB1F** – **PB5F^{Hex}** were further studied by cyclic voltammetry (CV) and square wave voltammetry (SWV) in THF solution (Figure 2.3.5). The voltammograms of the bisboranes reveal reversible reduction behavior with first half-wave potentials of $E_{1/2}$ = −2.29 V (**BB1F**), $E_{1/2}$ = −2.29 V (**BB2F**), and $E_{1/2}$ = −2.36 V (**BB3F**) relative to the Fc/Fc$^+$ couple. The bisboranes **BB2F** and **BB3F** show two distinct reductions, indicating a stepwise reduction of the two borane moieties (half-wave potential splittings $\Delta E_{1/2}$ = 395 mV (**BB2F**) and 140 mV (**BB3F**)). The second reduction of **BB1F** is beyond the solvent limit, suggesting a separation from the first reduction wave of about 1 V or greater.

Table 2.3.2: *GPC data, photophysical, and electrochemical properties of the polymers.*

compd	M_n [kDa]	DP_n	Đ	λ_{abs}[a] [nm]	λ_{em}[a] [nm]	Φ_f[b] [%]	τ[a,c] [ns]	$E_{1/2}$[d] [V]
PB1F	4.5	14	1.41	392, **412**	**423**, 447	78	1.19 (92 %), 2.57 (8 %)	−1.9
PB2F	3.8	10	1.18	425, **453**	**472**, 505	87	1.40 (79 %), 3.27 (21 %)	−2.0
PB3F	5.2	11	1.30	444, **472**	**496**, 530	59	1.30 (75 %), 2.44 (25 %)	−2.1
PB4F	7.0	13	1.65	450, **479**	**508**, 540	32	1.24 (70 %), 2.31 (30 %)	−2.2
PB5F	5.4	9	1.51	**452**, 482	**516**, 546	42	1.28 (67 %), 2.51 (34 %)	−2.2
PB5F^{Hex}	5.2	8	1.58	**458**, 486	**525**, 557	40	1.44 (73 %), 2.80 (27 %)	−2.2

[a]In THF solution, absorption and emission maxima bold. [b]Determined by using an integration sphere. [c]Fluorescence lifetime. [d]Determined by CV.

For **BB4F** and **BB5F**, multiple irreversible reduction processes with reduction onsets of −2.3 V (**BB4F**) and −2.4 V (**BB5F**) were observed as indicated by the emergence of corresponding oxidation peaks at −0.8 V (**BB4F**) and −1.0/−0.8 V (**BB5F**). For **BB5F** an additional oxidation event was observed at $E_{1/2}$ = 0.40 V (see Appendix, Figure S5.3.96), consistent with a narrowing of the HOMO–LUMO gap by elongation of the π-system.

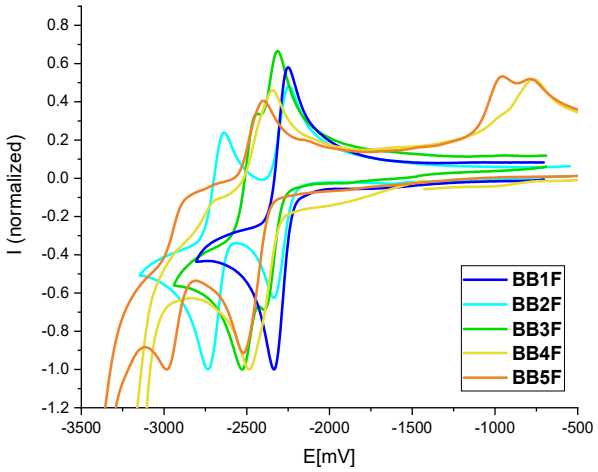

Figure 2.3.5: *Cyclic voltammograms (vs. Fc/Fc+ in THF containing 0.1 M [n-Bu$_4$N][PF$_6$] as the supporting electrolyte) in the cathodic of **BB1F** – **BB5F**.*

The observed splittings in the longer-chain derivatives thus indicate a gradual decrease of electronic communication between the two boron atoms due to their spacial distance as the number of furan units in the bridge increases.

CV measurements of the polymers show multiple reduction events with onsets between −1.9 and −2.2 V (Figure S5.3.97). While the reduction events for the polymers **PB1F**, **PB2F**, **PB5F** and **PB5F^{Hex}** show partial reversibility, polymers **PB3F** and **PB4F** undergo irreversible reduction processes as indicated by the emergence of a corresponding oxidation peak at −1.0 V.[31] With elongation of the furan bridge, the spacing between the different reductions becomes narrower due to a decrease of the interactions between the boron centers. For **PB5F** and **PB5F^{Hex}**, an additional oxidation event was observed at 0.40 V, which is consistent with the observations made for **BB5F**.

To gain deeper insight into the nature of the reduced species, we carried out spectroelectrochemistry studies on bisborane **BB2F** and **PB2F** in THF as representative examples (Figure 2.3.6; see also: Figures S5.3.58 – S5.3.59). For **BB2F**, new absorption features were observed when the applied voltage was gradually decreased, reaching their maximum at −1.95 V, while at the same time the bands for neutral **BB2F** continuously decreased and finally vanished. One new, structured band appeared at λ_{max} = 601 nm, besides two lower maxima at 546 and 569 nm. A second new, broad band appeared in the near infrared (NIR) region of the spectrum, having its maximum at λ_{max} = 1590 nm and a lower peak at

1302 nm. Such features are characteristic of a negative polaron, that is in this case, the radical anion [**BB2F**]$^{\bullet-}$. Upon further reduction of the applied voltage from −1.95 V to −2.85 V, the absorption bands for [**BB2F**]$^{\bullet-}$ decreased again in intensity at the expense of a new one at 816 nm with a shoulder at 740 nm, indicating the formation of the dipolaron [**BB2F**]$^{2-}$.

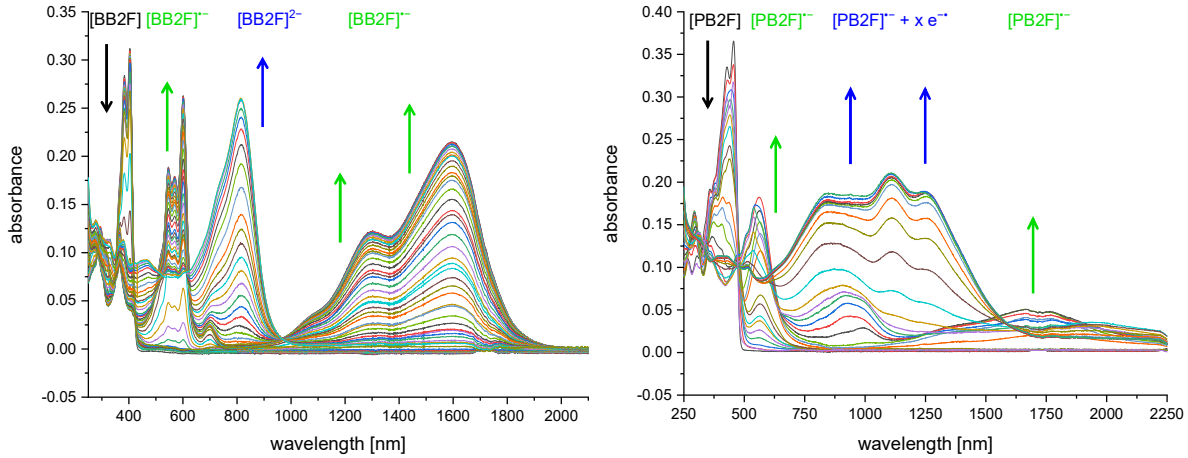

Figure 2.3.6: *UV/Vis/NIR absorption spectra recorded during the electrochemical reduction of* ***BB2F*** *(left, 0.0 to −3.0 V* vs. *Ag/AgCl in THF) and* ***PB2F*** *(right, 0.0 to −3.6 V* vs. *Ag/AgCl in THF).*

Full recovery of the initial spectrum was obtained by gradually returning back to 0.00 V, thus proving the full reversibility of the process.

This behavior is consistent with the observations made by Jäkle and co-workers for compound **B** (R = *t*Bu; see Figure 2.3.1)[20] and by Kaim and co-workers for related phenylene- and biphenylene-bridged bisboranes.[32] Also in these cases, the singly reduced species showed two absorption bands, one of which in the NIR range, and the doubly reduced species gave rise to an absorption band in the long-wavelength region of the visible spectrum. On the basis of computational studies, Kaim assigned the NIR band of the mono-anions to a SOMO → LUMO transition with intervalence charge transfer character, and the higher-energy band to a HOMO → SOMO excitation. The low-energy absorption for the dications was assigned to a HOMO → LUMO transition. In our case, the respective bands for both the singly and the doubly reduced species of **BB2F** are bathochromic shifted from those for the compounds investigated by Kaim and co-workers. They reported λ_{max} values for the mono-anions of 424 and 872 nm for [$Mes_2B-C_6H_4-BMes_2$]$^{\bullet-}$ and 522 and 1305 nm for [$Mes_2B-C_6H_4-C_6H_4-BMes_2$]$^{\bullet-}$. The corresponding dianions [$Mes_2B-C_6H_4-BMes_2$]$^{2-}$ and [$Mes_2B-C_6H_4-C_6H_4-BMes_2$]$^{2-}$ gave rise to absorption maxima at 665 and 736 nm, respectively. The spectral features for [**BB2F**]$^{\bullet-}$ and [**BB2F**]$^{2-}$ compare well with those for the reduced species of **B** reported by Jäkle and co-workers.[20] With respect to **[B]**$^{\bullet-}$ (λ_{max} = 640 and 1460 nm), the higher-energy band for the polaron [**BB2F**]$^{\bullet-}$ is slightly blue-shifted (by 1014 cm^{-1}), while its NIR band is red-shifted (by 560 cm^{-1}). For **[B]**$^{2-}$, the authors reported two

maxima, at λ_{max} = 760 and 840 nm, while the spectrum for [**BB2F**]$^{2-}$ displayed a band at λ_{max} = 816 nm. This is also close to that of a thiophene-bridged bisborole investigated by Braunschweig et al.,[33] which showed an absorption band at about λ_{max} = 800 nm.

Spectroelectrochemical investigations of **PB2F** revealed the emergence of two new bands, one at 564 nm and a broad NIR band at around 1667 nm, when the applied voltage was decreased to −1.0 V. By comparison with the observations made for the model compound **BB2F**, we assign these bands to a polaron. Upon further decreasing the potential to −2.0 V, these signals get replaced by a set of new, broad bands with maxima at 911, 1110, and 1245 nm. Also in this case the reduction processes are fully reversible when returning to 0.00 V.

We determined the HOMO and LUMO energy levels for the new bisboranes as well as for the polymers using the data from the electrochemical and the UV-vis absorption measurements (Figure 2.3.7). The values obtained compare well with those derived from our computations for the Mes-substituted model compounds. As the oligofuran chain is extended from **BB1F** to **BB5F**, the LUMO level stays rather constant, while the HOMO increases gradually in energy. This can be understood as an effect of successive addition of electron-rich furan rings. It results in continuously narrower band gaps down to E_g = 2.51 eV for **BB5F**. In comparison to the corresponding undoped α-oligofurans with the same number of conjugated furan rings,[12b] the energy levels for both frontier orbitals of **BB1F** – **BB5F** lie significantly lower (0.5 – 0.8 eV for the HOMO and 0.6 – 1.0 eV for the LUMO), and the overall electronic band gap is reduced by 0.12 – 0.14 eV.

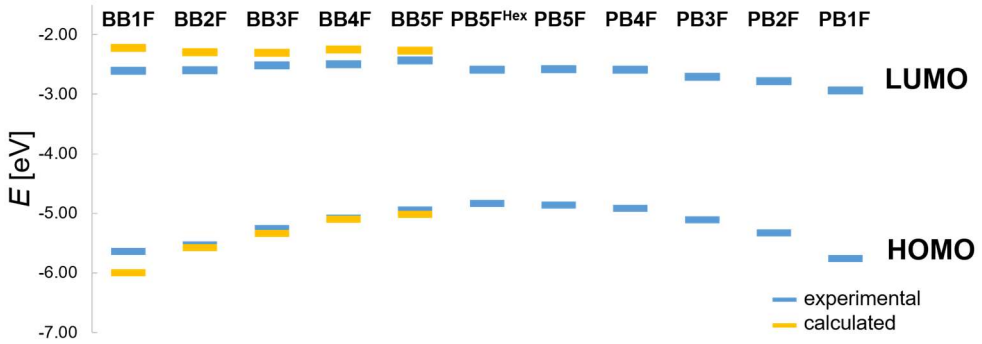

Figure 2.3.7: *Experimental and calculated HOMO and LUMO energies for the bisboranes and polymers. Calculated LUMO levels were determined as* $\varepsilon_{LUMO} = -(4.8 + E_{red})$ *eV and HOMO levels as* $\varepsilon_{HOMO} = \varepsilon_{LUMO} - E_g$. *The energy gap (*$E_g$*) was taken from UV-vis spectroscopy using the equation* $E_g = 1240/\lambda_{abs}$.

For the polymers a similar picture emerges: while the LUMO energy stays nearly constant, the HOMO energies increase progressively when the furan bridge is extended, which effectively narrows the band gap even further (down to E_g = 2.25 eV for **PB5F^{Hex}**).

2.3.3 Conclusion

We have presented a series of unprecedented poly(oligofuran boranes), which can be regarded as boron-doped polyfurans with varying doping density, as well as oligofuran-bridged bisboranes that serve as molecular model systems for the polymers. A comparison of the new compounds with conventional α-oligofurans[12b] sheds light on the effect of B-doping of such materials: it causes a decrease of the energy levels of both frontier orbitals and a reduction of the overall electronic band gap. This makes these materials oxidatively stable and processible under ambient conditions. The kinetically stabilizing bulky substituent at boron, furthermore, imparts pronounced robustness and ensures hydrolysis resistance. All oligomers and polymers prepared show considerable absorption and emission features in the visible range that arise from π–π* transitions involving the furan moieties and the boron centers. When going from the bisboranes to the corresponding polymers, these bands experience pronounced red-shifts, thus indicating effective π-conjugation along the main chain. The photophysical properties of both the molecular bisboranes and the polymers are effectively tuned via the length of the furan bridge between the boron centers. Elongation thereof leads to an increase of the HOMO energy while the LUMO level stays relatively constant. This results in progressive bathochromic shifts of the absorption and emission bands with increasing number of bridging furan units. Compared to their respective oligo- and poly(oligothiophene borane) congeners,[20] the positions of their maxima are very similar, however, they have significantly higher fluorescence quantum efficiencies. This is presumably a result of the lower probability for intersystem crossing (ISC) in the excited state of the furan- compared to the thiophene-based systems, which would be followed by non-radiative decay from low-lying triplet states, as has been hypothesized recently.[15u] The bisboranes with 2 – 5 furan rings bridging the boron centers show quantum yields between 89 and 97 %. These favorable emission properties are largely preserved upon polymerization. The highest quantum yield of about 87 % was found for **PB2F**. By cyclic voltammetry, two separate reduction events were observed for each boron center in the bisboranes, whose separation becomes narrower upon elongation of the bridging oligofuran moiety. Spectroelectrochemical investigations revealed a stepwise reduction of the bisborane **BB2F** to a radical anion (polaron) with absorption features in NIR region, which is then converted to a dianion (dipolaron) at higher reduction potentials. These processes proved to be fully reversible, once again demonstrating the high stability of these compounds. A similar behavior was observed for the respective polymer **PB2F**, indicating the resemblance of the electronic nature of the polymer and its model compound. Overall, the results presented herein demonstrate that the combination of furan moieties with trivalent boron allows to produce materials that benefit from the favorable optoelectronic properties of oligofuran species and pronounced stability as well as the special features of electron-deficient boranes. Our study clearly illustrates the great potential of furan-based organoboron materials for future

applications in organic optoelectronics, showing that they can certainly compete with their more-established thiophene congeners.

2.3.4 Experimental Section

General procedures. All manipulations were performed under an atmosphere of dry argon using standard Schlenk techniques or in an MBraun glove box. Solvents (toluene, dichloromethane, *n*-pentane, *n*-hexane, diethyl ether and tetrahydrofuran) were dried and degassed by means of an MBraun SPS-800 solvent purification system. Methanol was dried over magnesium turnings and freshly distilled prior to use. *o*-Xylene was dried over sodium and freshly distilled prior to use. Dimethylformamide was dried over molecular sieve (3 Å) and distilled prior to use.

Deuterated solvents for NMR spectroscopy were dried and degassed at reflux over CaH ($CDCl_3$) or Na (C_6D_6) and freshly distilled prior to use. Solvents for aqueous work up (*n*-hexane, dichloromethane, diethylether), and iodine were purchased from commercial sources and used as received. Solutions of *tert*-butyllithium (1.6 M and 1.7 M in *n*-pentane), *n*-butyllithium (2.5 M in *n*-hexane), trimethyltin chloride (1.0 M in THF), tributyltin chloride, triphenylarsine and tetrakis(triphenylphosphine)palladium(0) were purchased from Sigma Aldrich and used as received as well. *N,N,N′,N′*-Tetramethylethylenediamine (TMEDA) was purchased from Sigma Aldrich and distilled from sodium prior to use. **3**,[22a] **PB1F**,[22a] **BB1F**,[22b] **8**[24] were prepared according to procedures previously described by us. 2-Bromfuran,[34] 2,5-dibromofuran,[34] **S4**[35] and 2-(trimethylstannyl)furan[36] were prepared according to procedures described in the literature.

NMR spectra were recorded at 25 °C on a Bruker Avance III HD spectrometer operating at 300 MHz, on a Bruker Avance III Nanobay 400 operating at 400 MHz or on a Bruker Avance 500 spectrometer operating at 500 MHz. Chemical shifts were referenced to residual protic impurities in the solvent (^1H) or the deuterated solvent itself (^{13}C) and reported relative to external $SiMe_4$ (^1H, ^{13}C) or $BF_3{\cdot}OEt_2$ (^{11}B) standards.

Mass spectra were obtained with the use of a Thermo Scientific Exactive Plus Orbitrap MS system employing either atmospheric sample analysis probe (ASAP) or atmospheric pressure chemical ionization (APCI) and showed excellent congruence with the calculated isotopic distribution patterns.

MALDI-TOF measurements for polymers were performed on an UltrafleXtreme mass spectrometer (Bruker Daltonics, Bremen), equipped with a smartbeam II laser (355 nm). All MALDI-TOF spectra were acquired in the reflectron positive or negative mode. Calibration was performed externally with 1µl of a solution of Cesium triiodide. Trans-2[3-(4-tertbutylphenyl)-2-methyl-2-propenylidene]malononitrile (DCTB) was used as the matrix (10 mg/mL

dichloromethane). Samples were prepared in dichloromethane (1 mg/mL), mixed with the matrix in a 1:1 ratio, and then onto the stainless steel target (MTP 384 massive target; Bruker Daltonics #26755).

Elemental analyses were performed on an Elementar vario MICRO cube elemental analyzer.

Cyclic voltammetry experiments were performed using a Gamry Instruments Reference 600 potentiostat. A standard three-electrode cell configuration was employed using a platinum disk working electrode, a platinum wire counter electrode, and a silver wire, separated by a Vycor tip, serving as the reference electrode. Tetra-*n*-butylammonium hexafluorophosphate ([*n*-Bu_4N][PF_6]) was employed as the supporting electrolyte. Compensation for resistive losses (iR drop) was employed for all measurements. Cyclic voltammetry scans were conducted with a scan rate of 250 mV/s. The scans were referenced after the addition of a small amount of ferrocene as internal standard. The potentials are reported relative to the ferrocene/ferrocenium couple.

UV–vis spectra were obtained using a Jasco V-630 spectrophotometer. Emission spectra were recorded using an Edinburgh Instruments FLSP920 spectrometer equipped with a double monochromator for both excitation and emission, operating in right-angle geometry mode, and all spectra were fully corrected for the spectral response of the instrument. Fluorescence quantum yields were measured using a calibrated integrating sphere from Edinburgh Instruments combined with the FLSP920 spectrometer described above. Fluorescence lifetimes were determined on the same machine. Measurements were made in right-angle geometry mode, and the emission was collected through a polarizer set to the magic angle. All compounds were excited with pulsed diode lasers at wavelengths of either 376.6 nm (full-width-at-half-maximum (FWHM) of ca. 73 ps), 418.6 nm (FWHM of ca. 91 ps) or 472.6 nm (FWHM of ca. 91 ps), depending on the respective compounds absorption maxima. The instrument-response-function (IRF) were measured from the scatter of a colloidal SiO_2 solution at the respective excitation wavelengths, with a FWHM of ca. 1.0 ns. Decays were recorded to 10000 counts in the peak channel with a record length of at least 4800 channels. The band pass of the emission monochromator and a variable neutral density filter on the excitation side were adjusted to give a signal count rate of ca. 50 kHz.

Spectroelectrochemical experiments were carried out using an Agilent Cary 5000 spectrometer in combination with a designed sample compartment consisting of a cylindrical PTFE cell with an Infrasil® wedge window with an angle of 0.5°. An adjustable three-in-one electrode (6 mm platinum disc as working electrode, 1 mm platinum as counter electrode, and a pseudo reference electrode) was used. The potentials were adjusted with a Gamry 600 potentiostat. All experiments were measured at room temperature under an argon atmosphere.

TG measurements for thermal analyses were performed with a STA 449 F3 Perseus (Netzsch) in the temperature range of 50 to 600 °C with a heating rate of 10 K min^{-1}.

GPC chromatograms were recorded on an Agilent 1260 Infinity II Series, equipped with two PSS SDV 3 µm 1000Å (300x8 mm) columns and one PSS SDV 3 µm 10000Å (300x8 mm) column, at 25 °C with a flow rate of 1 mL min^{-1} and calibrated against polystyrene standards. The samples were diluted in THF and toluene as internal standard. Detection was carried out via UV signal ($\lambda = 254$ nm). Evaluation of the chromatograms was performed by using WinGPC software.

Syntheses

Synthesis of **4**. To a solution of **3** (585.9 mg, 1.50 mmol) in THF (15 mL) was added *tert*-butyllithium (1.7 M, 0.90 mL, 1.50 mmol) at −78 °C. Subsequently, the mixture was warmed to 0 °C and stirred at this temperature for further 1 h. Then, I_2 (474.6 mg, 1.88 mmol) was added to the solution at -78 °C. The reaction mixture was allowed to warm up to room temperature overnight. All volatiles were removed in vacuo, and the resulting solid was extracted with diethyl ether. The crude product was subjected to column chromatography (silica; *n*-hexane) to give **4** as a colorless solid. Yield: 170 mg (0.33 mmol, 22 %); ^{1}H NMR (500 MHz, $CDCl_3$): δ = 7.76 (d, *J* = 1.4 Hz, 1H, Fur-*H*), 7.46 – 7.30 (br, 1H, Fur-*H*), 7.42 (s, 2H, Mes*-*H*), 7.05 – 6.85 (br, 1H, Fur-*H*), 6.64 (d, *J* = 3.3 Hz, 1H, Fur-*H*), 6.54 (dd, *J* = 3.5 Hz, 1H, Fur-*H*), 1.38 (s, 9H, *p*-*t*BuC*H*$_3$), 1.16 (s, 18H, *o*-*t*BuC*H*$_3$); ^{11}B{^{1}H} NMR (160 MHz, $CDCl_3$): δ = 46.0 (s); ^{13}C{^{1}H} NMR (126 MHz, $CDCl_3$): δ = 171.2 (Fur-*C*-B), 163.5 (Fur-*C*-B), 152.4 (Mes*-*C*-*o*-*t*Bu), 148.7 (Fur-*C*H), 148.3 (Mes*-*C*-*p*-*t*Bu), 131.6 (Mes*-*C*-B), 130.7 (Fur-*C*H), 128.2 (Fur-*C*H), 122.2 (Fur-*C*H), 122.1 (Mes*-*C*H), 111.8 (Fur-*C*H), 97.2 (Fur-*C*-I), 38.4 (*p*-*t*Bu-*C*H$_3$), 34.9 (*p*-*t*Bu-*C*), 34.3 (*o*-*t*Bu-*C*H$_3$), 31.6 (*o*-*t*Bu-*C*); HRMS (ASAP): m/z $[M+H]^+$ calculated: 517.1769, found: 517.1762; elem. anal. calcd (%) for C26H34BIO2: C 60.49; H 6.64; found: C 60.48, H 6.73.

Synthesis of **5**. To a solution of **3** (390.4 mg, 1.00 mmol) in THF (10 mL) was added *tert*-butyllithium (1.6 M, 0.63 mL, 1.00 mmol) at −78 °C. Subsequently, the mixture was warmed to 0 °C and stirred at this temperature for further 1 h. Then, $ClSnMe_3$ (1.0 M, 1.1 mL, 1.10 mmol) was added to the solution at -78 °C. The reaction mixture was allowed to warm up to room temperature overnight. All volatiles were removed in vacuo, and the resulting solid was extracted with diethyl ether. The crude product was reprecipitated in MeOH to give **5** as a colorless solid. Yield: 193.7 mg (0.35 mmol, 35 %); ^{1}H NMR (500 MHz, $CDCl_3$): δ = 7.74 (dd, *J* = 1.6, 0.7 Hz, 1H, Fur-*H*), 7.42 (s, 2H, Mes*-*H*), 7.40 – 7.30 (br, 1H, Fur-*H*), 7.24 – 7.11 (br, 1H, Fur-*H*), 6.67 (d, *J* = 3.2 Hz, 1H, Fur-*H*), 6.53 (dd, *J* = 3.4, 1.6 Hz, 1H, Fur-*H*), 1.38 (s, 9H, *p*-*t*BuC*H*$_3$), 1.15 (s, 18H, *o*-*t*BuC*H*$_3$), 0.36 (s, 9H, Sn(C*H*$_3$)$_3$); ^{11}B{^{1}H} NMR (160 MHz, $CDCl_3$): δ = 46.5 (s); ^{119}Sn{^{1}H} NMR (187 MHz, $CDCl_3$): δ = -51.4 (s); ^{13}C{^{1}H} NMR (126 MHz, $CDCl_3$): δ = 168.9 (Fur-*C*-B), 168.5 (Fur-*C*-Sn), 164.5 (Fur-*C*-B), 152.2 (Mes*-*C*-*o*-*t*Bu), 148.3 (Mes*-

C-*p*-*t*Bu), 147.7 (Fur-*C*H), 133.2 (Mes*-*C*-B), 128.3 (Fur-*C*H), 127.2 (Fur-*C*H), 122.5 (Fur-*C*H), 121.9 (Mes*-*C*-H), 111.6 (Fur-*C*H), 38.3 (*p*-*t*Bu-*C*H_3), 34.9 (*p*-*t*Bu-*C*), 34.2 (*o*-*t*Bu-*C*H_3), 31.6 (*o*-*t*Bu-*C*), -8.9 (Sn*C*H_3); HRMS (APCI): m/z $[M+H]^+$ calculated: 555.2451, found: 555.2446; elem. anal. calcd (%) for C29H43BO2Sn: C, 62.97; H, 7.84; found: C 63.72, H 8.09.

Synthesis of **6a**. To a solution of furan (773.5 mg, 11.4 mmol) in OEt_2 (11 mL) was added *tert*-butyllithium (1.6 M, 15.6 mL, 25.0 mmol) at −78 °C. Subsequently, the mixture was stirred at that temperature for 1 h, followed by 2 h at room temperature. Then, $ClSnMe_3$ (1.0 M, 11.0 mL, 11.0 mmol) was added to the solution at -78 °C. The reaction mixture was allowed to warm up to room temperature overnight. All volatiles were removed in vacuo, and the resulting solid was extracted with diethylether. Distillation in high vacuum followed by filtration trough basic AlOx (*n*-hexane) to gave **6a** as a colorless oil. Yield: 3.42 g (8.7 mmol, 76 %); ^{1}H NMR (300 MHz, $CDCl_3$): δ = 6.63 (s, 2H, Fur-*H*), 0.33 (s, 18H, Sn(CH_3)$_3$); ^{119}Sn{^{1}H} NMR (112 MHz, $CDCl_3$): δ = -53.1 (s).

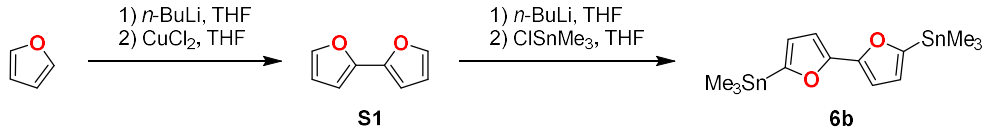

Scheme S2.3.1: *Stepwise synthesis of* ***6b****.*

Synthesis of **S1**. To a solution of furan (7.49 g, 110.0 mmol) and TMEDA (11.62 g, 100.0 mmol) in THF (130 mL) was added *n*-butyllithium (2.5 M, 40.0 mL, 100.0 mmol) at -78 °C. The mixture was stirred at that temperature for 1 h, then anhydrous $CuCl_2$ (18.75 g, 110.0 mmol) was added and the mixture was allowed to warm up to room temperature overnight. Water (50 mL) and diluted HCl (50 mL) were added and the mixture was extracted with *n*-pentane. The obtained crude product was purified by column chromatography (silica; *n*-hexane) to give **S1** as a colorless oil. Yield: 5.57 g (41.5 mmol, 83 %). ^{1}H NMR (300 MHz, $CDCl_3$): δ = 7.41 (dd, *J* = 1.8, 0.8 Hz, 2H, Fur-C*H*), 6.55 (dd, *J* = 3.3, 0.8 Hz, 2H, Fur-C*H*), 6.46 (dd, *J* = 3.4, 1.8 Hz, 2H, Fur-C*H*).

Synthesis of **6b**. To a solution of **S1** (670.7 mg, 5.00 mmol) in THF (50 mL) was added *n*-butyllithium (2.5M, 4.1 mL, 10.3 mmol) at -78 °C. Subsequently, the mixture was stirred at that temperature for 0.5 h, followed by 1 h at room temperature. Then, $ClSnMe_3$ (1.0 M, 10.5 mL, 10.5 mmol) was added to the solution at -78 °C and the reaction mixture was allowed to warm up to room temperature overnight. All volatiles were removed in vacuo and the remaining solid was dissolved in *n*-pentane. After filtration, the solvent was gradually removed in vacuo and **6b** was obtained as an off-white solid. Yield: 1.85 g (4.02 mmol, 80%). ^{1}H NMR (300 MHz,

C_6D_6): δ = 6.76 (d, *J* = 3.2 Hz, 2H, Fur-C*H*), 6.54 (d, *J* = 3.2 Hz, 2H, Fur-C*H*), 0.19 (s, 18H, Sn-CH_3); ^{119}Sn{^{1}H} NMR (MHz, C_6D_6): δ = -52.66 (s); ^{13}C{^{1}H} NMR (75 MHz, C_6D_6): δ = 160.4 (Fur-*C*-Sn), 152.5 (Fur-*C*), 123.3 (Fur- *C*H), 105.9 (Fur- *C*H), -9.3 (Sn- *C*H_3); HRMS (APCI) m/z [M+H]$^+$ calculated: 460.9731, found: 460.9732.

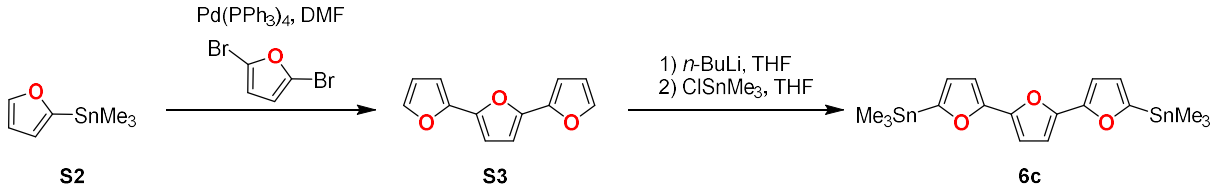

Scheme S2.3.2: *Stepwise synthesis of* ***6c****.*

Synthesis of **S3**. A solution of 2,5-dibromofuran (1.13 g, 5.00 mmol), 2-(trimethylstannyl)furan (2.51 g, 10.3 mmol) and $Pd(PPh_3)_4$ (288.9 mg, 0.25 mmol) in DMF (60 mL) was stirred at 105 °C for 15 h. Then, water was added (50 mL) and the mixture was extracted with *n*-pentane. The organic phase was washed with water and all volatiles were removed in vacuo. The obtained crude product was subjected to column chromatography (silica, *n*-hexane), giving **S3** as an off-white solid. Yield: 0.74 g (3.70 mmol, 74 %). ^{1}H NMR (300 MHz, $CDCl_3$): δ = 7.43 (dd, *J* = 1.8, 0.8 Hz, 2H, Fur-C*H*), 6.62 (dd, *J* = 3.4, 0.8 Hz, 2H, Fur-C*H*), 6.61 (s, 2H, Fur-C*H*), 6.48 (dd, *J* = 3.4, 1.8 Hz, 2H, Fur-C*H*).

Synthesis of **6c**. To a solution of **S3** (400.4 mg, 2.00 mmol) in THF (20 mL) was added *n*-butyllithium (2.5 M, 1.7 mL, 4.20 mmol) at -78 °C. Subsequently, the mixture was stirred for 0.5 h at that temperature, followed by 2 h at room temperature. Then, $ClSnMe_3$ (1.0 M, 4.40 mL, 4.40 mmol) was added at -78 °C and the reaction mixture was allowed to warm up to room temperature overnight. After all volatiles were removed in vacuo, the residue was dissolved in *n*-pentane, transferred to a separation funnel and was subsequently washed with methanol, water and methanol. All volatiles were removed in vacuo and **6c** was obtained as an orange oil. Yield: 937.2 mg (1.78 mmol, 89 %). ^{1}H NMR (300 MHz, C_6D_6): δ = 6.71 (d, *J* = 3.3 Hz, 2H, Fur-C*H*), 6.57 (s, 2H, Fur-C*H*), 6.51 (d, *J* = 3.3 Hz, 2H, Fur-C*H*), 0.20 (s, 18H, Sn-CH_3); ^{119}Sn{^{1}H} NMR (C_6D_6): δ = -52.24; ^{13}C{^{1}H} NMR (75 MHz, C_6D_6): δ =160.9 (Fur-*C*-Sn), 151.6 (Fur-*C*), 146.9 (Fur-*C*), 123.3 (Fur-*C*H), 107.5 (Fur-*C*H), 106.2 (Fur-*C*H), -9.3 (Sn-*C*H_3); HRMS (APCI) m/z [M+H]$^+$ calculated: 526.9836, found:526.9841.

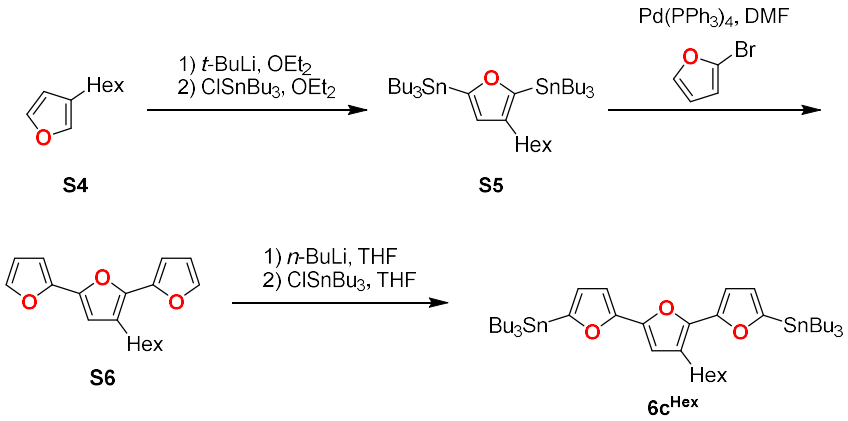

Scheme S2.2.3: *Stepwise synthesis of* ***6c^{Hex}***.

Synthesis of **S5**. To a solution of **S4** (304.4 g, 2.00 mmol) in OEt_2 (2.0 mL) was added *tert*-butyllithium (1.6 M, 2.63 mL, 4.20 mmol) at -78 °C. Subsequently, the mixture was stirred for 1 h at this temperature, followed by 2 h at room temperature. Then, $ClSnBu_3$ (1.43 g, 4.40 mmol) was added at -78 °C and the mixture was allowed to warm up to room temperature overnight. After all volatiles were removed in vacuo, the residue was dissolved in *n*-pentane, transferred to a separation funnel and was subsequently washed with methanol, water and methanol. All volatiles were again removed in vacuo and **S5** was obtained as an orange oil, which was then used without further purification. Yield: 1.21 g (1.66 mmol, 83 %). A fraction was purified by column chromatography (silica, *n*-hexane) for further characterization. ^{1}H NMR (300 MHz, C_6D_6): δ = 6.45 (s, 1H, Fur-C*H*), 2.40 (J = 7.8 Hz, 2H, hexyl-CH_2), 1.63 – 1.46 (m, 14H, hexyl/butyl-CH_2), 1.32 – 1.20 (m, 18H, hexyl/butyl-CH_2), 1.05 – 0.95 (m, 12H, butyl-CH_2), 0.88 (t, J = 7.3 Hz, 21H, hexyl/butyl-CH_3); ^{119}Sn{^{1}H} NMR (112 MHz, $CDCl_3$): δ = -65.41 (s), -65.72 (s); ^{13}C{^{1}H} NMR (75 MHz, $CDCl_3$): δ = 165.5 (Fur-*C*-Sn), 161.0 (Fur-*C*-Sn), 136.5 (Fur-*C*-CH_2), 122.2 (Fur-*C*H), 32.0 (hexyl-*C*H_2), 31.9 (hexyl-*C*H_2), 29.5 (butyl-*C*H_2), 29.5 (butyl-*C*H_2), 29.2 (hexyl-*C*H_3), 27.4(butyl-*C*H_2), 27.4 (butyl-*C*H_2), 26.3 (hexyl-*C*H_2), 22.8 (hexyl-*C*H_2), 14.3 (hexyl-*C*H_2), 13.9 (butyl-*C*H_2), 13.8 (butyl-*C*H_2), 10.3 (butyl-*C*H_3), 10.2 (butyl-*C*H_3); HRMS (APCI) m/z $[M+H]^+$ calculated: 731.3381, found: 731.3375.

Synthesis of **S6**. A solution of **S5** (2.26 g, 3.10 mmol), 2-bromofuran (1.14 g, 7.75 mmol) and $Pd(PPh_3)_4$ (173.3 mg, 0.15 mmol) in DMF (35 mL) was stirred at 105 °C for 15 h. Then, water was added (20 mL) and the mixture was extracted with *n*-pentane. The organic phase was washed with water and all volatiles were removed in vacuo. The obtained crude product was subjected to column chromatography (silica, *n*-hexane), giving **S6** as yellow oil. Yield: 436.4 mg (1.53 mmol, 50 %). ^{1}H NMR (300 MHz, C_6D_6): δ = 7.08 (dd, J = 1.8, 0.8 Hz, 1H, Fur-C*H*), 7.04 (dd, J = 1.8, 0.8 Hz, 1H, Fur- C*H*), 6.56 – 6.50 (m, 3H, Fur- C*H*), 6.13 (dd, J = 3.4, 1.8 Hz, 1H, Fur- C*H*), 6.09 (dd, J = 3.4, 1.8 Hz, 1H, Fur- C*H*), 2.66 (t, J = 7.7 Hz, 2H, hexyl-CH_2), 1.59 – 1.47 (m, 2H, hexyl-CH_2), 1.33 – 1.19 (m, 6H, hexyl-CH_2), 0.89 – 0.83 (m, 3H,

hexyl-C*H*$_3$); ^{13}C{^{1}H} NMR (75 MHz, C_6D_6): δ = 147.6 (Fur-*C*), 147.1 (Fur-*C*), 145.6 (Fur-*C*), 142.1 (Fur-*C*H), 141.8 (Fur-*C*H), 141.7 (Fur-*C*), 124.2 (Fur-*C*-CH$_2$), 111.8 (Fur-*C*H), 111.5 (Fur-*C*H), 109.2 (Fur-*C*H), 106.2 (Fur-*C*H), 105.7 (Fur-*C*H), 32.0 (hexyl-*C*H$_2$), 30.3 (hexyl-*C*H$_2$), 29.4 (hexyl-*C*H$_2$), 25.4 (hexyl-*C*H$_2$), 23.0 (hexyl-*C*H$_2$), 14.3 (hexyl-*C*H$_3$); HRMS (APCI) m/z [M+H]$^+$ calculated: 285.1485, found: 285.1483 [M+H]$^+$.

Synthesis of **6c^{Hex}**. To a solution of **S6** (436.2 mg, 1.53 mmol) in THF (15 mL) was added *n*-butyllithium (2.5 M, 1.3 mL, 3.21 mmol) at -78 °C. Subsequently, the mixture was stirred for 0.5 h at this temperature, followed by 2 h at room temperature. Then, ClSnBu$_3$ (1.10 g, 3.37 mmol) was added at -78 °C and the reaction mixture was allowed to warm up to room temperature overnight. After all volatiles were removed in vacuo, the residue was dissolved in *n*-pentane, transferred to a separation funnel and was subsequently washed with methanol, water and methanol. All volatiles were again removed in vacuo and the obtained crude product was subjected to column chromatography (silica, *n*-hexane), to give **6c^{Hex}** as an orange liquid. Yield: 523.3 mg (0.61 mmol, 40 %). ^{1}H NMR (300 MHz, C_6D_6): δ = 6.79 (d, *J* = 3.2 Hz, 1H, Fur-C*H*), 6.77 (d, *J* = 3.2 Hz, 1H, Fur- C*H*), 6.69 (s, 1H, Fur- C*H*), 6.65 (d, *J* = 3.2 Hz, 1H, Fur- C*H*), 6.63 (d, *J* = 3.2 Hz, 1H, Fur- C*H*), 2.82 (t, *J* = 7.6 Hz, 2H, hexyl-C*H*$_2$), 1.80 – 1.48 (m, 14H, hexyl/butyl-C*H*$_2$), 1.47 – 1.30 (m, 14H, hexyl/butyl-C*H*$_2$), 1.30 – 1.23 (m, 4H, hexyl-C*H*$_2$), 1.23 – 0.98 (m, 12H, butyl-C*H*$_2$), 0.92 (m, 21H, hexyl/butyl-C*H*$_3$); ^{119}Sn{^{1}H} NMR (112 MHz, C_6D_6): δ= -61.63; ^{13}C{^{1}H} NMR (75 MHz, C_6D_6): δ = 160.9 (Fur-*C*-Sn), 160.2 (Fur-*C*-Sn), 152.6 (Fur-*C*), 151.9 (Fur-*C*), 146.2 (Fur-*C*), 142.3 (Fur-*C*), 123.9 (Fur-*C*H), 123.9 (Fur-*C*-CH$_2$), 123.7 (Fur-*C*H), 109.2 (Fur-*C*H), 106.3 (Fur-*C*H), 105.9 (Fur-*C*H), 32.2 (hexyl-*C*H$_2$), 30.6 (hexyl-*C*H$_2$), 29.6 (hexyl-*C*H$_2$), 29.5 (butyl-*C*H$_2$), 29.4 (butyl-*C*H$_2$), 27.6 (butyl-*C*H$_2$), 27.6 (butyl-*C*H$_2$), 25.7 (hexyl-*C*H$_2$), 23.1 (hexyl-*C*H$_2$), 14.4 (hexyl-*C*H$_3$), 13.9 (butyl-*C*H$_3$), 10.5 (butyl-*C*H$_2$), 10.5 (butyl-*C*H$_2$); HRMS (APCI) m/z [M+H]$^+$ calculated: 863.3592, found: 863.3591.

Synthesis of **9**. To a solution of **3** (585.9 mg, 1.50 mmol) in THF (15 mL) was added *tert*-butyllithium (1.7 M, 1.81 mL, 3.08 mmol) at −78 °C. Subsequently, the mixture was warmed to 0 °C and stirred at for further 1 h. Then, ClSnMe$_3$ (1.0M, 3.1 mL, 3.08 mmol) was added to the solution at -78 °C. The reaction mixture was allowed to warm up to room temperature overnight. All volatiles were removed in vacuo and and the resulting solid was extracted with diethyl ether. The crude product was reprecipitated in methanol and *n*-pentane to give **9** as an off-white solid. Yield: 666 mg (0.93 mmol, 62 %); ^{1}H NMR (500 MHz, $CDCl_3$): δ = 7.42 (s, 2H, Mes*-*H*), 7.32 – 7.15 (br, 2H, Fur-*H*), 6.70 (d, *J* = 3.2 Hz, 2H, Fur-*H*), 1.41 (s, 9H, *p*-*t*BuC*H*$_3$), 1.16 (s, 18H, *o*-*t*BuC*H*$_3$), 0.35 (s, 18H, SnC*H*$_3$); ^{11}B{^{1}H} NMR (160 MHz, $CDCl_3$): δ = 47.8 (s); ^{119}Sn{^{1}H} NMR (187 MHz, $CDCl_3$): δ = -52.0 (s); ^{13}C{^{1}H} NMR (126 MHz, $CDCl_3$): δ = 169.3 (Fur-*C*-B), 168.0 (Fur-*C*-Sn), 152.2 (Mes*-*C*-*o*-*t*Bu), 148.0 (Mes*-*C*-*p*-*t*Bu), 134.0 (Mes*-*C*-B),

127.5 (Fur-*C*H), 122.5 (Fur-*C*H), 121.4 (Mes*-*C*-H), 38.3 (*p*-*t*Bu-*C*H_3), 34.9 (*p*-*t*Bu-*C*), 34.1 (*o*-*t*Bu-*C*H_3), 31.7 (*o*-*t*Bu-*C*), -8.9 (Sn*C*H_3); HRMS (ASAP): m/z $[M+H]^+$ calculated: 717.2093, found: 717.2089; elem. anal. calcd (%) for C32H51BO2Sn2: C 53.68, H 7.18; found: C 54.08, H 7.14.

Synthesis of **BB2F**. **4** (154.9 mg, 0.30 mmol), **5** (166.0 mg, 0.30 mmol), $Pd(PPh_3)_4$ (34.7 mg, 0.03 mmol), and $AsPh_3$ (9.2 mg, 0.03 mmol) were added in a reaction tube, followed by *o*-xylene (1.6 mL). Then, the tube was heated in a microwave reactor for 80 min (100 °C). The mixture was allowed to cool down to room temperature, diluted with THF and then filtered through silica gel to remove insoluble compounds and the catalyst. All volatiles were removed in vacuo and the crude product was subjected to column chromatography (AlOx; *n*-hexane:DCM 100:5) to give **BB2F** as a yellow solid. Yield: 155 mg (2.0 mmol, 66 %); ^{1}H NMR (500 MHz, $CDCl_3$): δ = 7.78 (d, *J* = 1.1 Hz, 2H, Fur-*H*), 7.58 (s, 2H, Fur-*H*), 7.44 (s, 4H, Mes*-*H*), 7.08 (s, 2H, Fur-*H*), 6.85 (d, *J* = 3.1 Hz, 2H, Fur-*H*), 6.57 (dd, *J* = 1.8 Hz, 2H, Fur-*H*), 1.39 (s, 18H, *p*-*t*BuC*H*$_3$), 1.20 (s, 36H, *o*-*t*BuC*H*$_3$); ^{11}B{^{1}H} NMR (96 MHz, $CDCl_3$): δ = 48.9 (s); ^{13}C{^{1}H} NMR (126 MHz, CDCl3): δ = 165.1 (Fur-*C*-B), 163.9 (Fur-*C*-B), 152.4 (Mes*-*C*-*o*-*t*Bu), 151.3 (Fur-*C*-C), 148.7 (Mes*-*C*-*p*-*t*Bu), 148.1 (Fur-*C*H), 132.2 (Mes*-*C*-B), 130.7 (Fur-*C*H), 127.7 (Fur-*C*H), 122.1 (Mes*-*C*H), 111.8 (Fur-*C*H), 109.2 (Fur-*C*H), 38.5 (*p*-*t*Bu-*C*H_3), 34.9 (*p*-*t*Bu-*C*), 34.4 (*o*-*t*Bu-*C*H_3), 31.6 (*o*-*t*Bu-*C*); HRMS (APCI): m/z $[M+H]^+$ calculated: 779.5376, found: 779.5370; UV–vis (THF): $\lambda_{abs,max}$ = 403 (ε = 42959 L mol^{-1} cm^{-1}), 382 (ε = 39818 L mol^{-1} cm^{-1}), 294 (ε = 22465 L mol^{-1} cm^{-1}) nm; fluorescence (THF): $\lambda_{em,max}$ (λ_{ex} = 382 nm) = 421 nm (Φ_f = 97 %).

Synthesis of **BB3F**. **4** (267.7 mg, 0.52 mmol), **6a** (96.2 mg, 0.24 mmol), $Pd(PPh_3)_4$ (60.1 mg, 0.05 mmol), and $AsPh_3$ (15.3 mg, 0.05 mmol) were added in a reaction tube, followed by *o*-xylene (1.8 mL). Then, the tube was heated in a microwave reactor for 80 min (100 °C). The mixture was allowed to cool down to room temperature, diluted with THF and then filtered through silica gel to remove insoluble compounds and the catalyst. All volatiles were removed in vacuo and the crude product was subjected to column chromatography (silica; *n*-hexane:DCM 100:10) to give **BB3F** as a yellow solid. Yield: 84 mg (0.10 mmol, 41 %); ^{1}H NMR (500 MHz, $CDCl_3$): δ = 7.78 (dd, *J* = 1.6, 0.6 Hz, 2H, Fur-*H*), 7.61 – 7.44 (s, 2H, Fur-*H*), 7.44 (s, 4H, Mes*-*H*), 7.19 – 7.03 (br, 2H, Fur-*H*), 6.86 (s, 2H, Fur-*H*), 6.75 (d, *J* = 3.5 Hz, 2H, Fur-*H*), 6.57 (dd, *J* = 3.4, 1.6 Hz, 2H, Fur-*H*), 1.39 (s, 18H, *p*-*t*BuC*H*$_3$), 1.19 (s, 36H, *o*-*t*BuC*H*$_3$); ^{11}B{^{1}H} NMR (96 MHz, $CDCl_3$): δ = 49.1 (s); ^{13}C{^{1}H} NMR (126 MHz, $CDCl_3$): δ = 164.6 (Fur-*C*-B), 164.0 (Fur-*C*-B), 152.4 (Mes*-*C*-*o*-*t*Bu), 150.9 (Fur-*C*-C), 148.6 (Mes*-*C*-*p*-*t*Bu), 148.0 (Fur-*C*H), 146.7 (Fur-*C*-C), 132.4 (Mes*-*C*-B), 130.7 (Fur-*C*H), 127.6 (Fur-*C*H), 122.1 (Mes*-

*C*H), 111.8 (Fur-*C*H), 109.5 (Fur-*C*H), 108.0 (Fur-*C*H), 38.5 (*p*-*t*Bu-*C*H_3), 34.9 (*p*-*t*Bu-*C*), 34.4 (*o*-*t*Bu-*C*H_3), 31.6 (*o*-*t*Bu-*C*); HRMS (APCI): m/z $[M+H]^+$ calculated: 845.5482, found: 845.5466; UV–vis (THF): $\lambda_{abs,max}$ = 432 (ε = 116930 L mol^{-1} cm^{-1}), 408 (ε = 125116 L mol^{-1} cm^{-1}), 294 (ε = 57711 L mol^{-1} cm^{-1}) nm; fluorescence (THF): $\lambda_{em,max}$ (λ_{ex} = 408 nm) = 455 nm (Φ_f = 94 %).

Synthesis of **BB4F**. **4** (258.1 mg, 0.50 mmol), **6b** (108.0 mg, 0.24 mmol), $Pd(PPh_3)_4$ (57.8 mg, 0.05 mmol), and $AsPh_3$ (15.3 mg, 0.05 mmol) were added in a reaction tube, followed by *o*-xylene (2.0 mL). Then, the tube was heated in a microwave reactor for 40 min (200 °C). The mixture was allowed to cool down to room temperature, diluted with THF and then filtered through silica gel to remove insoluble compounds and the catalyst. All volatiles were removed in vacuo and the crude product was subjected to column chromatography (silica; *n*-hexane:DCM 100:10) to give **BB4F** as a yellow solid. Yield: 160 mg (0.17 mmol, 73 %); ^{1}H NMR (500 MHz, $CDCl_3$): *δ* = 7.78 (s, 2H, Fur-*H*), 7.65 – 7.39 (br, 2H, Fur-*H*), 7.44 (s, 4H, Mes*-*H*), 7.23 – 7.01 (br, 2H, Fur-*H*), 6.85 (d, *J* = 3.5 Hz, 2H, Fur-*H*), 6.77 (d, *J* = 3.6 Hz, 2H, Fur-*H*), 6.75 (d, *J* = 3.5 Hz, 2H, Fur-*H*), 6.57 (dd, *J* = 3.4, 1.7 Hz, 2H, Fur-*H*), 1.39 (s, 18H, *p*-*t*BuCH_3), 1.20 (s, 36H, *o*-*t*BuCH_3); ^{11}B{^{1}H} NMR (96 MHz, $CDCl_3$): 47.7 (s); ^{13}C{^{1}H} NMR (126 MHz, $CDCl_3$): *δ* = 164.5 (Fur-*C*-B), 164.0 (Fur-*C*-B), 152.4 (Mes*-*C*-*o*-*t*Bu), 151.0 (Fur-*C*-C), 148.6 (Mes*-*C*-*p*-*t*Bu), 148.0 (Fur-*C*H), 146.3 (Fur-*C*-C), 146.3 (Fur-*C*-C), 132.4 (Mes*-*C*-B), 130.7 (Fur-*C*H), 127.5 (Fur-*C*H), 122.1 (Mes*-*C*H), 111.8 (Fur-*C*H), 109.5 (Fur-*C*H), 108.1 (Fur-*C*H), 107.8 (Fur-*C*H), 38.5 (*p*-*t*Bu-*C*H_3), 34.9 (*p*-*t*Bu-*C*), 34.4 (*o*-*t*Bu-*C*H_3), 31.6 (*o*-*t*Bu-*C*); HRMS (APCI): m/z $[M+H]^+$ calculated: 911.5588, found: 911.5573; UV–vis (THF): $\lambda_{abs,max}$ = 448 (ε = 46837 L mol^{-1} cm^{-1}), 424 (ε = 52683 L mol^{-1} cm^{-1}), 301 (ε = 18787 L mol^{-1} cm^{-1}) nm; fluorescence (THF): $\lambda_{em,max}$ (λ_{ex} = 424 nm) = 478 nm (Φ_f = 93 %).

Synthesis of **BB5F**. **4** (258.1 mg, 0.50 mmol), **6c** (123.6 mg, 0.24 mmol), $Pd(PPh_3)_4$ (57.8 mg, 0.05 mmol), and $AsPh_3$ (15.3 mg, 0.05 mmol) were added in a reaction tube, followed by *o*-xylene (2.0 mL). Then the tube was heated in a microwave reactor for 40 min (200 °C). The mixture was allowed to cool down to room temperature, diluted with THF and then filtered through silica gel to remove insoluble compounds and the catalyst. All volatiles were removed in vacuo and the crude product was subjected to column chromatography (silica; *n*-hexane:DCM 100:10) to give **BB5F** as a yellow solid. Yield: 174 mg (1.8 mmol, 75 %); ^{1}H NMR (500 MHz, $CDCl_3$): *δ* = 7.79 (d, *J* = 1.6 Hz, 2H, Fur-*H*), 7.63 – 7.43 (br, 2H, Fur-*H*), 7.46 (s, 4H, Mes*-*H*), 7.21 – 7.07 (br, 2H, Fur-*H*), 6.87 (d, *J* = 3.5 Hz, 2H, Fur-*H*), 6.82 – 6.72 (m, 6H, Fur-*H*), 6.62 – 6.56 (m, 2H, Fur-*H*), 1.41 (s, 18H, *p*-*t*BuCH_3), 1.22 (s, 36H, *o*-*t*BuCH_3); ^{11}B{^{1}H} NMR (96 MHz, $CDCl_3$): 47.2 (s); ^{13}C{^{1}H} NMR (126 MHz, $CDCl_3$): *δ* = 164.5 (Fur-*C*-B), 164.0 (Fur-

C-B), 152.4 (Mes*-*C*-*o*-*t*Bu), 151.0 (Fur-*C*-C), 148.6 (Mes*-*C*-*p*-*t*Bu), 148.0 (Fur-*C*H), 146.3 (Fur-*C*-C), 146.2 (Fur-*C*-C), 145.8 (Fur-*C*-C), 132.4 (Mes*-*C*-B), 130.7 (Fur-*C*H), 127.5 (Fur-*C*H), 122.1 (Mes*-*C*H), 111.8 (Fur-*C*H), 109.5 (Fur-*C*H), 108.1 (Fur-*C*H), 108.0 (Fur-*C*H), 107.7 (Fur-*C*H), 38.5 (*p*-*t*Bu-*C*H_3), 34.9 (*p*-*t*Bu-*C*), 34.4 (*o*-*t*Bu-*C*H_3), 31.6 (*o*-*t*Bu-*C*); HRMS (APCI): m/z $[M+H]^+$ calculated: 977.5693, found:977.5682; UV–vis (THF): $\lambda_{abs,max}$ = 457 (ε = 60501 L mol^{-1} cm^{-1}), 433 (ε = 73633 L mol^{-1} cm^{-1}), 291 (ε = 28380L mol^{-1} cm^{-1}) nm; fluorescence (THF): $\lambda_{em,max}$ (λ_{ex} = 433 nm) = 514 nm (Φ_f = 89 %).

General Procedure for Polymerization. In a glovebox, 0.30 mmol of both, the bis(trimethylstannane) and diiodo monomers, were placed in a 2 mL microwave tube. $Pd(PPh_3)_4$ (10%), $AsPh_3$ (10%), and *o*-xylene (2mL) were added. Then, the tube was heated in a microwave for 40 min (200 °C). The mixture was allowed to cool down to room temperature, diluted with 20 mL of THF and filtered through a glas filter to remove insoluble compounds and the catalyst. The polymer was precipitated in cold methanol (80mL).

PB2F: Yellow solid. Yield: 90 mg (0.21 mmol, 35 %); ^{1}H NMR (300 MHz, $CDCl_3$): δ = 7.57 – 7.20 (br, 2H, Fur-*H*), 7.42 (s, 2H, Mes*-*H*), 6.91 – 6.76 (br, 2H, Fur-*H*), 1.39 (s, 9H, *p*-*t*BuCH_3), 1.20 (s, 18H, *o*-*t*BuCH_3); ^{11}B{^{1}H} NMR (96 MHz, $CDCl_3$): no signal detectable; GPC: M_n = 3832, M_w = 4521, Đ = 1.17; UV–vis (THF): $\lambda_{abs,max}$ = 425, 453 nm; fluorescence (THF): $\lambda_{em,max}$ (λ_{ex} = 425 nm) = 505 nm (Φ_f = 87 %).

PB3F: Orange Solid. Yield: 57 mg (0.12 mmol, 20 %); ^{1}H NMR (300 MHz, $CDCl_3$): δ = 7.55 – 7.30 (br, 2H, Fur-*H*), 7.43 (s, 2H, Mes*-*H*), 6.90 – 6.64 (br, 4H, Fur-*H*), 1.40 (s, 9H, *p*-*t*BuCH_3), 1.22 (s, 18H, *o*-*t*BuCH_3); ^{11}B{^{1}H} NMR (96 MHz, $CDCl_3$): no signal detectable; GPC: M_n = 5205, M_w = 6764, Đ = 1.30; UV–vis (THF): $\lambda_{abs,max}$ = 444, 472 nm; fluorescence (THF): $\lambda_{em,max}$ (λ_{ex} = 444 nm) = 530 nm (Φ_f = 59 %).

PB4F: Dark orange solid. Yield: 48 mg (0.11 mmol, 18%); ^{1}H NMR (300 MHz, $CDCl_3$): δ = 7.59 – 7.35 (br, 2H, Fur-*H*), 7.44 (s, 2H, Mes*-*H*), 6.94 – 6.68 (br, 6H, Fur-*H*), 1.40 (s, 9H, *p*-*t*BuCH_3), 1.23 (s, 18H, *o*-*t*BuCH_3); ^{11}B{^{1}H} NMR (96 MHz, $CDCl_3$): no signal detectable; GPC: M_n = 6982, M_w = 11482, Đ = 1.64; UV–vis (THF): $\lambda_{abs,max}$ = 450, 479 nm; fluorescence (THF): $\lambda_{em,max}$ (λ_{ex} = 450 nm) = 540 nm (Φ_f = 32 %).

PB5F: Dark red solid. Yield: 96 mg (0.16 mmol, 27 %); ^{1}H NMR (300 MHz, $CDCl_3$): δ = 7.52 – 7.32 (br, 2H, Fur-*H*), 7.44 (s, 2H, Mes*-*H*), 6.93 – 6.62 (br, 8H, Fur-*H*), 1.40 (s, 9H, *p*-*t*BuCH_3),

1.23 (s, 18H, *o*-*t*BuC*H*$_3$); ^{11}B{^{1}H} NMR (96 MHz, $CDCl_3$): no signal detectable; GPC: M_n = 5385, M_w = 8115, Đ = 1.51; UV–vis (THF): $\lambda_{abs,max}$ = 482, 452 nm; fluorescence (THF): $\lambda_{em,max}$ (λ_{ex} = 452 nm) = 516 nm (Φ_f = 42 %).

PB5F^{Hex}: Orange solid. Yield: 76 mg (0.11 mmol, 19 %); ^{1}H NMR (400 MHz, $CDCl_3$): δ = 7.55 – 7.35 (br, 2H, Fur-*H*), 7.44 (s, 2H, Mes*-*H*), 6.91 – 6.60 (br, 7H, Fur-*H*), 2.86 – 2.76 (br, 2H, hexyl-*H*), 1.77 – 1.51 (m, 4H, hexyl-*H*), 1.41 (s, 9H, *p*-*t*BuC*H*$_3$), 1.23 (s, 18H, *o*-*t*BuC*H*$_3$), 0.96 – 0.81 (m, 6H, hexyl-*H*); ^{11}B{^{1}H} NMR (128 MHz, $CDCl_3$): no signal detectable; GPC: M_n = 5214, M_w = 8221, Đ = 1.58; UV–vis (THF): $\lambda_{abs,max}$ = 458, 486 nm; fluorescence (THF): $\lambda_{em,max}$ (λ_{ex} = 458 nm) = 525 nm (Φ_f = 40 %).

Crystallographic methods. Crystals suitable for single-crystal X-Ray diffraction were selected, coated in perfluoropolyether oil, and mounted on MiTeGen sample holders. Diffraction data were collected on Bruker X8 Apex II 4-circle diffractometers with CCD area detectors using M*o*-Kα radiation (**5**) or on XtaLAB Synergy, Dualflex, HyPix diffractometer equipped using CuKa radiation (micr*o*-focus sealed X-Ray tube, l = 1.54184 Å). The crystals were cooled using an Oxford Cryostreams low-temperature device. Data were collected at 100 K. The images were processed and corrected for Lorentz-polarization effects and absorption as implemented in the Bruker software packages (**5**) or as implemented in CrysAlisPro (Version 40_64.45a). The structures were solved using the intrinsic phasing method (SHELXT)[37] and Fourier expansion technique. All non-hydrogen atoms were refined in anisotropic approximation, with hydrogen atoms 'riding' in idealized positions, by full-matrix least squares against F2 of all data, using SHELXL[38] software and the SHELXLE graphical user interface.[39] Other structural information was extracted using OLEX2 software.[40] The structure of **BB1F** has been reported by us before,[22b] herewith we present a crystal of an improved dataset.

Table S2.3.1. *X-Ray crystallographic information.*

compound	**5**	**BB1F**	**BB2F**	**BB3F**	**BB4F**	**BB5F**
CCDC number	2063515	2064304	2064305	2064306	2079146	2079147
Size / mm	0.53 x 0.31 x 0.24	0.13 x 0.10 x 0.02	0.10 x 0.07 x 0.04	0.22 x 0.11 x 0.03	0.21 x 0.08 x 0.03	0.18 x 0.15 x 0.05
Empiric Formula	$C_{29}H_{43}BO_2Sn$	$C_{48}H_{66}B_2O_3$, C_6H_{14}	$C_{52}H_{68}B_2O_4$	$C_{56}H_{70}B_2O_5$	$C_{60}H_{72}B_2O_6$, $2(CH_2Cl_2)$	$C_{64}H_{74}B_2O_7$
M / g mol^{-1}	553.13	798.80	778.68	844.74	1080.64	976.85
Crystal system	monoclinic	triclinic	monoclinic	triclinic	triclinic	monoclinic
Space group	P 1 21/n 1	P -1	P 21/c	P -1	P -1	P 21/c
a / Å	13.342(2)	9.5877(2)	9.3592(2)	8.8186(2)	8.97010(10)	9.22400(10)
b / Å	9.4334(14)	15.4653(4)	22.9478(5)	16.4525(3)	9.12320(10)	33.4634(3)
c / Å	22.992(3)	17.7539(3)	10.8292(3)	17.5838(3)	20.1945(3)	40.2439(3)
α / deg	90	85.701(2)	90	88.200(2)	94.5630(10)	90
β / deg	91.715(8)	75.555(2)	99.593(2)	80.644(2)	99.6230(10)	95.1600(10)
γ / deg	90	75.461(2)	90	81.078(2)	108.139(2)	90
V / Å^3	2892.6(8)	2467.42(10)	2293.30(10)	2486.75(9)	1533.06(4)	12371.6(2)
Z	4	2	2	2	1	8
μ / mm^{-1}	0.905	0.478	0.525	0.538	2.119	0.518
T / K	100	100	100	100	100	100
$\theta_{min,max}$	1.742, 27.091	2.570, 72.122	3.853, 68.244	2.547, 72.125	2.241, 72.124	2.205, 70.075
Completeness	98.2	99.3	99.7	99.5	100	99.6
Reflections: total / independent	6254, 4974	9639, 7736	4651, 3940	9748, 8036	6020, 5241	23406, 18875
R_{int}	0.0901	0.0411	0.0431	-	0.0532	0.0432
Final R1 and wR2	0.0613, 0.1796	0.0509, 0.1361	0.0492, 0.1339	0.0796, 0.2376	0.0604, 0.2322	0.0474, 0.1261
Largest peak and hole / e Å^{-3}	1.044, -2.187	0.327, -0.294	0.453, -0.199	0.766, -0.375	0.587, -0.768	0.585, -0.259
ρ_{calc} / g cm^{-3}	1.270	1.075	1.128	1.128	1.171	1.049

Computational methods. DFT calculations were carried out with the TURBOMOLE V7.3 program package.[41] Optimizations were performed with Becke's three parameter exchange-correlation hybrid functional B3LYP[42] in combination with the valence-double-ζ basis set def2-SV(P).[43] The empirical dispersion correction DFT-D3 by Grimme was used including the three-body term and with Becke-Johnson (BJ) damping.[44] The stationary points were characterized as minima by analytical vibrational frequency calculations.[45] Vertical singlet excitations were calculated by means of time-dependent DFT[46] using the same density functional–basis set combination as specified above.

Table S2.3.2. *Results from TD-DFT calculations (π–π* excitation marked in bold).*

compound	No.	λ / nm	Oscillator strength *f*	Orbital contributions	$\|c\|^2$ / %
BB1F^{Mes}	**5**	**356.1**	**0.4620**	**HOM*O*-1 → LUMO**	**54.5**
				HOM*O*-3 → LUMO	**25.8**
				HOM*O*-4 → LUMO	**14.8**
	6	**303.1**	**0.1462**	**HOM*O*-5 → LUMO**	**88.9**
				HOM*O*-1 → LUMO+1	**8.0**
	11	**273.0**	**0.1631**	**HOM*O*-1 → LUMO+1**	**48.1**
				HOM*O*-3 → LUMO+1	**16.8**
				HOM*O*-8 → LUMO	**11.8**
				HOM*O*-4 → LUMO	**7.6**
				HOM*O*-5 → LUMO	**7.5**
BB2F^{Mes}	**1**	**417.8**	**1.1764**	**HOMO → LUMO**	**90.1**
	3	399.6	0.1826	HOM*O*-2 → LUMO	82.5
				HOM*O*-3 → LUMO+1	8.4
	13	**270.7**	**0.1795**	**HOM*O*-5 → LUMO+1**	**85.7**
				HOMO → LUMO+2	12.5
BB3F^{Mes}	**1**	**455.9**	**1.5597**	**HOMO → LUMO**	**98.0**
	13	**300.9**	**0.1334**	**HOM*O*-5 → LUMO+1**	**57.8**
				HOM*O*-6 → LUMO	**26.5**
				HOMO → LUMO+2	**14.0**
	14	**284.4**	**0.1829**	**HOMO → LUMO+2**	**42.9**
				HOM*O*-5 → LUMO+1	**35.2**
				HOM*O*-6 → LUMO	**16.1**
BB4F^{Mes}	**1**	**489.7**	**1.9515**	**HOMO → LUMO**	**98.3**
	8	**342.9**	**0.3565**	**HOMO → LUMO+2**	**72.9**
				HOM*O*-1 → LUMO+1	**11.2**
				HOM*O*-3 → LUMO+1	**8.0**
	14	**302.7**	**0.1023**	**HOM*O*-6 → LUMO+1**	**75.0**
				HOMO → LUMO+2	**14.5**
				HOM*O*-3 → LUMO+1	**4.7**

BB5F^{Mes}	**1**	**510.3**	**2.1647**	**HOMO → LUMO**	**98.0**
	6	**372.2**	**0.4046**	**HOMO → LUMO+2**	**75.4**
				HOM*O*-1 → LUMO+1	**17.6**
	9	**349.6**	**0.1030**	**HOM*O*-1 → LUMO+1**	**75.8**
				HOMO → LUMO+2	**12.7**
				HOM*O*-6 → LUMO	**6.7**

2.3.5 References

(1) Swager, T. M. 50th Anniversary Perspective: Conducting/Semiconducting Conjugated Polymers. A Personal Perspective on the Past and the Future. *Macromolecules* **2017**, *50*, 4867–4886.

(2) (a) Grimsdale, A. C.; Chan, K. L.; Martin, R. E.; Jokisz, P. G.; Holmes, A. B. Synthesis of light-emitting conjugated polymers for applications in electroluminescent devices. *Chem. Rev.* **2009**, *109*, 897–1091. (b) Liang, J.; Ying, L.; Huang, F.; Cao, Y. Recent advances in high performance solution processed WOLEDs for solid-state lighting. *J. Mater. Chem. C* **2016**, *4*, 10993–11006.

(3) (a) Allard, S.; Forster, M.; Souharce, B.; Thiem, H.; Scherf, U. Organic Semiconductors for Solution-Processable Field-Effect Transistors (OFETs). *Angew. Chem. Int. Ed.* **2008**, *47*, 4070–4098. (b) Beaujuge, P. M.; Fréchet, J. M. J. Molecular design and ordering effects in π-functional materials for transistor and solar cell applications. *J. Am. Chem. Soc.* **2011**, *133*, 20009–20029. (c) Wang, C.; Dong, H.; Hu, W.; Liu, Y.; Zhu, D. Semiconducting π-conjugated systems in field-effect transistors: a material odyssey of organic electronics. *Chem. Rev.* **2012**, *112*, 2208–2267. (d) Mei, J.; Diao, Y.; Appleton, A. L.; Fang, L.; Bao, Z. Integrated materials design of organic semiconductors for field-effect transistors. *J. Am. Chem. Soc.* **2013**, *135*, 6724–6746. (e) Sirringhaus, H. 25th Anniversary Article: Organic Field-Effect Transistors: The Path Beyond Amorphous Silicon. *Adv. Mater.* **2014**, *26*, 1319–1335.

(4) (a) Li, C.; Liu, M.; Pschirer, N. G.; Baumgarten, M.; Müllen, K. Polyphenylene-based materials for organic photovoltaics. *Chem. Rev.* **2010**, *110*, 6817–6855. (b) Boudreault, P.-L. T.; Najari, A.; Leclerc, M. Processable Low-Bandgap Polymers for Photovoltaic Applications. *Chem. Mater.* **2011**, *23*, 456–469. (c) Zhou, H.; Yang, L.; You, W. Rational design of high performance conjugated polymers for organic solar cells. *Macromolecules* **2012**, *45*, 607–632. (d) Dou, L.; You, J.; Hong, Z.; Xu, Z.; Li, G.; Street, R. A.; Yang, Y. 25th anniversary article: a decade of organic/polymeric photovoltaic research. *Adv. Mater.* **2013**, *25*, 6642–6671. (e) Lu, L.; Zheng, T.; Wu, Q.; Schneider, A. M.; Zhao, D.; Yu, L. Recent advances in bulk heterojunction polymer solar cells. *Chem. Rev.* **2015**, *115*, 12666–12731.

(5) (a) Thomas, S. W.; Joly, G. D.; Swager, T. M. Chemical sensors based on amplifying fluorescent conjugated polymers. *Chem. Rev.* **2007**, *107*, 1339–1386. (b) Zhou, Y.; Zhang, J. F.; Yoon, J. Fluorescence and colorimetric chemosensors for fluoride-ion detection. *Chem. Rev.* **2014**, *114*, 5511–5571.

(6) Zhu, C.; Liu, L.; Yang, Q.; Lv, F.; Wang, S. Water-soluble conjugated polymers for imaging, diagnosis, and therapy. *Chem. Rev.* **2012**, *112*, 4687–4735.

(7) (a) Osaka, I.; McCullough, R. D. Advances in molecular design and synthesis of regioregular polythiophenes. *Acc. Chem. Res.* **2008**, *41*, 1202–1214. (b) Mishra, A.; Ma, C.-Q.; Bäuerle, P. Functional oligothiophenes: molecular design for multidimensional nanoarchitectures and their applications. *Chem. Rev.* **2009**, *109*, 1141–1276. (c) Olivier, Y.; Niedzialek, D.; Lemaur, V.; Pisula, W.; Müllen, K.; Koldemir, U.; Reynolds, J. R.; Lazzaroni, R.; Cornil, J.; Beljonne, D. 25th Anniversary Article: High-Mobility Hole and Electron Transport Conjugated Polymers: How Structure Defines Function. *Adv. Mater.* **2014**, *26*, 2119–2136. (d) Qian, J.; Li, X.; Lunn, D. J.; Gwyther, J.; Hudson, Z. M.; Kynaston, E.; Rupar, P. A.; Winnik, M. A.; Manners, I. Uniform, High Aspect Ratio Fiber-like Micelles and Block Co-micelles with a Crystalline π-Conjugated Polythiophene Core by Self-Seeding. *J. Am. Chem. Soc.* **2014**, *136*, 4121–4124. (e) Kaloni, T. P.; Giesbrecht, P. K.; Schreckenbach, G.; Freund, M. S. Polythiophene: from fundamental perspectives to applications. *Chem. Mater.* **2017**, *29*, 10248–10283.

(8) Jeffries-EL, M.; Kobilka, B. M.; Hale, B. J. Optimizing the Performance of Conjugated Polymers in Organic Photovoltaic Cells by Traversing Group 16. *Macromolecules* **2014**, *47*, 7253–7271.

(9) (a) Carrera, E. I.; Seferos, D. S. Semiconducting polymers containing tellurium: perspectives toward obtaining high-performance materials. *Macromolecules* **2015**, *48*, 297–308. (b) Rivard, E. Tellurophenes and Their Emergence as Building Blocks for Polymeric and Light-emitting Materials. *Chem. Lett.* **2015**, *44*, 730–736. (c) Hoover, G. C.; Seferos, D. S. Photoactivity and optical applications of organic materials containing selenium and tellurium. *Chem. Sci.* **2019**, *10*, 9182–9188.

(10) (a) He, G.; Le Kang; Torres Delgado, W.; Shynkaruk, O.; Ferguson, M. J.; McDonald, R.; Rivard, E. The marriage of metallacycle transfer chemistry with Suzuki–miyaura cross-coupling to give main group element-containing conjugated polymers. *J. Am. Chem. Soc.* **2013**, *135*, 5360–5363. (b) Jahnke, A. A.; Djukic, B.; McCormick, T. M.; Buchaca Domingo, E.; Hellmann, C.; Lee, Y.; Seferos, D. S. Poly(3-alkyltellurophene)s are solution-processable polyheterocycles. *J. Am. Chem. Soc.* **2013**, *135*, 951–954. (c) Park, Y. S.; Wu, Q.; Nam, C.-Y.; Grubbs, R. B. Polymerization of Tellurophene Derivatives by Microwave-Assisted Palladium-Catalyzed *ipso*-Arylative Polymerization. *Angew. Chem. Int. Ed.* **2014**, *53*, 10691–10695. (d) Al-Hashimi, M.; Han, Y.; Smith, J.; Bazzi, H. S.; Alqaradawi, S. Y. A.; Watkins, S. E.; Anthopoulos, T. D.; Heeney, M. Influence of the heteroatom on the optoelectronic properties and transistor performance of soluble thiophene-, selenophene- and tellurophene–vinylene copolymers. *Chem. Sci.* **2016**, *7*, 1093–1099. (e) Kynaston, E. L.; Nazemi, A.; MacFarlane, L. R.; Whittell, G. R.; Faul, C. F. J.; Manners, I. Uniform Polyselenophene Block Copolymer Fiberlike Micelles and Block Co-micelles via Living Crystallization-Driven Self-Assembly. *Macromolecules* **2018**, *51*, 1002–1010. (f) Luppi, B.

T.; McDonald, R.; Ferguson, M. J.; Sang, L.; Rivard, E. Rapid access to (cycloalkyl)tellurophene oligomer mixtures and the first poly(3-aryltellurophene). *Chem. Commun.* **2019**, *55*, 14218–14221.

(11) (a) González-Tejera, M. J.; La Blanca, E. S. de; Carrillo, I. Polyfuran conducting polymers: Synthesis, properties, and applications. *Synth. Met.* **2008**, *158*, 165–189. (b) Bunz, U. H. F. α-Oligofurans: Molecules without a Twist. *Angew. Chem. Int. Ed.* **2010**, *49*, 5037–5040. (c) Swager, T. M.; Esser, B. α-Oligofurans: A Computational Study. *Synfacts* **2010**, *5*, 0536. (d) Gidron, O.; Bendikov, M. α-Oligofurans: an emerging class of conjugated oligomers for organic electronics. *Angew. Chem. Int. Ed.* **2014**, 2546–2555. (e) Cao, H.; Rupar, P. A. Recent Advances in Conjugated Furans. *Chem. Eur. J.* **2017**, *23*, 14670–14678.

(12) (a) Miyata, Y.; Nishinaga, T.; Komatsu, K. Synthesis and structural, electronic, and optical properties of oligo(thienylfuran)s in comparison with oligothiophenes and oligofurans. *J. Org. Chem.* **2005**, *70*, 1147–1153. (b) Gidron, O.; Diskin-Posner, Y.; Bendikov, M. α-Oligofurans. *J. Am. Chem. Soc.* **2010**, *132*, 2148–2150. (c) Gidron, O.; Dadvand, A.; Sheynin, Y.; Bendikov, M.; Perepichka, D. F. Towards “green” electronic materials. α-Oligofurans as semiconductors. *Chem. Commun.* **2011**, *47*, 1976–1978. (d) Sharma, S.; Bendikov, M. α-Oligofurans: A Computational Study. *Chem. Eur. J.* **2013**, *19*, 13127–13139. (e) Jin, X.-H.; Sheberla, D.; Shimon, L. J. W.; Bendikov, M. Highly coplanar very long oligo(alkylfuran)s: a conjugated system with specific head-to-head defect. *J. Am. Chem. Soc.* **2014**, *136*, 2592–2601. (f) Sheberla, D.; Patra, S.; Wijsboom, Y. H.; Sharma, S.; Sheynin, Y.; Haj-Yahia, A.-E.; Barak, A. H.; Gidron, O.; Bendikov, M. Conducting polyfurans by electropolymerization of oligofurans. *Chem. Sci.* **2015**, *6*, 360–371.

(13) (a) Woo, C. H.; Beaujuge, P. M.; Holcombe, T. W.; Lee, O. P.; Fréchet, J. M. J. Incorporation of furan into low band-gap polymers for efficient solar cells. *J. Am. Chem. Soc.* **2010**, *132*, 15547–15549. (b) Bijleveld, J. C.; Karsten, B. P.; Mathijssen, S. G. J.; Wienk, M. M.; Leeuw, D. M. de; Janssen, R. A. J. Small band gap copolymers based on furan and diketopyrrolopyrrole for field-effect transistors and photovoltaic cells. *J. Mater. Chem.* **2011**, *21*, 1600–1606. (c) Wang, X.; Chen, S.; Sun, Y.; Zhang, M.; Li, Y.; Li, X.; Wang, H. A furan-bridged D-π-A copolymer with deep HOMO level: synthesis and application in polymer solar cells. *Polym. Chem.* **2011**, *2*, 2872–2877. (d) Yiu, A. T.; Beaujuge, P. M.; Lee, O. P.; Woo, C. H.; Toney, M. F.; Frechet, J. M. J. Side-chain tunability of furan-containing low-band-gap polymers provides control of structural order in efficient solar cells. *J. Am. Chem. Soc.* **2012**, *134*, 2180–2185. (e) Wang, X.; Sun, Y.; Chen, S.; Guo, X.; Zhang, M.; Li, X.; Li, Y.; Wang, H. Effects of π-conjugated bridges on photovoltaic properties of donor-π-acceptor conjugated copolymers. *Macromolecules* **2012**, *45*, 1208–1216. (f) Li, Y.; Sonar, P.; Singh, S. P.; Ooi, Z. E.; Lek, E. S. H.; Loh, M. Q. Y. Poly(2,5-

bis(2-octyldodecyl)-3,6-di(furan-2-yl)-2,5-dihydro-pyrrolo[3,4-c]pyrrole-1,4-dione-co-thieno[3,2-b]thiophene): a high performance polymer semiconductor for both organic thin film transistors and organic photovoltaics. *Phys. Chem. Chem. Phys.* **2012**, *14*, 7162–7169. (g) Yuan, J.; Zang, Y.; Dong, H.; Liu, G.; Di, C.-a.; Li, Y.; Ma, W. Effect of a furan π-bridge on polymer coplanarity and performance in organic field effect transistors. *Polym. Chem.* **2013**, *4*, 4199–4206. (h) Luzio, A.; Fazzi, D.; Nübling, F.; Matsidik, R.; Straub, A.; Komber, H.; Giussani, E.; Watkins, S. E.; Barbatti, M.; Thiel, W.; Gann, E.; Thomsen, L.; McNeill, C. R.; Caironi, M.; Sommer, M. Structure–Function Relationships of High-Electron Mobility Naphthalene Diimide Copolymers Prepared Via Direct Arylation. *Chem. Mater.* **2014**, *26*, 6233–6240. (i) Huo, L.; Liu, T.; Fan, B.; Zhao, Z.; Sun, X.; Wei, D.; Yu, M.; Liu, Y.; Sun, Y. Organic Solar Cells Based on a 2D Benzo[1,2-b:4,5-b′]difuran-Conjugated Polymer with High-Power Conversion Efficiency. *Adv. Mater.* **2015**, *27*, 6969–6975. (j) Xiong, Y.; Tao, J.; Wang, R.; Qiao, X.; Yang, X.; Wang, D.; Wu, H.; Li, H. A Furan–Thiophene-Based Quinoidal Compound: A New Class of Solution-Processable High-Performance n-Type Organic Semiconductor. *Adv. Mater.* **2016**, *28*, 5949–5953. (k) Yan, T.; Bin, H.; Yang, Y.; Xue, L.; Zhang, Z.-G.; Li, Y. Effect of furan π-bridge on the photovoltaic performance of DA copolymers based on bi(alkylthio-thienyl) benzodithiophene and fluorobenzotriazole. *Sci. China Chem.* **2017**, *60*, 537–544. (l) Cao, H.; Brettell-Adams, I. A.; Qu, F.; Rupar, P. A. Bridged Difurans: Stabilizing Furan with p-Block Elements. *Organometallics* **2017**, *36*, 2565–2572.

(14) (a) Gandini, A. Polymers from renewable resources: a challenge for the future of macromolecular materials. *Macromolecules* **2008**, *41*, 9491–9504. (b) Gandini, A. The irruption of polymers from renewable resources on the scene of macromolecular science and technology. *Green Chem.* **2011**, *13*, 1061–1083. (c) Mooney, M.; Nyayachavadi, A.; Rondeau-Gagné, S. Eco-friendly semiconducting polymers: from greener synthesis to greener processability. *J. Mater. Chem. C* **2020**, *8*, 14645–14664.

(15) (a) Entwistle, C. D.; Marder, T. B. Boron chemistry lights the way: optical properties of molecular and polymeric systems. *Angew. Chem. Int. Ed.* **2002**, *41*, 2927–2931. (b) Wade, C. R.; Broomsgrove, A. E. J.; Aldridge, S.; Gabbaï, F. P. Fluoride ion complexation and sensing using organoboron compounds. *Chem. Rev.* **2010**, *110*, 3958–3984. (c) Jäkle, F. Advances in the synthesis of organoborane polymers for optical, electronic, and sensory applications. *Chem. Rev.* **2010**, *110*, 3985–4022. (d) Hudson, Z. M.; Wang, S. Metal-containing triarylboron compounds for optoelectronic applications. *Dalton Trans* **2011**, *40*, 7805–7816. (e) Tanaka, K.; Chujo, Y. Advanced Luminescent Materials Based on Organoboron Polymers. *Macromol. Rapid Commun.* **2012**, *33*, 1235–1255. (f) Zhao, H.; Leamer, L. A.; Gabbaï, F. P. Anion capture and sensing with cationic boranes: on the synergy of Coulombic effects and onium ion-centred Lewis acidity. *Dalton Trans.* **2013**, *42*,

8164–8178. (g) Wakamiya, A.; Yamaguchi, S. Designs of Functional π-Electron Materials based on the Characteristic Features of Boron. *Bull. Chem. Soc. Jpn.* **2015**, *88*, 1357–1377. (h) Escande, A.; Ingleson, M. J. Fused polycyclic aromatics incorporating boron in the core: fundamentals and applications. *Chem. Commun.* **2015**, *51*, 6257–6274. (i) Jäkle, F. Recent advances in the synthesis and applications of organoborane polymers. *Top. Organomet. Chem.* **2015**, *49*, 297–325. (j) Helten, H. B=N Units as Part of Extended π-Conjugated Oligomers and Polymers. *Chem. Eur. J.* **2016**, *22*, 12972–12982. (k) Mukherjee, S.; Thilagar, P. Stimuli and shape responsive 'boron-containing' luminescent organic materials. *J. Mater. Chem. C* **2016**, *4*, 2647–2662. (l) Su, B.; Kinjo, R. Construction of Boron-Containing Aromatic Heterocycles. *Synthesis* **2017**, *49*, 2985–3034. (m) Ji, L.; Griesbeck, S.; Marder, T. B. Recent developments in and perspectives on three-coordinate boron materials: a bright future. *Chem. Sci.* **2017**, *8*, 846–863. (n) Li, S.-Y.; Sun, Z.-B.; Zhao, C.-H. Charge-Transfer Emitting Triarylborane π-Electron Systems. *Inorg. Chem.* **2017**, *56*, 8705–8717. (o) von Grotthuss, E.; John, A.; Kaese, T.; Wagner, M. Doping Polycyclic Aromatics with Boron for Superior Performance in Materials Science and Catalysis. *Asian J. Org. Chem.* **2018**, *7*, 37–53. (p) Ren, Y.; Jäkle, F. Incorporation of Group 13 Elements into Polymers. In Main Group Strategies towards Functional Hybrid Materials; Baumgartner, T., Jäkle, F.; Eds.; Wiley, Hoboken, 2018, pp 79–110. (q) Helten, H. Doping the Backbone of π-Conjugated Polymers with Tricoordinate Boron: Synthetic Strategies and Emerging Applications. *Chem. Asian J.* **2019**, *14*, 919–935. (r) Mellerup, S. K.; Wang, S. Boron-based stimuli responsive materials. *Chem. Soc. Rev.* **2019**, *48*, 3537–3549. (s) Hirai, M.; Tanaka, N.; Sakai, M.; Yamaguchi, S. Structurally Constrained Boron-, Nitrogen-, Silicon-, and Phosphorus-Centered Polycyclic π-Conjugated Systems. *Chem. Rev.* **2019**, *119*, 8291–8331. (t) Wang, X.-Y.; Yao, X.; Narita, A.; Müllen, K. Heteroatom-Doped Nanographenes with Structural Precision. *Acc. Chem. Res.* **2019**, *52*, 2491–2505. (u) Yin, X.; Liu, J.; Jäkle, F. Electron-Deficient Conjugated Materials via p–π* Conjugation with Boron: Extending Monomers to Oligomers, Macrocycles, and Polymers. *Chem. Eur. J.* **2021**, *27*, 2973–2986.

(16) Examples of main-chain B-doped polymers: (a) Matsumi, N.; Naka, K.; Chujo, Y. Extension of π-Conjugation Length via the Vacant p-Orbital of the Boron Atom. Synthesis of Novel Electron Deficient π-Conjugated Systems by Hydroboration Polymerization and Their Blue Light Emission. *J. Am. Chem. Soc.* **1998**, *120*, 5112–5113. (b) Sundararaman, A.; Victor, M.; Varughese, R.; Jäkle, F. A family of main-chain polymeric Lewis acids: synthesis and fluorescent sensing properties of boron-modified polythiophenes. *J. Am. Chem. Soc.* **2005**, *127*, 13748–13749. (c) Heilmann, J. B.; Scheibitz, M.; Qin, Y.; Sundararaman, A.; Jäkle, F.; Kretz, T.; Bolte, M.; Lerner, H.-W.; Holthausen, M. C.; Wagner, M. A synthetic route to borylene-bridged poly(ferrocenylene)s. *Angew. Chem. Int. Ed.* **2006**, *45*, 920–925. (d) Nagai, A.; Murakami, T.; Nagata, Y.; Kokado, K.; Chujo, Y. Synthesis and

Photostability of Poly(*p*-phenylenevinylene-borane)s. *Macromolecules* **2009**, *42*, 7217–7220. (e) Lorbach, A.; Bolte, M.; Li, H.; Lerner, H.-W.; Holthausen, M. C.; Jäkle, F.; Wagner, M. 9,10-Dihydro-9,10-diboraanthracene: supramolecular structure and use as a building block for luminescent conjugated polymers. *Angew. Chem. Int. Ed.* **2009**, *48*, 4584–4588. (f) Li, H.; Jäkle, F. Universal scaffold for fluorescent conjugated organoborane polymers. *Angew. Chem. Int. Ed.* **2009**, *48*, 2313–2316. (g) Zhao, W.; Zhuang, X.; Wu, D.; Zhang, F.; Gehrig, D.; Laquai, F.; Feng, X. Boron-π-nitrogen-based conjugated porous polymers with multi-functions. *J. Mater. Chem. A* **2013**, *1*, 13878–13884. (h) Reus, C.; Guo, F.; John, A.; Winhold, M.; Lerner, H.-W.; Jäkle, F.; Wagner, M. Air-and Water-Stable, Fluorescent Oligomers of 9,10-Dihydro-9,10-diboraanthracene. *Macromolecules* **2014**, *47*, 3727–3735. (i) Adams, I. A.; Rupar, P. A. A Poly(9-Borafluorene) Homopolymer: An Electron-Deficient Polyfluorene with "Turn-On" Fluorescence Sensing of NH3 Vapor. *Macromol. Rapid Commun.* **2015**, *36*, 1336–1340. (j) Baggett, A. W.; Guo, F.; Li, B.; Liu, S.-Y.; Jäkle, F. Regioregular synthesis of azaborine oligomers and a polymer with a *syn* conformation stabilized by N-H···π interactions. *Angew. Chem. Int. Ed.* **2015**, *54*, 11191–11195. (k) Wang, X.-Y.; Zhuang, F.-D.; Wang, J.-Y.; Pei, J. Incorporation of polycyclic azaborine compounds into polythiophene-type conjugated polymers for organic field-effect transistors. *Chem. Commun.* **2015**, *51*, 17532–17535. (l) Kawai, S.; Saito, S.; Osumi, S.; Yamaguchi, S.; Foster, A. S.; Spijker, P.; Meyer, E. Atomically controlled substitutional boron-doping of graphene nanoribbons. *Nat. Commun.* **2015**, *6*, 8098. (m) Cloke, R. R.; Marangoni, T.; Nguyen, G. D.; Joshi, T.; Rizzo, D. J.; Bronner, C.; Cao, T.; Louie, S. G.; Crommie, M. F.; Fischer, F. R. Site-specific substitutional boron doping of semiconducting armchair graphene nanoribbons. *J. Am. Chem. Soc.* **2015**, *137*, 8872–8875. (n) Lorenz, T.; Lik, A.; Plamper, F. A.; Helten, H. Dehydrocoupling and Silazane Cleavage Routes to Organic–Inorganic Hybrid Polymers with NBN Units in the Main Chain. *Angew. Chem. Int. Ed.* **2016**, *55*, 7236–7241. (o) Ayhan, O.; Eckert, T.; Plamper, F. A.; Helten, H. Poly(iminoborane)s: An Elusive Class of Main-Group Polymers? *Angew. Chem. Int. Ed.* **2016**, *55*, 13321–13325. (p) Lorenz, T.; Crumbach, M.; Eckert, T.; Lik, A.; Helten, H. Poly(*p*-phenylene iminoborane): A Boron-Nitrogen Analogue of Poly(*p*-phenylene vinylene). *Angew. Chem. Int. Ed.* **2017**, *56*, 2780–2784. (q) Marinelli, D.; Fasano, F.; Najjari, B.; Demitri, N.; Bonifazi, D. Borazino-doped polyphenylenes. *J. Am. Chem. Soc.* **2017**, *139*, 5503–5519. (r) Hu, K.; Zhang, Z.; Burke, J.; Qin, Y. Boron “Doped” Polyacetylenes. *J. Am. Chem. Soc.* **2017**, *139*, 11004–11007. (s) Ayhan, O.; Riensch, N. A.; Glasmacher, C.; Helten, H. Cyclolinear Oligo- and Poly(iminoborane)s: The Missing Link in Inorganic Main-Group Macromolecular Chemistry. *Chem. Eur. J.* **2018**, *24*, 5883–5894. (t) Zhang, W.; Li, G.; Xu, L.; Zhuo, Y.; Wan, W.; Yan, N.; He, G. 9,10-Azaboraphenanthrene-containing small molecules and conjugated polymers: synthesis and their application in chemodosimeters for the ratiometric detection

of fluoride ions. *Chem. Sci.* **2018**, *9*, 4444–4450. (u) Wang, X.-Y.; Urgel, J. I.; Barin, G. B.; Eimre, K.; Di Giovannantonio, M.; Milani, A.; Tommasini, M.; Pignedoli, C. A.; Ruffieux, P.; Feng, X.; Fasel, R.; Müllen, K.; Narita, A. Bottom-up synthesis of heteroatom-doped chiral graphene nanoribbons. *J. Am. Chem. Soc.* **2018**, *140*, 9104–9107. (v) Brosge, F.; Lorenz, T.; Helten, H.; Bolm, C. BN- and BO-Doped Inorganic-Organic Hybrid Polymers with Sulfoximine Core Units. *Chem. Eur. J.* **2019**, *25*, 12708–12711. (w) Fu, Y.; Yang, H.; Gao, Y.; Huang, L.; Berger, R.; Liu, J.; Lu, H.; Cheng, Z.; Du, S.; Gao, H.-J.; Feng, X. On-Surface Synthesis of NBN-Doped Zigzag-Edged Graphene Nanoribbons. *Angew. Chem. Int. Ed.* **2020**, *59*, 8873–8879.

(17) (a) Ren, Y.; Jäkle, F. Merging thiophene with boron: new building blocks for conjugated materials. *Dalton Trans* **2016**, *45*, 13996–14007. (b) Dhiman, A.; Giribabu, L.; Trivedi, R. π-conjugated Materials Derived From Boron-chalcogenophene Combination. A Brief Description of Synthetic Routes and Optoelectronic Applications. *Chem. Rec.* **2021**, *21*, 1–34.

(18) Examples: (a) Sundararaman, A.; Venkatasubbaiah, K.; Victor, M.; Zakharov, L. N.; Rheingold, A. L.; Jäkle, F. Electronic communication and negative binding cooperativity in diborylated bithiophenes. *J. Am. Chem. Soc.* **2006**, *128*, 16554–16565. (b) Wakamiya, A.; Mori, K.; Araki, T.; Yamaguchi, S. AB− B Bond-Containing Polycyclic π-Electron System: Dithieno-1,2-dihydro-1,2-diborin and Its Dianion. *J. Am. Chem. Soc.* **2009**, *131*, 10850–10851. (c) Lepeltier, M.; Lukoyanova, O.; Jacobson, A.; Jeeva, S.; Perepichka, D. F. New azaborine-thiophene heteroacenes. *Chem. Commun.* **2010**, *46*, 7007–7009. (d) Iida, A.; Yamaguchi, S. Thiophene-fused ladder boroles with high antiaromaticity. *J. Am. Chem. Soc.* **2011**, *133*, 6952–6955. (e) Poon, C.-T.; Lam, W. H.; Yam, V. W.-W. Gated photochromism in triarylborane-containing dithienylethenes: a new approach to a “lock–unlock” system. *J. Am. Chem. Soc.* **2011**, *133*, 19622–19625. (f) Braunschweig, H.; Damme, A.; Jimenez-Halla, J. O. C.; Hörl, C.; Krummenacher, I.; Kupfer, T.; Mailänder, L.; Radacki, K. 1-Heteroaromatic-Substituted Tetraphenylboroles: π–π Interactions Between Aromatic and Antiaromatic Rings Through a B–C Bond. *J. Am. Chem. Soc.* **2012**, *134*, 20169–20177. (g) Mercier, L. G.; Piers, W. E.; Harrington, R. W.; Clegg, W. Benzo[b]thiophene-Fused Boron and Silicon Ladder Acenes. *Organometallics* **2013**, *32*, 6820–6826. (h) Levine, D. R.; Siegler, M. A.; Tovar, J. D. Thiophene-fused borepins as directly functionalizable boron-containing π-electron systems. *J. Am. Chem. Soc.* **2014**, *136*, 7132–7139. (i) Sarkar, S. K.; Kumar, G. R.; Thilagar, P. White light emissive molecular siblings. *Chem. Commun.* **2016**, *52*, 4175–4178. (j) Kumar, G. R.; Sarkar, S. K.; Thilagar, P. Aggregation-Induced Emission and Sensing Characteristics of Triarylborane–Oligothiophene–Dicyanovinyl Triads. *Chem. Eur. J.* **2016**, *22*, 17215–17225. (k) Yan, Y.; Sun, Z.; Li, C.; Zhang, J.; Lv, L.; Liu, X.; Liu, X. Thiophene-Fused 1,4-Thiaborins: Synthesis,

Structures and Properties. *Asian J. Org. Chem.* **2017**, *6*, 496–502. (l) Messersmith, R. E.; Yadav, S.; Siegler, M. A.; Ottosson, H.; Tovar, J. D. Benzo[b]thiophene Fusion Enhances Local Borepin Aromaticity in Polycyclic Heteroaromatic Compounds. *J. Org. Chem.* **2017**, *82*, 13440–13448. (m) Cao, Y.; Wang, X.; Shi, X.; Clee, S. M.; McGeer, P. L.; Wolf, M. O.; Orvig, C. Biological Imaging with Medium-Sensitive Bichromatic Flexible Fluorescent Dyes. *Angew. Chem. Int. Ed.* **2017**, *56*, 15603–15606. (n) Araki, T.; Hirai, M.; Wakamiya, A.; Piers, W. E.; Yamaguchi, S. Antiaromatic Dithieno-1,2-dihydro-1,2-diborin Splits Diatomic Hydrogen. *Chem. Lett.* **2017**, *46*, 1714–1717. (o) Shimogawa, H.; Yoshikawa, O.; Aramaki, Y.; Murata, M.; Wakamiya, A.; Murata, Y. 4,7-Bis[3-(dimesitylboryl)thien-2-yl]benzothiadiazole: Solvato-, Thermo-, and Mechanochromism Based on the Reversible Formation of an Intramolecular B−N Bond. *Chem. Eur. J.* **2017**, *23*, 3784–3791. (p) Adachi, Y.; Ohshita, J. Synthesis and Properties of Benzo[d]dithieno[b,f]borepins. *Organometallics* **2018**, *37*, 869–881. (q) Mitsudo, K.; Shigemori, K.; Mandai, H.; Wakamiya, A.; Suga, S. Synthesis and Properties of Dithieno-fused 1,4-Azaborine Derivatives. *Org. Lett.* **2018**, *20*, 7336–7340. (r) Ito, M.; Ito, E.; Hirai, M.; Yamaguchi, S. Donor−π–Acceptor Type Unsymmetrical Triarylborane-Based Fluorophores: Synthesis, Fluorescence Properties, and Photostability. *J. Org. Chem.* **2018**, *83*, 8449–8456. (s) Stennett, T. E.; Bissinger, P.; Griesbeck, S.; Ullrich, S.; Krummenacher, I.; Auth, M.; Sperlich, A.; Stolte, M.; Radacki, K.; Yao, C.-J.; Würthner, F.; Steffen, A.; Marder, T. B.; Braunschweig, H. Near-Infrared Quadrupolar Chromophores Combining Three-Coordinate Boron-Based Superdonor and Superacceptor Units. *Angew. Chem. Int. Ed.* **2019**, *58*, 6449–6454. (t) Zhang, W.; Yu, D.; Wang, Z.; Zhang, B.; Xu, L.; Li, G.; Yan, N.; Rivard, E.; He, G. Dibora10annulenes: Construction, Properties, and Their Ring-Opening Reactions. *Org. Lett.* **2019**, *21*, 109–113. (u) Cao, Y.; Arsenault, N. E.; Hean, D.; Wolf, M. O. Fluorescence Switching of Intramolecular Lewis Acid–Base Pairs on a Flexible Backbone. *J. Org. Chem.* **2019**, *84*, 5394–5403. (v) Adachi, Y.; Arai, F.; Jäkle, F. Extended conjugated borenium dimers via late stage functionalization of air-stable borepinium ions. *Chem. Commun.* **2020**, *56*, 5119–5122. (w) Crumbach, M.; Bachmann, J.; Fritze, L.; Helbig, A.; Krummenacher, I.; Braunschweig, H.; Helten, H. Dithiophene-Fused Oxadiborepins and Azadiborepins: A New Class of Highly Fluorescent Heteroaromatics. *Angew. Chem. Int. Ed.* **2021**, *60*, 9290–9295.

(19) (a) Yin, X.; Chen, J.; Lalancette, R. A.; Marder, T. B.; Jäkle, F. Highly electron-deficient and air-stable conjugated thienylboranes. *Angew. Chem. Int. Ed.* **2014**, *53*, 9761–9765. (b) Meng, B.; Ren, Y.; Liu, J.; Jäkle, F.; Wang, L. p–π Conjugated Polymers Based on Stable Triarylborane with n-Type Behavior in Optoelectronic Devices. *Angew. Chem.* **2018**, *130*, 2205–2209. (c) Adachi, Y.; Ooyama, Y.; Ren, Y.; Yin, X.; Jäkle, F.; Ohshita, J. Hybrid conjugated polymers with alternating dithienosilole or dithienogermole and tricoordinate boron units. *Polym. Chem.* **2018**, *9*, 291–299.

(20) Yin, X.; Guo, F.; Lalancette, R. A.; Jäkle, F. Luminescent Main-Chain Organoborane Polymers: Highly Robust, Electron-Deficient Poly(oligothiophene borane)s via Stille Coupling Polymerization. *Macromolecules* **2016**, *49*, 537–546.

(21) (a) Yin, X.; Liu, K.; Ren, Y.; Lalancette, R. A.; Loo, Y.-L.; Jäkle, F. Pyridalthiadiazole acceptor-functionalized triarylboranes with multi-responsive optoelectronic characteristics. *Chem. Sci.* **2017**, *8*, 5497–5505. (b) Yu, Y.; Dong, C.; Alahmadi, A. F.; Meng, B.; Liu, J.; Jäkle, F.; Wang, L. A p-π* conjugated triarylborane as an alcohol-processable n-type semiconductor for organic optoelectronic devices. *J. Mater. Chem. C* **2019**, *7*, 7427–7432. (c) Welsh, T. A.; Laventure, A.; Alahmadi, A. F.; Zhang, G.; Baumgartner, T.; Zou, Y.; Jäkle, F.; Welch, G. C. Borane incorporation in a non-fullerene acceptor to tune steric and electronic properties and improve organic solar cell performance. *ACS Appl. Energy Mater.* **2019**, *2*, 1229–1240. (d) Yu, Y.; Meng, B.; Jäkle, F.; Liu, J.; Wang, L. Molecular acceptors based on a triarylborane core unit for organic solar cells. *Chem. Eur. J.* **2020**, *26*, 873–880. (e) Adachi, Y.; Nabeya, T.; Kawakami, K.; Yamaji, K.; Jäkle, F.; Ohshita, J. Optical Characteristics of Hybrid Macrocycles with Dithienogermole and Tricoordinate Boron Units. *Chem. Eur. J.* **2021**, *27*, 3306–3314.

(22) (a) Lik, A.; Fritze, L.; Müller, L.; Helten, H. Catalytic B-C Coupling by Si/B Exchange: A Versatile Route to π-Conjugated Organoborane Molecules, Oligomers, and Polymers. *J. Am. Chem. Soc.* **2017**, *139*, 5692–5695. (b) Lik, A.; Jenthra, S.; Fritze, L.; Müller, L.; Truong, K.-N.; Helten, H. From Monodisperse Thienyl- and Furylborane Oligomers to Polymers: Modulating the Optical Properties through the Hetarene Ratio. *Chem. Eur. J.* **2018**, *24*, 11961–11972.

(23) Fritze, L.; Riensch, N. A.; Helten, H. Catalytic Si/B Exchange Condensation: A Green B–C Coupling Method That Provides Access to Monodisperse (Het)arylborane 'Trimers'. *Synthesis* **2019**, *51*, 399–406.

(24) Riensch, N. A.; Fritze, L.; Schindler, T.; Kremer, M.; Helten, H. Difuryl(supermesityl)borane: a versatile building block for extended π-conjugated materials. *Dalton Trans.* **2018**, *47*, 10399–10403.

(25) Riensch, N. A.; Fest, M.; Fritze, L.; Helbig, A.; Krummenacher, I.; Braunschweig, H.; Helten, H. Bifuran-bridged bisboranes: highly luminescent B-doped oligohetarenes. *New J. Chem.* **2021**, DOI: 10.1039/D0NJ04297H.

(26) Riensch, N. A.; Swoboda, L.; Lik, A.; Krummenacher, I.; Braunschweig, H.; Helten, H. Conjugated Bis(triarylboranes) with Disconnected Conjugation. *Z. Anorg. Allg. Chem.* **2021**, *647*, 421–424.

(27) (a) Köhler, T.; Faderl, J.; Pritzkow, H.; Siebert, W. Synthesis and Properties of Bis(2-heteroaryl) borane Derivatives. *Eur. J. Inorg. Chem.* **2002**, 2942–2946. (b) Braunschweig,

H.; Dewhurst, R. D.; Hörl, C.; Phukan, A. K.; Pinzner, F.; Ullrich, S. Direct Hydroboration of B–B Bonds: A Mild Strategy for the Proliferation of B– B Bonds. *Angew. Chem. Int. Ed.* **2014**, *53*, 3241–3244. (c) Braunschweig, H.; Dewhurst, R. D.; Kramer, T. Synthesis of the First Heteroaryl-Substituted Boryl Complexes: Strong Stabilizing Effects of Boron–Aryl π-Conjugation. *Inorg. Chem.* **2015**, *54*, 3619–3623. (d) Chen, B.; Nie, H.; Hu, R.; Qin, A.; Zhao, Z.; Tang, B.-Z. Red fluorescent siloles with aggregation-enhanced emission characteristics. *Sci. China Chem.* **2016**, *59*, 699–706. (e) Shishido, R.; Sasaki, I.; Seki, T.; Ishiyama, T.; Ito, H. Direct Dimesitylborylation of Benzofuran Derivatives by an Iridium-Catalyzed C-H Activation with Silyldimesitylborane. *Chem. Eur. J.* **2019**, *25*, 12924–12928.

(28) The wavelength of the emission maximum as well as the quantum yield for polymer **C** varies somewhat with the degree of polymerization. While we have previously obtained and reported[22] Φ_f values of 70 and 71 %, we have now obtained a higher polymer of **C** with a fluorescence quantum yield of 78 %.

(29) The tetrafuran derivative of **F** we have reported in reference 25. The synthesis from bifuran, described therein, however, was only successful with 2,4,6-triisopropylphenyl as the third substituent at boron. The Mes*-derivative of **F** corresponds to compound **BB2F**, the synthesis of which is described herein.

(30) The TD-DFT calculations for **BB2F^{Mes}** have been reported by us previously.[25] As we also reported recently,[22b] in the case of **BB1F^{Mes}**, the HOMO–LUMO excitation corresponds to a charge transfer from the Mes group to the furylborane-chain's π system. This transition, however, is of very low oscillator strength, and therefore insignificant. π–π* transitions analogous to those in **BB2F^{Mes}** – **BB5F^{Mes}** are in this case HOMO-1–LUMO transitions.

(31) Increasing the scan rate did not change the CV response (Figure S5.3.98), indicating that the following chemical step is fast relative to the CV time scale.

(32) Fiedler, J.; Zališ, S.; Klein, A.; Hornung, F. M.; Kaim, W. Electronic Structure of π-Conjugated Redox Systems with Borane/Borataalkene End Groups. *Inorg. Chem.* **1996**, *35*, 3039–3043.

(33) Braunschweig, H.; Dyakonov, V.; Engels, B.; Falk, Z.; Hörl, C.; Klein, J. H.; Kramer, T.; Kraus, H.; Krummenacher, I.; Lambert, C.; Walter, C. Multiple reduction of 2,5-bis(borolyl)thiophene: isolation of a negative bipolaron by comproportionation. *Angew. Chem. Int. Ed.* **2013**, *52*, 12852–12855.

(34) Keegstra, M. A.; Klomp, A. J. A.; Brandsma, L. Convenient Synthetic Procedures for 2-Bromofuran and 2,5-Dibromofuran. *Synthetic Communications* **2006**, *20* (21), 3371–3374.

(35) Qiu, Y.; Fortney, A.; Tsai, C.-H.; Baker, M. A.; Gil, R. R.; Kowalewski, T.; Noonan, K. J. T. Synthesis of Polyfuran and Thiophene-Furan Alternating Copolymers Using Catalyst-Transfer Polycondensation. *ACS Macro Lett.* **2016**, *5* (3), 332–336.

(36) Sasabe, M.; Houda, Y.; Takagi, H.; Sugane, T.; Bo, X.; Yamamura, K. A versatile and efficient method for the synthesis of benz[a]azulenic enones starting from readily available o-(2-furyl)cycloheptatrienylbenzenes. *J. Chem. Soc., Perkin Trans. 1* **2000** (22), 3786–3790.

(37) Sheldrick, G. M. SHELXT - integrated space-group and crystal-structure determination. *Acta crystallographica. Section A, Foundations and advances* **2015**, *71* (Pt 1), 3–8.

(38) Sheldrick, G. M. A short history of SHELX. *Acta crystallographica. Section A, Foundations of crystallography* **2008**, *64* (Pt 1), 112–122.

(39) Hübschle, C. B.; Sheldrick, G. M.; Dittrich, B. ShelXle: a Qt graphical user interface for SHELXL. *Journal of applied crystallography* **2011**, *44* (Pt 6), 1281–1284.

(40) Dolomanov, O. V.; Bourhis, L. J.; Gildea, R. J.; Howard, J. A. K.; Puschmann, H. OLEX2: a complete structure solution, refinement and analysis program. *Journal of applied crystallography* **2009**, *42* (2), 339–341.

(41) Ahlrichs, R.; Bär, M.; Häser, M.; Horn, H.; Kölmel, C. Electronic structure calculations on workstation computers: The program system turbomole. *Chemical Physics Letters* **1989**, *162* (3), 165–169.

(42) a) Quantum mechanics of many-electron systems. *Proc. R. Soc. Lond. A* **1929**, *123* (792), 714–733; b) Slater, J. C. A Simplification of the Hartree-Fock Method. *Phys. Rev.* **1951**, *81* (3), 385–390; c) Becke. Density-functional exchange-energy approximation with correct asymptotic behavior. *Physical review. A, General physics* **1988**, *38* (6), 3098–3100; d) Lee; Yang; Parr. Development of the Colle-Salvetti correlation-energy formula into a functional of the electron density. *Physical review. B, Condensed matter* **1988**, *37* (2), 785–789; e) Becke, A. D. Density-functional thermochemistry. III. The role of exact exchange. *The Journal of Chemical Physics* **1993**, *98* (7), 5648–5652.

(43) Schäfer, A.; Horn, H.; Ahlrichs, R. Fully optimized contracted Gaussian basis sets for atoms Li to Kr. *The Journal of Chemical Physics* **1992**, *97* (4), 2571–2577.

(44) a) Grimme, S.; Antony, J.; Ehrlich, S.; Krieg, H. A consistent and accurate ab initio parametrization of density functional dispersion correction (DFT-D) for the 94 elements H-Pu. *The Journal of Chemical Physics* **2010**, *132* (15), 154104; b) Grimme, S.; Ehrlich, S.; Goerigk, L. Effect of the damping function in dispersion corrected density functional theory. *Journal of computational chemistry* **2011**, *32* (7), 1456–1465.

(45) Deglmann, P.; Furche, F.; Ahlrichs, R. An efficient implementation of second analytical derivatives for density functional methods. *Chemical Physics Letters* **2002**, *362* (5-6), 511–518; b) Deglmann, P.; Furche, F. Efficient characterization of stationary points on potential energy surfaces. *J. Am. Chem. Soc.* **2002**, *117* (21), 9535–9538.

(46) a) Bauernschmitt, R.; Ahlrichs, R. Treatment of electronic excitations within the adiabatic approximation of time dependent density functional theory. *Chemical Physics Letters* **1996**, *256* (4-5), 454–464; b) Bauernschmitt, R.; Ahlrichs, R. Stability analysis for solutions of the closed shell Kohn–Sham equation. *Chemical Physics Letters* **1996**, *104* (22), 9047–9052; c) Furche, F.; Rappoport, D. {III}-density functional methods for excited states: Equilibrium structure and electronic spectra. *Computational photochemistry* **2005**, *16*, 93–128.

2.4 Mechanistic Investigations on the Catalytic Si/B Exchange Condensation to Form Di(het)aryl-bromoboranes

2.4.1 Introduction

Boron−carbon bond formation reactions constitute the key aspect of synthetic organoboron chemistry.[1] There are several synthetic methods available, many of them involve the use of Rh, Pd or Ru catalysts – all come with their own advantages and disadvantages (Scheme 2.4.1).[2–5]

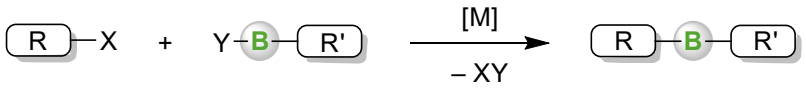

Scheme 2.4.1: *General scheme for the formation of B−C bonds by organometallic metathesis reactions.*

We became interested in such transformations in the course of our investigations on π-conjugated organoborane polymers and oligomers with B−C_{aryl} linkages. Hydroboration reactions, for instance, cannot be used to form such bonds. Chujo and coworkers applied their approach to polymers **1a-c** containing B-C_{vinyl} bonds, which were kinetically stabilized by bulky 2,4,6-trimethylphenyl (mesityl, Mes) or 2,4,6-triisopropylylphenyl (Tip) substituents (Scheme 2.4.2a).[6,7] Subsequently, they used dilithiated substrates to produce poly(ethynylene-phenyleneethynylene borane)s **2a-b** (Scheme 2.4.2b).[8]

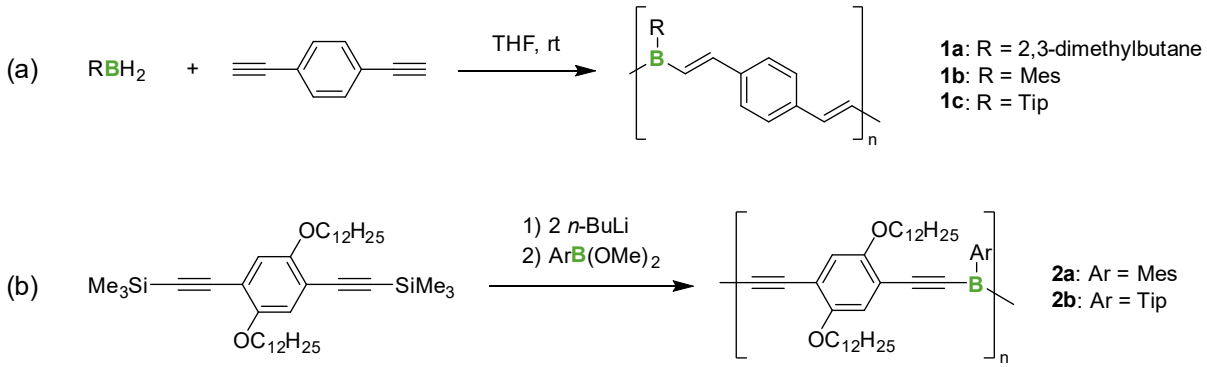

Scheme 2.4.2: *a: Synthesis of poly(vinylene-p-phenylenevinylene-borane)s **1a-c** by hydroboration polymerization; b: Synthesis of poly(ethynylenephenyleneethynylene borane)s **2a-b** by organometallic metathesis reaction.*

For B–C_{aryl} bond formation, different organometallic metathesis reactions have been explored. Chujo and coworkers synthesized a series of poly(*p*-phenylene borane)s **3a-d** by utilization of difunctional Grignard reagents (Scheme 2.4.3).[9] For this reaction, heating of up to 70 °C was required.

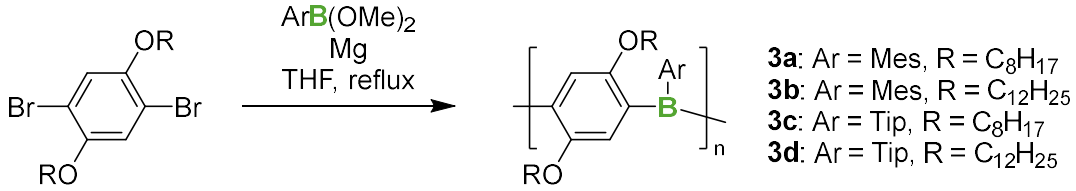

Scheme 2.4.3: *Synthesis of poly(p-phenylene borane)s* ***3a-d*** *by Grignard reaction.*

Sn/B exchange condensations have been explored by the workgroups of Jäkle[10,11] (Scheme 2.4.4) and Jia[12] as a potential milder and more selective method, which has proved to be particularly feasible to produce B–C_{aryl} linkages. However, a disadvantage is the toxicity of the organotin substrates and condensation by-products, as well as side reactions like Sn–C_{alkyl} cleavage.[13] These polymerizations can be conducted in noncoordinating solvents such as CH_2Cl_2 or toluene. This avoids the need for ether solvents, which are typically used for Grignard and organolithium reagents, but tend to react with highly Lewis acidic borane centers under formation of Lewis acid–base complexes or ether cleavage.[3]

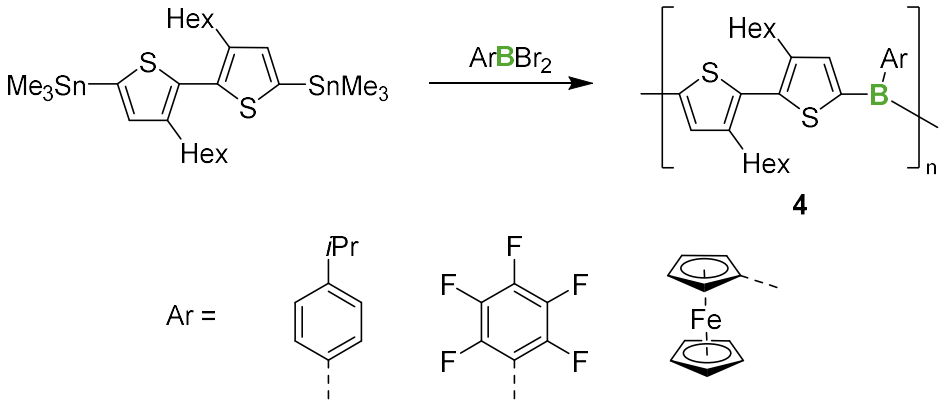

Scheme 2.4.4: *Synthesis of poly-thienylboranes* ***4*** *by Sn/B exchange condensation.*

Recently, we found that Si/B exchange condensation reactions can also be successfully applied for this purpose. In general, Si/B exchange condensation reactions are well-established, but for the formation of a second B–C_{aryl} bond at one boron center, relatively harsh reaction conditions are required, as demonstrated by the reaction to give bromo-(diphenyl)boranes **5** previously reported by Haubold and coworkers (Scheme 2.4.5).[14]

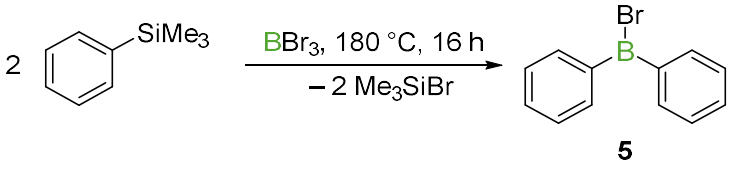

Scheme 2.4.5: *Preparation of bromo(diphenyl)borane* ***5*** *under harsh conditions.*

However, we found that catalytic amounts of electrophilic silyl reagents, Me_3SiOTf and, particularly, Me_3SiNTf_2 significantly accelerate such reactions, which gave the possibility to synthesize a series of mixed triarylboranes (Scheme 2.4.6).[15–18]

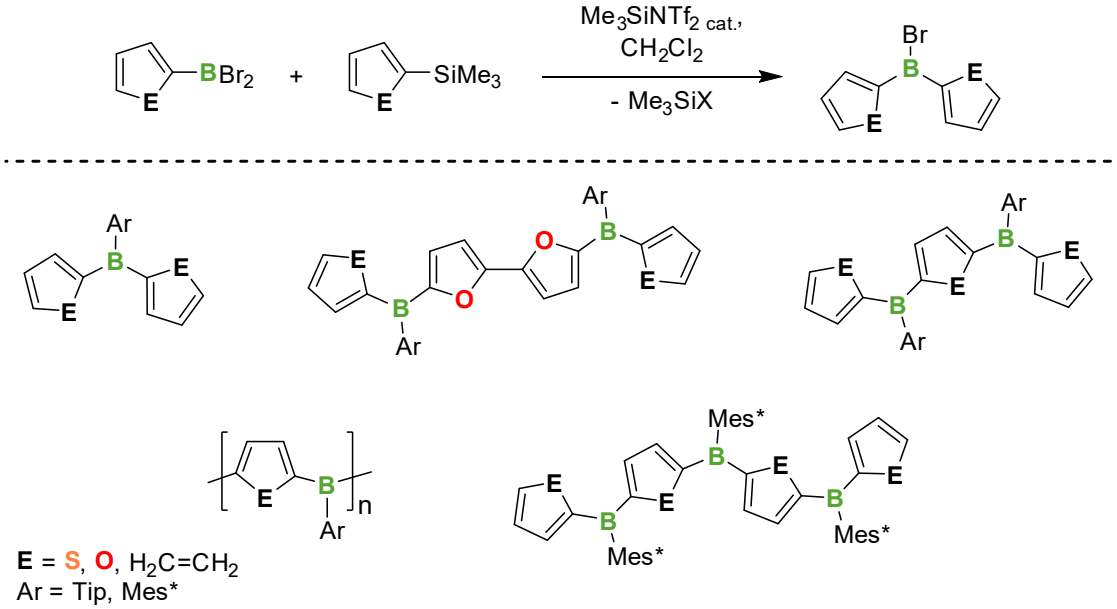

Scheme 2.4.6: *General scheme of catalytic Si/B exchange condensation and resulting materials.*

This metal-free procedure allows Si/B exchange reactions to take place under mild conditions and avoiding toxic substrates or by-products. To gain more information on the mechanisms involving Me_3SiNTf_2 as the catalyst, we conducted an extended study of the system.

2.4.2 Results and Discussion

We started our investigations with the reaction between dibromo(2-thienyl)borane (**6a**) and 2-(trimethylsilyl)thiophene (**7a**). First, we monitored the reaction without a catalyst (Scheme 2.4.7a) by ^1H and $^{11}B\{^1H\}$ NMR spectroscopy. We found that the resonances of the product, **8a**, increased over time at the expense of those of the reactants, **6a** and **7a**; the generation of an intermediate in the course of the reaction could not be observed. This means that the formation of **8a** either proceeds in a single step or through an intermediate that is rather short-lived. So, the rate-determining step (rds) is the reaction between **6a** and **7a**, rather than the transformation of a possible intermediate into the final product. Overall, the reaction proceeded slowly and remained incomplete. We conclude that the rate acceleration in the presence of an electrophilic silyl reagent (i.e. its catalytic activity) is based on the initial reaction between the catalyst and either of the two reactants. Therefore, in the next step, we explored stoichiometric reactions of Me_3SiNTf_2 with **6a** (Scheme 2.4.7b) and **7a** (c), respectively.

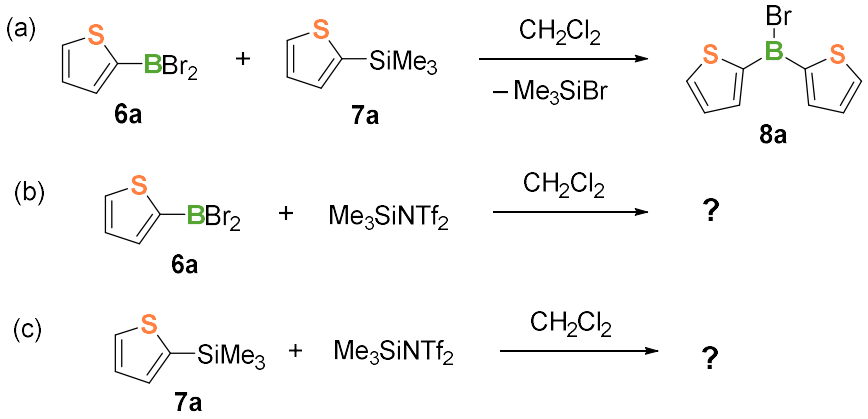

Scheme 2.4.7: *Stoichiometric reactions of catalyst and substrates. Substrates **6a** and **7a** without a catalyst (a), and stoichiometric reactions between Me_3SiNTf_2 and **6a** (b), and between Me_3SiNTf_2 and **7a** (c).*

No reaction was observed between Me_3SiNTf_2 and **7a** within 24 h (Figure 2.4.1b). For the reaction of Me_3SiNTf_2 with **6a**, on the other hand, $^{11}B\{^1H\}$ NMR analysis revealed the rapid formation of new species. While the signal for unreacted **6a** still dominated the spectrum after 14 d, two additional resonances were detected. Based on their chemical shifts (δ = 40.7, 6.5 ppm) we propose the structures shown in Figure 2.4.1c. In the corresponding ^1H NMR spectrum, the resonance for Me_3SiBr was detected (δ = 0.61 ppm), which additionally supports the hypothesis that a substitution reaction has occurred. In the further course of the reaction, in the $^{11}B\{^1H\}$ NMR spectrum an additional broad signal at 49.5 ppm emerged, which we assign to the product **8°** of an oligomerization reaction.

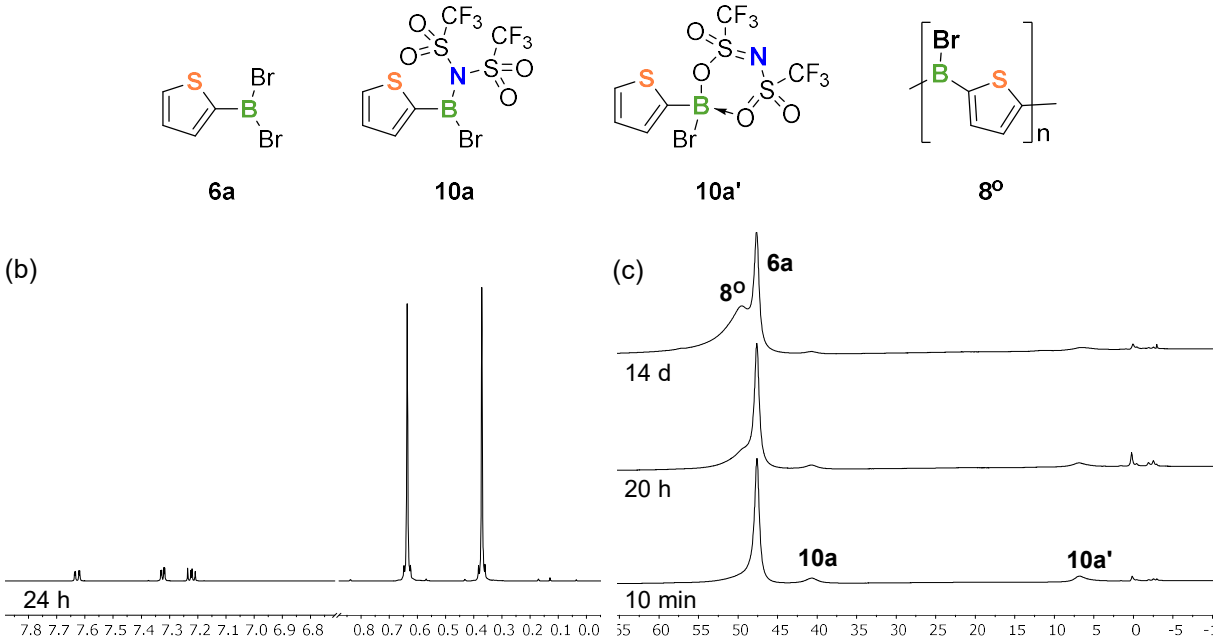

Figure 2.4.1: *In situ NMR spectra of the reactions of substrates **7a** (^1H NMR, b) and **6a** ($^{11}B\{^1H\}$ NMR, c) with stoichiometric amounts of Me_3SiNTf_2.*

These results are consistent with the following catalytic cycle (Scheme 2.4.8): In the first step, the catalyst, **9**, reacts with substrate **6a** under formation of the putative reactive intermediate **10a**. Via this reaction, the leaving group Br gets replaced by an even better leaving group: NTf_2, which we assume is very loosely bound. Therefore, compound **10a** may be termed a "masked borinium cation". This means that it shows pronounced electrophilic reactivity, i.e. it reacts like a cation, although it is a neutral compound.

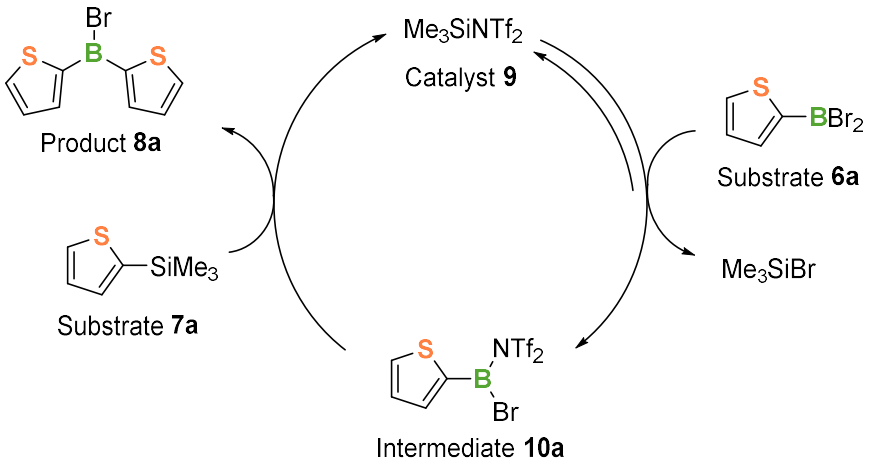

Scheme 2.4.8: *Initial postulated catalytic cycle for the Si/B exchange reaction between **6a** and **7a**.*

When monitoring the catalytic reaction between **6a** and **7a** in the presence of Me_3SiNTf_2 via ^1H NMR spectroscopy (Figure 2.4.2), at an early stage (after 10 min.) we detected, beside the reactant (**6a** and **7a**) and product signals (**8a**), one signal at δ = 7.20 – 7.16 (m) that is assigned to thiophene (the other signal at around δ = 7.40 ppm is overlapped by a signal of product **8a**; for a COSY NMR of a later stage of the reaction, see Figure S5.4.4), and another set of resonances (**8b**) corresponding to a compound with one 2-substituted and one 2,5-disubstituted thiophene ring, and one $SiMe_3$ group.

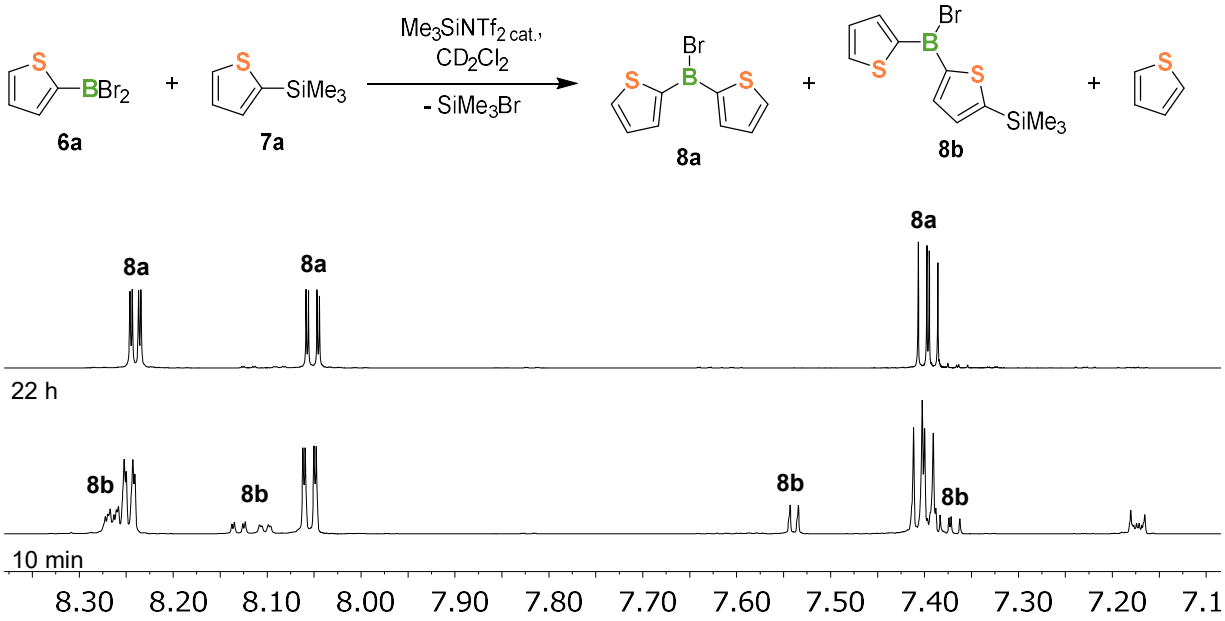

Figure 2.4.2: *Extended reaction scheme for the catalytic reaction of* ***6a*** *and* ***7a****. Aromatic region of the* ^{1}H *NMR spectrum of the reaction mixture.*

We assign the latter resonances to compound **8b**, which we confirmed by independent synthesis thereof from **6a** and **7b** (Scheme 2.4.9). Subsequent derivatization of **8b** with Mes*Li yielded the air- and water-stable compound **11b**, which was obtained in pure form after column chromatographic workup.

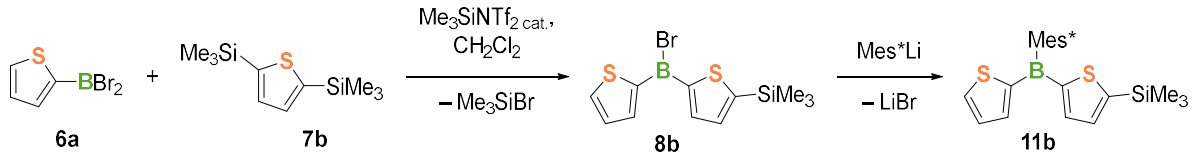

Scheme 2.4.9: *Synthesis of triarylborane* ***6b*** *via bromo(dithienyl)borane* ***8b****.*

Further monitoring of the catalytic reaction between **6a** and **7a** revealed that compound **8b** and thiophene were formed in quantities up to 35 % relative to the desired product in the mixture (Figure S5.4.3). However, both of them did not persist. After their initial buildup, towards the end of the reaction, their signals decreased again in intensity. After 22 h, compound **8a** was the only observable product and, besides Me_3SiBr and the re-formed catalyst, no further by-products were detected.

The observation of the formation of **8b** in the catalytic reaction of **6a** with **7a** can be explained by assuming an S_EAr type mechanism (Scheme 2.4.10). This involves an electrophilic attack of the reactive species **10a** at the aromatic (thienyl) ring of **7a** under formation of an intermediate arene σ-complex. This may occur in either of two different regiochemistries. Route 1: Attack at C2 yields the zwitterionic *Wheland-like* intermediate **Int-I**. Subsequent elimination of Me_3SiNTf_2, i.e., abstraction of the $SiMe_3$ group by NTf_2, associated with re-aromatization of the heterocycle, gives the observed product **8a**. On the other hand, the

electrophilic attack of **10a** at **7a** may alternatively occur at the 5-position of the latter (route 2), thus leading to the *Wheland* intermediate **Int-II**. According to our computational studies (RI-BP86/def2-SV(P)), this should actually be favored over the attack at C2. The Gibbs free energy of the **Int-I** formation ($\Delta_R G$ = 60 kJ mol^{-1}) is higher than for the formation of **Int-II** ($\Delta_R G$ = 47 kJ mol^{-1}), making it the less likely reaction route under the same reaction conditions. Subsequent elimination of $HNTf_2$ from **Int-II** thus leads to the observed species **8b**.

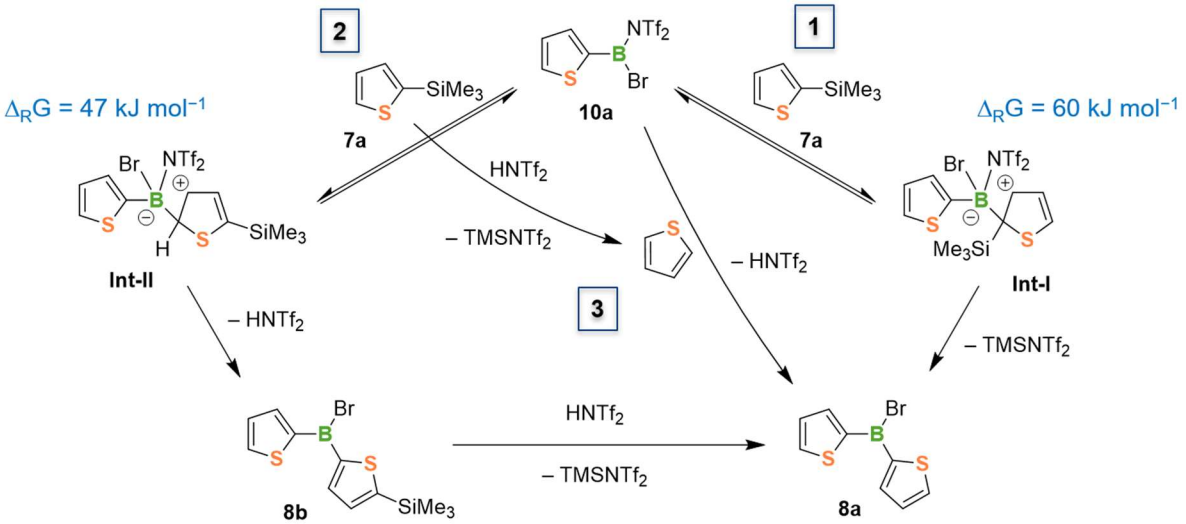

Scheme 2.4.10: *Feasible reaction pathways for the formation of **8a**. Route 1: Si/B exchange. Routes 2 and 3: C–H activation.*

As we have observed that **8b** transforms into **8a** in the further course of the reaction (cf. Figure 2.4.2), it is plausible that this occurs via abstraction of the $SiMe_3$ group of the former by the action of $HNTf_2$, which had been previously formed as the byproduct in the formation of **8b**. To prove this hypothesis, we treated pure **11b** in CH_2Cl_2 with $HNTf_2$ (Scheme 2.4.11, Figure S5.4.5). After 12 minutes, the reaction showed 93 % conversion to **11a** and Me_3SiNTf_2. Consequently, **8b** is indeed an intermediate in the formation of **8a**, hence, route 2 is one feasible pathway for the catalytic Si/B exchange condensation between **6a** and **7a**.

The formed $HNTf_2$ is furthermore also able to abstract a $SiMe_3$ group from the reactant **7a**. This explains the formation of thiophene in the mixture. Subsequently, thiophene can react with **10a** to yield the desired product **8a** through route 3 via C–H borylation. First indications that C–H borylation reactions may be operative were already noted in our above-mentioned study of the stoichiometric reaction of Me_3SiNTf_2 with **6a** (cf. Scheme 2.4.7 and Figure 2.4.1). In this case, an oligomerization reaction was observed that must have proceeded via such a reaction mechanism.

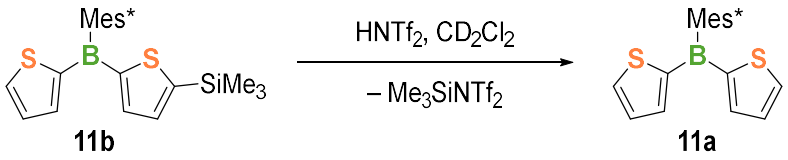

Scheme 2.4.11: *Desilylation reaction of* ***11b*** *to give* ***11a****.*

The reaction to **8a** via **8b** is reminiscent of a tin/boron exchange reaction at a stannylferrocene previously reported by Jäkle et al.[19] In that case, the reaction was also found to proceed via electrophilic C–H borylation, which was facilitated by intramolecular reaction of a pyridyl group attached to the ferrocene unit. Subsequent destannylation at a different position of the molecule led to the final product.

For the C–H borylation pathway in the reaction between **6a** and **7a**, the final desilylation step is crucial, as it completes the catalytic cycle by regeneration of the catalyst, Me_3SiNTf_2. This is clearly demonstrated by the inability of Me_3SiNTf_2 to catalyze an intermolecular borylation of thiophene by **6a** if no further additives are present (Scheme 2.4.12a). Without regeneration of Me_3SiNTf_2, the maximum yield of the desired product is equivalent to the amount of Me_3SiNTf_2 used (Figure S5.4.6a). We conclude that $HNTf_2$ is not capable of generating the reactive species **10a** from **6a**. We hypothesized that the catalyst, Me_3SiNTf_2, may also be regenerated through an external $SiMe_3$ source. To demonstrate this, we performed a three-component reaction of **6a**, thiophene, and trimethyl(phenyl)silane **7j** (Scheme 2.4.12b). We have previously noticed that **7j** is a relatively poor substrate for catalytic Si/B exchange reactions.[15,16] Indeed, our three-component reaction resulted in selective borylation of thiophene by **6a** in the presence of **7j** with concomitant desilylation of the latter.[20] The reaction yielded full conversion to **8a** (besides benzene and Me_3SiCl) after 24 h (Figure S5.4.6b).

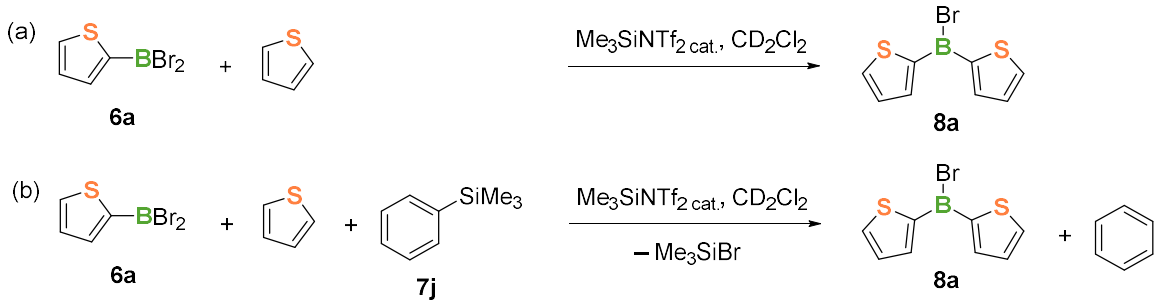

Scheme 2.4.12: *C-H activation capabilities of* Me_3SiNTf_2*. Reaction schemes without (a) and with (b)* $SiMe_3$ *source.*

These results raise the question if route 2 of Scheme 2.4.10 might be the major pathway and whether the initially postulated route 1 is operative at all. Several observations unambiguously evidence that an *ipso*-borodesilylation in the manner of route 1 is in principle indeed possible. One of these observations is the successful synthesis of **8b** (see Scheme 2.4.9). In this case, a competing C–H borylation pathway is very unlikely because both positions at the thiophene

ring in **7b** that are usually involved in such reactions are blocked with $SiMe_3$ groups. Furthermore, successful polymerization reactions (cf. Scheme 2.4.6)[15,16] as well as Si/B exchange condensations using 2-methyl-5-(trimethylsilyl)thiophene **7g** as the substrate (vide infra) lead to the same conclusion.

With a view to get an estimate of the relative preference of Si/B exchange vs. C–H borylation, we additionally performed catalytic reactions involving 3- and 4-substituted substrates **6c-f** and **7c-f** (Scheme 2.4.13). These reactants were chosen because the positions of the two substituents can be clearly distinguished in the product and, furthermore, both alkyl substituents have different steric demand compared to each other and compared to an unsubstituted position (C_{Thi}–H); so, steric effects on the reaction course should also be observed.

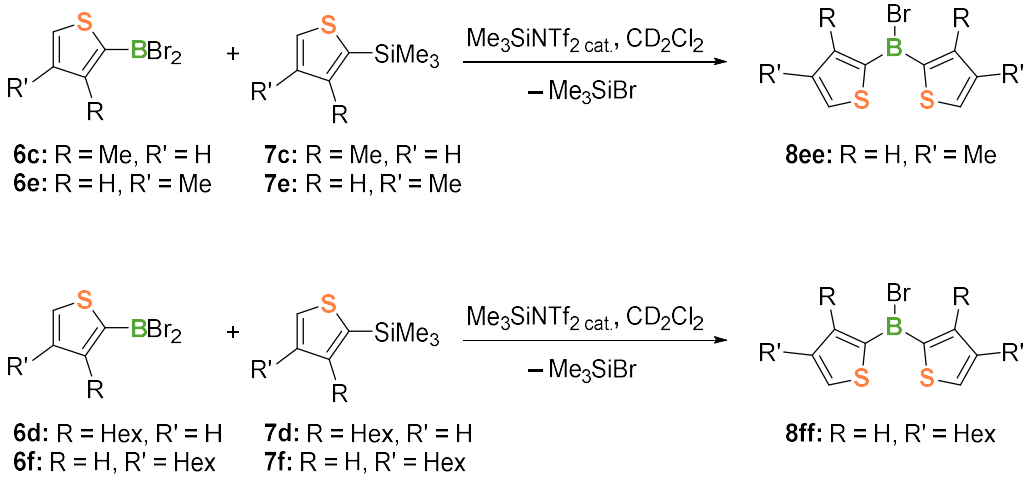

Scheme 2.4.13: *Si/B exchange reactions of substrates **1c-f** and **2c-f**.*

The different reaction pathways and their products are illustrated in Scheme 2.4.14 using the reaction of **6c** and **7c** as an example. Si/B exchange and C–H activation would give two by ^{1}H NMR spectroscopy clearly distinguishable products **8cc** and **8ce.** A disilylation of substrate **7c** on the other hand could give either of both products, via C–H activation processes.

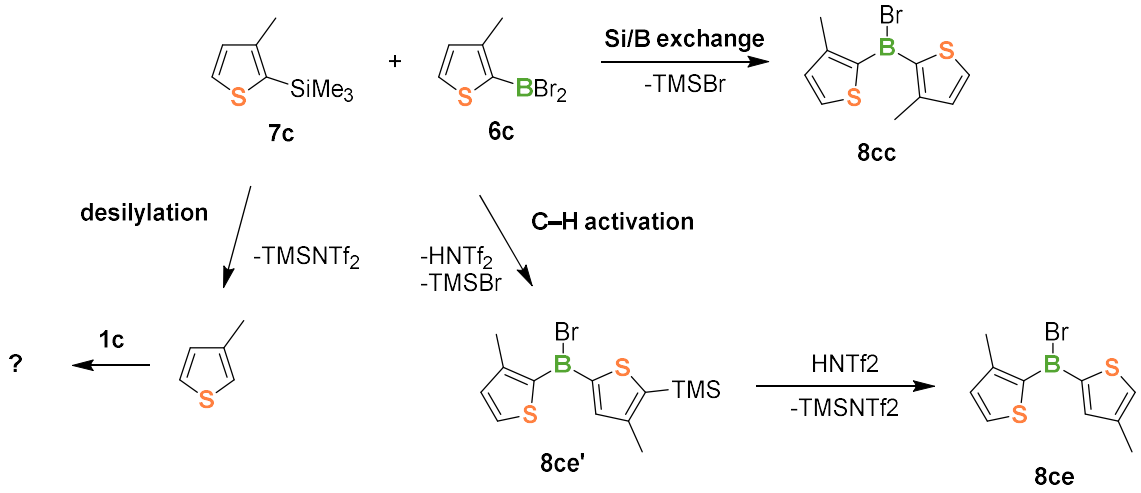

Scheme 2.4.14: *Different reaction pathways for the catalytic reaction of* ***6c*** *and* ***7c****: Si/B exchange, C–H activation and disilylation of* ***7c****.*

During the first 3 h of the reactions, the formation of different species was observed (Figure S5.4.7, Figure S5.4.8), which correspond to the different species described in Scheme 2.4.14. The first C–H activation product (**8ce'**) has a characteristic aromatic singlet signal in the ^{1}H NMR spectrum for C_{Thi}–H at the silylated thiophene, which could be observed in almost all of the reactions involving the hexyl-thiophene substrates. These reactions were slower than the ones with the methyl-thiophene substrates. This study revealed that although different reaction pathways were initially conceivable for the reactions, at extended reaction times of 48 h only one product was obtained in each case (Scheme 2.4.13). Independent of the combination of substituents, species **8ee** or **8ff** were ultimately formed, which represent the 4,4'-substituted products. This made a final evaluation of the dominant regiochemistry or a ratio between the reaction routes impossible under the applied conditions. Observations of the early stages of the reactions, however, allow for a visual estimation of the ratios (Figure S5.4.7, Figure S5.4.8). In all of the investigated reactions, the C–H activation route seemed to be preferred.

In order to eliminate competing C–H activation pathways (routes 2 and 3), we decided to carry out further investigations on the model reaction between **6g** and **7g**, in which the 5-position is blocked with a methyl group (Scheme 2.4.15a). In this case, we observed a follow-up reaction of the product, **8g**, with substrate **7g** leading to the triarylborane **12g** (Scheme 2.4.15b). However, this was only observed if an excess of **7g** was present as well as higher catalyst loadings of 20% or more. Under these conditions, the reaction to **12g** was complete within 72 h (Figure S5.4.9). This kind of follow-up reaction has also been observed in the reaction between **6a** and an excess of **7a**, though at significantly slower rates. With 2 equiv of **7a**, about 90% conversion to product **12a** was observed after 18 d when a catalyst loading of 5% was employed (Figure S5.4.11).

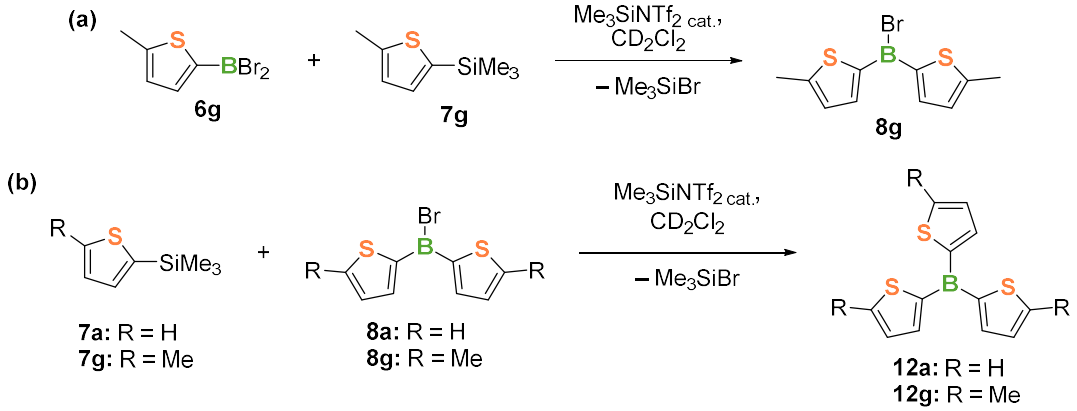

Scheme 2.4.15: *Reactivity of 5-methylated substrates* ***6g*** *and* ***7g*** *and the follow up reaction with higher catalyst loading.*

In the next step, we explored stoichiometric reactions of Me_3SiNTf_2 with **6g** and **7g**, respectively. Compound **7g** showed no reactivity towards Me_3SiNTf_2 even after 24 h, analogous to **7a**. For **6g**, on the other hand, $^{11}B\{^1H\}$ NMR analysis revealed rapid formation of additional species, similar to **6a**. The signal for **6g** remained the main signal, while mainly two additional species were formed with resonances at δ = 41.8 and 6.9 ppm, suggesting a trivalent boron species, which we assign to **10g**, and a quaternary boron species. The absence of a signal for a linear oligomer as observed in the reaction of **6a** (cf. Figure 2.4.1) evidences the successful suppression of C–H activation processes.

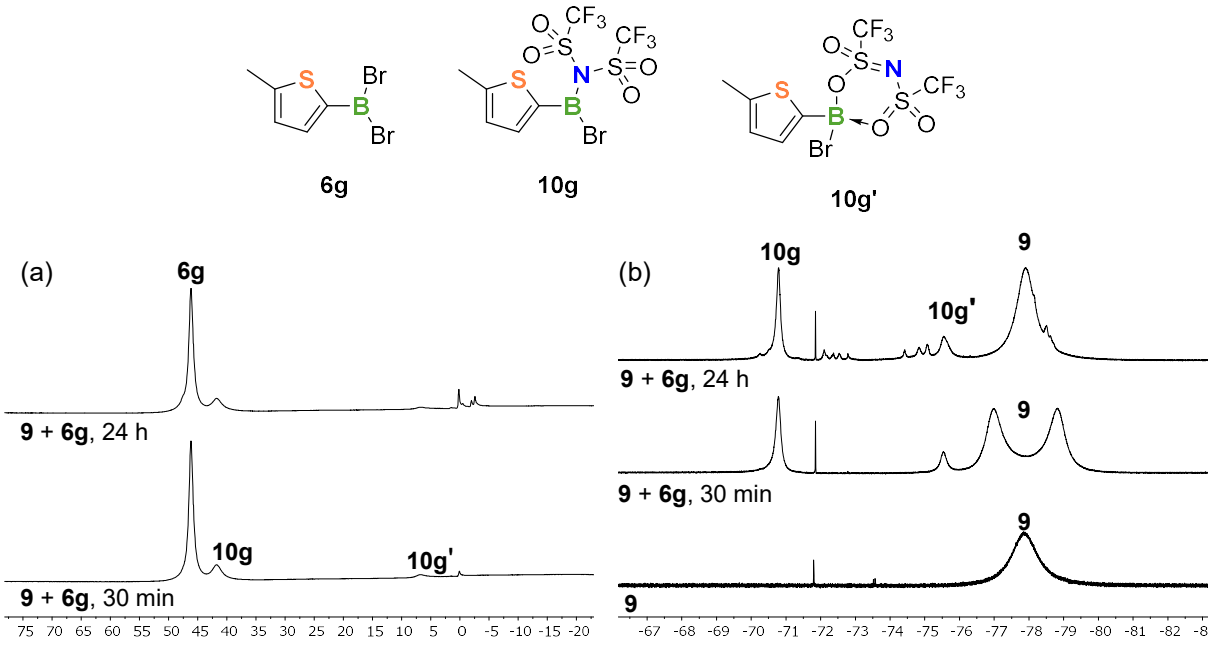

Figure 2.4.3: *$^{11}B\{^1H\}$ NMR (a) and $^{19}F\{^1H\}$ NMR (b) spectra of substrate* ***6g*** *with stoichiometric amounts of Me_3SiNTf_2* ***9*** *after 30 min and after 24 h.*

$^{19}F\{^1H\}$ NMR analysis of that mixture revealed a change of the initial broad singlet for Me_3SiNTf_2 (δ = −77.9 ppm) to four signals (δ = −78.8, −77.0; −75.5; −70.8), that can be assigned to three species. This furthermore confirms a contribution of the triflimide group in

the formation of the new species (Figure 2.4.3). After 24 h, side reactions were observed, which lead to the formation of more species with resonances between 0 and −2.5 ppm in the $^{11}B\{^1H\}$ NMR spectrum and −72.1 and −75.1 in the $^{19}F\{^1H\}$ NMR spectrum.

We observed that the $^{19}F\{^1H\}$ NMR signal (δ = −77.9 ppm) for the CF_3 groups in pure Me_3SiNTf_2 **9** was unexpectedly broad (FWHM: 380 Hz) at room temperature. Experiments at varying temperature (VT NMR) show decoalescence to two signals of the same integral (δ = −78.9, −77.0 at −90 °C; Figure 2.4.5, left); the coalescence temperature is between 0 and −20 °C (cf. Figure S5.4.15). Earlier investigations on triflimide species have shown that such kind of signal set is a sign of an asymmetrically substituted triflimide.[21,22] Berionni and coworkers synthesized NTf_2^- Lewis adducts of 9-boratriptycene **13** (Figure 2.4.4).

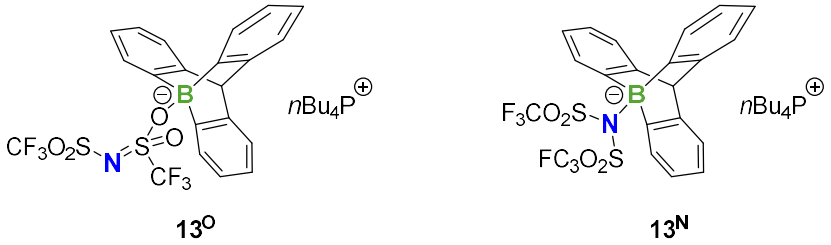

Figure 2.4.4: *NTf_2^- Lewis adducts of 9-boratriptycene **13^O** and **13^N**.*

In the described reaction, three signals in the ^{19}F NMR spectrum were detected (in CD_2Cl_2): Two of them were observed as sharp signals at δ = −78.8 and −76.0 ppm and were assigned to an *O*-isomer **13^O**. The third signal appeared broad at δ = −79.0 ppm, which was assigned to an *N*-isomer **13^N**.[21]

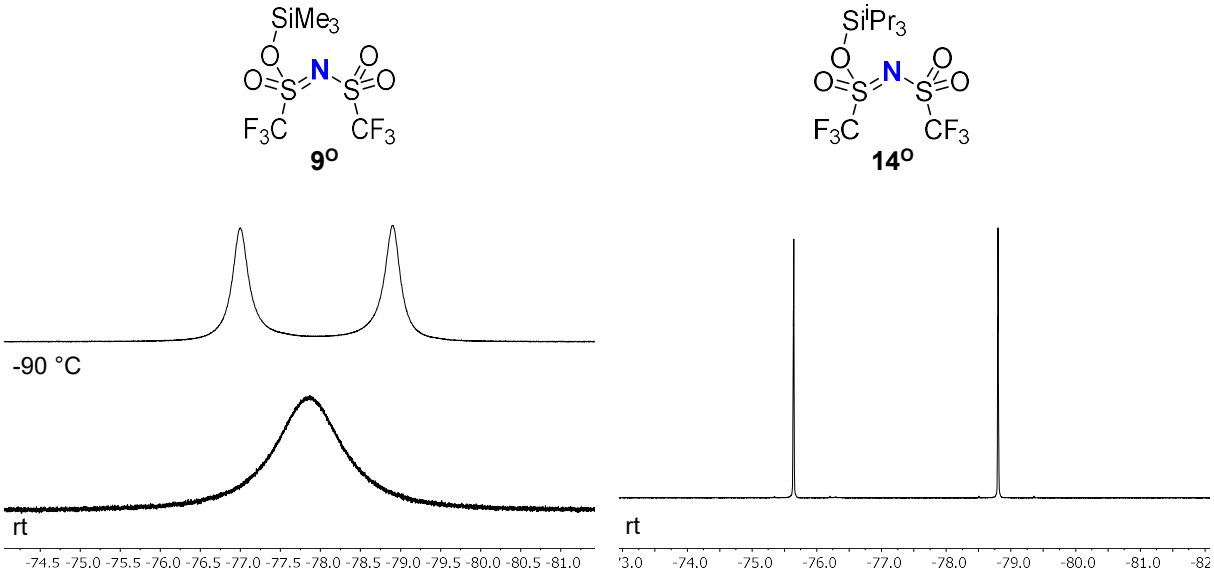

Figure 2.4.5: *$^{19}F\{^1H\}$ NMR of Me_3SiNTf_2 at room temperature and -90 °C (left), and $TIPSNTf_2$ at room temperature (right).*

These results suggest that Me_3SiNTf_2 is present in an asymmetric O–Si bond structure **9^O** when in CH_2Cl_2 solution at room temperature. Our computational investigations (B3LYP/6-311++G**; PCM method for solvent effects) underline that statement (Table 2.4.1). They revealed that structure **9^O** is favored over the N–Si structure **9^N** by ΔE = 20 kJ mol^{-1} (in CH_2Cl_2 solution).

Table 2.4.1: *Energy differences between the different structures of the catalysts Me_3SiNTf_2 **9** and $TIPSNTf_2$ **14** in CH_2Cl_2 or $CHCl_3$ solution (B3LYP/6-311++G**; PCM method for solvent effects). Lower energy was set to 0.*

ΔE [kJ mol^{-1}]	9^N	9^O	14^N	14^O
CH_2Cl_2	+19.9	0	+57.0[a]	0
$CHCl_3$	+19.3	0	+55.9[a]	0

[a]single-point calculations.

Additionally, we synthesized a silyl triflimide having the bulkier triisopropylsilyl group (TIPS), compound **14**, as a potential further Si/B exchange catalyst. It features a set of sharp signals in the $^{19}F\{^1H\}$ NMR spectrum at room temperature (Figure 2.4.5, right), which we assign to the Si–O structure **14^O**. The thermodynamic energy difference to the respective N–Si isomer **14^N** is computationally predicted to be significantly higher (ΔE = 60 kJ mol^{-1}, in CH_2Cl_2 solution) in comparison to the Me_3SiNTf_2 (Table 2.4.1). Apparently, the sterically more demanding TIPS group causes a stronger preference of the Si–O structure **14^O**. The barrier for the migration of the $SiMe_3$ group in Me_3SiNTf_2 from an oxygen atom on one triflate group to one on the other one is significantly lower, which allows for this process to occur at room temperature.

After discovering a change in the catalyst structure, we investigated the structure of the catalyst before, during, and after the catalysis (Figure 2.4.6). To this end, we recorded $^{19}F\{^1H\}$ NMR spectra from different stages of the catalysis. We discovered that the formation of the species **10g** resulting from the interaction of catalyst and **6g** was proportionally slow (ii → iii). **10g** is formed under the formation of Me_3SiBr (Figure S5.4.18). When **7g** was added to the mixture, all previously formed signals disappear in favor of a single, more sharp singlet at δ = -78.8 ppm (iv). Therefore, we propose that Me_3SiNTf_2 is re-formed as **9^N** after one iteration of the catalysis. VT NMR analysis at -90 °C confirmed this statement, giving only a single sharp signal for Me_3SiNTf_2 with no peak separation (Figure S5.4.19). After the reaction was finished, a second portion of **6g** (v) was added. Now, only a broadened $^{19}F\{^1H\}$ NMR signal at δ = -77.6 ppm was formed, which can be assigned to a species with a quaternary boron that resonated at δ_B = 10.0 ppm. This time, species **10g"** is feasible. Additionally, no trivalent boron species was formed, which was evident by absence of signals at around δ = 41 ppm in $^{11}B\{^1H\}$ NMR (Figure S5.4.20) and around δ = -70 ppm in the $^{19}F\{^1H\}$ NMR spectrum, which we believe to describe the species **10g** (Figure 2.4.3). When **7g** was added to complete the second

catalysis iteration, $^{19}F\{^{1}H\}$ NMR analysis suggested the formation of **9^{N}** as in the first iteration of the catalysis.

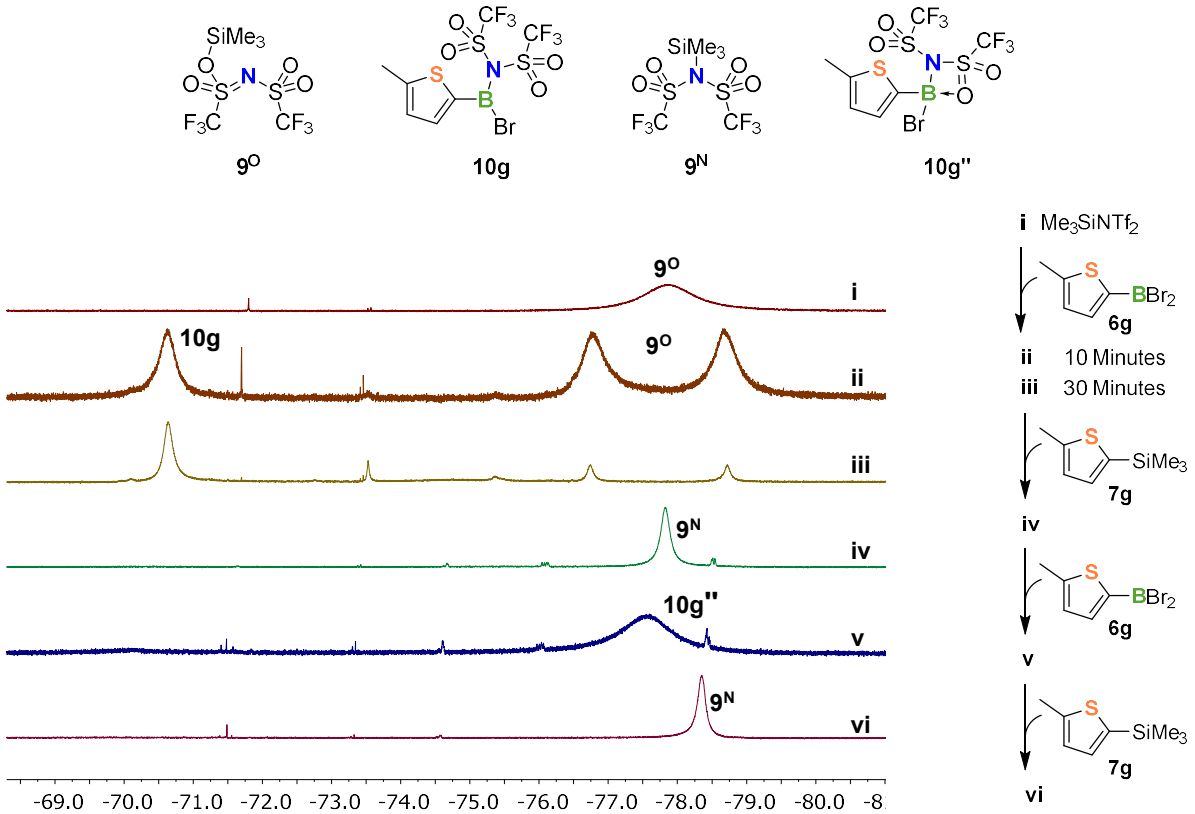

Figure 2.4.6: *$^{19}F\{^{1}H\}$ NMR spectra of the reaction mixture using Me_3SiNTf_2 at different stages of the reaction.*

Similar observations pointing to the formation of an N–Si species **9^{N}** during the reaction was also made when using $TIPSNTf_2$ **14** as catalyst for the reaction of **6g** and **7g** (Figure 2.4.7). Compared to using Me_3SiNTf_2, this reaction is about five times slower. During the reaction, the two CF_3 signals broadened and changed from their initial 1:1 integral ratio, which we interpret as a slow formation of a single signal that is overlapping with one of the original signals. In this case, the formed species is Me_3SiNTf_2, which can be clearly distinguished after 20 h of reaction time (ix). During the reaction, no other species were observed in $^{19}F\{^{1}H\}$ NMR.

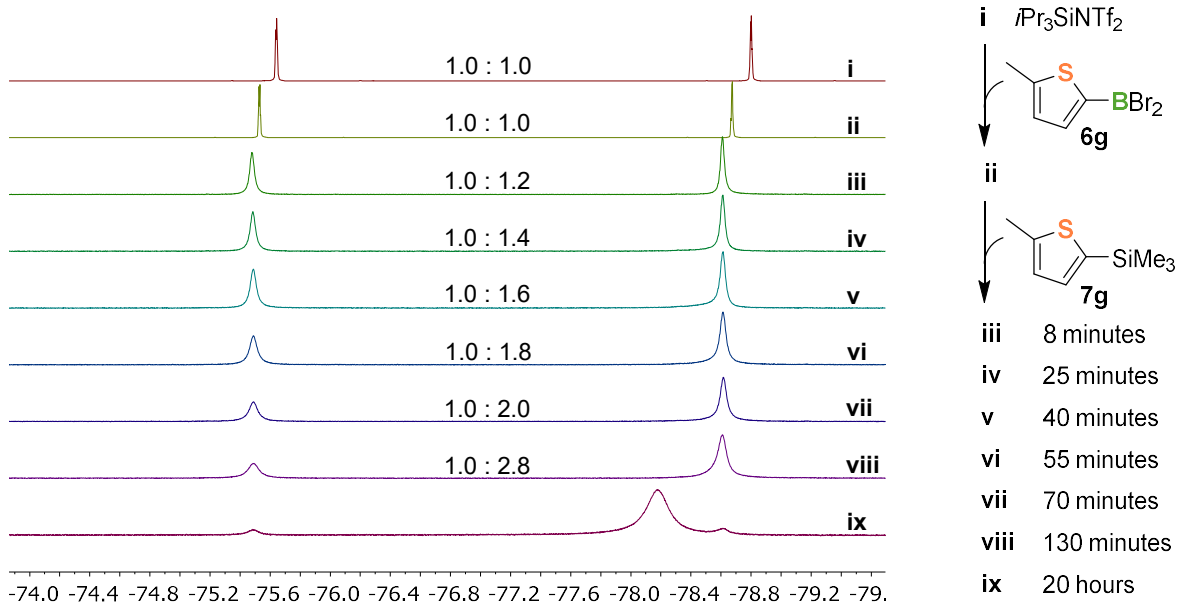

Figure 2.4.7: *$^{19}F\{^{1}H\}$ NMR spectra of the reaction mixture using $TIPSNTf_2$ at different stages of the reaction.*

This information led us to the proposal of a modified reaction scheme (Scheme 2.4.16). It involves a first reaction (1) in which species **10g** is formed from precatalyst $\mathbf{9^O}$ and **6g** under formation of Me_3SiBr. Subsequently, **10g** reacts with **7g** to product **8g**, after which $\mathbf{9^N}$ persists. In the following iterations (2) this species reacts with **6g** to give quaternary boron species **10g"**. Together with **7g**, this species re-forms the N–Si catalyst $\mathbf{9^N}$ under the formation of Me_3SiBr and formation of product **8g**.

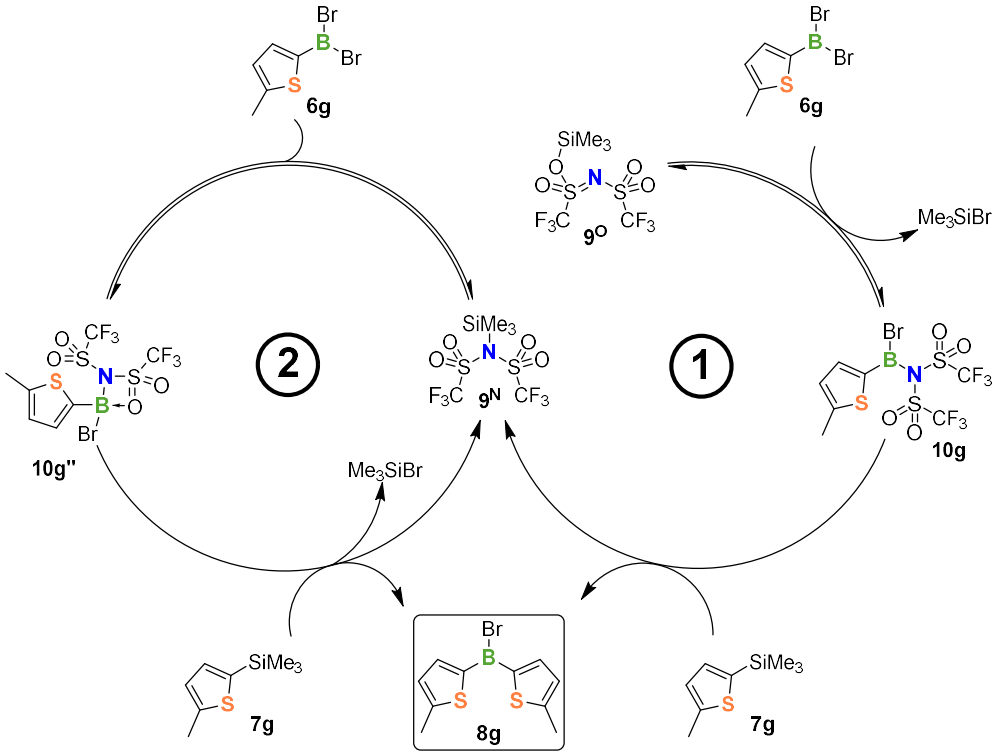

Scheme 2.4.16: *Proposed catalytic cycle of the Si/B exchange reaction between **6g** and **7g**.*

To obtain kinetic information from that reaction, variable time normalization analysis (VTNA) according to the model of Burés was applied (Figure 2.4.8).[23–26] This analysis enables the visual comparison of concentration reaction profiles by variable normalization of their reaction time scale and determination of the kinetic orders in the substrates and catalyst. To this end, the time-dependent concentration profiles of the substrates and the product in the reaction mixture were determined via ^{1}H NMR analysis (Figure S5.4.22 – Figure S5.4.26). The profiles of conducted experiments differ by the starting concentration of one reactant (Figure 2.4.8a-d) but need to be overlaying to be comparable. They will only overlay when the time axis is replaced by the time integral of the concentration of **6g** raised to the correct power α (Equation 1).[24] Analogously, the concentration of **7g** has raised to the correct power β (Equation 2). Variables α and β then directly give the respective order in substrates (Figure 2.4.8a-d, red exponents). Our observations of the reaction mixture showed that the concentration of the catalyst **9** remained constant during the reaction, which simplifies its mathematical term compared to the other reactants (Equation 3).[24]

$$\int_{t=0}^{t=n}[\mathbf{6g}]^{\alpha}dt = \sum_{i=1}^{n}\left(\frac{[\mathbf{6g}]_i+[\mathbf{6g}]_{i-1}}{2}\right)^{\alpha}(t_i - t_{i-1}) \quad (1)$$

$$\int_{t=0}^{t=n}[\mathbf{7g}]^{\beta}dt = \sum_{i=1}^{n}\left(\frac{[\mathbf{7g}]_i+[\mathbf{7g}]_{i-1}}{2}\right)^{\beta}(t_i - t_{i-1}) \quad (2)$$

$$\int_{t=0}^{t=n}[\mathbf{9}]^{\gamma}dt = t[\mathbf{9}]_0\Delta t \quad (3)$$

Through variation of the catalyst loading and starting concentrations of the substrates **6g** and **7g**, their kinetic orders could be determined: α = 1, β = 0, and γ = 0.75 (Figure 2.4.8a-c). Additionally, the observed rate constant of the reaction was determined by comparison of multiple reactions and assess the slope of a linear regression line (k_{obs} = 1.42 M^{-2} min^{-1}, Figure 2.4.8d). The determined values are in accordance with the proposed catalysis cycle. From the information of the kinetic orders, combined with our previous observations, the free catalyst Me_3SiNTf_2 **9** could be designated as resting state of the catalyst. Additionally, the studies allowed for determination of the rate determining step, which is the formation of species **10g** and **10g"**.

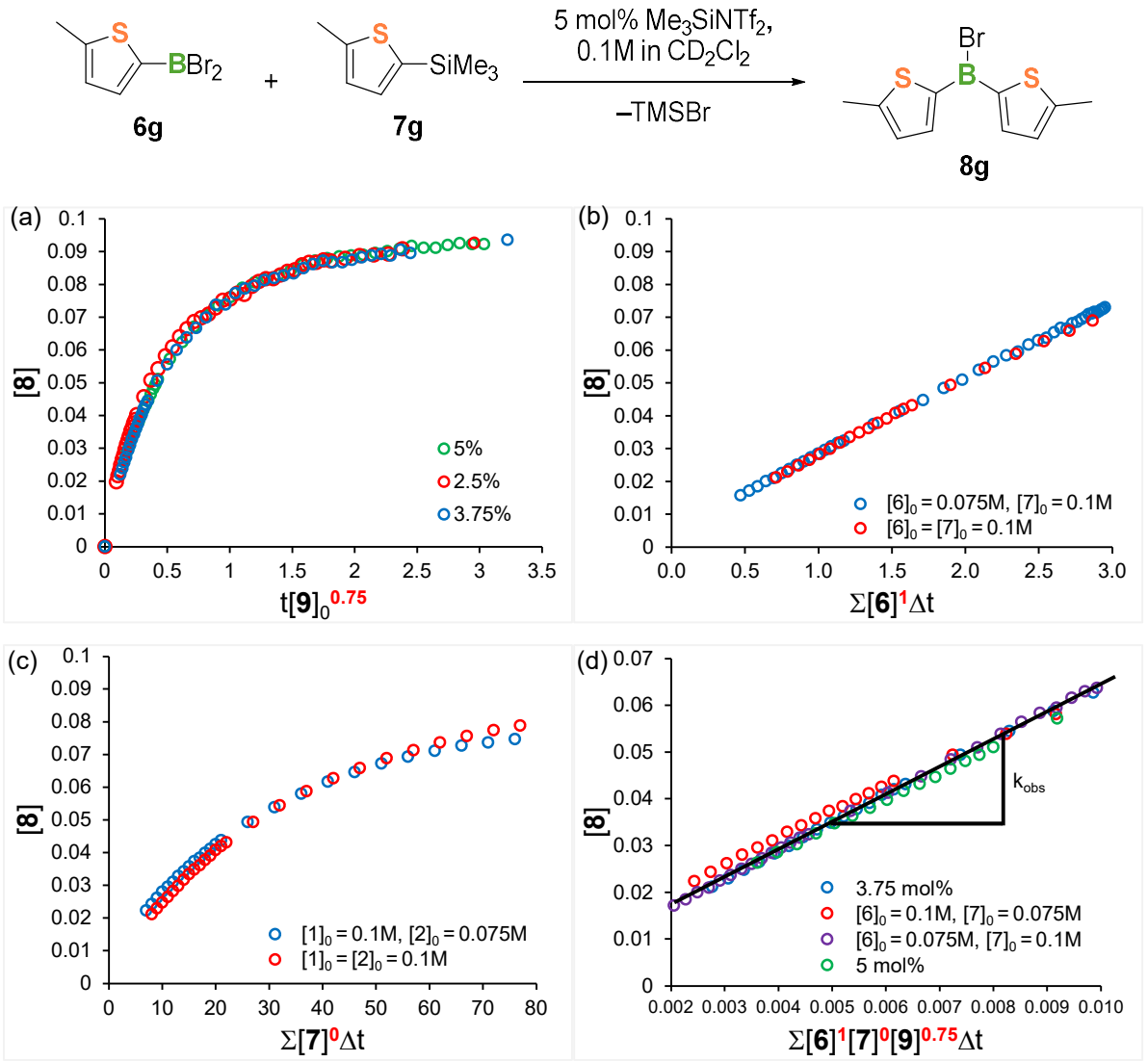

Figure 2.4.8: *Results of the VTNA analysis of the Si/B exchange reaction between* ***6g*** *and* ***7g****. General reaction scheme (top), variation of catalyst loading (a), variation of starting concentration of* ***6g*** *(b), variation of starting concentration of* ***7g*** *(c), and determination of observed rate constant* k_{obs} *(d).*

Finally, we performed cross reactions between different (het)aryl-reactants and studied the time of the complete consumption of the (het)aryl-$SiMe_3$ species **7** via ^1H NMR analysis (Table 2.4.2, see Figure S5.4.27 – Figure S5.4.38). Here, this guiding value was used for putting the reactivity of the systems in relation to each other. It is important to note, that this does not describe the time of the reaction until full conversion to the expected products **8** by Si/B exchange reaction. As described earlier, routes 2 and 3 (Scheme 2.4.10) also lead to formal consumption of the (het)aryl-$SiMe_3$ species **7** by desilylation.

We found that a more electron-poor substituent on the BBr_2 species **6** and a more electron-rich substituent on the $SiMe_3$ species **7** seemed to have a favorable effect on the reaction. The use of species 2-methyl-5-(trimethylsilyl)thiophene **7g** and 2-(trimethylsilyl)furan **7i** led to very similar consumption times, thereby underlining the similarity of their electronic situation. For trimethyl(phenyl)silane **7j**, the slowest conversion rates of the investigated trimethylsilyl

substrates were observed. The corresponding reactions featured <20 % conversion of **2j** in 24 h reaction time. The fastest conversion was observed for the reaction between **6j** (most electron-poor) and **7g** (most electron-rich). Here, **7g** was consumed in less than 7 min. The choice of species **7** turned out to have a much greater effect on the reaction time than the choice of species **6**.

Table 2.4.2: *Consumption time of species **2** when using different (het)aryl species in minutes.*

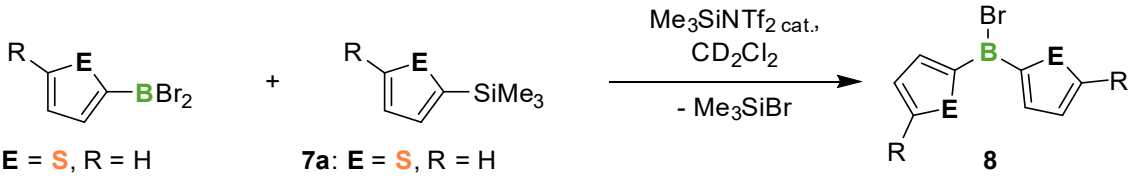

6a: **E** = S, R = H
6g: **E** = S, R = Me
6j: **E** = $H_2C{=}CH_2$, R = H

7a: **E** = S, R = H
7g: **E** = S, R = Me
7i: **E** = O, R = H
7j: **E** = $H_2C{=}CH_2$, R = H

substrates	time of full conversion [min]			
	7i	**7g**	**7a**	**7j**
6g	25	24	37	10%[a]
6a	17	22	66	15%[a]
6j	15	8[b]	82	20%[a]

[a]Conversion after 24 h reaction time. [b]First data point in our investigations is usually collected after 8 minutes.

2.4.3 Conclusion

In this chapter, the mechanism of the catalytic Si/B exchange reaction by Me_3SiNTf_2 was investigated in detail. In the model reaction of substrates **6a** and **7a**, besides expected Si/B exchange processes, the occurrence of C–H activation routes was additionally observed. Interactions between the dibromo(thienyl)borane **6a** and the catalyst were evidenced by the observation of new intermediates via in situ ^{1}H, $^{11}B\{^{1}H\}$ and $^{19}F\{^{1}H\}$ NMR spectroscopy. Blocking the 5-position of the substrates allowed for prevention of the C–H activation routes, which enabled the observation and analysis of the Si/B exchange mechanism of **6g** and **7g**. A structural change of the catalyst from $\mathbf{9^O}$ to $\mathbf{9^N}$ during the process was proposed. The position of the silyl substituent at the triflimide was found to have an effect on the catalysts' behavior in the reaction. Via VTNA, important characteristics of the catalysis were determined: kinetic orders in the substrates **6g** (α = 1) and **7g** (β = 0), the order in the catalyst **9** (γ = 0.75), as well as the observed rate constant of the reaction (k_{obs} = 1.42 M^{-2} min^{-1}). Ultimately, a catalytic cycle was proposed (Scheme 2.4.16). In addition, it was found that a more electron-poor species **6** and a more electron-rich species **7** favored the overall reaction rate. Me_3SiNTf_2 shows its versatility, being highly effective as catalyst in B–C bond formation reactions, whether C–Si or

C–H bond activation. Additionally, the possibility of threefold arylation of the boron center of **6a,g** was discovered, though it proceeded significantly slower than the formation of the second B–C bond.

Further investigations should include computational studies towards the structure of intermediates and transition states, especially with regards to the triflimide substituent, to support the experimentally established proposals.

2.4.4 Experimental Section

General procedures. All manipulations were performed under an atmosphere of dry argon using standard Schlenk techniques or in a MBraun glove box. Solvents (CH_2Cl_2, *n*-hexane, *n*-pentane, toluene) were dried and degassed by means of a MBraun SPS-800 solvent purification system. Deuterated solvents for NMR spectroscopy were dried and degassed at reflux over CaH (CD_2Cl_2, $CDCl_3$) and freshly distilled prior to use. **9**,[27] 2,4,6-tritertbutylphenyl lithium,[28] **6a,b,g,j** and **7a-j** were prepared according to procedures described in the literature.[15,16,29] Tribromoborane was purchased from commercial sources and used as received.

NMR spectra were recorded at 25 °C on a Bruker Avance III HD spectrometer operating at 300 MHz or on a Bruker Avance III Nanobay 400 operating at 400 MHz. Chemical shifts were referenced to residual protic impurities in the solvent (^{1}H) or the deuterated solvent itself (^{13}C) and reported relative to external $SiMe_4$ (^{1}H, ^{13}C), $BF_3{\cdot}OEt_2$ (^{11}B) or $CFCl_3$ (^{19}F) standards.

general procedure for the synthesis of 6c-g. To a solution of BBr_3 (2.63 g, 10.0 mmol) in CH_2Cl_2 (10 mL) was added **7c-g** (10 mmol) at 0 °C and stirred for 2 h. All volatiles were removed in vacuo at 0 °C. The crude product was purified by distillation and **6c-f** was obtained as colorless to brown liquids.

6c: Yield: 82 %; ^{1}H NMR (500 MHz, $CDCl_3$): δ = 7.88 (d, *J* = 4.7 Hz, 1H; Thi-*H*), 7.16 (d, *J* = 4.7 Hz, 1H, Thi-*H*), 2.66 (s, 3H, C*H*$_3$); ^{11}B{^{1}H} NMR (160 MHz, $CDCl_3$): δ = 46.1 (s); ^{13}C{^{1}H} NMR (126 MHz, $CDCl_3$): δ = 155.4 (Thi-*C*-C), 139.9 (Thi-*C*-H), 135.1 (Thi-*C*-H), 18.9 (*C*H$_3$).

6d: Yield: 74 %; ^{1}H NMR (500 MHz, $CDCl_3$): δ = 7.88 (d, *J* = 4.7 Hz, 1H, Thi-*H*), 7.20 (d, *J* = 4.7 Hz, 1H, Thi-*H*), 3.13 – 3.06 (m, 2H, hex-*H*), 1.69 – 1.60 (m, 2H, hex-*H*), 1.43 – 1.35 (m, 2H, hex-*H*), 1.35 – 1.27 (m, 4H, hex-*H*), 0.94 – 0.84 (m, 3H, hex-*H*); ^{11}B{^{1}H} NMR (160 MHz, $CDCl_3$): δ = 46.1 (s); ^{13}C{^{1}H} NMR (126 MHz, $CDCl_3$): δ = 160.9 (Thi-*C*-C), 140.1 (Thi-*C*-H), 134.0 (Thi-*C*-H), 31.8 (hex-*C*), 31.8 (hex-*C*), 31.6 (hex-*C*), 29.5 (hex-*C*), 22.8 (hex-*C*), 14.2 (hex-*C*).

6e: Yield: 84 %; ^{1}H NMR (500 MHz, $CDCl_3$): δ = 7.84 (s, 1H, Thi-*H*), 7.70 (s, 1H, Thi-*H*), 2.34 (s, 3H, C*H*$_3$); ^{11}B{^{1}H} NMR (160 MHz, $CDCl_3$): δ = 47.4 (s); ^{13}C{^{1}H} NMR (126 MHz, $CDCl_3$): δ = 145.9 (Thi-*C*-H), 141.3 (Thi-*C*-C), 138.7 (Thi-*C*-H), 15.4 (*C*H$_3$).

6f: Yield: 76 %; ^{1}H NMR (500 MHz, $CDCl_3$): δ = 7.86 (d, *J* = 1.3 Hz, 1H, Thi-*H*), 7.72 (d, *J* = 1.4 Hz, 1H, Thi-*H*), 2.69 – 2.63 (m, 2H, hex-*H*), 1.68 – 1.59 (m, 2H, hex-*H*), 1.39 – 1.26 (m, 6H, hex-*H*), 0.89 (s, 3H, hex-*H*); ^{11}B{^{1}H} NMR (160 MHz, $CDCl_3$): δ = 47.4 (s); ^{13}C{^{1}H} NMR (126 MHz, $CDCl_3$): δ = 147.0 (Thi-*C*-C), 145.1 (Thi-*C*-H), 138.1 (Thi-*C*-H), 31.7 (hex-*C*), 30.7 (hex-*C*), 30.1 (hex-*C*), 29.0 (hex-*C*), 22.7 (hex-*C*), 14.2 (hex-*C*).

6g: Yield: 85 %; ^{1}H NMR (500 MHz, $CDCl_3$): δ = 7.89 (d, *J* = 3.7 Hz, 1H, Thi-*H*), 7.03 (dq, *J* = 3.7, 0.9 Hz, 1H, Thi-*H*), 2.56 (dd, *J* = 0.9, 0.5 Hz, 3H, C*H*$_3$); ^{11}B{^{1}H} NMR (160 MHz, $CDCl_3$): δ = 46.3 (s); ^{13}C{^{1}H} NMR (126 MHz, $CDCl_3$): δ = 159.0 (Thi-*C*-C), 145.1 (Thi-*C*-H), 129.6 (Thi-*C*-H), 16.4 (*C*H$_3$).

Synthesis of **11b**. To a solution of 2,5-bis(trimethylsilyl)thiophene (685.3 mg, 3.0 mmol) and Me_3SiNTf_2 (53.0 mg, 0.15 mmol) in CH_2Cl_2 (3 mL) was added dibromo(thienyl)borane (761.3 mg, 3.0 mmol) at rt. After 16 h, all volatiles were removed in vacuo. Toluene (3 mL) was added to the residue, followed by Mes*Li (1.01 g, 4.0 mmol) in toluene (7 mL). This suspension was stirred for 24 h. After aqueous workup, the crude product was purified by column chromatography (silica, *n*-hexane) to give **11b** as a colorless solid. Yield: 778.4 mg (1.57 mmol, 52 %); ^{1}H NMR (400 MHz, $CDCl_3$): δ = 7.81 (dd, *J* = 4.7, 1.0 Hz, 1H, Thi-*H*), 7.75 (s, 1H Thi-*H*), 7.71 (d, *J* = 3.4 Hz, 1H, Thi-*H*), 7.45 (s, 2H, Mes*-*H*), 7.30 (d, *J* = 3.4 Hz, 1H, Thi-*H*), 7.20 (dd, *J* = 4.7, 3.6 Hz, 1H, Thi-*H*), 1.41 (s, 9H, *p*-*t*BuC*H*$_3$), 1.17 (s, 18H, *o*-*t*BuC*H*$_3$), 0.38 (s, 9H, Si(C*H*$_3$)$_3$); ^{11}B{^{1}H} NMR (128 MHz, $CDCl_3$): δ = 53.8 (s); ^{13}C{^{1}H} NMR (101 MHz, $CDCl_3$): δ = 153.4 (Mes*-*C*-B), 152.1 (Thi-*C*-Si), 151.8 (Mes*-*C*-*o*-*t*Bu), 148.7 (Thi-*C*-B), 148.6 (Mes*-*C*-*p*-*t*Bu), 142.6 (Thi-*C*H), 141.3 (Thi-*C*H), 135.6 (Thi-*C*H), 135.1 (Thi-*C*H), 128.6 (Thi-*C*H), 122.7 (Mes*-*C*H), 38.8 (*p*-*t*Bu-*C*H$_3$), 35.1 (*o*-*t*Bu-*C*H$_3$), 34.9 (*p*-*t*Bu-*C*), 31.6 (*o*-*t*Bu-*C*), 0.2 (Si(*C*H$_3$)$_3$); ^{29}Si NMR (79 MHz, $CDCl_3$): δ = -6.35 (s); HRMS (EI): m/z = 494.2665 [M]$^+$, calcd. for $C_{29}H_{43}BS_2Si$: 494.2668.

general procedure for stoichiometric reactions of substrates and catalyst 9. In a glovebox, **6** (0.6 mmol) in CD_2Cl_2 (0.3 mL) or **7** (0.6 mmol) in CD_2Cl_2 (0.3 mL) were added to a solution of **9** (0.6 mmol) in CD_2Cl_2 (0.3 mL) were added together in a Young NMR tube, which resulted in a clear, colorless to brown solution. The mixture was shaken vigorously, and the reaction process was observed via ^{1}H, ^{11}B{^{1}H} and ^{19}F{^{1}H} NMR analysis.

general procedure for reactions between 6a-j and 7a-j. In a glovebox, **6** (0.6 mmol) in CD_2Cl_2 (0.2 mL), **7** (0.6 mmol) in CD_2Cl_2 (0.2 mL) and **9** (10.6 mg, 0.03 mmol) in CD_2Cl_2 (0.2 mL) were added together in a Young NMR tube, which resulted in a clear, colorless to brown solution. The mixture was shaken vigorously, and the reaction process was observed via ^1H NMR analysis.

Synthesis of **11a.** To a solution of **11b** (12.4 mg, 0.025 mmol) in CD_2Cl_2 (0.25 mL) was added $HNTf_2$ (7.0 mg, 0.025 mmol) in CD_2Cl_2 (0.25 mL) in a Young NMR tube at rt. The mixture was shaken vigorously, and the reaction process was observed via ^1H NMR analysis.

catalytic reaction between 6a and thiophene. In a glovebox, **6a** (152.5 mg, 0.6 mmol) in CD_2Cl_2 (0.2 mL), thiophene (50.5 mg, 0.6 mmol) in CD_2Cl_2 (0.2 mL) and **9** (10.6 mg, 0.03 mmol) in CD_2Cl_2 (0.2 mL) were added together in a Young NMR tube, which resulted in a clear brown solution. The mixture was shaken vigorously, and the reaction process was observed via ^1H NMR analysis.

catalytic reaction between 6a, thiophene and 7j. In a glovebox, to a solution of **6a** (152.5 mg, 0.6 mmol), **7j** (90.2 mg, 0.6 mmol), and **9** (10.6 mg, 0.03 mmol) in CD_2Cl_2 (0.6 mL) was added thiophene (50.5 mg, 0.6 mmol) in a Young NMR tube, which resulted in a clear brown solution. The mixture was shaken vigorously, and the reaction process was observed via ^1H NMR analysis.

Synthesis of **17a**. To a solution of **6a** (152.3 mg, 0.6 mmol) in CD_2Cl_2 (0.6 mL) was added **7a** (93.8 mg, 0.6 mmol) and **9** (10.6 mg, 0.03 mmol) in a Young NMR tube at rt, which resulted in a clear brown solution. The mixture was shaken vigorously. After the reaction to **8a** was complete (confirmed by ^1H NMR), **7a** (93.8 mg, 0.6 mmol) was added to the mixture. The mixture was shaken vigorously, and the reaction process was observed via ^1H NMR analysis.

Synthesis of **17g**. To a solution of **6g** (42.6 mg, 0.25 mmol) in CD_2Cl_2 (0.5 mL) was added **7g** (85.18 mg, 0.50 mmol) and **9** (17.7 mg, 0.05 mmol) in a Young NMR tube at rt, which resulted in a clear brown solution. The mixture was shaken vigorously, and the reaction process was observed via ^1H NMR analysis.

Synthesis of **14.** To $HNTf_2$ (2.25 g, 8.0 mmol) was added 2-triisopropylsilyl-thiophene (2.02 g, 8.4 mmol) at rt and stirred for 16 h. After removal of all volatiles, **14** was obtained as a yellow oil. Yield: 2.52 g (5.8 mmol, 72 %). ^1H NMR (400 MHz, $CDCl_3$): δ = 1.47 (dp, J = 14.5, 7.5 Hz,

3H, C*H*-(CH_3)$_3$), 1.20 (s, 9H, CH_3), 1.18 (s, 9H, CH_3); $^{19}F\{^1H\}$ NMR (377 MHz, $CDCl_3$): δ = -75.27 (q, J = 2.0 Hz), -78.23 (q, J = 2.0 Hz).

$^{19}F\{^1H\}$ NMR analysis of catalysis using catalyst 9. (Through this process, $^{19}F\{^1H\}$ NMR of the reaction mixture were taken, which will be indicated by the roman numeral analogue to Figure 2.4.6.) A solution of **9** (10.6 mg, 0.03 mmol) in CD_2Cl_2 (0.6 mL) was given in a Young NMR tube at rt (i). To that solution, **6g** (160.7 mg, 0.6 mmol) was added (ii). The solution was again analyzed after 30 minutes (iii). Afterwards, **7g** (102.2 mg, 0.6 mmol) was added to the mixture and the solution was analyzed after 60 minutes reaction time (iv). To that solution, **6g** (160.7 mg, 0.6 mmol) was added (v). Afterwards, **7g** (102.2 mg, 0.6 mmol) was added to the mixture (vi). After all additions, the mixture was shaken vigorously before taking the $^{19}F\{^1H\}$ NMR.

$^{19}F\{^1H\}$ NMR analysis of catalysis using catalyst 14. (Through this process, $^{19}F\{^1H\}$ NMR of the reaction mixture were taken, which will be indicated by the roman numeral analogue to Figure 2.4.7.) A solution of **14** (13.1 mg, 0.03 mmol) in CD_2Cl_2 (0.6 mL) was given in a Young NMR tube at rt (i). To that solution, **6g** (160.7 mg, 0.6 mmol) was added (ii). Afterwards, **7g** (102.2 mg, 0.6 mmol) was added to the mixture (iii) and the solution was analyzed after 25 (iv), 40 (v), 55 (vi), 70 (vii), and 130 minutes (viii), as well as after 20 h reaction time (ix). After all additions, the mixture was shaken vigorously before taking the $^{19}F\{^1H\}$ NMR.

general procedure for VTNA reactions. 4 stock solutions were prepared in a glovebox and stored under inert conditions and low temperatures (-40° C): I. **6g** (240.9 mg, 0.9 mmol) in CD_2Cl_2 (3 mL, conc: 0.3 M), II. **7g** (153.5 mg, 0.9 mmol) in CD_2Cl_2 (3 mL, conc: 0.3 M), III. **9** (15.8 mg, 0.045 mmol) in CD_2Cl_2 (3 mL, conc: 0.015M), and IV. CD_2Cl_2.

In a glovebox, different volumes of the stock solutions (Table S2.4.1) were added together in a Young NMR tube at rt. For that, solution I was added first, followed by solutions IV, II, and III in that order. That resulted in a clear, colorless to brown solution. The mixture was shaken vigorously, and the reaction process was observed via ^1H NMR analysis.

To examine different aspects of the reaction, the starting concentrations of the reactants were varied (Table S2.4.1).

Table S2.4.1: *Key figures for the reaction procedure used for VTNA.*

number	characteristic	added volume of stock solution [mL]					starting concentration of reactant [mol L-1]			catalyst loading [%]	Figure
		I	II	III	IV	total	6g	7g	9		
1	standard conditions	0.2	0.2	0.2	0	0.6	0.100	0.100	5.00E-03	5.00	Figure S5.4.22
2	2.5% cat loading	0.2	0.2	0.1	0.1	0.6	0.100	0.100	2.50E-03	2.50	Figure S5.4.23
3	3.75% cat loading	0.2	0.2	0.15	0.05	0.6	0.100	0.100	3.75E-03	3.75	Figure S5.4.24
4	excess of **7g**	0.15	0.2	0.2	0.05	0.6	0.075	0.100	5.00E-03	5.00	Figure S5.4.25
5	excess of **6g**	0.2	0.15	0.2	0.05	0.6	0.100	0.075	5.00E-03	5.00	Figure S5.4.26

Computational methods. DFT calculations were carried out with the Gaussian 09 program package, revision D.01.[30] Becke's three parameter exchange-correlation hybrid functional B3LYP[31] was used in combination with the 6-311++G** basis set. The PCM method was added to simulate the solvent effects on the geometry.[32] **14^N** molecules were optimized without solvent due to convergence problems, which can be ascribed to the sterical influence of the TIPS-group on the Nitrogen. For comparison of the energetical differences the molecule with the lowest energy eigenvalue was set to zero.

Table S2.4.2: *Total energies for geometric optimization species $9^{O,N}$ and $14^{O,N}$ in CH_2Cl_2 and $CHCl_3$.*

compound	solvent	E [Hartree]	ΔE [kJ mol^{-1}]
9^O	CH_2Cl_2	-2236.863818	0
9^O	$CHCl_3$	-2236.862070	+4.59
9^N	CH_2Cl_2	-2236.856251	+19.87
9^N	$CHCl_3$	-2236.854714	+23.90
14^O	CH_2Cl_2	-2472.782041	0
14^O	$CHCl_3$	-2472.780413	+4.27
14^N	CH_2Cl_2	-2472.760327[a]	+57.01[a]
14^N	$CHCl_3$	-2472.759079[a]	+60.20[a]

[a]single-point calculations.

2.4.5 References

(1) Priegert, A. M.; Rawe, B. W.; Serin, S. C.; Gates, D. P. Polymers and the p-block elements. *Chem. Soc. Rev.* **2016**, *45* (4), 922–953.

(2) Mkhalid, I. A. I.; Barnard, J. H.; Marder, T. B.; Murphy, J. M.; Hartwig, J. F. C-H activation for the construction of C-B bonds. *Chem. Rev.* **2010**, *110* (2), 890–931.

(3) Jäkle, F. Advances in the synthesis of organoborane polymers for optical, electronic, and sensory applications. *Chem. Rev.* **2010**, *110* (7), 3985–4022.

(4) Braunschweig, H.; Shang, R. Reactivity of transition-metal borylene complexes: recent advances in B-C and B-B bond formation via borylene ligand coupling. *Inorganic chemistry* **20110**, *54* (7), 3099–3106.

(5) Yan, G.; Huang, D.; Wu, X. Recent Advances in C-B Bond Formation through a Free Radical Pathway. *Adv. Synth. Catal.* **2018**, *360* (6), 1040–1053.

(6) Chujo, Y.; Sasaki, Y.; Kinomura, N.; Matsumi, N. Stable organoboron polymers prepared by hydroboration polymerization of diynes with mesitylborane. *Polymer* **2000**, *41* (13), 5047–5051.

(7) Chujo, Y.; Tomita, I.; Hashiguchi, Y.; Tanigawa, H.; Ihara, E.; Saegusa, T. Hydroboration polymerization. 1. Synthesis of organoboron polymers by polyaddition between diene and monoalkylborane. *Macromolecules* **1991**, *24* (2), 345–348.

(8) Matsumi, N.; Umeyama, T.; Chujo, Y. Novel π-conjugated organoboron polymers: Poly (ethynylene-phenylene-ethynylene-borane)s. *Polym. Bull.* **2000**, *44* (5-6), 431–436.

(9) Matsumi, N.; Naka, K.; Chujo, Y. Poly(p -phenylene-borane)s. Novel Organoboron π-Conjugated Polymers via Grignard Reagent. *J. Am. Chem. Soc.* **1998**, *120* (41), 10776–10777.

(10) Sundararaman, A.; Victor, M.; Varughese, R.; Jäkle, F. A family of main-chain polymeric Lewis acids: synthesis and fluorescent sensing properties of boron-modified polythiophenes. *J. Am. Chem. Soc.* **20010**, *127* (40), 13748–13749.

(11) Li, H.; Jäkle, F. Universal scaffold for fluorescent conjugated organoborane polymers. *Angew. Chem. Int. Ed.* **2009**, *48* (13), 2313–2316.

(12) Chai, J.; Wang, C.; Jia, L.; Pang, Y.; Graham, M.; Cheng, S. Z.D. Synthesis and electrochemical properties of a new class of boron-containing n-type conjugated polymers. *Synthetic Metals* **2009**, *159* (14), 1443–1449.

(13) Cordovilla, C.; Bartolomé, C.; Martínez-Ilarduya, J. M.; Espinet, P. The Stille Reaction, 38 Years Later. *ACS Catal.* **20110**, *5* (5), 3040–3053.

(14) Haubold, W.; Herdtle, J.; Gollinger, W.; Einholz, W. Darstellung von arylhalogenboranen. *Journal of Organometallic Chemistry* **1986**, *315* (1), 1–8.

(15) Lik, A.; Fritze, L.; Müller, L.; Helten, H. Catalytic B-C Coupling by Si/B Exchange: A Versatile Route to pi-Conjugated Organoborane Molecules, Oligomers, and Polymers. *J. Am. Chem. Soc.* **2017**, *139* (16), 5692–5695.

(16) Lik, A.; Jenthra, S.; Fritze, L.; Müller, L.; Truong, K.-N.; Helten, H. From Monodisperse Thienyl- and Furylborane Oligomers to Polymers: Modulating the Optical Properties through the Hetarene Ratio. *Chem. Eur. J.* **2018**, *24* (46), 11961–11972.

(17) Riensch, N. A.; Fest, M.; Fritze, L.; Helbig, A.; Krummenacher, I.; Braunschweig, H.; Helten, H. Bifuran-bridged bisboranes: highly luminescent B-doped oligohetarenes. *New J. Chem.*, doi: 10.1039/D0NJ04297H.

(18) Fritze, L.; Riensch, N. A.; Helten, H. Catalytic Si/B Exchange Condensation: A Green B–C Coupling Method That Provides Access to Monodisperse (Het)arylborane 'Trimers'. *Synthesis* **2019**, *51* (02), 399–406.

(19) Chen, J.; Lalancette, R. A.; Jäkle, F. Stereoselective Ortho Borylation of Pyridylferrocenes. *Organometallics* **2018**, *32* (20), 5843–5851.

(20) Me_3SiNTf_2 can actually be synthesized by the reaction of $HNTf_2$ with **7j**.

(21) Chardon, A.; Osi, A.; Mahaut, D.; Doan, T.-H.; Tumanov, N.; Wouters, J.; Fusaro, L.; Champagne, B.; Berionni, G. Controlled Generation of 9-Boratriptycene by Lewis Adduct Dissociation: Accessing a Non-Planar Triarylborane. *Angew. Chem. Int. Ed.* **2020**, *59* (30), 12402–12406.

(22) Schroeder, S.; Strauch, C.; Gaelings, N.; Niggemann, M. Vinyl Triflimides-A Case of Assisted Vinyl Cation Formation. *Angew. Chem. Int. Ed.* **2019**, *58* (15), 5119–5123.

(23) Burés, J. A Simple Graphical Method to Determine the Order in Catalyst. *Angew. Chem. Int. Ed.* **2016**, *55* (6), 2028–2031.

(24) Burés, J. Variable Time Normalization Analysis: General Graphical Elucidation of Reaction Orders from Concentration Profiles. *Angew. Chem. Int. Ed.* **2016**, *55* (52), 16084–16087.

(25) Martínez-Carrión, A.; Howlett, M. G.; Alamillo-Ferrer, C.; Clayton, A. D.; Bourne, R. A.; Codina, A.; Vidal-Ferran, A.; Adams, R. W.; Burés, J. Kinetic Treatments for Catalyst Activation and Deactivation Processes based on Variable Time Normalization Analysis. *Angew. Chem. Int. Ed.* **2019**, *58* (30), 10189–10193.

(26) Nielsen, C. D.-T.; Burés, J. Visual kinetic analysis. *Chem. Sci.* **2019**, *10* (2), 348–353.

(27) Mathieu, B.; Ghosez, L. Trimethylsilyl bis(trifluoromethanesulfonyl)imide as a tolerant and environmentally benign Lewis acid catalyst of the Diels–Alder reaction:TMS-NTf2. *Tetrahedron* **2002**, *58* (41), 8219–8226.

(28) Yin, X.; Chen, J.; Lalancette, R. A.; Marder, T. B.; Jäkle, F. Highly electron-deficient and air-stable conjugated thienylboranes. *Angew. Chem. Int. Ed.* **2019**, *53* (37), 9761–9765.

(29) Lik, A. Thienyl- and Furylborane Oligomers, Polymers, and Macrocycles - Development of a Catalytic Si/B Exchange Reaction As a Novel B–C Bond Formation Method. Doctoral dissertation, RWTH Aachen, Aachen, 2017.

(30) Frisch, M.; Clemente, F. Gaussian 09, Revision A. 01, MJ Frisch, GW Trucks, HB Schlegel, GE Scuseria, MA Robb, JR Cheeseman, G. *Scalmani, V. Barone, B. Mennucci, GA Petersson, H. Nakatsuji, M. Caricato, X. Li, HP Hratchian, AF Izmaylov, J. Bloino, G. Zhe* **2009**.

(31) (a) Dirac. P. M. A. *Quantum mechanics of many-electron systems. Proc. R. Soc. Lond. A* ***1929****, 123 (792), 714–733;* (b) Slater, J. C. A Simplification of the Hartree-Fock Method. *Phys. Rev.* **19101**, *81 (3)*, 385–390; (c) Becke. Density-functional exchange-energy approximation with correct asymptotic behavior. *Physical review. A, General physics* **1988**, *38* (6), 3098–3100; (d) Lee; Yang; Parr. Development of the Colle-Salvetti correlation-energy formula into a functional of the electron density. *Physical review. B, Condensed matter* **1988**, *37* (2), 785–789; (e) Becke, A. D. Density-functional thermochemistry. III. The role of exact exchange. *The Journal of Chemical Physics* **1998**, *98* (7), 5648–5652.

(32) (a) Miertuš, S.; Scrocco, E.; Tomasi, J. Electrostatic interaction of a solute with a continuum. A direct utilizaion of AB initio molecular potentials for the prevision of solvent effects. *Chemical Physics* **1981**, *55* (1), 117–129; (b) Lipparini, F.; Scalmani, G.; Mennucci, B.; Cancès, E.; Caricato, M.; Frisch, M. J. A variational formulation of the polarizable continuum model. *The Journal of Chemical Physics* **2010**, *133* (1), 14106; (c) Miertuš, S.; Tomasi, J. Approximate evaluations of the electrostatic free energy and internal energy changes in solution processes. *Chemical Physics* **1982**, *65* (2), 239–245; (d) Cossi, M.; Barone, V.; Cammi, R.; Tomasi, J. Ab initio study of solvated molecules: a new implementation of the polarizable continuum model. *Chemical Physics Letters* **1996**, *255* (4-6), 327–335; (e) Barone, V.; Cossi, M.; Tomasi, J. A new definition of cavities for the computation of solvation free energies by the polarizable continuum model. *Chemical Physics Letters* **1997**, *107* (8), 3210–3221; (f) Cancès, E.; Mennucci, B.; Tomasi, J. A new integral equation formalism for the polarizable continuum model: Theoretical background and applications to isotropic and anisotropic dielectrics. *The Journal of Chemical Physics* **1997**, *107* (8), 3032–3041; (g) Mennucci, B.; Tomasi, J. Continuum solvation models: A new approach to the problem of solute's charge distribution and cavity boundaries. *The Journal of Chemical Physics* **1997**, *106* (12), 5151–5158; (h) Mennucci, B.; Cancès, E.; Tomasi, J. Evaluation of Solvent Effects in Isotropic and Anisotropic Dielectrics and in Ionic Solutions with a Unified Integral Equation Method: Theoretical Bases, Computational Implementation, and Numerical Applications. *J. Phys. Chem. B* **1997**, *101* (49), 10506–10517; (i) Barone, V.; Cossi, M. Quantum Calculation of Molecular Energies and Energy Gradients in Solution by a Conductor Solvent Model. *J. Phys. Chem. A* **1998**, *102* (11),

1995–2001; (j) Cossi, M.; Barone, V.; Mennucci, B.; Tomasi, J. Ab initio study of ionic solutions by a polarizable continuum dielectric model. *Chemical Physics Letters* **1998**, *286* (3-4), 253–260; (k) Barone, V.; Cossi, M.; Tomasi, J. Geometry optimization of molecular structures in solution by the polarizable continuum model. *J. Comput. Chem.* **1998**, *19* (4), 404–417; (l) Cammi, R.; Mennucci, B.; Tomasi, J. Second-Order Møller−Plesset Analytical Derivatives for the Polarizable Continuum Model Using the Relaxed Density Approach. *J. Phys. Chem. A* **1999**, *103* (45), 9100–9108; (m) Cossi, M.; Barone, V.; Robb, M. A. A direct procedure for the evaluation of solvent effects in MC-SCF calculations. *The Journal of Chemical Physics* **1999**, *111* (12), 5295–5302; (n) Tomasi, J.; Mennucci, B.; Cancès, E. The IEF version of the PCM solvation method: an overview of a new method addressed to study molecular solutes at the QM ab initio level. *Journal of Molecular Structure: THEOCHEM* **1999**, *464* (1-3), 211–226; (o) Cammi, R.; Mennucci, B.; Tomasi, J. Fast Evaluation of Geometries and Properties of Excited Molecules in Solution: A Tamm-Dancoff Model with Application to 4-Dimethylaminobenzonitrile. *J. Phys. Chem. A* **2000**, *104* (23), 5631–5637; (p) Cossi, M.; Barone, V. Solvent effect on vertical electronic transitions by the polarizable continuum model. *The Journal of Chemical Physics* **2000**, *112* (5), 2427–2435; (q) Cossi, M.; Barone, V. Time-dependent density functional theory for molecules in liquid solutions. *The Journal of Chemical Physics* **2001**, *115* (10), 4708–4717; (r) Cossi, M.; Rega, N.; Scalmani, G.; Barone, V. Polarizable dielectric model of solvation with inclusion of charge penetration effects. *The Journal of Chemical Physics* **2001**, *114* (13), 5691–5701; (s) Cossi, M.; Scalmani, G.; Rega, N.; Barone, V. New developments in the polarizable continuum model for quantum mechanical and classical calculations on molecules in solution. *The Journal of Chemical Physics* **2002**, *117* (1), 43–54; (t) Cammi, R. Quantum cluster theory for the polarizable continuum model. I. The CCSD level with analytical first and second derivatives. *The Journal of Chemical Physics* **2009**, *131* (16), 164104; (u) Cammi, R. Coupled-cluster theories for the polarizable continuum model. II. Analytical gradients for excited states of molecular solutes by the equation of motion coupled-cluster method. *Int. J. Quantum Chem.* **2010**, *110* (15), 3040–3052; (v) Cossi, M.; Rega, N.; Scalmani, G.; Barone, V. Energies, structures, and electronic properties of molecules in solution with the C-PCM solvation model. *J. Comput. Chem.* **2003**, *24* (6), 669–681; (w) Scalmani, G.; Frisch, M. J. Continuous surface charge polarizable continuum models of solvation. I. General formalism. *The Journal of Chemical Physics* **2010**, *132* (11), 114110; (x) Nottoli, M.; Cupellini, L.; Lipparini, F.; Granucci, G.; Mennucci, B. Multiscale Models for Light-Driven Processes. *Annual review of physical chemistry* **2021**, *72*, 489–513; (y) Caricato, M. Absorption and Emission Spectra of Solvated Molecules with the EOM-CCSD-PCM Method. *Journal of chemical theory and computation* **2012**, *8* (11), 4494–4502.

2.5 Selective C–H Activation of Heterocyclic Systems by Intermolecular Electrophilic Borylation

2.5.1 Introduction

Organoboranes are organic-inorganic hybrid compounds containing B–C bonds.[1] The introduction of boron into small molecules and polymers gives the opportunity to create materials with new properties.[1,2,3] If a vacant p orbital is introduced into an extended organic π-system via the formation of a B–C bond, it can interact with the π-electron system, creating a new electronic structure. In this case, it is a formal n-doping of the system, which alters the optoelectronic properties of the molecule.[4] This enables the use of such molecules as semiconductor materials for Organic Light Emitting Diodes (OLEDs).[2,5] Furthermore, the vacant p-orbital enables the coordination of Lewis bases and nucleophiles, thus changing the electronic structure at the boron center. This not only allows for the detection of toxic amines and other nucleophiles, but also allows for additional reactivities.[6,7] Additionally, the trigonal-planar geometry of boron may give advantages when used as a building block for complex structures.[2]

So far, it has been shown that the formation of a second B–C bond via selective substitution of dihaloboranes with one aryl group is challenging. Either harsh reaction conditions (Scheme 2.5.1) or highly toxic tin compounds were required to prepare diaryl(halo)boranes.[8]

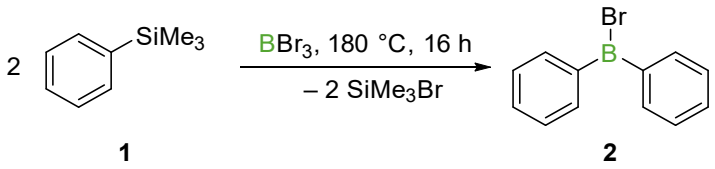

Scheme 2.5.1: *Preparation of bromo(diphenyl)borane* ***2*** *under harsh conditions.*

Helten and coworkers recently presented a versatile catalytic route that allowed for synthesis of diaryl(halo)boranes via silicon/boron exchange condensation, avoiding toxic or harsh reaction conditions (Scheme 2.5.2). To this end, the electrophilic silyl reagent trimethylsilyl triflimide (Me_3SiNTf_2) was used as catalyst.[9]

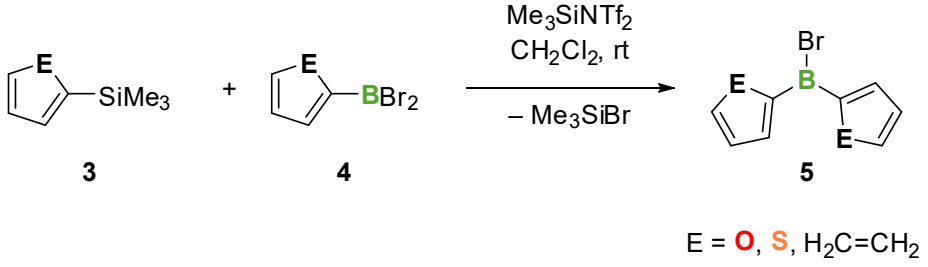

Scheme 2.5.2: *General reaction scheme for catalytic Si/B exchange reaction.*

Recent studies by Oestreich and coworkers show that the use of boron cations allows for new metal-free methods of borylating arenes (Scheme 2.5.3). They presented an initial formation of a boron cation by reaction of *N*,*N*-dimethylaniline **6**, the strong Lewis acid tris(pentafluorophenyl)borane ($B(C_6F_5)_3$) and CatBH, which then reacts with a second molecule of **6** to product **7** via electrophilic aromatic substitution (S_EAr) mechanism.[10]

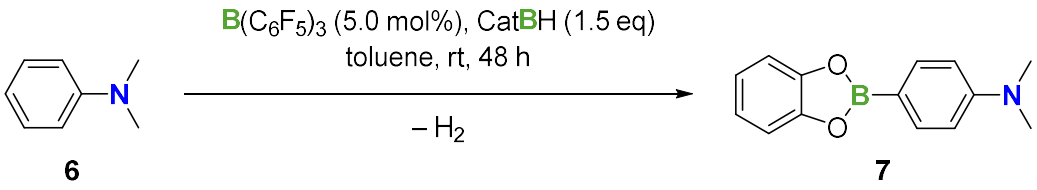

Scheme 2.5.3: *Electrophilic aromatic substitution of N,N-dimethylaniline* ***6****.*

The electrophilicity of boron, thus its Lewis acidity significantly increases when a positive charge is introduced at the boron center. Boron cations are classified according to their coordination number (Figure 2.5.1). The reactivity of the cations generally decreases with saturation of the coordination sphere or increase of the electron density at the boron center by neutral two-electron donors.[11]

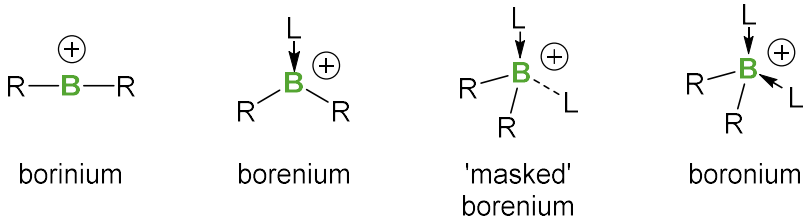

Figure 2.5.1: *Terminology of boron cations with varying coordination number (R: formal monoanionic substituent, L: formal neutral two-electron donor).*

In a borinium ion, the boron is linearly coordinated by two σ-bonding substituents R. The unoccupied p orbitals can be partially occupied by free electron pairs of the covalently bonded substituents (π donation), which can relieve the electron deficiency at the boron. That partial occupation of the p orbitals stabilizes this cation. Stabilization may also be achieved by addition of sterically demanding substituents, which shield the positive charge.[11] If a neutral two-electron donor L coordinates at the boron in addition to the two σ-bonding substituents R, the trigonal planar borenium cation is formed. Compared to the borinium cation, the additional σ-donor ligand provides an increase in the electron density at the boron center which further stabilizes the borenium cation. Less π backbonding occurs in this state.[11] When a weakly coordinating Lewis acid (for example a solvent molecule or a weakly coordinating anion (WCA)) occupies the fourth coordination site, a “masked” borenium cation is formed.[7] Investigations of Vedejs and coworkers have shown, that weakly stabilized primary borenium

cations are capable of forming dimeric structures in solution.[12] By successively introducing another neutral two-electron donor L, a boronium cation is formed. This is tetrahedrally coordinated and thus sp^3 hybridized. The coordination sphere provides spatially shielding and through a total of four σ-donors the boronium cation is the most stabilized of the categories shown.[11]

Experimental and theoretical studies suggest an electrophilic aromatic substitution for the reaction of a borenium ion with an aromatic or heteroaromatic compound (Scheme 2.5.4), giving a metal-free reaction route for a C–H borylation reaction on aryl species.[7,13,14] For a catecholato borane, two feasible routes for the formation of the product were reported.[15] In this example an amine acts as a neutral two-electron donor L.

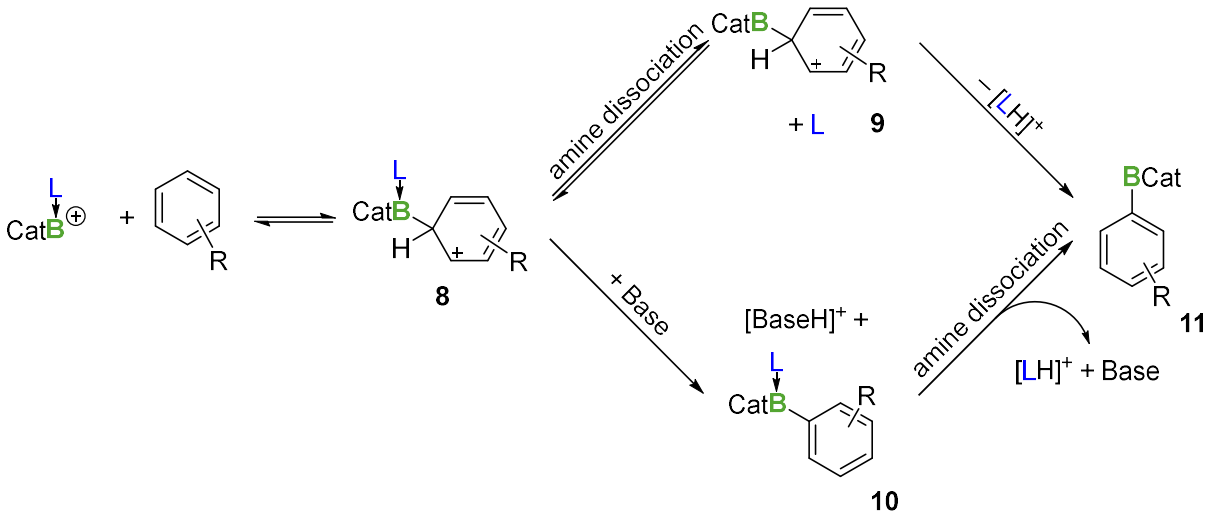

Scheme 2.5.4: *Intermolecular electrophilic borylation of aromatic or heteroaromatic compounds via an S_EAr mechanism (Cat: catecholato substituent, L: formal neutral two-electron donor).*

If an amine ligand of low nucleophilicity, for example 2,6-dimethylpyridine, is involved, it can be readily dissociated. In consequence, the borylated σ-complex **9** is formed with dissociation of the amine ligand. After deprotonation of $[H(arene)]^+$ by the amine, the borane product **11** is formed. If a more nucleophilic amine, such as triethylamine, coordinates to the boron center, an additional base is required. This deprotonates the σ-complex, resulting in the neutral, tetrahedrally coordinated borane **10**. Dissociation of the amine ligand yields product **11**. The formation of a B-C bond via the S_EAr mechanism offers, despite its complex chemistry with respect to the boron cation and other reagents, an attractive one-step method.[7,13,15]

Ingleson and coworkers used the S_EAr capabilities of borenium cations to synthesize a series of pinacol-substituted arenes **16** (Scheme 2.5.5).[16] To this end, the borenium cation **13** was generated from *B*-chlorocatecholborane **12** (CatBCl) using an amine and aluminium chloride ($AlCl_3$). In the next reaction step, species **14** was synthesized via S_EAr mechanism besides the

by-product **15**. The latter represents the $[LH]^+$ species shown in Scheme 2.5.4. Finally, **14** was converted to the desired pinacol species **16**.

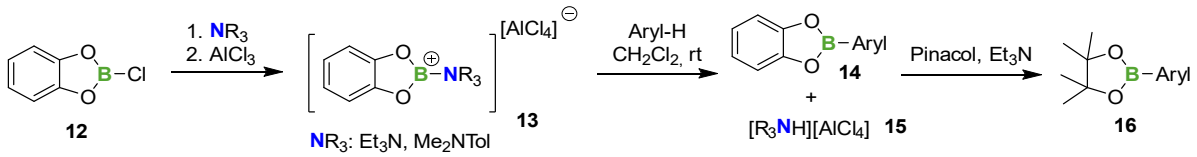

Scheme 2.5.5: *Synthesis of pinacol-substituted arenes **16** using borenium cation **13**.*

Subsequently, the same group presented a similar reaction route using electrophiles derived from trichloroborane (BCl_3).[17] As amines, 2,6-lutidine or *N*,*N*-dimethyl-*p*-toluidine were used (Scheme 2.5.6). In the end, this route gave a series of pinacol arenes **17**.

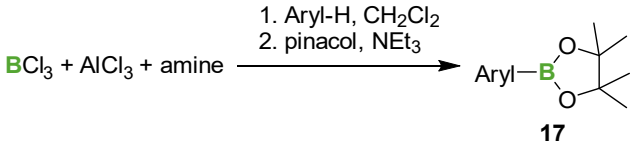

Scheme 2.5.6: *Synthesis of pinacol-substituted arenes **17** using electrophiles derived from BCl_3.*

Herein we present a study in which we explore the intermolecular electrophilic borylation reaction to form halo(dithienyl)boranes **20** (Scheme 2.5.7). For our investigations di(halo)thienylboranes $\mathbf{18^{Br}}$ and $\mathbf{18^{Cl}}$ were chosen to perform C–H activation of thiophene **19**.

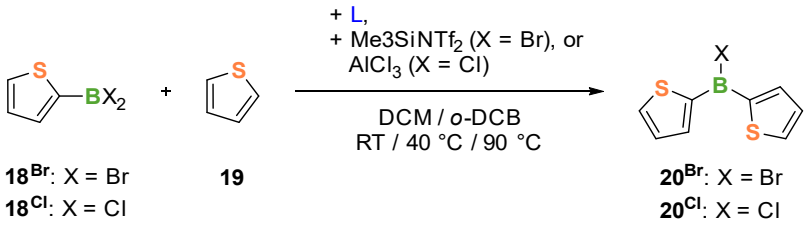

Scheme 2.5.7: *Intermolecular electrophilic borylation at thiophene **19** to give di(thienyl)haloboranes **20** (L: formal neutral two-electron donor).*

2.5.2 Results and Discussion

2.5.2.1 Synthesis of reactive intermediates

At the beginning of our investigations, the interactions of the substrates $\mathbf{18^{Br}}$ and $\mathbf{18^{Cl}}$ with two different amines, 2,6-lut **21** and Me_2NTol **22**, were examined (Scheme 2.5.8). Both are frequently used as auxiliary bases in electrophilic borylation reactions.[16,17,18] Goal of these investigations was the isolation of the respecting amine adducts, to possibly use them as substrates in the desired S_EAr reaction. This would guarantee a fixed 1:1 ratio of the dihalo(thienyl)borane and the amine.

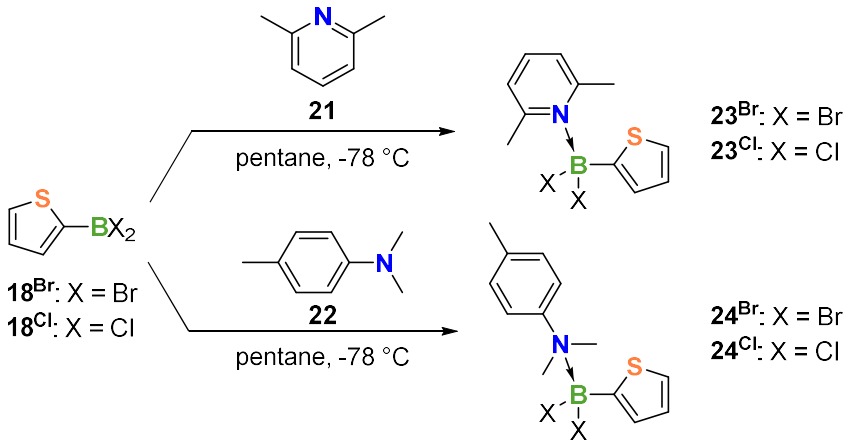

Scheme 2.5.8: *Reactions of* ***18^{Br}*** *and* ***18^{Cl}*** *with amines* ***21*** *and* ***22****.*

Both substrates exhibited strong reactivity towards both amines, even at -78 °C in pentane, indicated by immediate precipitation of the adducts **23** and **24**. For both 2,6-lut adducts **23^{Br}** and **23^{Cl}**, even small increase of temperature to -40 °C or removal of the solvent resulted in the reaction mixture turning dark brown and tar-like, which prevented analysis of the initial reaction outcome. The amine adducts **24** showed higher stability. Nonetheless, while **24^{Cl}** was isolated and fully characterized, **24^{Br}** underwent a slow decomposition process at room temperature both in solution and as a solid. The instability of 2,6-lut adducts **23** is probably caused by the amine **21** being less nucleophilic compared to Me_2NTol **22**.

Then, the selective formation and isolation of the corresponding borenium salts **25** and **26** was investigated (Scheme 2.5.9). Indeed, these compounds could be used as substrates for the S_EAr reaction. An isolation was attempted by covering a mixture of substrates **18**, amines **21** or **22**, and $AlCl_3$ for **18^{Cl}** or Me_3SiNTf_2 for **18^{Br}** in dichloromethane (CH_2Cl_2) with *n*-pentane to achieve precipitation of the desired products at the solvent interface. In this reaction, $AlCl_3$ should act as a Lewis acid, while Me_3SiNTf_2 should initiate a condensation reaction, where trimethylsilyl bromide (Me_3SiBr) is formed, to give the desired borenium cation salts **25** or **26**.

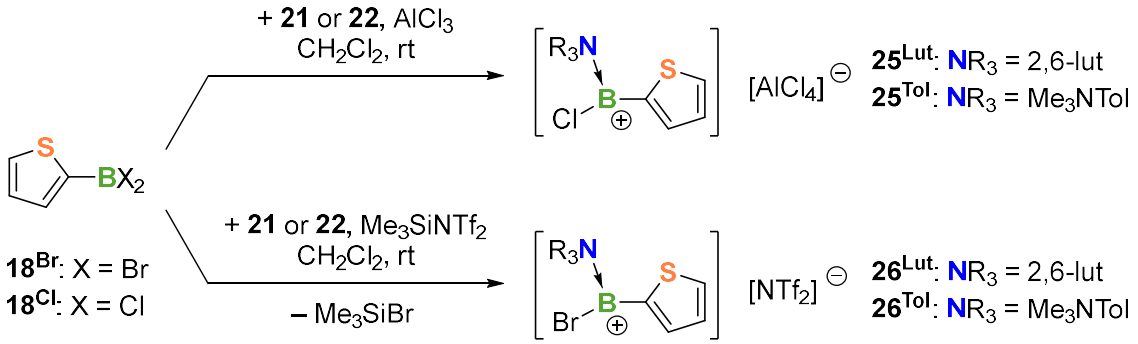

Scheme 2.5.9: *Formation of borenium salts* ***25*** *and* ***26*** *from substrates* ***18****.*

Unfortunately, no formation of the desired products was observed. Modification of the precipitation method like lowering of the temperature or concentration of the solution via

slow evaporation of the solvents did not lead to observable formation of the products. Without isolation of any of the feasible substrates, the S_EAr reaction to halo(dithienyl)boranes **20** was attempted as a one-pot reaction with the initially chosen reactants (Scheme 2.5.7).

2.5.2.2 Synthesis of halo(dithienyl)boranes $\mathbf{20^{Br}}$ and $\mathbf{20^{Cl}}$ via S_EAr reaction

To investigate the formation of halo(dithienyl)boranes $\mathbf{20^{Br}}$ and $\mathbf{20^{Cl}}$, different reaction parameters were varied (Scheme 2.5.10). The influence of solvents (CH_2Cl_2 and *o*-dichlorobenzene (*o*-DCB)), reaction temperature, as well as the amines on the reaction was examined.

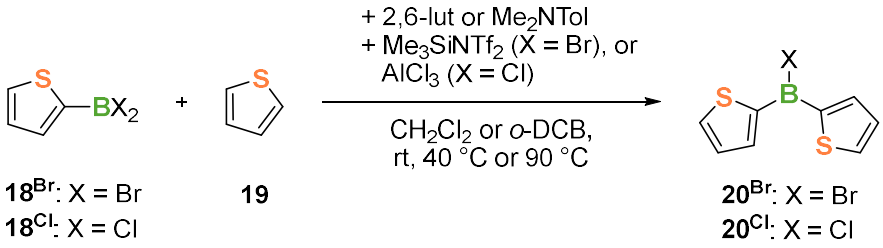

Scheme 2.5.10: *Varied reaction conditions towards the synthesis of halo(dithienyl)boranes* ***20****.*

Variation of the amine had a considerable effect on the reaction process, as shown as an example for the reaction of dichloro(thienyl)borane $\mathbf{18^{Cl}}$ (Figure 2.5.2).

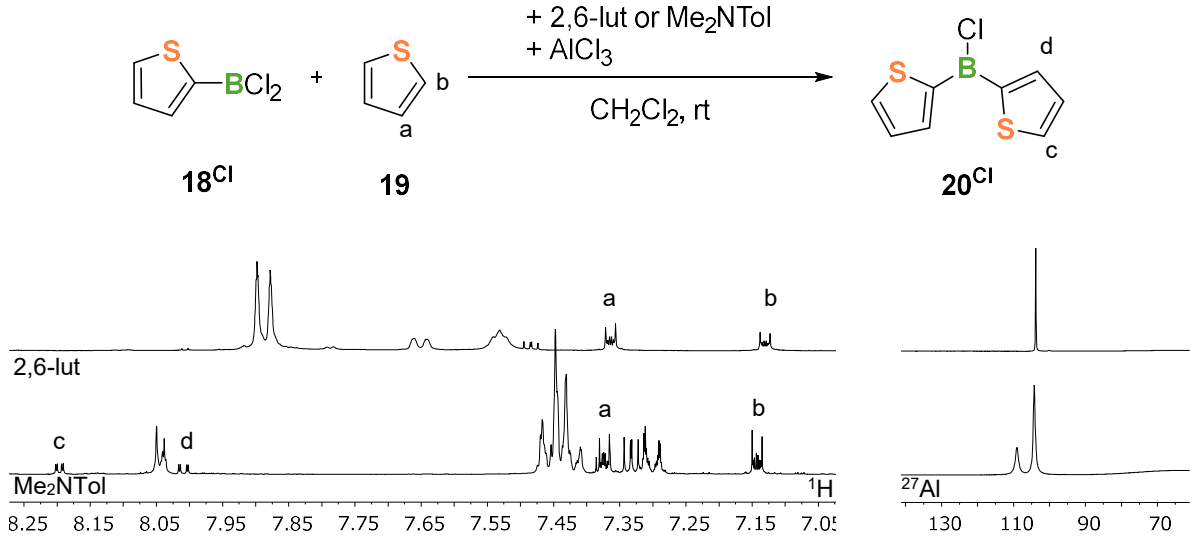

Figure 2.5.2: *Variation of the amine in the synthesis of halo(dithienyl)borane* $\mathbf{20^{Cl}}$ *via* S_EAr *reaction. Corresponding* ^1H *and* ^{27}Al *NMR spectra after 24 h reaction time (in* CD_2Cl_2*).*

While using Me_2NTol, the formation of the desired product $\mathbf{20^{Cl}}$ was observed by ^1H NMR within the first 24 h of the reaction (Figure 2.5.2; signals c, d). After 7 days, only 15 % yield were achieved (determined with cyclohexane as internal standard). This is also evident by the remaining thiophene substrate in the reaction mixture (Figure 2.5.2; signals a, b). Using

2,6-tol on the other hand, led to no observable formation of the desired product. ^{27}Al NMR spectra of the two reactions revealed one signal around δ = 104.2 ppm, which can be assigned to an $[AlCl_4]^-$ species. Additionally, when using Me_2NTol, a second signal emerges at δ = 109.0 ppm, which can be assigned to $Me_2NTol–AlCl_3$.[17] Similarly, to the observations of the formation of 2,6-lut-based species **23^{Cl}**, the amine appears not suitable for the reaction. One possible reason is the insufficient stability of the putative intermediates. Additionally, the lack of steric hindrance at the 4-position of the pyridine ring could lead to borylation of the of the amine and open up the possibilities for unwanted side reactions.[10]

When using **18^{Br}** as substrate, a second species was formed beside the desired product **20^{Br}** (Figure 2.5.3). A follow-up reaction of the desired product **20^{Br}** with a second **18^{Br}** was observed, forming bisborane **27^{Br}**. The free 5,5'-positions of the thienyl substituents of **20^{Br}** are similarly susceptible to S_EAr attacks as substrate **19** and the higher reactivity of bromoboranes in comparison to chloroboranes leads to the formation of **27^{Br}**.

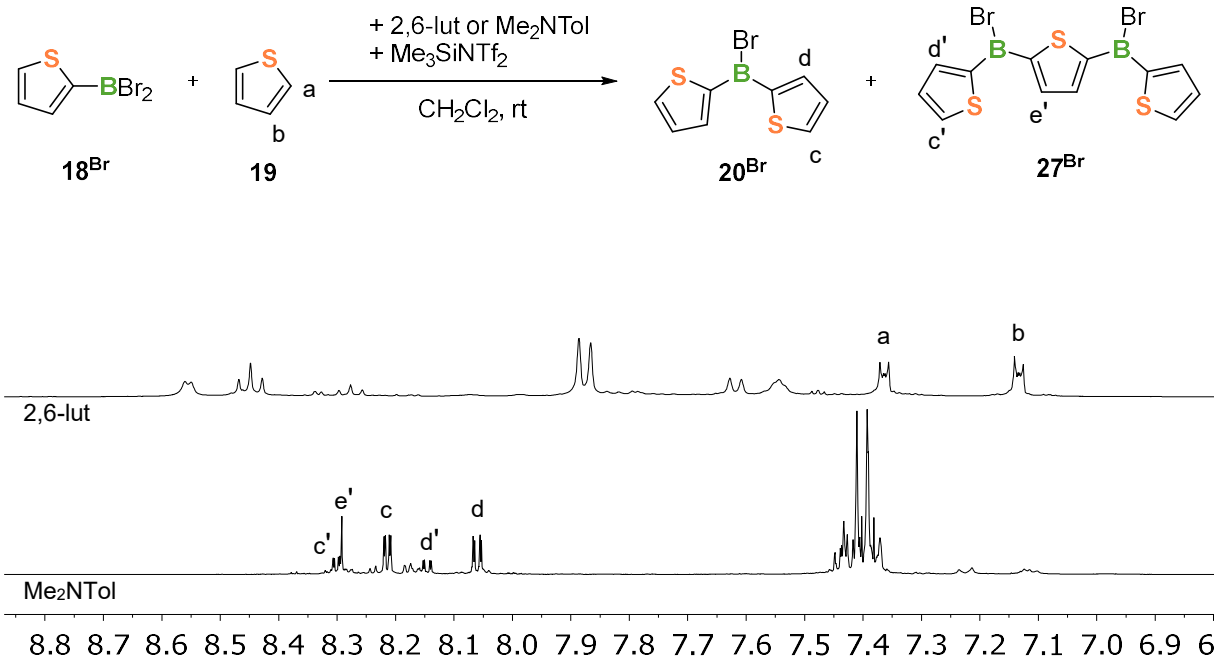

Figure 2.5.3: *Variation of the amine in the attempted synthesis of halo(dithienyl)borane **20^{Br}** via S_EAr reaction. Corresponding ^{1}H NMR spectra after 24 h reaction time (in CD_2Cl_2).*

To improve the yield of the reactions, they were carried out at higher temperatures. In order to exceed the boiling temperature of CH_2Cl_2, the *o*-DCB was used for a reaction at 90 °C. Figure 2.5.4 shows the results for substrate **18^{Cl}**.

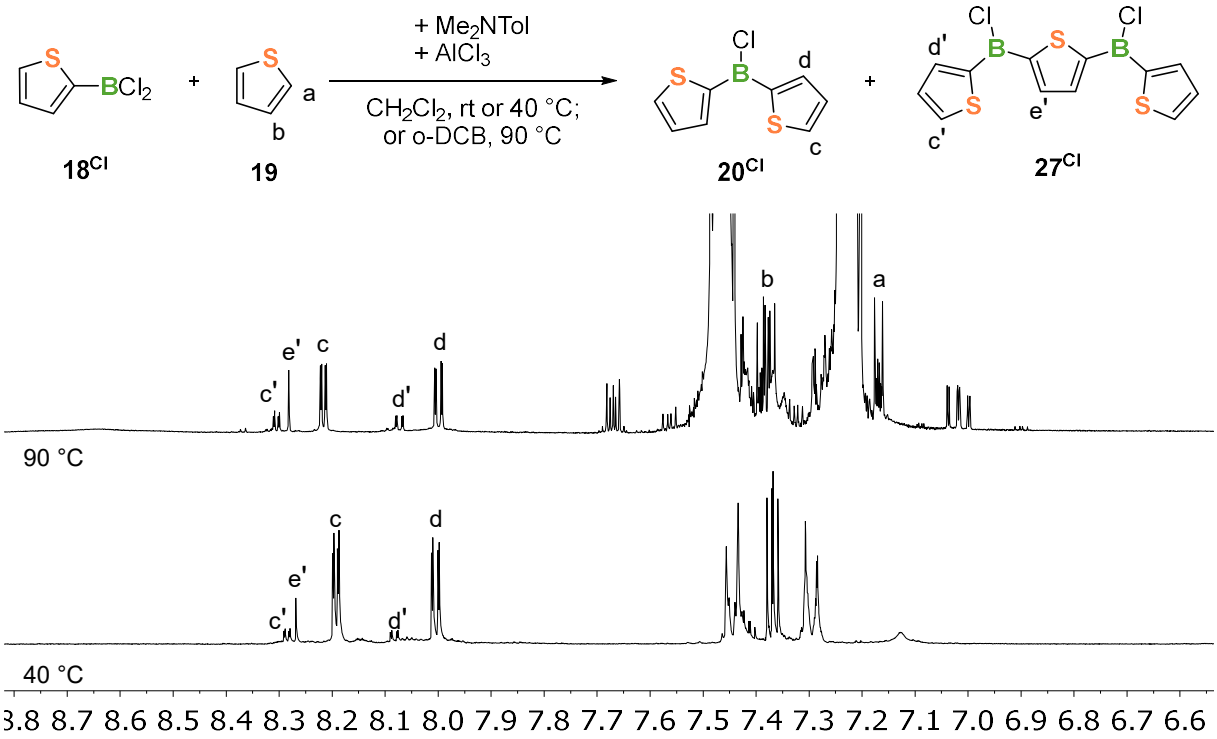

Figure 2.5.4: *Variation of the temperature in the synthesis of halo(dithienyl)borane* ***20^{Cl}*** *via S_EAr reaction. Corresponding ^1H NMR spectra at 40 °C and 90 °C after 24 h reaction time (in CD_2Cl_2).*

At both elevated temperatures, the formation of a bisborane **27^{Cl}** was observed. Again, a follow-up reaction of the desired **20^{Cl}** with a second **18^{Cl}** had occurred. At 40 °C, the ratio between **20^{Cl}** and **27^{Cl}** amounts to 9:1, at 90 °C it amounts to 5:1. Elevation of the temperature enhances the reactivity of the substrates, leading to higher conversion rates at the cost of selectivity. However, while the ^1H NMR spectra suggest a selective reaction, $^{11}B\{^1H\}$ NMR spectra show some side products (Figure S5.5.11). Additionally, the determined yield of **20^{Cl}** is still below 20 % after 6 days reaction time (determined with cyclohexane as internal standard).

For **18^{Br}** and the product **20^{Br}**, very similar observations were made. ^1H NMR and $^{11}B\{^1H\}$ NMR analysis showed very similar signals and thus reaction processes (Figure S5.5.15, Figure S5.5.16). The ratios between **20^{Br}** and **27^{Br}** change to 1:1.5 at 40 °C and 1:1 at 90 °C. Again, the higher reactivity of bromoboranes leads to a higher percentage of follow-up reactions.

The observed follow-up reaction made an evaluation of the reaction more challenging. In order to block that possible 5-position attack, the methylated substrates **18'^{Br}** was used (Figure 2.5.5).

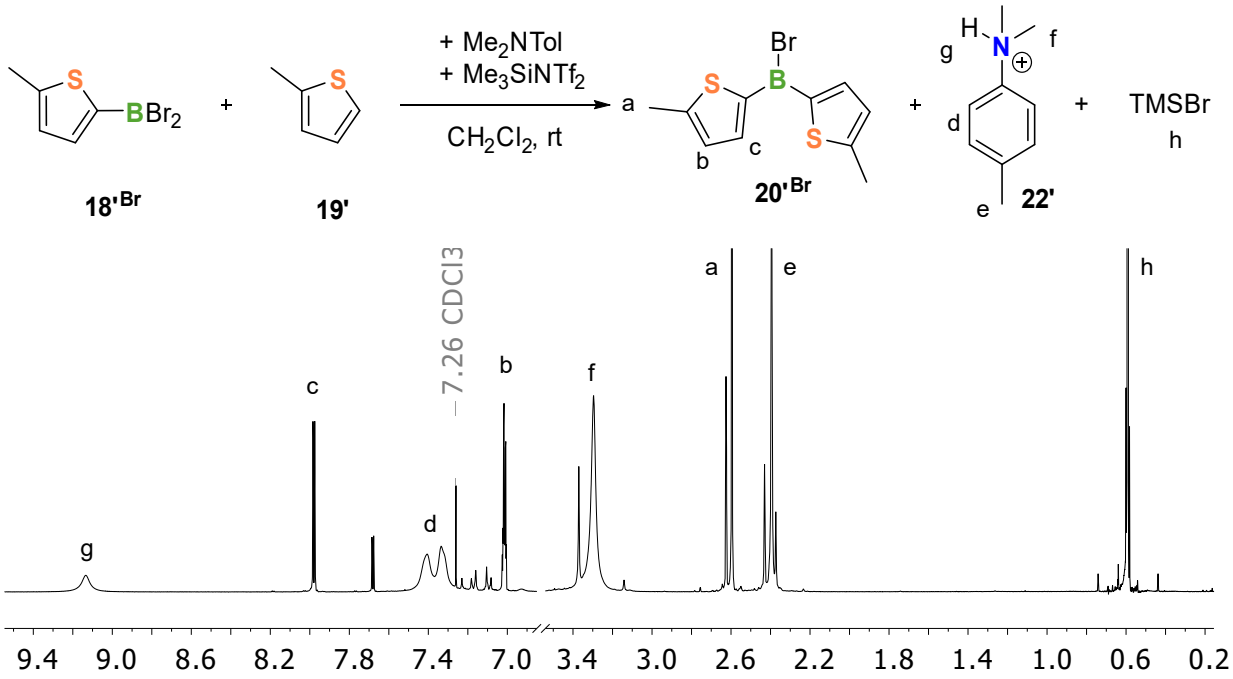

Figure 2.5.5: *Synthesis of halo(dithienyl)boranes* ***20'Br*** *via* S_EAr *mechanism. Corresponding* ^1H *NMR spectra at rt after 48 h reaction time (in* $CDCl_3$*).*

The ^1H NMR spectrum after 48 h reaction time shows the expected product **20'Br** and by-products $[HMe_2NTol]^+$ **22'** and Me_3SiBr. The reactant Me_3SiNTf_2 was completely consumed as well. Besides preventing attack at the 5-position of the thiophene ring, the methyl group's +I-effect also seems to favor the reactivity of one or both substrates.

2.5.3 Conclusion

First studies on the formation of halo(dithienyl)boranes via S_EAr reactions have been carried out. For this purpose, different amines, solvents and temperatures have been investigated (Scheme 2.5.11). While the yield of the desired products **20** was relatively low (< 20 % yield after 6 days), its formation in general was confirmed. While the evaluation of the reaction performance was complicated by a follow-up reaction to bisborane **27**, improvement of the reaction's selectivity by addition of a methyl group at the 5-position of the substrates also led to improved results.

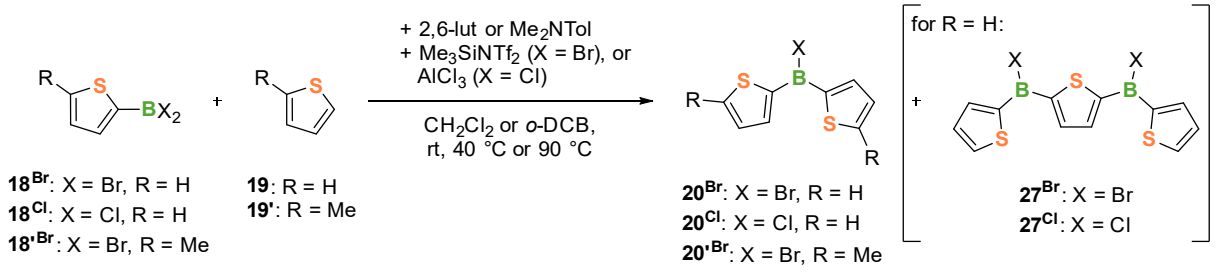

Scheme 2.5.11: *Summarizing reaction scheme of investigated conditions to form halo(dithienyl)boranes* ***20*** *and* ***20'****.*

Future investigations in this field may involve using this reaction protocol for the synthesis of thiophene-based organoborane polymer scaffold **28** (Scheme 2.5.12). A characteristic of this route would be the head-to-tail selectivity of the polymerization, which can be beneficial for introduction of functional groups in the thienyl backbone.

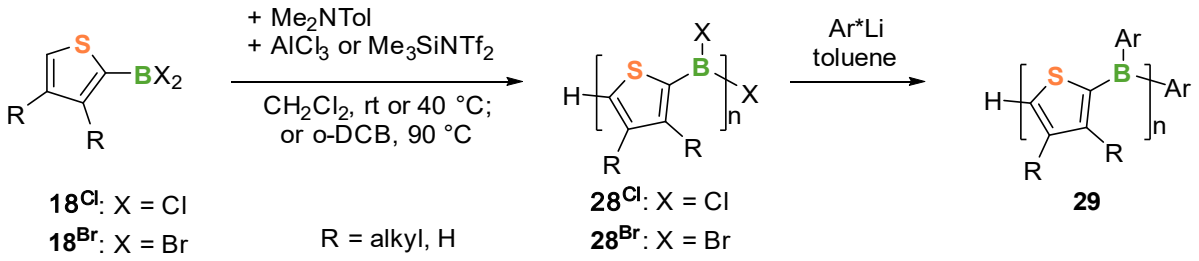

Scheme 2.5.12: *Polycondensation reaction pathway applying the intermolecular electrophilic C–H borylation.*

2.5.4 Experimental Section

General procedures. All manipulations were performed under an atmosphere of dry argon using standard Schlenk techniques or in an MBraun glove box. Solvents (CH_2Cl_2, hexane, pentane) were dried and degassed by means of an MBraun SPS-800 solvent purification system. Deuterated solvents for NMR spectroscopy were dried and degassed at reflux over CaH (CD_2Cl_2, $CDCl_3$) and freshly distilled prior to use. 2,6-Toluidine, *N*,*N*-dimethyl-*p*-toluidine, thiophene and 2-methylthiophene were degassed and freshly distilled prior to use. $AlCl_3$ was purified via sublimation under inert conditions. Me_3SiNTf_2, **12^{Br}**, **12^{Cl}** and **12'^{Br}** were prepared according to procedures described in the literature.[19]

NMR spectra were recorded at 25 °C on a Bruker Avance II HD spectrometer operating at 400 MHz. Chemical shifts were referenced to residual protic impurities in the solvent (^{1}H) or the deuterated solvent itself (^{13}C) and reported relative to external $SiMe_4$ (^{1}H, ^{13}C), $BF_3{\cdot}OEt_2$ (^{11}B) or $CFCl_3$ (^{19}F) standards. Mass spectra were obtained with the use of a Finnigan MAT95 spectrometer employing electron ionization (EI) using a 70 eV electron impact ionization source. Elemental analysis was performed with a CHN-O-Rapid VarioEL by Heraeus.

General procedure for the synthesis of 20 and 20'. To a solution of **18^{Cl}**, **18^{Br}** or **18'^{Br}** (0.10 mmol) and **19** (0.10 mmol) in CD_2Cl_2 or *o*-DCB (0.50 mL) was added 2,6-lut or Me_2NTol (0.10 mmol) at rt. Afterwards, $AlCl_3$ or Me_3SiNTf_2 (0.10 mmol) was added at the same temperature. The reaction was stirred at rt, 40 °C or 90 °C for up to 14 days.

Table 2.5.1: *Key figures for the syntheses of **20** and **20'**.*

number	substrate	temperature [°C]	solvent	Lewis base	reactant
1	**18^{Cl}**	rt	CD_2Cl_2	2,6-Lut	$AlCl_3$
2	**18^{Cl}**	rt	CD_2Cl_2	Me_2NTol	$AlCl_3$
3	**18^{Br}**	rt	CD_2Cl_2	2,6-Lut	Me_3SiNTf_2
4	**18^{Br}**	rt	CD_2Cl_2	Me_2NTol	Me_3SiNTf_2
5	**18^{Cl}**	40	CD_2Cl_2	Me_2NTol	$AlCl_3$
6	**18^{Cl}**	90	*o*-DCB	Me_2NTol	$AlCl_3$
7	**18^{Br}**	40	CD_2Cl_2	Me_2NTol	Me_3SiNTf_2
8	**18^{Br}**	90	*o*-DCB	Me_2NTol	Me_3SiNTf_2
9	**18'^{Br}**	rt	CD_2Cl_2	Me_2NTol	Me_3SiNTf_2

General procedure for the synthesis of 23. To a solution of 2,6-Lut (1.31 g, 12.25 mmol) in *n*-pentane (9.4 mL) was added **18^{Br}** or **18^{Cl}** (9.4 mmol) in *n*-pentane (9.4 mL) at -78 °C. The solution was filtered at -60 °C, and the residue repeatedly washed with cold pentane (2 x 20 mL). **23^{Br}** and **23^{Cl}** were obtained as off-white solids, which underwent slow decomposition at that temperature.

Synthesis of **24^{Cl}**. A solution of **18^{Cl}** (1.65 g, 10.0 mmol) in *n*-pentane (10 mL) was added to a solution of Me_2NTol **22** (1.80 g, 13.3 mmol) in pentane (10 mL) at -78 °C. The solution was stirred over night at ambient temperature. The solution was filtered, and the residue repeatedly washed with pentane (2 x 20 mL). **24^{Cl}** was obtained as a colorless solid. Yield: 2.85 g (9.50 mmol, 95%); ^{1}H NMR (400 MHz, CD_2Cl_2): δ = 7.39 (dd, *J* = 4.6, 1.3 Hz, 1H, Thi-*H*), 7.11 (s, 4H, Ph-*H*), 7.02 (dd, *J* = 3.4, 1.3 Hz, 1H, Thi-*H*), 7.00 (dd, *J* = 4.6, 3.4 Hz, 1H, Thi-*H*), 3.36 (s, 6H, N-(CH_3)$_2$), 2.34 (s, 3H, Ph-CH_3); ^{11}B{^{1}H} NMR (128 MHz, CD_2Cl_2): δ = 9.2 (s); ^{13}C{^{1}H} NMR (126 MHz, CD_2Cl_2): δ = 143.7 (Ph-*C*-N(CH_3)$_2$), 138.5 (Ph-*C*-CH_3), 134.9 (Thi-*C*H), 129.5 (Thi-*C*H), 129.0 (Ph-*C*H), 127.7 (Thi-*C*H), 123.6 (Ph-*C*H), 50.0 (N(*C*H_3)$_2$), 20.9 (Ph-*C*H_3); MS (EI): m/z = 135.2 (Me_2NTol, 82 %), 299.0 ([M]$^+$, 0 %); elem. anal. calcd. (%) for C13H16BCl2NS: C 52.04; H 5.38, N 4.67 found: C 51.97, H 5.49, N 4.85.

Synthesis of **24^{Br}**. A solution of **18^{Br}** (203.2 mg, 0.80 mmol) in *n*-pentane (1 mL) was added to a solution of Me_2NTol **22** (140.6 g, 1.04 mmol) in pentane (1 mL) at -78 °C. The solution was stirred over night at ambient temperature. The solution was filtered at -60 °C, and the residue repeatedly washed with cold pentane (2 x 20 mL). **24^{Br}** was obtained as a colorless solid, which underwent decomposition at ambient temperature. ^{1}H NMR (400 MHz, CD_2Cl_2): δ = 7.44 (d, *J* = 4.7 Hz, 1H, Thi-*H*), 7.11 – 7.05 (m, 4H, Ph-*H*), 7.05 – 7.01 (m, 2H, Thi-*H*), 3.51 (s, 6H, N-(CH_3)$_2$), 2.34 (s, 3H, Ph-CH_3); ^{11}B{^{1}H} NMR (128 MHz, CD_2Cl_2): δ = 4.3 (s).

General procedure for the synthesis of 25. To a solution of 2,6-Lut or Me_2NTol (0.80 mmol) and **18^{Cl}** (131.9 mg, 0.80 mmol) in CH_2Cl_2 (2 mL) was added $AlCl_3$ (106.7 mg, 0.80 mmol) in an NMR tube and the mixture was shaken until it resulted in a clear solution. Afterwards, *n*-pentane was slowly added to cover the mixture. No precipitation of **25** was observed.

General procedure for the synthesis of 26. To a solution of 2,6-Lut or Me_2NTol (0.80 mmol) and **18^{Br}** (203.0 mg, 0.80 mmol) in CH_2Cl_2 (2 mL) was added Me_3SiNTf_2 (282.7 mg, 0.80 mmol) in an NMR tube and the mixture was shaken until it resulted in a clear solution. Afterwards, *n*-pentane was slowly added to cover the mixture. No precipitation of **26** was observed.

2.5.5 References

[1] A. M. Priegert, B. W. Rawe, S. C. Serin, D. P. Gates, *Chem. Soc. Rev.* **2016**, *45*, 922–953.

[2] S. Yamaguchi, A. Wakamiya, *Pure and Applied Chemistry* **2006**, *78*, 1413–1424.

[3] a) I. Manners, *Angew. Chem. Int. Ed.* **1996**, *35*, 1602–1621; b) X. He, T. Baumgartner, *RSC Adv.* **2013**, *3*, 11334; c) F. Vidal, F. Jäkle, *Angew. Chem.* **2019**, *131*, 5904–5929.

[4] F. Jäkle, *Chem. Rev.* **2010**, *110*, 3985–4022.

[5] a) T. M. Swager, *Macromolecules* **2017**, *50*, 4867–4886; b) C. Li, M. Liu, N. G. Pschirer, M. Baumgarten, K. Müllen, *Chem. Rev.* **2010**, *110*, 6817–6855; c) C. Wang, H. Dong, W. Hu, Y. Liu, D. Zhu, *Chem. Rev.* **2012**, *112*, 2208–2267; d) A. C. Grimsdale, K. L. Chan, R. E. Martin, P. G. Jokisz, A. B. Holmes, *Chem. Rev.* **2009**, *109*, 897–1091.

[6] a) F. P. Gabbaï, *Angew. Chem. Int. Ed.* **2012**, *51*, 6316–6318; b) C. R. Wade, A. E. J. Broomsgrove, S. Aldridge, F. P. Gabbaï, *Chem. Rev.* **2010**, *110*, 3958–3984.

[7] E. Fernández, A. Whiting (Eds.) *Topics in Organometallic Chemistry*, Springer International Publishing, Cham, **2015**.

[8] W. Haubold, J. Herdtle, W. Gollinger, W. Einholz, *Journal of Organometallic Chemistry* **1986**, *315*, 1–8.

[9] a) A. Lik, L. Fritze, L. Müller, H. Helten, *J. Am. Chem. Soc.* **2017**, *139*, 5692–5695; b) A. Lik, S. Jenthra, L. Fritze, L. Müller, K.-N. Truong, H. Helten, *Chem. Eur. J.* **2018**, *24*, 11961–11972; c) L. Fritze, N. A. Riensch, H. Helten, *Synthesis* **2019**, *51*, 399–406; d) N. A. Riensch, M. Fest, L. Fritze, A. Helbig, I. Krummenacher, H. Braunschweig, H. Helten, *New J. Chem.*, doi: 10.1039/D0NJ04297H.

[10] Q. Yin, H. F. T. Klare, M. Oestreich, *Angew. Chem. Int. Ed.* **2017**, *56*, 3712–3717.

[11] W. E. Piers, S. C. Bourke, K. D. Conroy, *Angew. Chem. Int. Ed.* **2005**, *44*, 5016–5036.

[12] A. Prokofjevs, J. W. Kampf, A. Solovyev, D. P. Curran, E. Vedejs, *J. Am. Chem. Soc.* **2013**, *135*, 15686–15689.

[13] S. A. Solomon, A. Del Grosso, E. R. Clark, V. Bagutski, J. J. W. McDouall, M. J. Ingleson, *Organometallics* **2012**, *31*, 1908–1916.

[14] M. J. Ingleson in *Topics in Organometallic Chemistry* (Eds.: E. Fernández, A. Whiting), Springer International Publishing, Cham, **2015**.

[15] V. Bagutski, A. Del Grosso, J. A. Carrillo, I. A. Cade, M. D. Helm, J. R. Lawson, P. J. Singleton, S. A. Solomon, T. Marcelli, M. J. Ingleson, *J. Am. Chem. Soc.* **2013**, *135*, 474–487.

[16] A. Del Grosso, P. J. Singleton, C. A. Muryn, M. J. Ingleson, *Angew. Chem. Int. Ed.* **2011**, *50*, 2102–2106.

[17] A. Del Grosso, M. D. Helm, S. A. Solomon, D. Caras-Quintero, M. J. Ingleson, *Chem. Commun.* **2011**, *47*, 12459–12461.

[18] a) P. Eisenberger, C. M. Crudden, *Dalton Trans* **2017**, *46*, 4874–4887; b) A. Escande, D. L. Crossley, J. Cid, I. A. Cade, I. Vitorica-Yrezabal, M. J. Ingleson, *Dalton Trans* **2016**, *45*, 17160–17167; c) T. S. de Vries, A. Prokofjevs, E. Vedejs, *Chem. Rev.* **2012**, *112*, 4246–4282.

[19] A. Lik, *Doctoral dissertation*, RWTH Aachen, Aachen, **2017**.

2.6 A Conjugated Boron-doped Tetraoxaporphyrinogen

2.6.1 Introduction

Porphine and its structural motif **1** (Figure 2.6.1) plays a key role in many essential processes in living organisms. Porphyrin complexes are best known for the transport of O_2 in the human blood and the conversion of light into usable energy in the process of photosynthesis. Additionally, they are important organic dyes. Porphyrins and related macrocycles also have various important technological applications. In recent years, there has been an increasing interest in the incorporation thereof in dye-sensitized solar cells,[1] molecular electronics[2] and in organic photovoltaic cells.[3,4] A very active field of current research is the design of new materials with tailored opto-electronic properties for such applications.[3,4]

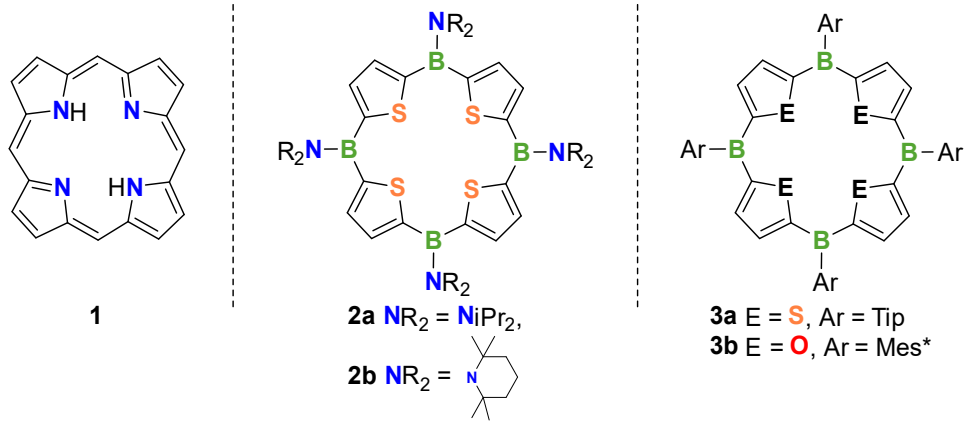

Figure 2.6.1: *Structures of porphine* ***1****, the boron-bridged tetrathiaporphyrinogens* ***2a,b****[5] and the tetrabora-porphyrinogens* ***3a,b****.[6]*

Incorporation of the vacant p orbital of boron in an organic π system leads to very interesting optic and electronic properties, enabling the resulting materials to be used for sensory and imaging applications. π-Conjugated organoboranes and respective polymers have emerged as important classes of organic−inorganic hybrid compounds in materials science.[7] Recently, the workgroups of Jäkle and Gabbai introduced highly luminescent conjugated organoboron bora-cyclophanes containing two to six Lewis acidic boron centers, which are capable of fluoride and cyanide sensing.[8,9]

In 1998, Corriu, Douglas, Siebert and coworkers reported the synthesis of the boron-bridged tetrathiaporphyrinogen **2a**.[5] Later, Siebert and coworkers added another derivative **2b** with more bulky substituents on the boron centers (Figure 2.6.1).[10] The compounds showed no evidence of macrocyclic π conjugation. Interestingly, the solid-state structure revealed a heavy twist between the thiophene rings. It has been noted that the stabilizing amino groups limit the Lewis acidity of the boron centers of **2**.[8] It seems reasonable, that the double bond

character of the BN bonds suppresses possible π-electron delocalization across the boron atoms and thus the whole macrocycle.

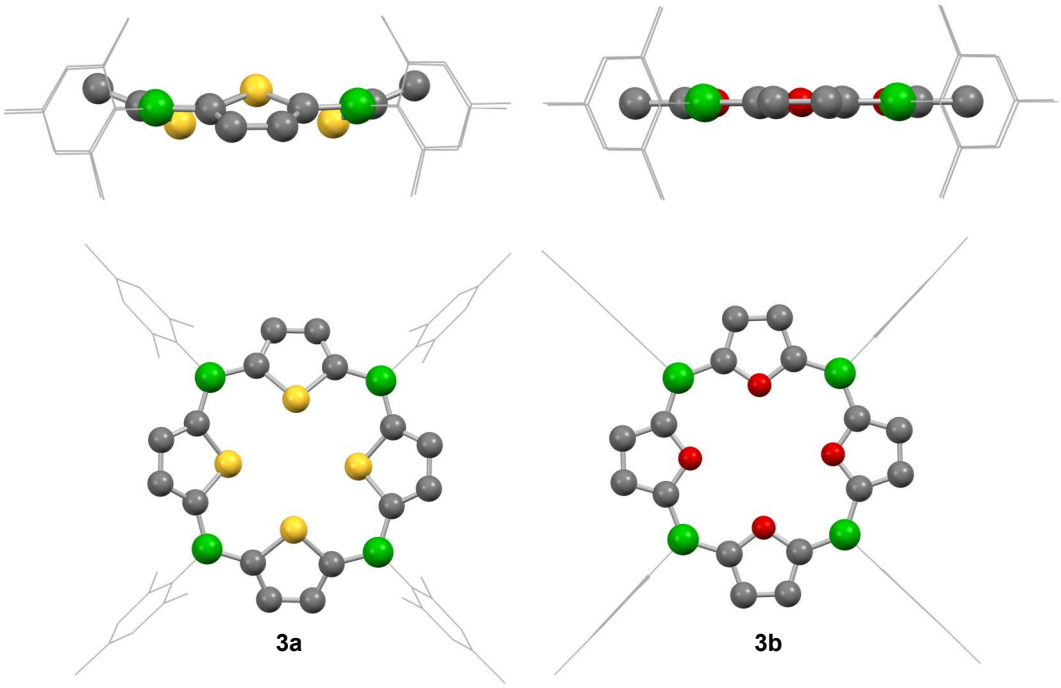

Figure 2.6.2: *DFT calculated basic structures of **3a** and **3b** (B3LYP-D3(BJ)/def2-SV(P)). Heteroatoms in green (boron), orange (sulfur) and red (oxygen).*

The Helten group has been working on the synthesis of the tetrathiaporphyrinogen **3a**, anticipating that macrocyclic conjugation should be favored if the substituent attached to the boron center is not π-donating.[6] This assumption was furthermore supported by DFT calculations done on the basic ring structure (B3LYP-D3(BJ)/def2-SV(P), Figure 2.6.2). Introduction of a bulky substituent like 2,4,6-triisopropylphenyl (Tip) not only kinetically stabilizes the boron centers, it also flattens the macrocyclic structure even further to possibly enhance π-conjugation.

Recent investigations in our workgroup have shown the benefits of implementing furan in π-conjugated boron-containing structures to enhance their opto-electronic properties.[11,12,13] Therefore, we decided to target a boraporphyrinoid structure motif containing furan rings. Herein, we present the attempted synthesis of the first fully π-conjugated tetraoxaporphyrinogen **3b**. An initial idea for the reaction route was given from previous work in our group, where the synthesis of tetrathiaporphyrinogen **3a** was attempted (Scheme 2.6.1).[6]

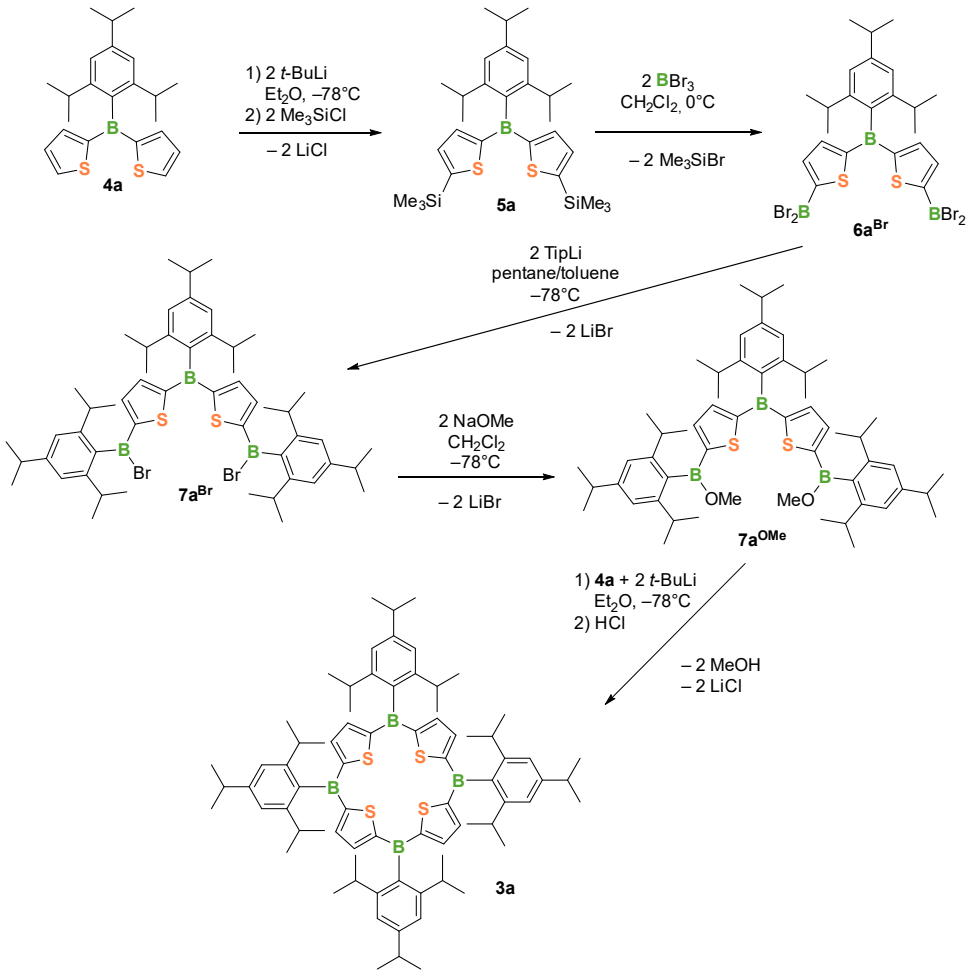

Scheme 2.6.1: *Multi-step synthesis of tetrathiaporphyrinogen **3a** starting from triarylborane **4a**.*

The tetraboratetrathiaporphyrinogen **3a** was synthesized in a multi-step synthesis starting from triarylborane **4a**. After consecutive steps of disilylation to **5a**, diborylation to **6a**, diarylation to **7a^{Br}** and salt metathesis to **7a^{OMe}**, the ring-closing reaction to **3a** was performed.

Thiophene-based organoboranes are well-known and have been recently well-explored, which led to many examples of highly stable compounds. Those characteristics can be transferred to the shown reaction route, in which all intermediate stages are reasonably stable and isolable. In general, furan-based organoboranes were found to be more reactive and therefore less stable.[14] Previous investigations of our workgroup underline that statement.[11,12] To enhance the kinetic stabilization at the boron atoms of aryl(difuryl)boranes, 2,4,6-tri-*tert*-butylphenyl (supermesityl, Mes*) was considered as an even bulkier substituent.

2.6.2 Results and Discussion

Analogous to the synthesis of tetraboratetrathiaporphyrinogen **3a**, the starting point of the multi-step route to tetraoxaporphyrinogen **3b** was triarylborane **4b**, which has been synthesized via a silicon/boron exchange procedure described by us previously.[11] To introduce further functionality, **4b** was disilylated at its 5,5'-positions to form **5b** (Scheme 2.6.2).

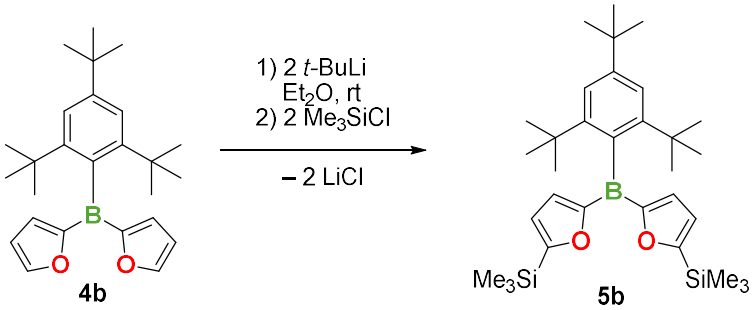

Scheme 2.6.2: *Synthesis of* ***5b****.*

The differences in stability between thienyl- and furylboranes became apparent in the following reaction step. Similar to their smaller analogues, dibromo(thiophen-2-yl)borane and dibromo(fur-2-yl)borane, the stability of the furan-based compounds **6b** was drastically decreased compared to thiophene-based compound **6a**. In an attempt to synthesize and isolate the species **6b**, compound **5b** was treated with different trihaloboranes (BX_3) in dichloromethane (DCM, Scheme 2.6.3).

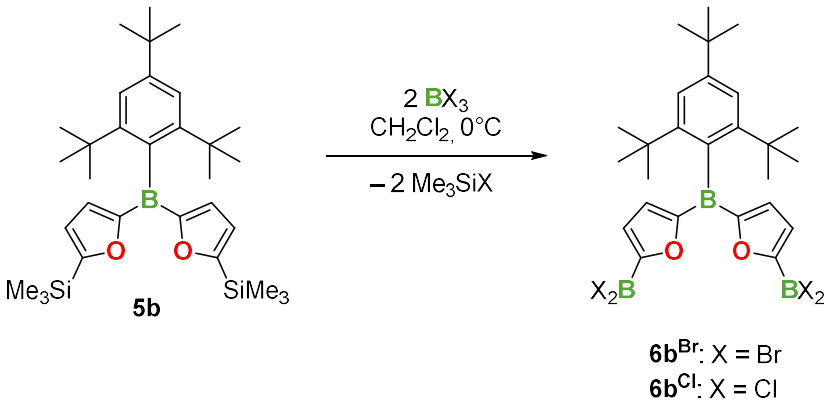

Scheme 2.6.3: *Synthesis of* ***6b****.*

While the reaction to **6b^{Br}** was complete in 30 minutes, about four times as fast compared to **6a^{Br}**,[15] a decomposition of the desired product and, among other unidentified compounds, the formation of Mes* was observed (Figure S5.6.1). Even after this short reaction time, about 5% decomposition was took place. Similar results were obtained for its less reactive, but more stable analogue **6b^{Cl}**. Removal of the solvent or other isolation techniques like precipitation failed because of fast decomposition of the products.

As a consequence of the labile nature of the dihaloborane (BX_2) species, attempts of converting these species to more stable compounds were made. Those attempts were performed *in situ*. For that purpose, different approaches were chosen (Scheme 2.6.4).

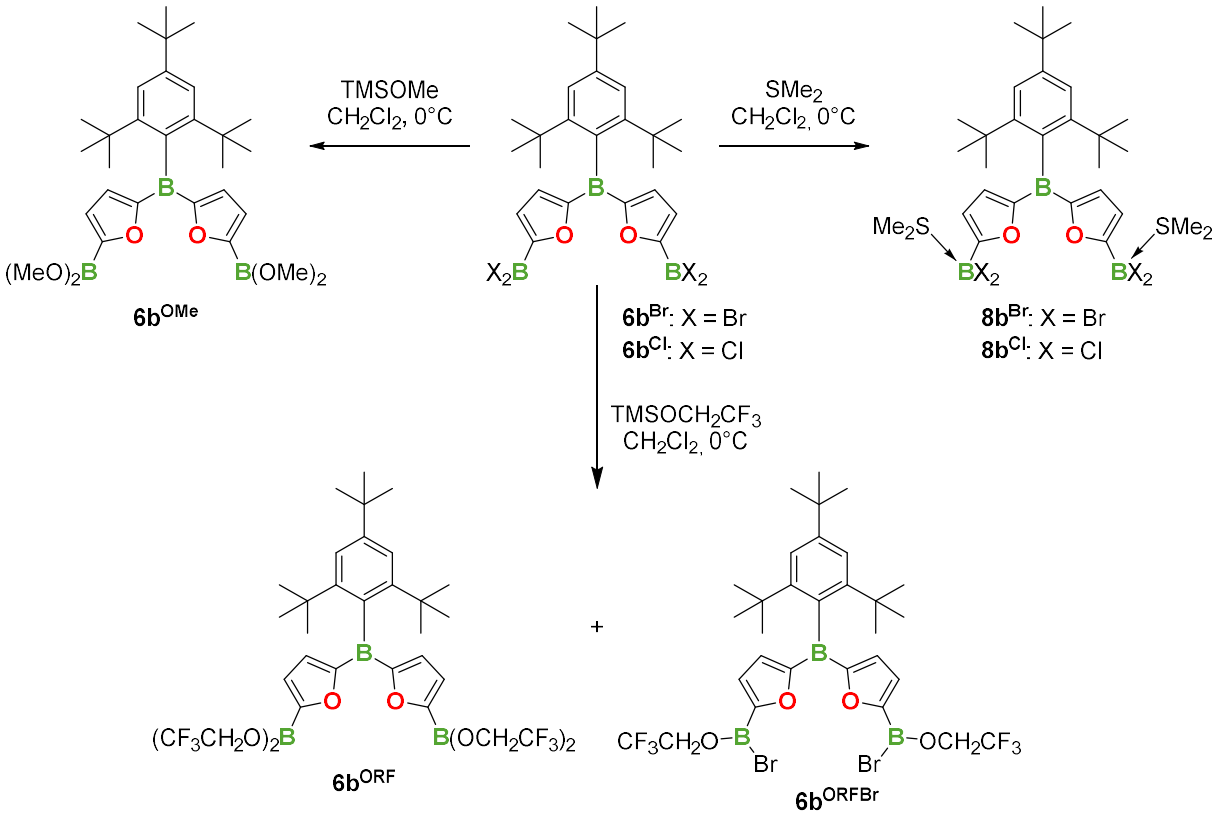

Scheme 2.6.4: *In situ reactions of* ***6b****.*

One approach to stabilize the compounds was the substitution of the halide substituents by alkoxy groups. An attempt to perform a salt metathesis procedure by adding sodium methoxide (NaOMe) to **6b^{Br}**, however, led to complete decomposition of the substrate. As another possible way to the desired dialkoxyboranes, reactions of **6b^{Br}** with alkoxytrimethylsilanes were explored. The addition of methoxytrimethylsilane (TMSOMe) to **6b^{Br}** rapidly gave the desired compound **6b^{OMe}**. Additionally, the use of TMSOMe offered the opportunity of facile removal of the formed trimethylsilylhalides (TMSX) in vacuo at ambient temperature.

The addition of trimethyl(2,2,2-trifluoroethoxy)silane (TMSORF), however, did not lead to the formation of the desired compound **6b^{ORF}**. $^{11}B\{^1H\}$ NMR spectroscopic analysis of the reaction mixture suggested the formation of a mixed species **6b^{ORFBr}** (δ = 34.4 ppm, Figure S5.6.2) alongside with **6b^{ORF}** (δ = 23.9 ppm) and tris(2,2,2-trifluoroethoxy)borane ($B(OR^F)_3$, δ = 17.8 ppm). Isolation of **6b^{ORF}** via separation of the different species was unsuccessful. Removal of all volatiles resulted in a brown oil and severe broadening of the $^{11}B\{^1H\}$ NMR signals. A continuous intermolecular exchange of Br and OCH_2CF_3 substituents was feasible, hindering the successful separation. For the selective synthesis of **6b^{ORF}**, a different route was chosen (Scheme 2.6.5). Dilithiation of **4b**, followed by addition of a large excess of $B(OR^F)_3$, successfully yielded compound **6b^{ORF}**. Compared to **6b^{OMe}**, this species should favor subsequent substitution reactions with aryllithium reagents, because of the more electron-withdrawing (EW) character of the fluoroalkoxy substituents. Additionally, it should remain

stable in ethers such as diethylether (OEt_2) or tetrahydrofuran (THF), enabling reactions to be performed in such solvents, in which the lithiated reactant should show increased reactivity.

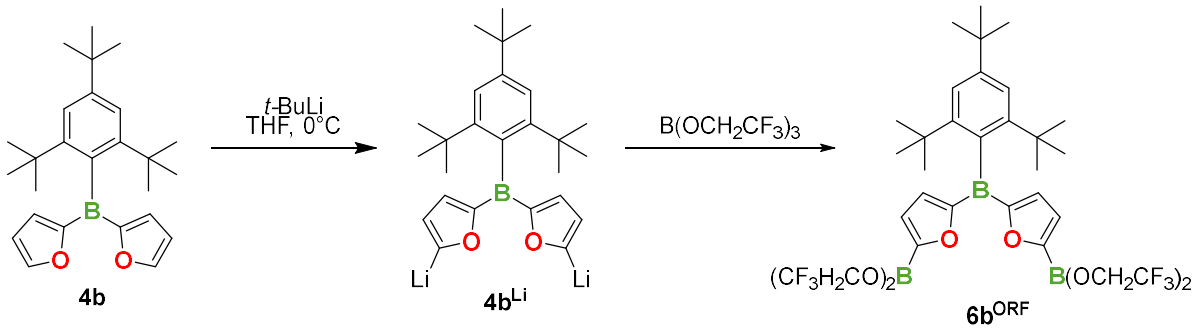

Scheme 2.6.5: *Synthesis of* ***6b^{ORF}****.*

In a different attempt, the stabilization of the highly reactive compounds **6b^{Br}** and **6b^{Cl}** through coordination of the electrophilic boron center was investigated. Addition of dimethyl sulfide (SMe_2) to species **6b** as stabilizing agent to coordinate to the boron centers led to formation of **8b^{Br}** and **8b^{Cl}**. After removal of all volatiles, **8b^{Br}** decomposed slowly even at low temperatures of -78 °C. **8b^{Cl}** on the other hand was reasonably stable, even when stored at room temperature and being solved in ethers such as OEt_2.

In summary, the conversions of the labile BX_2 species to more stable moieties were partially successful. Changing the substituents to alkoxy groups seemed to have the most effect in the stability of the resulting compounds. SMe_2 adduct formation also improved the stability of the compounds, but did not give a stable species in case of bis(dibromo)borane **6b^{Br}**.

In the next step, the synthesis of **7b** and analogues thereof was attempted. First, the reactivity of compound **8b^{Cl}** towards 2,4,6-tri-*tert*-butylphenyl)lithium (Mes*Li) was investigated by adding both reactants together in either toluene or OEt_2 (Scheme 2.6.6).

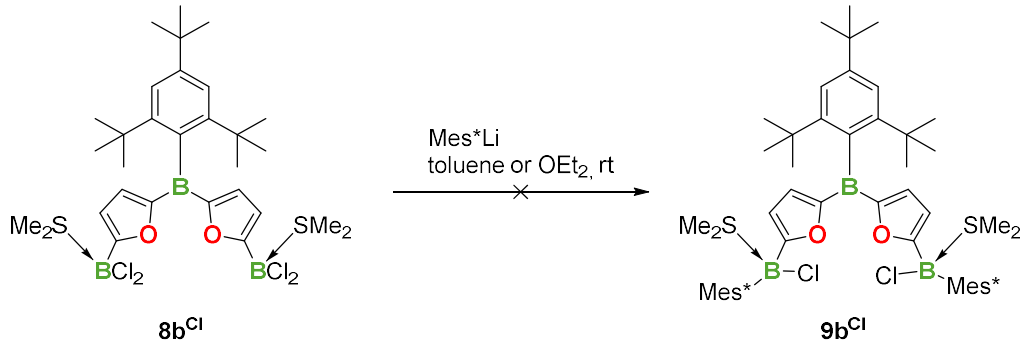

Scheme 2.6.6: *Attempted synthesis of* ***9b^{Cl}****.*

However, no reaction to the desired **9b^{Cl}** could be observed in both solvents. Furthermore, the addition of Mes*Li led to formation of an insoluble solid in the reaction mixture. ^{1}H NMR

spectroscopic analysis of the solution suggested decomposition of the substrate initiated by the dissociation of the SMe_2 ligand.

For this reason, the focus was on the substitution of dialkoxyboranes **6b^{OR}** and the synthesis of **7b^{OMe}** was attempted. After addition of Mes*Li to the substrate in either toluene or OEt_2, the reaction was stirred for 16 h, showing a full conversion of the substrate **6b^{OMe}** to a boron species with an $^{11}B\{^1H\}$ NMR shift of δ = 3.4 ppm, a region where quaternary boron species are expected. Earlier investigations in our workgroup on that reaction type have shown that a formation of a lithium borate **7'b^{OMe}** is feasible, which could possibly be transformed into the desired product **7b^{OMe}** by a salt metathesis reaction (Figure 2.6.3).

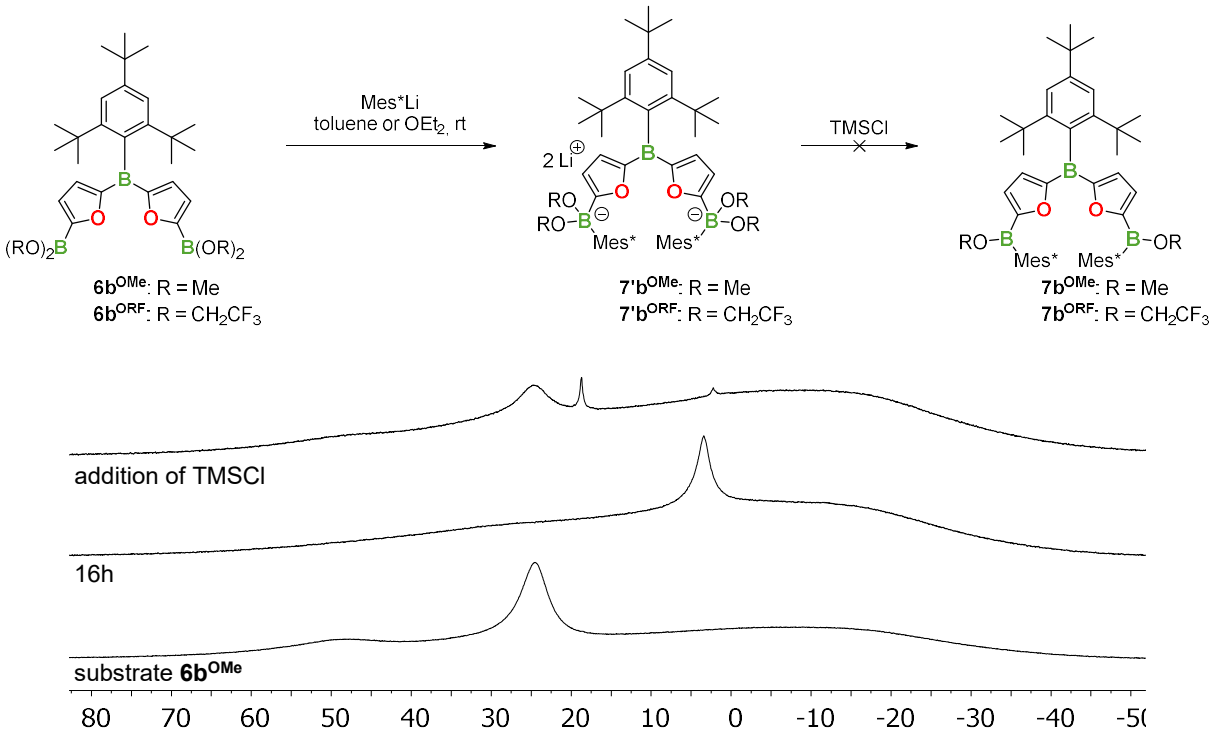

Figure 2.6.3: *Attempted reaction of **6b^{OR}** with Mes*Li and corresponding $^{11}B\{^1H\}$ NMR spectra of **6b^{OMe}** ($CDCl_3$).*

The isolation of **7b^{OMe}** was attempted by addition of chlorotrimethylsilane (TMSCl) or hydrogen chloride (HCl) to the reaction mixture to induce abstraction of the OMe^- leaving group. These attempts always led to re-formation of the substrate **6b^{OMe}** (Figure 2.6.3). In the reaction, additionally formation of trimethyl borate ($B(OMe)_3$) was observed after the addition (δ = 18.7 ppm) of TMSCl when using toluene as solvent. This suggested partial decomposition of the reaction partners. In OEt_2, the reaction took a similar path, with an $^{11}B\{^1H\}$ signal for a quaternary boron species that was slightly shifted (δ = 4.4 ppm), and no observable formation of $B(OMe)_3$. If species **7'b^{OMe}** was formed, the elimination of the bulky Mes* substituent seems to be favored over B–O bond cleavage and accompanying elimination of the methoxy substituent. Using the corresponding Grignard reagent (2,4,6-tri-*tert*-butylphenyl)magnesium

bromide (Mes*MgBr) instead of Mes*Li did not give the desired product either, rather leading to decomposition of the system under formation of $B(OMe)_3$.

For **6b^{ORF}**, very similar results were obtained. At first, a quaternary boron species was formed in both solvents after adding Mes*Li to the substrate (in OEt_2: δ = 3.8 ppm, in toluene: δ = 2.7 ppm). Addition of TMSCl had no effect on the reaction mixture, while addition of HCl led to regeneration of **6b^{ORF}** and $B(OR^F)_3$ (Figure S5.6.3).

A model reaction of the smaller dimethoxy(furan-2-yl)borane **10** with Mes*Li in OEt_2 also showed similar results (Figure 2.6.4).

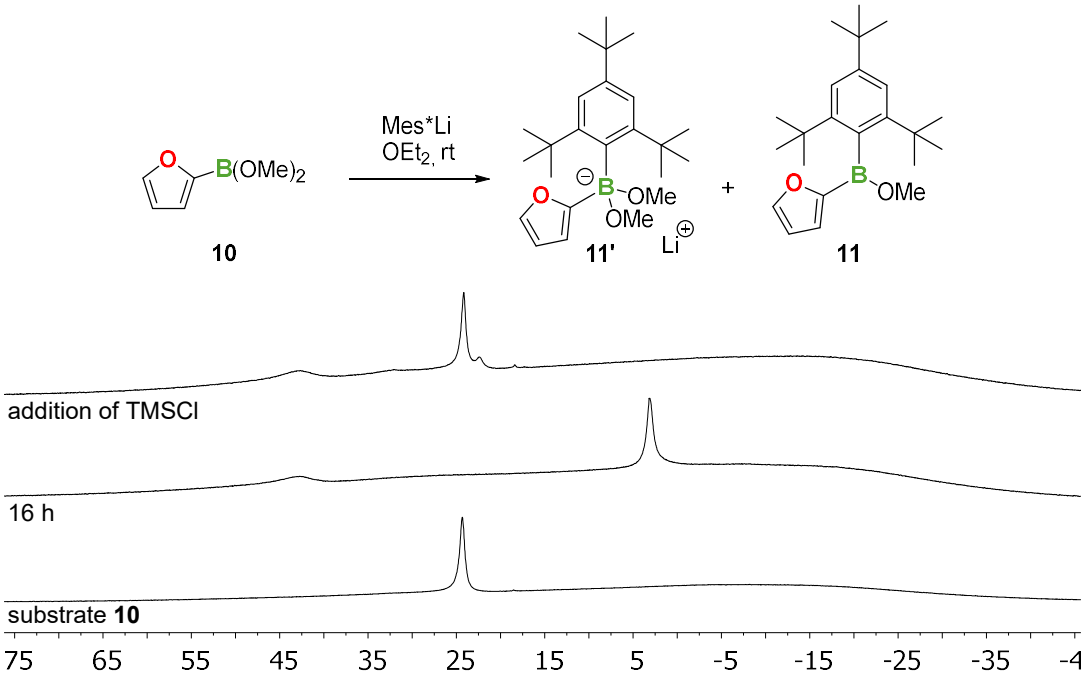

Figure 2.6.4: *Reaction of **10** with Mes*Li and $^{11}B\{^1H\}$ NMR spectra of the corresponding reaction mixture ($CDCl_3$).*

After 16h reaction time all of the substrate was converted, mainly to another quaternary boron species **11'** (δ = 3.1 ppm), very similar to the attempted reaction to **7b^{OMe}**. In this reaction, approximately 20% was converted to a species with a chemical shift of δ = 42.7 ppm, a feasible region for the desired product **11**. Addition of TMSCl and HCl transformed the quaternary boron species back to the substrate **10** with small formation of $B(OMe)_3$ (δ = 18.3 ppm). Heating this reaction to 40 °C had no effect on its selectivity or conversion. Obviously, the formation of the quaternary boron species represents a competing reaction to the formation of the desired product. Comparison of the reactivities of **10** and **6b^{OMe}** revealed that the electronic structure of **6b^{OMe}** should have a lower reactivity due to the triarylborane group at the 5-position of the furan ring. This electron-withdrawing group (EWG) seems to drastically lower the reactivity in the applied substitution procedure.

A further route that was attempted to obtain the desired diarylborane was the direct transformation of the dihaloboranes **6b** to **7b**. Here, a much higher stability could be expected from the desired product compared to the substrate. Again, **6b** had to be transformed *in situ* using Mes*Li. Since the borylation to **6b** was previously performed in DCM, which cannot be used in combination with a lithiated species, a different protocol had to be applied. To this end, **6b** was synthesized in toluene. As expected, the lower reactivity of the substrates in toluene led to a reaction time of around 16 h (Scheme 2.6.7).

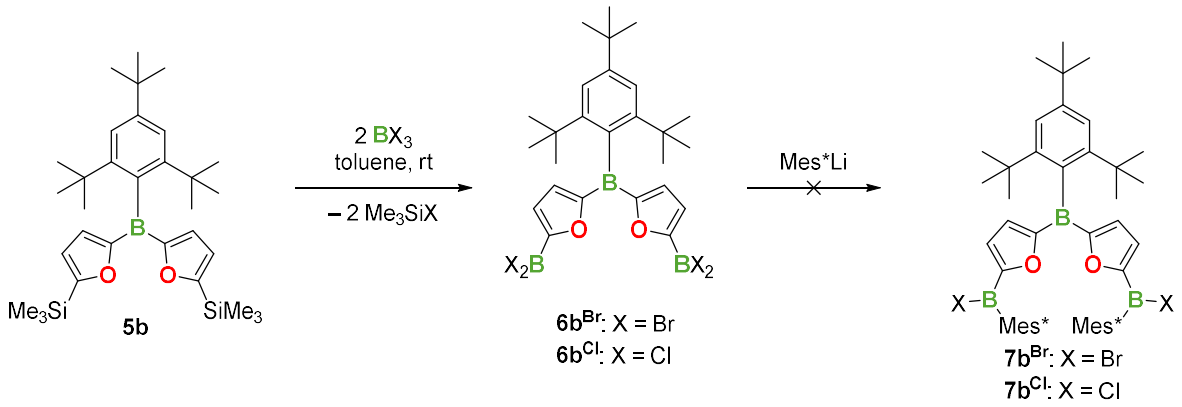

Scheme 2.6.7: *Attempted synthesis of haloboranes* ***7b****.*

After the formation of **6b** was complete, remaining BX_3 species and TMSX were removed under reduced pressure (100 mbar). Then, Mes*Li was added to the reaction mixture which has proven to be stable in toluene. Severe broadening and overlapping of the $^{11}B\{^1H\}$ NMR signals complicated the evaluation of the reaction outcome (Figure S5.6.4), but mass spectrometry analysis of the reaction mixture showed no traces of the desired products **7b^{Br}** (Figure S5.6.5) or **7b^{Cl}** (Figure S5.6.6). Instead, they both showed two main signals at m/z = 473.28 Da and 966.91 Da, which do not resemble any of the partaken substances. To enhance the reactivity of the arylation reagent in toluene, small amounts of OEt_2 were added to the reaction mixture in the case of that of **6b^{Br}**. This led to complete transformation of the substrate to a dialkoxyborane.

The substitution of the boron centers turned out to be more difficult than expected. As an alternative approach, the Mes* substituent was introduced to the boron center first and the resulting supermesitylborane was used as a reactant for the reaction with **4b^{Li}**. To this end, the lithiated species **4b^{Li}** was generated, which then was attempted to react with different aryl(dimethoxy)boranes to directly yield diarylborates **7b^{OMe}**, **12b^{OMe}** or **13b^{OMe}** (Scheme 2.6.8).

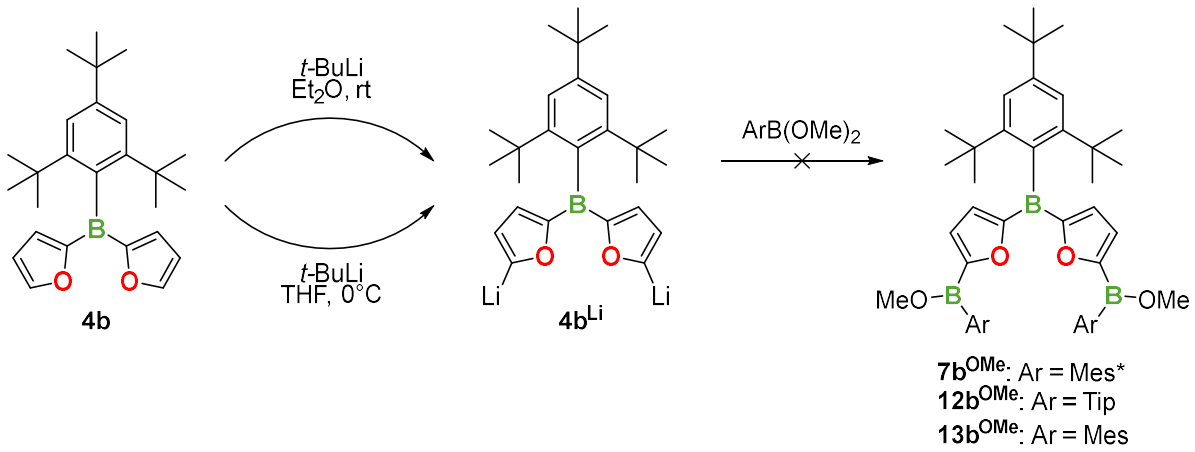

Scheme 2.6.8: *Attempted synthesis of methoxyboranes* ***7b****,* ***12b*** *and* ***13b****.*

In the first step, the lithiation was performed similar to the synthesis of compound **5b**. To this end, **4b** was stirred with *tert*-butyllithium in OEt_2 at room temperature for 3 h. After the lithiation was complete, dimethoxy(supermesityl)borane ($Mes^*B(OMe)_2$) was added to the reaction mixture, which was then stirred overnight. $^{11}B\{^1H\}$ NMR spectroscopic analysis of the reaction mixture revealed that no reaction took place. Only the two signals of the substrates were observed: A broadened peak for **4b** (δ = 47.6 ppm) and a sharp signal for $Mes^*B(OMe)_2$ (δ = 32.4 ppm) (Figure S5.6.7). Additionally, ^1H NMR spectroscopic analysis confirmed this result. Using tetramethylethylenediamine (TMEDA) as an additive to enhance the reactivity of **4b^{Li}** did not change the reaction outcome. To prove the formation of **4b^{Li}** and assess its reactivity in this reaction, other aryl(dimethoxy)boranes were used: dimethoxy-(2,4,6-tri-iso-propylphenyl)borane ($TipB(OMe)_2$) and dimethoxy(2,4,6-tri-methylphenyl)borane ($MesB(OMe)_2$) to yield **12b^{OMe}** and **13b^{OMe}**, respectively. While the reaction mixtures in both cases were also heated to reflux, and $MesB(OMe)_2$ was added to the lithiated species in THF, low conversion was observed to quaternary boron species with resonances at δ = −3.0 ppm (Ar = Tip) and δ = −5.0 ppm (Ar = Mes) in the $^{11}B\{^1H\}$ NMR spectra (Figure S5.6.8). In both cases, addition of TMSCl or HCl did not convert these species to the desired product. Here, the influence of the steric demand of the aryl substituents became apparent, drastically lowering the reactivity of the reactants. Additionally, the lithiated compound **4b^{Li}** appeared to have relatively low reactivity as well. In the next step, dibromo(supermesityl)borane (Mes^*BBr_2) and dichloro(supermesityl)borane (Mes^*BCl_2) were used. Since the lithiation took place in an ether as the solvent, which is not compatible with the BX_2 species, the solvent was removed in vacuo after the lithiation of **4b** was complete and, to ensure stability of all reactants in the solvent, it was changed to pentane or toluene (Scheme 2.6.9). Stability of **4b^{Li}** through this process was beforehand investigated by adding TMSCl in pentane to form **5b** in >90% yield.

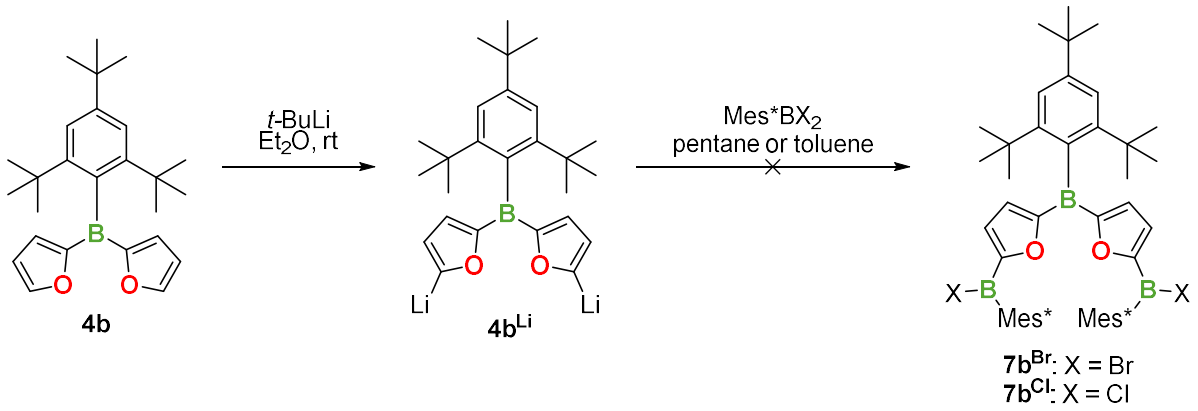

Scheme 2.6.9: *Attempted synthesis of haloboranes* ***7b****.*

Again, $^{11}B\{^{1}H\}$ NMR spectroscopic analysis revealed low conversions to quaternary boron species for both reactants at δ = -6.2 ppm (X = Br) and δ = -12.7 ppm (X = Cl) which could not be transferred to the desired product (Figure S5.6.9). Additionally, no direct formation of the desired species **7b** was observed.

Concluding, the substitution of the boron centers to yield the ring precursor **7b** or its analogues was not successful. Carrying the bulky Mes* group as a first or a substituent on the boron centers seems to lower the amount of space around it so drastically that no further substitution at those positions was possible under the applied conditions.

A different approach that was attempted to synthesize tetraoxaporphyrinogen **3b** is a [2+2]-cycloaddition reaction first to give the partially unprotected ring **14b**, then adding the bulky substituent Mes* in a follow-up reaction (Scheme 2.6.10).

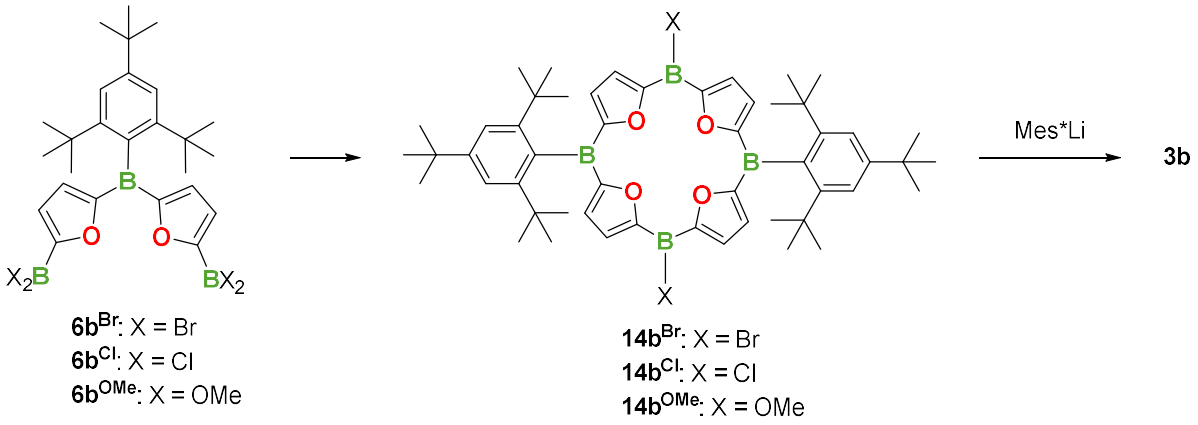

Scheme 2.6.10: *Alternative route to tetraoxaporphyrinogen* ***3b****.*

This route would give the macrocyclic framework first, potentially yielding a stable intermediate, in which then the bulky substituent Mes* could be introduced. This approach is analogous to the synthesis of **4b**.[11] On one hand, the procedure would also allow a more facile variation of the third aryl substituent on the boron centers, since it can happen in the last reaction step. On the other hand, the higher reactivity of the compounds **6b** in comparison to their kinetically

stabilized analogues **7b** may be prone to unwanted side reactions in the ring-closing reaction step. [2+2]-Cycloadditions are highly sensitive to the reaction parameters like temperature and concentration. As a competitive reaction, linear molecules could form, drastically lowering the yield of the desired product. The procedure for the ring-closing reaction significantly changes for the existing substituent X.

For X = Br and Cl, the silicon/boron exchange procedure developed in our workgroup was performed (Scheme 2.6.11). To guarantee the stability of all reaction partners and to control the reaction rate, **6**^{Br} or **6**^{Cl} were first synthesized in toluene. Afterwards, **5b** and catalyst (for X = Br: $TMSNTf_2$, for X = Cl: $Ag[Al(OC(CF_3)_3)_4]$) were added at room temperature. A detailed discussion of the silicon/boron exchange reaction can be found in chapter 2.4 of this work.

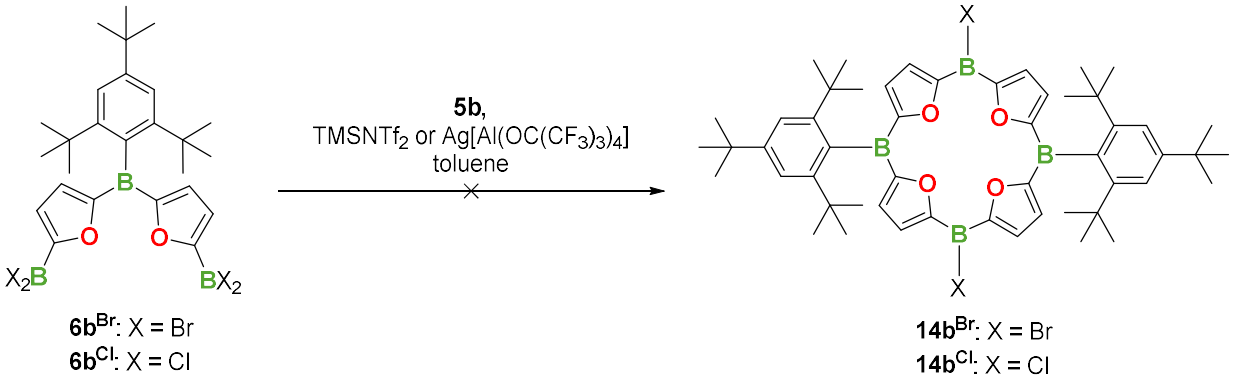

Scheme 2.6.11: *Attempted synthesis of* ***14b*** *via silicon/boron exchange.*

Both reactions were examined via mass spectrometry and no evidence of a successful reaction to macrocycle **14b** was found (Figure S5.6.10 and Figure S5.6.11). The reactivity of the system seemed to be too low in the unpolar solvent to perform the silicon/boron exchange reaction. Paired with side reactions and partial decomposition processes, that rendered this procedure to be not effective.

For X = OMe, model reactions were performed to test the behavior of the compounds towards lithiated furan species. To this end, furyllithium (FurLi) was added to the compounds **6b**^{OMe} and **10** in OEt_2 or THF at room temperature to evaluate the influence of the EWG in the 5-position of the furan ring (Figure 2.6.5).

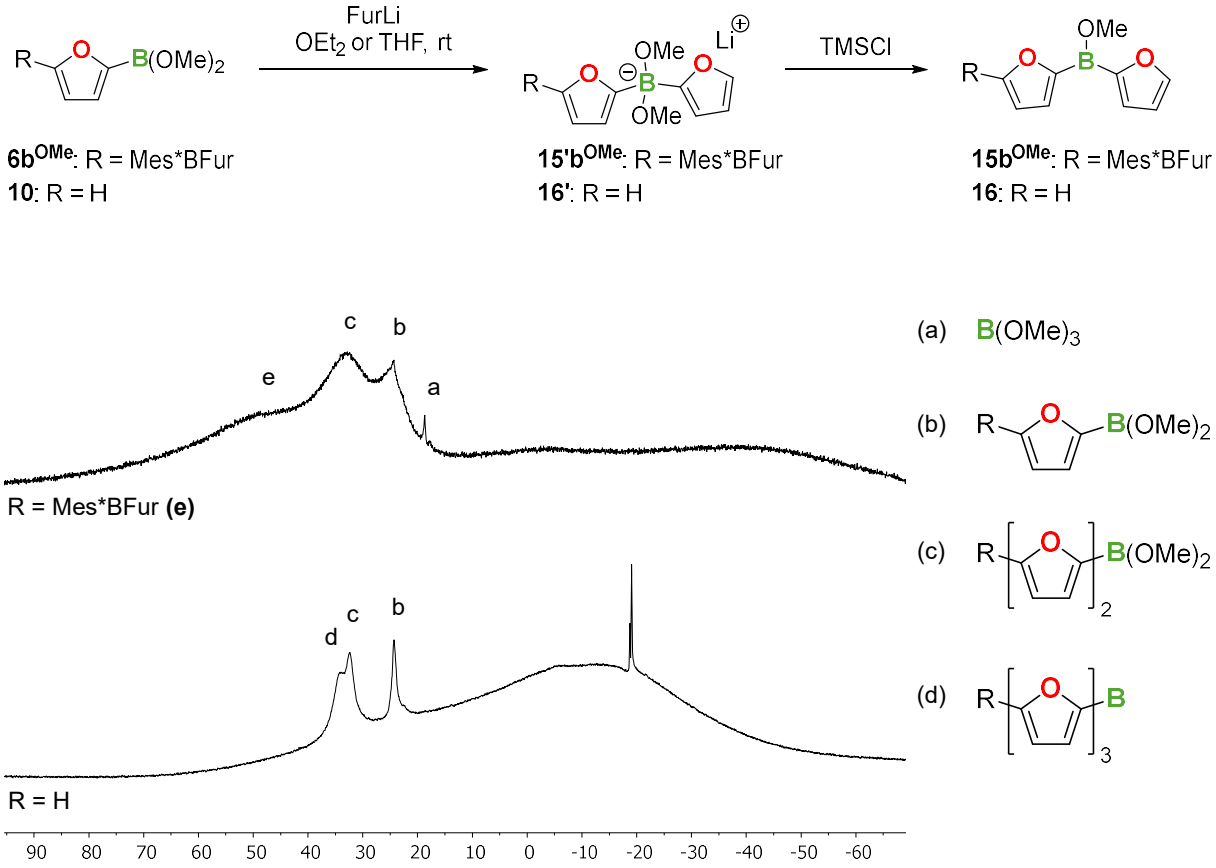

Figure 2.6.5: *Reaction of* ***6b^{OMe}*** *and* ***10*** *with FurLi and $^{11}B\{^1H\}$ NMR spectra of the reaction mixture after addition of TMSCl (in $CDCl_3$).*

Both reactions gave similar results. At first, quaternary boron species were formed, which could be transformed to the desired compounds by addition of TMSCl. Both reactions showed an unselective formation of a mixture of mono-, di- and triarylboranes, which indeed confirmed the suitable reactivity of the aryl(dimethoxy)borane species, while also advising caution before the unwanted third substitution with furan.

In the next step, **6b^{OMe}** and **4b^{Li}** were used to reproduce these reactions (Scheme 2.6.12). In a first test reaction, a relatively high concentration of the substrates (c = 0.75 mol/L) was chosen, to test their general reactivity. For this, formation of linear products was taken into consideration.

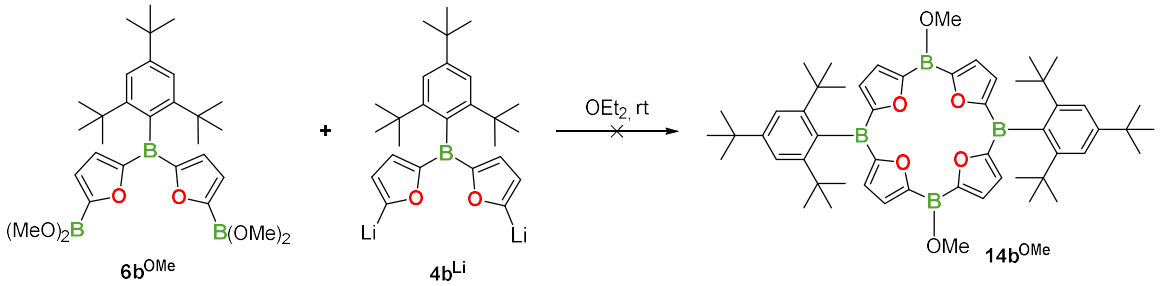

Scheme 2.6.12: *Attempted reaction to* ***14b^{OMe}***.

Again, a quaternary boron species was formed (δ = -2.9 ppm), which could be transformed by addition of TMSCl. The resulting $^{11}B\{^{1}H\}$ NMR spectrum of the reaction mixture revealed that no reaction took place (Figure S5.6.12). Furthermore, mass spectrometry analysis of the reaction mixture showed no traces of the desired product **14b^{OMe}**. It showed mainly the substrate **6b^{OMe}** (Figure S5.6.13). The elimination of the furyl substituent again seemed to be preferred over the B–O bond cleavage and accompanying elimination of the methoxy group.

Following that reaction path, the next step would be the third substitution of a difuryl(methoxy)borane species. Another set of model reactions was performed, testing the third substitution capabilities of **16** (Scheme 2.6.13).

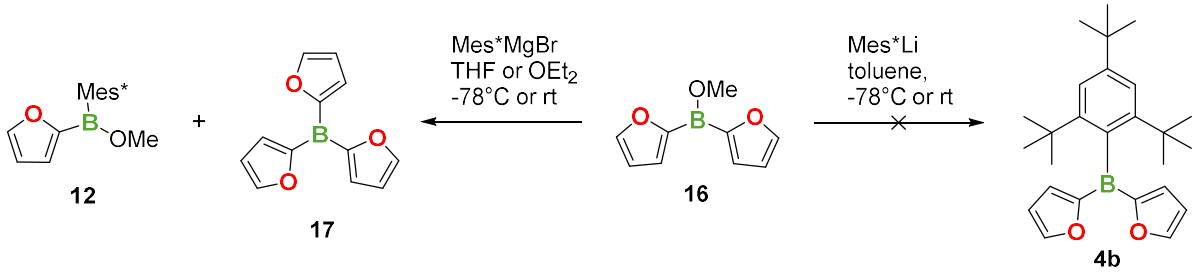

Scheme 2.6.13: *Attempted reaction of **16b^{OMe}** with Mes*Li and Mes*MgBr.*

The reactions were carried out in different solvents like THF, OEt_2 or toluene, and temperatures between -78 and 40 °C. While both aryl reagents caused a reaction to one or more different quaternary boron species (Figure S5.6.14), no formation of the desired product was observed. Again, no transformation of those species to the desired product succeeded. For Mes*MgBr, small amounts of furyl(supermesityl)(methoxy)borane **12** and trifurylborane **17** were formed, underlining the competition of the furyl, Mes* and OMe substituents at the boron center and showing their very similar prioritization. A third substitution on the boron center of a di(furyl)methoxyborane was not feasible. These model reactions show that additional adaptions would have to be made when further perusing the formation to the tetraoxaporphyrinogen **3b** via **14b^{OMe}**. A substitution of the OMe substituent with a more reactive halogen like Br or Cl to yield **14b^{Br}** or **14b^{Cl}** could help in the third substitution step (Scheme 2.6.14).

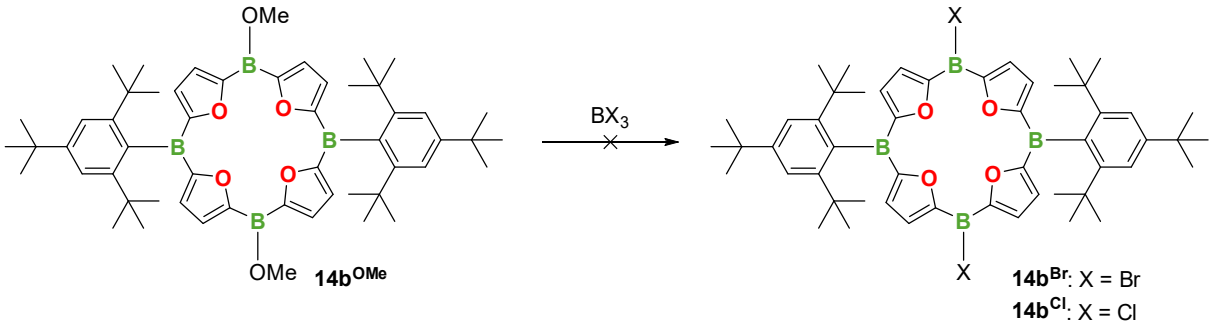

Scheme 2.6.14: *Transformation of* ***14b^{OMe}*** *to* ***14b^{Br}*** *or* ***14b^{Cl}****.*

2.6.3 Conclusion

The applied reaction routes did not lead to a successful formation of tetraoxaporphyrinogen **3b**. Central problems of the different reaction routes is the low reactivity of the reactants caused by either electric or steric hindrance. Further research in this field may involve the reaction of a bisstannyl compound **17** with compounds **6b** in a highly diluted solution (Scheme 2.6.15). The major advantage of this is the reaction proceeding in the absence of a catalyst, which could be beneficial for the formation of macrocycle **14b**. The higher reactivity of the organotin compounds compared to silylated compounds offers the opportunity to further tailor the reaction conditions by variation of the solvent's polarity. Furthermore, the preservation of the halide substituents should allow for better third substitution possibilities to give tetraoxaporphyrinogen **3b** in the final step of the protocol.

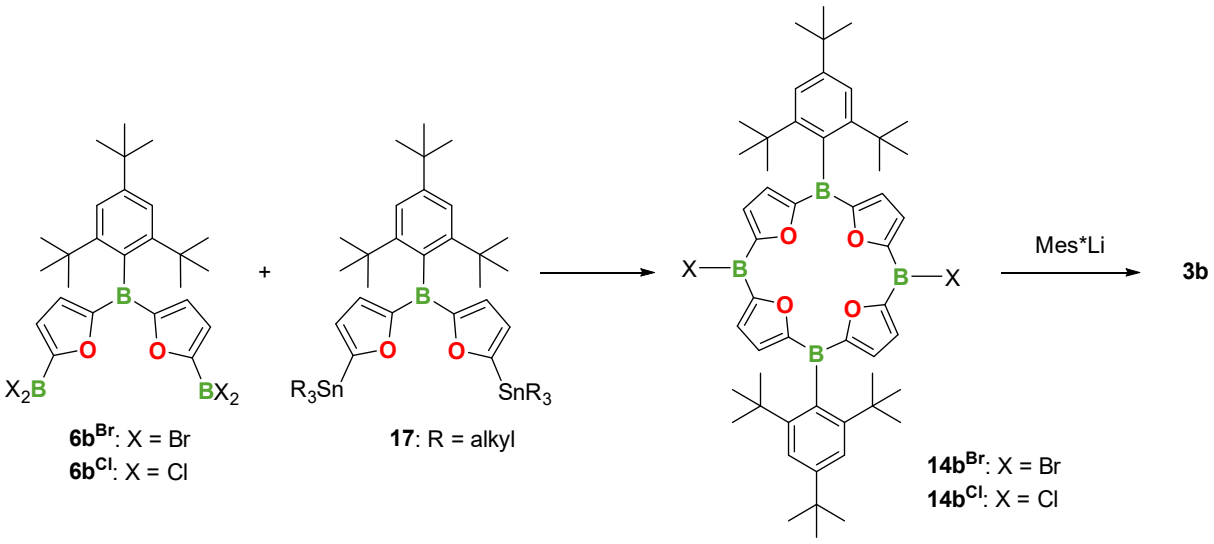

Scheme 2.6.15: *Reaction scheme of* ***6b*** *and* ***17*** *to yield* ***14b*** *and possible follow-up reaction to* ***3b****.*

2.6.4 Experimental Section

General procedures. All manipulations were performed under an atmosphere of dry argon using standard Schlenk techniques or in an MBraun glove box. Solvents (diethylether, toluene and tetrahydrofuran) were dried and degassed by means of an MBraun SPS-800 solvent purification system.

Deuterated solvents for NMR spectroscopy were dried and degassed at reflux over CaH ($CDCl_3$) or Na (C_6D_6) and freshly distilled prior to use. Solutions of *tert*-butyllithium (1.6 M and 1.7 M in *n*-pentane), trichloroborane (1 M in DCM and hexane) and tribromoborane were purchased from Sigma Aldrich and used as received as well. 2,2,2-Trifluoroethanol, dimethylsulfide and trimethoxyborane were degassed and freshly distilled prior to use. **4b** was prepared according to procedures previously described by us.[11] Mes*Li[16] and Mes*MgBr[17] were prepared according to procedures described in the literature.

NMR spectra were recorded at 25 °C on a Bruker Avance III HD spectrometer operating at 300 MHz, on a Bruker Avance III Nanobay 400 operating at 400 MHz. Chemical shifts were referenced to residual protic impurities in the solvent (^1H) or the deuterated solvent itself (^{13}C) and reported relative to external $SiMe_4$ (^1H, ^{13}C) or $BF_3{\cdot}OEt_2$ (^{11}B) standards.

Mass spectra were obtained with the use of a Thermo Scientific Exactive Plus Orbitrap MS system employing either atmospheric sample analysis probe (ASAP), atmospheric pressure chemical ionization (APCI) or liquid injection field desorption ionization (LIFDI).

Synthesis of **6b^{Br}**. To a solution of **5b** (53.5 mg, 0.10 mmol) in DCM (0.2 mL) was added BBr_3 (51.4 mg, 0.21 mmol) at 0 °C and stirred for 1 h. Alternatively, the reaction was performed in toluene (0.2 mL) and stirred overnight. ^1H NMR (400 MHz, $CDCl_3$): δ = 7.72 (d, J = 3.6 Hz, 2H, Fur-*H*), 7.46 – 7.41 (br, 2H, Fur-*H*), 7.43 (s, 2H, Mes*-*H*), 1.39 (s, 9H, *p*-*t*BuC*H*$_3$), 1.15 (s, 18H, *o*-*t*BuC*H*$_3$); $^{11}B\{^1H\}$ NMR (160 MHz, $CDCl_3$): δ = 47.6 (s).

Synthesis of **6b^{Cl}**. To a solution of **5b** (53.5 mg, 0.10 mmol) in DCM (0.2 mL) was added BCl_3 (1.0 M, 0.21 mL, 0.21 mmol) at 0 °C and stirred for 4 h. Alternatively, the reaction was taken out in toluene (0.2 mL) and stirred overnight. ^1H NMR (400 MHz, $CDCl_3$): δ = 7.59 (d, J = 3.6 Hz, 2H, Fur-*H*), 7.41 (s, 2H, Mes*-*H*), 7.39 – 7.35 (br, 2H, Fur-*H*), 1.38 (s, 9H, *p*-*t*BuC*H*$_3$), 1.13 (s, 18H, *o*-*t*BuC*H*$_3$); $^{11}B\{^1H\}$ NMR (160 MHz, $CDCl_3$): δ = 47.5 (s).

Synthesis of $B(OCH_2CF_3)_3$. To a solution of BCl_3 (14.46g, 123.4 mmol) in DCM (120 mL) was added 2,2,2-trifluoroethane (37.17 g, 370.23 mmol) at -78 °C. Subsequently, the mixture was warmed to rt overnight. All volatiles were removed in vacuo (100 mbar) and the crude product was distilled in vacuo (bp: 42 °C at 30 mbar) to yield $B(OCH_2CF_3)_3$ as a colorless liquid. Yield:

31.54 mg (102.4 mmol, 83 %); ^{1}H NMR (300 MHz, $CDCl_3$): δ = 4.22 (q, J_{HF} = 8.3 Hz, 6H); $^{11}B\{^{1}H\}$ NMR (96 MHz, $CDCl_3$): δ = 17.8 (s).

Synthesis of **8b^{Br}**. To a solution of **5b** (53.5 mg, 0.10 mmol) in DCM (0.2 mL) was added BBr_3 (51.4 mg, 0.21 mmol) at 0 °C and stirred for 1 h. Then, SMe_2 (13.0 mg, 0.21 mmol) was added to the reaction mixture at 0 °C. The mixture was stirred for 2 h and all volatiles were removed in vacuo. ^{1}H NMR (300 MHz, $CDCl_3$): δ = 7.40 (s, 2H, Mes*-*H*), 7.39 – 7.25 (br, 2H, Fur-*H*), 6.92 (d, *J* = 3.4 Hz, 2H, Fur-*H*), 2.19 (s, 12 H, S(CH_3)$_2$), 1.36 (s, 9H, *p*-*t*BuCH_3), 1.15 (s, 18H, *o*-*t*BuCH_3); $^{11}B\{^{1}H\}$ NMR (96 MHz, $CDCl_3$): δ = 49.1 (s), -4.3 (s).

Synthesis of **8b^{Cl}**. To a solution of **5b** (53.5 mg, 0.10 mmol) in DCM (0.2 mL) was added BCl_3 (1.0 M, 0.21 mL, 0.21 mmol) at 0 °C and stirred for 4 h. Then, SMe_2 (13.0 mg, 0.21 mmol) was added to to the reaction mixture at 0 °C. The reaction was stirred for 2 h and all volatiles were removed in vacuo. ^{1}H NMR (300 MHz, $CDCl_3$): δ = 7.39 (s, 2H, Mes*-*H*), 7.34 – 7.22 (br, 2H, Fur-*H*), 6.85 (d, *J* = 3.3 Hz, 2H, Fur-*H*), 2.22 (s, 24 H, S(CH_3)$_2$), 1.35 (s, 9H, *p*-*t*BuCH_3), 1.14 (s, 18H, *o*-*t*BuCH_3); $^{11}B\{^{1}H\}$ NMR (96 MHz, $CDCl_3$): δ = 49.1 (s), -4.9 (s).

Synthesis of **6b^{OMe}**. To a solution of **4b** (390.4 mg, 1.00 mmol) in THF (10 mL) was added *tert*-butyllithium (1.7 M, 1.20 mL, 2.05 mmol) at −78 °C. Subsequently, the mixture was warmed to 0 °C and stirred for further 1 h. Then, the solution was added to neat $B(OMe)_3$ (2.08 g, 20.00 mmol) at 0 °C. The reaction mixture was allowed to warm up to room temperature overnight. TMSCl (325.9 mg, 3.00 mmol) was added, and the resulting suspension was filtered off. All volatiles were removed in vacuo, and the crude product was reprecipitated in MeOH to give **6b^{OMe}** as an off-white solid. Yield: 240 mg (0.45 mmol, 45 %); ^{1}H NMR (500 MHz, $CDCl_3$): δ = 7.37 (s, 2H, Mes*-*H*), 7.26 – 7.34 (br, 2H, Fur-*H*), 7.07 (d, *J* = 3.3 Hz, 2H, Fur-*H*), 3.77 (s, 12H, BOCH_3), 1.34 (s, 9H, *p*-*t*BuCH_3), 1.12 (s, 18H, *o*-*t*BuCH_3); $^{11}B\{^{1}H\}$ NMR (160 MHz, $CDCl_3$): δ = 49.1 (s), 24.4 (s); $^{13}C\{^{1}H\}$ NMR (126 MHz, $CDCl_3$): δ = 167.8 (Fur-*C*-B), 158.4 (Fur-*C*-B(OCH_3)$_2$), 152.1 (Mes*-*C*–*o*-*t*Bu), 148.5 (Mes*-*C*–*p*-*t*Bu), 132.9 (Mes*-*C*-B), 127.5 (Fur-*C*H), 124.0 (Fur-*C*H), 121.7 (Mes*-*C*H), 52.6 (B(O*C*H_3)$_2$), 38.3 (*p*-*t*Bu-*C*H_3), 34.8 (*p*-*t*Bu-*C*), 34.3 (*o*-*t*Bu-*C*H_3), 31.6 (*o*-*t*Bu-*C*); HRMS (LIFDI): m/z = 534.3473 $[M]^+$, calcd. for $C_{30}H_{45}B_3O_6$: 534.3495; elem. anal. calcd. (%) for $C_{30}H_{45}B_3O_6$: C 67.46; H 8.49, found: C 67.12, H 8.69.

Synthesis of **6b^{ORF}**. To a solution of **4b** (390.4 mg, 5.00 mmol) in THF (10 mL) was added *tert*-butyllithium (1.7 M, 6.41 mL, 10.25 mmol) at −78 °C. Subsequently, the mixture was warmed to 0 °C and stirred at for further 1 h. Then, the solution was added to neat $B(OCH_2CF_3)_3$ (31.59 g, 20.00 mmol) at 0 °C. The reaction mixture was allowed to warm up to room temperature

overnight. All volatiles were removed in vacuo and the resulting solid was washed with hexane (30 mL) and filtered. All volatiles were removed from the filtrate to give the crude product, which was reprecipitated in hexane to give **6b^{ORF}** as a white solid. Yield: 2.22 g (2.75 mmol, 55 %); ^{1}H NMR (400 MHz, $CDCl_3$): δ = 7.40 (s, 2H, Mes*-*H*), 7.35 (d, *J* = 3.5 Hz, 2H, Fur-*H*), 7.28 (d, *J* = 3.6 Hz, 2H, Fur-*H*), 4.44 (q, J_{HF} = 8.4 Hz, 8H, BOCH_2CF_3), 1.33 (s, 9H, *p*-*t*BuCH_3), 1.10 (d, *J* = 0.9 Hz, 18H, *o*-*t*BuCH_3); ^{19}F{^{1}H} NMR (377 MHz, $CDCl_3$): δ = -76.32 (t, J_{HF} = 8.3 Hz, OCH_2CF_3); ^{11}B{^{1}H} NMR (160 MHz, $CDCl_3$): δ = 49.9 (s), 24.7 (s); ^{13}C{^{1}H} NMR (101 MHz, $CDCl_3$): δ = 168.4 (Fur-*C*-B), 155.3 (Fur-*C*-B(OR)$_2$), 151.9 (Mes*-*C*–*o*-*t*Bu), 149.4 (Mes*-*C*–*p*-*t*Bu), 131.4 (Mes*-*C*-B), 126.7 (Fur-*C*H), 126.6 (Fur-*C*H), 123.6 (q, J_{CF} = 277.8 Hz, OCH_2CF_3), 122.2 (Mes*-*C*H), 62.6 (q, J_{CF} = 36.5 Hz, OCH_2CF_3), 38.2 (*p*-*t*Bu-*C*H_3), 34.9 (*p*-*t*Bu-*C*), 34.2 (*o*-*t*Bu-*C*H_3), 31.4 (*o*-*t*Bu-*C*); HRMS (LIFDI): m/z = 806.2985 $[M]^+$, calcd. for $C_{34}H_{41}B_3F_{12}O_6$: 806.2991.

Computational methods. DFT calculations were carried out with the Gaussian 09 program package, revision D.01.[18] Becke's three parameter exchange-correlation hybrid functional B3LYP[19] was used in combination with the 6-311++G** basis set.

2.6.5 References

[1] a) M. G. Walter, A. B. Rudine, C. C. Wamser, *J. Porphyrins Phthalocyanines* **2010**, *14*, 759–792; b) A. Yella, H.-W. Lee, H. N. Tsao, C. Yi, A. K. Chandiran, M. K. Nazeeruddin, E. W.-G. Diau, C.-Y. Yeh, S. M. Zakeeruddin, M. Grätzel, *Science* **2011**, *334*, 629–634.

[2] J. P. Lewtak, D. T. Gryko, *Chem. Commun.* **2012**, *48*, 10069–10086.

[3] M. V. Martínez-Díaz, G. de La Torre, T. Torres, *Chem. Commun.* **2010**, *46*, 7090–7108.

[4] G. Bottari, G. de La Torre, D. M. Guldi, T. Torres, *Chem. Rev.* **2010**, *110*, 6768–6816.

[5] F. H. Carré, R. J.-P. Corriu, T. Deforth, W. E. Douglas, W. S. Siebert, W. Weinmann, *Angew. Chem. Int. Ed.* **1998**, *37*, 652–654.

[6] A. Lik, N. A. Riensch, H. Helten, *manuscript in preparation*.

[7] a) Y. Ren, F. Jäkle, *Dalton Trans* **2016**, *45*, 13996–14007; b) A. Wakamiya, S. Yamaguchi, *BCSJ* **2015**, *88*, 1357–1377; c) G. Bélanger-Chabot, H. Braunschweig, D. K. Roy, *Eur. J. Inorg. Chem.* **2017**, *38*, 4353–4368; d) C. D. Entwistle, T. B. Marder, *Angew. Chem. Int. Ed.* **2002**, *41*, 2927–2931; e) C. D. Entwistle, T. B. Marder, *Chem. Mater.* **2004**, *16*, 4574–4585; f) S. Griesbeck, M. Ferger, C. Czernetzi, C. Wang, R. Bertermann, A. Friedrich, M. Haehnel, D. Sieh, M. Taki, S. Yamaguchi et al., *Chem. Eur. J.* **2019**, *25*, 7679–7688; g) S. Griesbeck, E. Michail, C. Wang, H. Ogasawara, S. Lorenzen, L. Gerstner, T. Zang, J. Nitsch, Y. Sato, R. Bertermann et al., *Chem. Sci.* **2019**, *10*, 5405–5422; h) X. He, T. Baumgartner, *RSC Adv.* **2013**, *3*, 11334; i) H. Helten in *Encyclopedia of Inorganic and Bioinorganic Chemistry* (Ed.: R. A. Scott), John Wiley & Sons, Ltd, Chichester, UK, **2011**; j) H. Helten, *Chem. Eur. J.* **2016**, *22*, 12972–12982; k) F. Jäkle, *Chem. Rev.* **2010**, *110*, 3985–4022; l) L. Ji, S. Griesbeck, T. B. Marder, *Chem. Sci.* **2017**, *8*, 846–863; m) I. Manners, *Angew. Chem. Int. Ed.* **1996**, *35*, 1602–1621; n) A. J. V. Marwitz, A. N. Lamm, L. N. Zakharov, M. Vasiliu, D. A. Dixon, S.-Y. Liu **2012**; o) N. Matsumi, Y. Chujo, *Polym J* **2008**, *40*, 77–89; p) K. Tanaka, Y. Chujo, *Macromol. Rapid Commun.* **2012**, *33*, 1229; q) F. Vidal, F. Jäkle, *Angew. Chem.* **2019**, *131*, 5904–5929.

[8] F. P. Gabbaï, *Angew. Chem. Int. Ed.* **2012**, *51*, 6316–6318.

[9] a) P. Chen, F. Jäkle, *J. Am. Chem. Soc.* **2011**, *133*, 20142–20145; b) P. Chen, R. A. Lalancette, F. Jäkle, *Angew. Chem. Int. Ed.* **2012**, *51*, 7994–7998; c) P. Chen, X. Yin, N. Baser-Kirazli, F. Jäkle, *Angew. Chem. Int. Ed.* **2015**, *54*, 10768–10772.

[10] T. Köhler, H. Pritzkow, W. Siebert, *Z. Naturforsch.* **2002**, *57 b*, 1101–1107.

[11] A. Lik, L. Fritze, L. Müller, H. Helten, *J. Am. Chem. Soc.* **2017**, *139*, 5692–5695.

[12] A. Lik, S. Jenthra, L. Fritze, L. Müller, K.-N. Truong, H. Helten, *Chem. Eur. J.* **2018**, *24*, 11961–11972.

[13] a) N. A. Riensch, M. Fest, L. Fritze, A. Helbig, I. Krummenacher, H. Braunschweig, H. Helten, *New J. Chem.* **2020**, *41*, 1202–1206; b) L. Fritze, N. A. Riensch, H. Helten, *Synthesis* **2019**, *51*, 399–406; c) N. A. Riensch, L. Fritze, T. Schindler, M. Kremer, H. Helten, *Dalton Trans.* **2018**, *47*, 10399–10403.

[14] B. Wrackmeyer, H. Nöth, *Chem. Ber.* **1976**, *109*, 1075–1088.

[15] A. Lik, *Doctoral dissertation*, RWTH Aachen, Aachen, **2017**.

[16] X. Yin, J. Chen, R. A. Lalancette, T. B. Marder, F. Jäkle, *Angew. Chem. Int. Ed.* **2014**, *53*, 9761–9765.

[17] K. V. Bukhryakov, R. R. Schrock, A. H. Hoveyda, P. Müller, J. Becker, *Organic letters* **2017**, *19*, 2607–2609.

[18] Gaussian 09, Revision D.01, M. J. Frisch, G. W. Trucks, H. B. Schlegel, G. E. Scuseria, M. A. Robb, J. R. Cheeseman, G. Scalmani, V. Barone, G. A. Petersson, H. Nakatsuji, X. Li, M. Caricato, A. Marenich, J. Bloino, B. G. Janesko, R. Gomperts, B. Mennucci, H. P. Hratchian, J. V. Ortiz, A. F. Izmaylov, J. L. Sonnenberg, D. Williams-Young, F. Ding, F. Lipparini, F. Egidi, J. Goings, B. Peng, A. Petrone, T. Henderson, D. Ranasinghe, V. G. Zakrzewski, J. Gao, N. Rega, G. Zheng, W. Liang, M. Hada, M. Ehara, K. Toyota, R. Fukuda, J. Hasegawa, M. Ishida, T. Nakajima, Y. Honda, O. Kitao, H. Nakai, T. Vreven, K. Throssell, J. A. Montgomery, Jr., J. E. Peralta, F. Ogliaro, M. Bearpark, J. J. Heyd, E. Brothers, K. N. Kudin, V. N. Staroverov, T. Keith, R. Kobayashi, J. Normand, K. Raghavachari, A. Rendell, J. C. Burant, S. S. Iyengar, J. Tomasi, M. Cossi, J. M. Millam, M. Klene, C. Adamo, R. Cammi, J. W. Ochterski, R. L. Martin, K. Morokuma, O. Farkas, J. B. Foresman, D. J. Fox, *Gaussian Inc.*, *Wallingford CT*, **2016**.

[19] a) P. A. M. Dirac, *Proc. R. Soc. London, Ser. A* **1929**, *123*, 714–733; b) J. C. Slater, *Phys. Rev.* **1951**, *81*, 385–390; c) A. D. Becke, *Phys. Rev. A.* **1988**, *38*, 3098–3100; d) C. Lee, W. Yang, R. G. Parr, *Phys. Rev. B* **1988**, *37*, 785–89; e) A. D. Becke, *J. Chem. Phys.* **1993**, *98*, 5648–5652.

3 Conclusion

In this work syntheses of a series of inorganic-organic hybrid materials with favorable optical and electronic properties and potential applications in state-of-the-art technologies have been presented. The strategies to prepare those organoboron molecules, oligomers, polymers, and macrocycles varied from catalytic C–C coupling routes to new and highly effective B–C coupling procedures like catalytic boron/silicon exchange.

In chapters 2.1 – 2.3, various reaction protocols were applied to synthesize a range of different organoborane compounds with difurylborane units in the main chain, demonstrating the versatility of this unit as potent building block (Scheme 3.1).

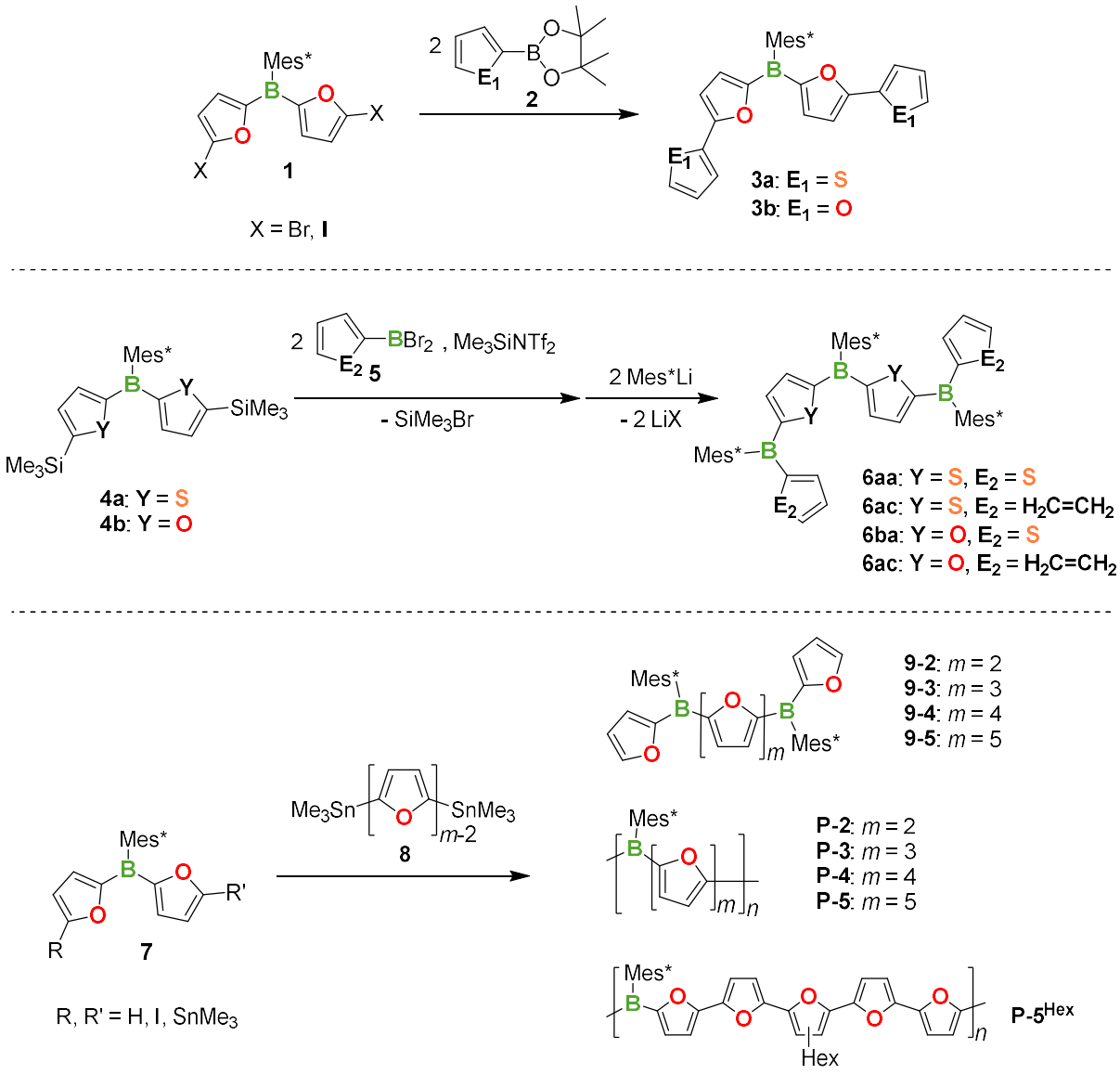

Scheme 3.1: *Synthetic protocols to different furyl-based organoboranes. Top: Suzuki-Miyaura cross-coupling reaction to give compounds* ***3****. Center: Boron/silicon exchange reaction to give trisboranes* ***6****. Bottom: Microwave-assisted Stille cross-coupling reaction to give furyl-based bisboranes* ***9*** *and polymers* ***P-1*** *–* ***P-5****.*

In chapter 2.1, Suzuki-Miyaura cross-coupling was used to effectively extend the π-system of bis-halogenated moieties **1** by coupling with pinacol boronates **2** to give organoboranes **3** (Scheme 3.1, top). In chapter 2.2, it was demonstrated that catalytic silicon/boron exchange is an effective and versatile route to yield defined organoborane oligomers **6** by coupling of di-silylated substrates **4** with aryl(dibromo)boranes **5** and subsequent arylation using Mes*Li (Scheme 3.1, center). Chapter 2.3 covers the synthesis of furyl-based bisboranes **9** and polymers **P-1** – **P-5** by microwave-assisted Stille cross-coupling reaction between iodinated substrate **7** and stannyl compounds **8** (Scheme 3.1, bottom).

The sterically demanding Mes* substituents kinetically stabilize the compounds, making them stable towards air- and moisture. These investigations show the influence of different degrees of boron-doping of oligo(het)aryl chains, as well as the choice of aromatic moieties on the electronic and optic properties of the materials. In chapters 2.1 – 2.2 furyl, thienyl and phenyl substituents were successfully incorporated to give compounds **3** and **6**. In chapter 2.3, the focus was on varying the extent of boron-doping, using furyl-based substrates **7** and **8**. In UV-Vis measurements, compounds **3**, **6**, **9** and **P-1** – **P-5** showed strong bathochromic shifts compared to the respective monomers, showing the effective extension of their respective π-systems.

Further investigations focused on the luminescence properties of the products, especially when compared to analogue thiophene-based materials. The highest fluorescence quantum yield gave **9-2** (Φ_f = 97 %). Bisboranes **9** and polymers **P-1** – **P-5** showed tunability of their emission color by variation of the furyl bridge length (Figure 3.1).

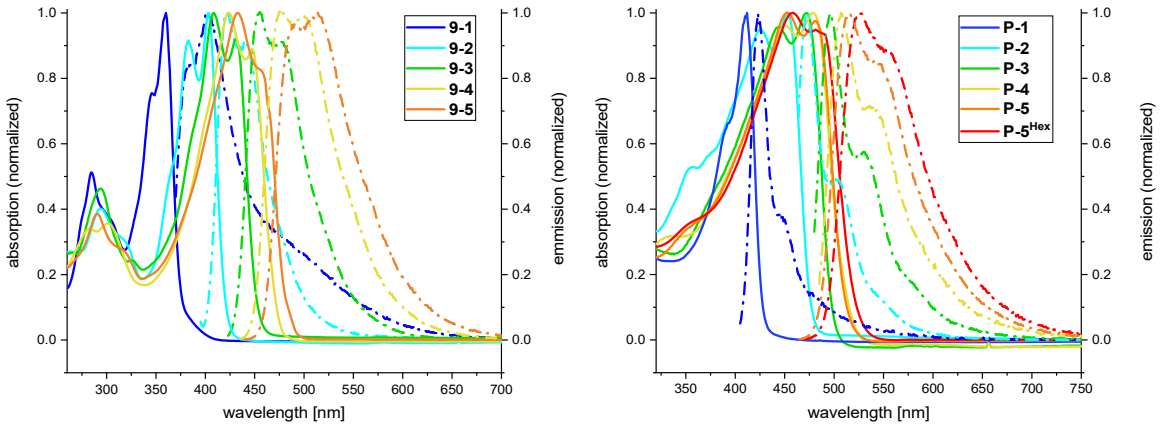

Figure 3.1: *UV-vis absorption (solid lines) and fluorescence (dashed lines) spectra for* ***9-1*** *–* ***9-5*** *(left) and* ***P-1*** *–* ***P-5^{Hex}*** *(right).*

Cyclic voltammetry (CV) measurements revealed reversible redox events for the smaller molecules (**3**, **6**, **9-2**, **9-3**, **P-1**, **P-2**). Elongation of the furyl bridge led to irreversible redox events for **9-4**, **9-5** and polymers **P-3** – **P-5**, but also an appearance of a re-oxidation event.

X-Ray analysis of compounds **9** and **3a** revealed a largely co-planar structure of the hetarene rings, as well as their anti-arrangement (Figure 3.2).

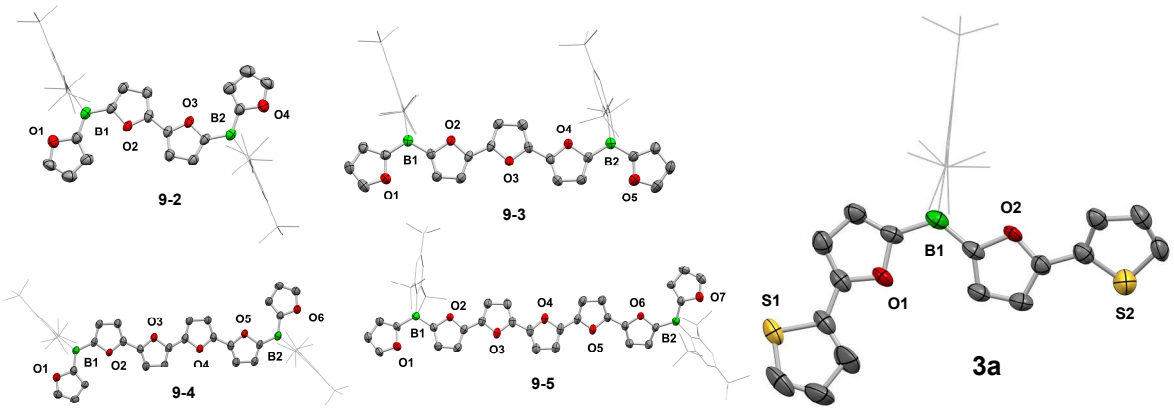

Figure 3.2: *Solid-state structures of bisboranes **9** and monoborane **3a**.*

Chapters 2.4 – 2.5 are devoted to B–C coupling reactions. In chapter 2.4, investigations on the catalytic silicon/boron exchange mechanism were shown. The effects of the addition of trimethylsilyl triflimide in catalytic amounts to a reaction between dibromo(2-thienyl)borane **10a** and 2-trimethylsilylthiophene **11a** in CH_2Cl_2 were investigated (Scheme 3.2). A second and third feasible reaction route via C–H activation mechanisms were discovered, which represent competitive reaction pathways to the silicon/boron exchange. Introduction of methyl groups at the 5-postion of the substrates (**10b** and **11b**) hindered these side reactions and made exclusive observation of the silicon/boron exchange possible.

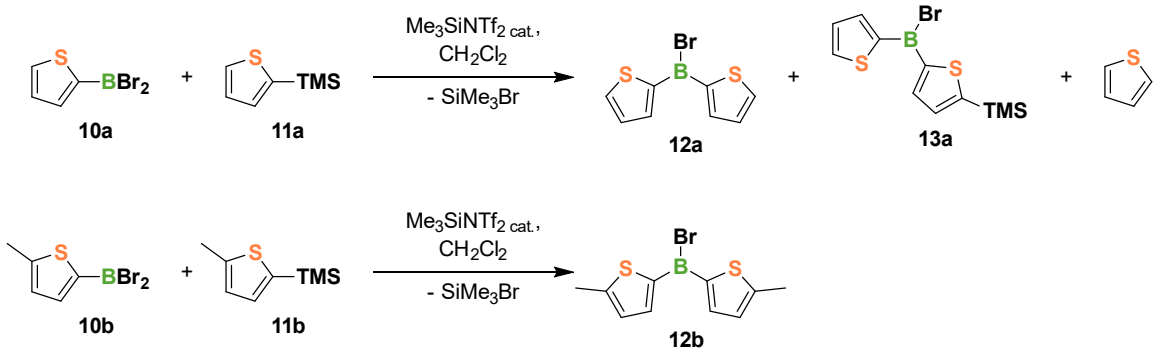

Scheme 3.2: *Catalytic silicon/boron exchange reactions of **10a** and **11a** (top) and **10b** and **11b** (bottom).*

During our investigations, a structural change of the catalyst has been observed, where the $SiMe_3$ group changes its position from oxygen to nitrogen (Figure 3.3). VTNA analysis of the catalysis revealed key features of the mechanism like reaction orders in the substrates (α = 1 (**10b**), β = 0 (**11b**)) and in catalyst (γ = 0.75). Based on this information, a catalytic cycle was proposed (Figure 3.3).

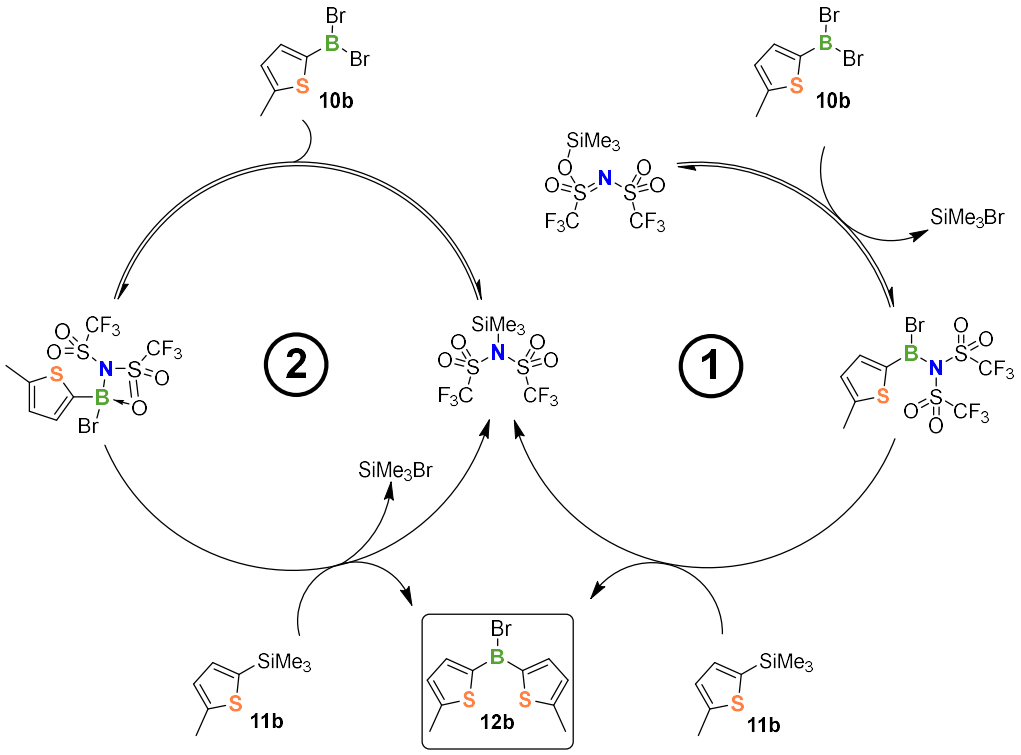

Figure 3.3: *Proposed catalytic cycle of the catalytic silicon/boron exchange reaction of* ***10b*** *and* ***11b****.*

In chapter 2.5, formation of halo(dithienyl)boranes **12** via intermolecular electrophilic borylation reaction was presented (Scheme 3.3). Halo(dithienyl)boranes **12** were synthesized by selective C–H activation via S_EAr mechanism. This reaction should proceeds via the *in situ* formation of a borenium cation from substrate **10**. When using substrates **10a,c** and **13a**, formation of monoboranes **12a,c** and bisboranes **14a,c** was observed. It is conceivable that **14a,c** is the product of a follow-up reaction between **12a,c** and a second borenium cation. Introduction of a methyl group at the 5-position of the substrates (**10b** and **13b**), prevented a second C–H activation step and facilitated the reaction to the desired product **12b**.

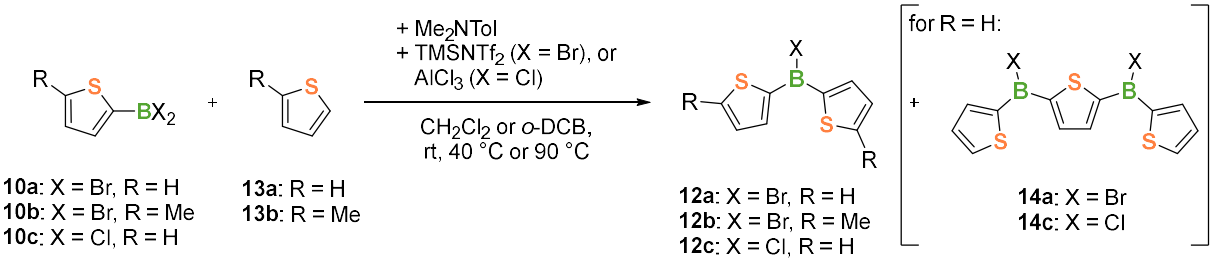

Scheme 3.3: *Reactions of substrates* ***10*** *and* ***13*** *performing intermolecular electrophilic borylation.*

While the yield of the reaction still has room for improvement, the general reactivity of the system was confirmed.

In chapter 2.6, the synthesis of tetraoxaporphyrinogen **18** was investigated. For that, two main routes were tested (Scheme 3.4). Starting from supermesityl(difuryl)borane **14**, a multi-step

synthesis to diborylated triarylborane **15** was performed. The high reactivity of the resulting dihaloboranes (R = Br, Cl) made further investigations more challenging because of their labile nature. On the other hand, the low reactivity of the dialkoxyboranes (R = OMe, OCH_2CF_3) prevented further reaction steps. Conversion of species **15** to the larger moieties **17** by addition of a second aryl substituent failed for all substituents R under the applied conditions.

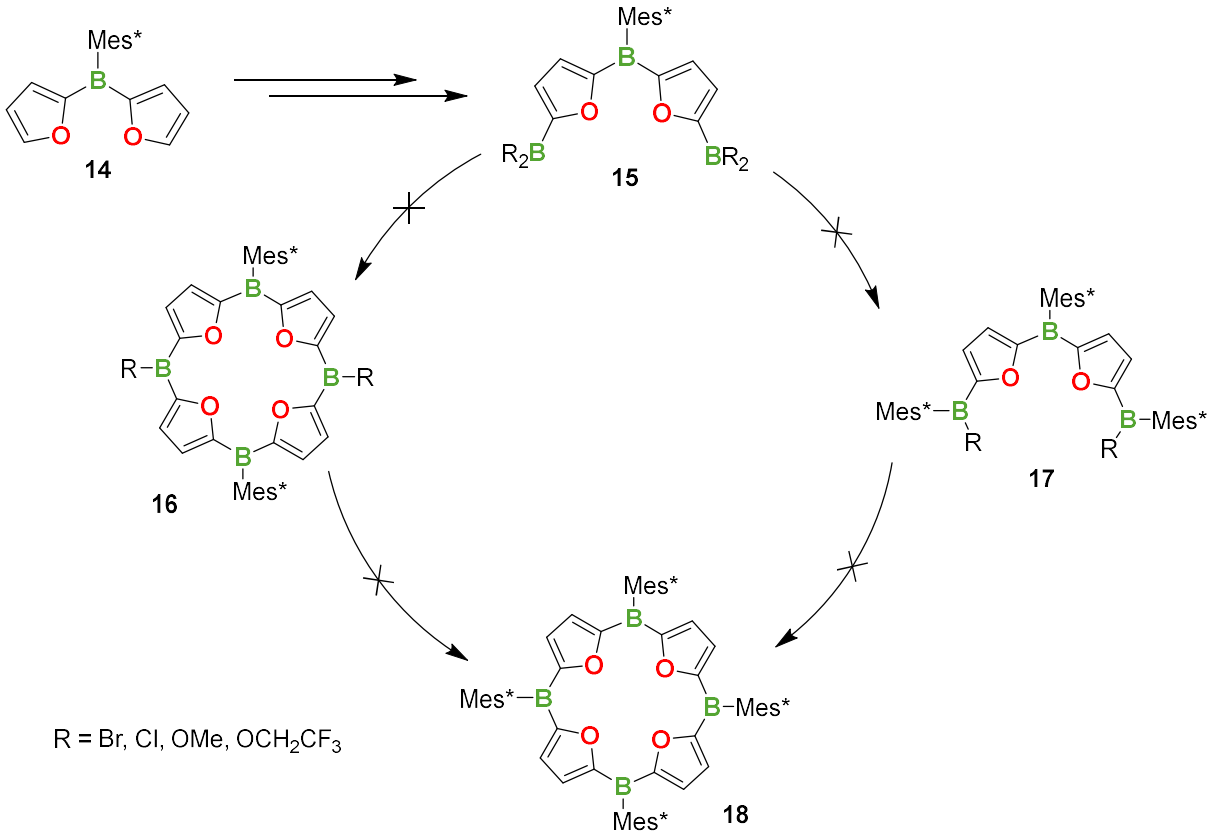

Scheme 3.4: *Investigated routes to tetraoxaporphyrinogen **18**.*

Accompanying model reactions and earlier investigations on Mes* substituted organoboranes in our workgroup suggested a different order of substitution, where the bulky substituent is added last. That led to ring-closing attempts directly using compounds **15** as a substrate to give the partially unprotected ring **16**. Catalytic attempts (R = Br, Cl) using Si/B exchange procedures, as well as reactions with dilithiated species did not yield the desired ring system. Furthermore, model reactions gave information about the follow-up reaction step to tetraoxaporphyrinogen **18**, suggesting an unsuccessful third substitution with Mes*, when using R = OMe. The chosen reaction routes gave important information on the investigated system, for further investigations the use of organo-tin compounds could be considered. The Sn/B exchange condensation protocol could offer the crucial advantages in the synthesis of the macrocycle.

In conclusion, this work provided relevant information on the work on tri(het)arylborane molecules, oligomers, and polymers, as well as various synthetic approaches thereof.

4 Zusammenfassung

In dieser Arbeit wurden Synthesen einer Reihe von anorganisch-organischen Hybridmaterialien mit interessanten optischen und elektronischen Eigenschaften und potenziellen Anwendungen in modernsten Technologien vorgestellt. Die Strategien zur Herstellung dieser Organobormoleküle, -oligomere, -polymere und -makrocyclen variierten von katalytischen C–C-Kupplungsrouten bis hin zu neuen und hocheffektiven B–C-Kupplungsverfahren wie dem katalytischen Bor/Silicium-Austausch.

In den Kapiteln 2.1 – 2.3 wurden verschiedene Reaktionsprotokolle angewandt, um eine Reihe unterschiedlicher Organoboranverbindungen mit Difurylboran-Einheiten in der Hauptkette zu synthetisieren, was die Vielseitigkeit dieser Einheit als potenten Baustein demonstriert (Schema 4.1).

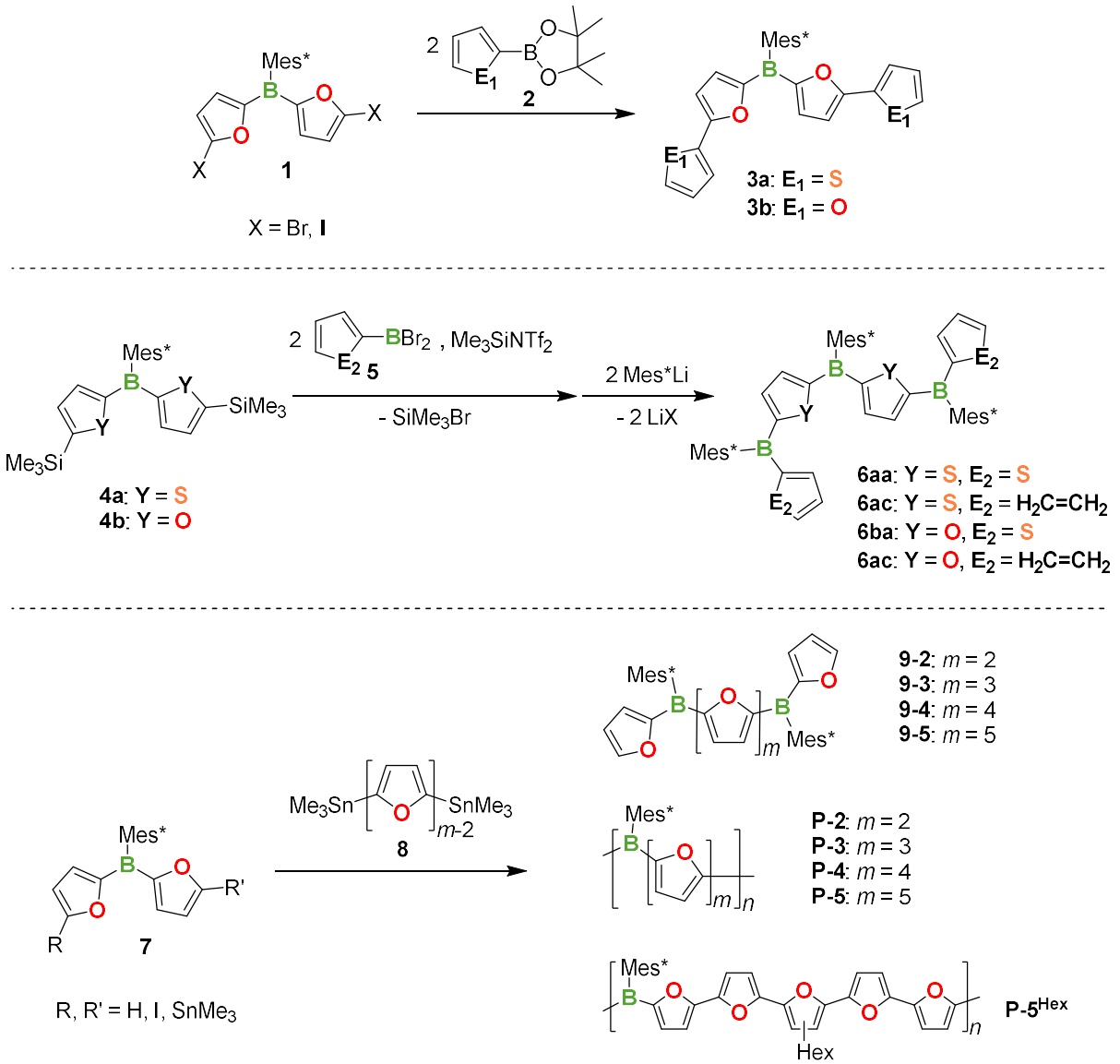

Schema 4.1: *Syntheseprotokolle zu verschiedenen furylbasierten Organoboranen. Oben: Suzuki-Miyaura-Kreuzkupplungsreaktion zu den Verbindungen **3**. Mitte: Bor/Silicium-Austauschreaktion zu Trisboranen **6**. Unten: Mikrowellen-unterstützte Stille-Kreuzkupplungsreaktion zu furylbasierten Bisboranen **9** und Polymeren **P-1** – **P-5**.*

In Kapitel 2.1 wurde die Suzuki-Miyaura-Kreuzkupplung zur effektiven Erweiterung des π-Systems von bis-halogenierten Verbindungen **1** durch Kupplung mit Pinacolboronaten **2** zu Organoboranen **3** verwendet (Schema 4.1, oben). In Kapitel 2.2 wurde gezeigt, dass der katalytische Silicium/Bor-Austausch ein effektiver und vielseitiger Weg ist, um definierte Organoboran-Oligomere **6** durch Kupplung von di-silylierten Substraten **4** mit Aryl(dibromo)boranen **5** und anschließender Arylierung mit Mes*Li zu erhalten (Schema 4.1, Mitte). Kapitel 2.3 behandelt die Synthese von Furyl-basierten Bisboranen **9** und Polymeren **P-1** – **P-5** durch mikrowellenunterstützte Stille-Kreuzkupplungsreaktion zwischen iodiertem Substrat **7** und Stannylverbindungen **8** (Schema 4.1, unten).

Die sterisch anspruchsvollen Mes*-Substituenten stabilisieren die Verbindungen kinetisch und machen sie stabil gegenüber Luft- und Feuchtigkeit. Diese Untersuchungen zeigen den Einfluss unterschiedlicher Grade der Bor-Dotierung von Oligo(het)arylketten sowie die Wahl der aromatischen Reste auf die elektronischen und optischen Eigenschaften der Materialien. In den Kapiteln 2.1 – 2.2 wurden Furyl-, Thienyl- und Phenylsubstituenten erfolgreich zu den Verbindungen **3** und **6** eingebaut. In Kapitel 2.3 lag der Fokus auf der Variation des Ausmaßes der Bor-Dotierung unter Verwendung der Furyl-basierten Substrate **7** und **8**. In UV-Vis-Messungen zeigten die Verbindungen **3**, **6**, **9** und **P-1** – **P-5** starke bathochrome Verschiebungen im Vergleich zu den jeweiligen Monomeren, was die effektive Erweiterung ihrer jeweiligen π-Systeme zeigt.

Weitere Untersuchungen konzentrierten sich auf die Lumineszenzeigenschaften der Produkte, insbesondere im Vergleich zu analogen Thiophen-basierten Materialien. Die höchste Fluoreszenzquantenausbeute ergab **9-2** (Φ_f = 97 %). Bisborane **9** und Polymere **P-1** – **P-5** zeigten eine Abstimmbarkeit ihrer Emissionsfarbe durch Variation der Furylbrückenlänge (Abbildung 4.1).

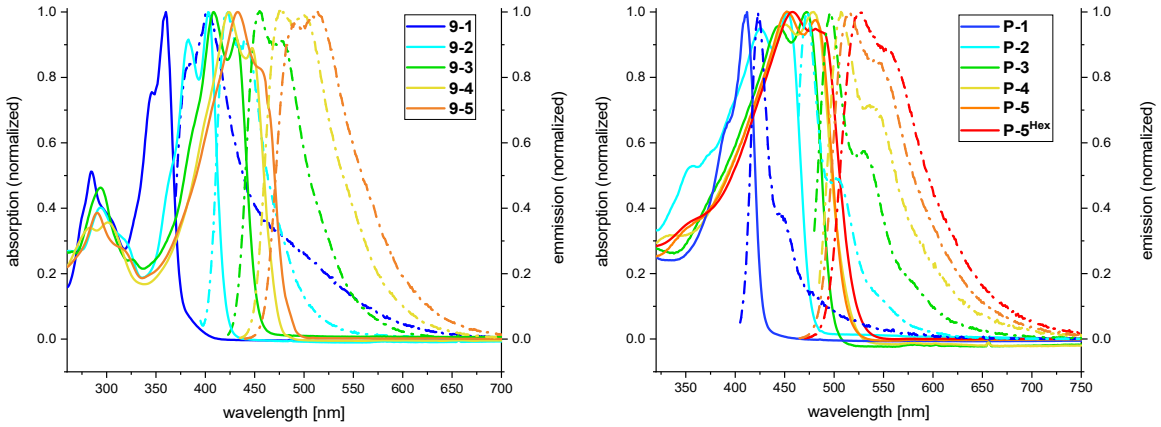

Abbildung 4.1: *UV-vis-Absorptions- (durchgezogene Linien) und Fluoreszenzspektren (gestrichelte Linien) für* ***9-1*** *–* ***9-5*** *(links) und* ***P-1*** *–* ***P-5^{Hex}*** *(rechts).*

Cyclovoltammetrie (CV)-Messungen zeigten reversible Redoxereignisse für die kleineren Moleküle (**3**, **6**, **9-2**, **9-3**, **P-1**, **P-2**). Die Verlängerung der Furylbrücke führte zu irreversiblen Redoxereignissen für **9-4**, **9-5** und die Polymere **P-3** – **P-5**, aber auch zum Auftreten eines Reoxidationsereignisses. Die Röntgenanalyse der Verbindungen **9** und **3a** zeigte eine weitgehend koplanare Struktur der Arylringe sowie deren Antikonformation (Abbildung 4.2).

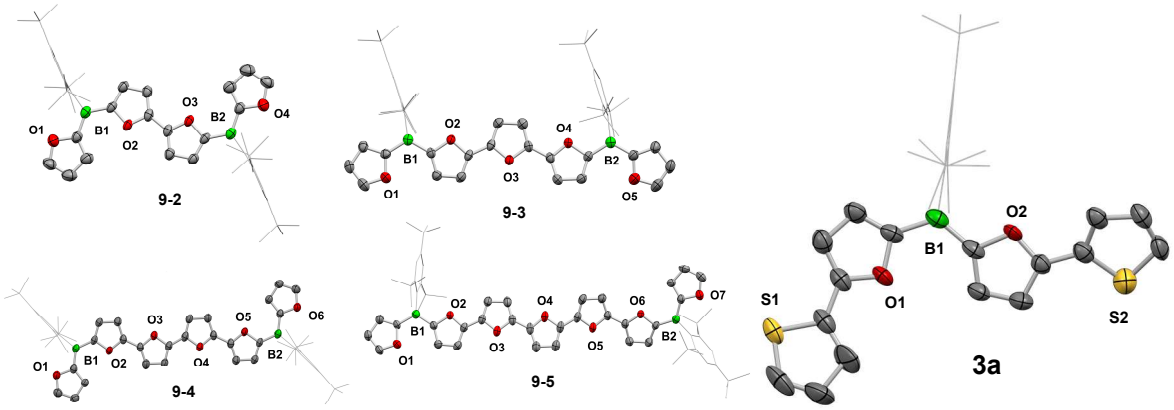

Abbildung 4.2: *Festkörperstrukturen der Bisborane **9** und Monoboran **3a**.*

Die Kapitel 2.4 – 2.5 sind den B–C-Kupplungsreaktionen gewidmet. In Kapitel 2.4 wurden Untersuchungen zum katalytischen Silicium/Bor-Austauschmechanismus gezeigt. Die Auswirkungen der Zugabe von Trimethylsilyltriflimid in katalytischen Mengen zu einer Reaktion zwischen Dibromo(2-thienyl)boran **10a** und 2-Trimethylsilylthiophen **11a** in CH_2Cl_2 wurden untersucht (Schema 4.2). Es wurden ein zweiter und ein dritter möglicher Reaktionsweg über C–H-Aktivierungsmechanismen entdeckt, die konkurrierende Reaktionswege zum Silicium/Bor-Austausch darstellen. Die Einführung von Methylgruppen an der 5-Position der Substrate (**10b** und **11b**) verhinderte diese Nebenreaktionen und ermöglichte die ausschließliche Beobachtung des Silicium/Bor-Austauschs.

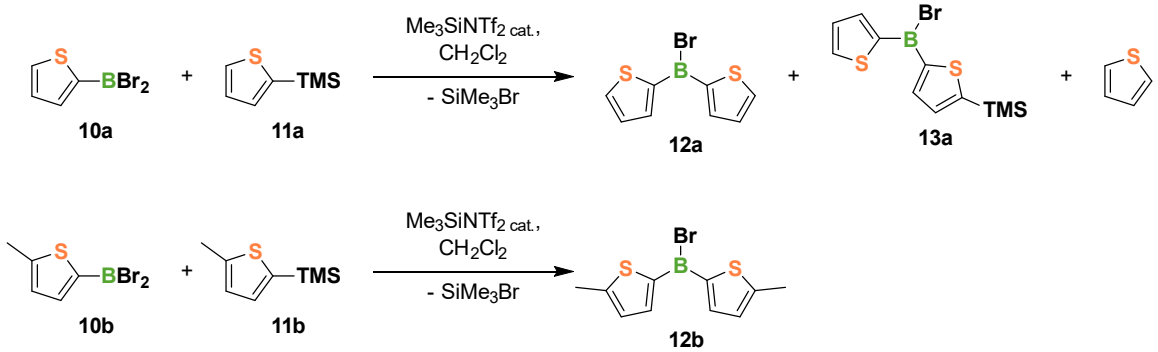

Schema 4.2: *Katalytische Silizium/Bor-Austauschreaktionen von **10a** und **11a** (oben) und **10b** und **11b** (unten).*

Während unserer Untersuchungen wurde eine Strukturänderung des Katalysators beobachtet, bei der die $SiMe_3$-Gruppe ihre Position von Sauerstoff zu Stickstoff ändert (Abbildung 4.3). Die VTNA-Analyse der Katalyse zeigte Schlüsselmerkmale des Mechanismus wie

Reaktionsordnungen der Substrate (α = 1 (**10b**), β = 0 (**11b**)) und des Katalysators (γ = 0.75). Basierend auf diesen Informationen wurde ein katalytischer Zyklus vorgeschlagen (Abbildung 4.3).

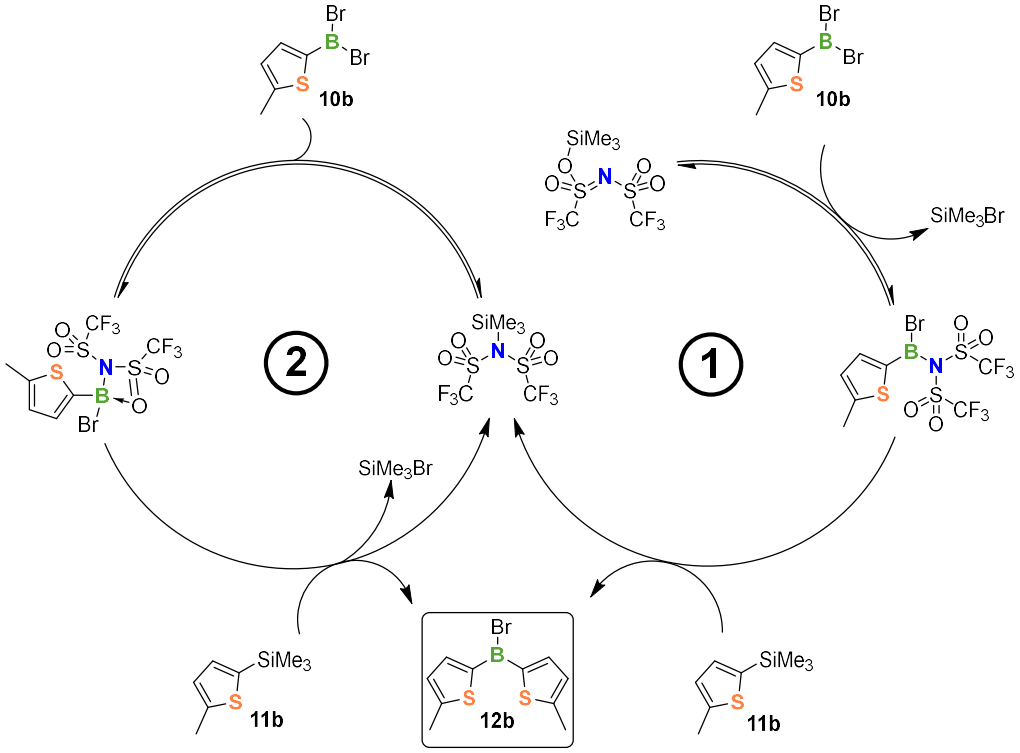

Abbildung 4.3: *Vorgeschlagener katalytischer Zyklus der katalytischen Silizium/Bor-Austauschreaktion von **10b** und **11b**.*

In Kapitel 2.5 wurde die Bildung von Halo(dithienyl)boranen **12** über eine intermolekulare elektrophile Borylierungsreaktion vorgestellt (Schema 4.3). Die Halo(dithienyl)borane **12** wurden durch selektive C–H-Aktivierung über einen S_EAr-Mechanismus synthetisiert. Diese Reaktion sollte über die *in situ* Bildung eines Borenium-Kations aus Substrat **10** ablaufen. Bei Verwendung der Substrate **10a,c** und **13a** wurde die Bildung von Monoboranen **12a,c** und Bisboranen **14a,c** beobachtet. Es ist denkbar, dass **14a,c** das Produkt einer Folgereaktion zwischen **12a,c** und einem zweiten Boreniumkation ist. Die Einführung einer Methylgruppe an der 5-Position der Substrate (**10b** und **13b**), verhinderte einen zweiten C–H-Aktivierungsschritt und erleichterte die Reaktion zum gewünschten Produkt **12b**.

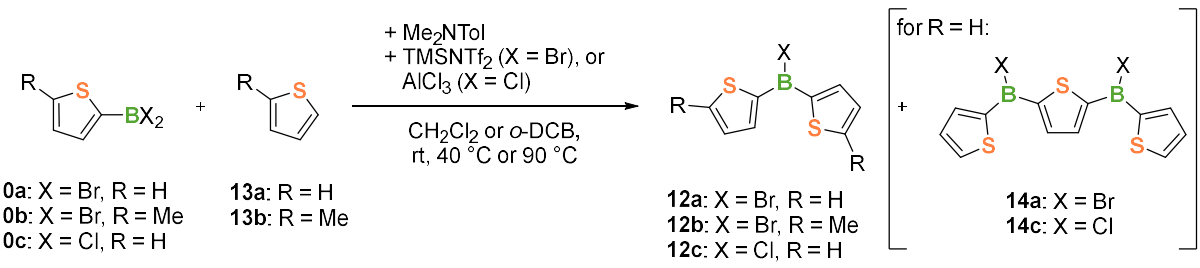

10a: X = Br, R = H
10b: X = Br, R = Me
10c: X = Cl, R = H

13a: R = H
13b: R = Me

12a: X = Br, R = H
12b: X = Br, R = Me
12c: X = Cl, R = H

14a: X = Br
14c: X = Cl

Schema 4.3: *Reaktionen der Substrate **10** und **13** durch intermolekulare elektrophile Borylierung.*

Während die Ausbeute der Reaktion noch verbesserungswürdig ist, konnte die generelle Reaktivität des Systems bestätigt werden.

In Kapitel 2.6 wurde die Synthese von Tetraoxaporphyrinogen **18** untersucht. Dazu wurden zwei Hauptrouten getestet (Schema 4.4). Ausgehend vom Supermesityl(difuryl)boran **14** wurde eine mehrstufige Synthese zum diborylierten Triarylboran **15** durchgeführt. Die hohe Reaktivität der resultierenden Dihalogenborane (R = Br, Cl) erschwerte weitere Untersuchungen aufgrund ihrer Labilität. Andererseits verhinderte die geringe Reaktivität der Dialkoxyborane (R = OMe, OCH_2CF_3) weitere Reaktionsschritte. Die Umwandlung der Spezies **15** in die größeren Verbindungen **17** durch Addition eines zweiten Arylsubstituenten scheiterte für alle Substituenten R unter den angewandten Bedingungen.

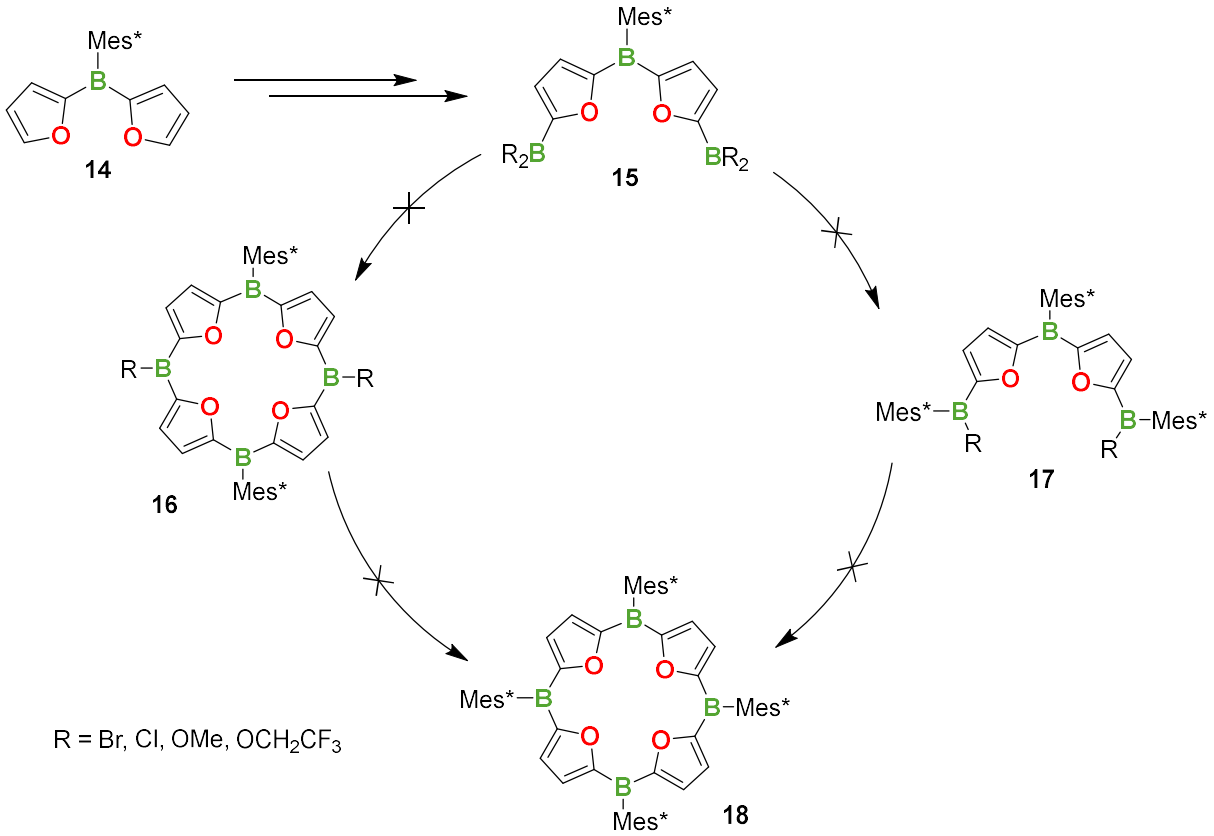

Schema 4.4: *Untersuchte Syntheserouten zu Tetraoxaporphyrinogen **18**.*

Begleitende Modellreaktionen und frühere Untersuchungen an Mes*-substituierten Organoboranen in unserer Arbeitsgruppe legten eine andere Substitutionsreihenfolge nahe, bei der der sperrige Substituent zuletzt hinzugefügt wird. Das führte zu Ringschlussversuchen direkt mit Verbindungen **15** als Substrat, um den teilweise ungeschützten Ring **16** zu erhalten. Katalytische Versuche (R = Br, Cl) mit Si/B-Austauschverfahren sowie Reaktionen mit dilithiierten Spezies ergaben nicht das gewünschte Ringsystem. Darüber hinaus gaben Modellreaktionen Aufschluss über den Folgereaktionsschritt zum Tetraoxaporphyrinogen **18**, was bei Verwendung von R = OMe auf eine erfolglose dritte Substitution mit Mes* hindeutet. Die gewählten Reaktionswege lieferten wichtige Informationen über das untersuchte System,

für weitere Untersuchungen könnten in Zukunft zinnorganische Verbindungen einbezogen werden. Die Verwendung der Sn/B-Austauschkondensation könnte die entscheidenden Vorteile bei der Synthese des Makrozyklus bieten.

Zusammenfassend liefert diese Arbeit relevante Informationen über die Arbeit an Tri(het)arylboranmolekülen, -oligomeren und -polymeren sowie über verschiedene Ansätze zu ihrer Synthese.

5 Appendix

5.1 Difuryl(supermesityl)borane: A Versatile Building Block for Extended π-conjugated Materials

NMR spectra

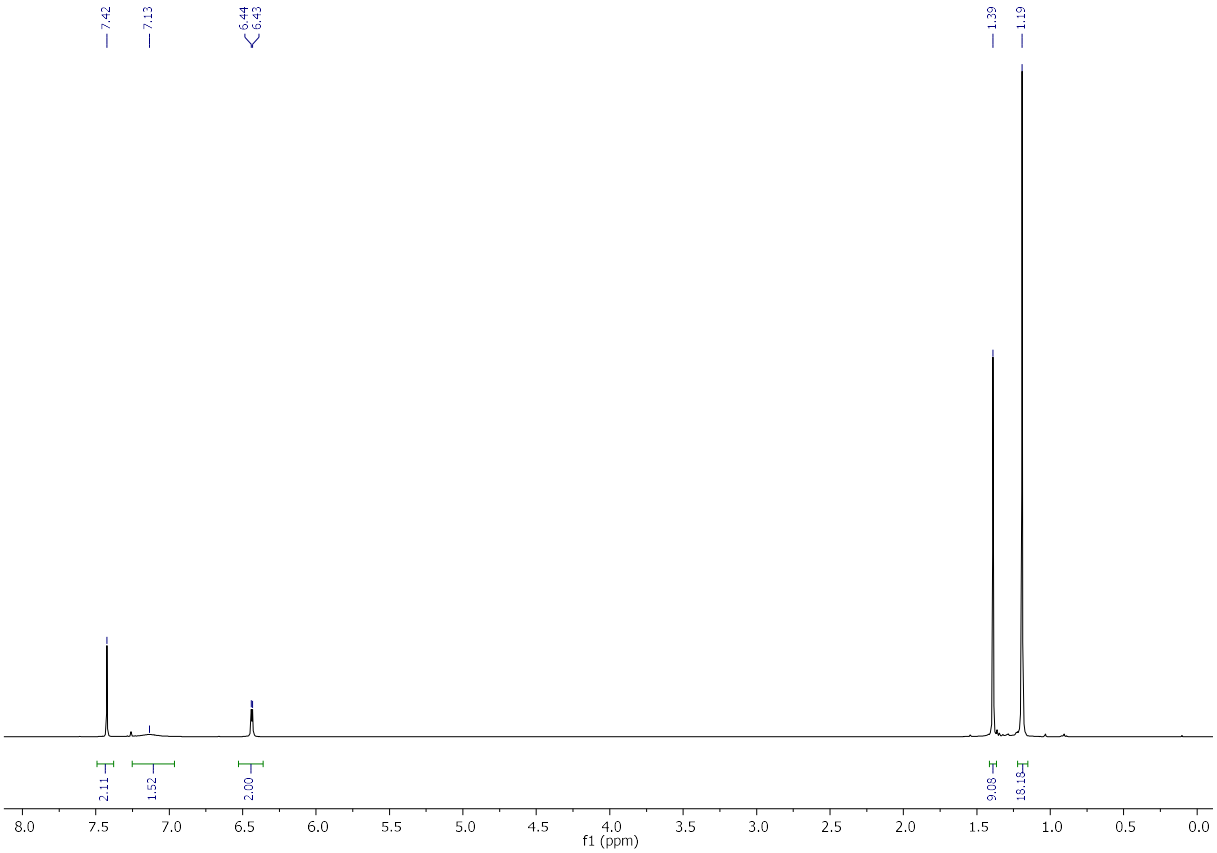

Figure S5.1.1. *^{1}H NMR spectrum of **2a** (in $CDCl_3$, 400 MHz).*

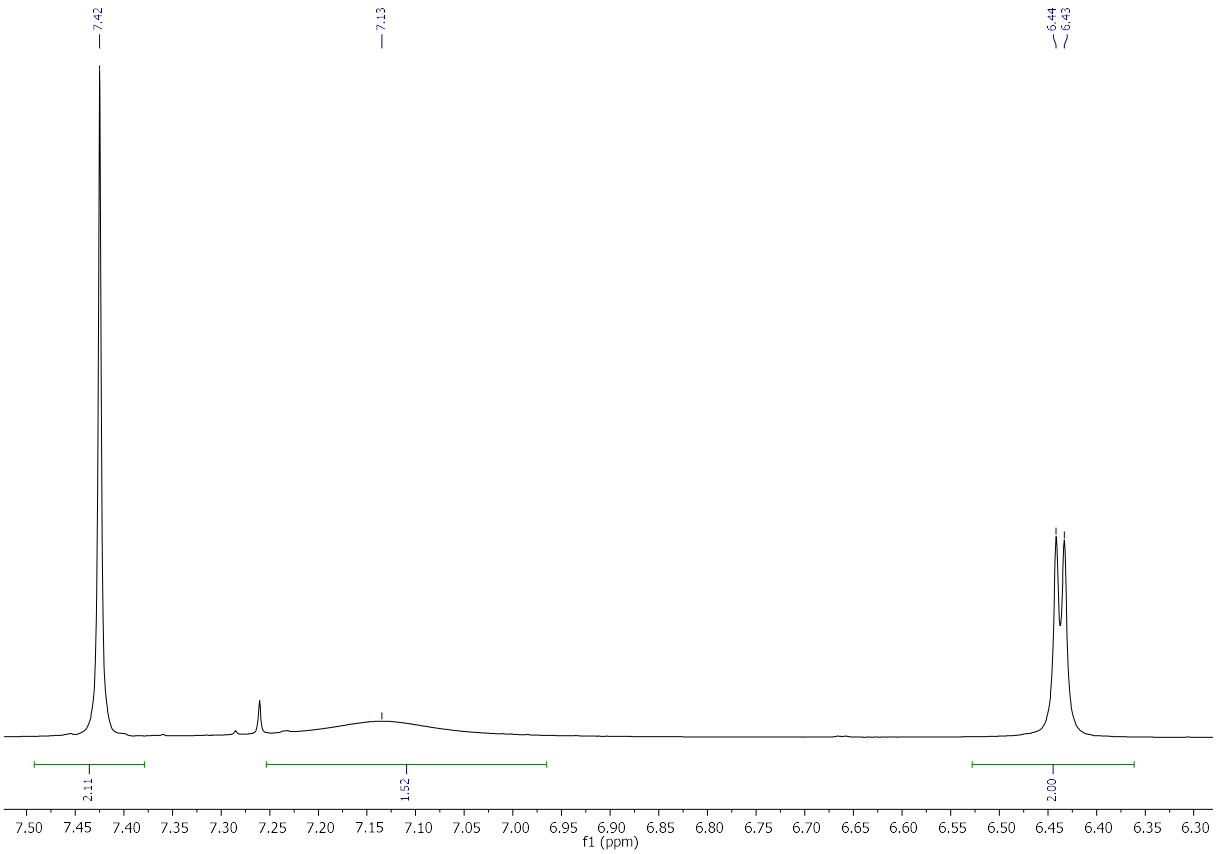

Figure S5.1.2. *Detail (aromatic region) of the ^{1}H NMR spectrum of* ***2a*** *(in $CDCl_3$, 400 MHz).*

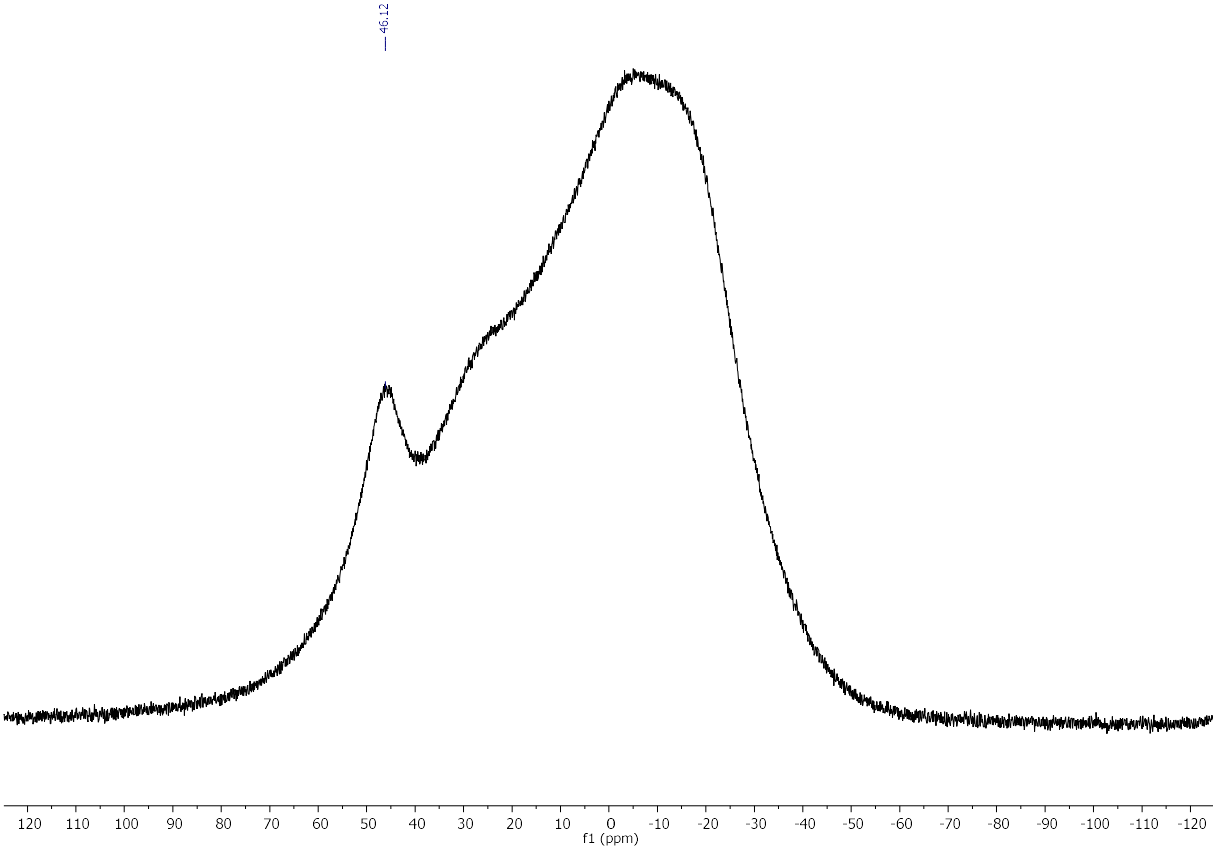

Figure S5.1.3. *$^{11}B\{^{1}H\}$ NMR spectrum of* ***2a*** *(in $CDCl_3$, 128 MHz).*

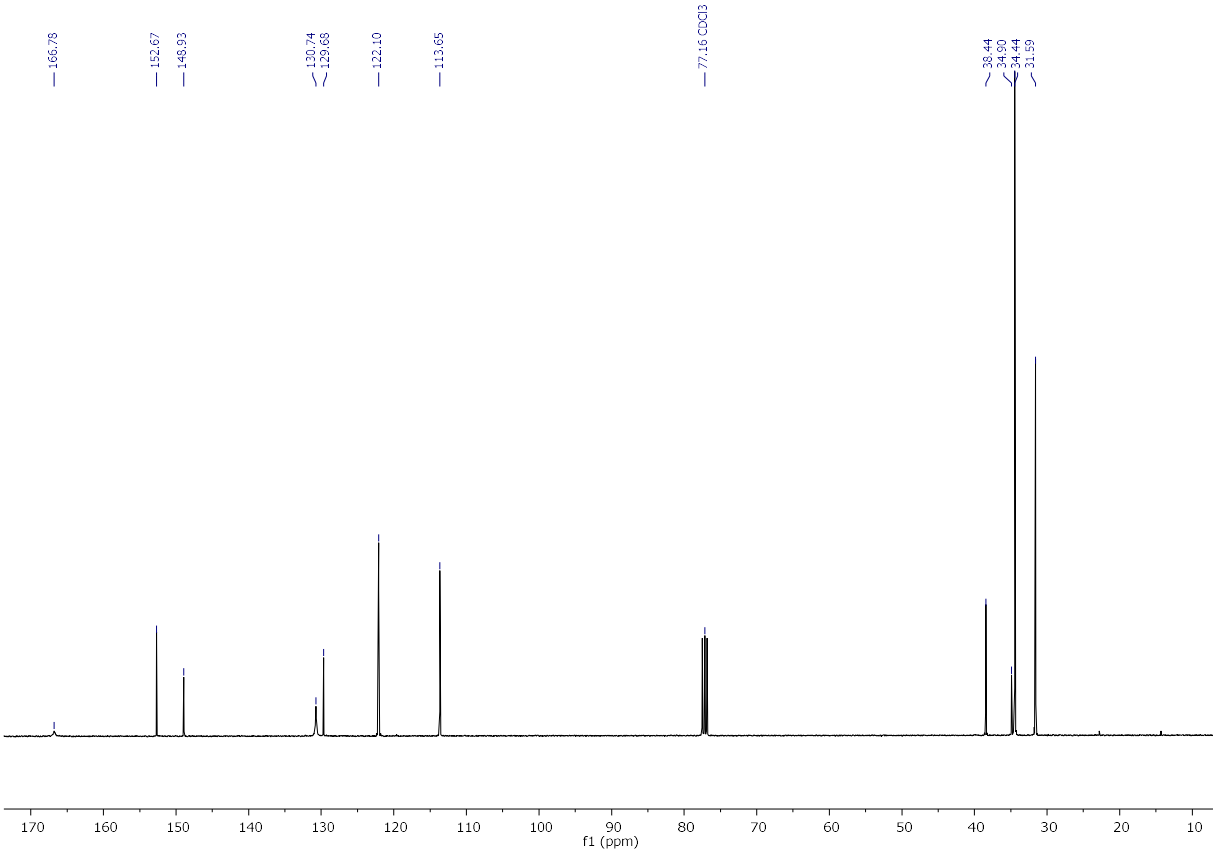

Figure S5.1.4. *^{13}C NMR spectrum of 2a (in $CDCl_3$, 101 MHz).*

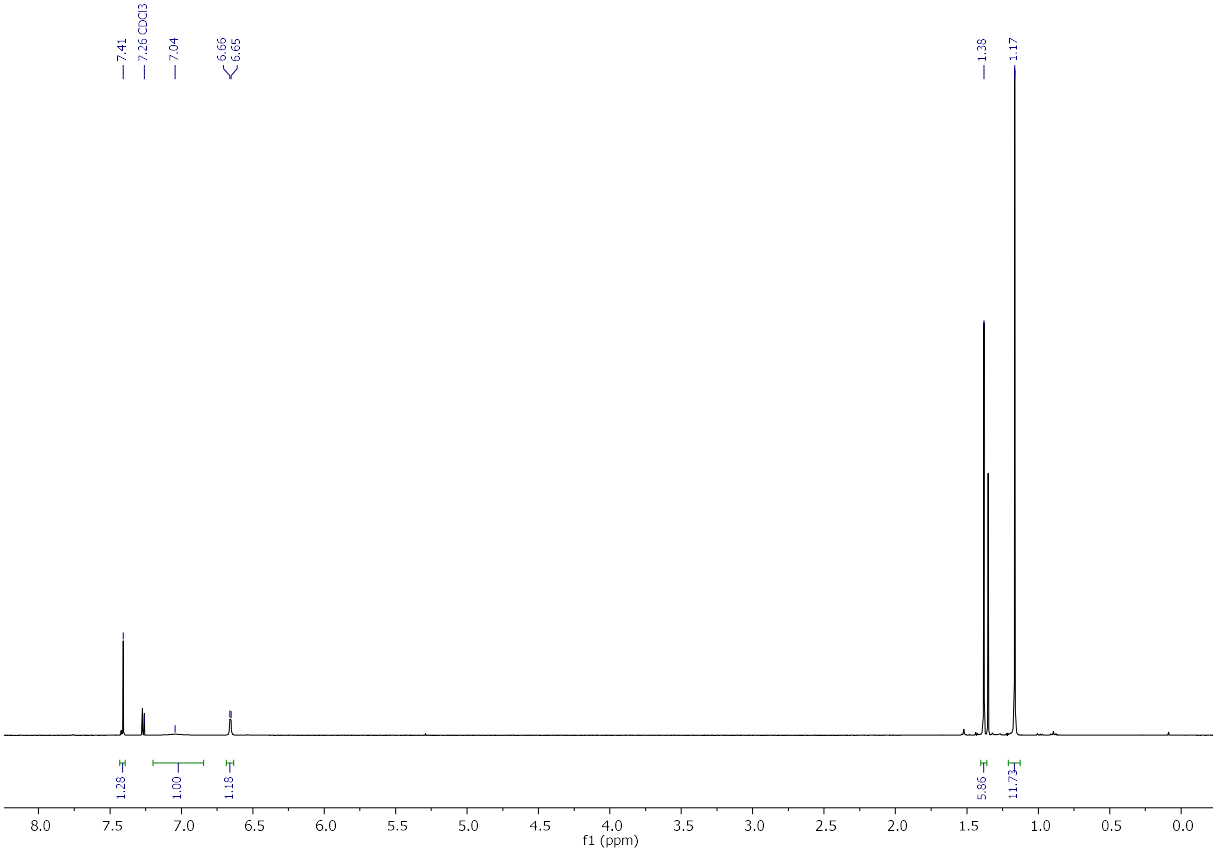

Figure S5.1.5. *^{1}H NMR spectrum of **2b** (in $CDCl_3$, 400 MHz).*

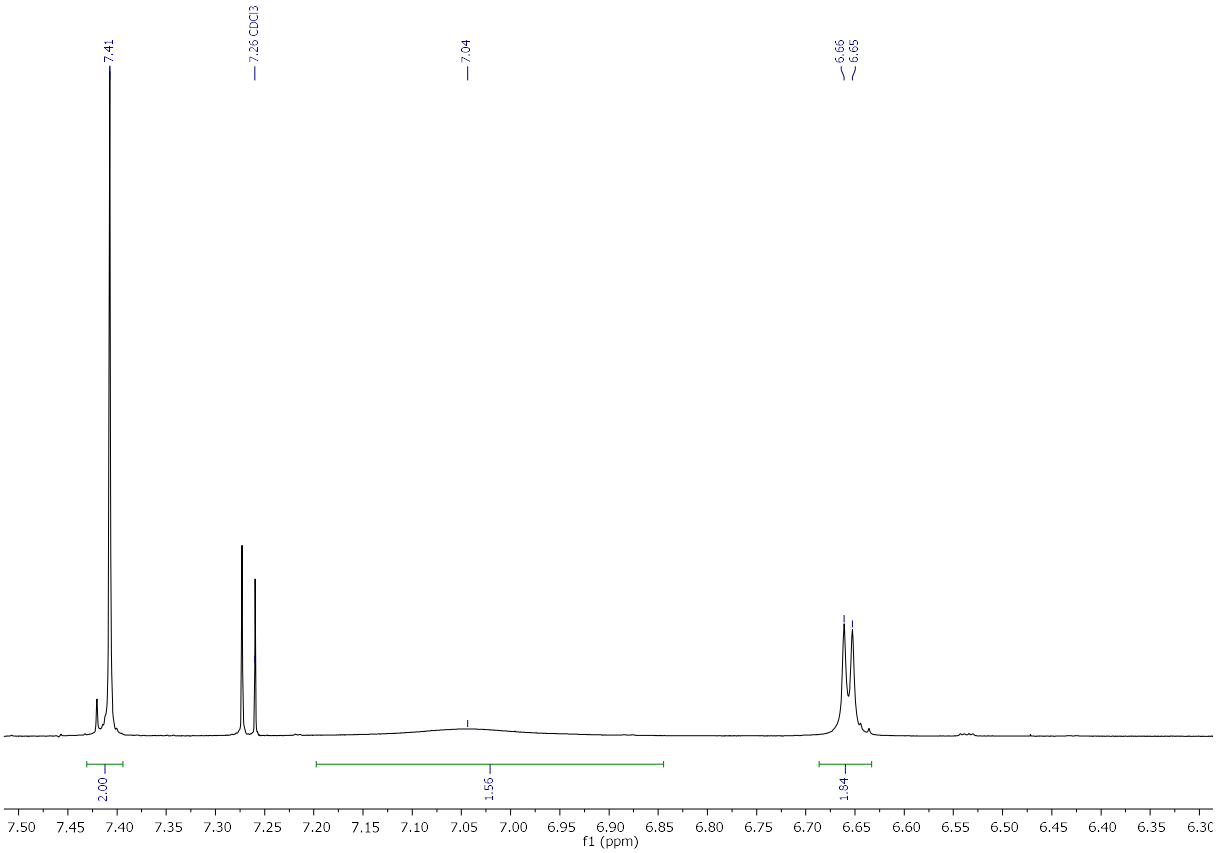

Figure S5.1.6. *Detail (aromatic region) of the ^{1}H NMR spectrum of* ***2b*** *(in $CDCl_3$, 400 MHz).*

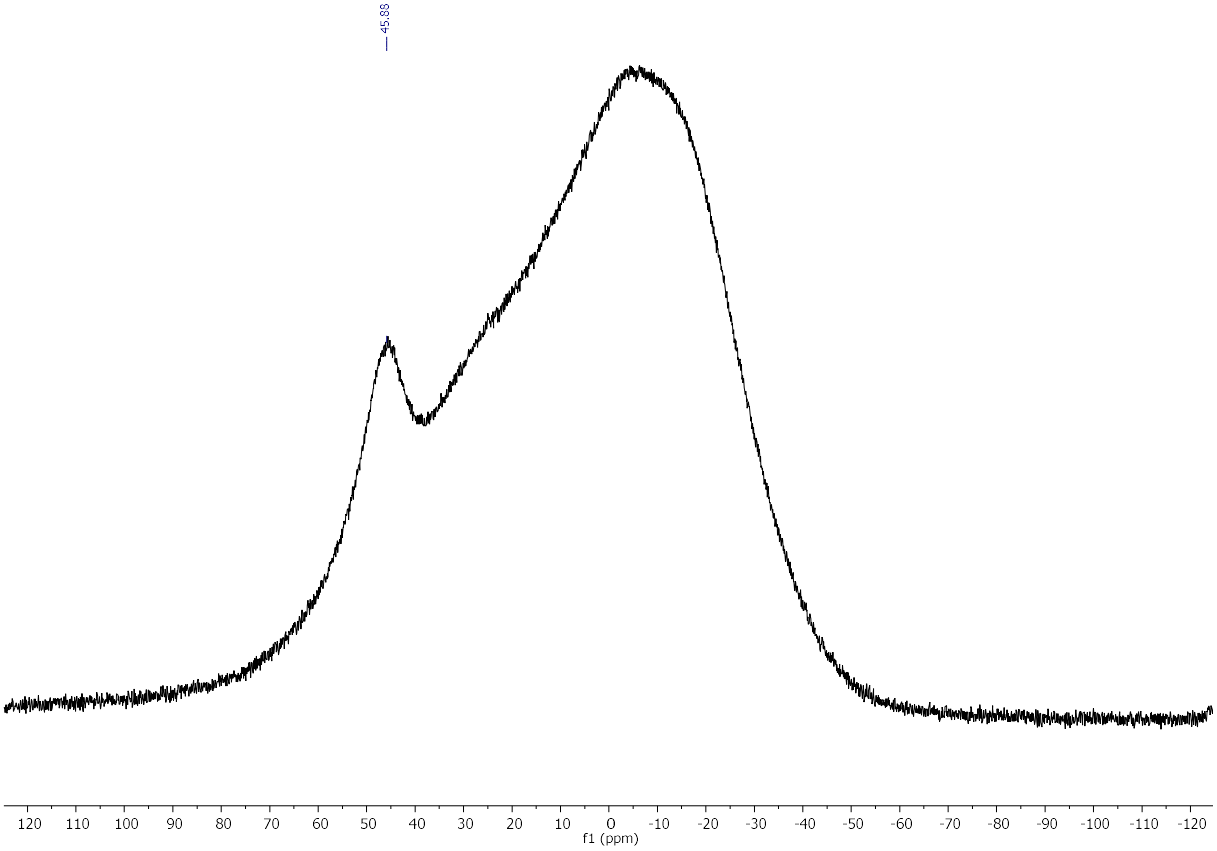

Figure S5.1.7. *$^{11}B\{^{1}H\}$ NMR spectrum of* ***2b*** *(in $CDCl_3$, 128 MHz).*

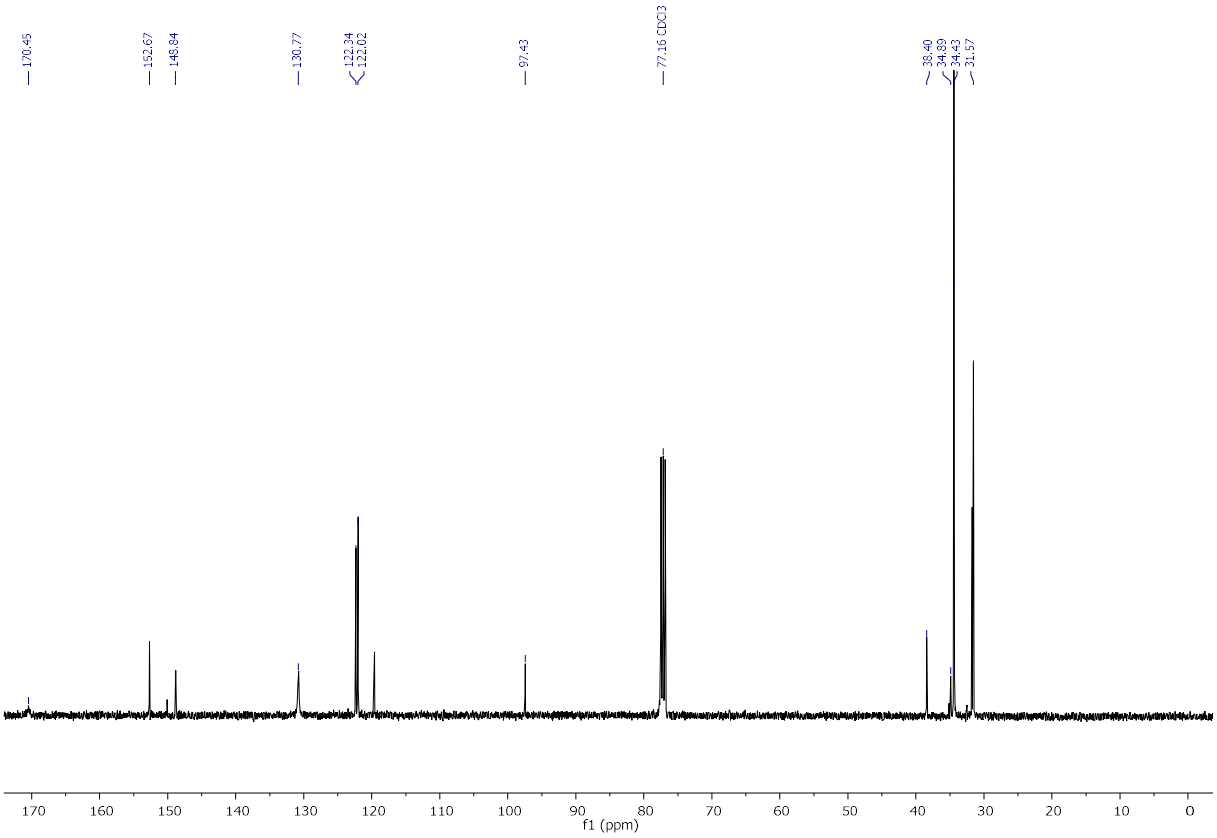

Figure S5.1.8. *^{13}C NMR spectrum of* ***2b*** *(in $CDCl_3$, 101 MHz).*

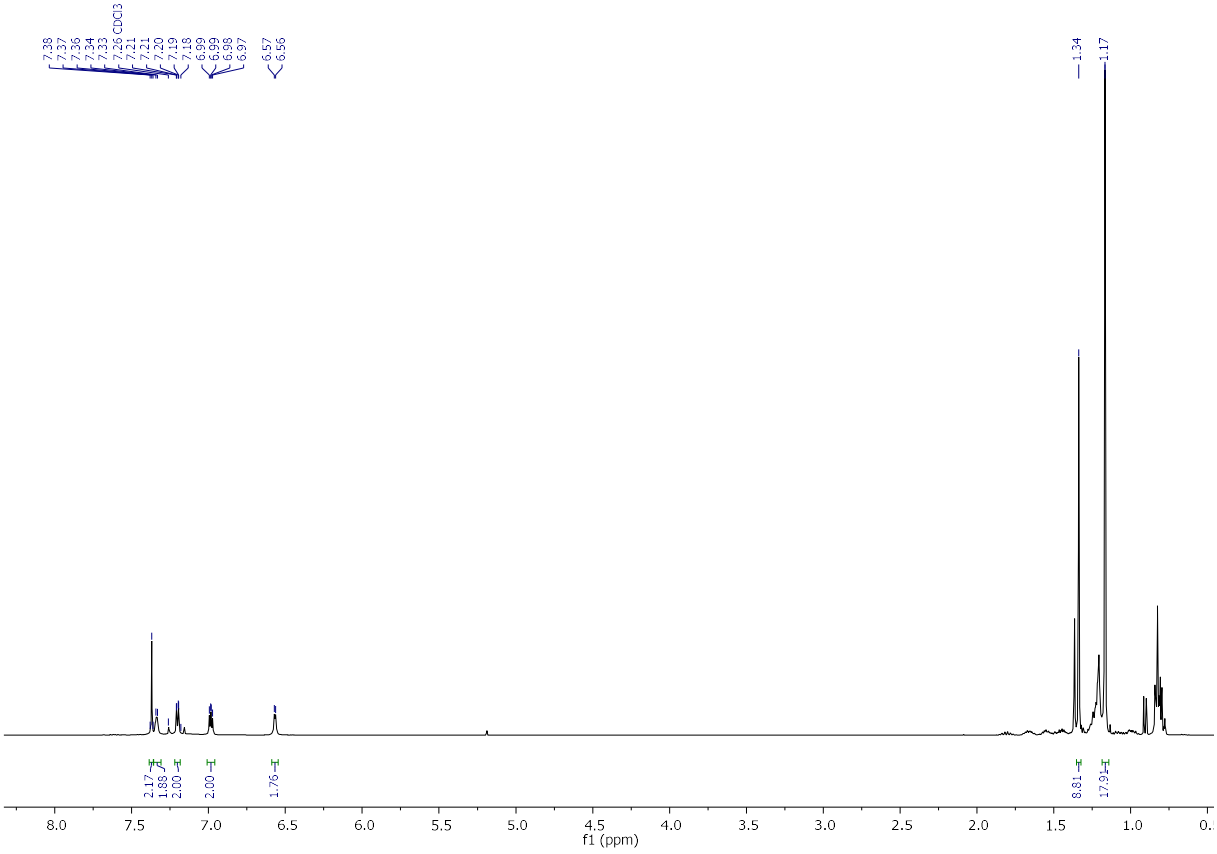

Figure S5.1.9. *^{1}H NMR spectrum of* ***3*** *(in $CDCl_3$, 400 MHz).*

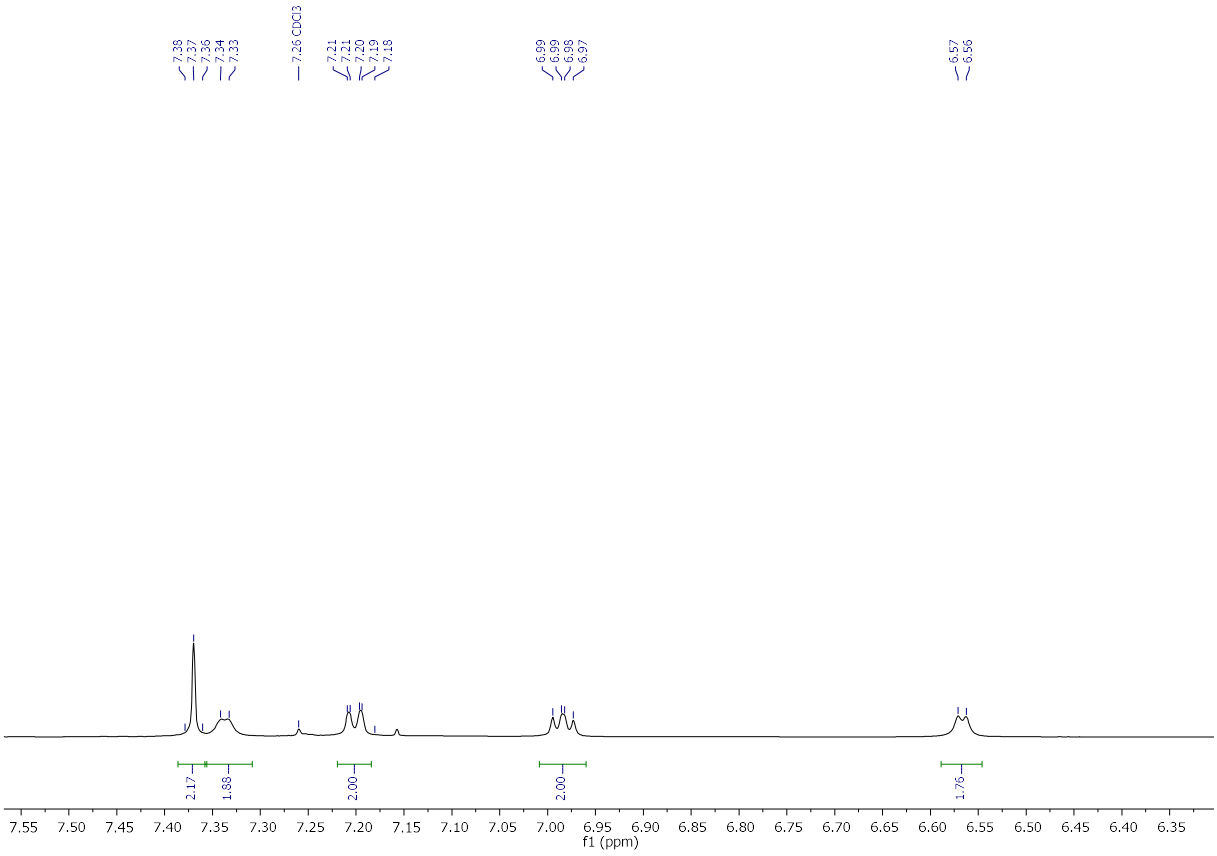

Figure S5.1.10. *Detail (aromatic region) of the ^{1}H NMR spectrum of **3** (in $CDCl_3$, 400 MHz).*

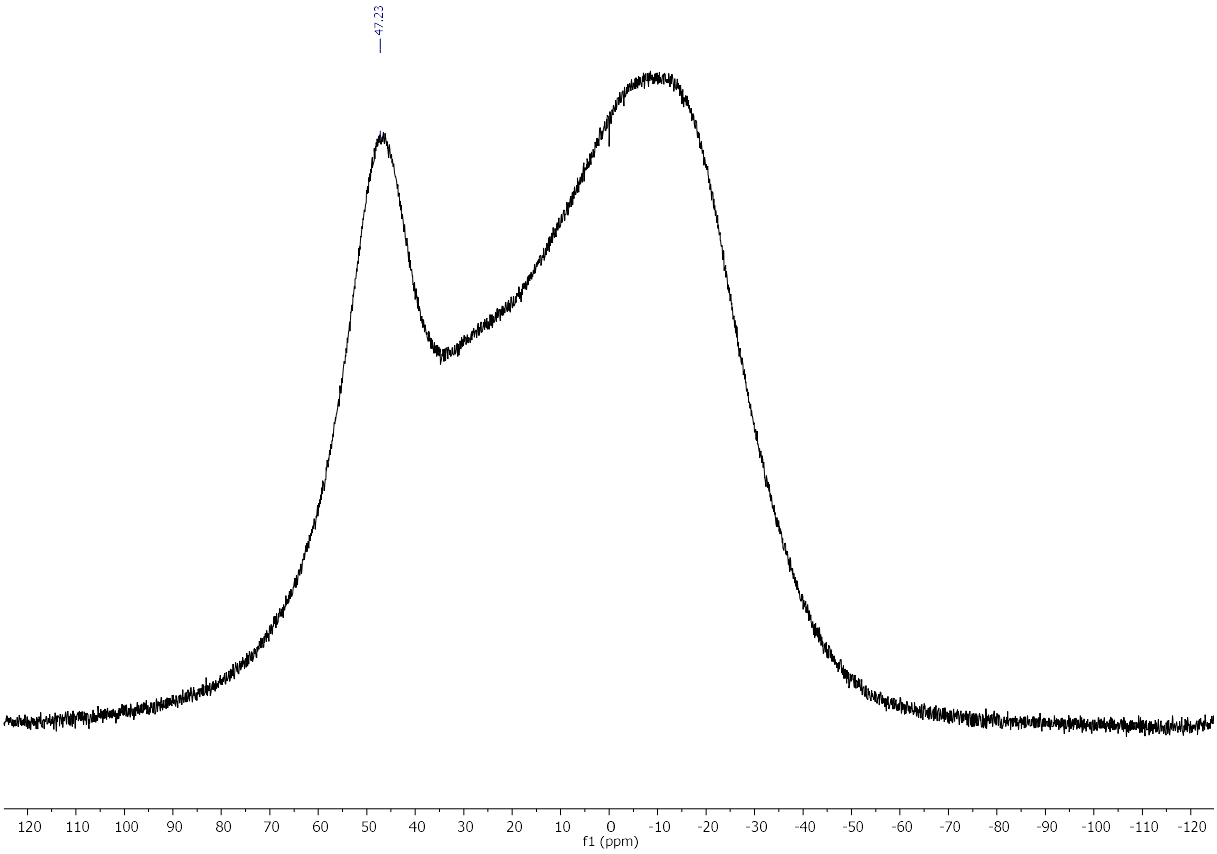

Figure S5.1.11. *$^{11}B\{^{1}H\}$ NMR spectrum of **3** (in $CDCl_3$, 128 MHz).*

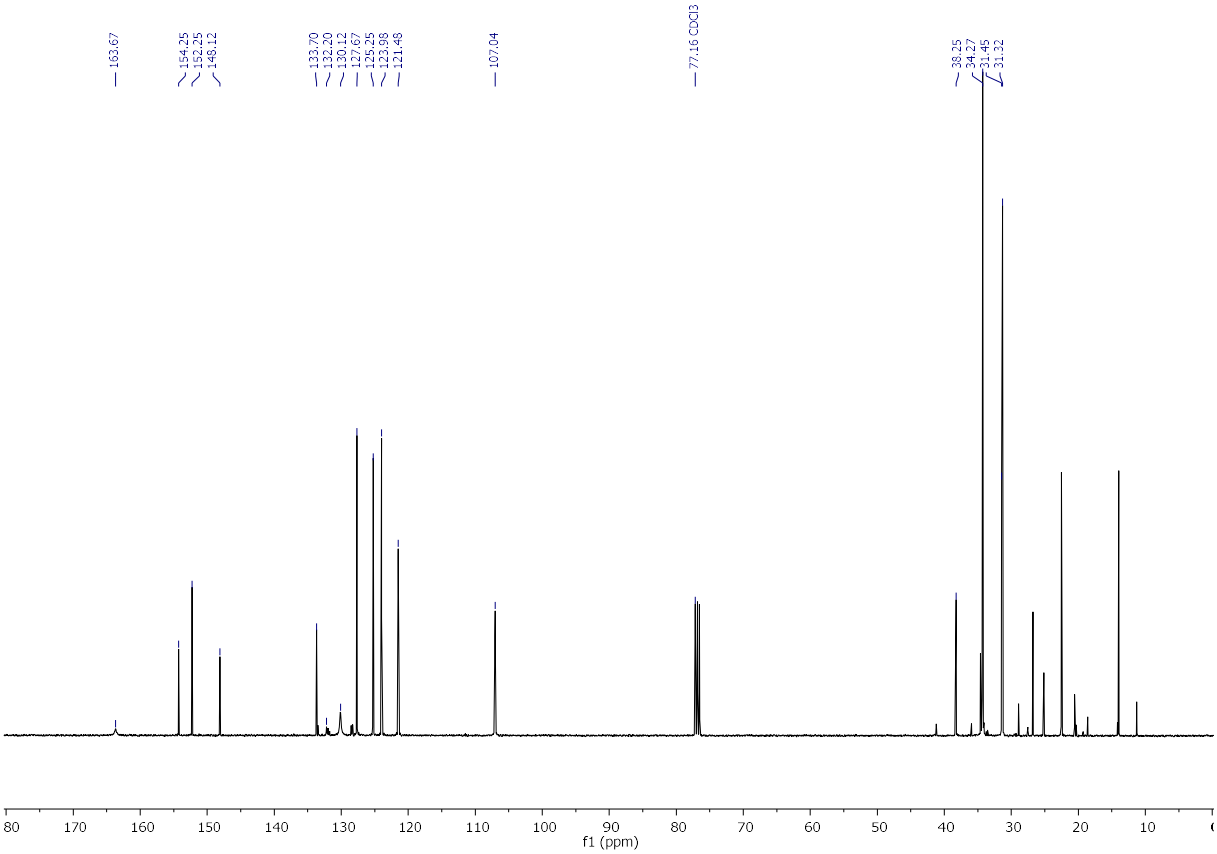

Figure S5.1.12. *^{13}C NMR spectrum of **3** (in $CDCl_3$, 101 MHz).*

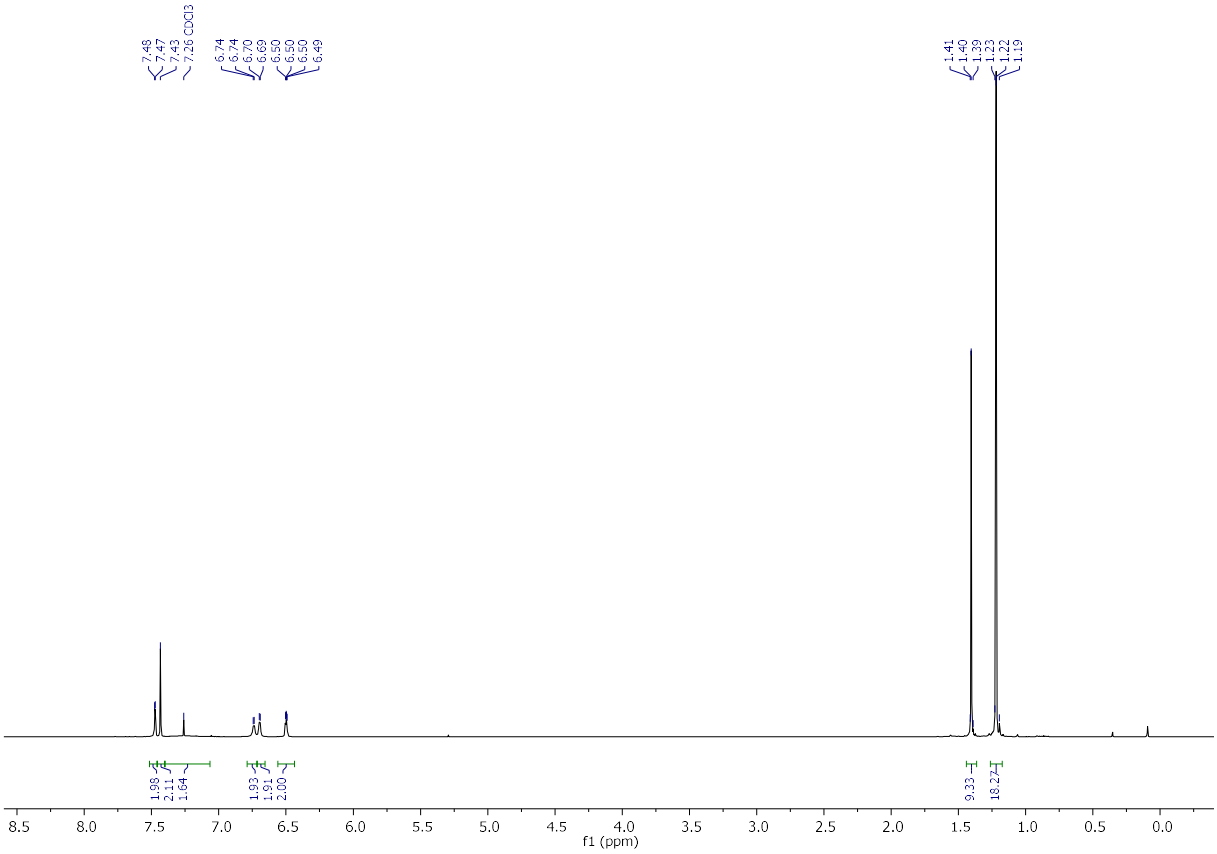

Figure S5.1.13. *^{1}H NMR spectrum of **4** (in $CDCl_3$, 400 MHz).*

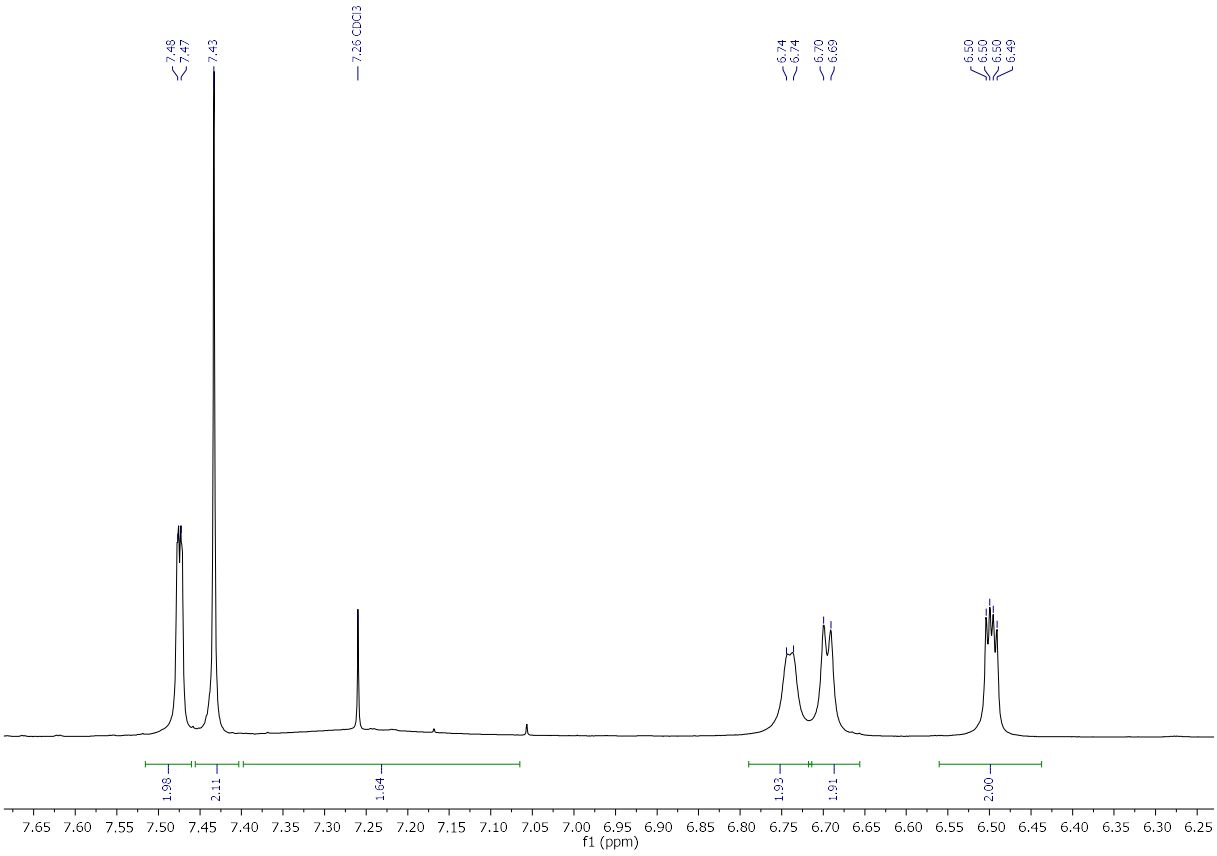

Figure S5.1.14. *Detail (aromatic region) of the ^{1}H NMR spectrum of **4** (in $CDCl_3$, 400 MHz).*

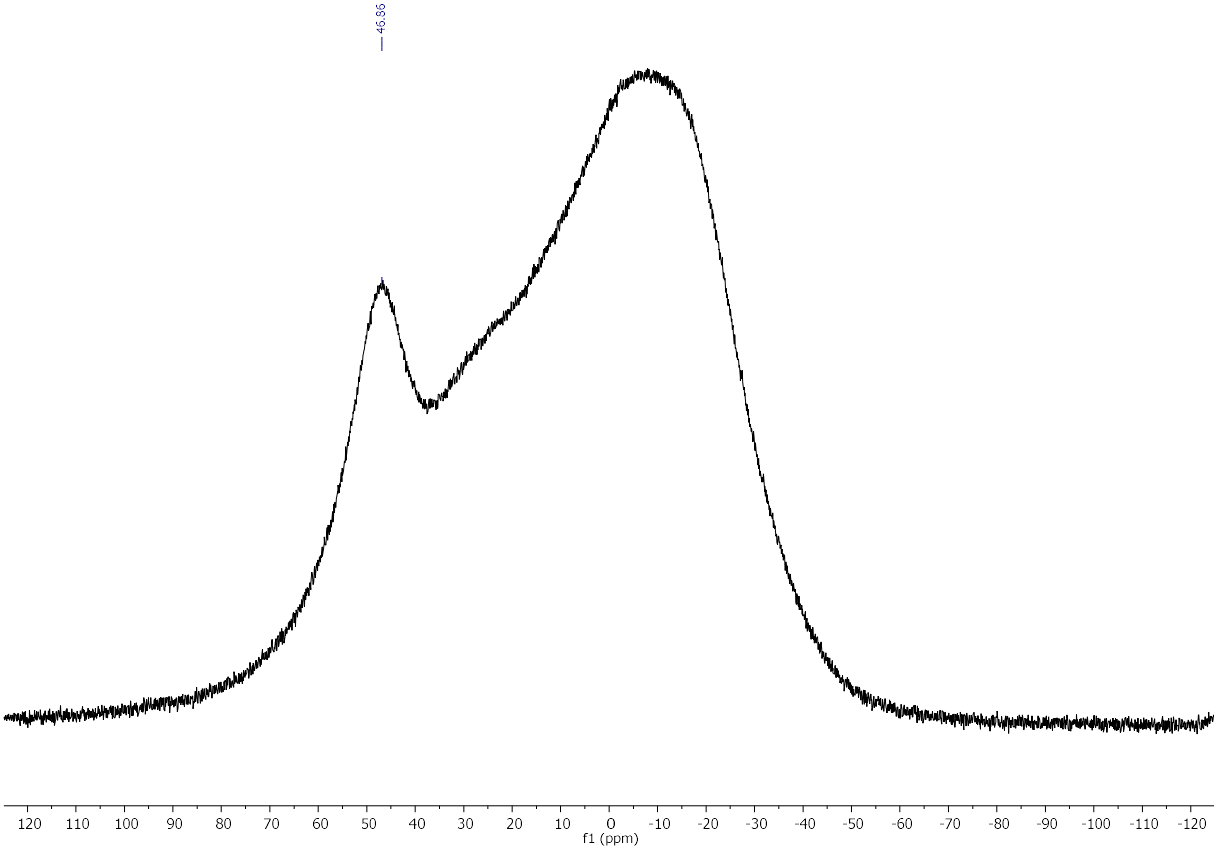

Figure S5.1.15. *$^{11}B\{^{1}H\}$ NMR spectrum of **4** (in $CDCl_3$, 128 MHz).*

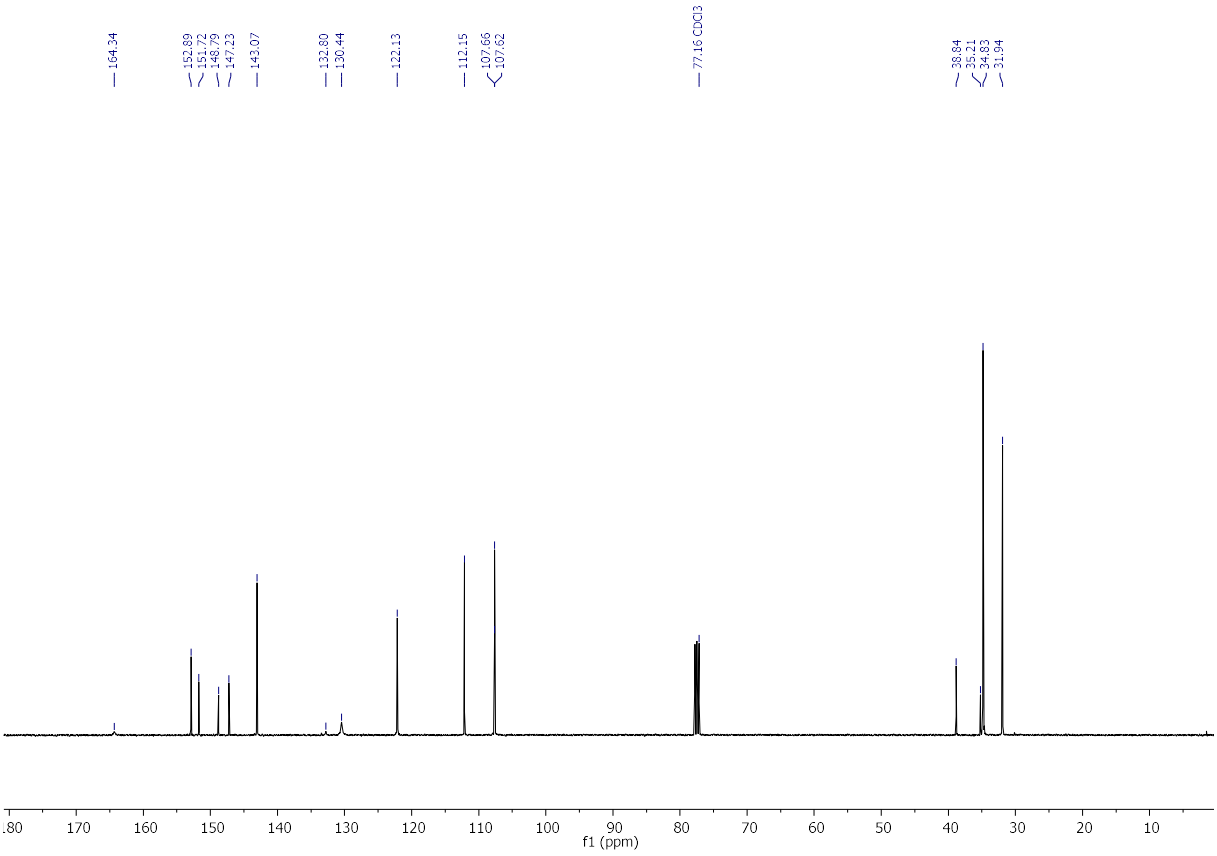

Figure S5.1.16. *^{13}C NMR spectrum of **4** (in $CDCl_3$, 101 MHz).*

UV–vis Spectra

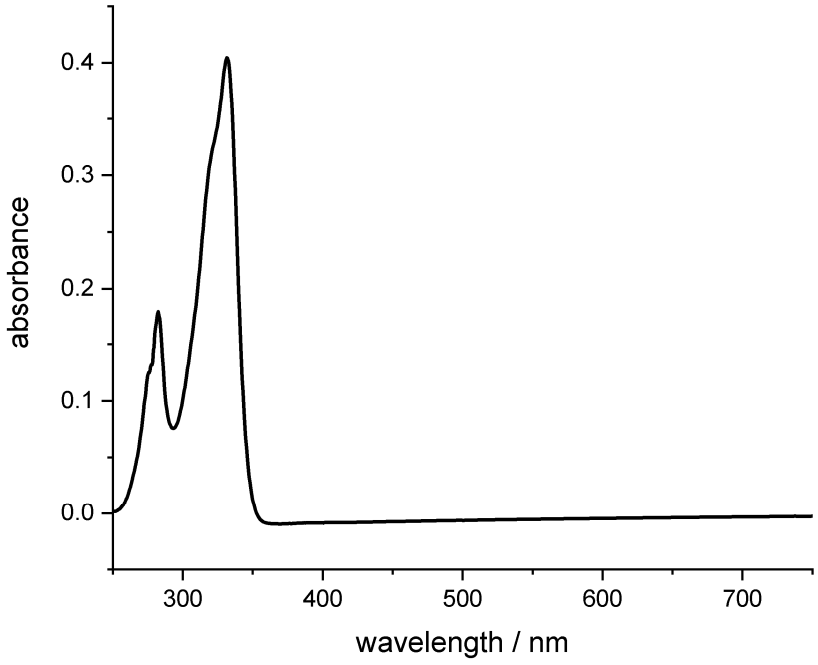

***Figure S5.1.17**. UV–vis spectrum of **2a** (in THF).*

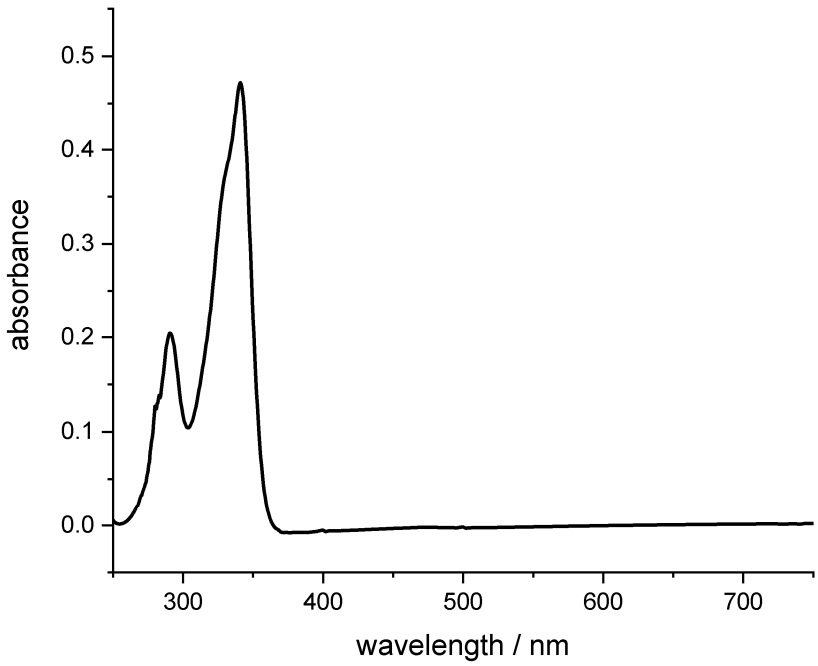

***Figure S5.1.18.** UV–vis spectrum of **2b** (in THF).*

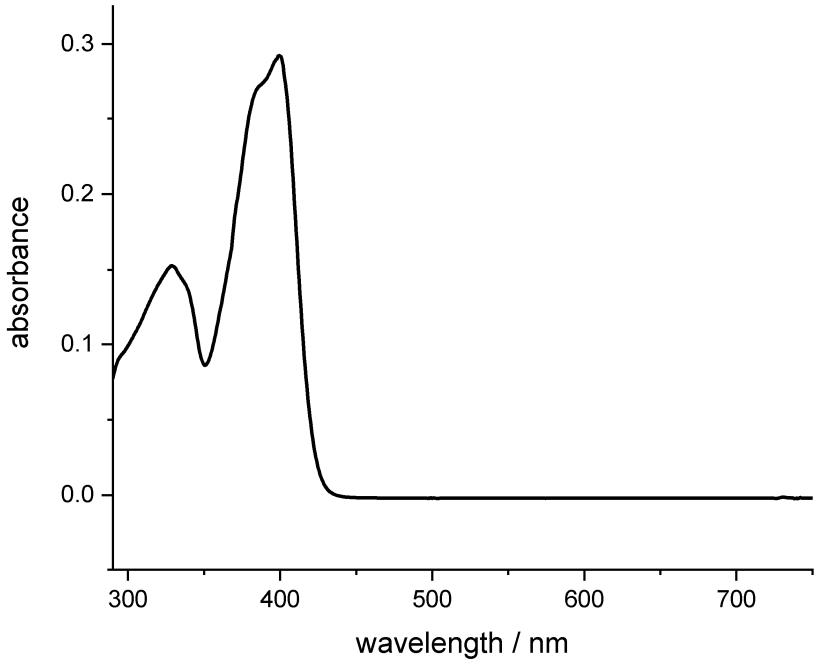

Figure S5.1.19. *UV–vis spectrum of* ***3*** *(in THF).*

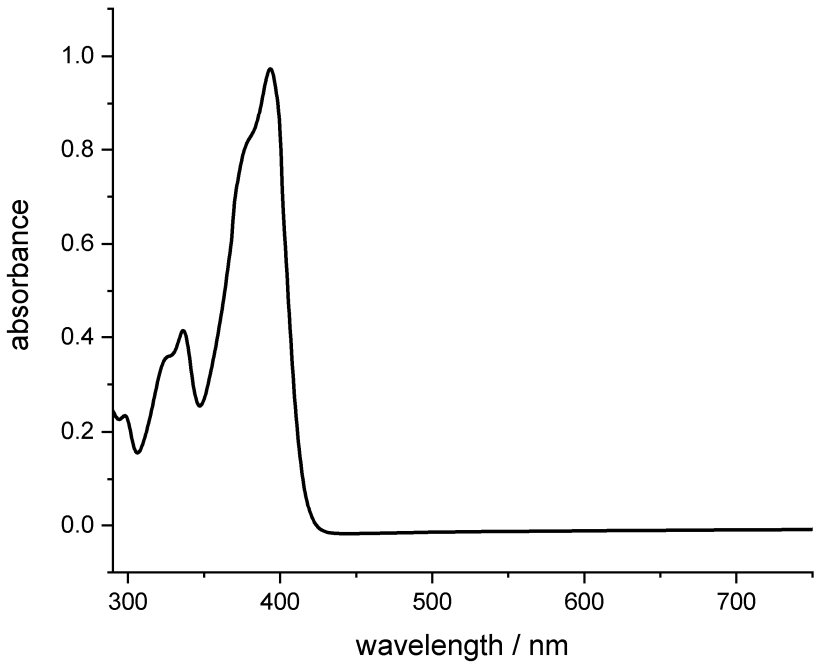

Figure S5.1.20. *UV–vis spectrum of* ***4*** *(in THF).*

Fluorescence spectra

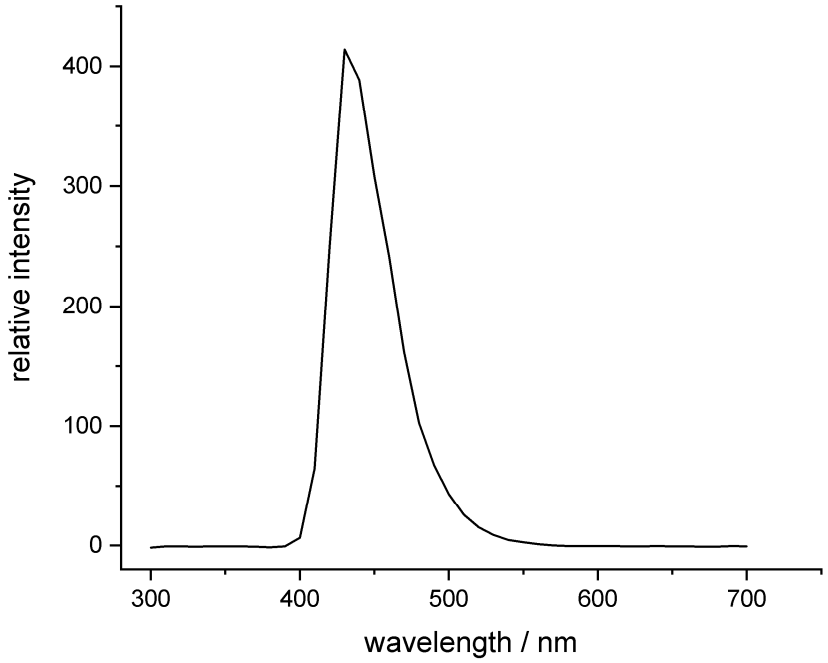

Figure S5.1.21. *Fluorescence spectrum of* ***3*** *(in THF,* λ_{ex} *= 400 nm).*

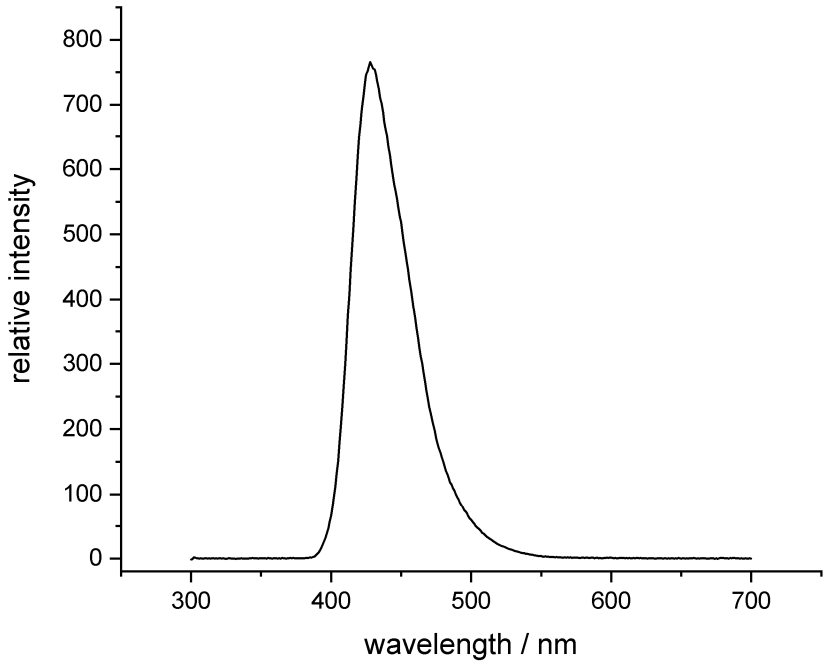

Figure S5.1.22. *Fluorescence spectrum of* ***4*** *(in THF,* λ_{ex} *= 394 nm).*

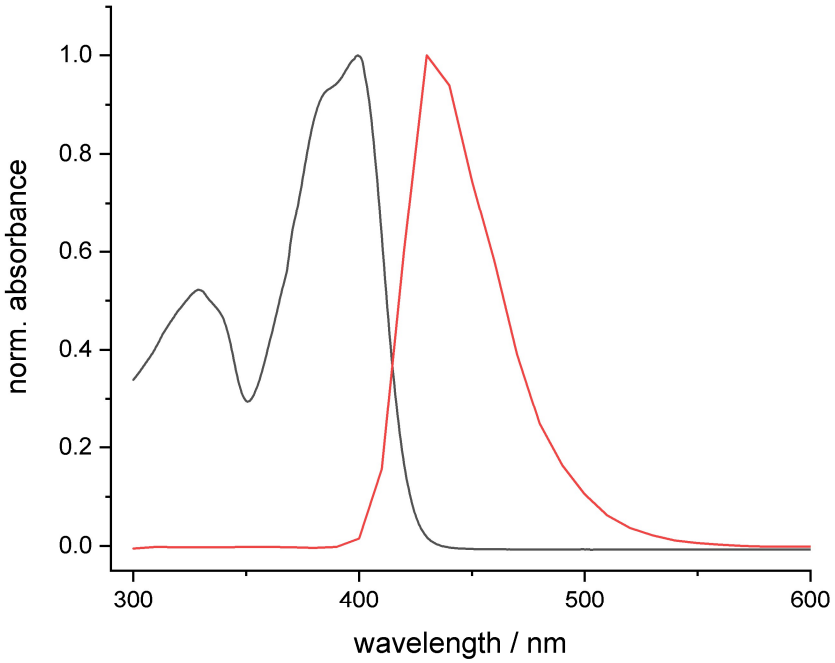

Figure S5.1.23. *UV–vis (black) and fluorescence (red) spectra of* ***3*** *(in THF).*

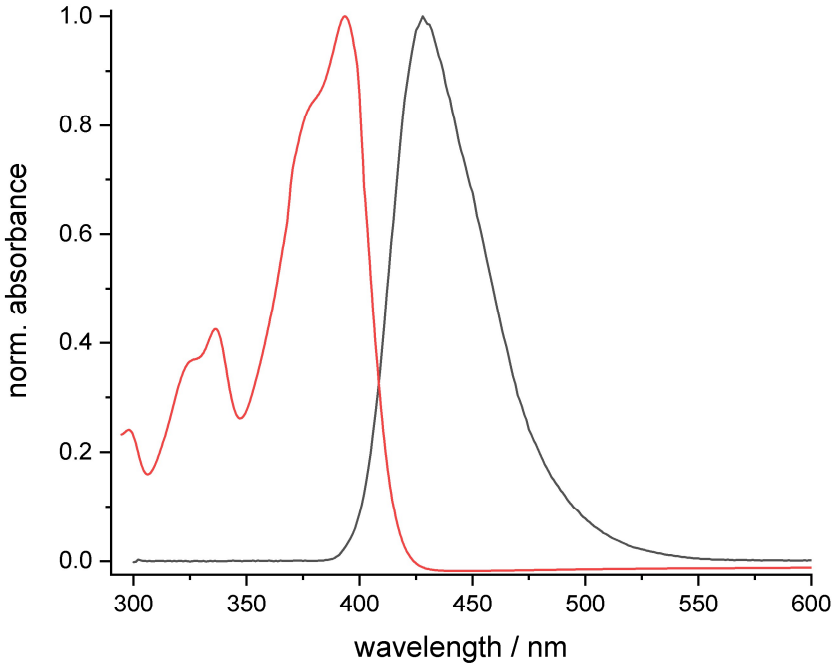

Figure S5.1.24. *UV–vis (red) and fluorescence (black) spectra of* ***4*** *(in THF).*

Mass spectra

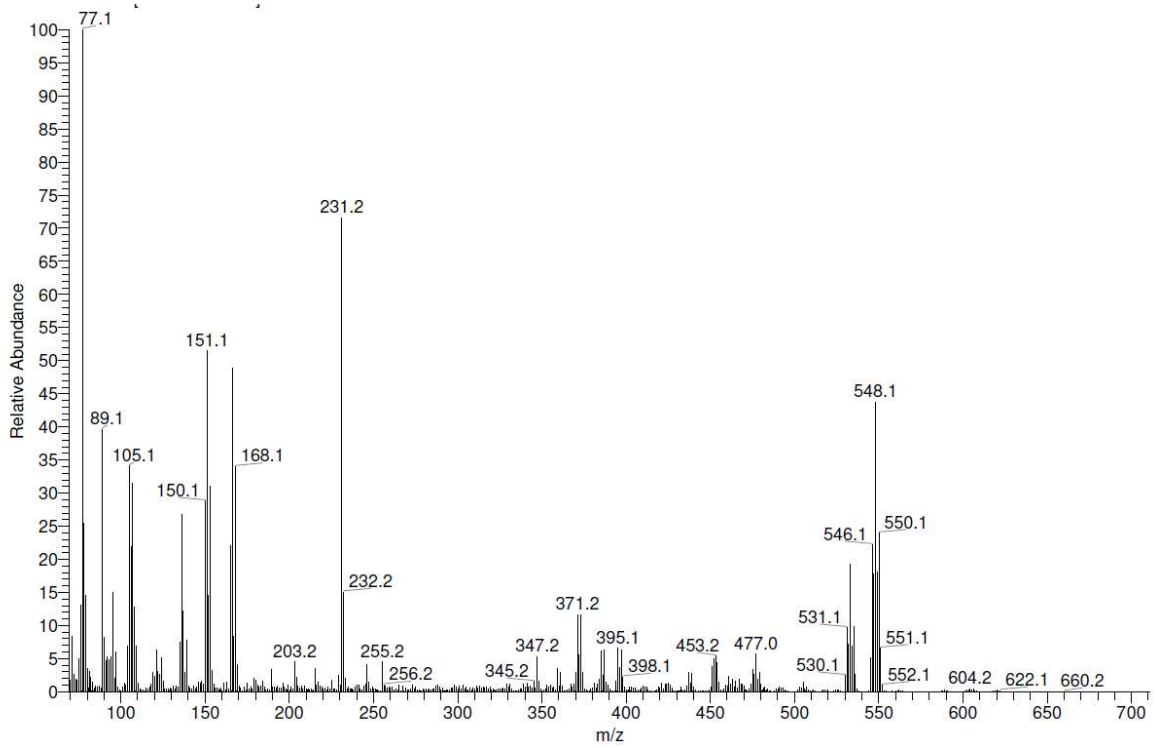

Figure S5.1.25. *EI mass spectrum of* ***2a****.*

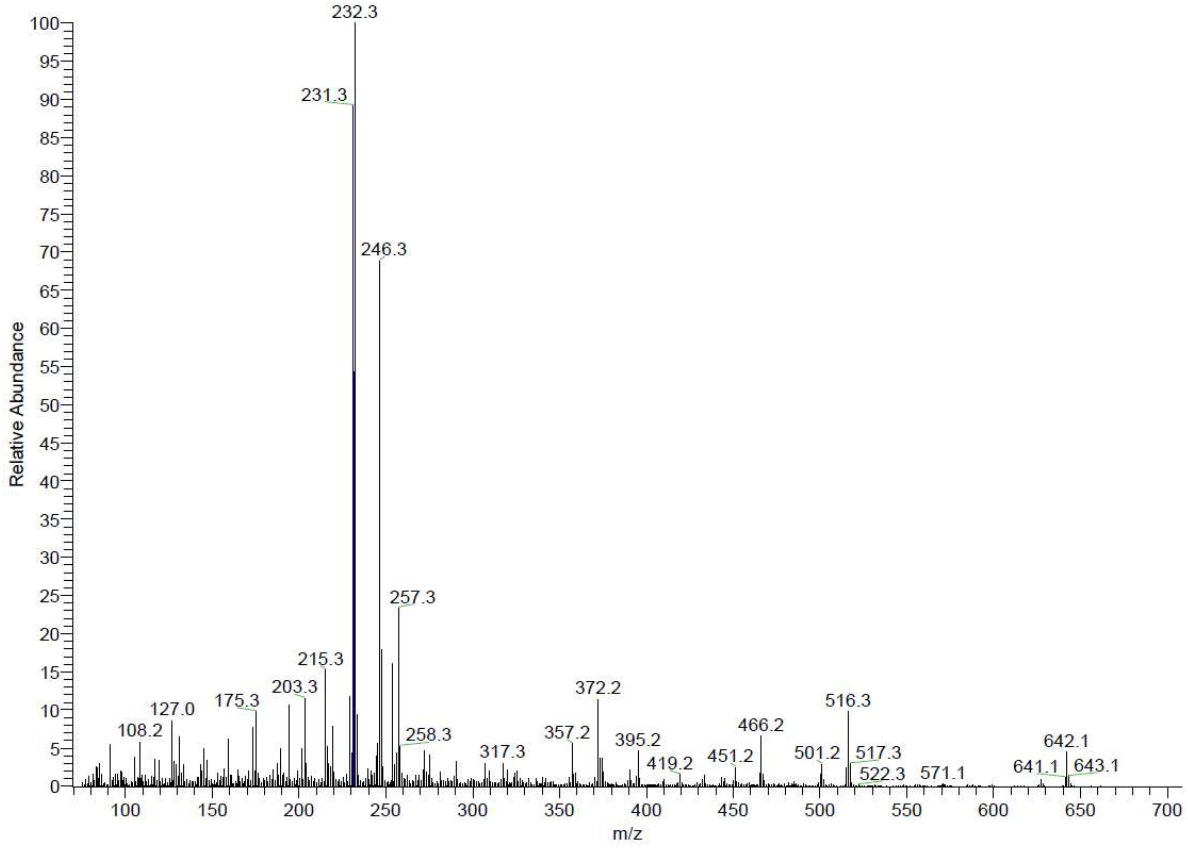

Figure S5.1.26. *EI mass spectrum of* ***2b****.*

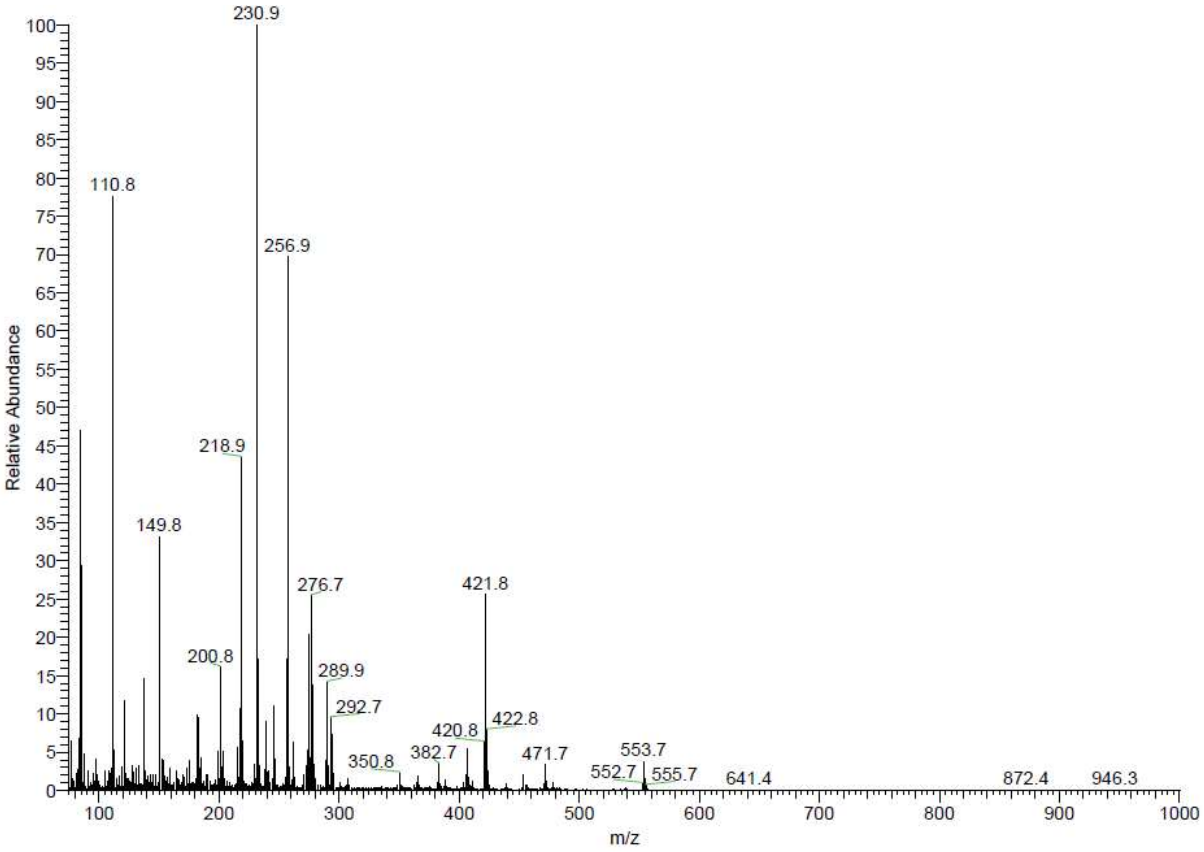

Figure S5.1.27. *EI mass spectrum of* ***3****.*

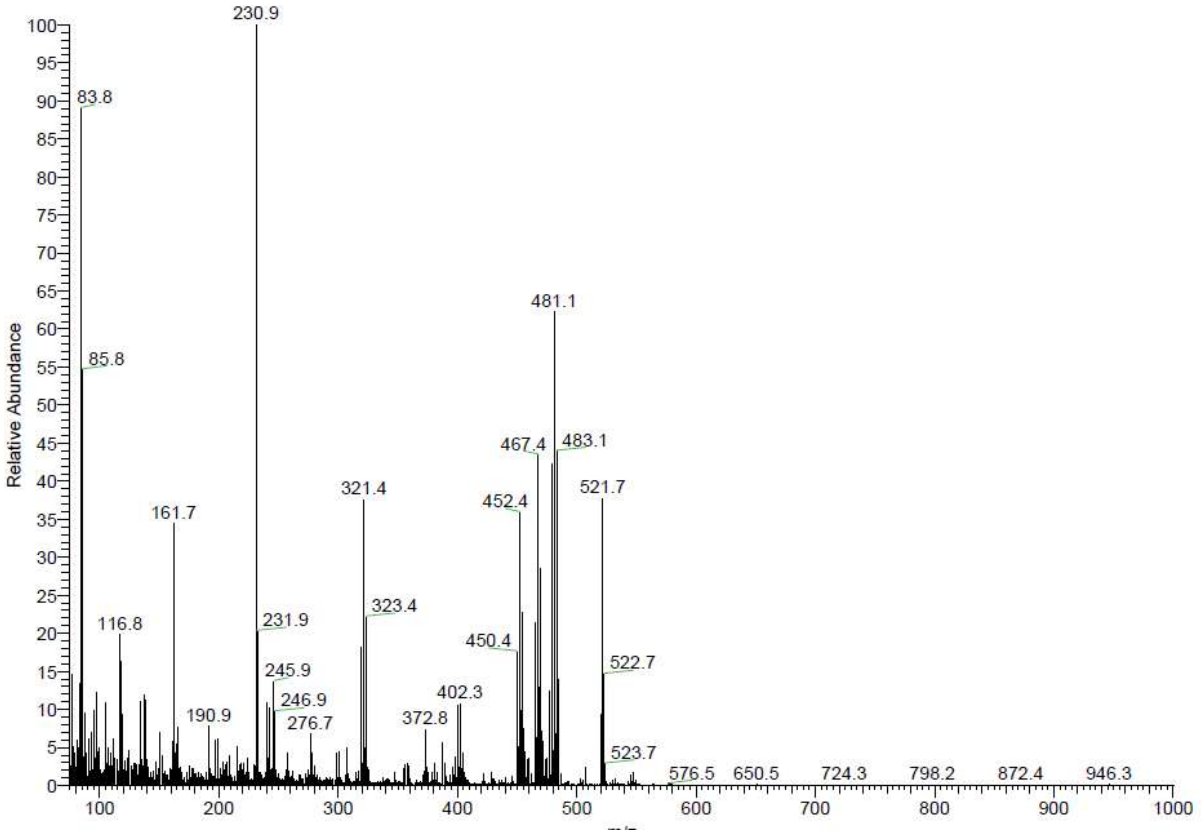

Figure S5.1.28. *EI mass spectrum of* ***4****.*

Cyclic Voltammetry

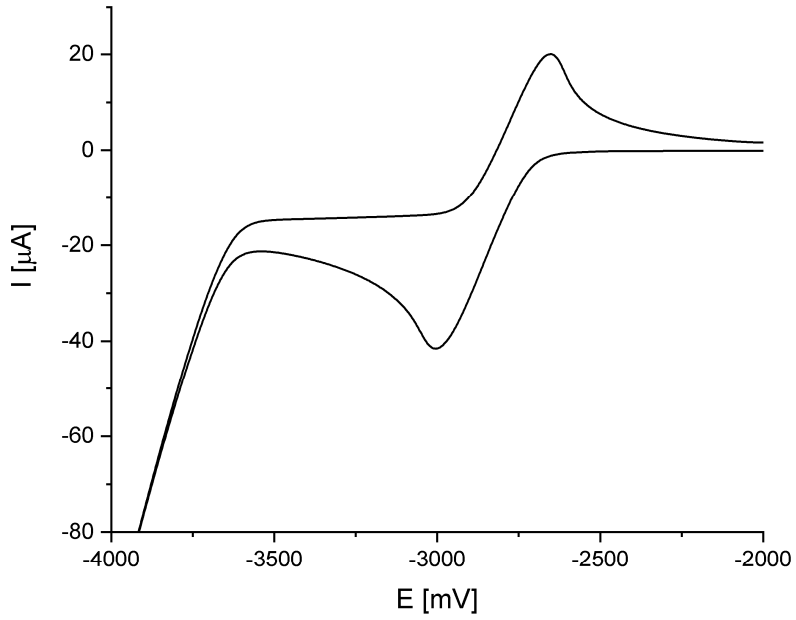

Figure S5.1.29. *Cyclic voltammogram of **1** in THF ($1 \cdot 10^{-3}$ M), recorded vs the ferrocene/ferrocenium couple as internal standard (scan rate: 100 mV s^{-1}).*

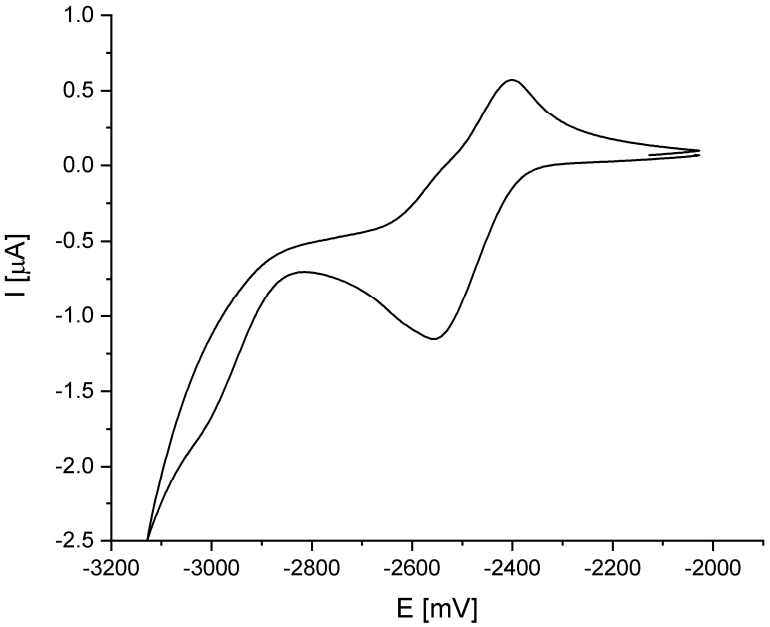

Figure S5.1.30. *Cyclic voltammogram of **3** in THF ($1 \cdot 10^{-3}$ M), recorded vs the ferrocene/ferrocenium couple as internal standard (scan rate: 100 mV s^{-1}).*

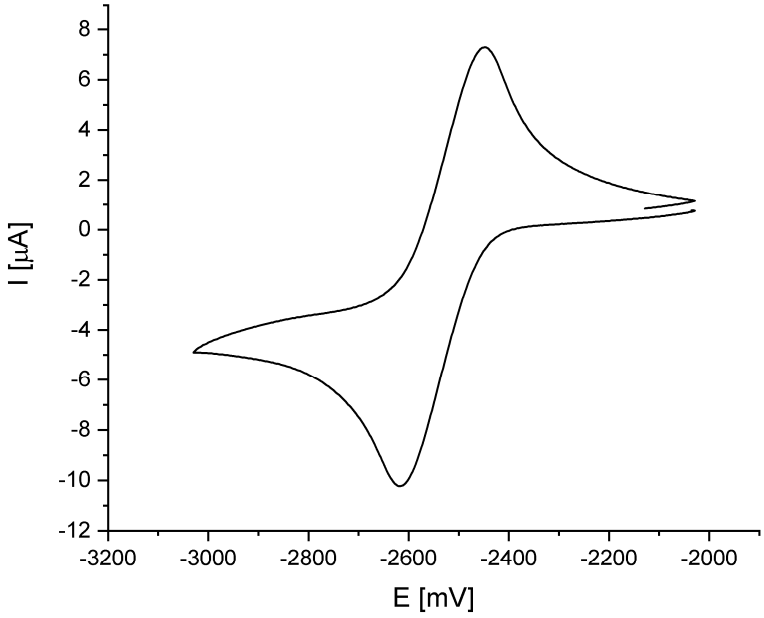

Figure S5.1.31. *Cyclic voltammogram of* ***4*** *in THF ($1 \cdot 10^{-3}$ M), recorded vs the ferrocene/ferrocenium couple as internal standard (scan rate: 100 mV s^{-1}).*

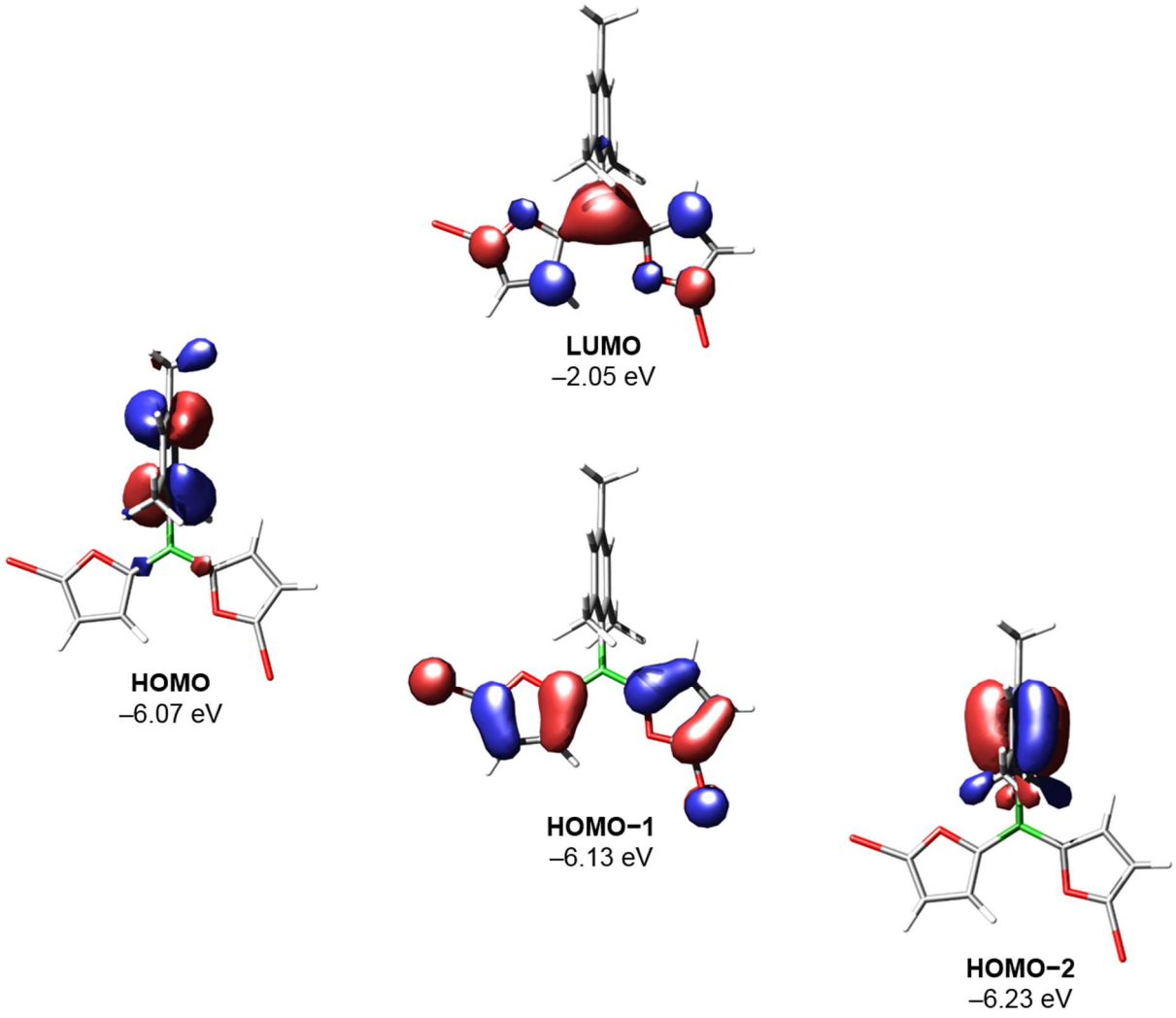

Figure S5.1.32. *Calculated frontier orbitals of* ***2a*** *(isovalue 0.04 a.u.).*

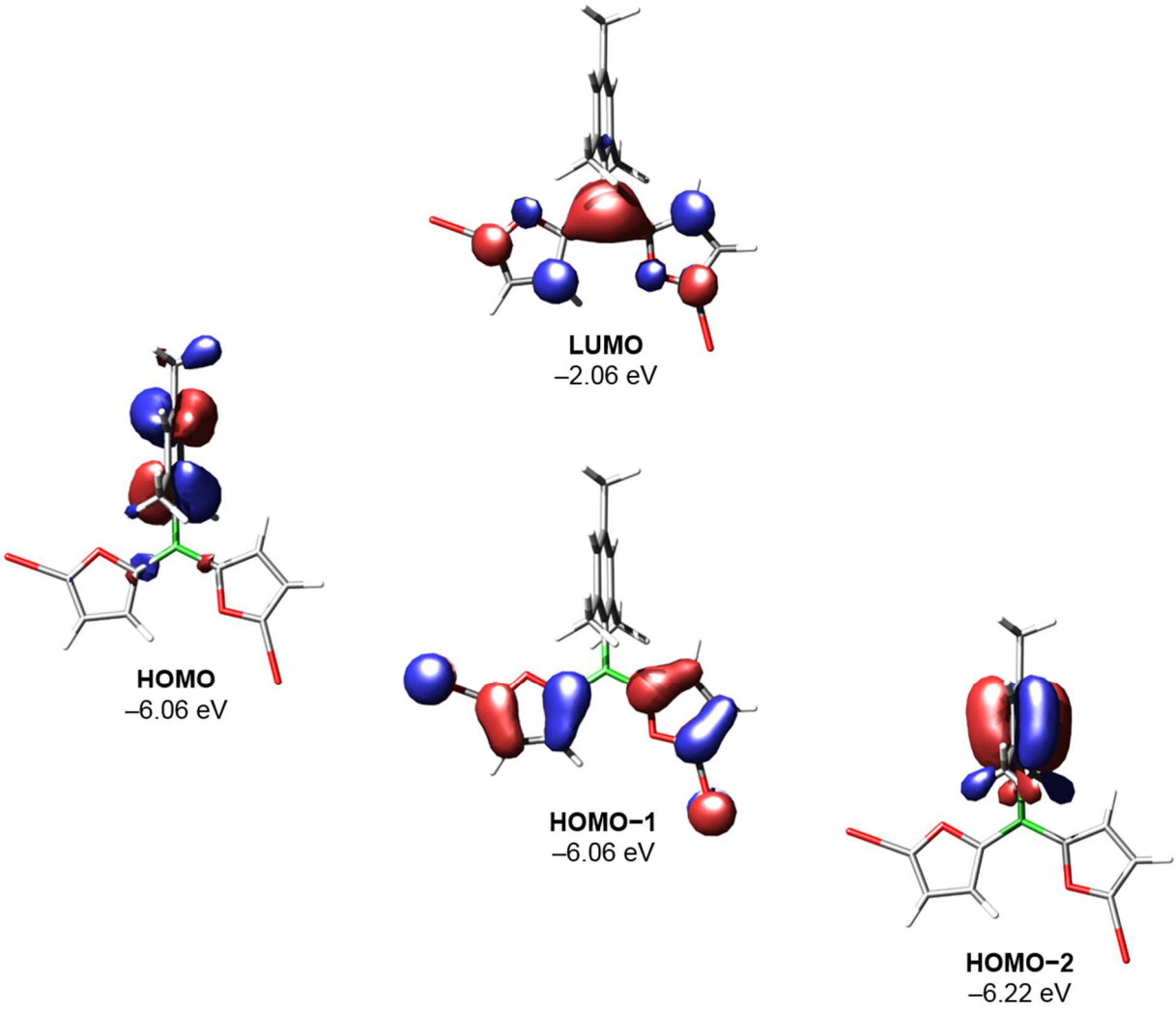

Figure S5.1.33. *Calculated frontier orbitals of* ***2b*** *(isovalue 0.04 a.u.).*

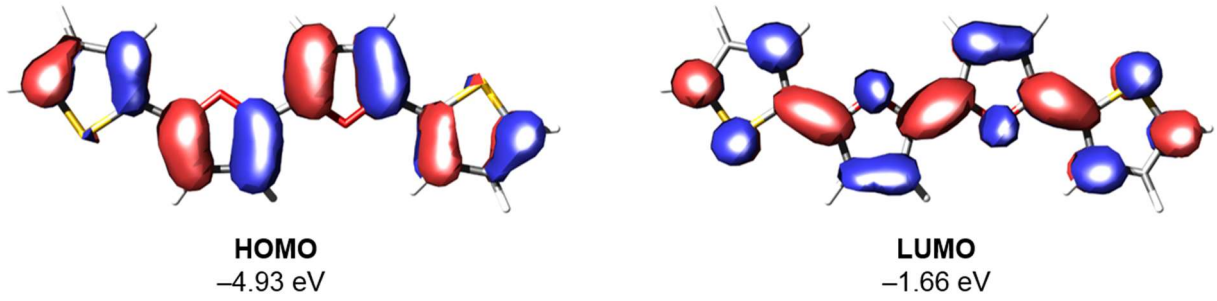

Figure S5.1.34. *Calculated frontier orbitals of* ***5*** *(isovalue 0.03 a.u.).*

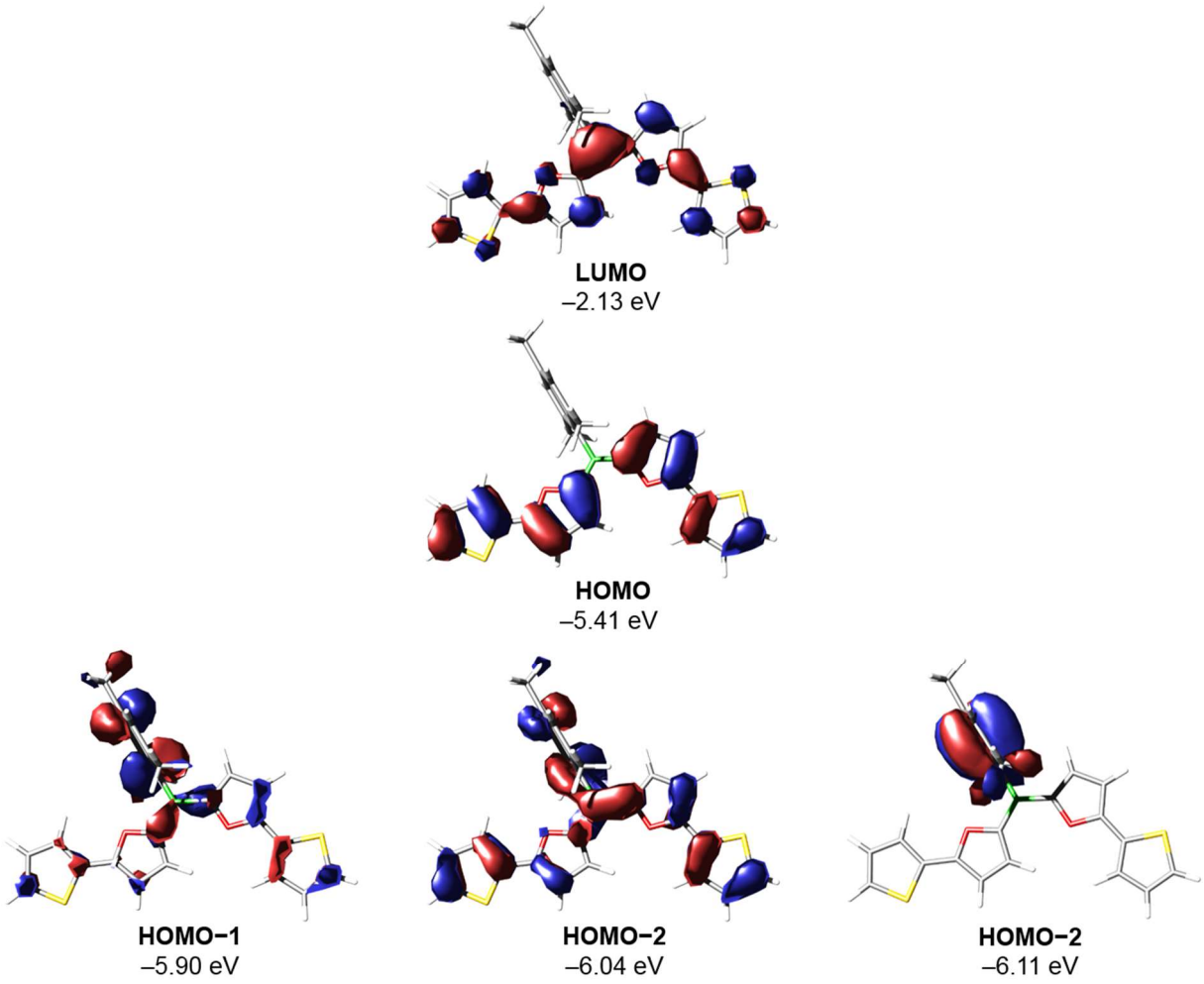

Figure S5.1.35. *Calculated frontier orbitals of* ***3*** *(isovalue 0.03 a.u.).*

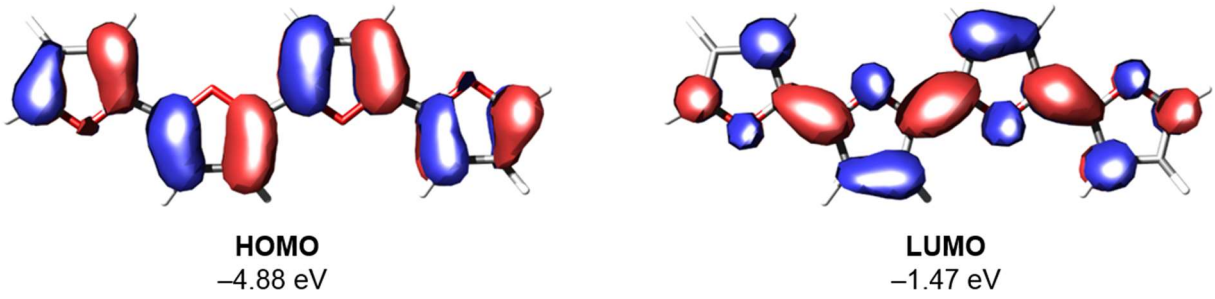

Figure S5.1.36. *Calculated frontier orbitals of* ***6*** *(isovalue 0.03 a.u.).*

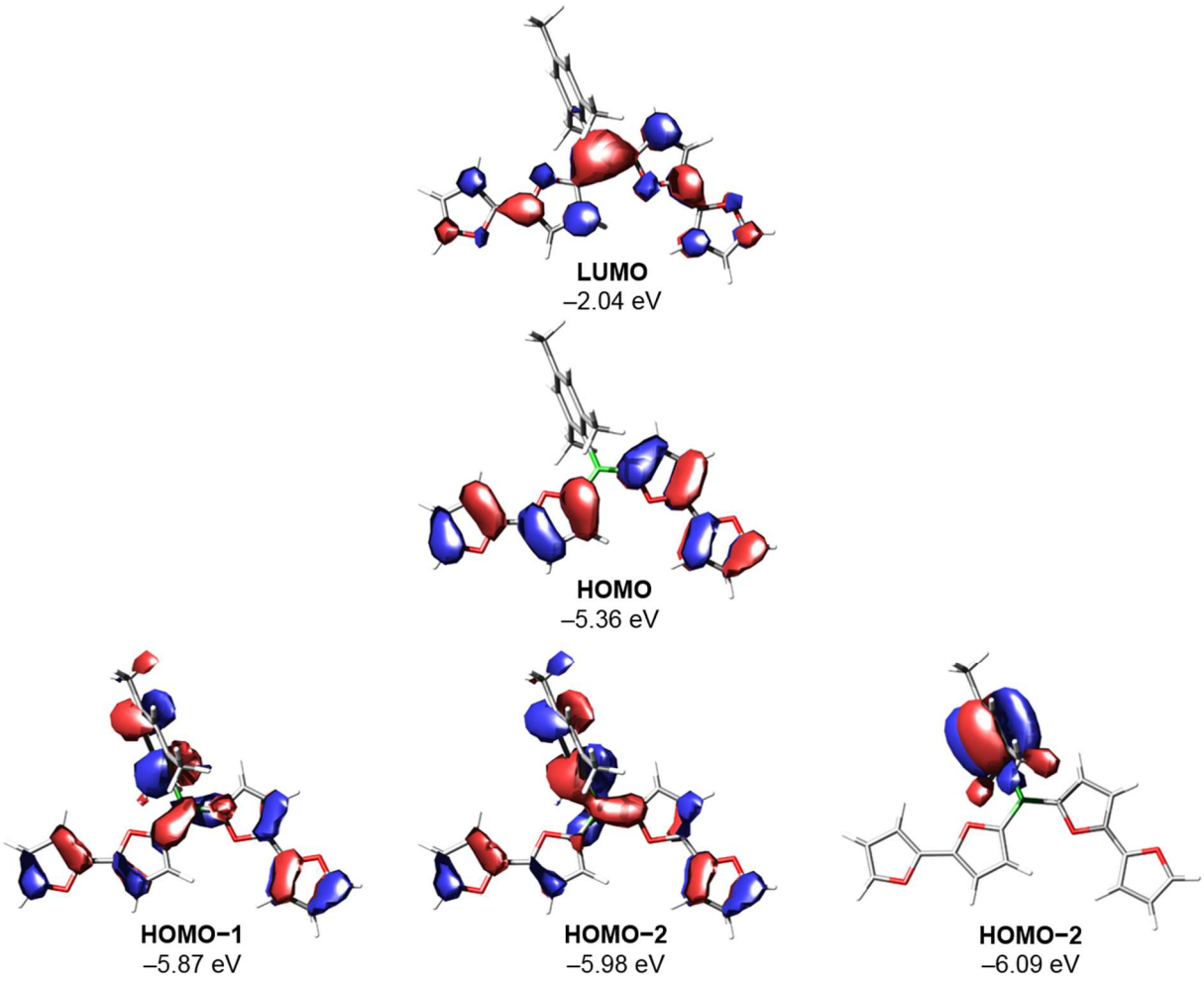

Figure S5.1.37. *Calculated frontier orbitals of* ***4*** *(isovalue 0.03 a.u.).*

Cartesian coordinates [Å] and total energies [a.u.] of optimized stationary points

2a:

Total energy (B3LYP-D3(BJ)/def2-SV(P)): −5978.533161529

O	0.754565	−0.025894	−2.497581
C	1.476939	−0.023971	−1.306010
C	2.823051	−0.027201	−1.640999
C	2.927392	−0.030531	−3.058272
C	1.624982	−0.028099	−3.506248
B	0.691916	−0.015286	0.007844
C	−0.882491	−0.012943	0.025058
C	−1.593117	1.187375	−0.193562
C	−2.992961	1.182969	−0.152132
C	−3.718005	0.010041	0.091499
C	−3.001702	−1.176979	0.289209
C	−1.601435	−1.204990	0.263484
C	−0.846639	2.468902	−0.488833
C	−5.226049	0.028541	0.164484
C	−0.866737	−2.510975	0.472670

C	1.423792	0.010819	1.357117
C	0.944384	0.073916	2.653996
C	2.058225	0.087907	3.540967
C	3.159917	0.031849	2.719752
O	2.813652	−0.013333	1.429724
Br	4.981254	0.010862	3.119679
H	2.063441	0.133283	4.628001
H	−0.112163	0.107494	2.919882
H	−0.073376	2.675488	0.274274
H	−1.527526	3.336260	−0.522900
H	−0.329021	2.407805	−1.464195
H	−0.257476	−2.491041	1.395040
H	−1.566610	−3.360375	0.548618
H	−0.172574	−2.719917	−0.362683
H	−3.549622	−2.109718	0.465218
H	−3.533586	2.121318	−0.320398
H	3.823817	−0.033135	−3.675020
Br	0.937480	−0.025508	−5.239041
H	3.639722	−0.026828	−0.920873
H	−5.651653	0.835404	−0.457431
H	−5.659491	−0.929424	−0.172731
H	−5.574597	0.197029	1.202303

2b:

Total energy (B3LYP-D3(BJ)/def2-SV(P)): −1426.465505390

O	0.750724	−0.016409	−2.493144
C	1.475551	−0.019124	−1.304459
C	2.820733	−0.022240	−1.642628
C	2.920453	−0.020384	−3.060405
C	1.616924	−0.015507	−3.507757
B	0.692149	−0.014328	0.011060
C	−0.882014	−0.012154	0.027979
C	−1.593195	1.186150	−0.200211
C	−2.993107	1.180696	−0.161878
C	−3.717674	0.008800	0.088240
C	−3.000800	−1.176209	0.295512
C	−1.600486	−1.203206	0.272914
C	−0.847393	2.466751	−0.501206
C	−5.225887	0.026594	0.157852
C	−0.865573	−2.507704	0.490545
C	1.425622	0.007167	1.360115
C	0.946781	0.069468	2.657228
C	2.061720	0.078054	3.542873
C	3.165096	0.019685	2.722534
O	2.814222	−0.022027	1.431754
I	5.197584	−0.010972	3.171693
H	2.063958	0.121338	4.630300
H	−0.109453	0.105681	2.924225

H	−0.078185	2.680135	0.264154
H	−1.529631	3.332652	−0.544573
H	−0.325204	2.399507	−1.473639
H	−0.258080	−2.482768	1.413876
H	−1.565308	−3.356939	0.569539
H	−0.169794	−2.720842	−0.342392
H	−3.548299	−2.108363	0.475840
H	−3.534200	2.117450	−0.337567
H	3.817694	−0.021110	−3.676444
I	0.844744	−0.004573	−5.440362
H	3.639680	−0.025163	−0.925053
H	−5.650915	0.826976	−0.472818
H	−5.657753	−0.935038	−0.170854
H	−5.576736	0.204973	1.193255

5:

Total energy (B3LYP-D3(BJ)/def2-SV(P)): −1561.207217474

C	0.252447	−0.387049	2.568198
C	1.371948	−0.568249	3.353528
C	2.491461	−0.491229	2.475561
C	1.990179	−0.268108	1.208953
O	0.626217	−0.205103	1.269342
H	1.376648	−0.735143	4.428618
H	3.543705	−0.588183	2.739093
C	2.594876	−0.100525	−0.087517
S	4.329195	−0.163997	−0.293125
C	4.187051	0.106231	−1.998045
C	2.875979	0.237759	−2.386492
C	1.963160	0.120489	−1.298856
H	0.878147	0.193656	−1.388165
H	2.571679	0.413457	−3.421032
H	5.084342	0.152253	−2.615717
C	−1.150085	−0.357966	2.857176
C	−2.269255	−0.170495	2.072844
C	−3.388999	−0.251899	2.950120
C	−2.888198	−0.484059	4.215293
O	−1.524274	−0.547794	4.154787
H	−2.273571	0.003647	0.998903
H	−4.441113	−0.152517	2.686971
C	−3.493497	−0.662952	5.509969
S	−5.227861	−0.600390	5.715483
C	−5.086671	−0.888729	7.417510
C	−3.775877	−1.025495	7.805089
C	−2.862484	−0.897292	6.719169
H	−1.777586	−0.972572	6.808111
H	−3.472183	−1.212696	8.837788
H	−5.984260	−0.940463	8.034298

6:

Total energy (B3LYP-D3(BJ)/def2-SV(P)): −915.4046364487

C	0.274378	−0.362287	2.483932
C	1.420791	−0.532174	3.232064
C	2.512648	−0.447732	2.319319
C	1.962673	−0.231292	1.073862
O	0.603240	−0.178619	1.172043
H	1.460227	−0.697366	4.306786
H	3.574764	−0.534274	2.539179
C	2.532241	−0.062463	−0.233184
C	1.981763	0.156345	−1.476360
C	3.082600	0.235351	−2.389339
O	3.890367	−0.121356	−0.332455
C	4.213386	0.059589	−1.639751
H	5.275666	0.036745	−1.873011
H	3.036270	0.401577	−3.464965
H	0.920440	0.247501	−1.698066
C	−1.118806	−0.348657	2.817443
C	−2.265293	−0.179846	2.069165
C	−3.357625	−0.274867	2.980311
C	−2.807771	−0.494987	4.225182
O	−1.447983	−0.539573	4.128204
H	−2.304518	−0.009310	0.995257
H	−4.420004	−0.193603	2.759655
C	−3.377912	−0.676661	5.530254
C	−2.827338	−0.894499	6.773549
C	−3.929103	−0.994219	7.683368
O	−4.736985	−0.637858	5.626466
C	−5.060516	−0.830932	6.931909
H	−6.123600	−0.825272	7.162560
H	−3.882964	−1.165628	8.758184
H	−1.765371	−0.971934	6.997332

3:

Total energy (B3LYP-D3(BJ)/def2-SV(P)): −1935.189219178

C	0.346012	−1.137169	7.912612
C	−1.019654	−1.123680	7.689509
S	−1.895228	−1.384527	9.178766
C	−0.424222	−1.507734	10.079941
C	0.682445	−1.356942	9.278626
C	−1.712788	−0.928816	6.439831
C	−3.057357	−0.879936	6.107570
C	−3.105202	−0.655127	4.708944
C	−1.800968	−0.576525	4.243255
O	−0.961737	−0.749864	5.331936
B	−1.255949	−0.362565	2.826657
C	−2.287316	−0.132462	1.656013
C	−2.878380	1.134923	1.455118

C	−3.789055	1.319140	0.407042
C	−4.141803	0.272383	−0.454190
C	−3.543777	−0.976724	−0.249408
C	−2.622880	−1.191298	0.784518
C	−2.518609	2.295819	2.356196
C	−5.156281	0.481459	−1.553014
C	−1.978486	−2.548797	0.954495
C	0.246955	−0.388227	2.542245
O	0.661441	−0.202050	1.232482
C	2.005021	−0.268141	1.182026
C	2.511930	−0.496179	2.453401
C	1.388789	−0.572217	3.312158
C	2.621810	−0.099505	−0.110301
S	4.354681	−0.173513	−0.314884
C	4.213025	0.107742	−2.015786
C	2.902120	0.250498	−2.405270
C	1.989253	0.132710	−1.319121
H	3.564145	−0.594801	2.717127
H	1.387981	−0.744782	4.386737
H	−2.854811	2.121793	3.394840
H	−1.423904	2.447287	2.398647
H	−2.976182	3.236524	2.005331
H	−6.190189	0.376975	−1.169620
H	−5.032273	−0.256716	−2.364470
H	−5.074712	1.491415	−1.992874
H	−4.233872	2.309531	0.255873
H	−3.798545	−1.807925	−0.916905
H	−0.895791	−2.501848	0.734701
H	−2.079961	−2.920176	1.990967
H	−2.427728	−3.298274	0.280755
H	−3.991299	−0.558509	4.082208
H	−3.893102	−0.992902	6.796774
H	0.903935	0.212874	−1.402343
H	2.600056	0.434690	−3.438879
H	5.110117	0.151990	−2.634100
H	1.072732	−0.990878	7.111748
H	1.706992	−1.401617	9.655134
H	−0.460654	−1.685490	11.155155

4:

Total energy (B3LYP-D3(BJ)/def2-SV(P)): −1289.386741232

O	3.916438	−0.112992	−0.348410
C	2.557358	−0.061474	−0.252090
C	2.007398	0.159538	−1.494990
C	3.108294	0.248259	−2.404909
C	4.239201	0.075374	−1.652458
C	1.975061	−0.234522	1.049511
O	0.634541	−0.183869	1.135732

C	0.265420	−0.371639	2.459946
C	1.433852	−0.539909	3.193093
C	2.530163	−0.453257	2.300426
B	−1.226856	−0.359144	2.795663
C	−2.302265	−0.136843	1.663761
C	−2.894076	1.131390	1.471836
C	−3.846517	1.308302	0.460292
C	−4.240216	0.253277	−0.372662
C	−3.640882	−0.996749	−0.177484
C	−2.679256	−1.204095	0.820219
C	−2.490124	2.300281	2.343105
C	−5.298432	0.454920	−1.430898
C	−2.035894	−2.563046	0.981997
C	−1.720146	−0.575729	4.230747
C	−3.006415	−0.653263	4.744551
C	−2.910484	−0.877311	6.141608
C	−1.555041	−0.925715	6.417957
O	−0.840373	−0.748622	5.288495
C	−0.828783	−1.121142	7.642354
O	−1.559500	−1.302744	8.779033
C	−0.686970	−1.464391	9.804881
C	0.602509	−1.391197	9.351112
C	0.514944	−1.167263	7.940264
H	3.592341	−0.537557	2.521691
H	1.467609	−0.708302	4.267871
H	−2.770831	2.134137	3.399398
H	−1.394942	2.453647	2.326447
H	−2.967335	3.237407	2.009211
H	−6.316014	0.359658	−1.003863
H	−5.211385	−0.292880	−2.238357
H	−5.230816	1.459488	−1.885225
H	−4.292042	2.299344	0.315634
H	−3.927735	−1.834582	−0.823357
H	−0.959354	−2.522235	0.732430
H	−2.110330	−2.926284	2.023710
H	−2.506553	−3.315603	0.326520
H	−3.914073	−0.555729	4.149497
H	−3.713560	−0.991167	6.866926
H	0.944625	0.245860	−1.713199
H	3.063827	0.418887	−3.479884
H	5.301890	0.060065	−1.885207
H	1.331737	−1.053350	7.230162
H	1.507931	−1.485363	9.949348
H	−1.131212	−1.620052	10.785739

5.2 Catalytic Si/B Exchange Condensation: A Green B–C Coupling Method That Provides Access to Monodisperse (Het)arylborane 'Trimers'

NMR spectra

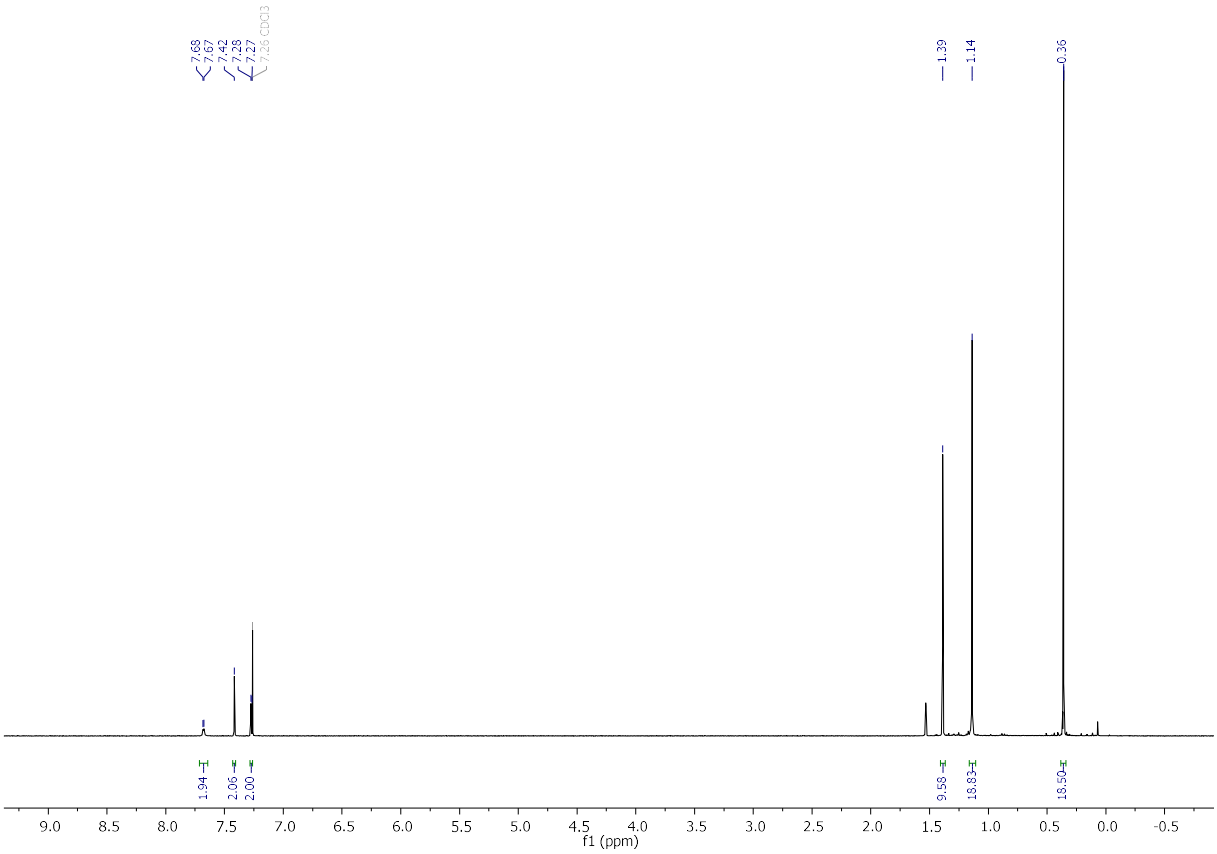

Figure S5.2.1. *^{1}H NMR spectrum of **4a** (in $CDCl_3$, 400 MHz).*

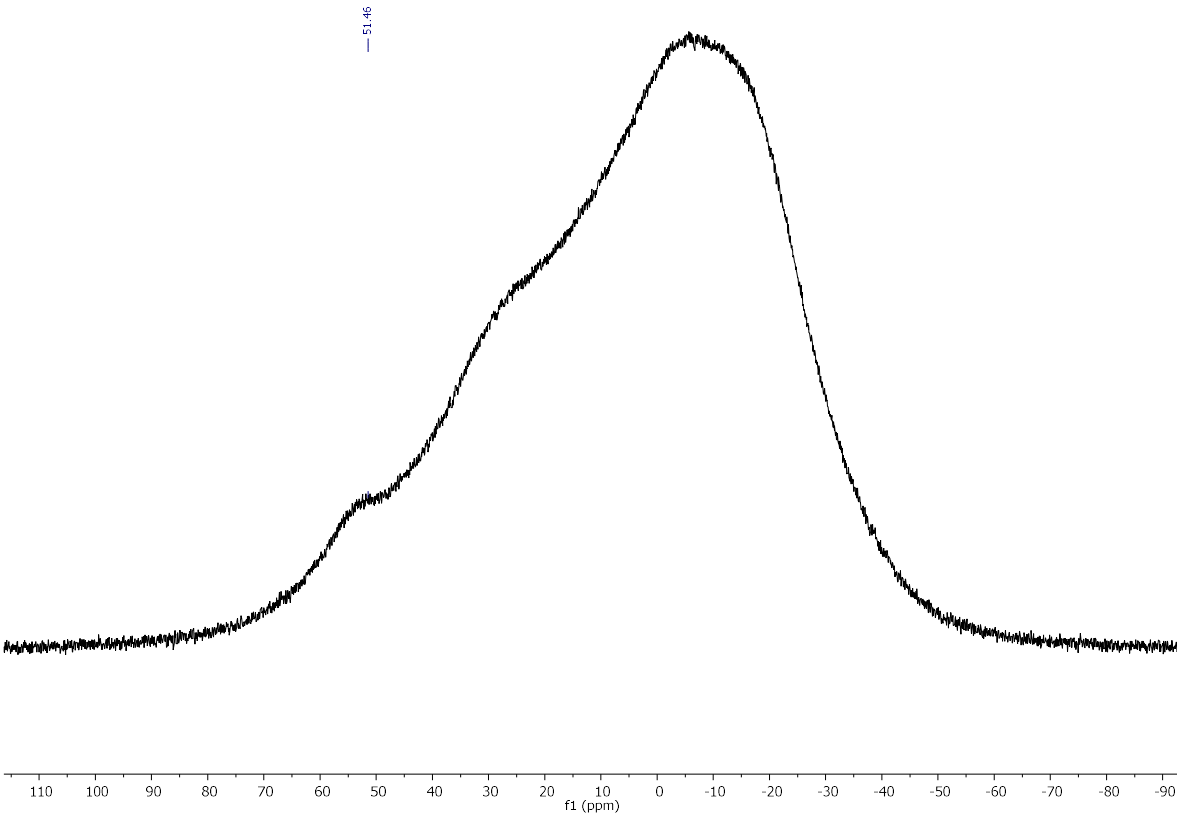

Figure S5.2.2. *$^{11}B\{^1H\}$ NMR spectrum of **4a** (in $CDCl_3$, 128 MHz).*

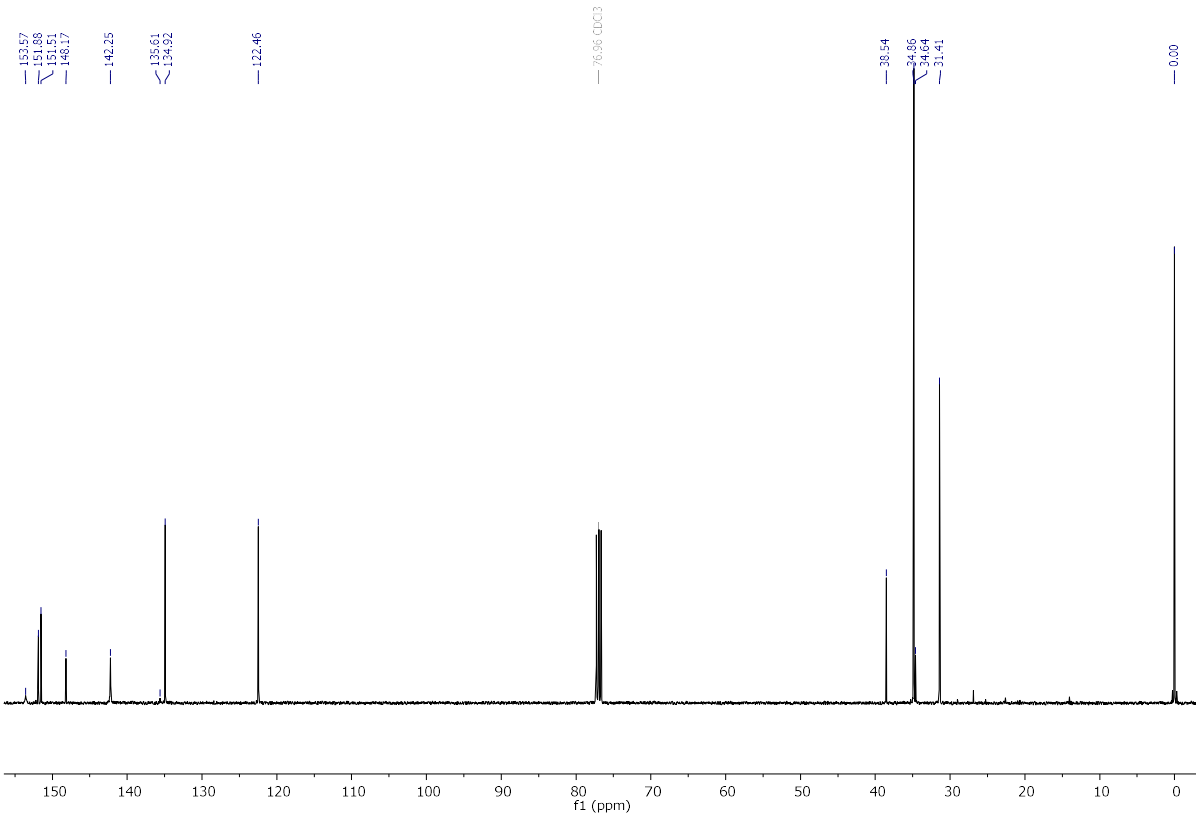

Figure S5.2.3. *^{13}C NMR spectrum of **4a** (in $CDCl_3$, 101 MHz).*

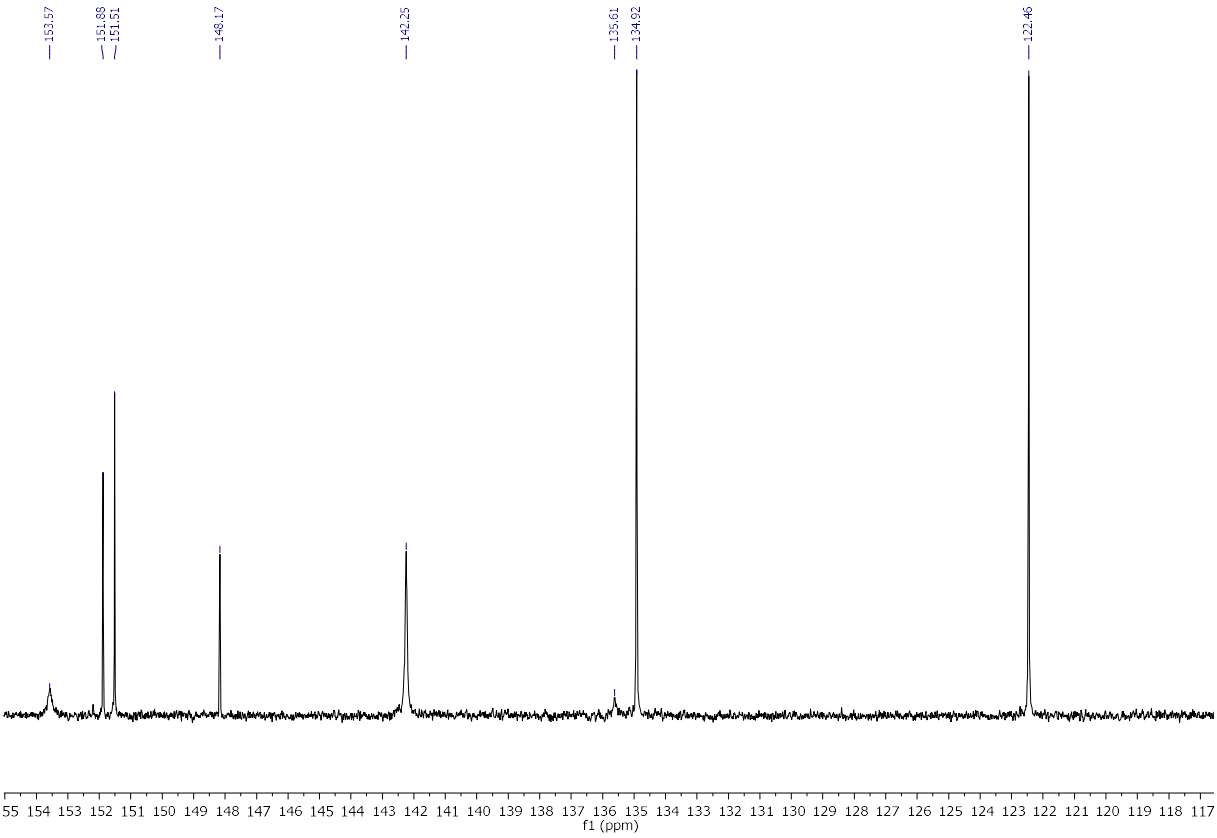

Figure S5.2.4. *Detail (aromatic region) of the ^{13}C NMR spectrum of* ***4a*** *(in $CDCl_3$, 101 MHz).*

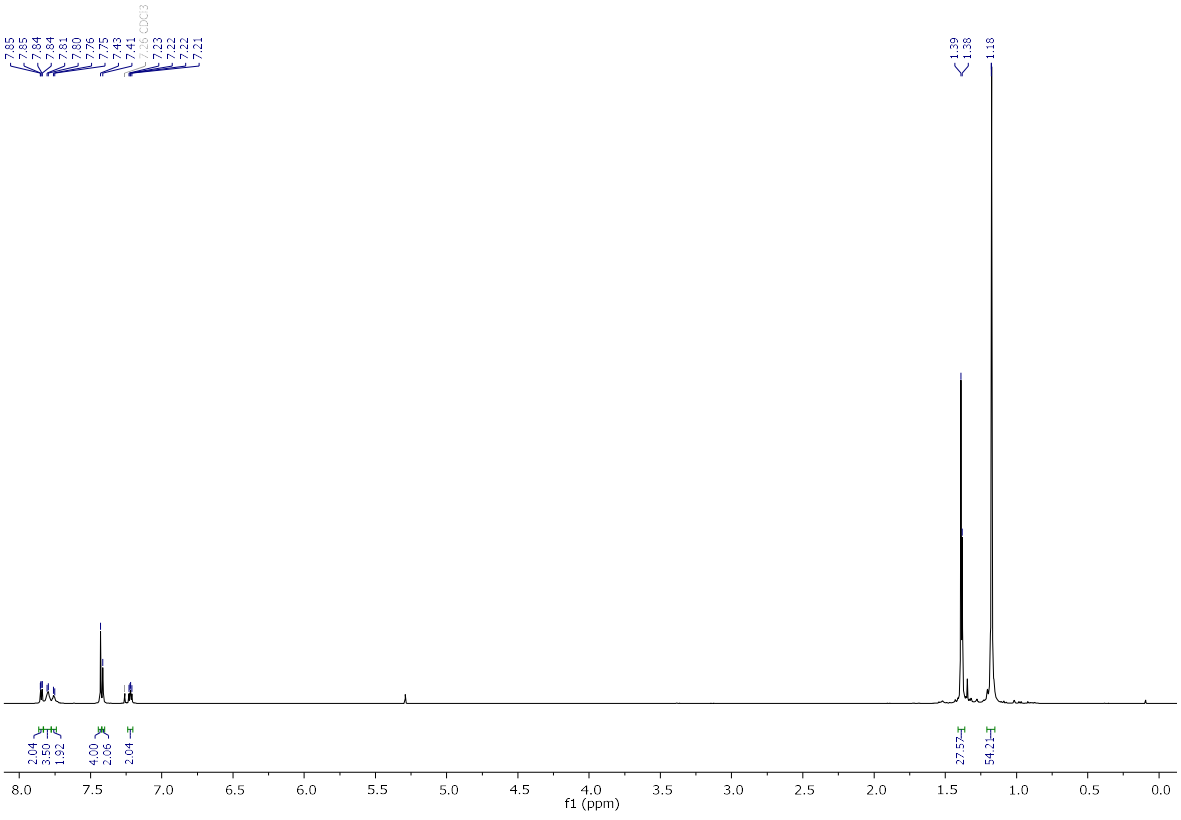

Figure S5.2.5. *^{1}H NMR spectrum of* ***5aa*** *(in $CDCl_3$, 400 MHz).*

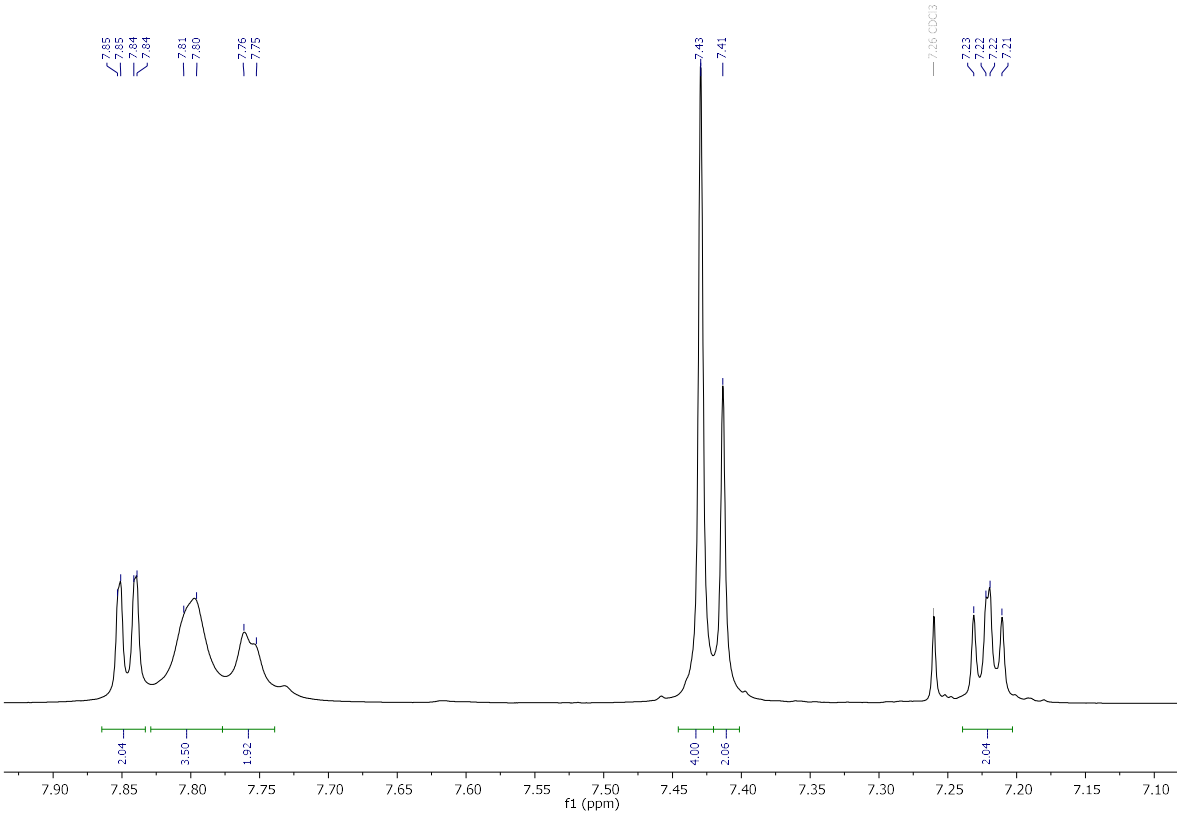

Figure S5.2.6. *Detail (aromatic region) of the ^{1}H NMR spectrum of* ***5aa*** *(in $CDCl_3$, 400 MHz).*

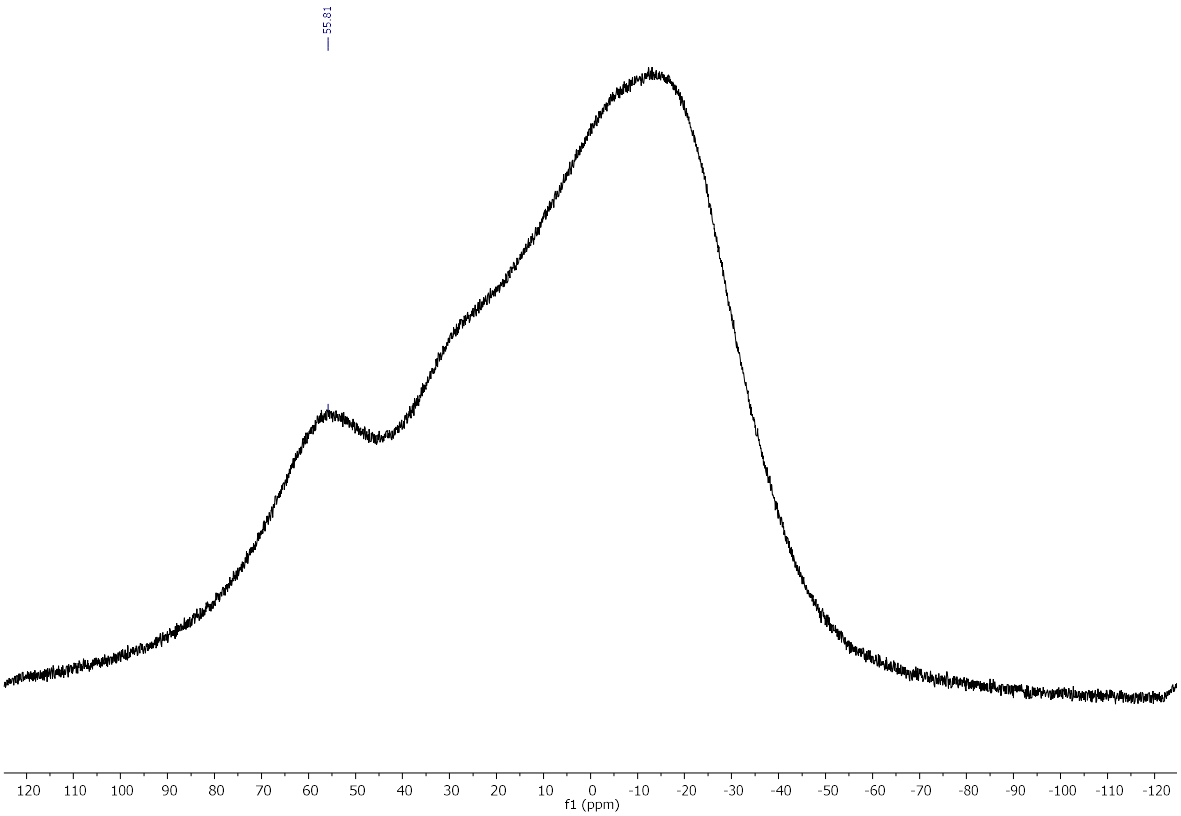

Figure S5.2.7. *$^{11}B\{^{1}H\}$ NMR spectrum of* ***5aa*** *(in $CDCl_3$, 128 MHz).*

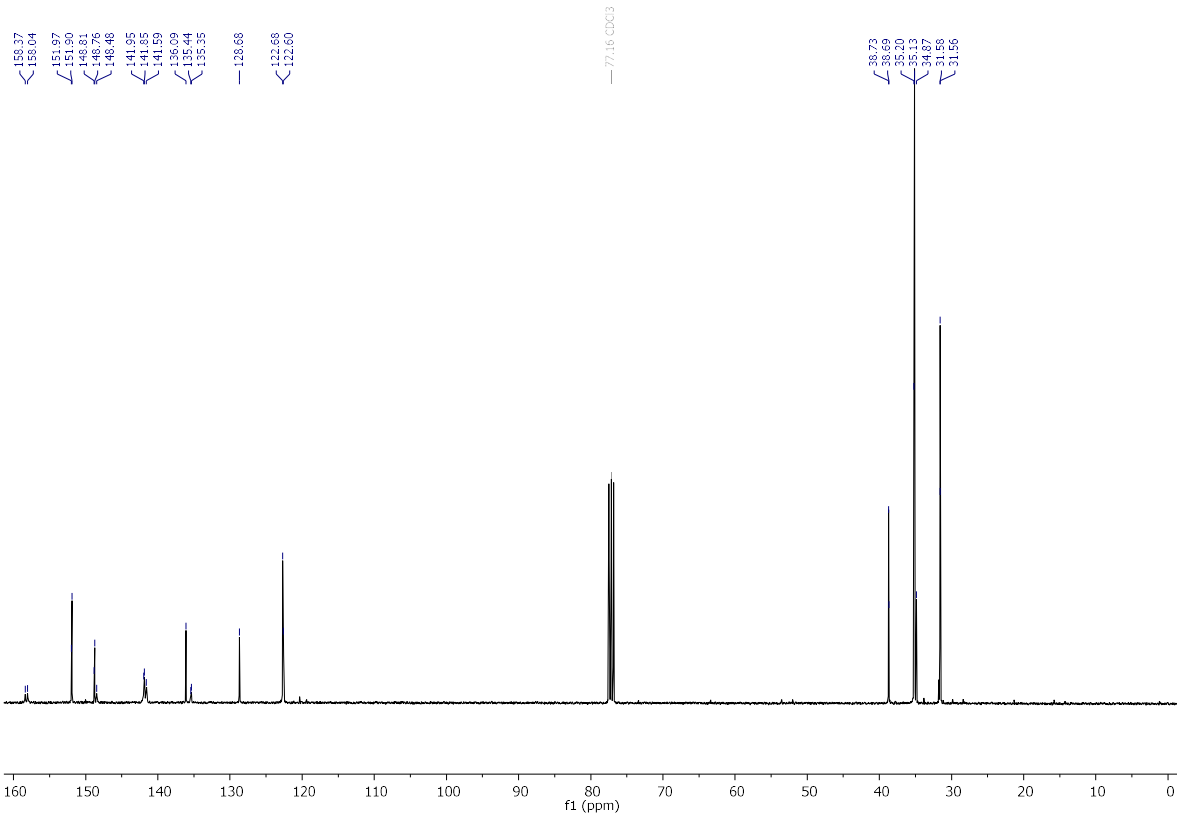

Figure S5.2.8. *^{13}C NMR spectrum of **5aa** (in $CDCl_3$, 101 MHz).*

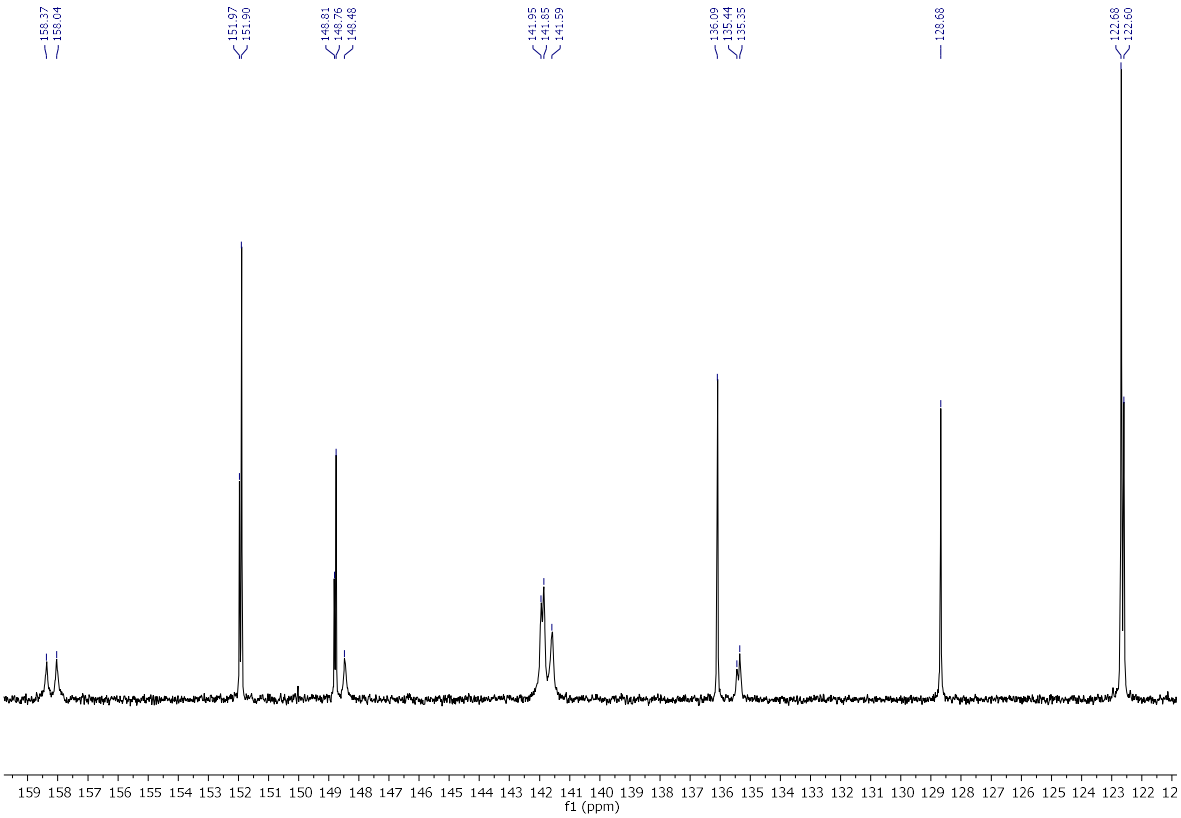

Figure S5.2.9. *Detail (aromatic region) of the ^{13}C NMR spectrum of **5aa** (in $CDCl_3$, 101 MHz).*

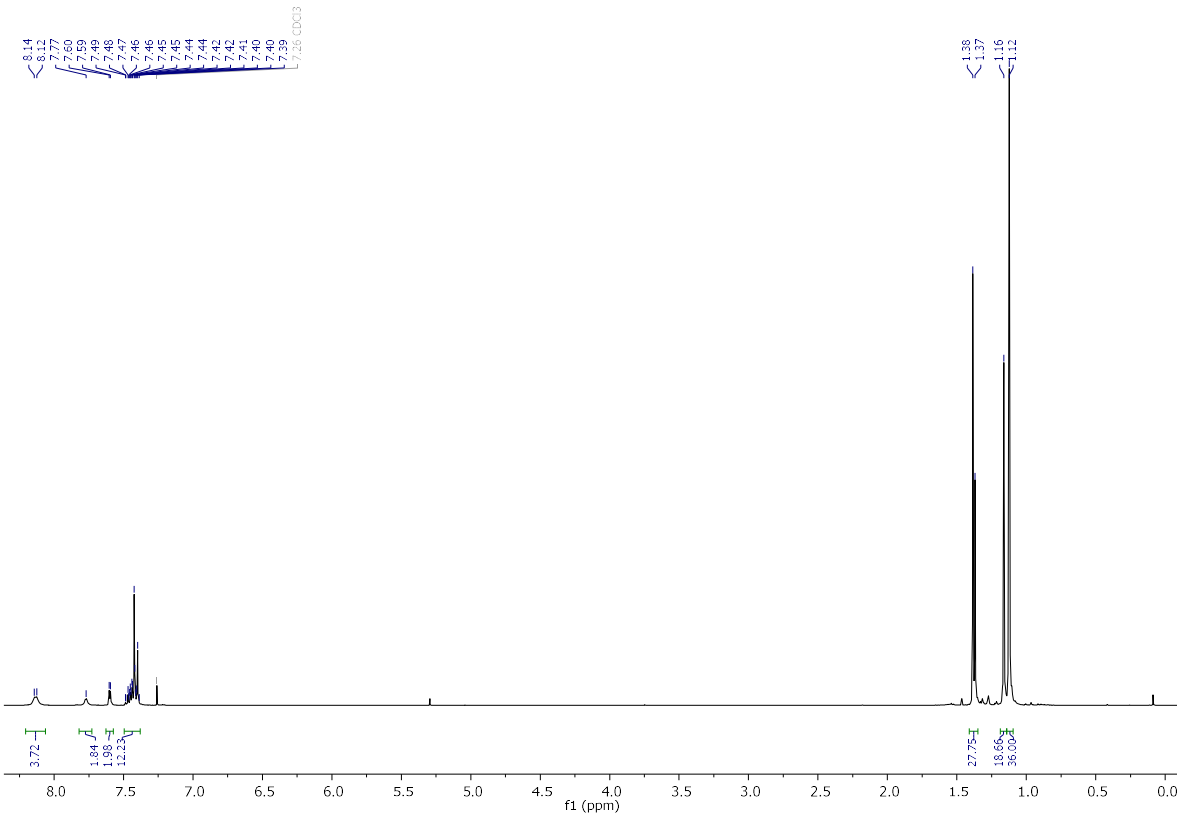

Figure S5.2.10. *^{1}H NMR spectrum of* ***5ac*** *(in $CDCl_3$, 400 MHz).*

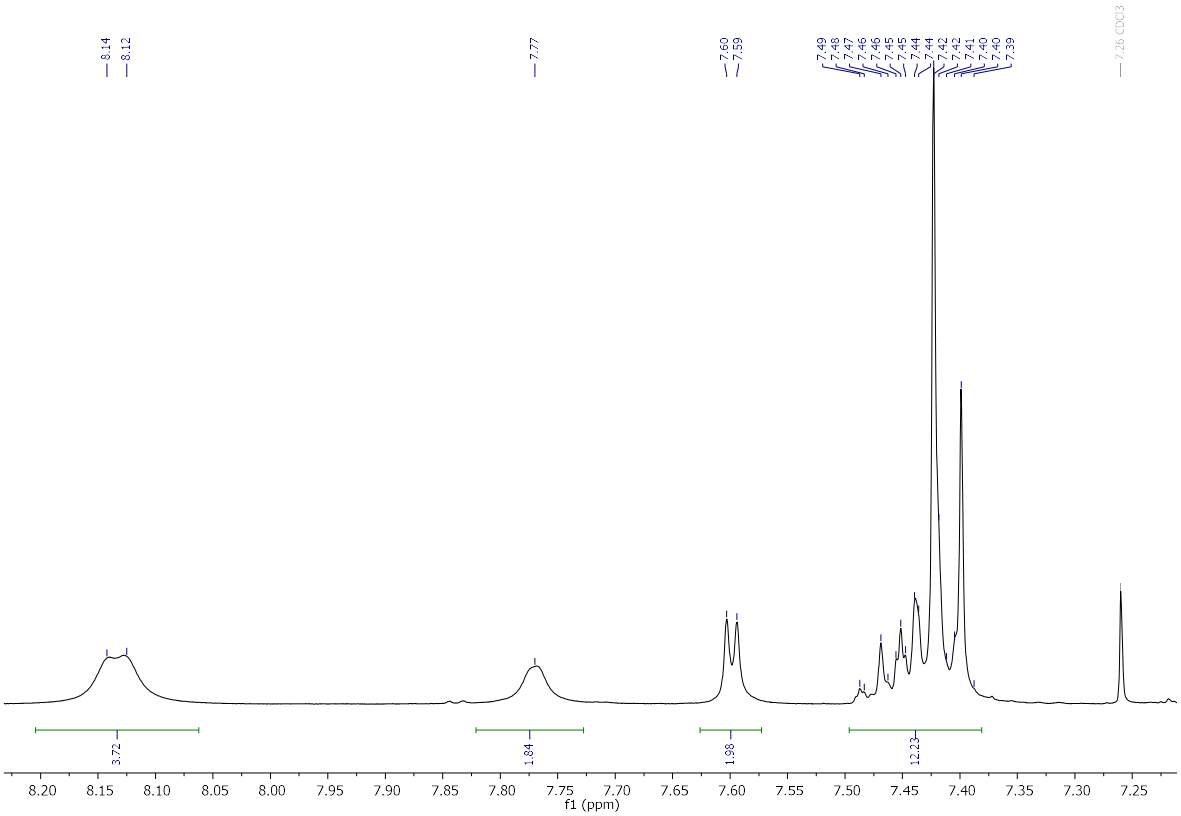

Figure S5.2.11. *Detail (aromatic region) of the ^{1}H NMR spectrum of* ***5ac*** *(in $CDCl_3$, 400 MHz).*

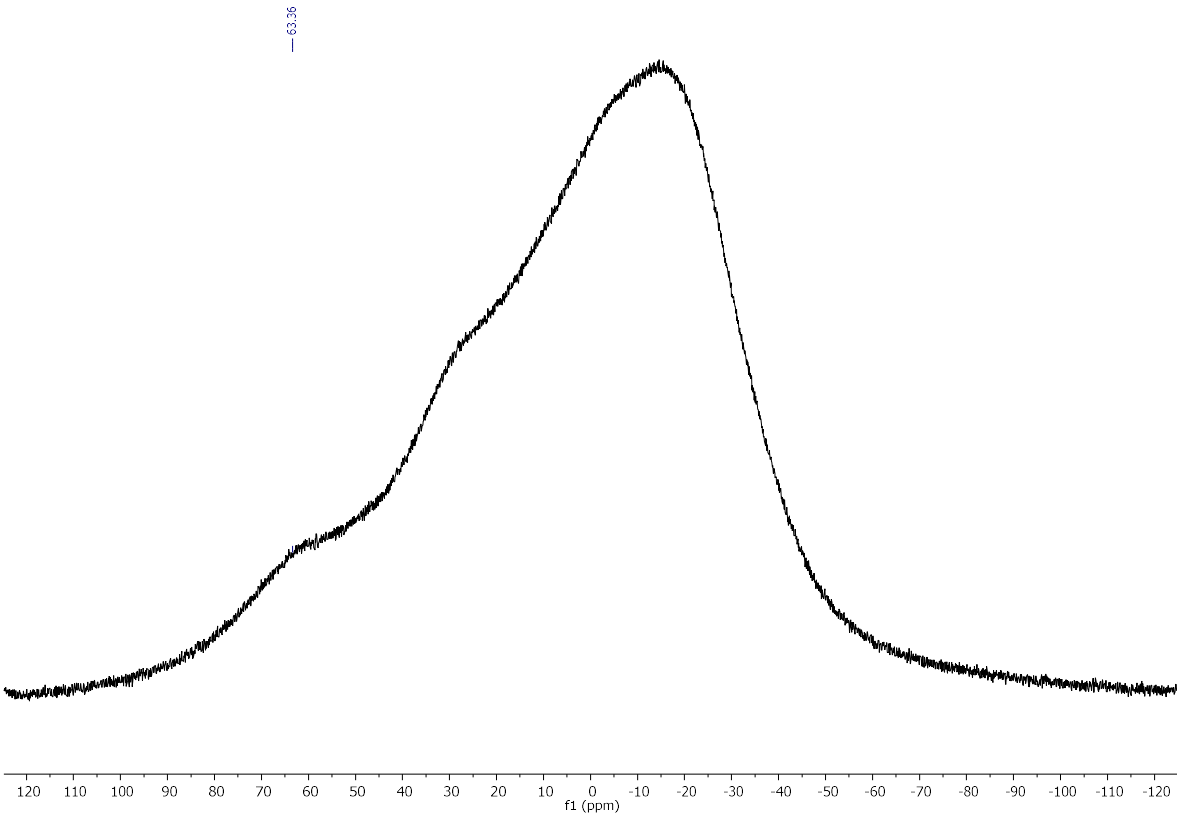

Figure S5.2.12. *$^{11}B\{^1H\}$ NMR spectrum of* ***5ac*** *(in $CDCl_3$, 128 MHz).*

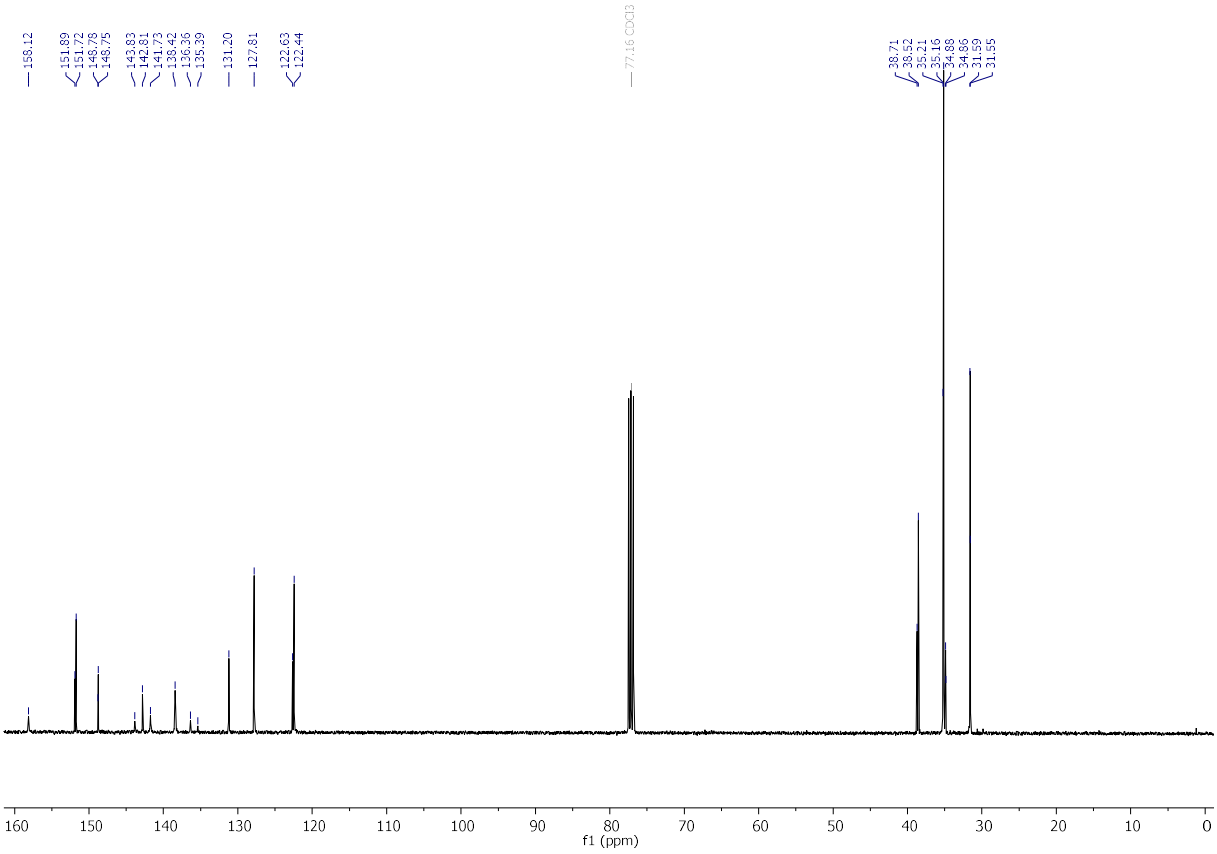

Figure S5.2.13. *^{13}C NMR spectrum of* ***5ac*** *(in $CDCl_3$, 101 MHz).*

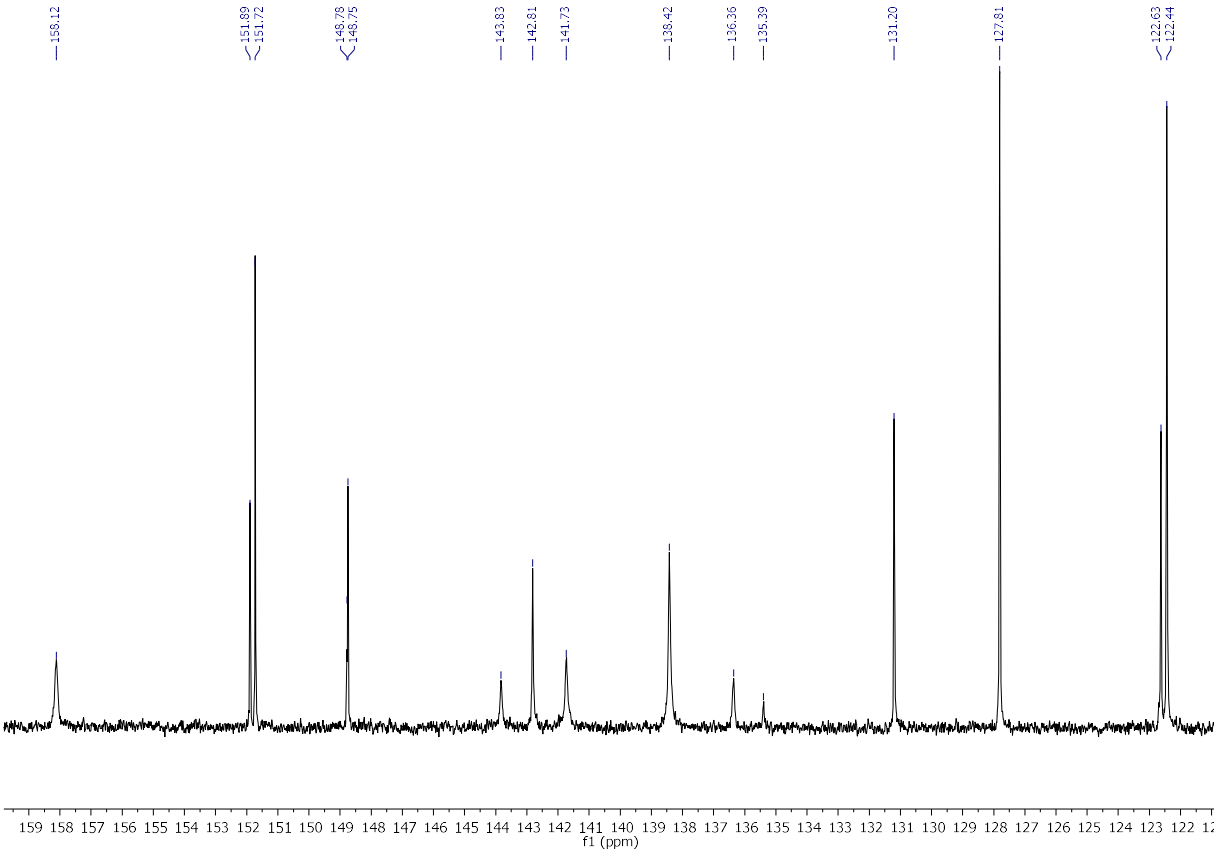

Figure S5.2.14. *Detail (aromatic region) of the ^{13}C NMR spectrum of* ***5ac*** *(in $CDCl_3$, 101 MHz).*

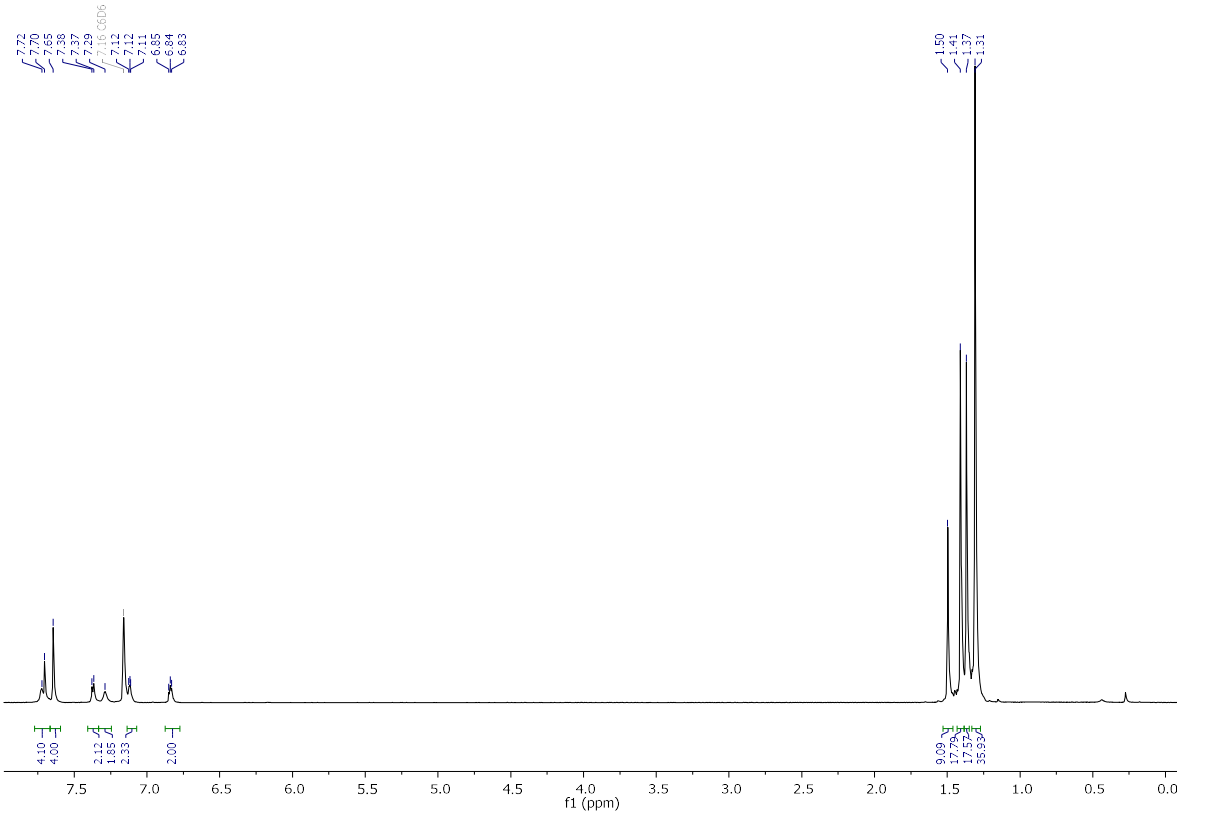

Figure S5.2.15. *^1H NMR spectrum of* ***5ba*** *(in C_6D_6, at 70°C, 400 MHz).*

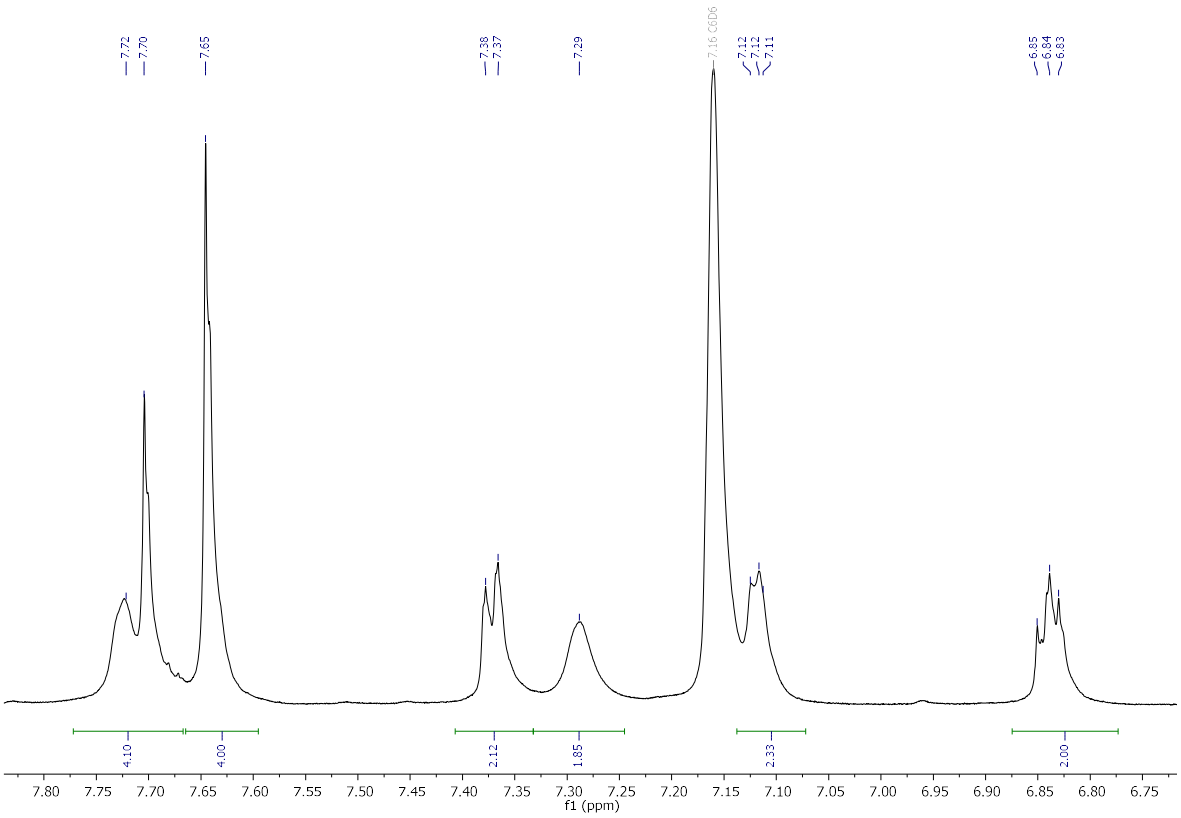

Figure S5.2.16. *Detail (aromatic region) of the ^{1}H NMR spectrum of* ***5ba*** *(in C_6D_6, at 70°C, 400 MHz).*

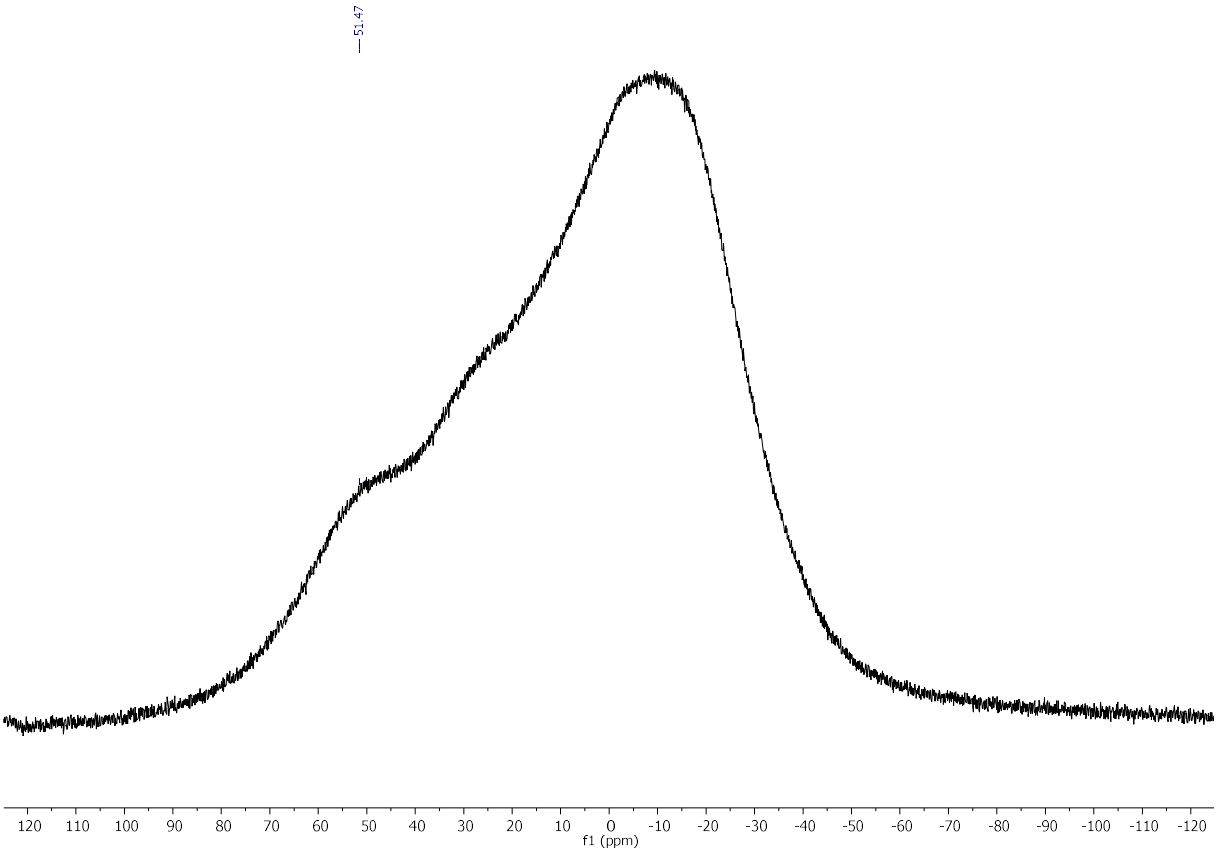

Figure S5.2.17. *$^{11}B\{^{1}H\}$ NMR spectrum of* ***5ba*** *(in C_6D_6, at 70°C, 128 MHz).*

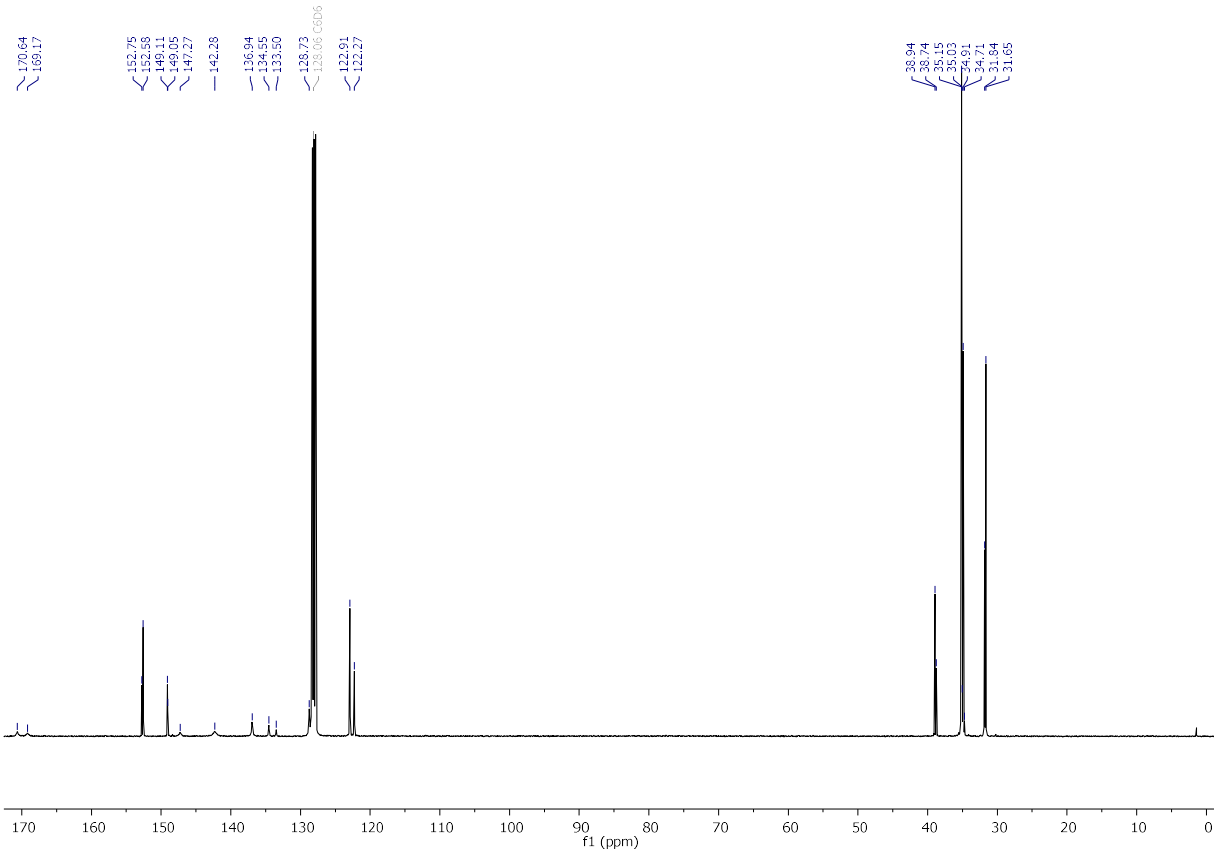

Figure S5.2.18. *^{13}C NMR spectrum of **5ba** (in C_6D_6, at 70°C, 101 MHz).*

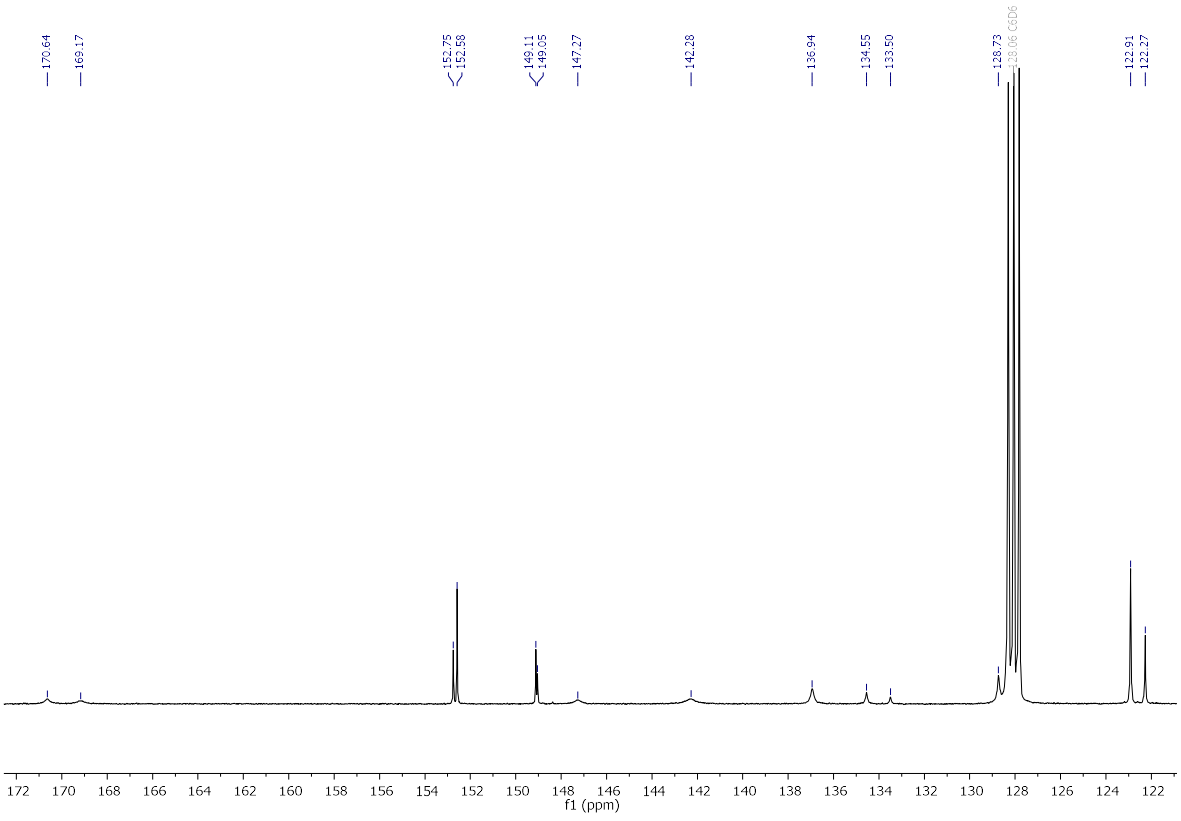

Figure S5.2.19. *Detail (aromatic region) of the ^{13}C NMR spectrum of **5ba** (in C_6D_6, at 70°C, 101 MHz).*

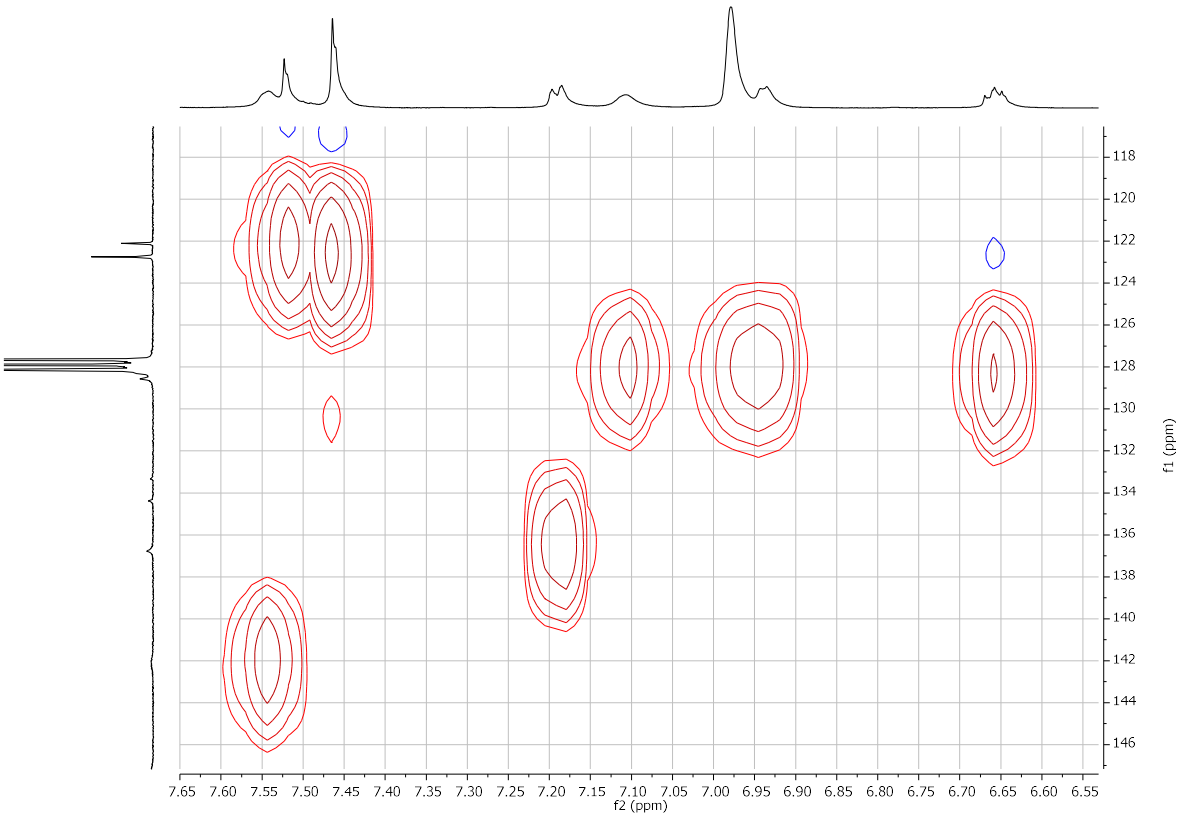

Figure S5.2.20. *Detail of HSQC spectrum of* ***5ba*** *(in C_6D_6, at 70°C, 101 MHz).*

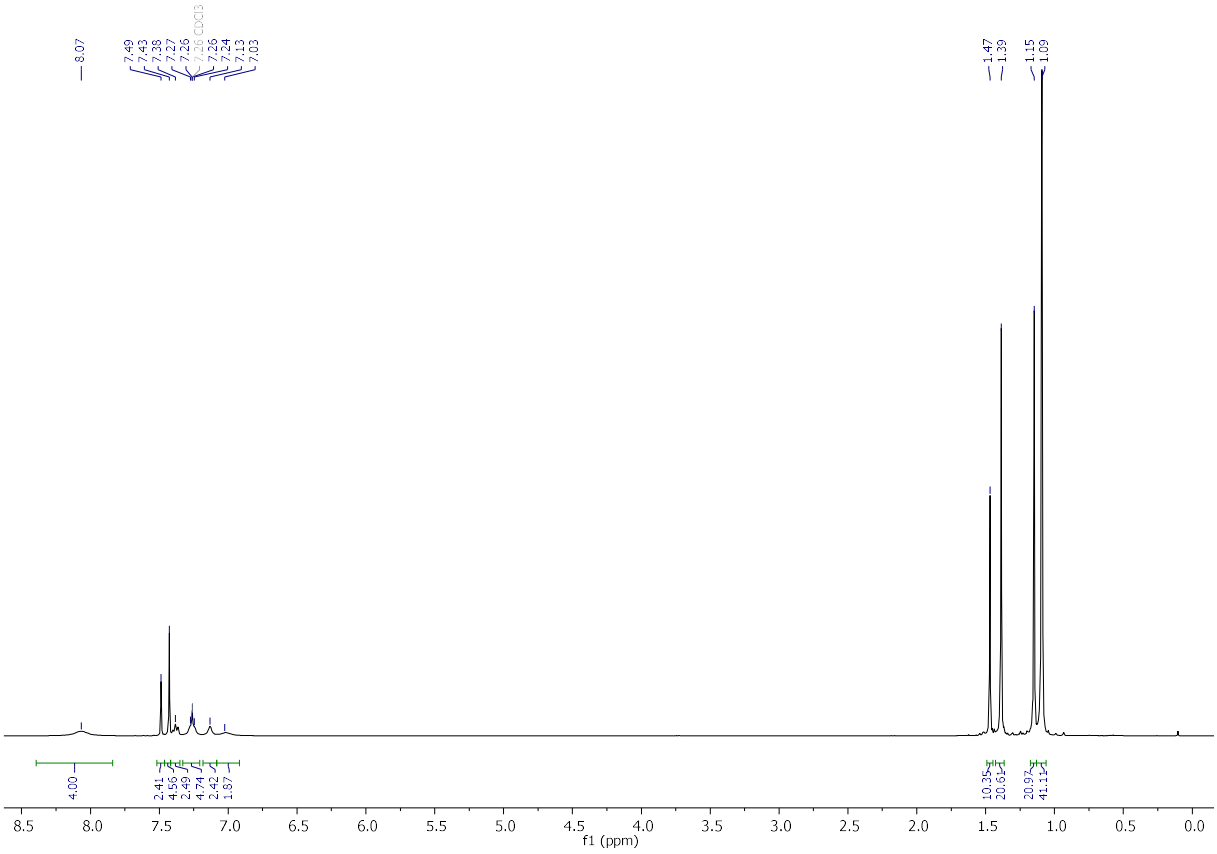

Figure S5.2.21. *^{1}H NMR spectrum of* ***5bc*** *(in $CDCl_3$, 400 MHz).*

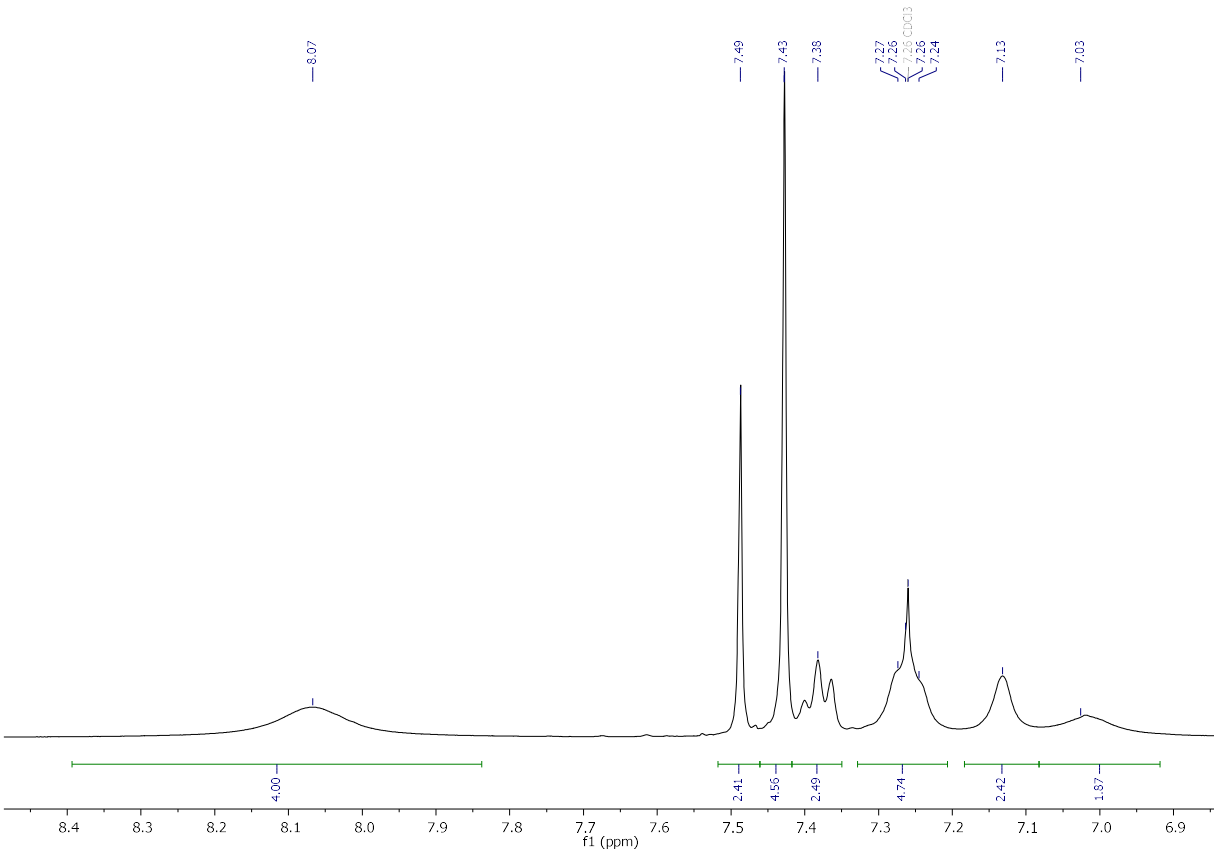

Figure S5.2.22. *Detail (aromatic region) of the ^{1}H NMR spectrum of* ***5bc*** *(in $CDCl_3$, 400 MHz).*

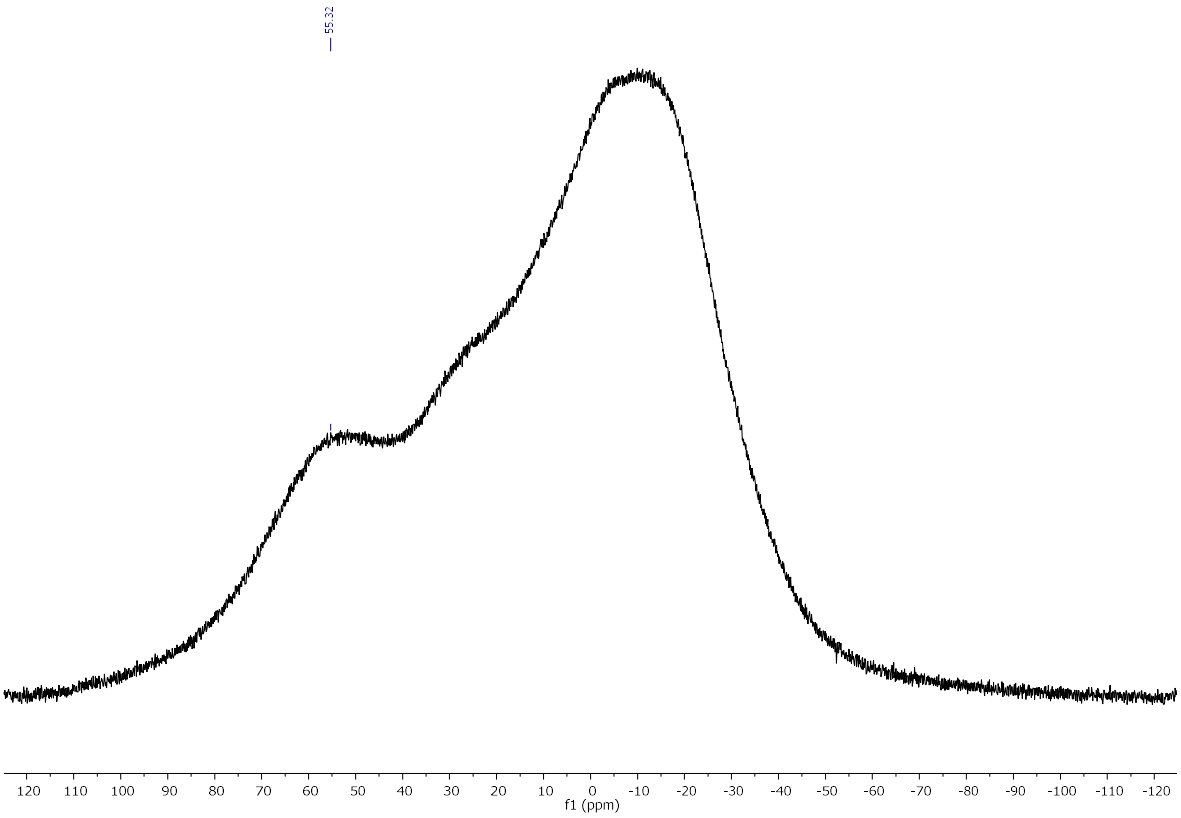

Figure S5.2.23. *$^{11}B\{^{1}H\}$ NMR spectrum of* ***5bc*** *(in $CDCl_3$, 128 MHz).*

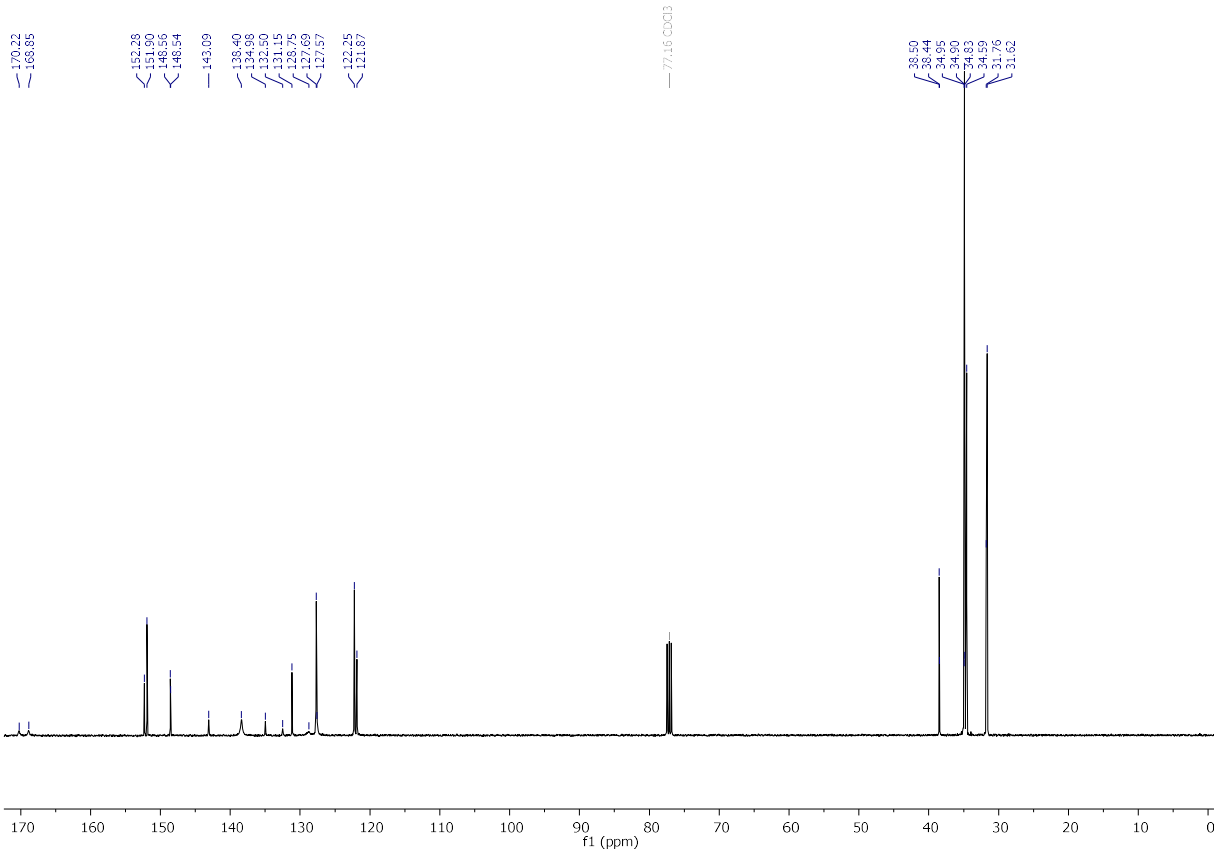

Figure S5.2.24. *^{13}C NMR spectrum of* ***5bc*** *(in $CDCl_3$, 101 MHz).*

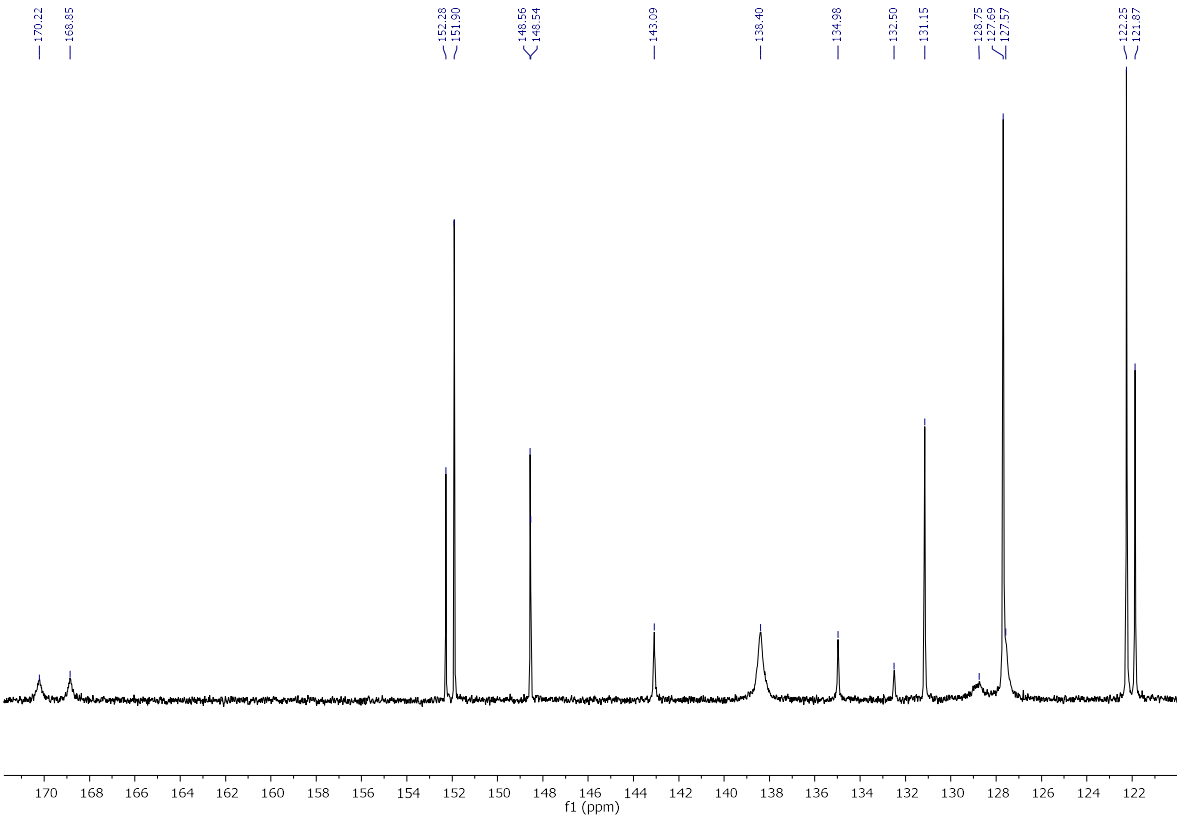

Figure S5.2.25. *Detail (aromatic region) of the ^{13}C NMR spectrum of* ***5bc*** *(in $CDCl_3$, 101 MHz).*

UV–vis spectra

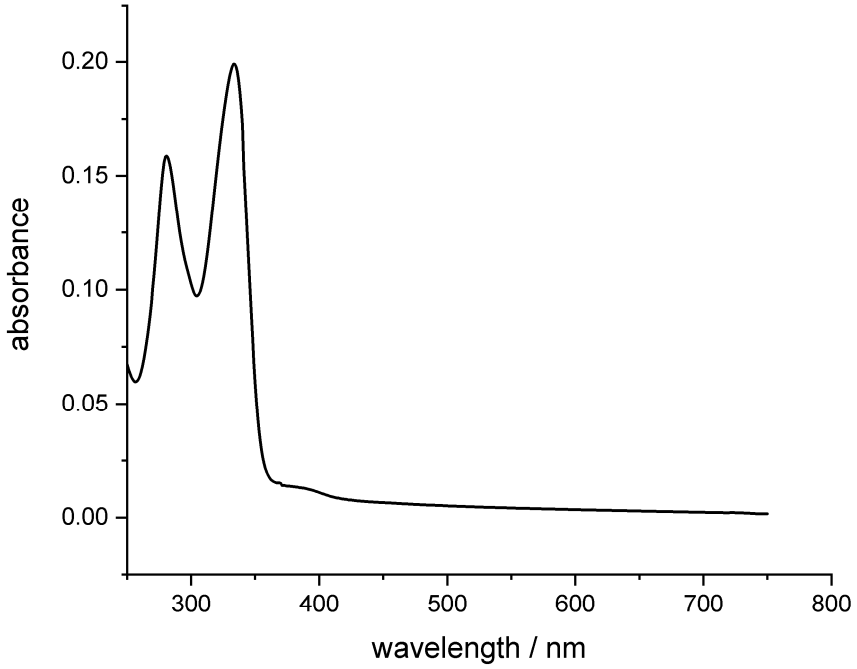

Figure S5.2.26. *UV–vis spectrum of* ***4a*** *(in THF).*

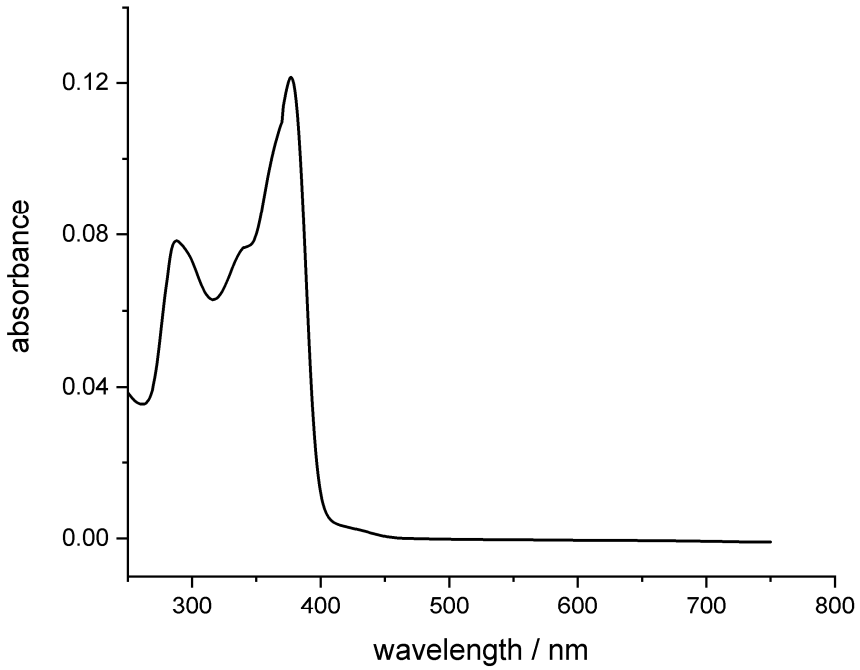

Figure S5.2.27. *UV–vis spectrum of* ***5aa*** *(in THF).*

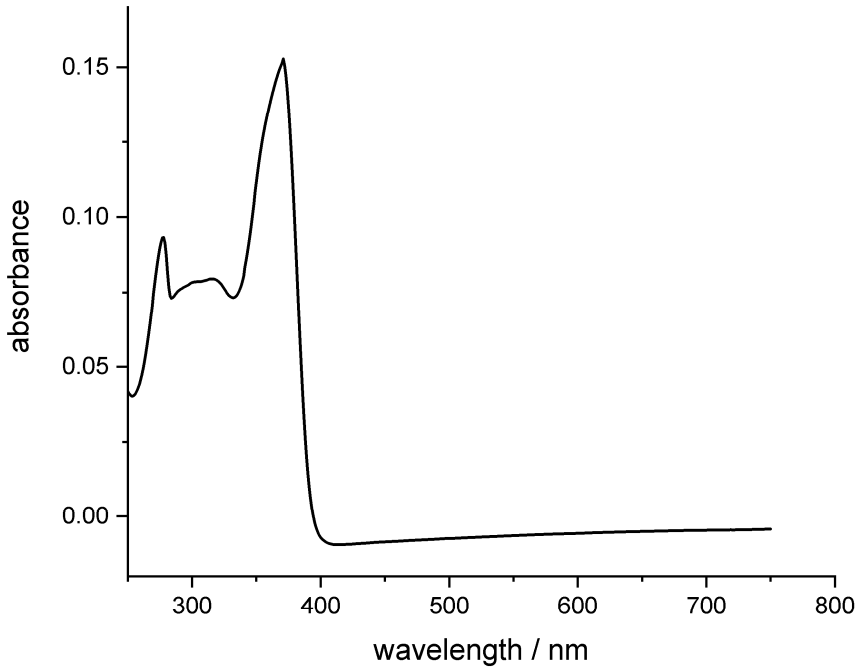

Figure S5.2.28. *UV–vis spectrum of* ***5ac*** *(in THF).*

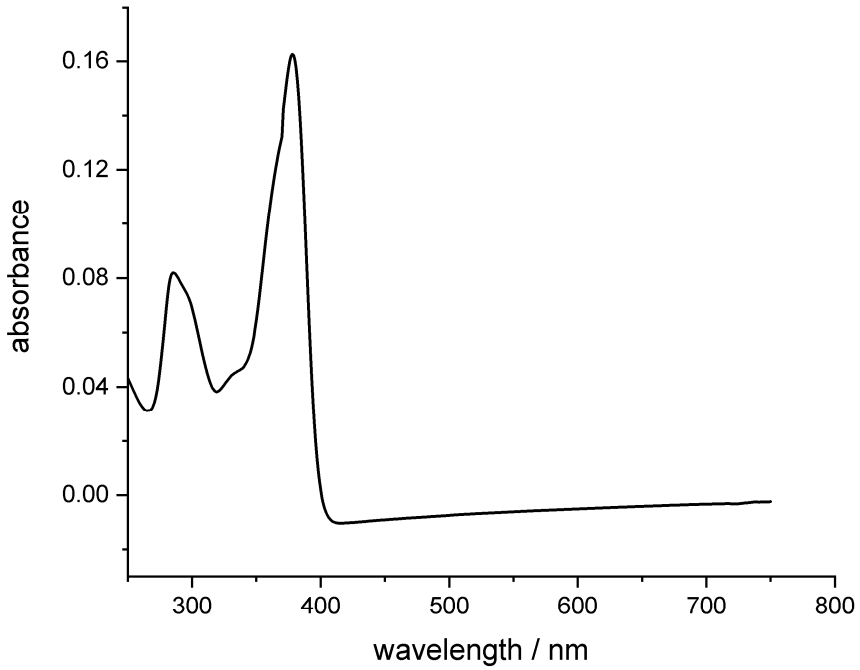

Figure S5.2.29. *UV–vis spectrum of* ***5ba*** *(in THF).*

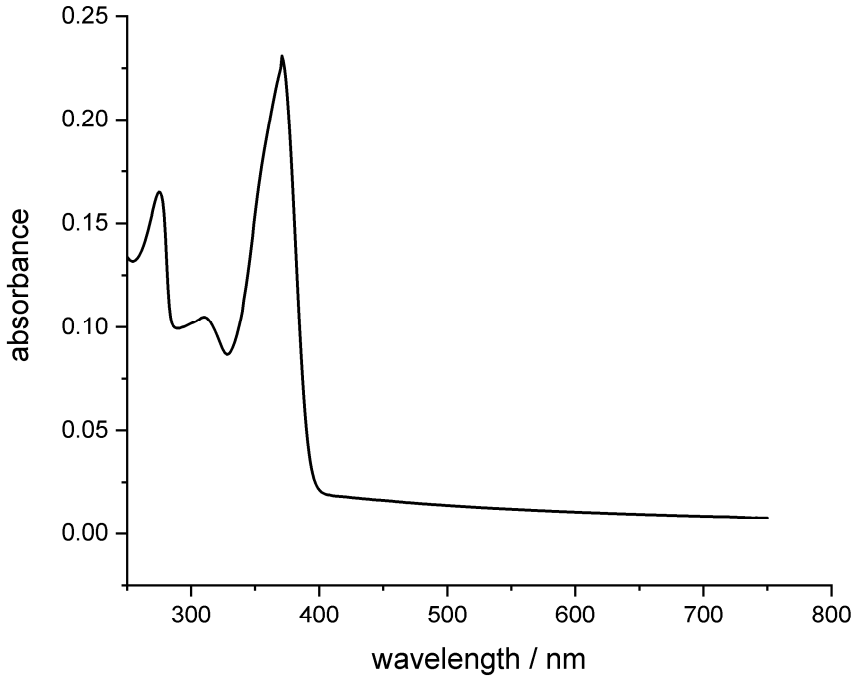

Figure S5.2.30. *UV–vis spectrum of* ***5bc*** *(in THF).*

Fluorescence spectra

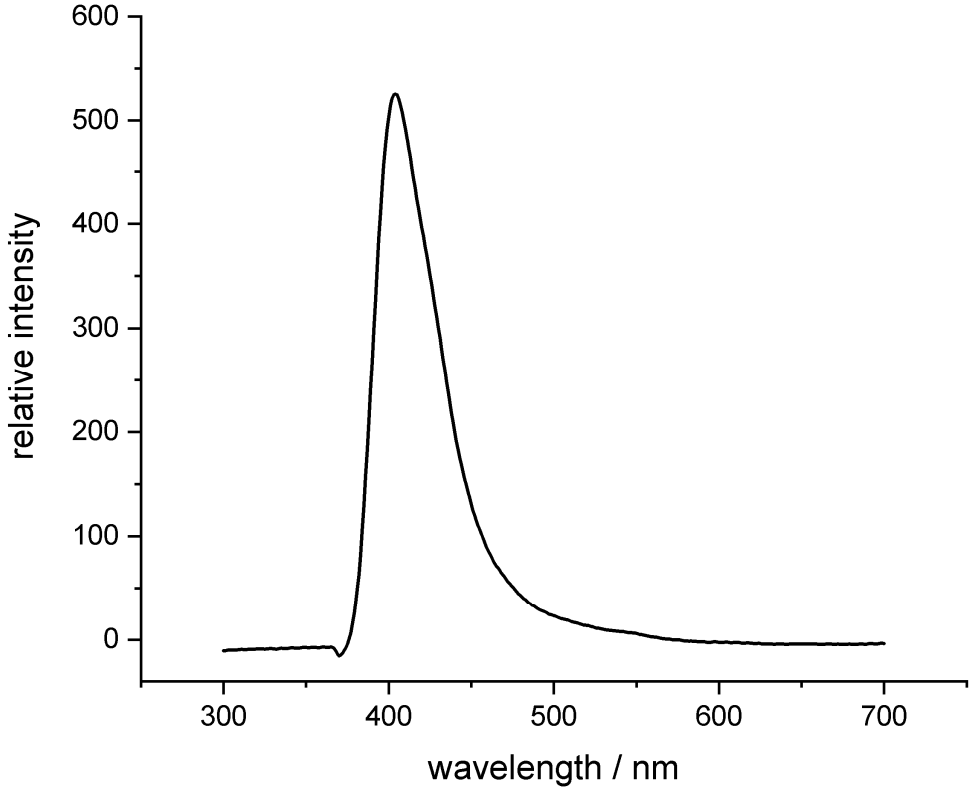

Figure S5.2.31. *Fluorescence spectrum of* ***5ba*** *(in THF, λ_{ex} = 378 nm).*

Mass spectra

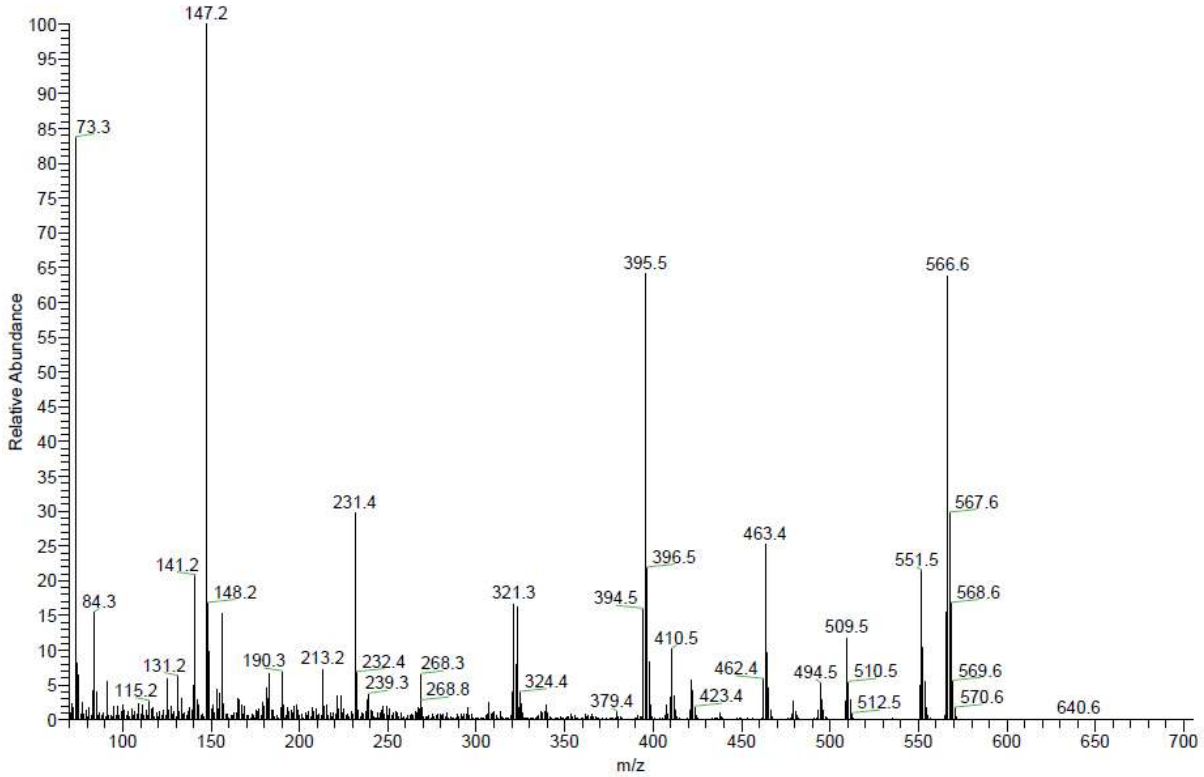

Figure S5.2.32. *EI mass spectrum of* ***4a****.*

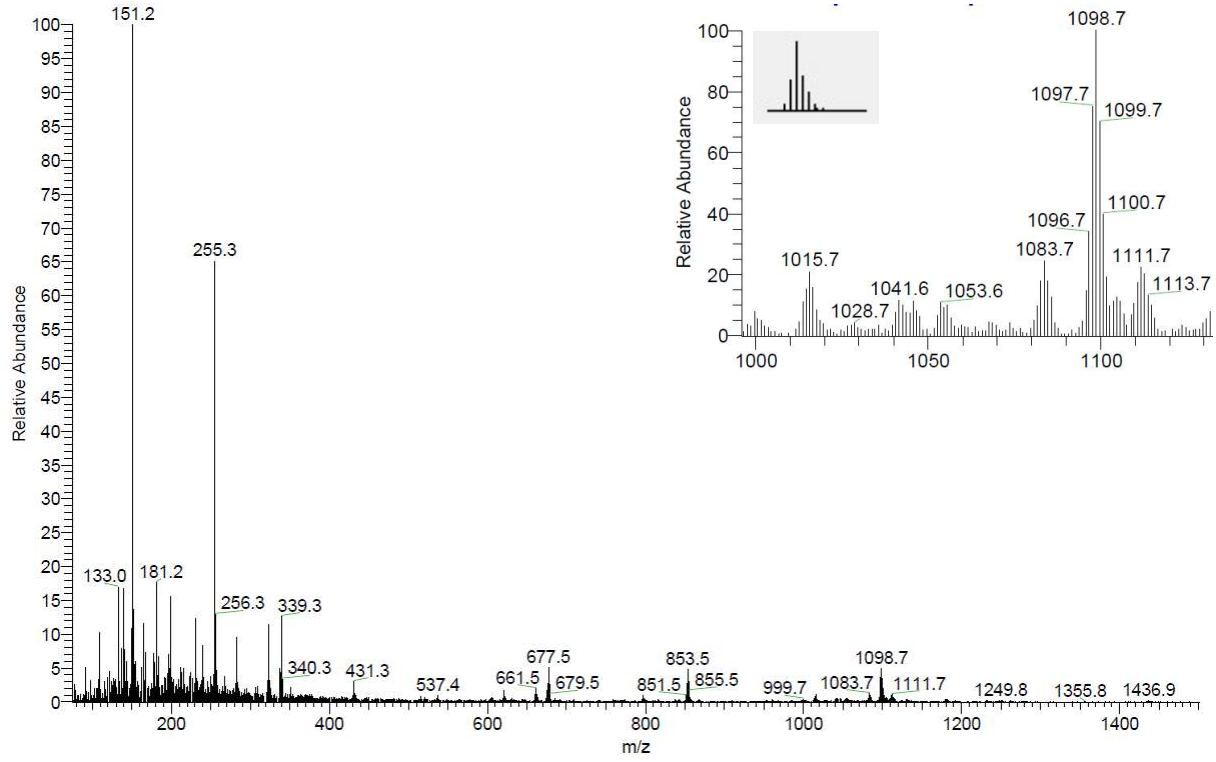

Figure S5.2.33. *SIMS mass spectrum of* ***5aa****.*

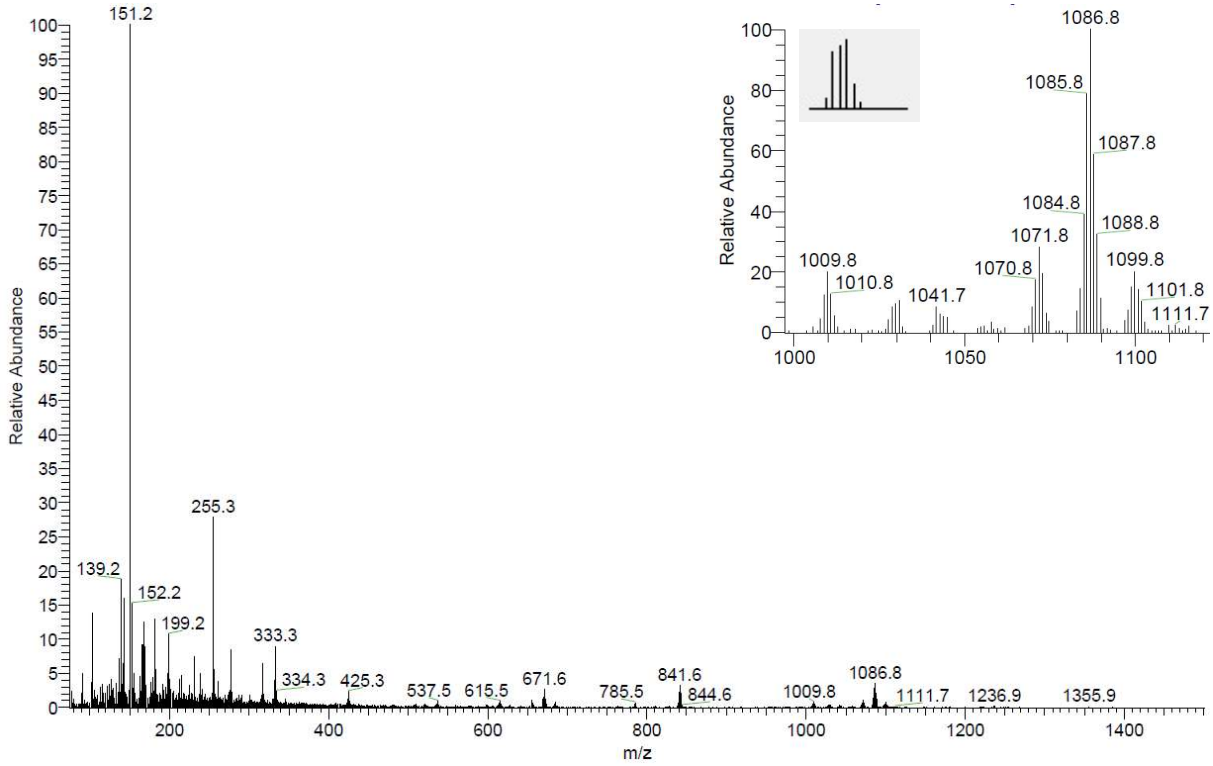

Figure S5.2.34. *SIMS mass spectrum of* ***5ac****.*

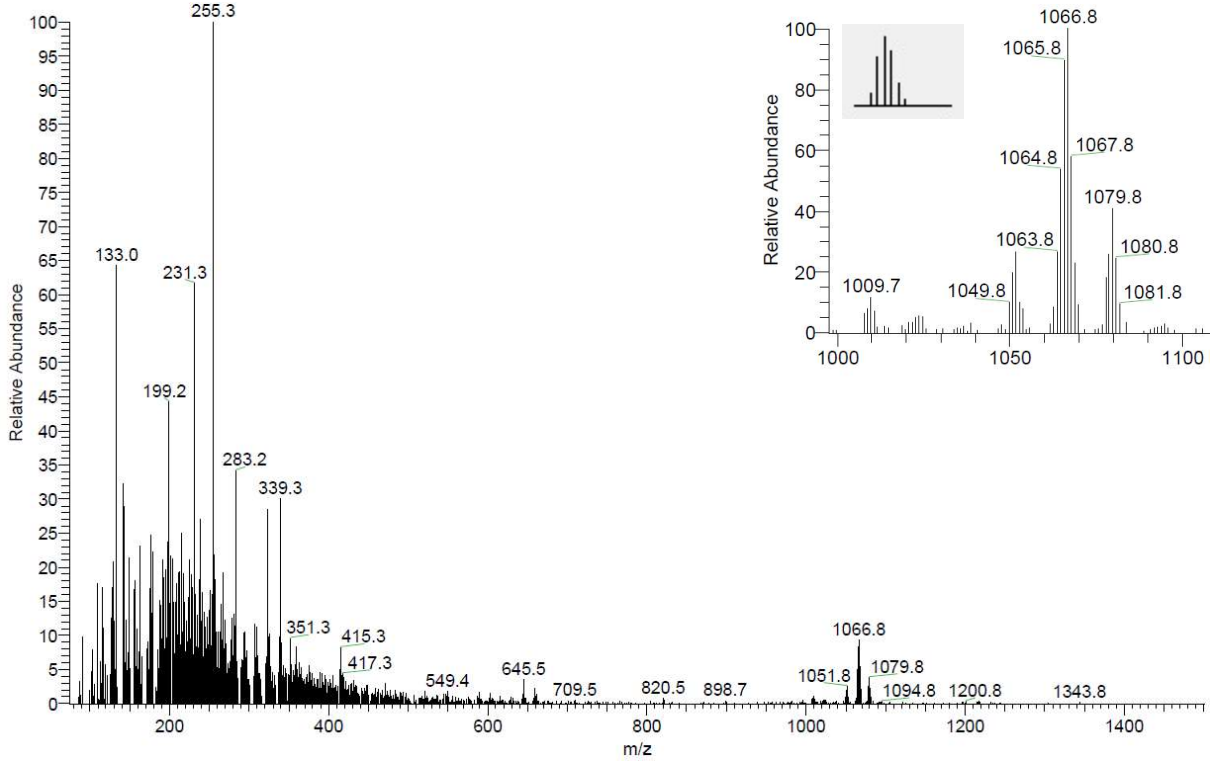

Figure S5.2.35. *SIMS mass spectrum of* ***5ba****.*

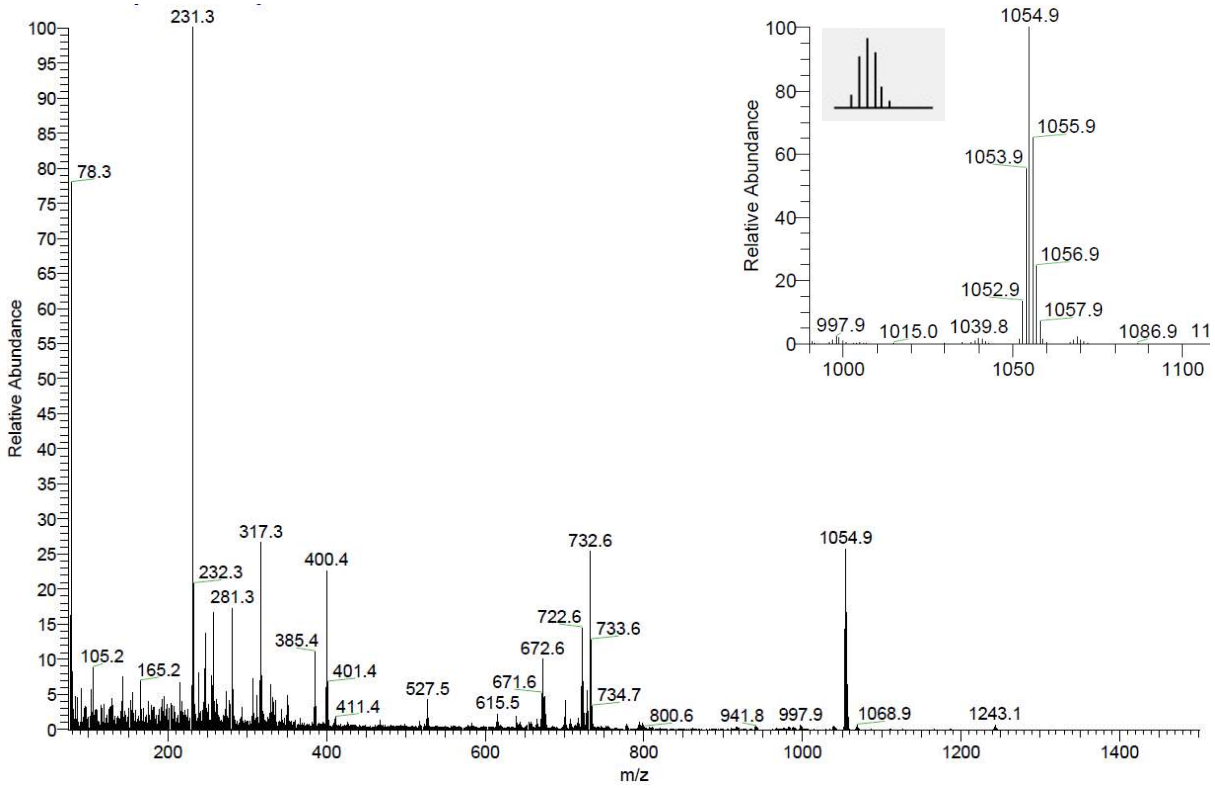

Figure S5.2.36. *EI mass spectrum of* ***5bc****.*

Cyclic Voltammetry

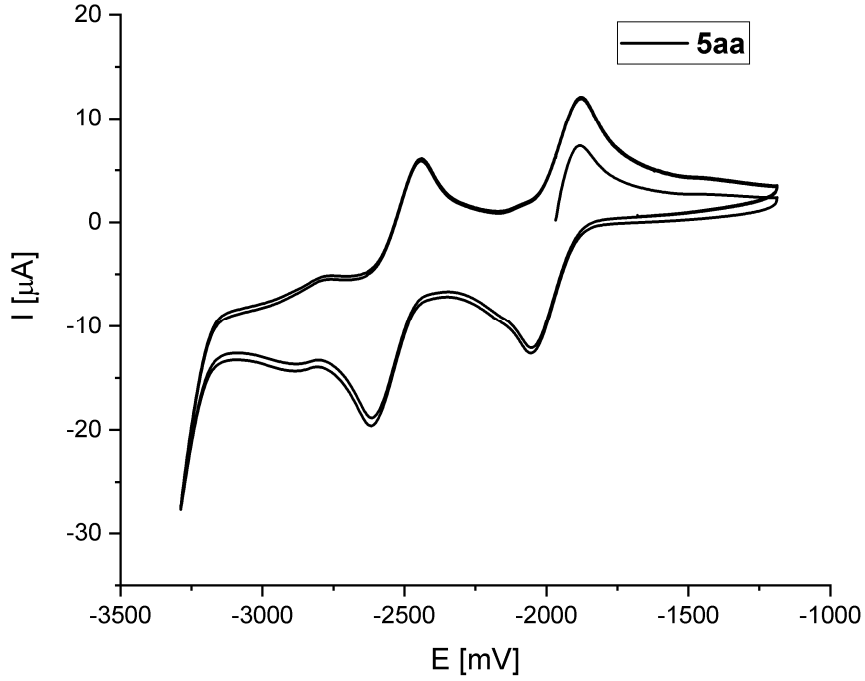

Figure S5.2.37. *Cyclic voltammogram of* ***5aa*** *in THF ($1 \cdot 10^{-3}$ M), recorded vs the ferrocene/ferrocenium couple as internal standard (scan rate: 100 mV s^{-1}).*

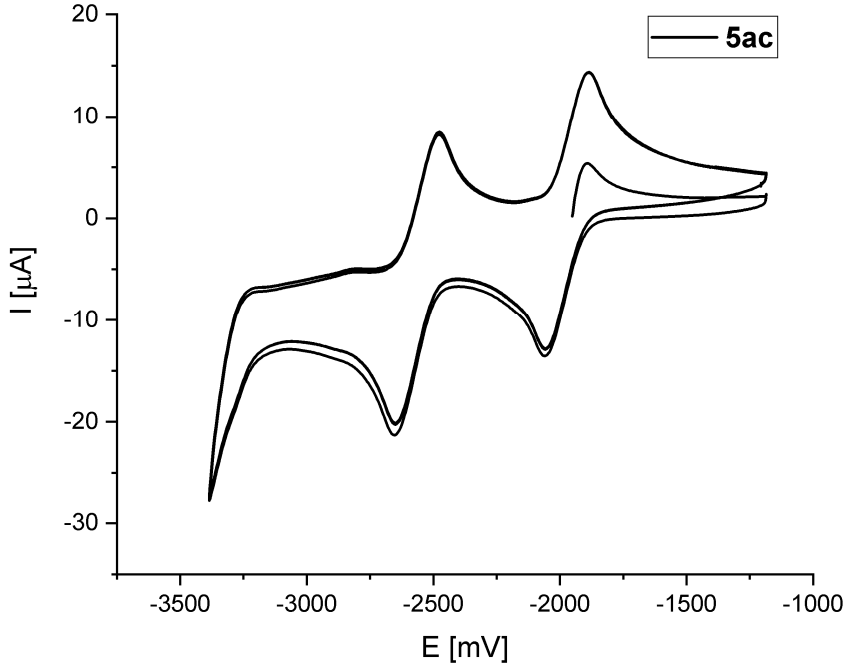

Figure S5.2.38. *Cyclic voltammogram of* ***5ac*** *in THF ($1 \cdot 10^{-3}$ M), recorded vs the ferrocene/ferrocenium couple as internal standard (scan rate: 100 mV s^{-1}).*

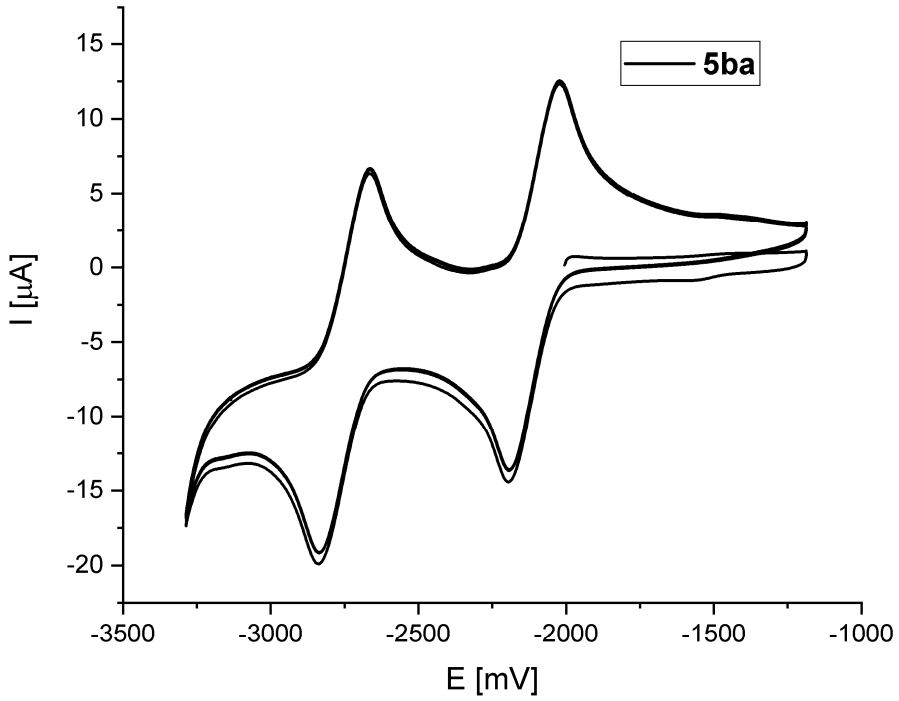

Figure S5.2.39. *Cyclic voltammogram of* ***5ba*** *in THF ($1 \cdot 10^{-3}$ M), recorded vs the ferrocene/ferrocenium couple as internal standard (scan rate: 100 mV s^{-1}).*

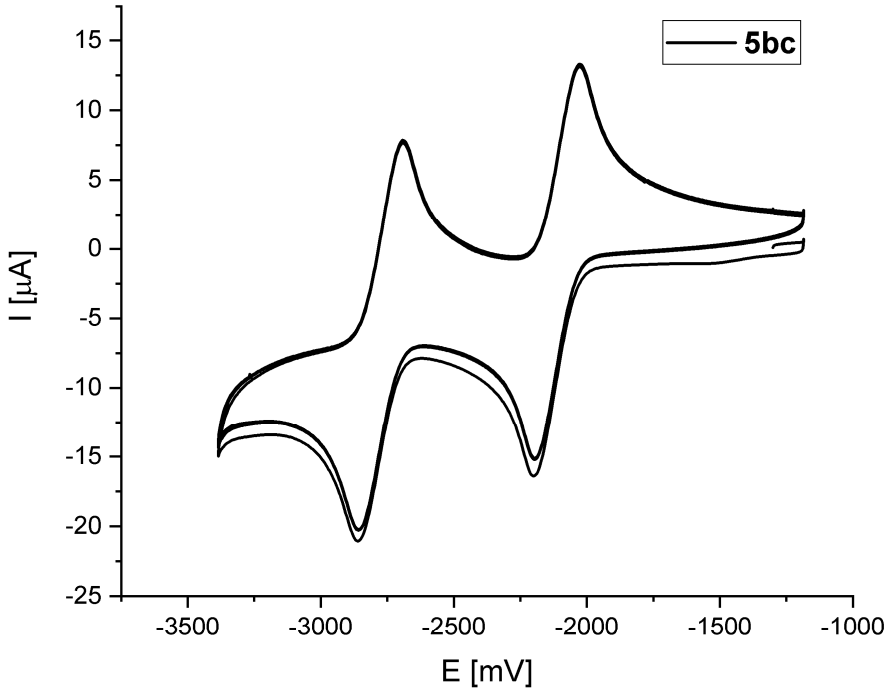

Figure S5.2.40. *Cyclic voltammogram of* ***5bc*** *in THF ($1 \cdot 10^{-3}$ M), recorded vs the ferrocene/ferrocenium couple as internal standard (scan rate: 100 mV s^{-1}).*

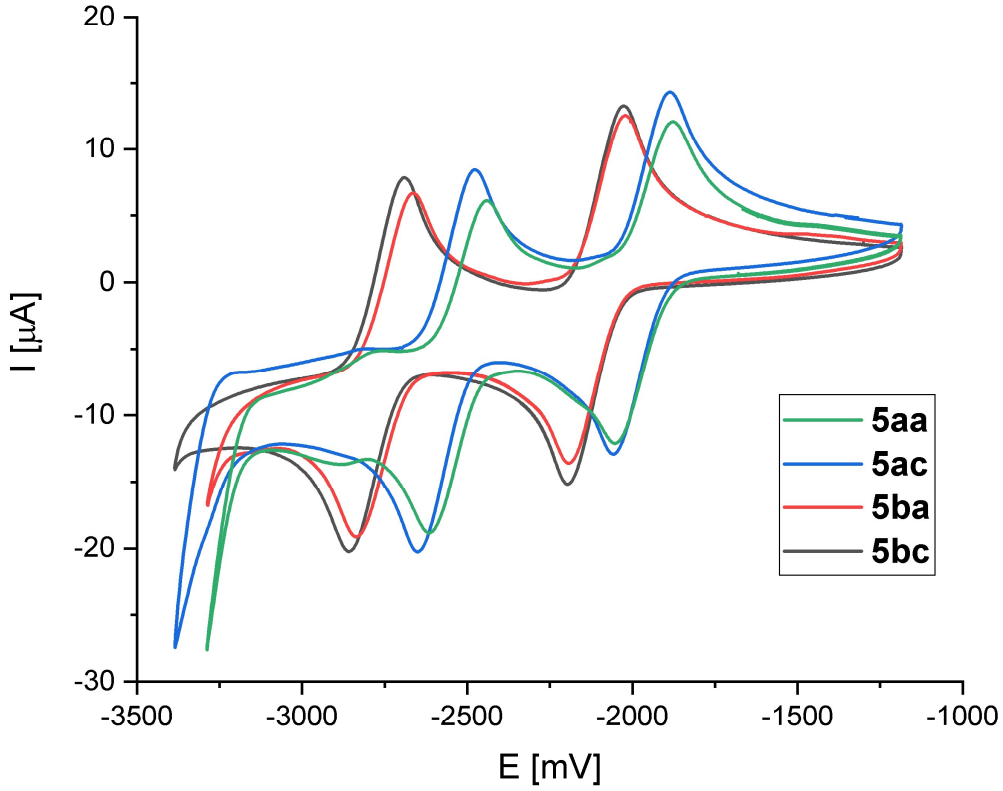

Figure S5.2.41. *Comparison of the cyclic voltammograms of* ***5*** *in THF ($1 \cdot 10^{-3}$ M), recorded vs the ferrocene/ferrocenium couple as internal standard (scan rate: 100 mV s^{-1}).*

5.3 Boron-Doped α-Oligo- and Polyfurans: Highly Luminescent Hybrid Materials, Color-Tunable through the Doping Density

NMR spectra

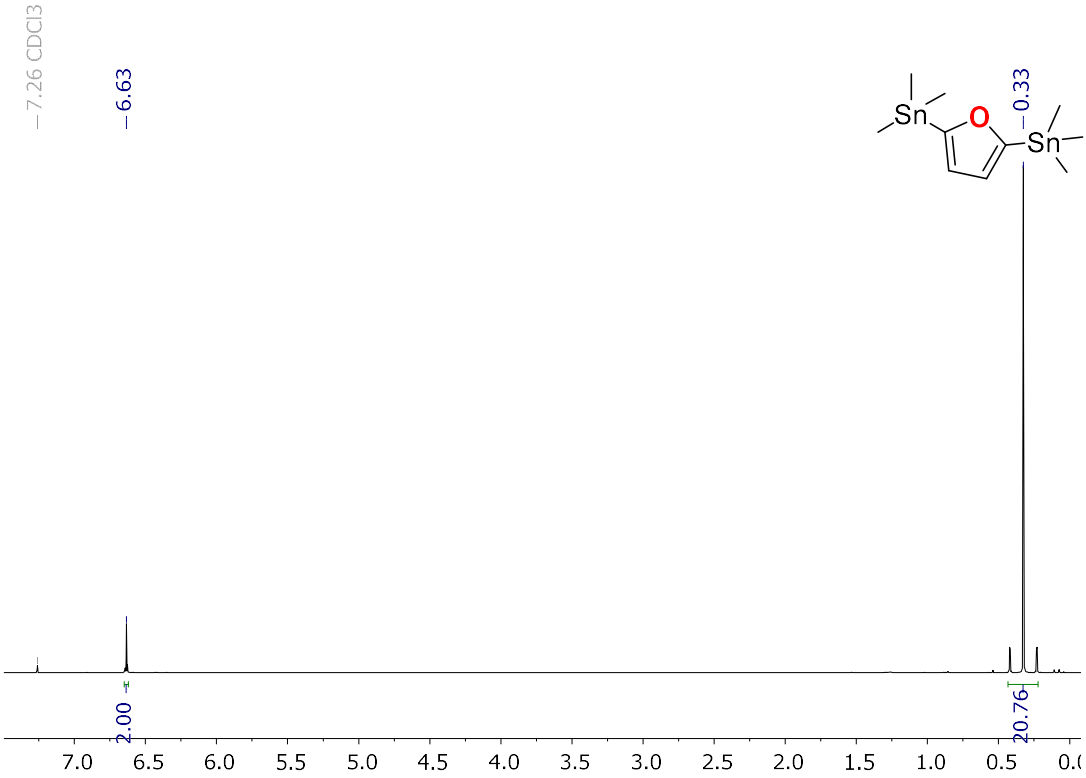

Figure S5.3.1. *^{1}H NMR spectrum of **6a** (300 MHz, in $CDCl_3$).*

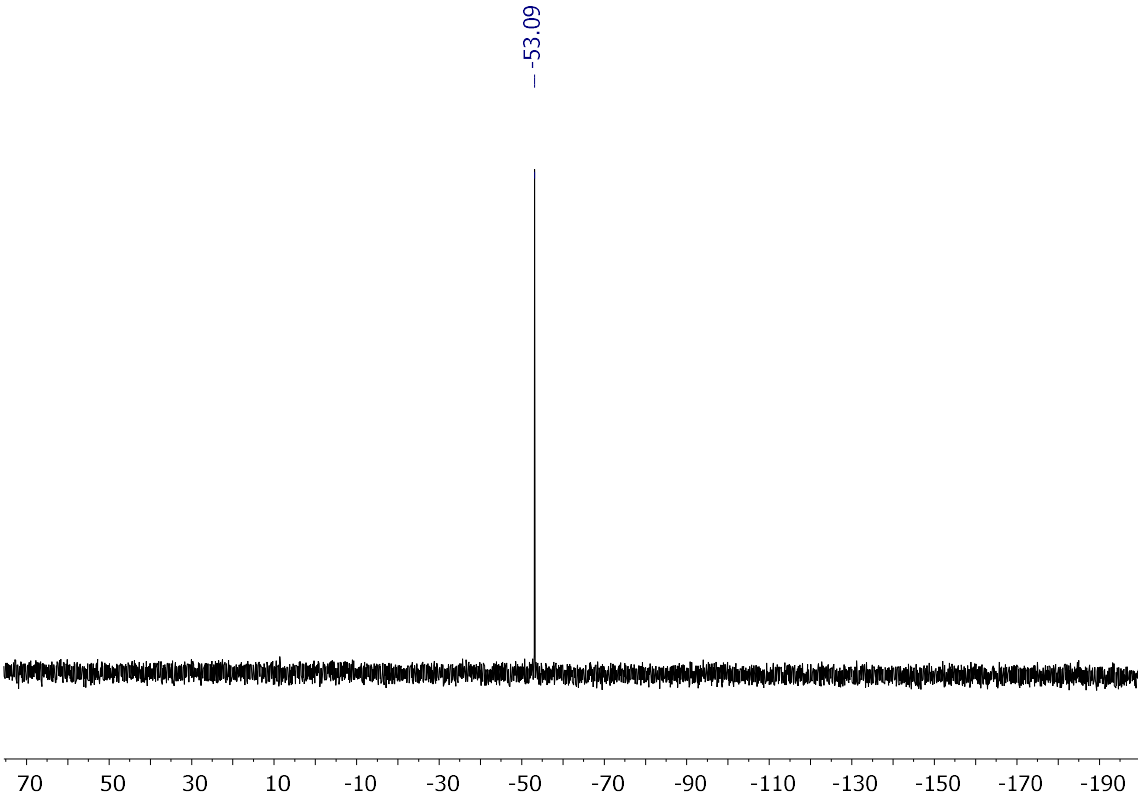

Figure S5.3.2. *^{119}Sn{^{1}H} NMR spectrum of **6a** (112 MHz, in $CDCl_3$).*

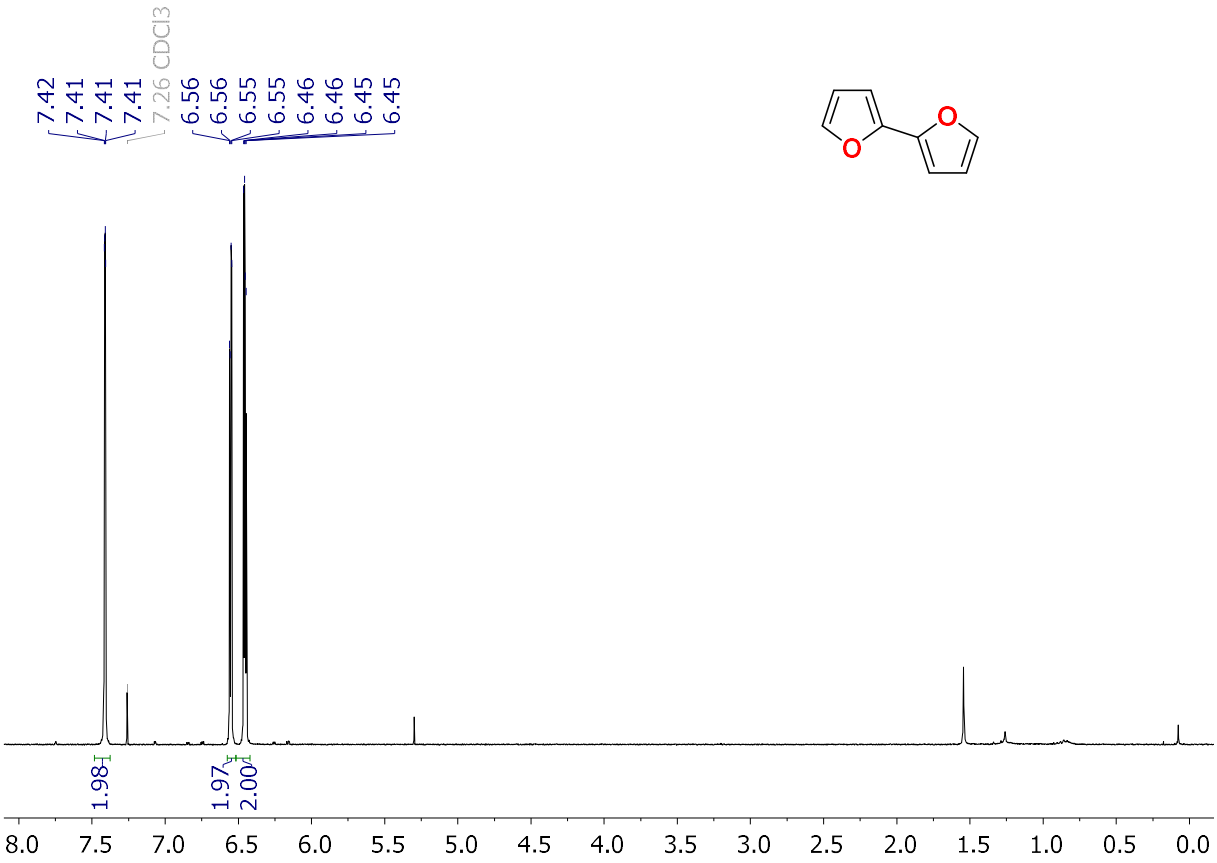

***Figure S5.3.3**: [1]H NMR of **S1** (300 MHz, in $CDCl_3$).*

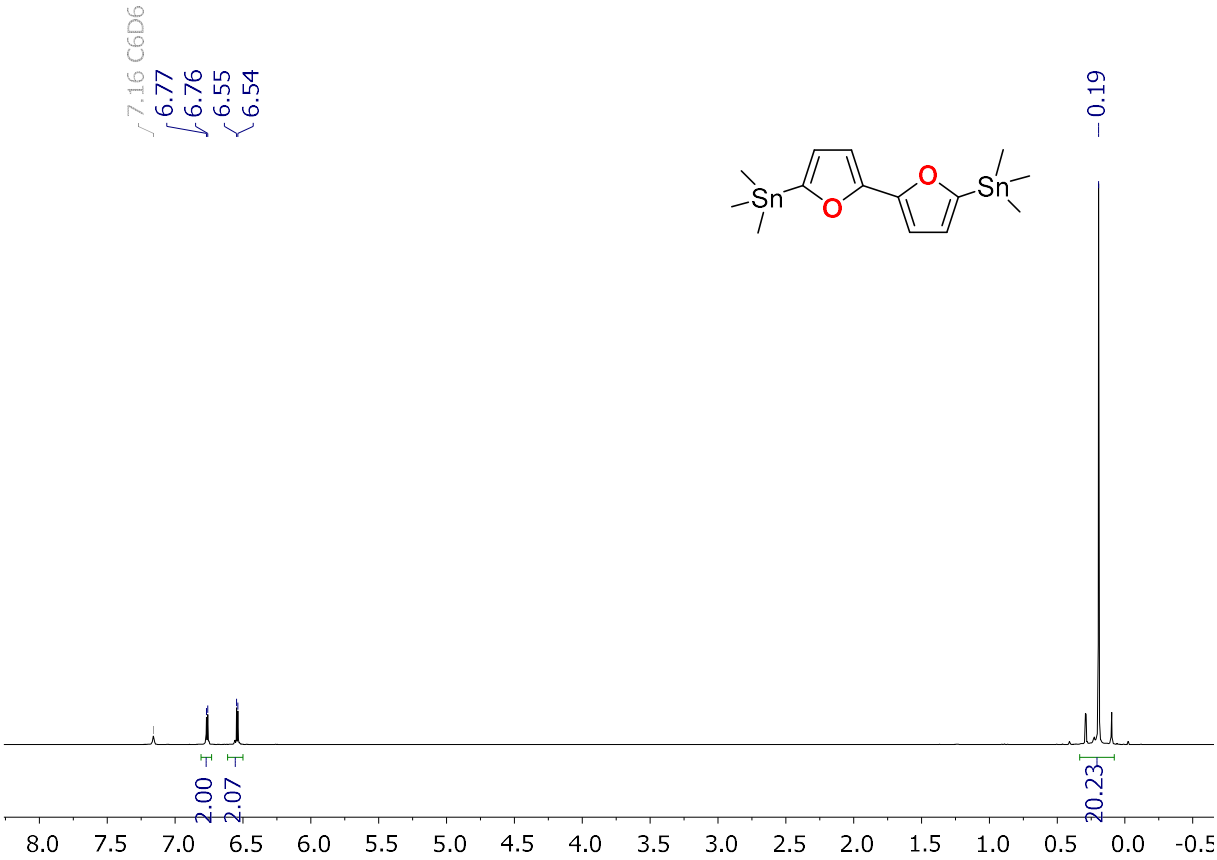

***Figure S5.3.4**: [13]C{[1]H} NMR of **6b** (75 MHz, in C_6D_6).*

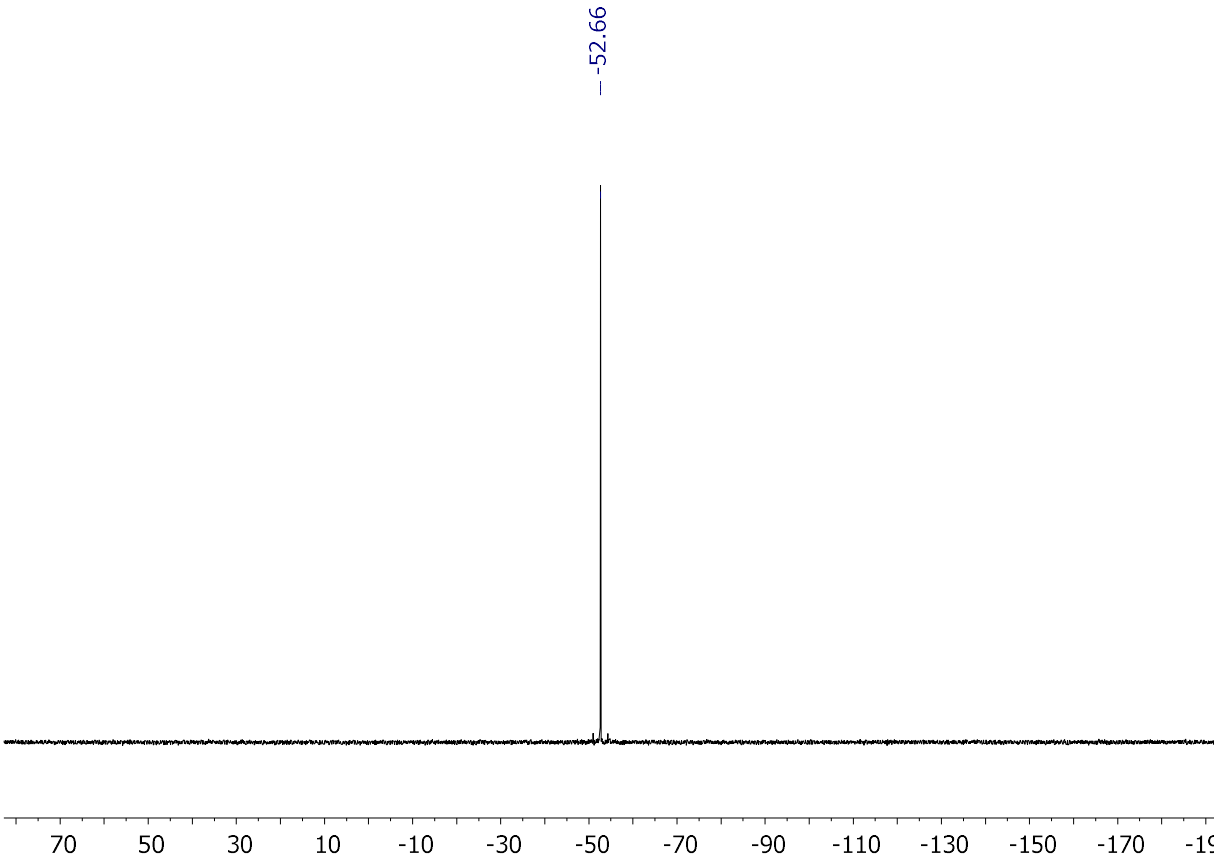

***Figure S5.3.5**: $^{119}Sn\{^{1}H\}$ NMR of **6b** (112 MHz, in C_6D_6).*

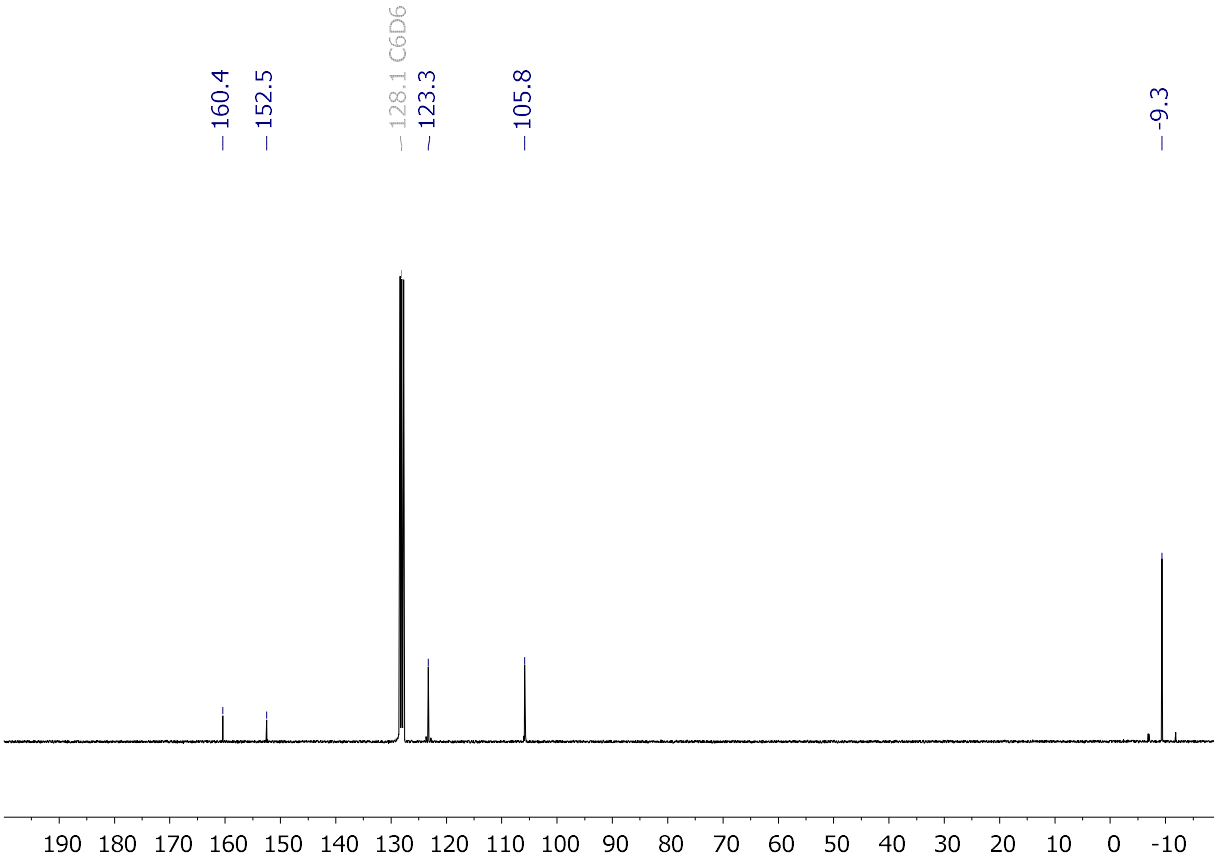

***Figure S5.3.6**: $^{13}C\{^{1}H\}$ NMR of **6b** (75 MHz, in C_6D_6).*

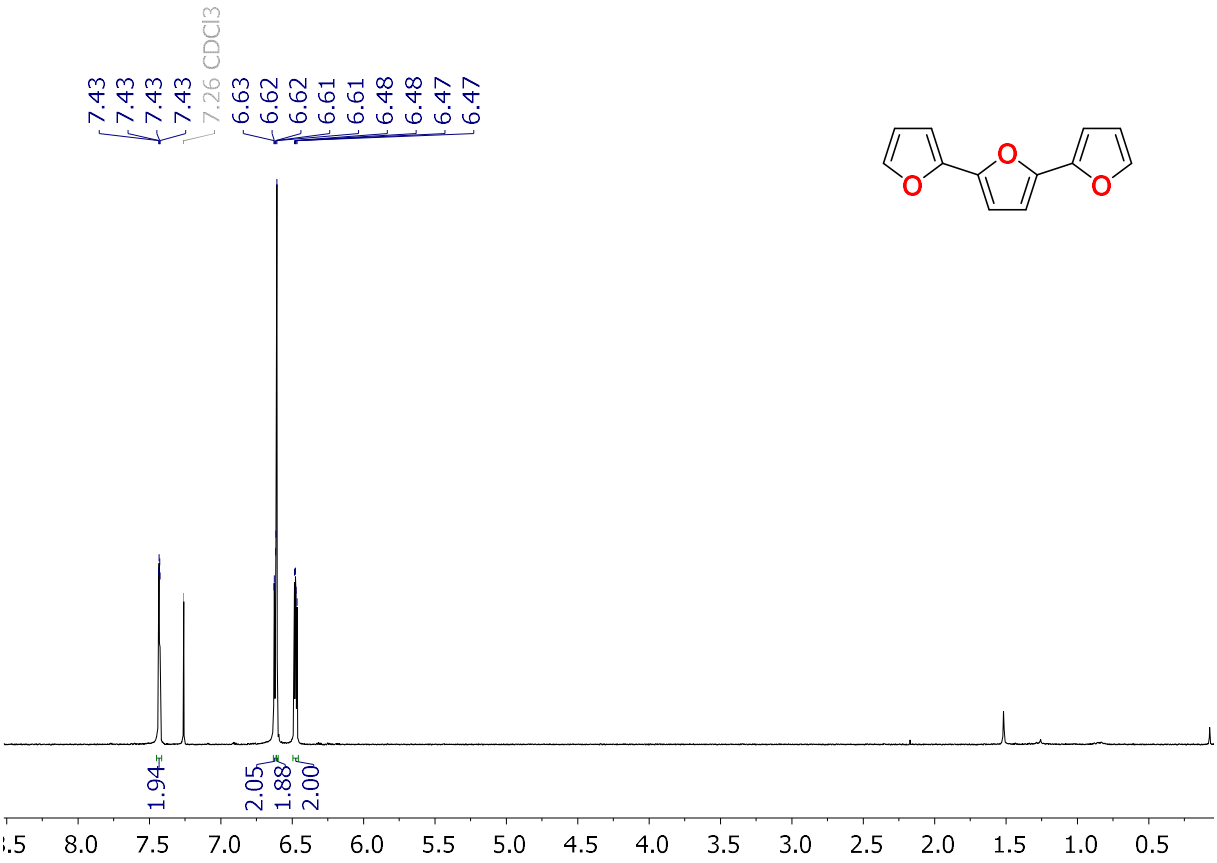

***Figure S5.3.7**: [1]H NMR of **S3** (300 MHz, in $CDCl_3$).*

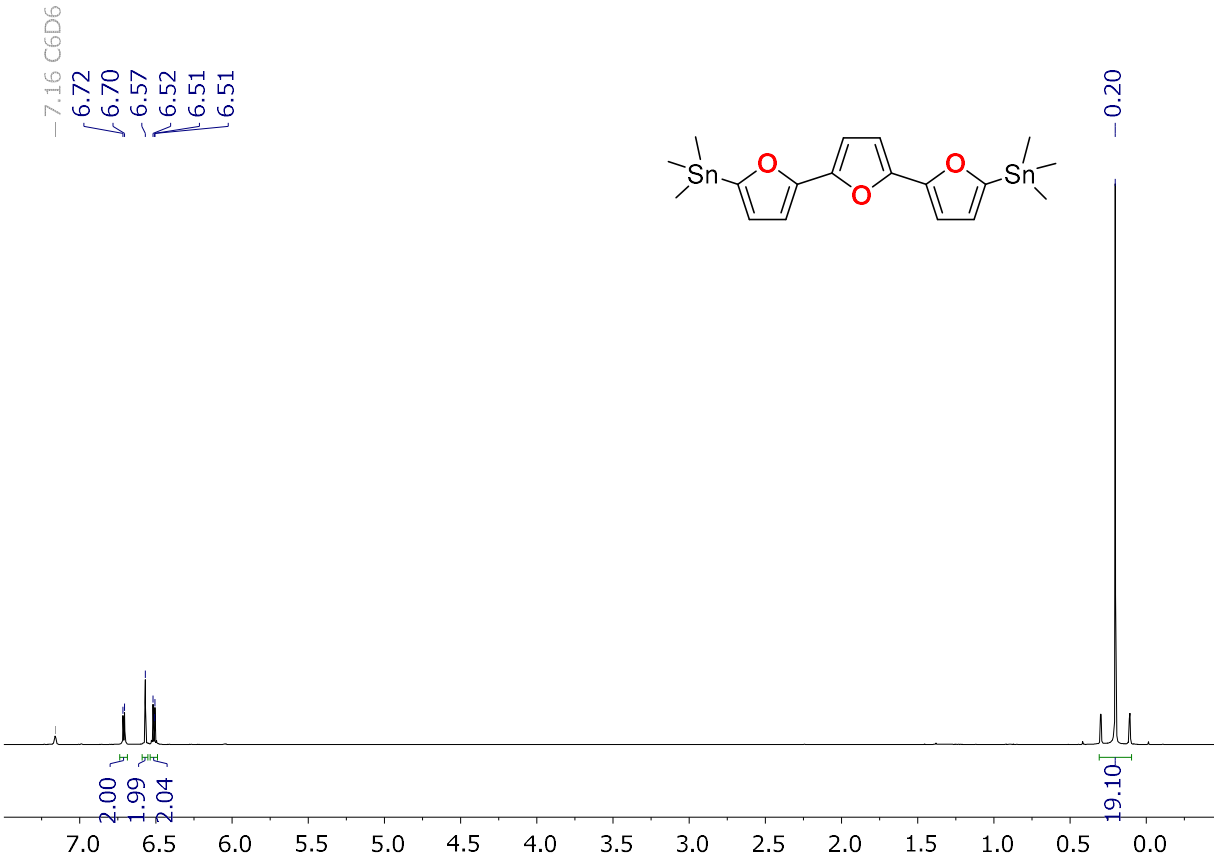

***Figure S5.3.8**: [1]H NMR of **6c** (300 MHz, in C_6D_6).*

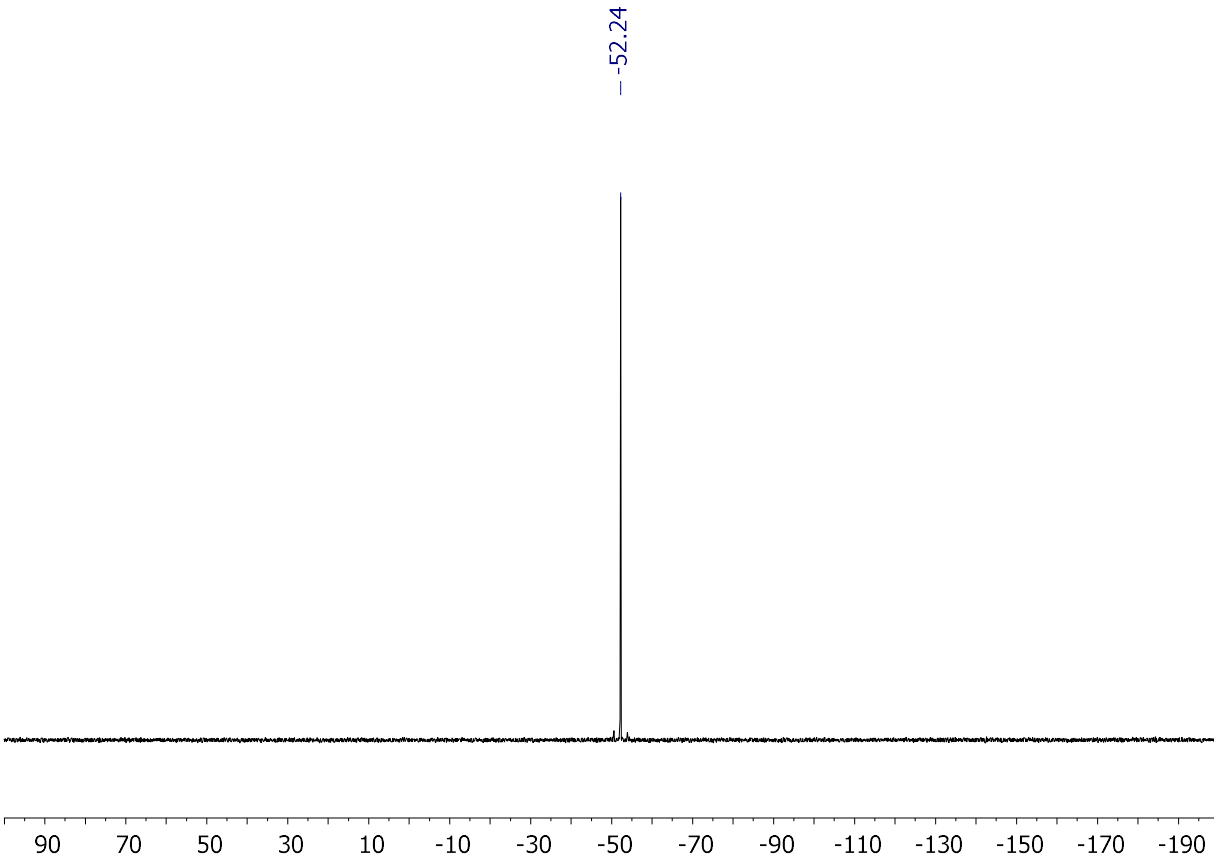

***Figure S5.3.9**: [119]Sn{[1]H} NMR of **6c** (112 MHz, in C_6D_6).*

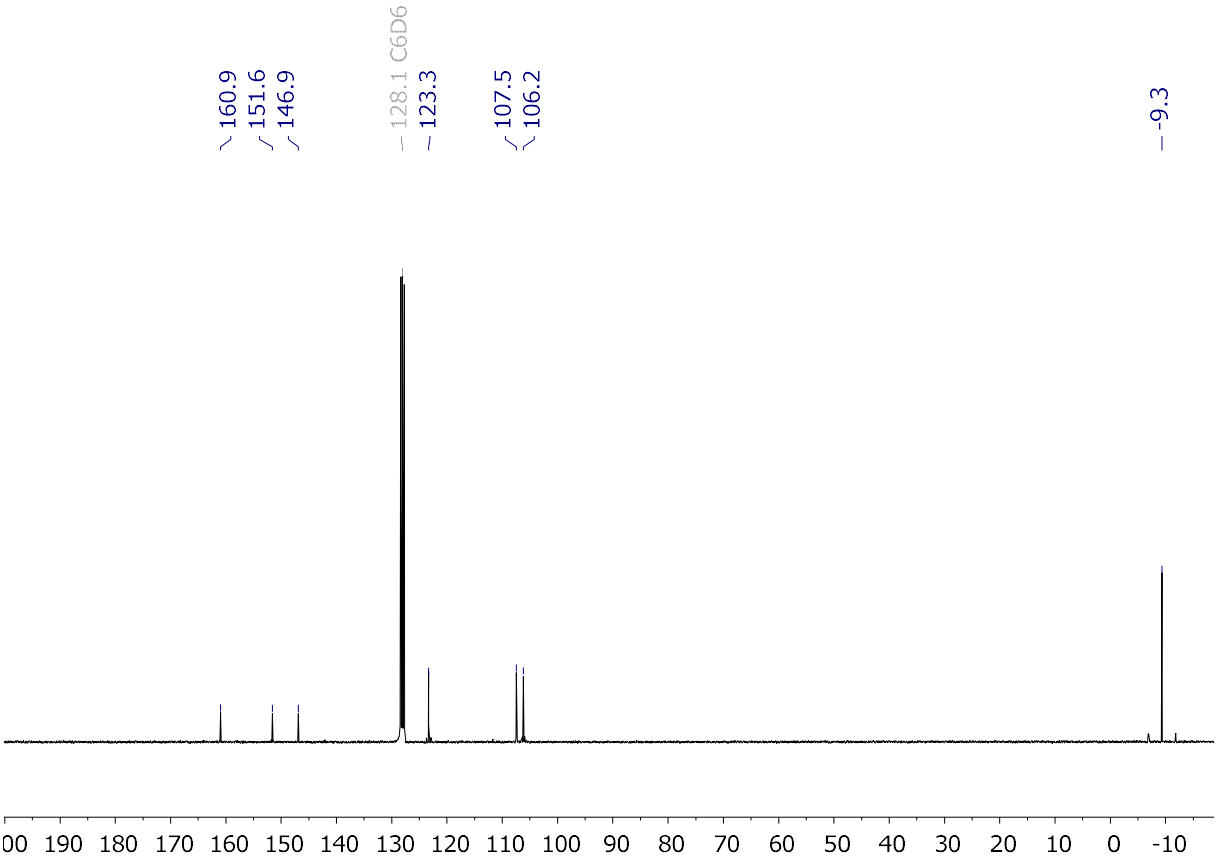

***Figure S5.3.10**: [13]C{[1]H} NMR of **6c** (75 MHz, in C_6D_6).*

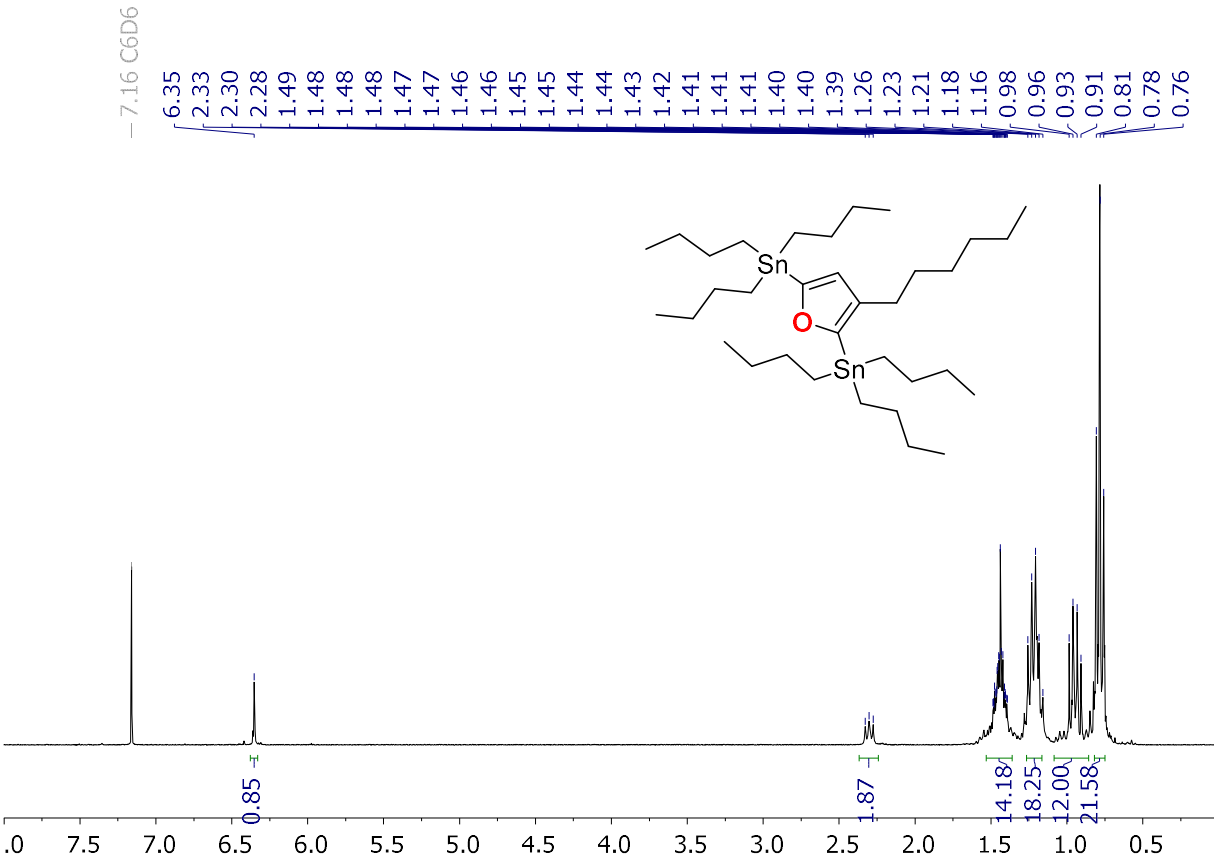

***Figure S5.3.11**: ^{1}H NMR of **S5** (300 MHz, in C_6D_6).*

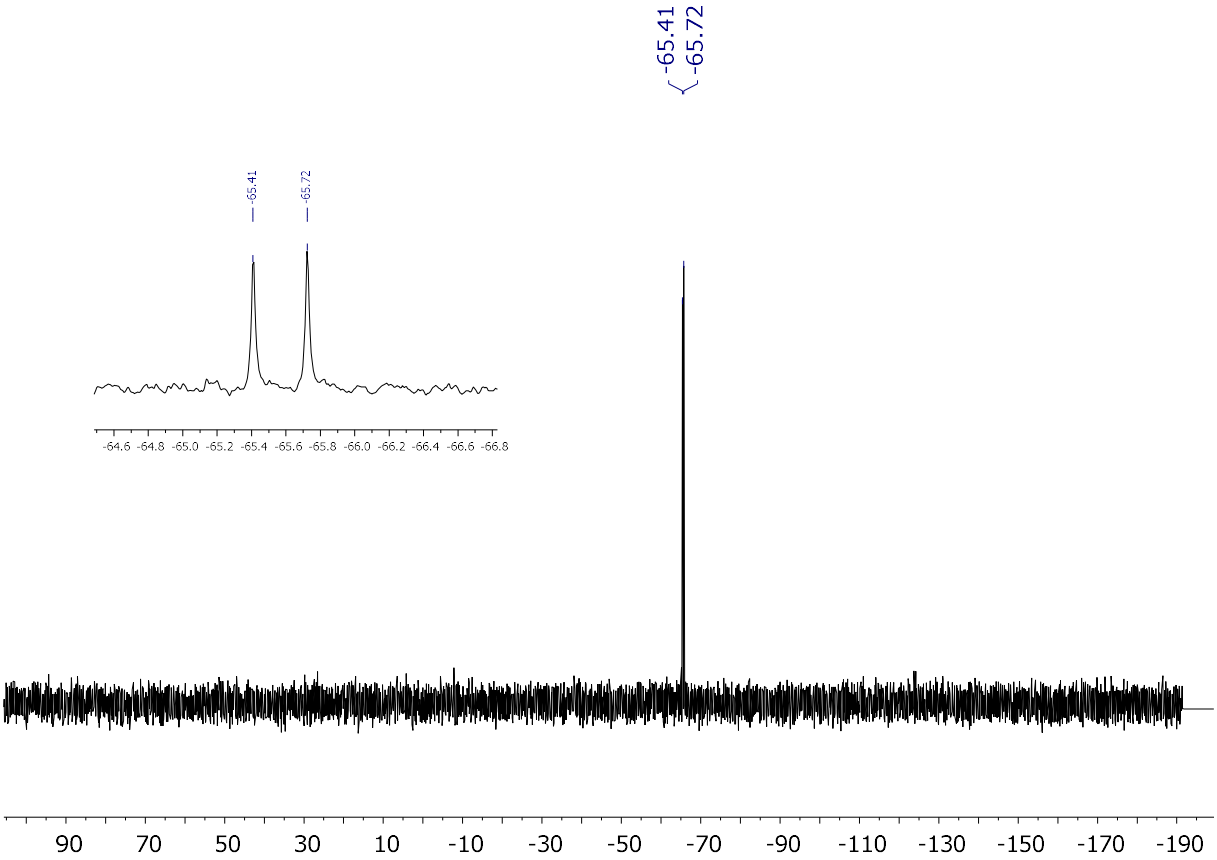

***Figure S5.3.12**: $^{119}Sn\{^{1}H\}$ NMR of **S5** (112 MHz, in C_6D_6).*

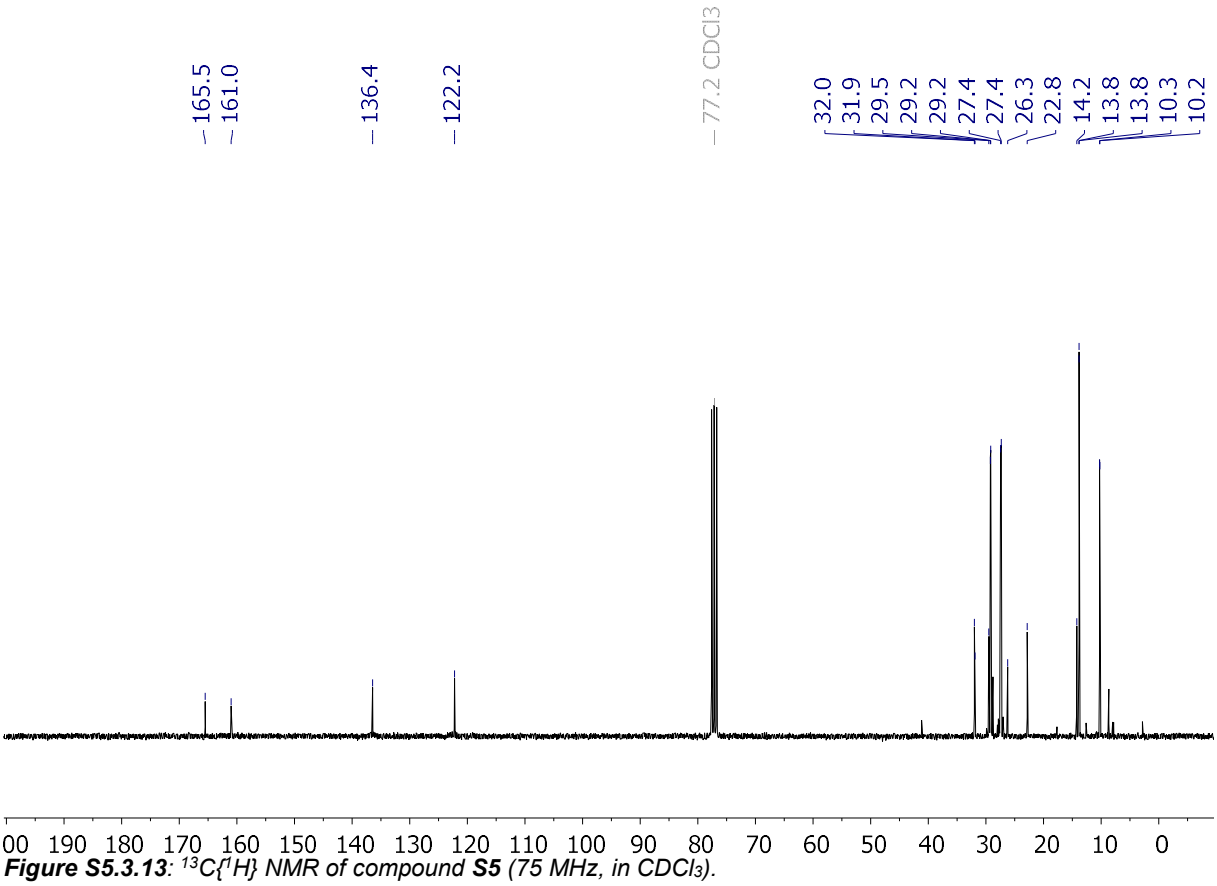

***Figure S5.3.13**: $^{13}C\{^{1}H\}$ NMR of compound **S5** (75 MHz, in $CDCl_3$).*

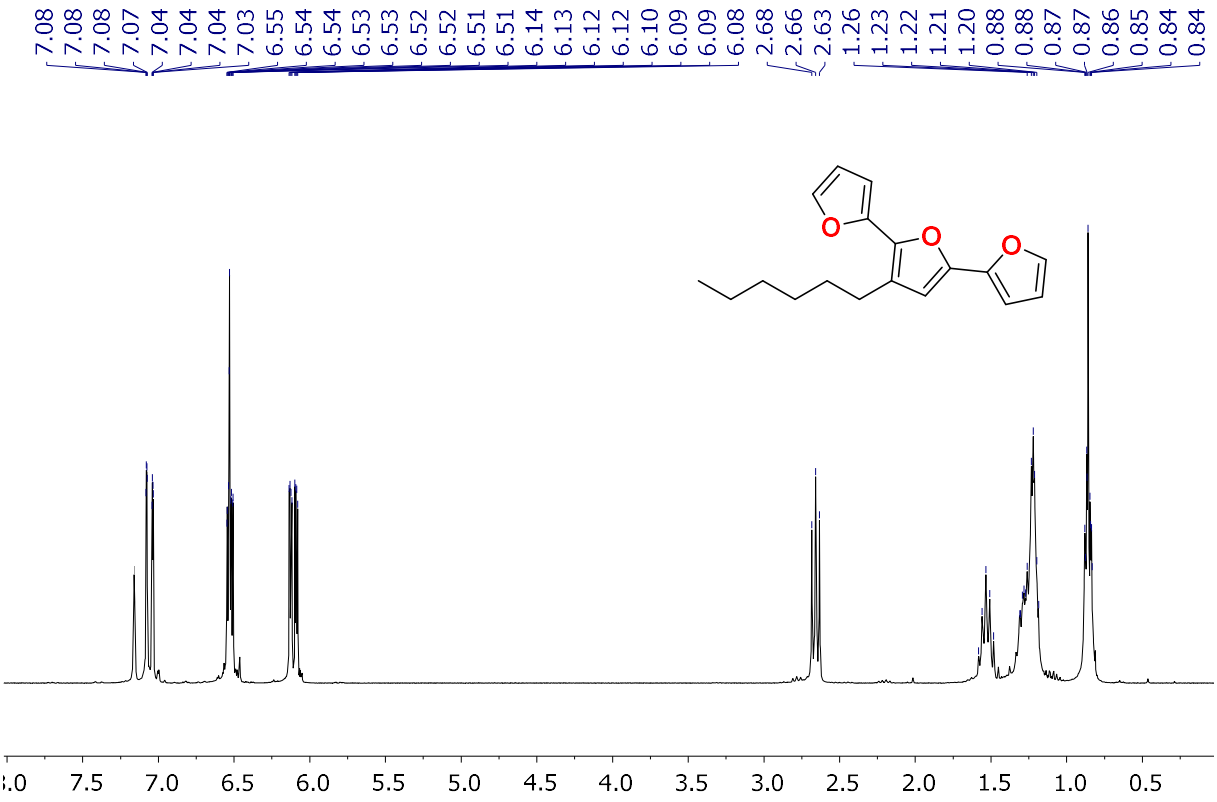

***Figure S5.3.14**: ^{1}H NMR of **S6** (300 MHz, in C_6D_6).*

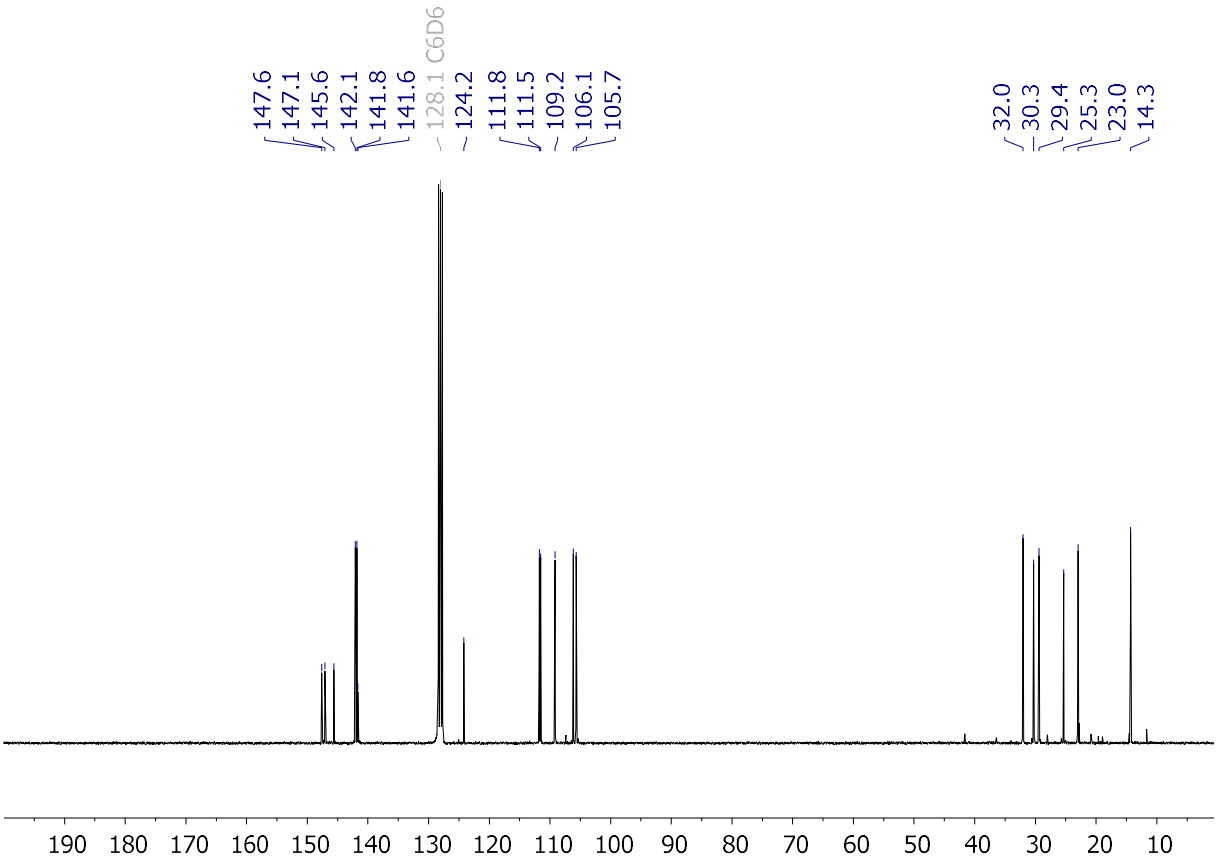

Figure S5.3.15: *$^{13}C\{^{1}H\}$ NMR of* ***S6*** *(75 MHz, in C_6D_6).*

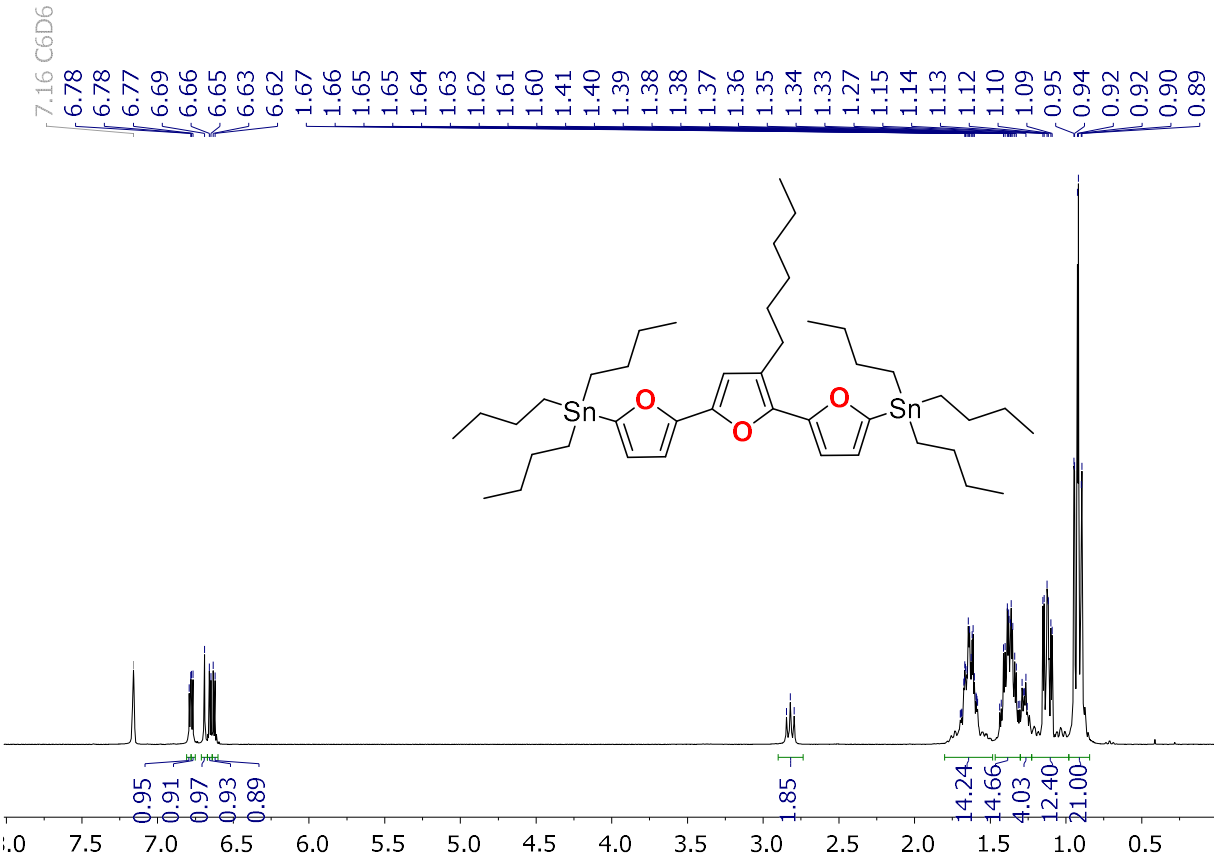

Figure S5.3.16: *^{1}H NMR of* ***6c^{Hex}*** *(300 MHz, in C_6D_6).*

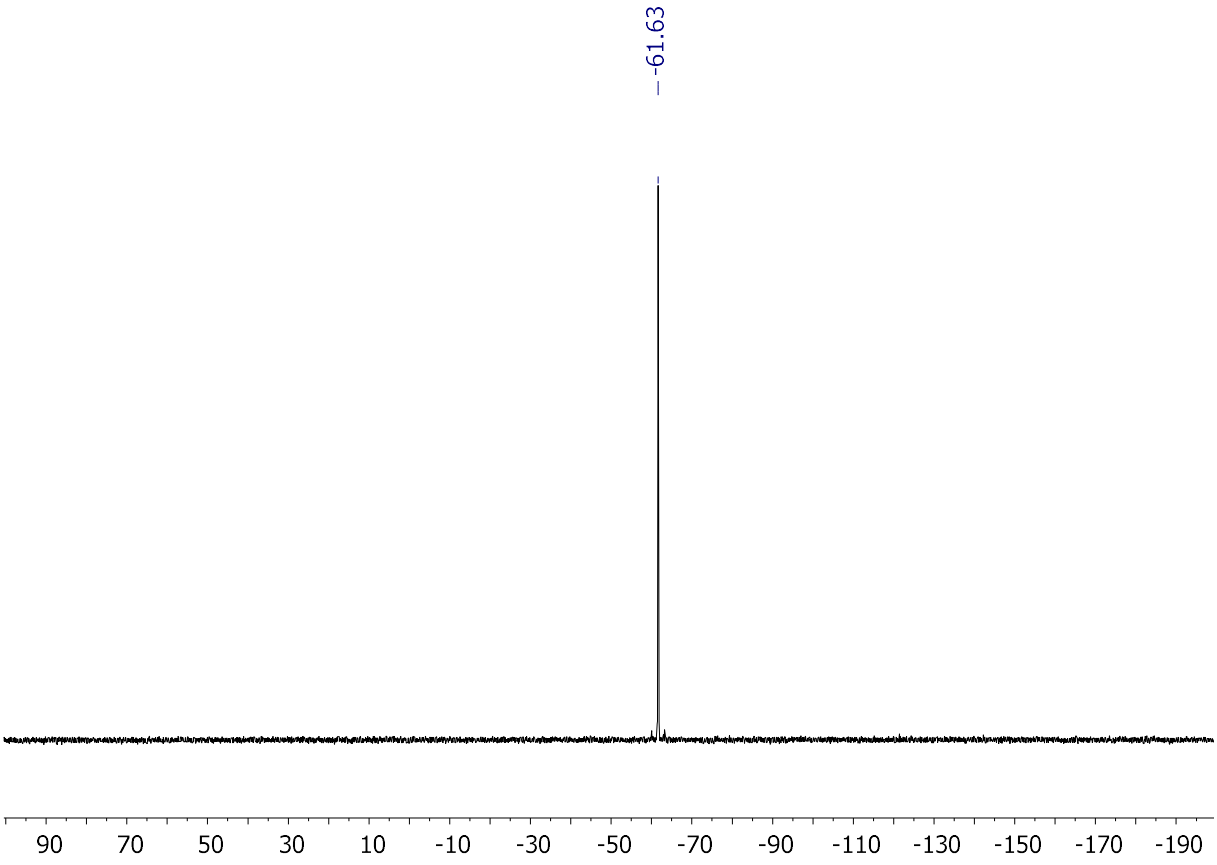

***Figure S5.3.17**: $^{119}Sn\{^{1}H\}$ NMR of **6c^{Hex}** (112 MHz, in C_6D_6).*

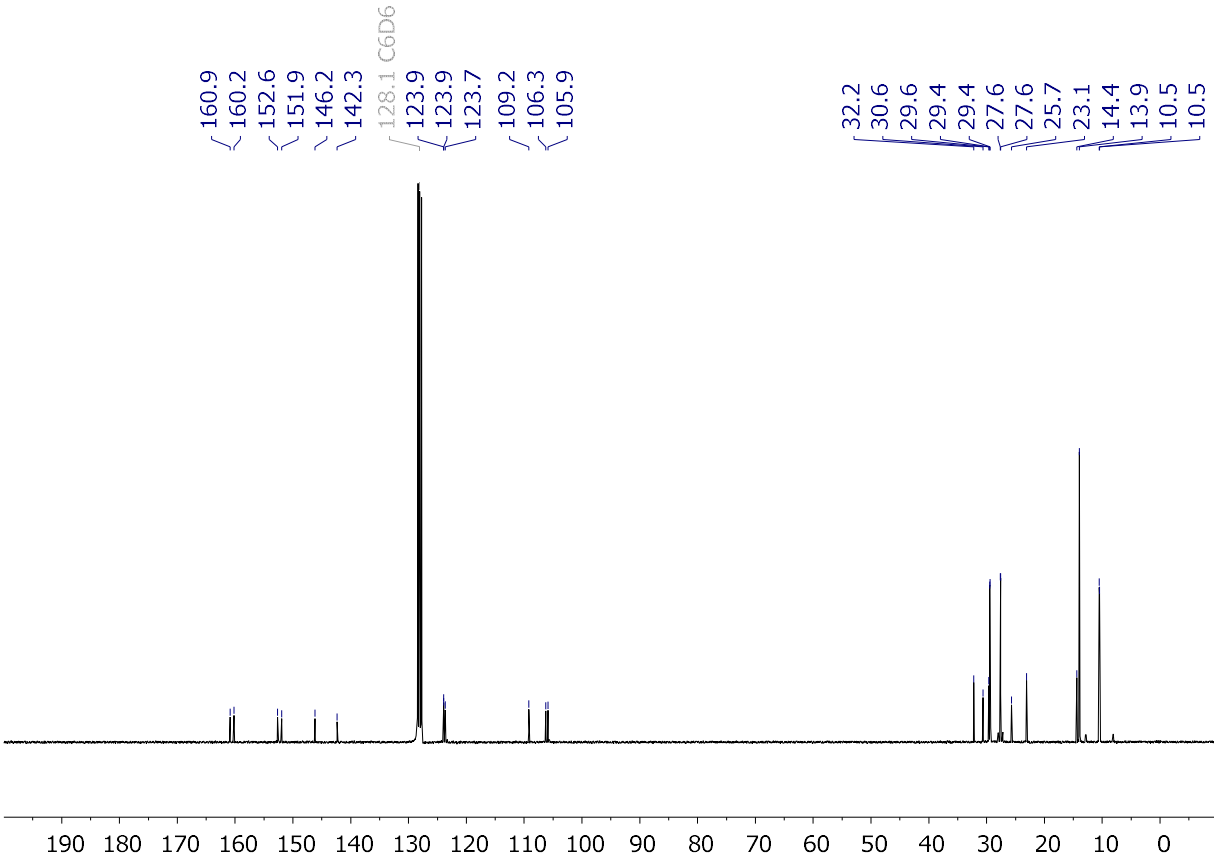

***Figure S5.3.18**: $^{13}C\{^{1}H\}$ NMR of **6c^{Hex}** (75 MHz, in C_6D_6).*

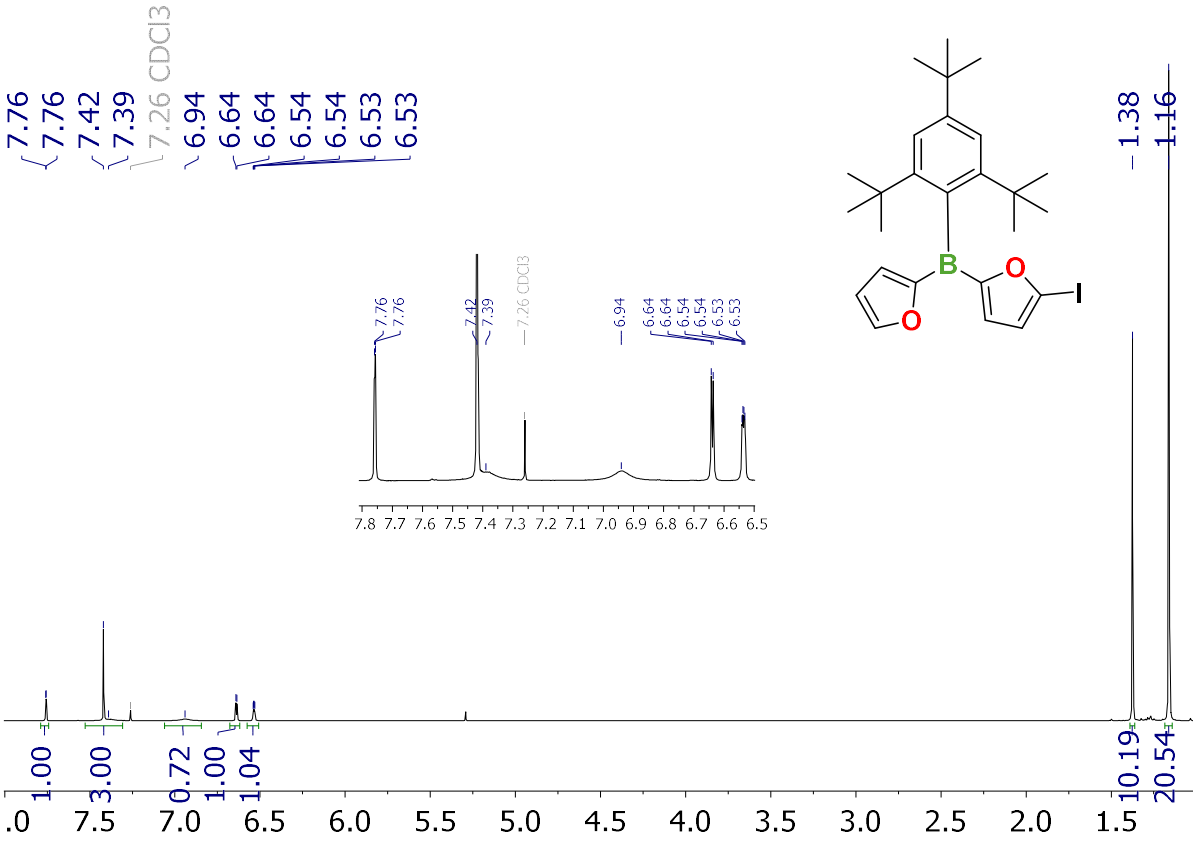

Figure S5.3.19. *^{1}H NMR spectrum of **4** (500 MHz, in $CDCl_3$).*

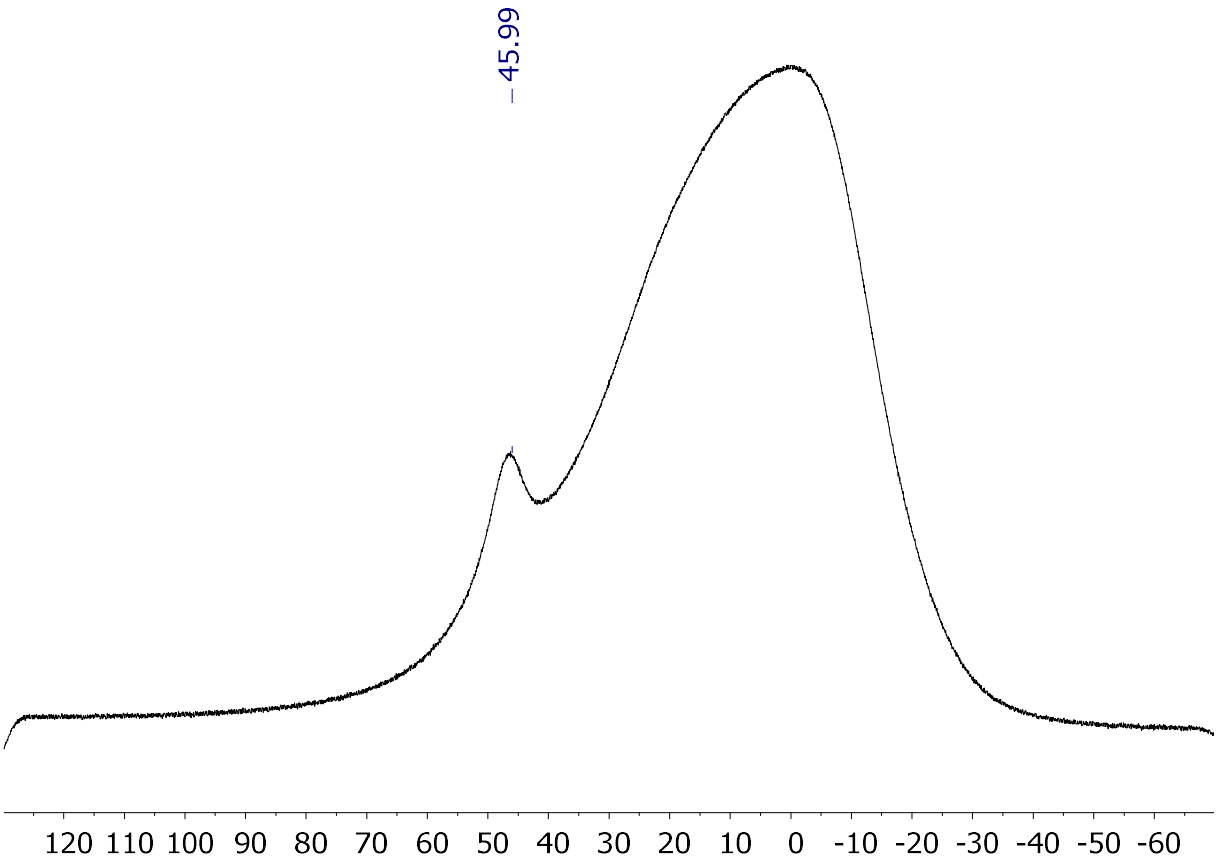

Figure S5.3.20. *$^{11}B\{^{1}H\}$ NMR spectrum of **4** (160 MHz, in $CDCl_3$).*

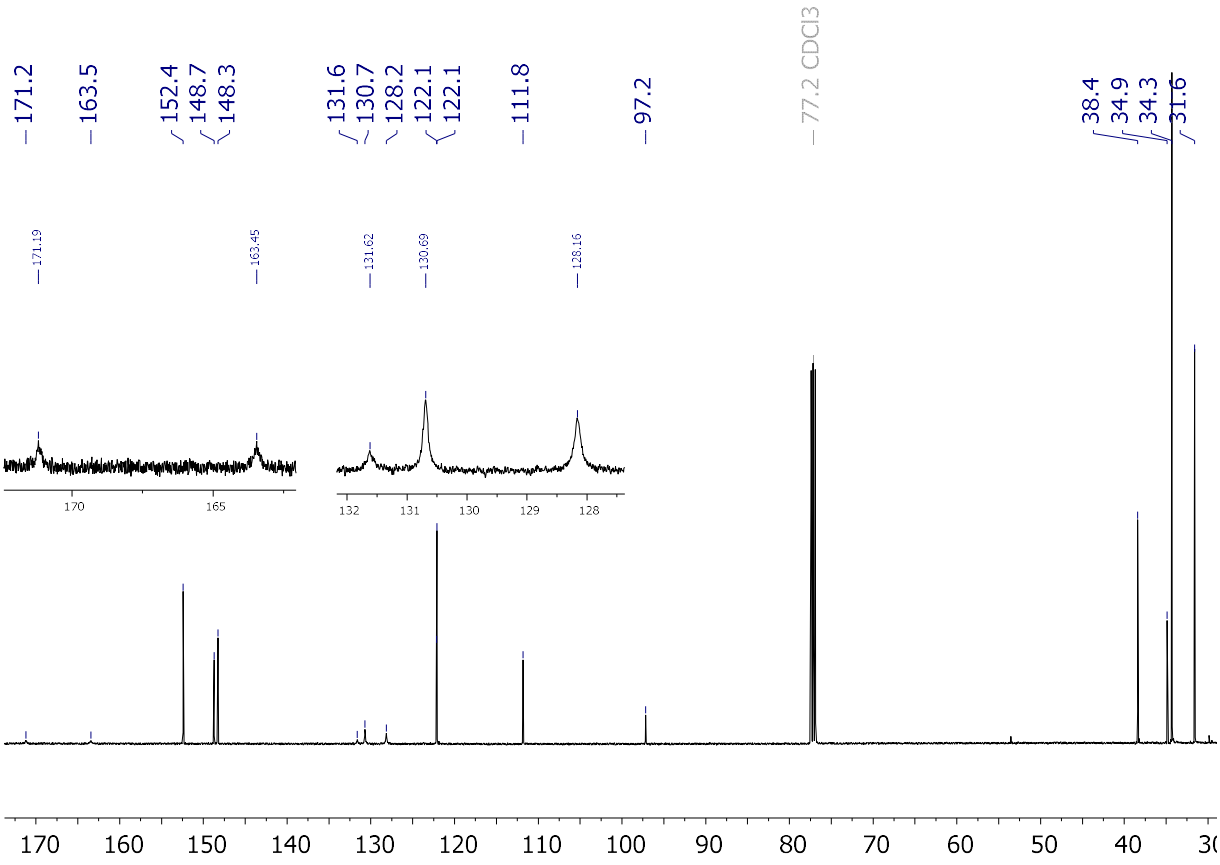

Figure S5.3.21. *$^{13}C\{^{1}H\}$ NMR spectrum of **4** (126 MHz, in $CDCl_3$).*

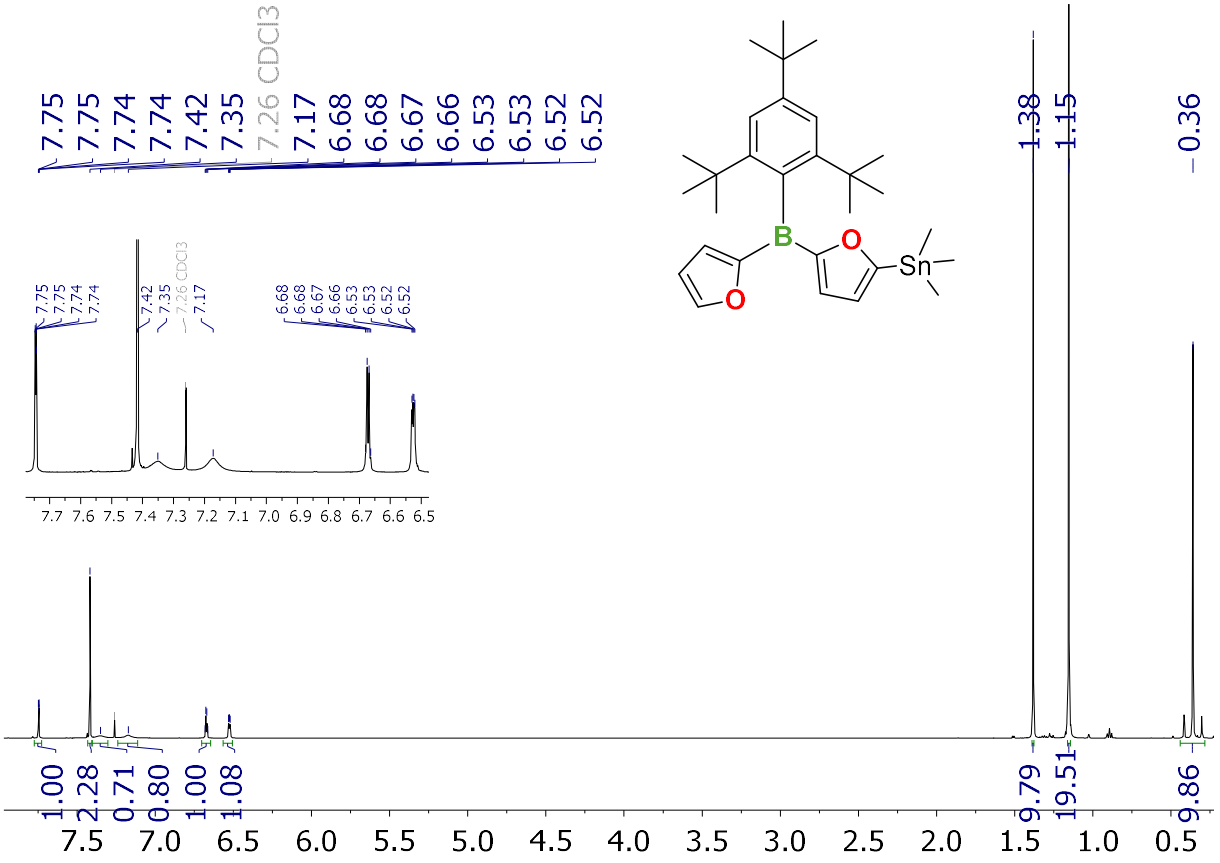

Figure S5.3.22. *^{1}H NMR spectrum of **5** (500 MHz, in $CDCl_3$).*

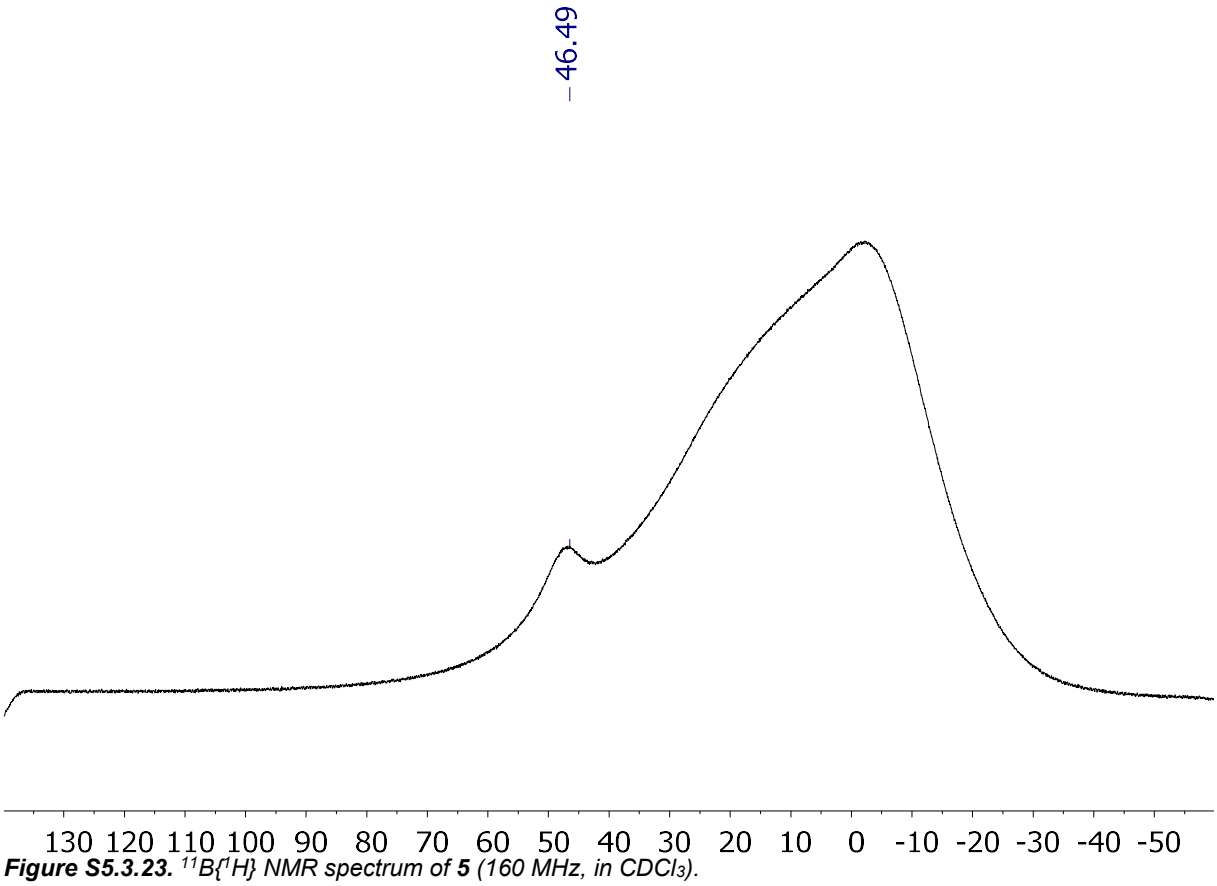

Figure S5.3.23. *$^{11}B\{^1H\}$ NMR spectrum of **5** (160 MHz, in $CDCl_3$).*

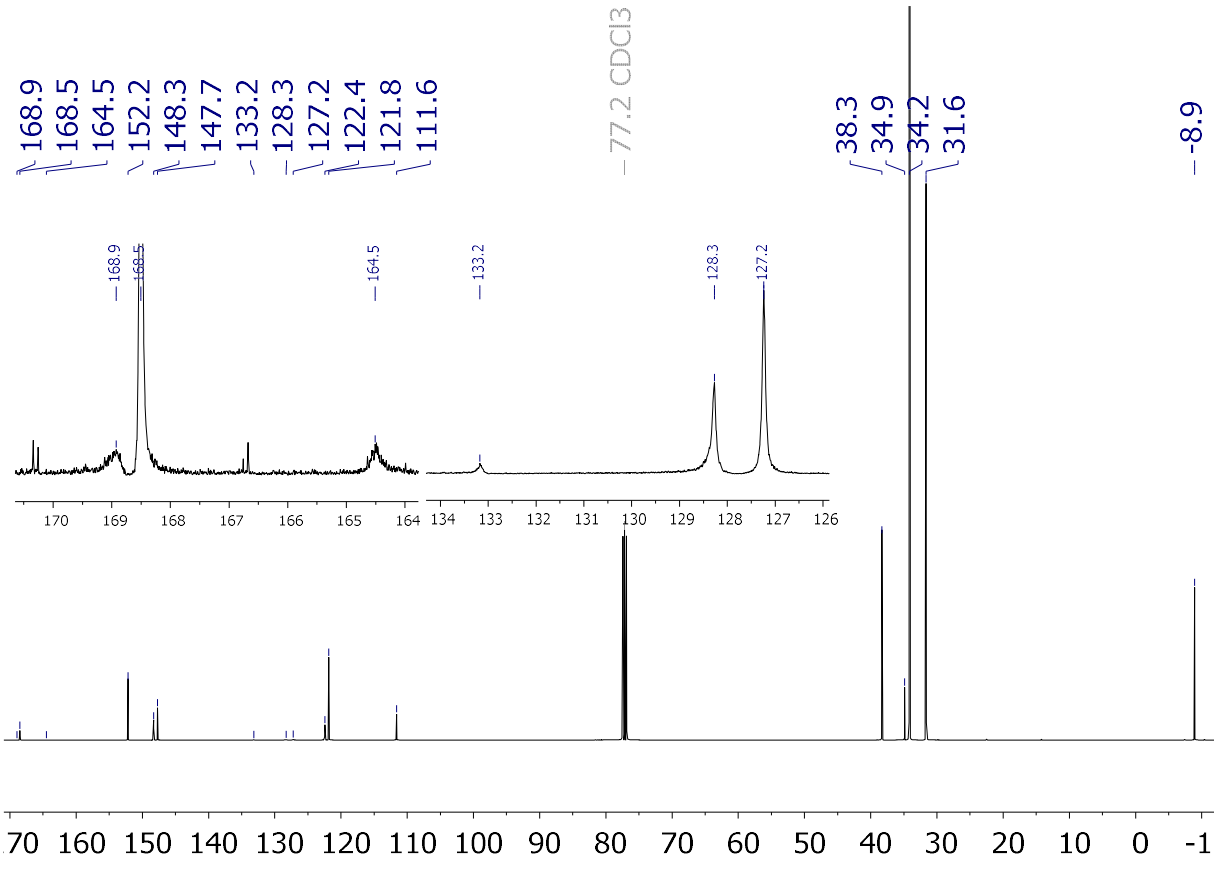

Figure S5.3.24. *$^{13}C\{^1H\}$ NMR spectrum of **5** (126 MHz, in $CDCl_3$).*

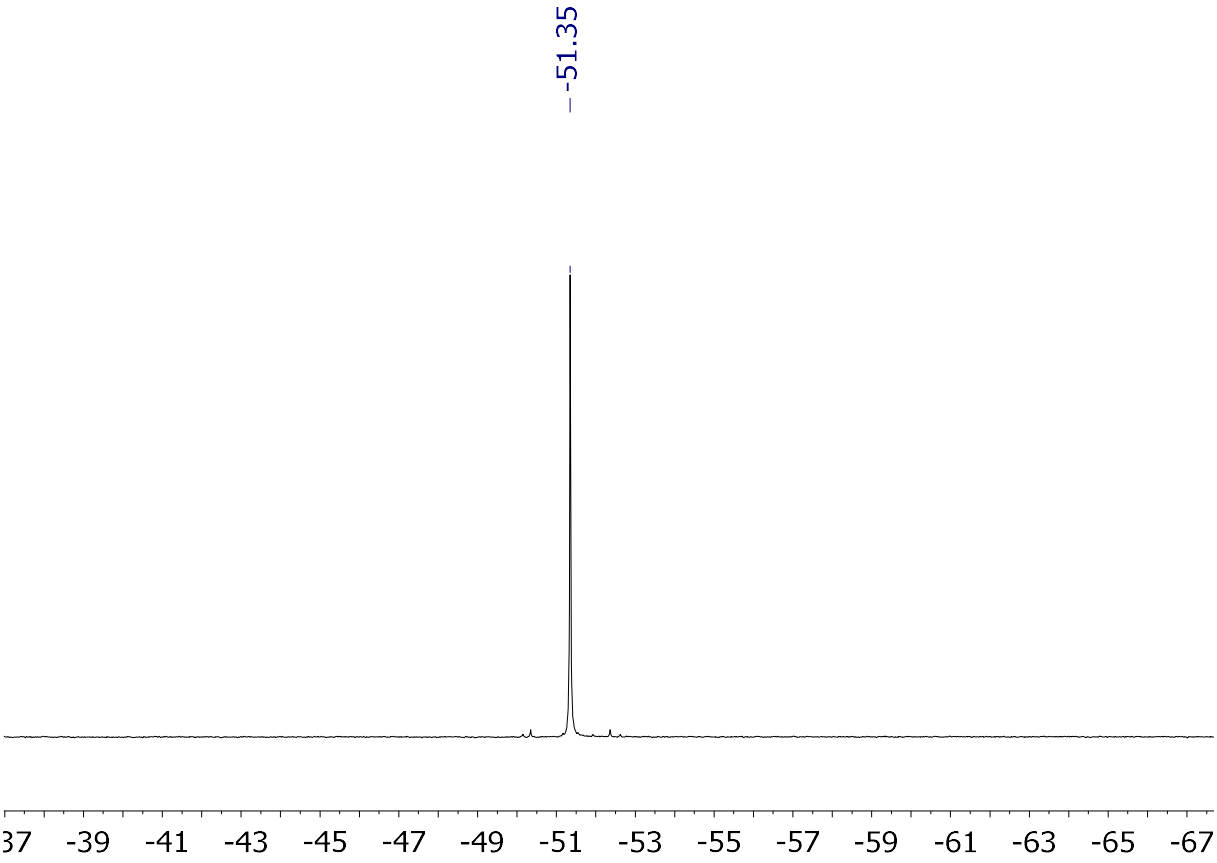

Figure S5.3.25. *$^{119}Sn\{^{1}H\}$ NMR spectrum of **5** (187 MHz, in $CDCl_3$).*

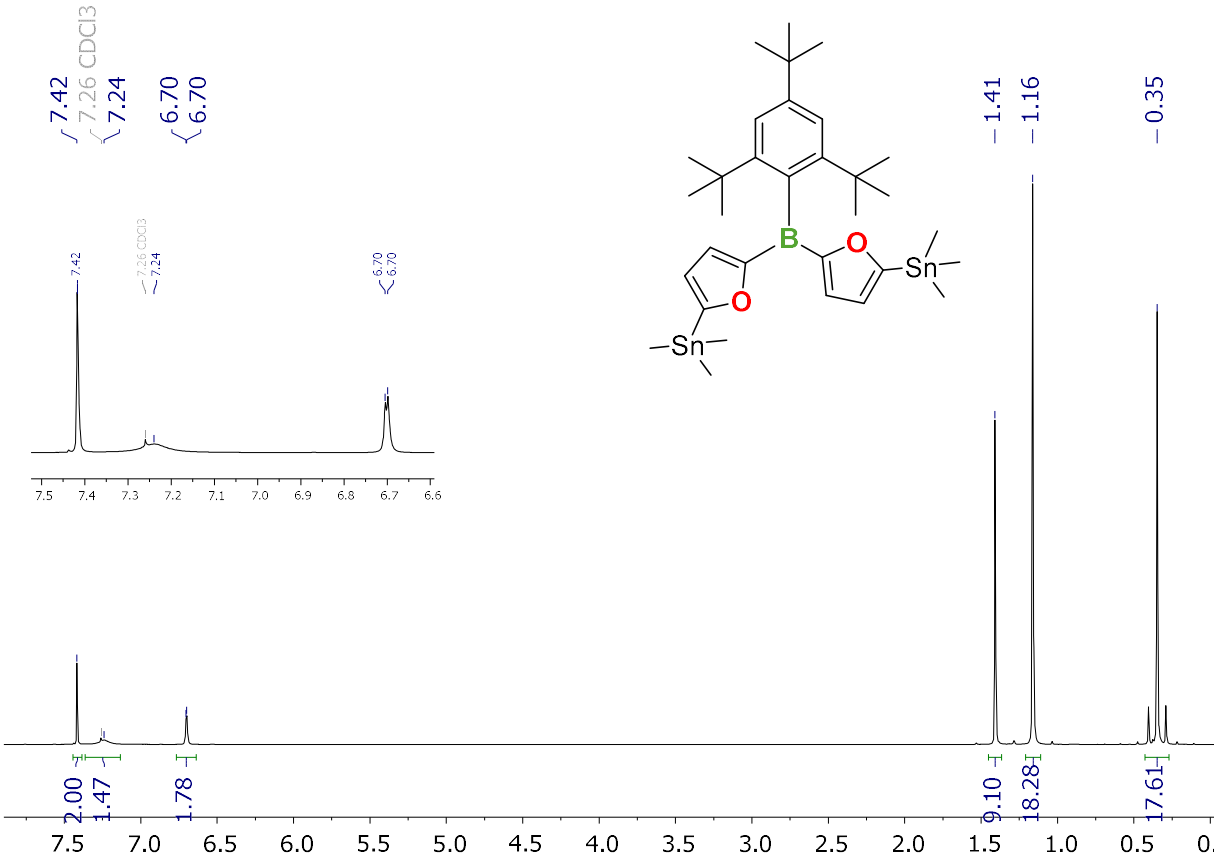

Figure S5.3.26. *^{1}H NMR spectrum of **9** (500 MHz, in $CDCl_3$).*

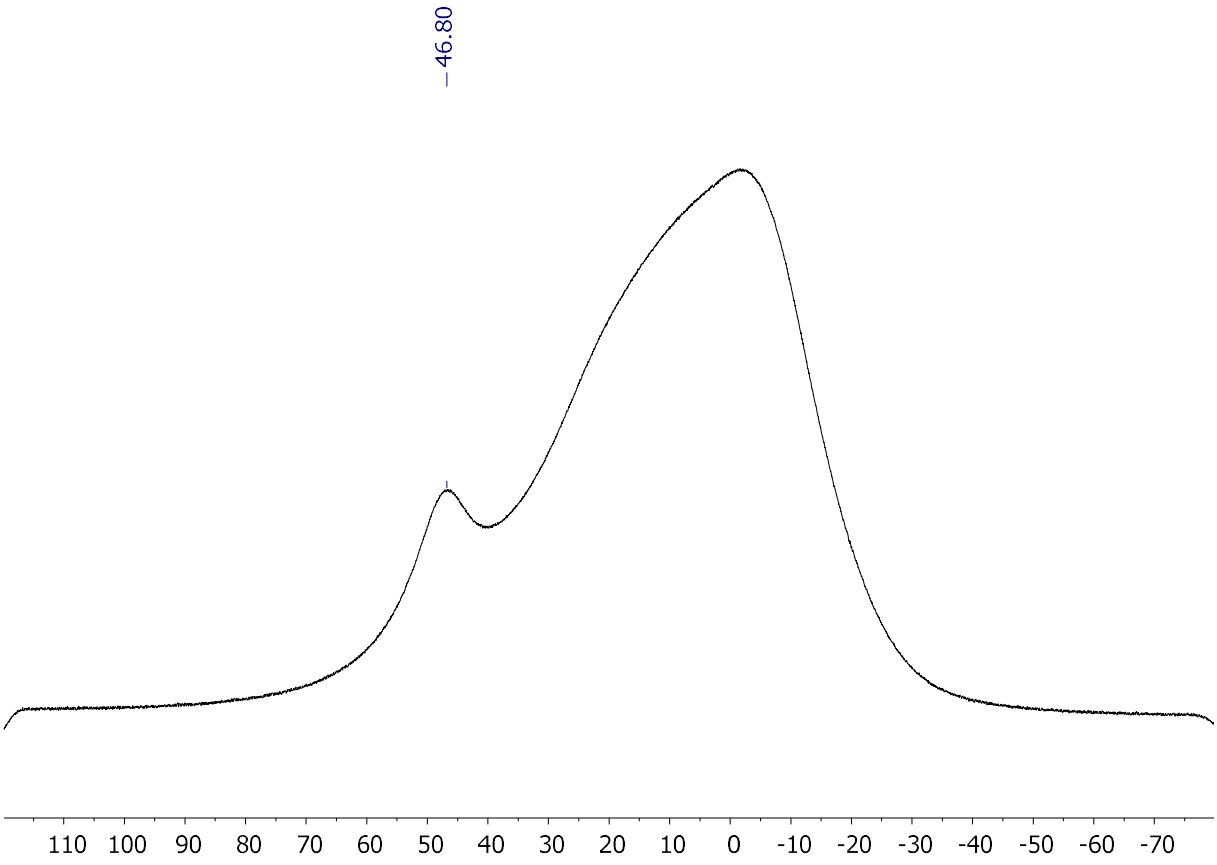

Figure S5.3.27. *$^{11}B\{^1H\}$ NMR spectrum of **9** (160 MHz and 96 MHz, in $CDCl_3$).*

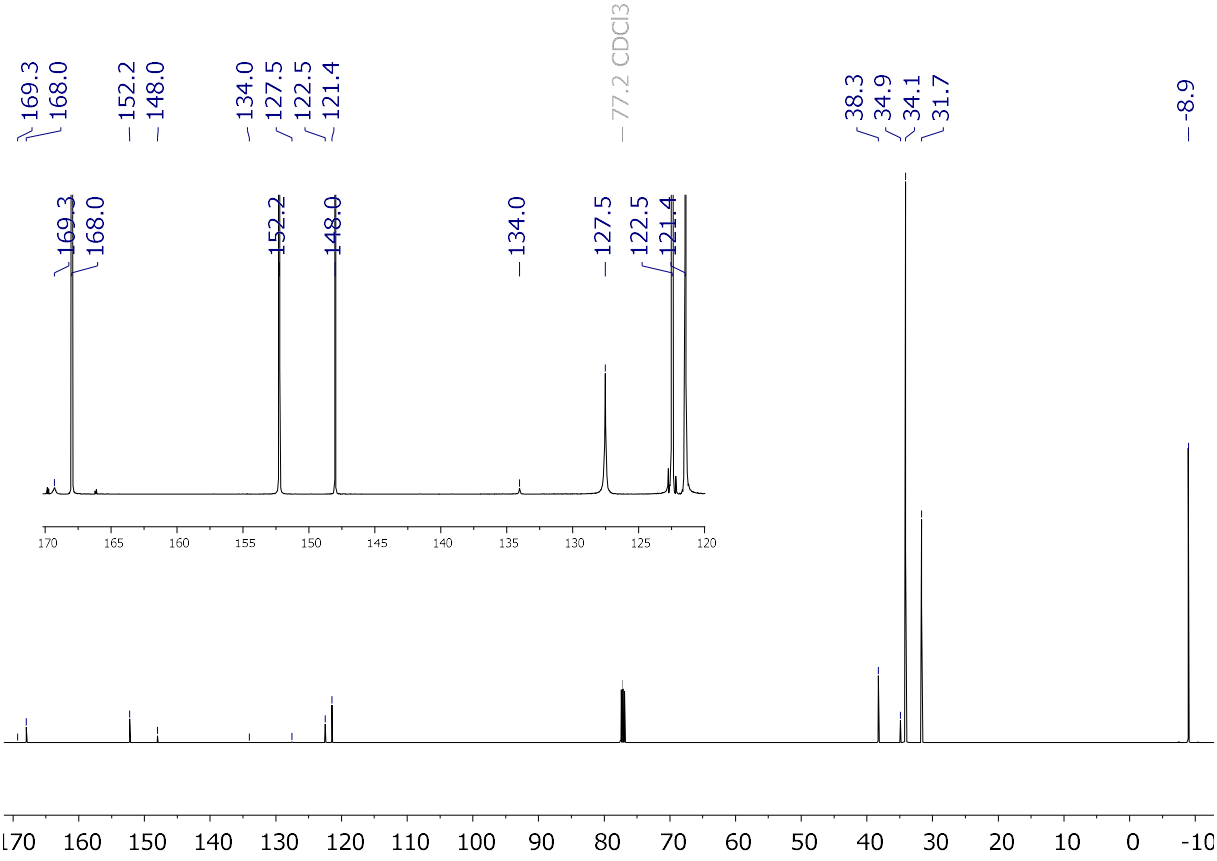

Figure S5.3.28. *$^{13}C\{^1H\}$ NMR spectrum of **9** (126 MHz, in $CDCl_3$).*

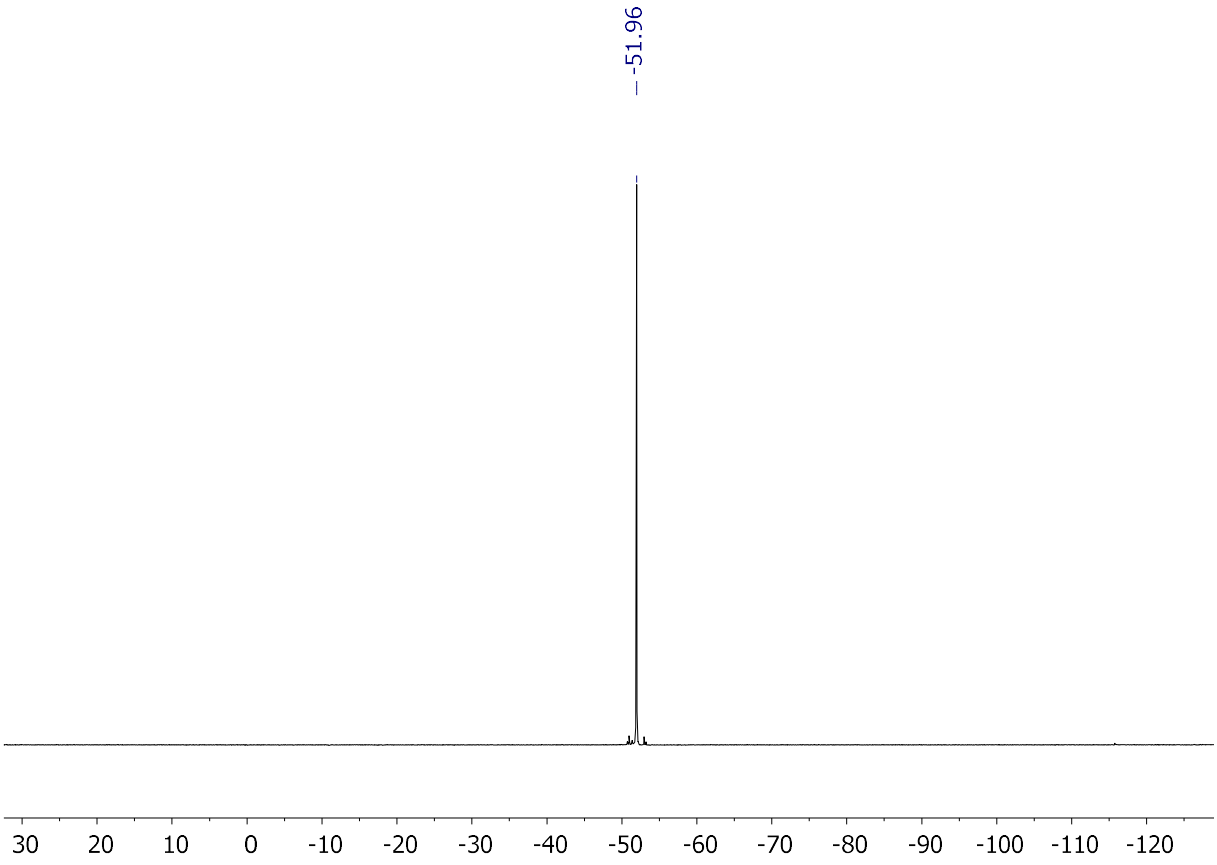

Figure S5.3.29. *$^{119}Sn\{^{1}H\}$ NMR spectrum of **9** (187 MHz, in $CDCl_3$).*

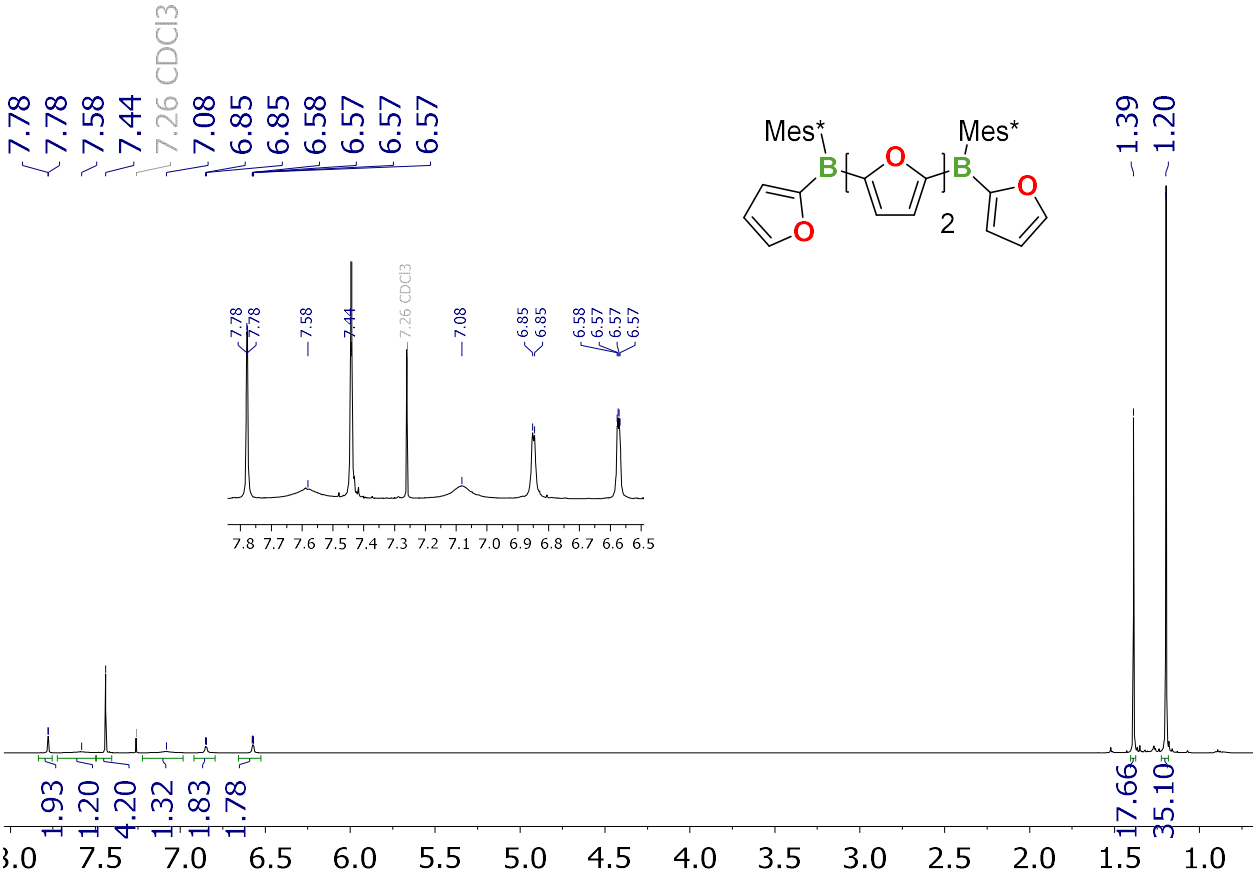

Figure S5.3.30. *^{1}H NMR spectrum of **BB2F** (500 MHz, in $CDCl_3$).*

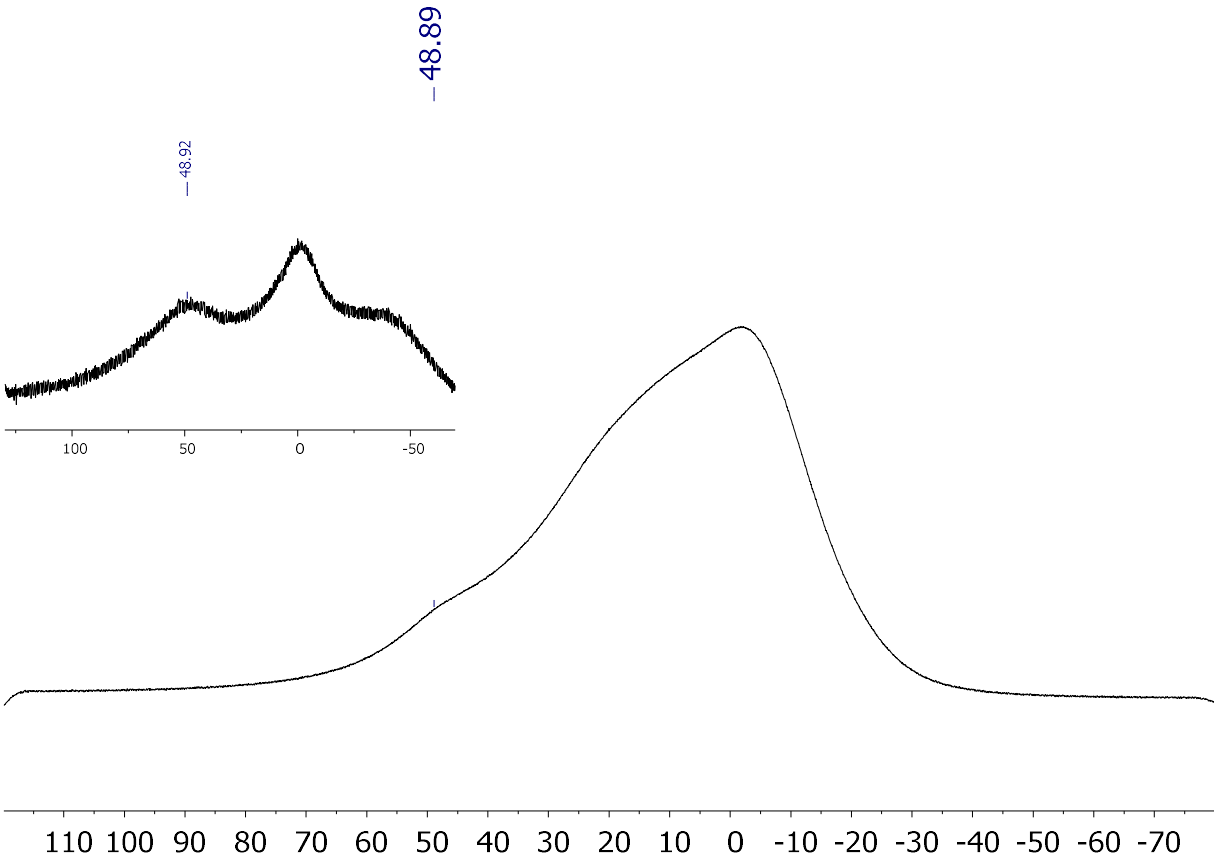

Figure S5.3.31. *$^{11}B\{^1H\}$ NMR spectrum of* ***BB2F*** *(160 MHz and 96 MHz, in $CDCl_3$).*

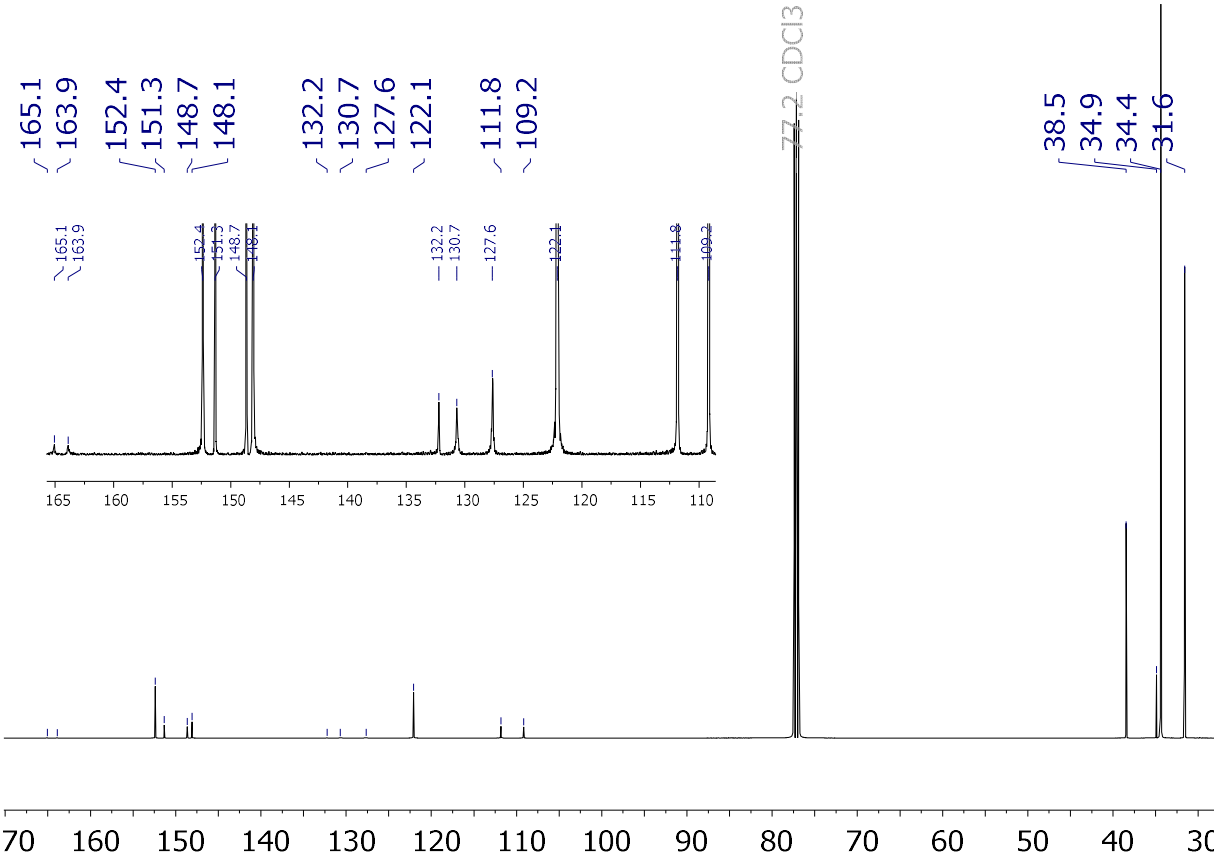

Figure S5.3.32. *$^{13}C\{^1H\}$ NMR spectrum of* ***BB2F*** *(126 MHz, in $CDCl_3$).*

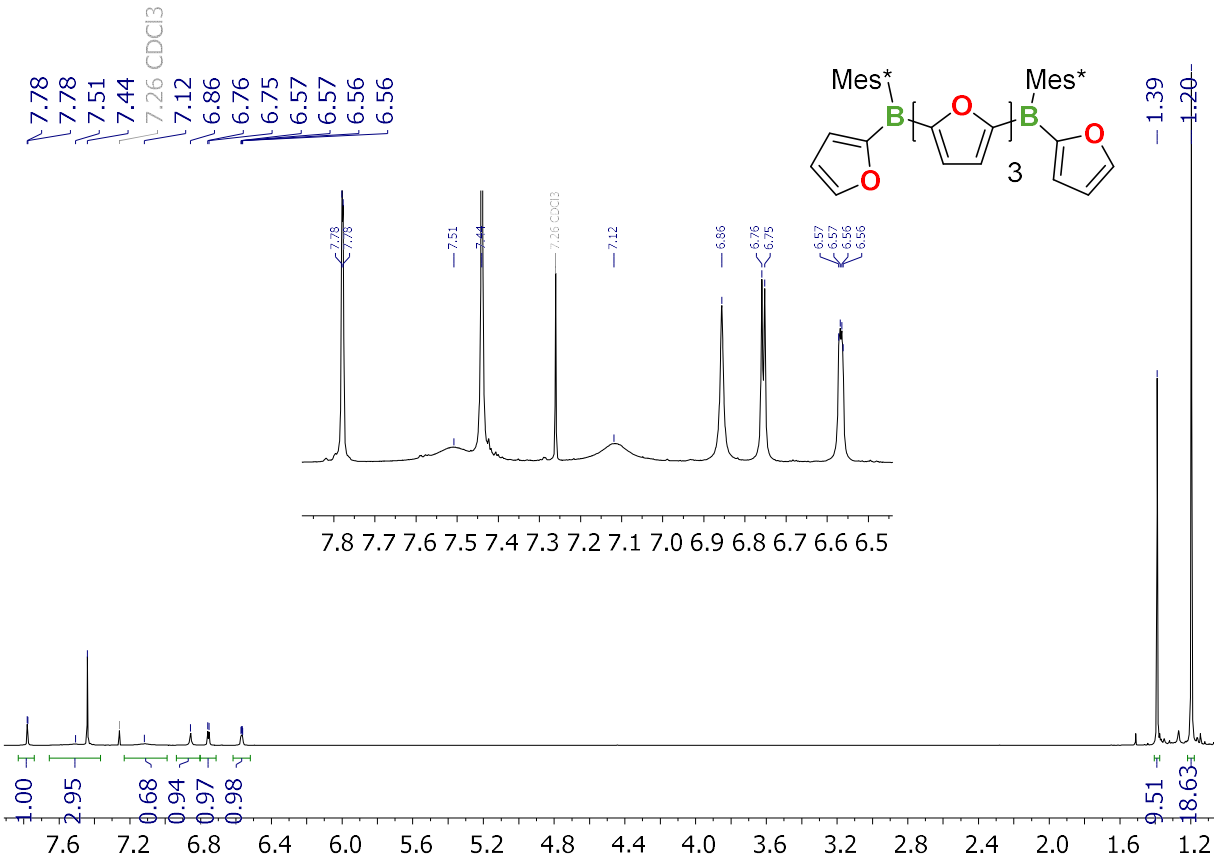

Figure S5.3.33. *^{1}H NMR spectrum of **BB3F** (500 MHz, in $CDCl_3$).*

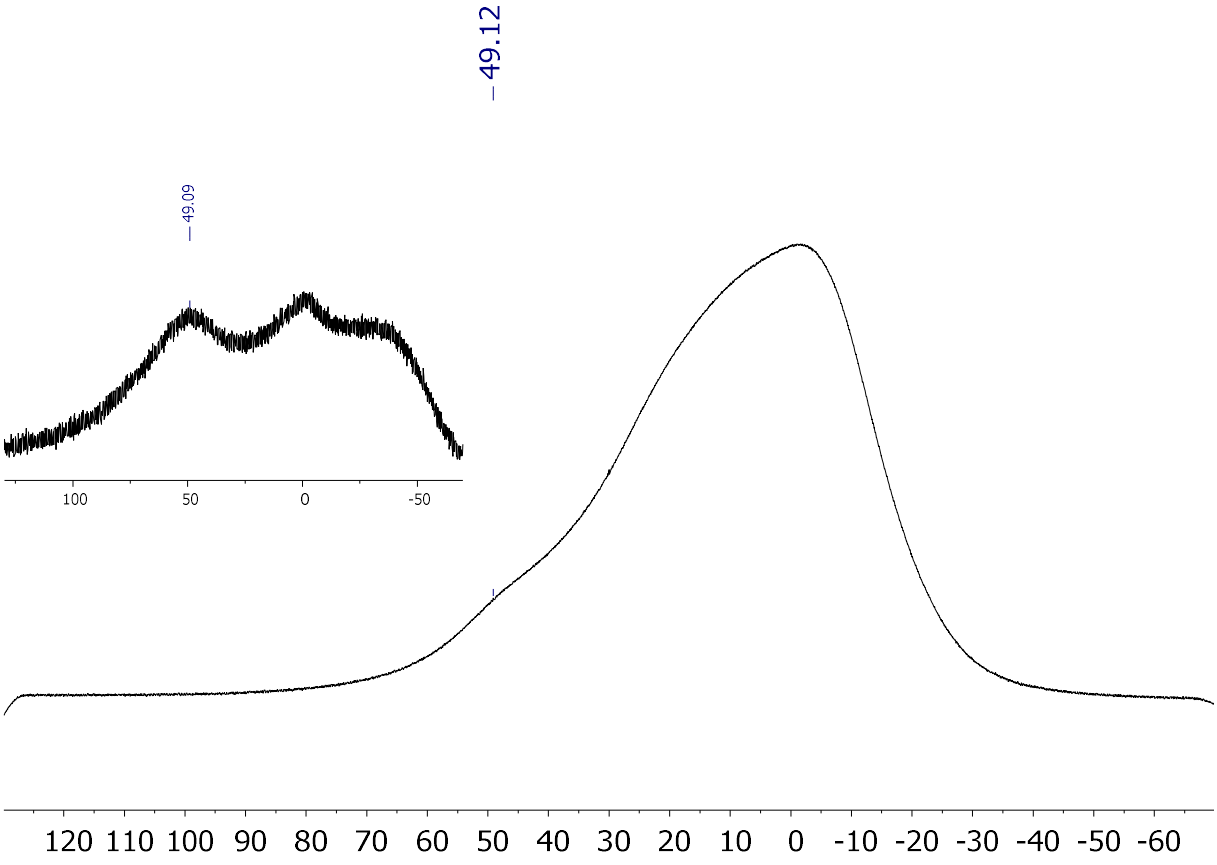

Figure S5.3.34. *$^{11}B\{^{1}H\}$ NMR spectrum of **BB3F** (160 MHz and 96 MHz, in $CDCl_3$).*

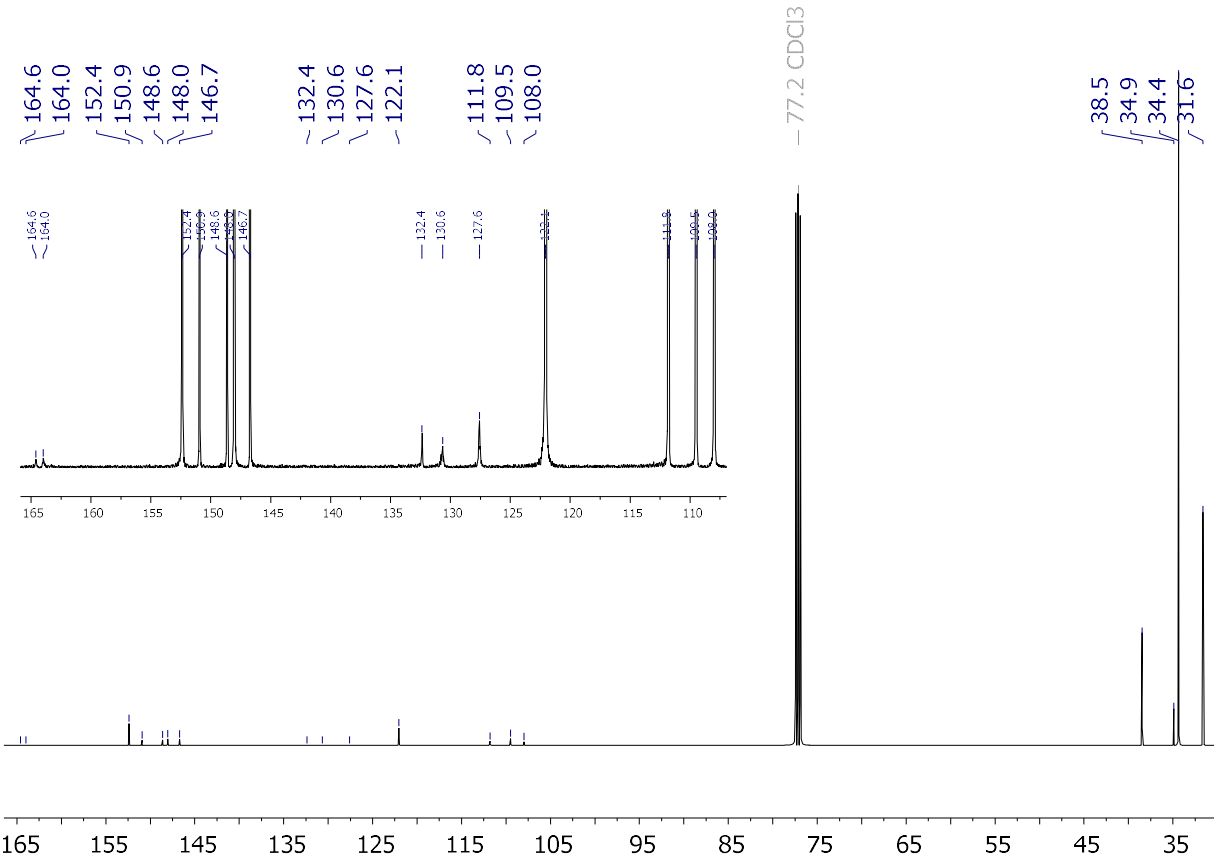

Figure S5.3.35. *$^{13}C\{^{1}H\}$ NMR spectrum of* ***BB3F*** *(126 MHz, in $CDCl_3$).*

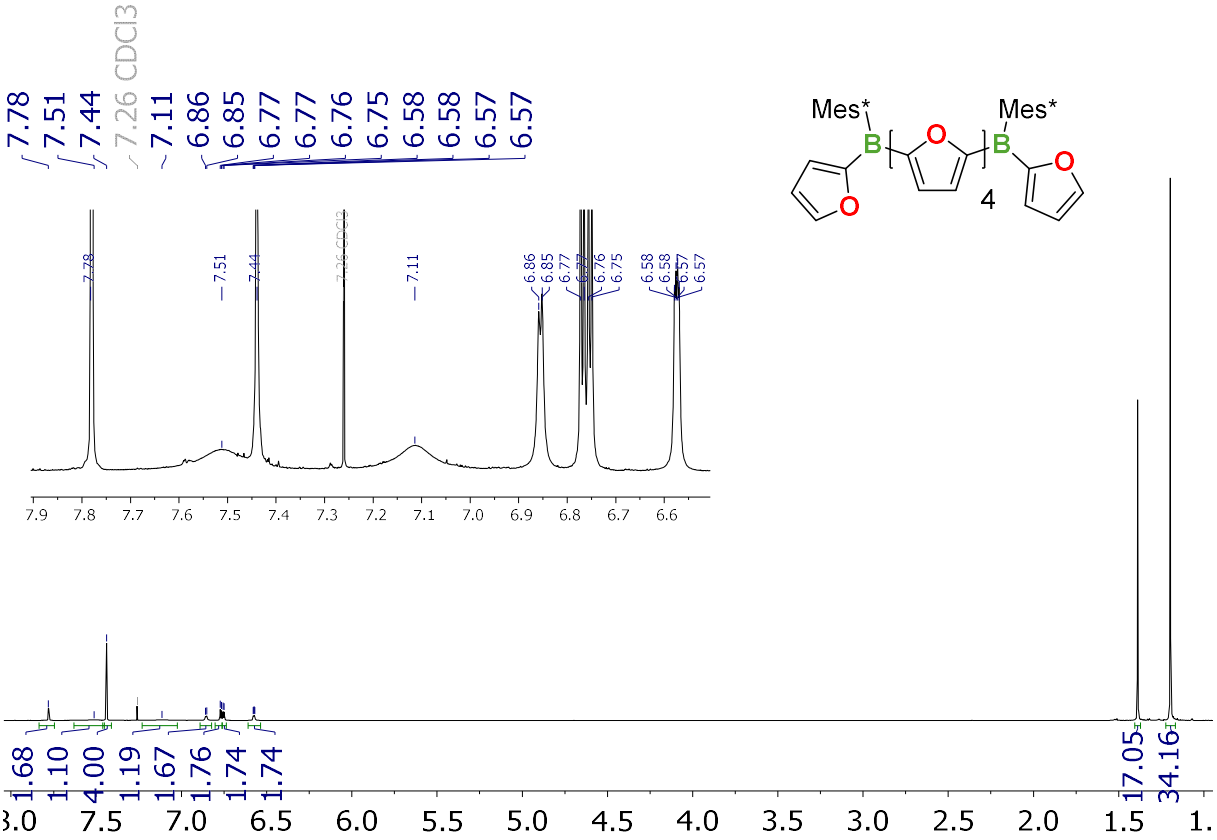

Figure S5.3.36. *^{1}H NMR spectrum of* ***BB4F*** *(500 MHz, in $CDCl_3$).*

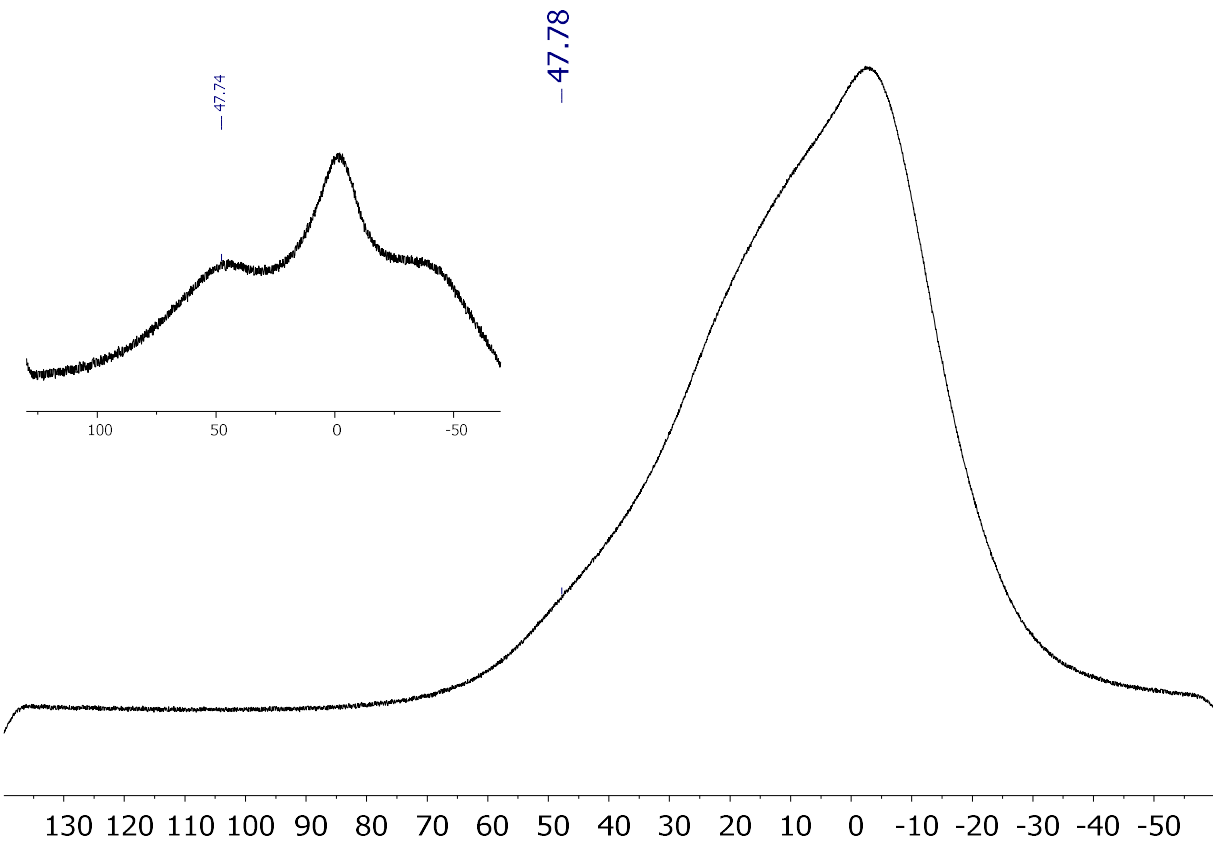

Figure S5.3.37. *$^{11}B\{^1H\}$ NMR spectrum of* ***BB4F*** *(160 MHz and 96 MHz, in $CDCl_3$).*

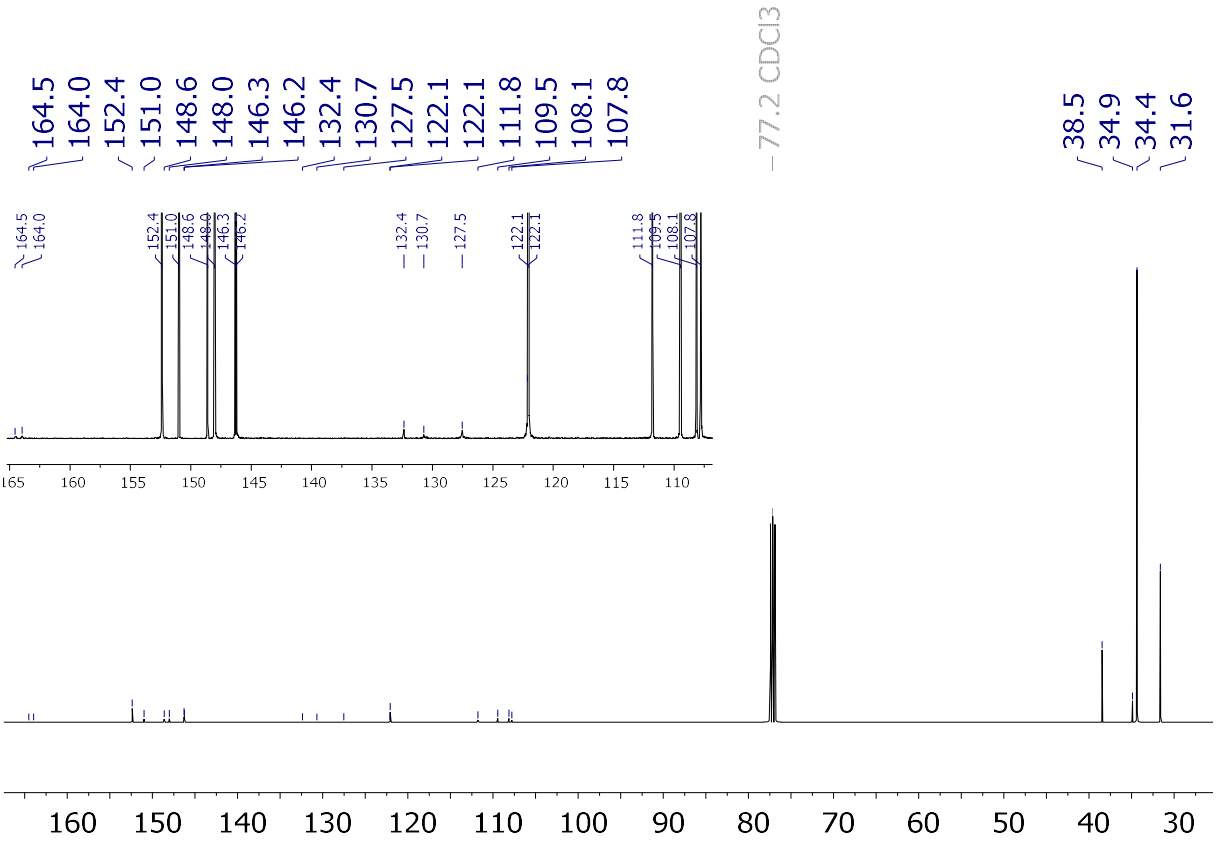

Figure S5.3.38. *$^{13}C\{^1H\}$ NMR spectrum of* ***BB4F*** *(126 MHz, in $CDCl_3$).*

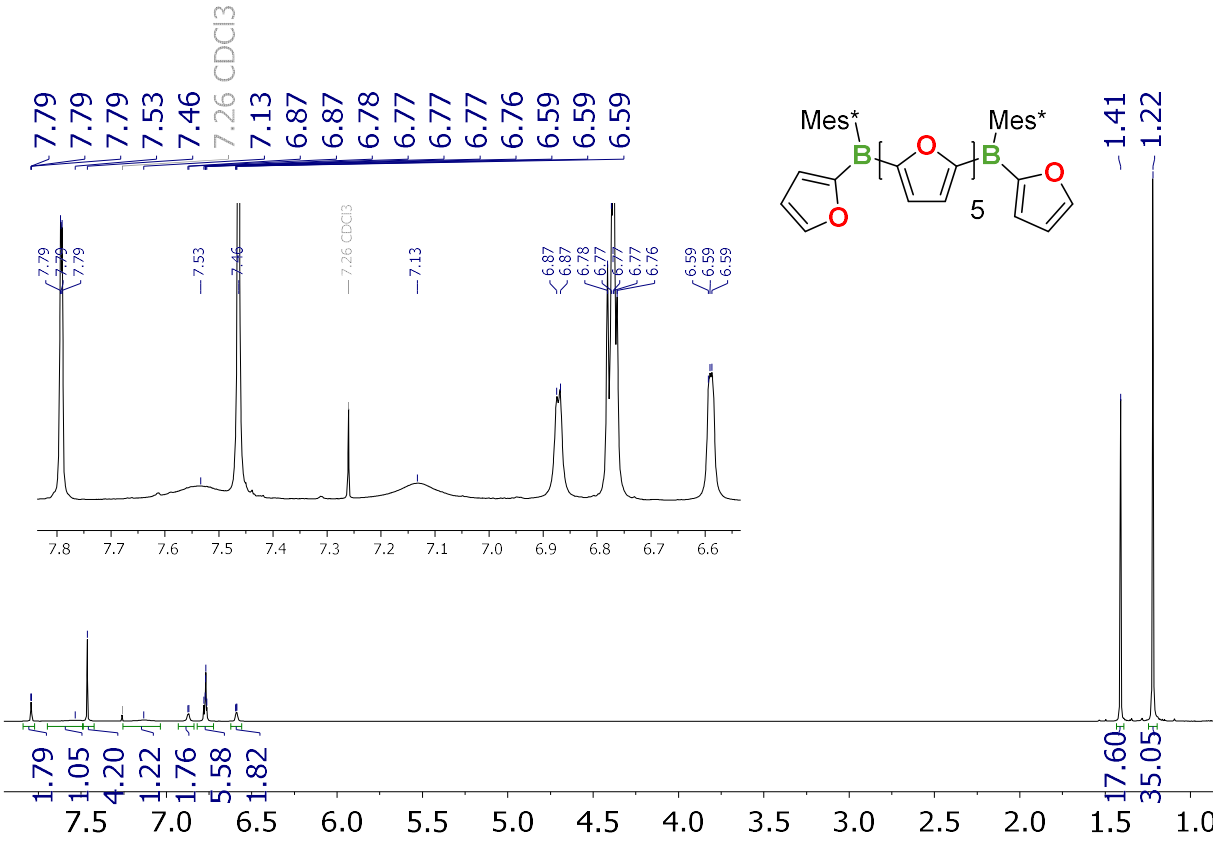

Figure S5.3.39. *^{1}H NMR spectrum of* ***BB5F*** *(500 MHz, in $CDCl_3$).*

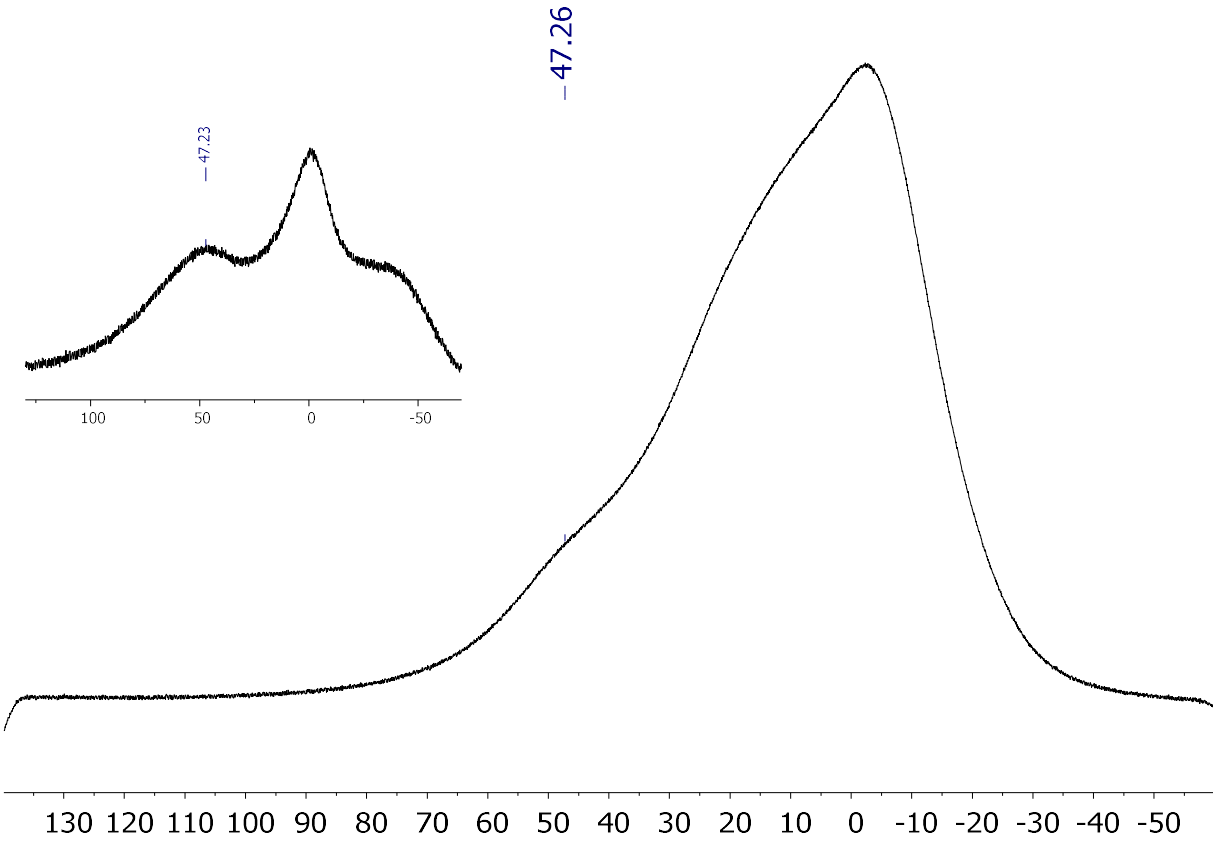

Figure S5.3.40. *$^{11}B\{^{1}H\}$ NMR spectrum of* ***BB5F*** *(160 MHz and 96 MHz, in $CDCl_3$).*

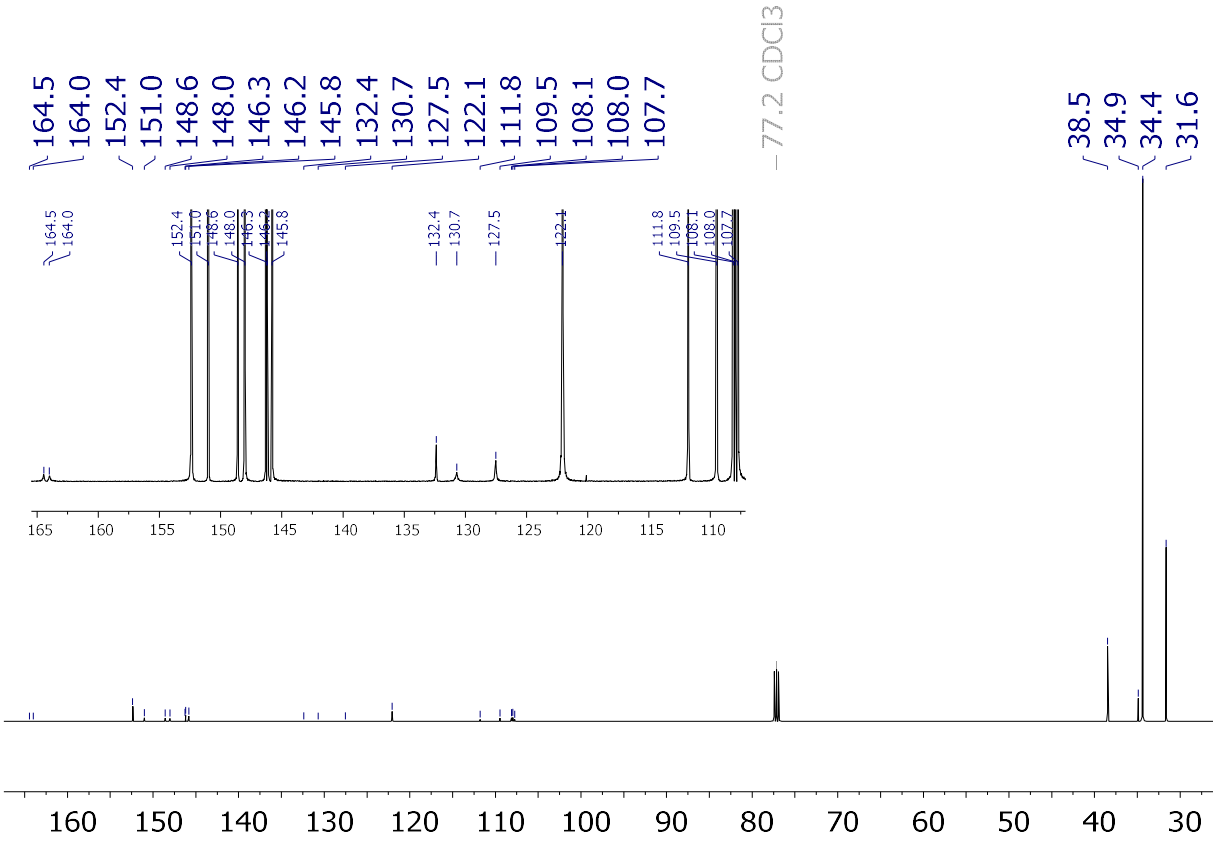

Figure S5.3.41. *$^{13}C\{^{1}H\}$ NMR spectrum of* ***BB5F*** *(126 MHz, in $CDCl_3$).*

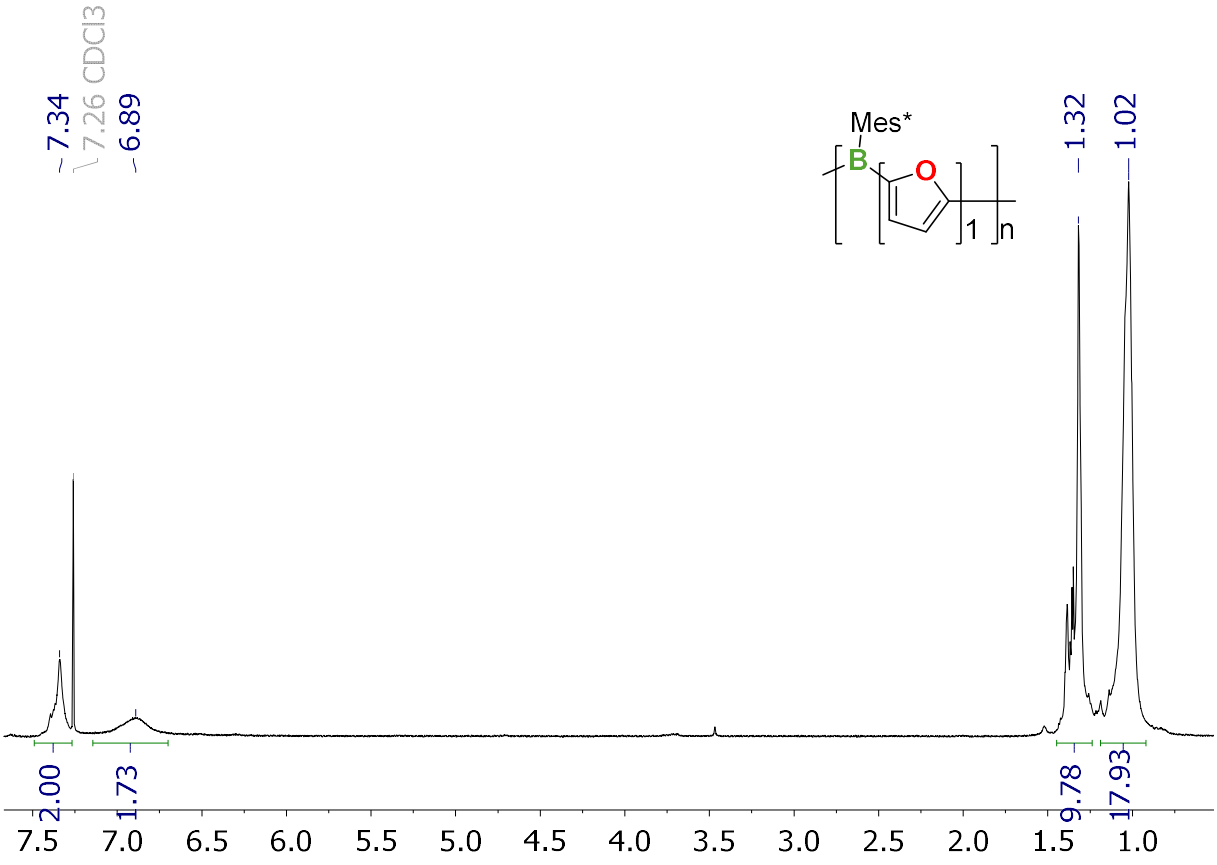

Figure S5.3.42. *^{1}H NMR spectrum of* ***PB1F*** *(300 MHz, in $CDCl_3$).*

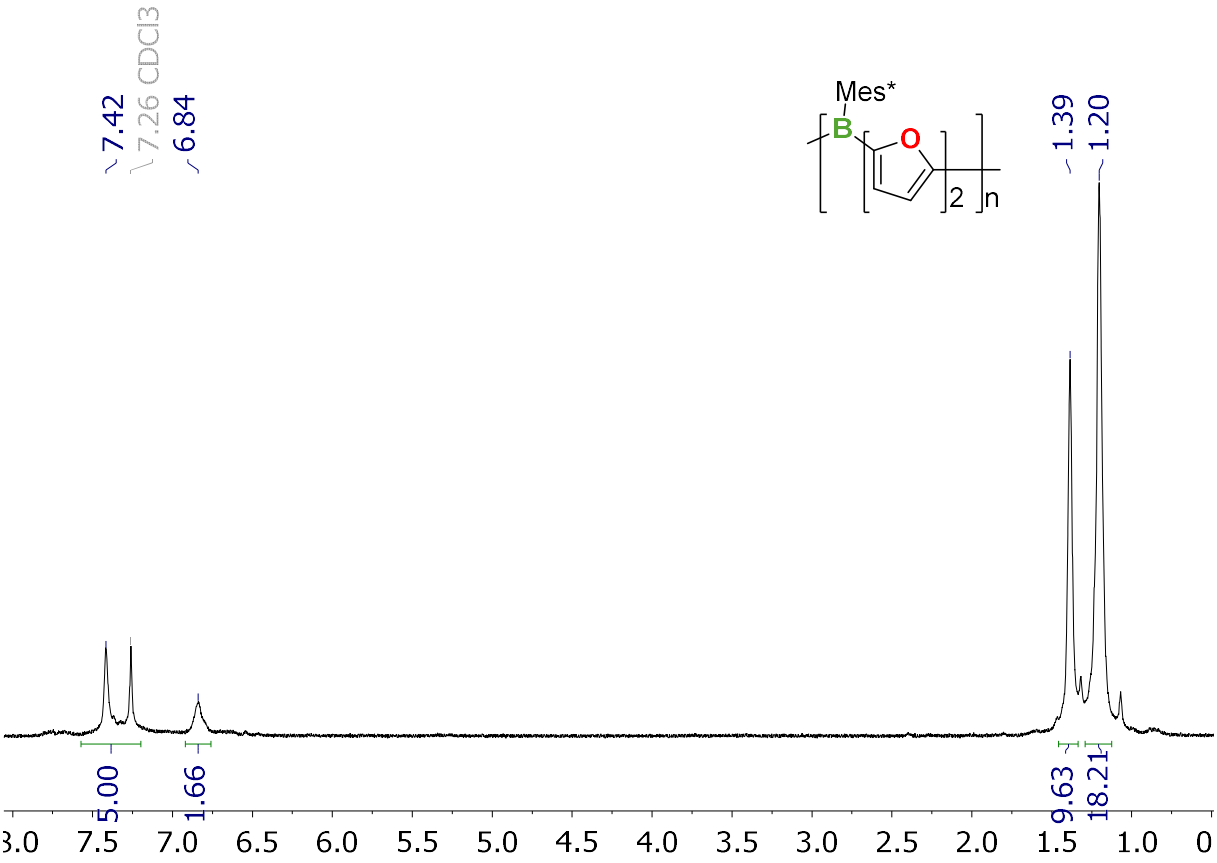

Figure S5.3.43. *^{1}H NMR spectrum of **PB2F** (300 MHz, in $CDCl_3$).*

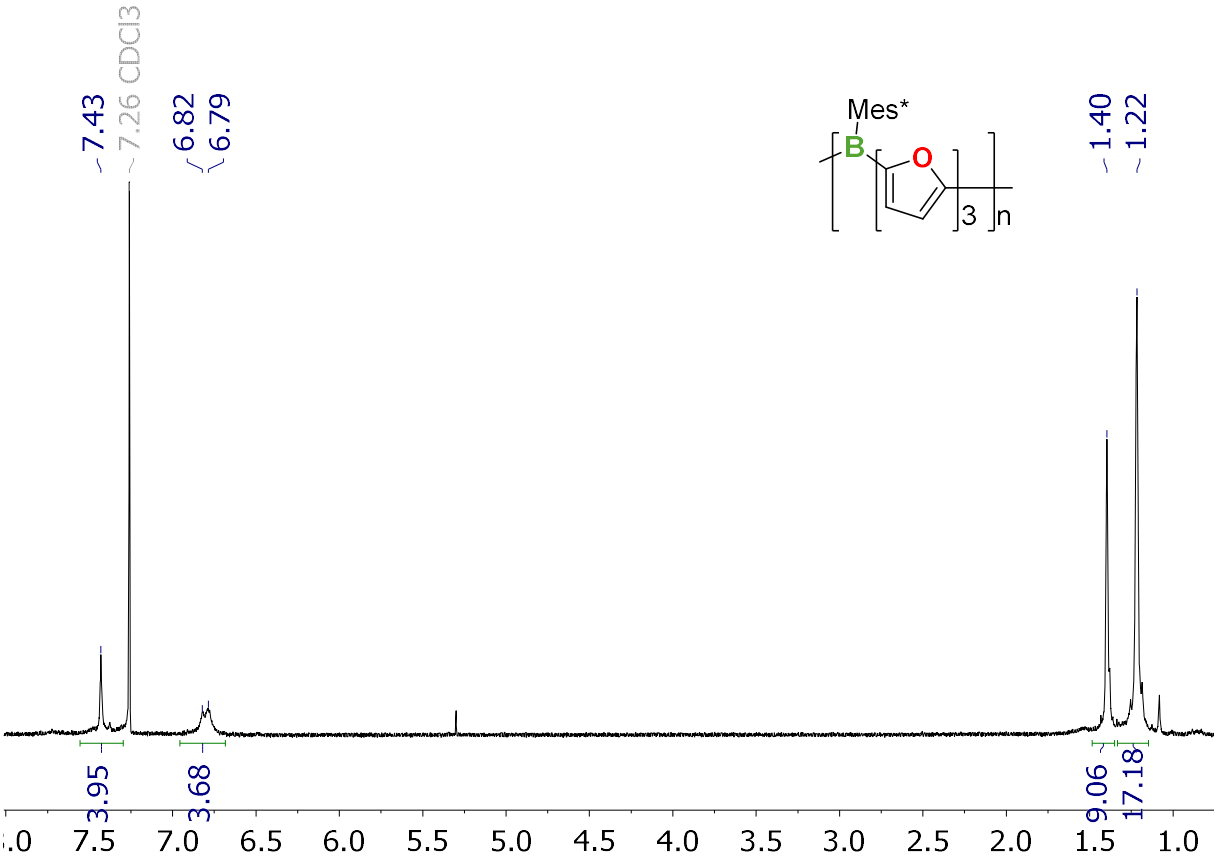

Figure S5.3.44. *^{1}H NMR spectrum of **PB3F** (300 MHz, in $CDCl_3$).*

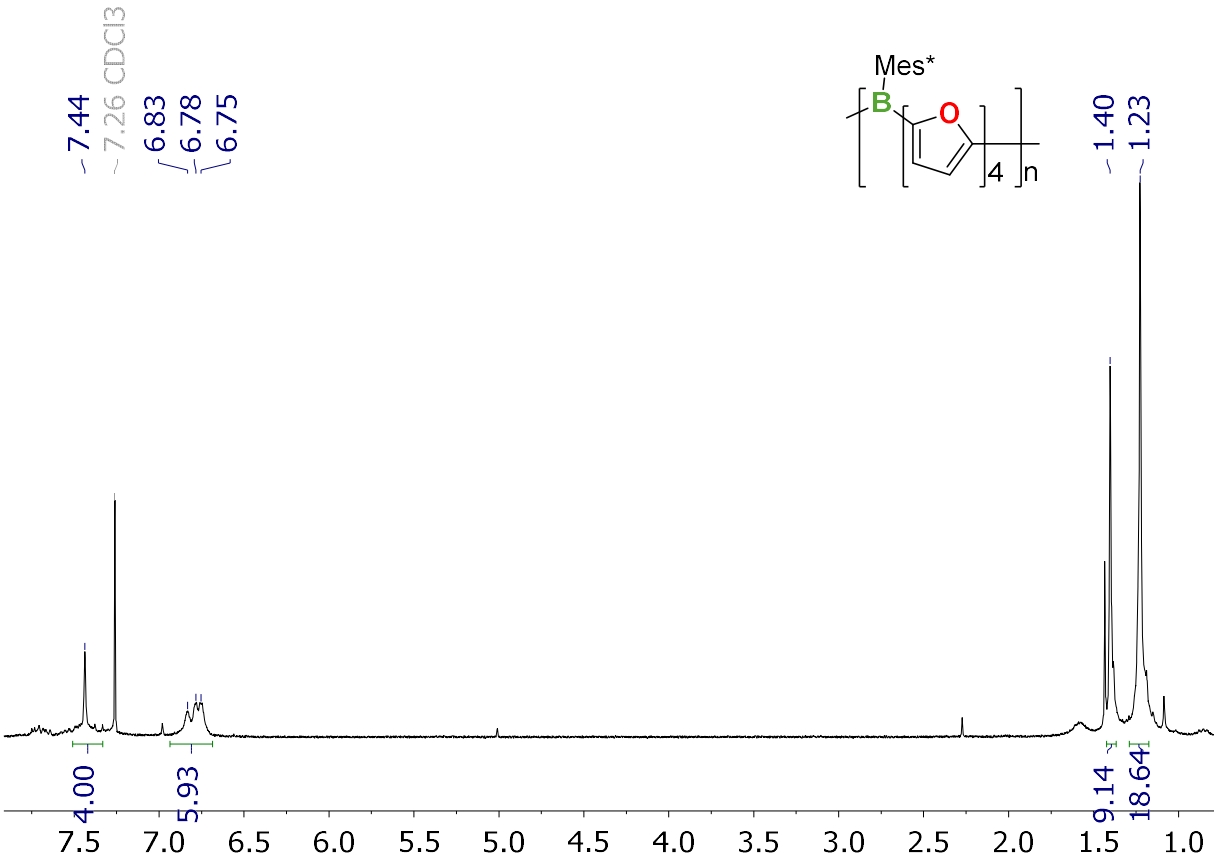

Figure S5.3.45. *^{1}H NMR spectrum of **PB4F** (300 MHz, in $CDCl_3$).*

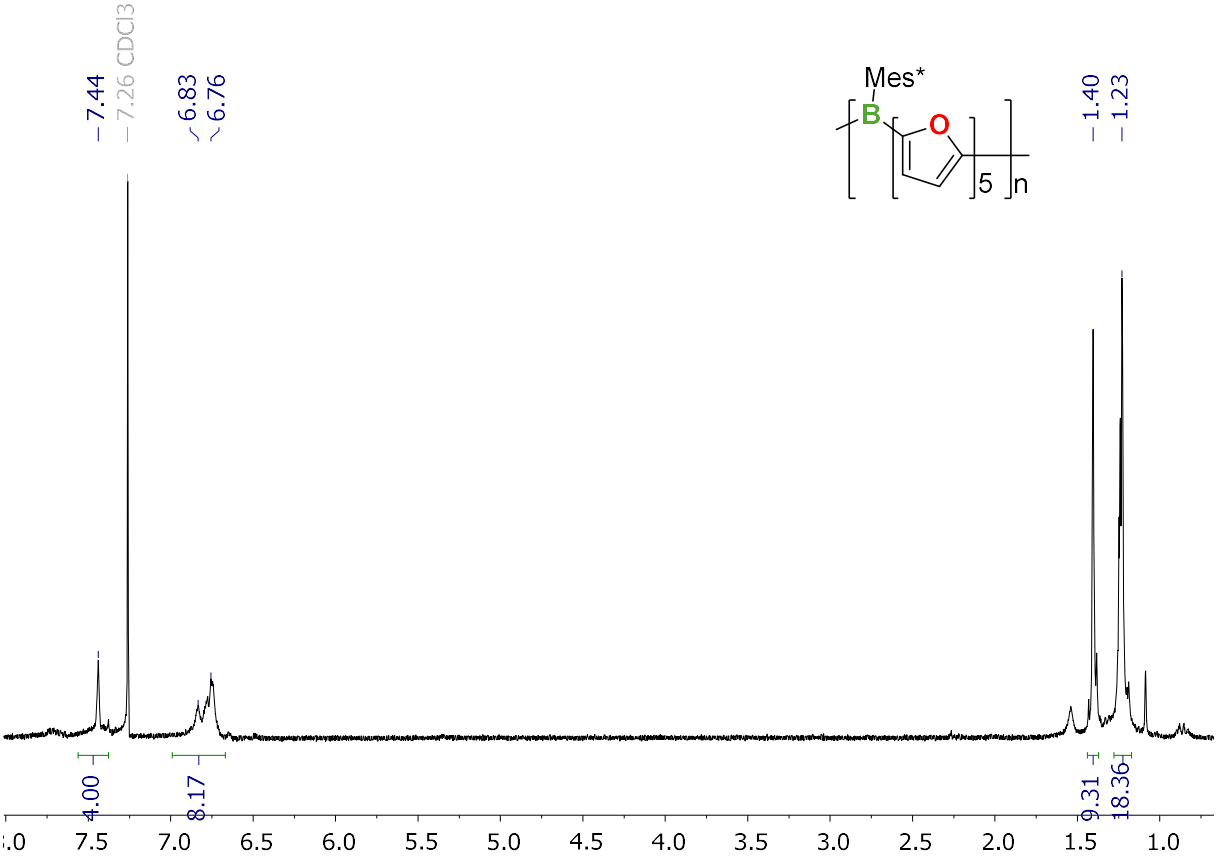

Figure S5.3.46. *^{1}H NMR spectrum of **PB5F** (300 MHz, in $CDCl_3$).*

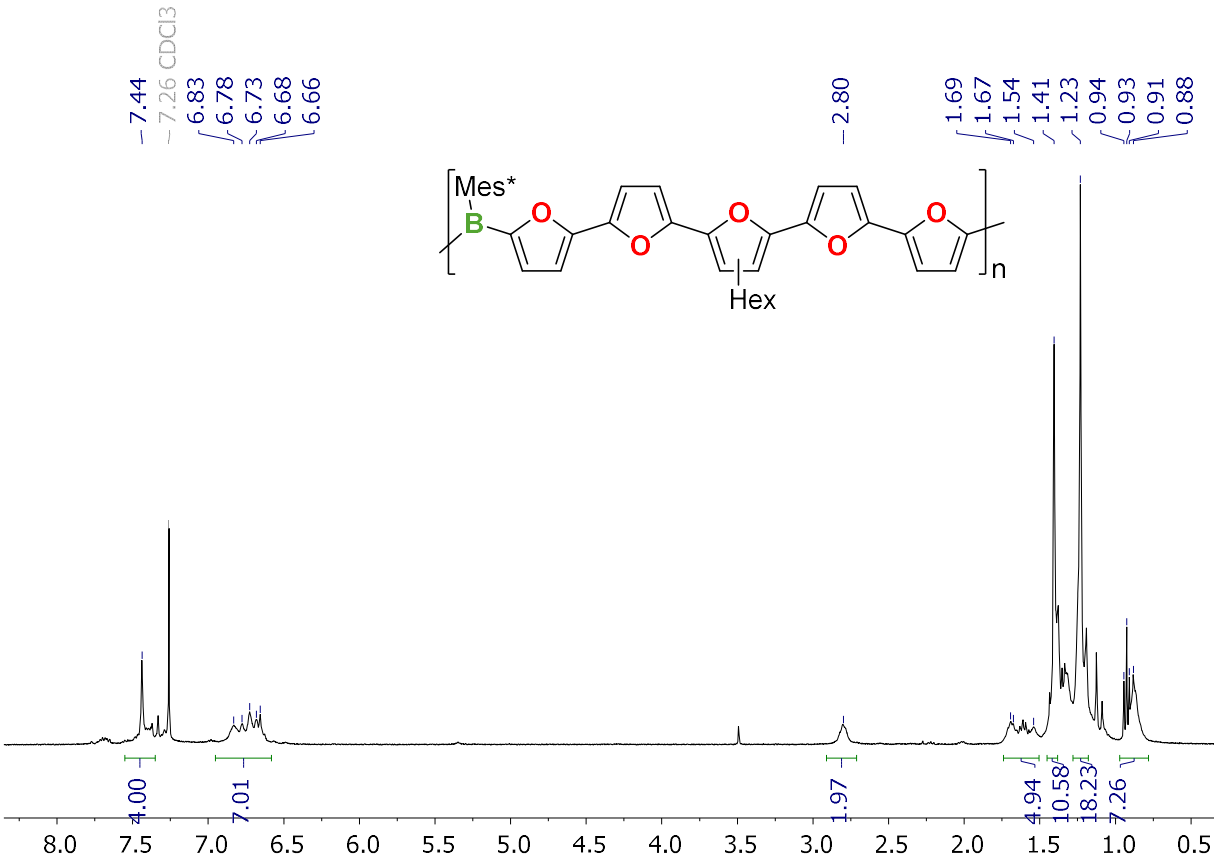

Figure S5.3.47. *^{1}H NMR spectrum of* ***PB5FHex*** *(400 MHz, in $CDCl_3$).*

UV-VIS spectra

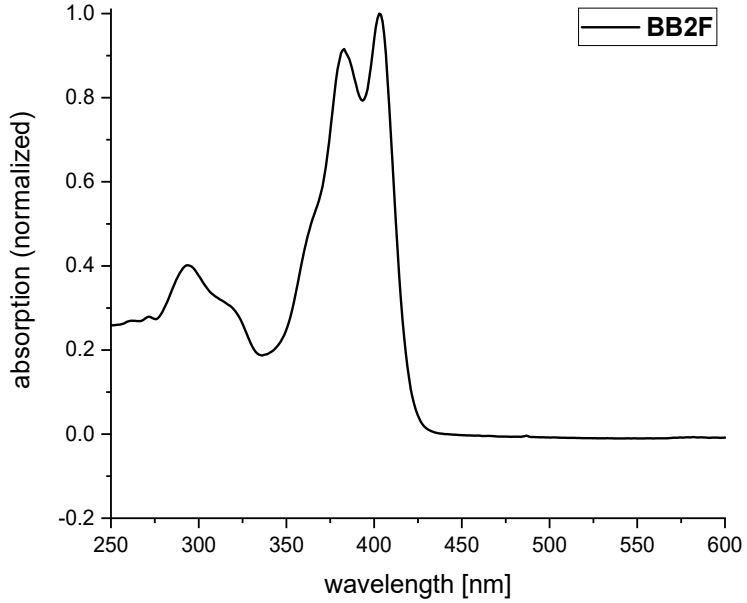

Figure S5.3.48. *UV-Vis spectrum of* ***BB2F*** *(in THF).*

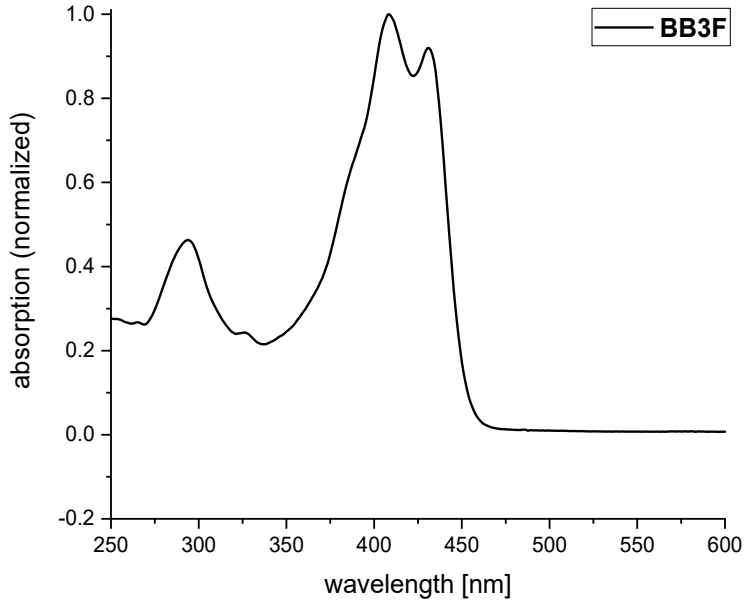

Figure S5.3.49. *UV-Vis spectrum of* ***BB3F*** *(in THF).*

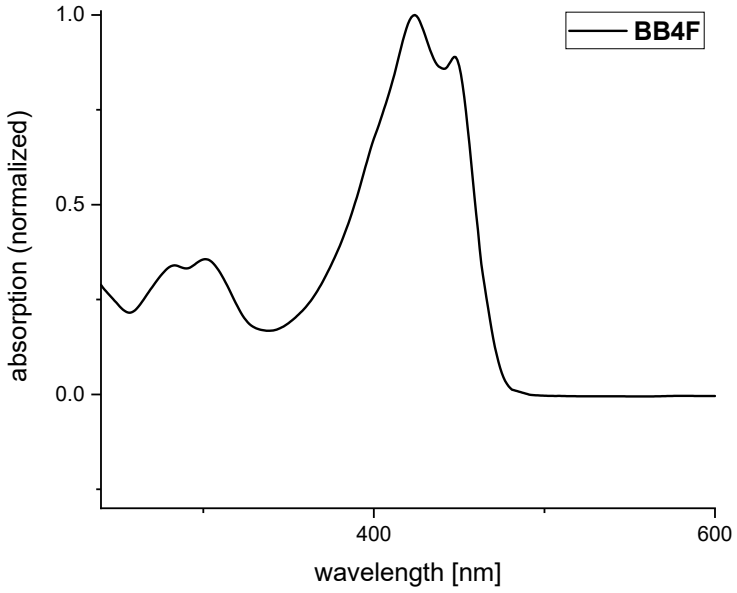

Figure S5.3.50. *UV-Vis spectrum of* ***BB4F*** *(in THF).*

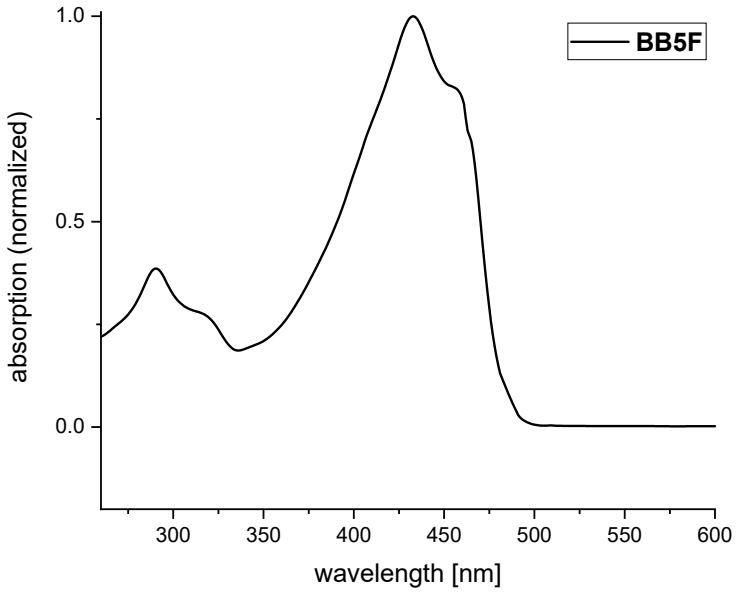

Figure S5.3.51. *UV-Vis spectrum of* ***BB5F*** *(in THF).*

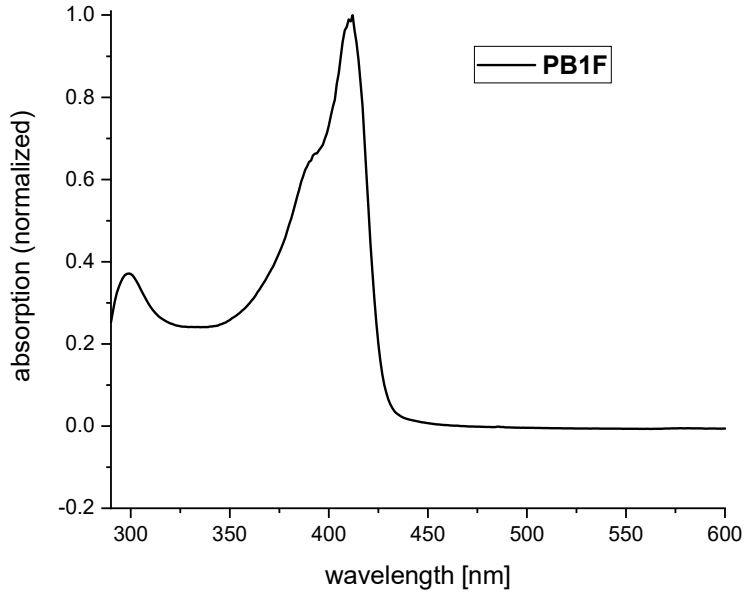

Figure S5.3.52. *UV-Vis spectrum of* ***PB1F*** *(in THF).*

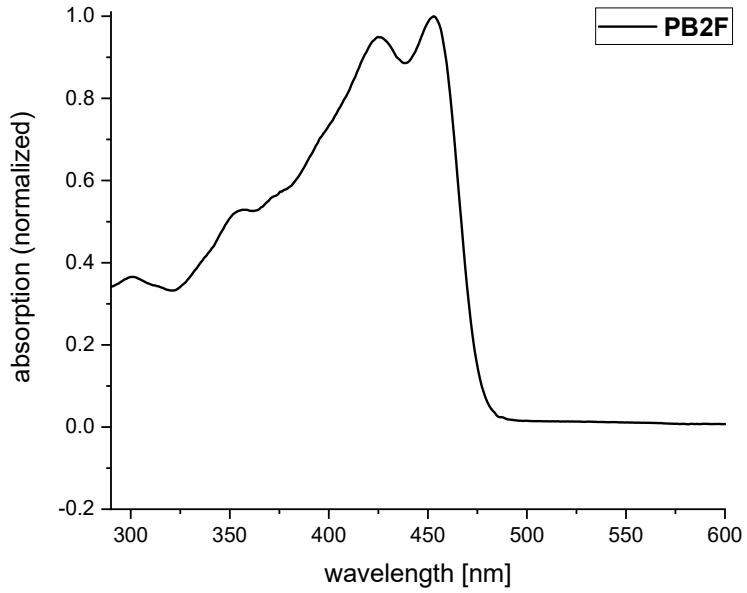

Figure S5.3.53. *UV-Vis spectrum of* ***PB2F*** *(in THF).*

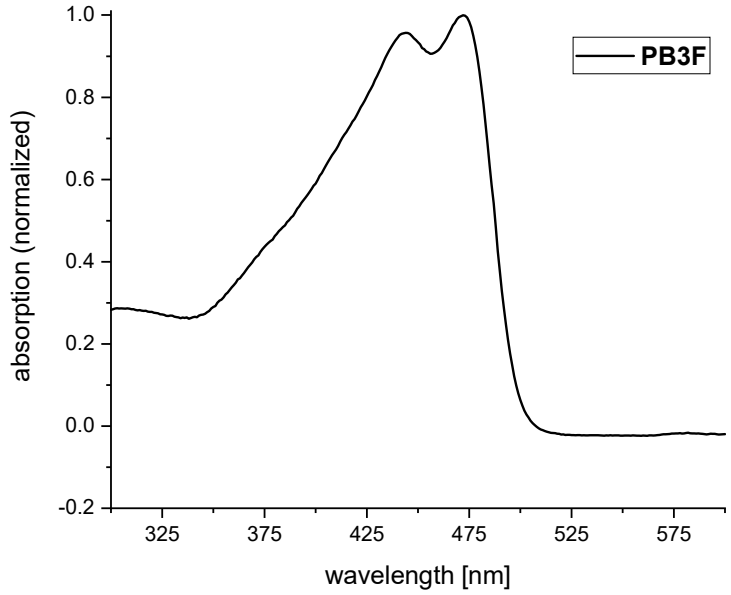

Figure S5.3.54. *UV-Vis spectrum of* ***PB3F*** *(in THF).*

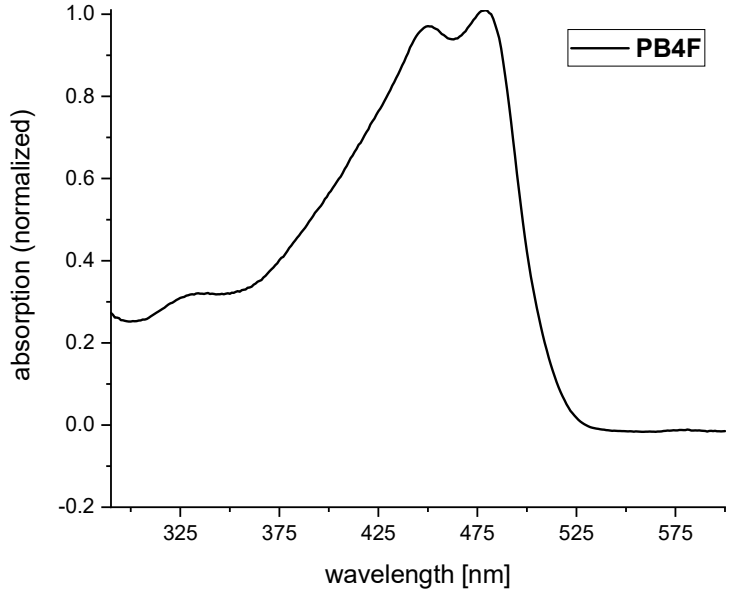

Figure S5.3.55. *UV-Vis spectrum of* ***PB4F*** *(in THF).*

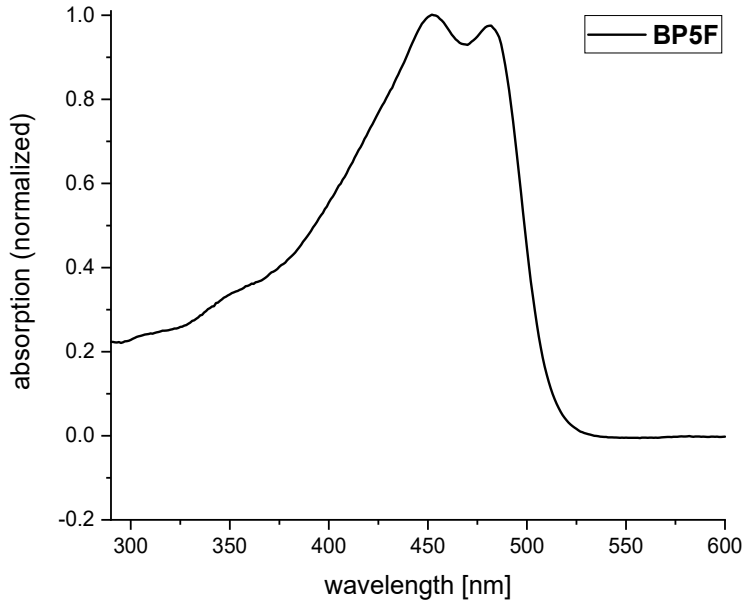

Figure S5.3.56. *UV-Vis spectrum of* ***PB5F*** *(in THF).*

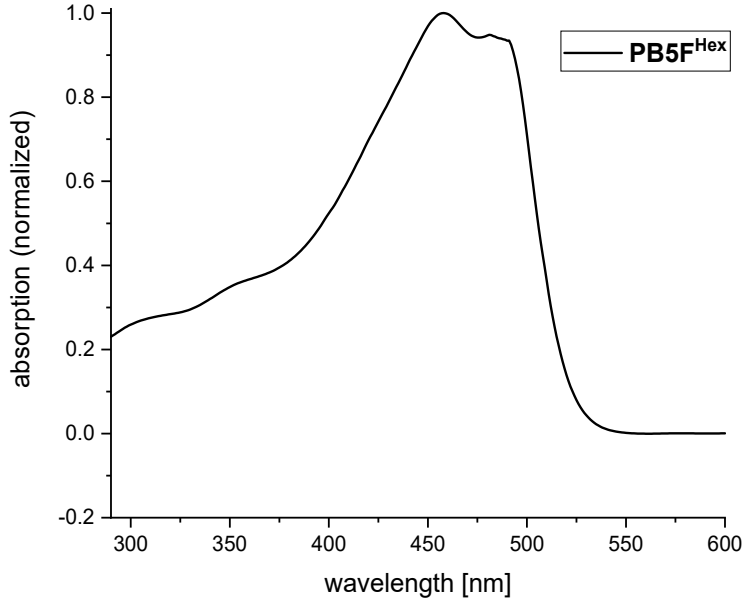

Figure S5.3.57. *UV-Vis spectrum of* ***PB5F^{Hex}*** *(in THF).*

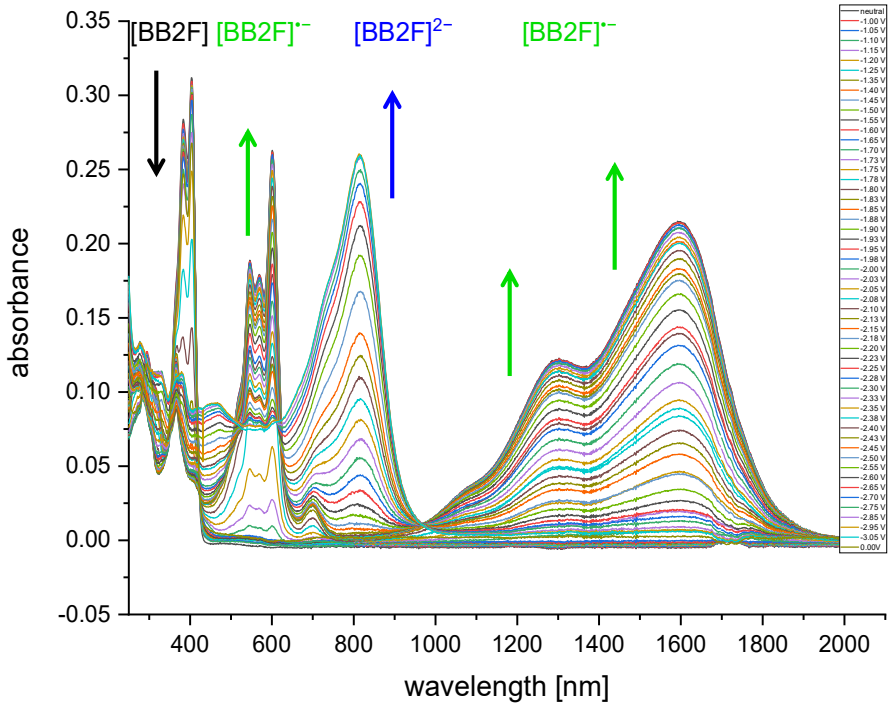

Figure S5.3.58. *Changes in UV-vis in spectroelectrochemical investigations of* ***BB2F*** *(potential vs. Ag/AgCl in THF).*

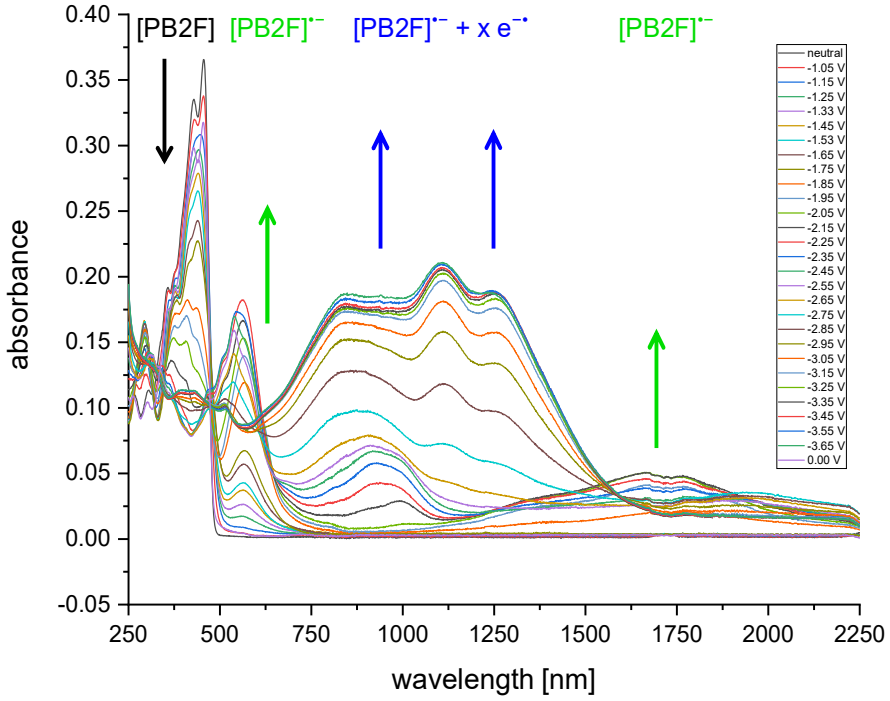

Figure S5.3.59. *Changes in UV-vis in spectroelectrochemical investigations of* ***PB2F*** *(potential vs. Ag/AgCl in THF).*

Fluorescence spectra

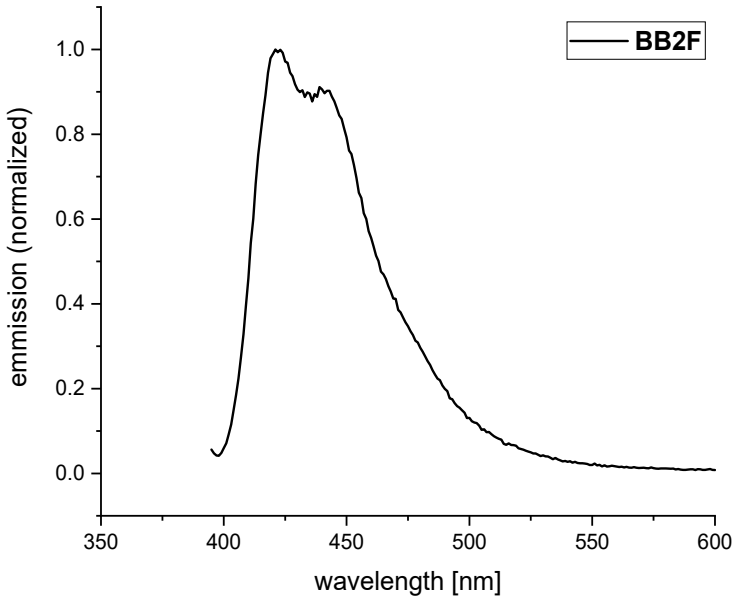

Figure S5.3.60. *Fluorescence spectrum of* ***BB2F*** *(in THF).*

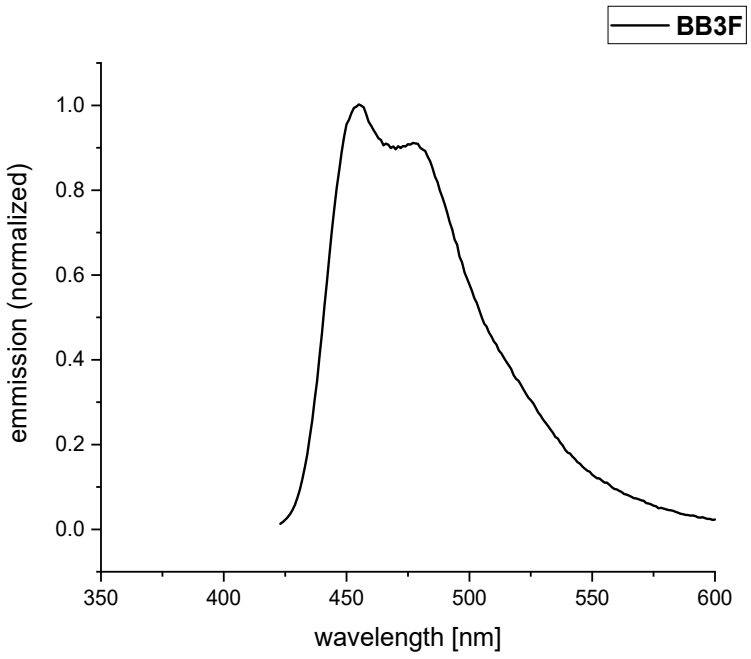

Figure S5.3.61. *Fluorescence spectrum of* ***BB3F*** *(in THF).*

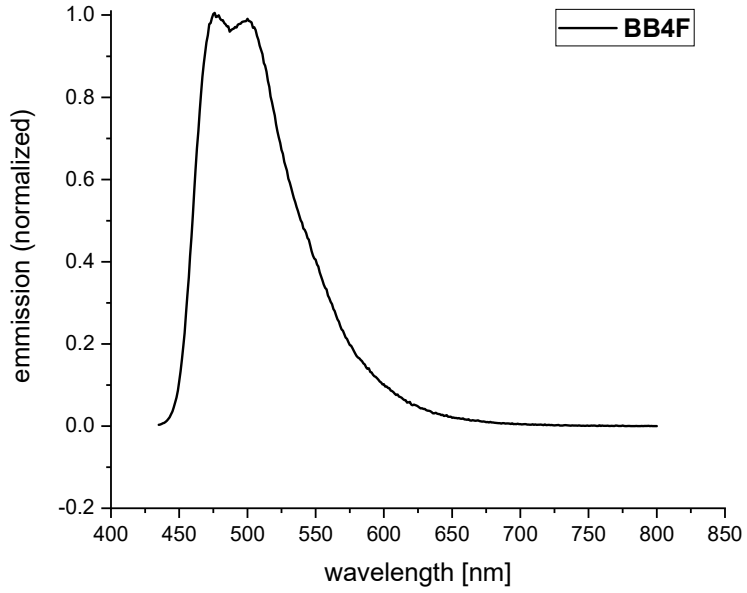

Figure S5.3.62. *Fluorescence spectrum of* ***BB4F*** *(in THF).*

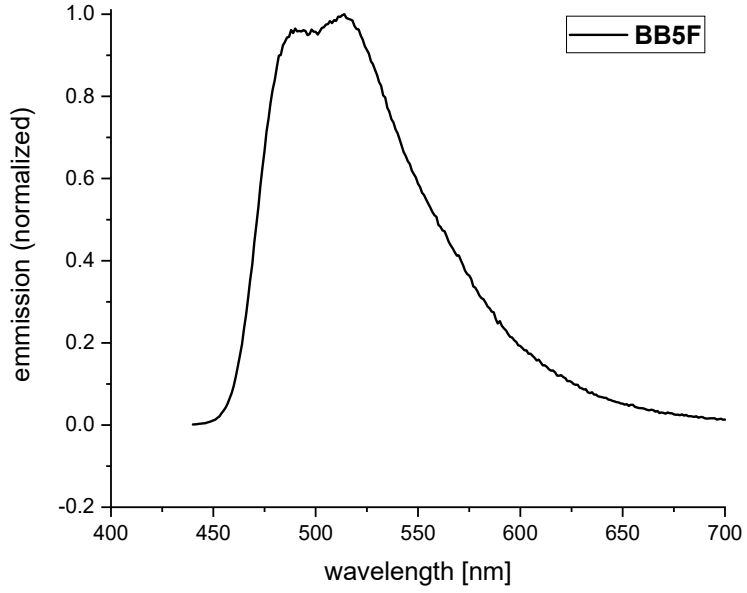

Figure S5.3.63. *Fluorescence spectrum of* ***BB5F*** *(in THF).*

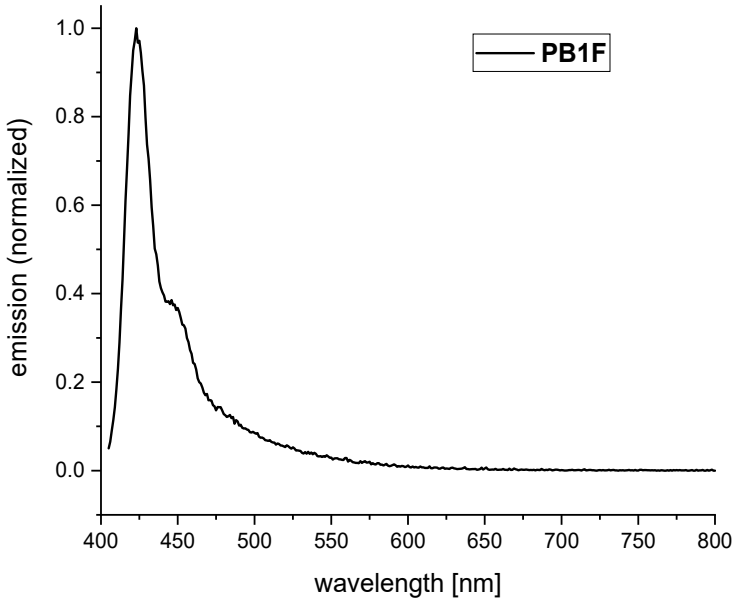

Figure S5.3.64. *Fluorescence spectrum of* ***PB1F*** *(in THF).*

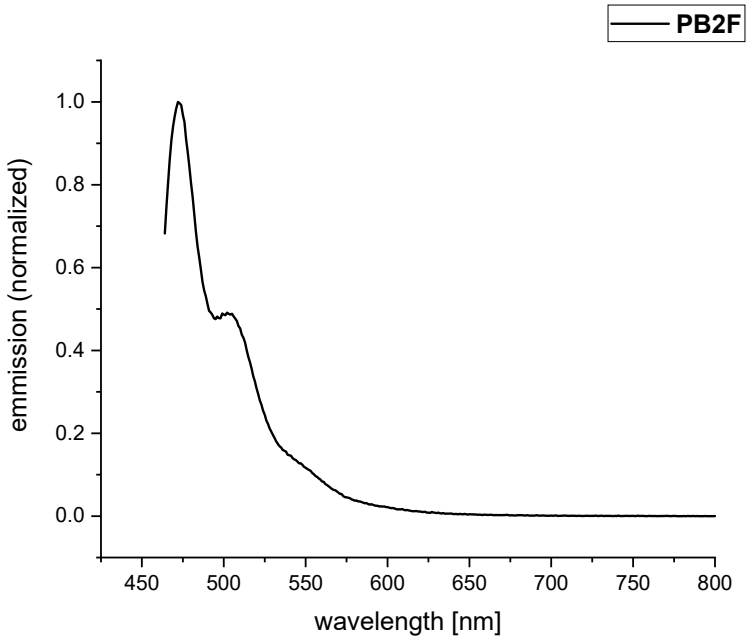

Figure S5.3.65. *Fluorescence spectrum of* ***PB2F*** *(in THF).*

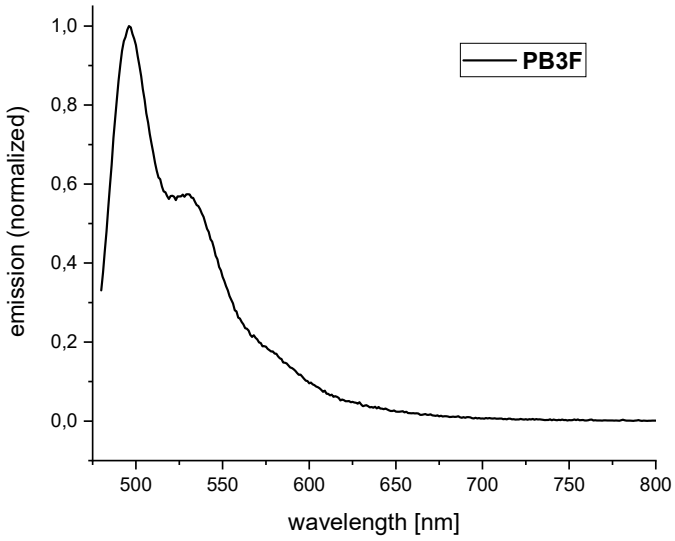

Figure S5.3.66. *Fluorescence spectrum of* ***PB3F*** *(in THF).*

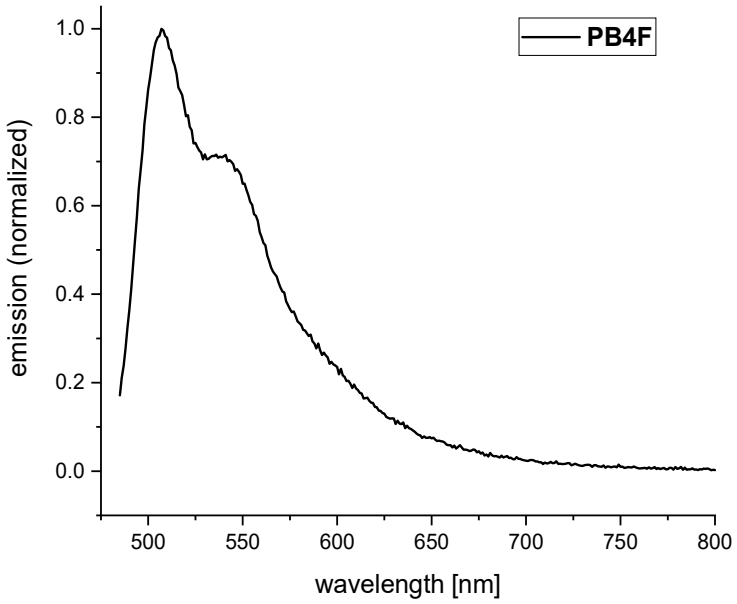

Figure S5.3.67. *Fluorescence spectrum of* ***PB4F*** *(in THF).*

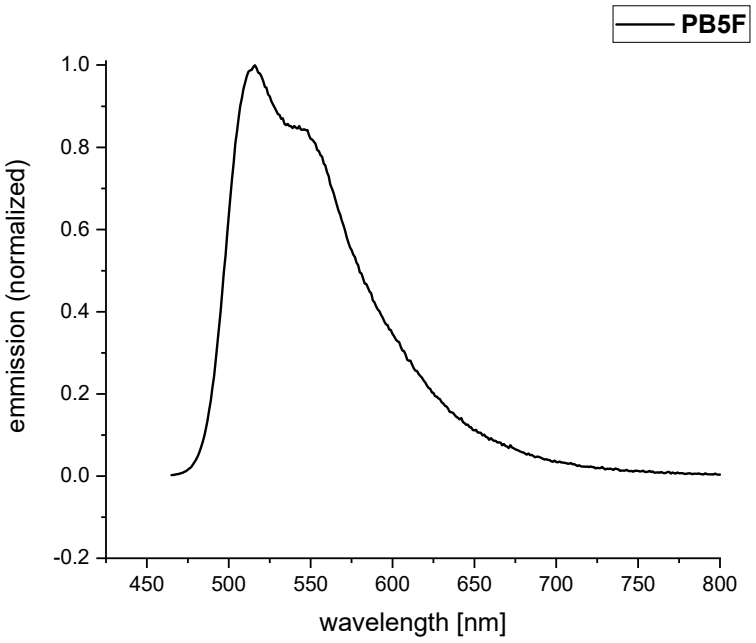

Figure S5.3.68. *Fluorescence spectrum of* ***PB5F*** *(in THF).*

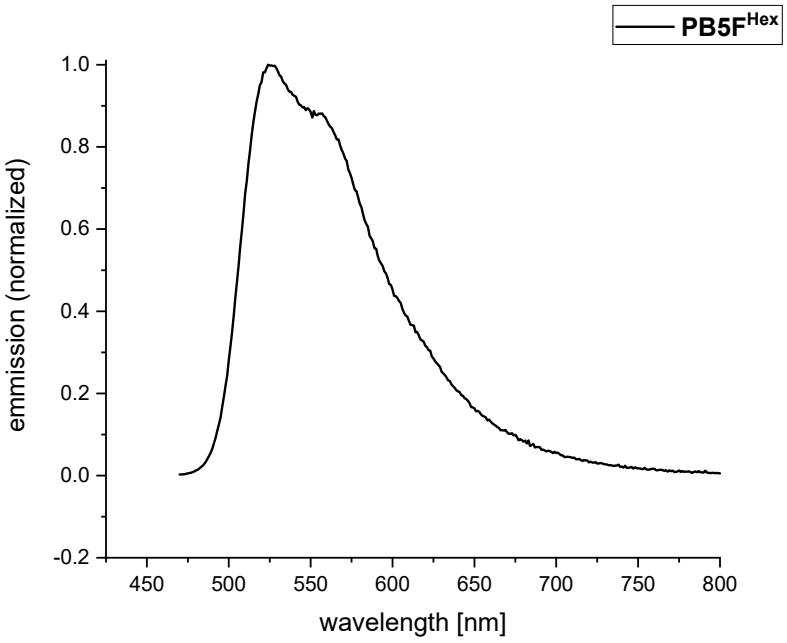

Figure S5.3.69. *Fluorescence spectrum of* ***PB5F^{Hex}*** *(in THF).*

Mass spectra

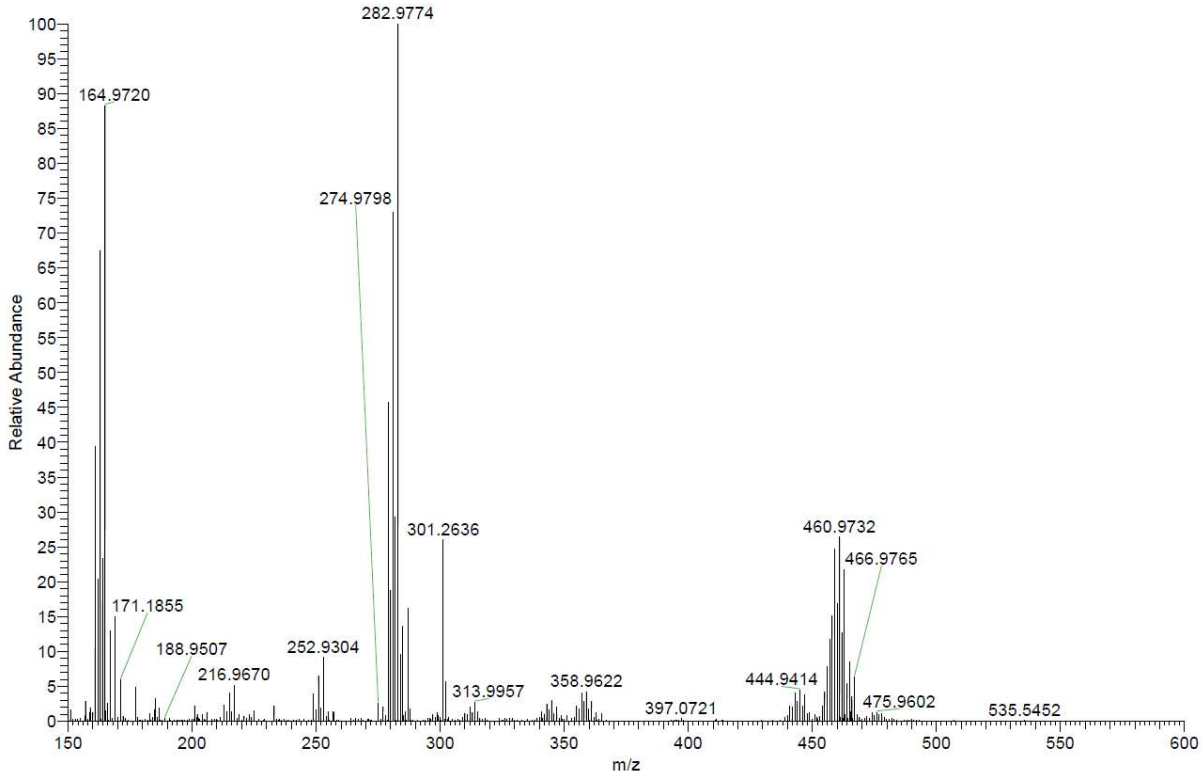

Figure S5.3.70. *HRMS (APCI) spectrum of* ***6b****.*

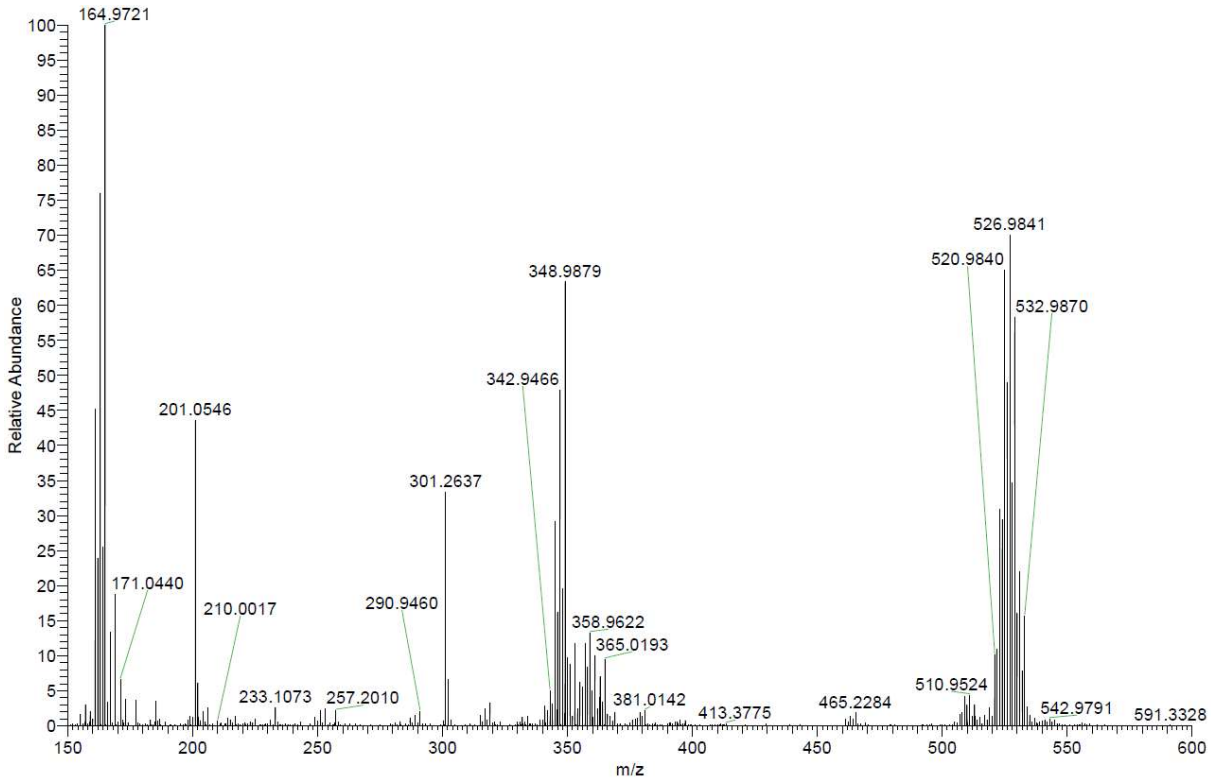

Figure S5.3.71. *HRMS (APCI) spectrum of* ***6c****.*

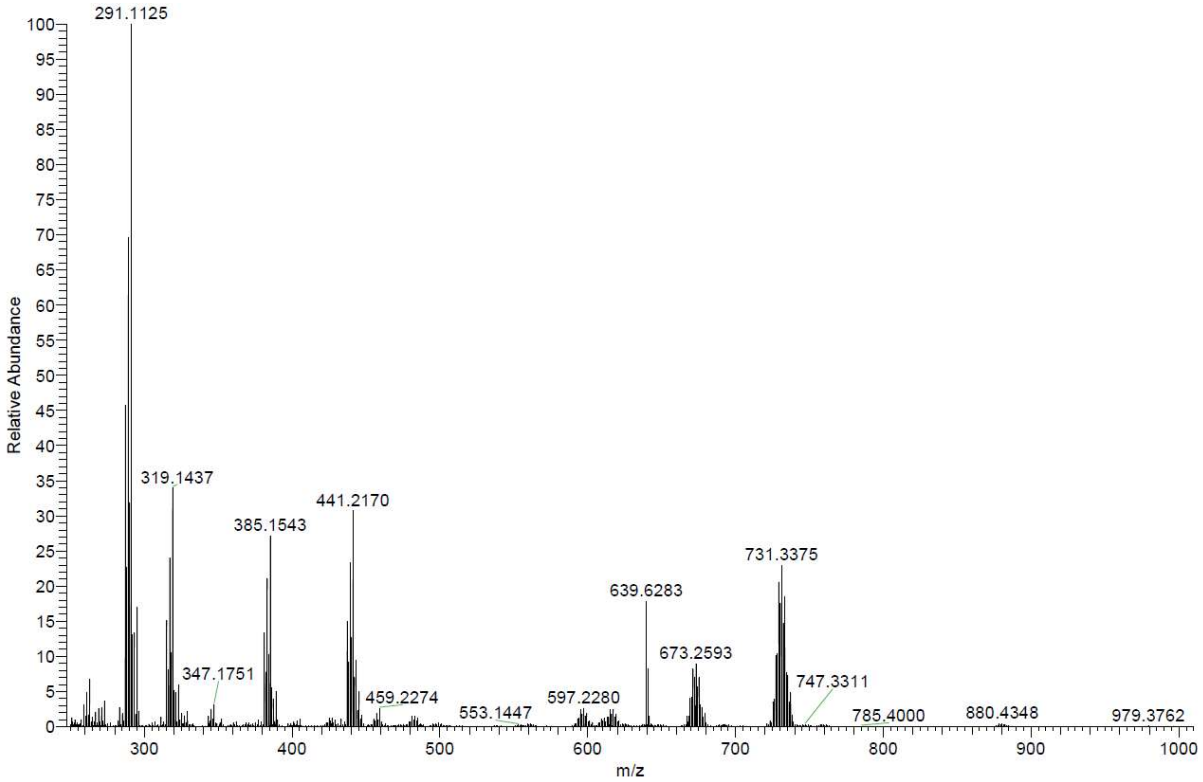

Figure S5.3.72. *HRMS (APCI) spectrum of* ***S5****.*

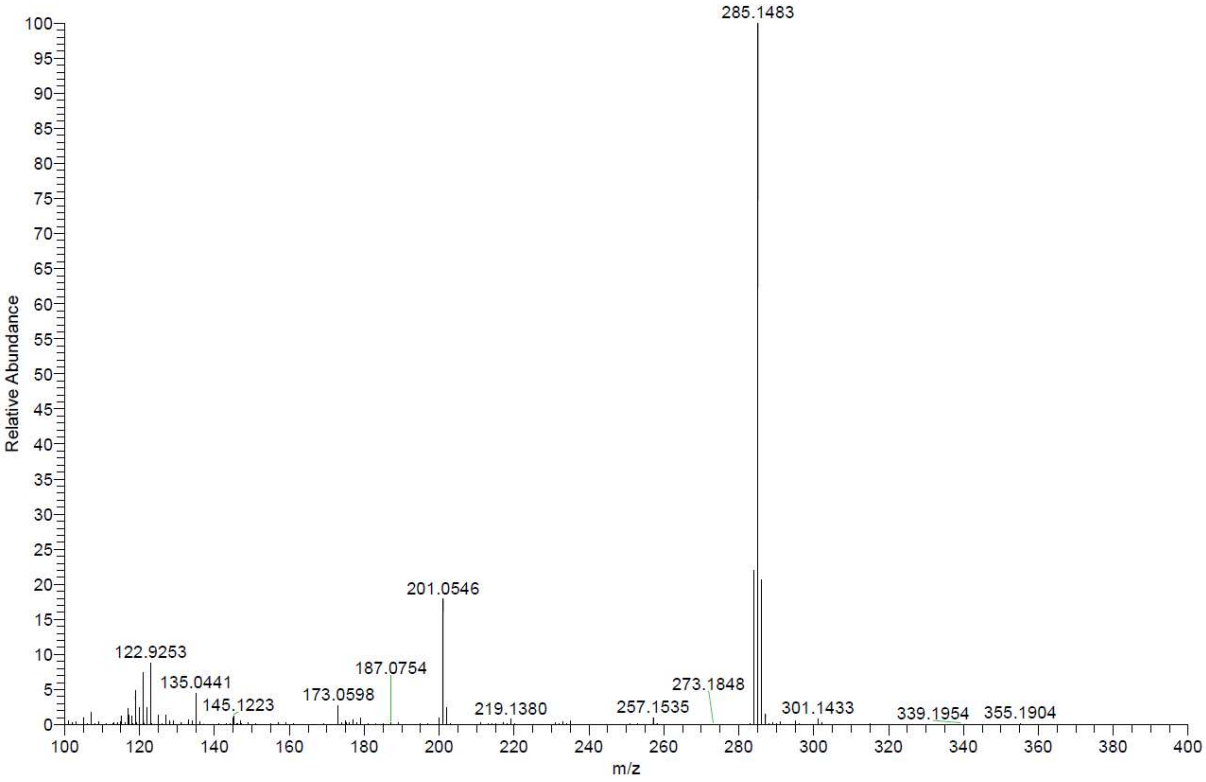

Figure S5.3.73. *HRMS (APCI) spectrum of* ***S6****.*

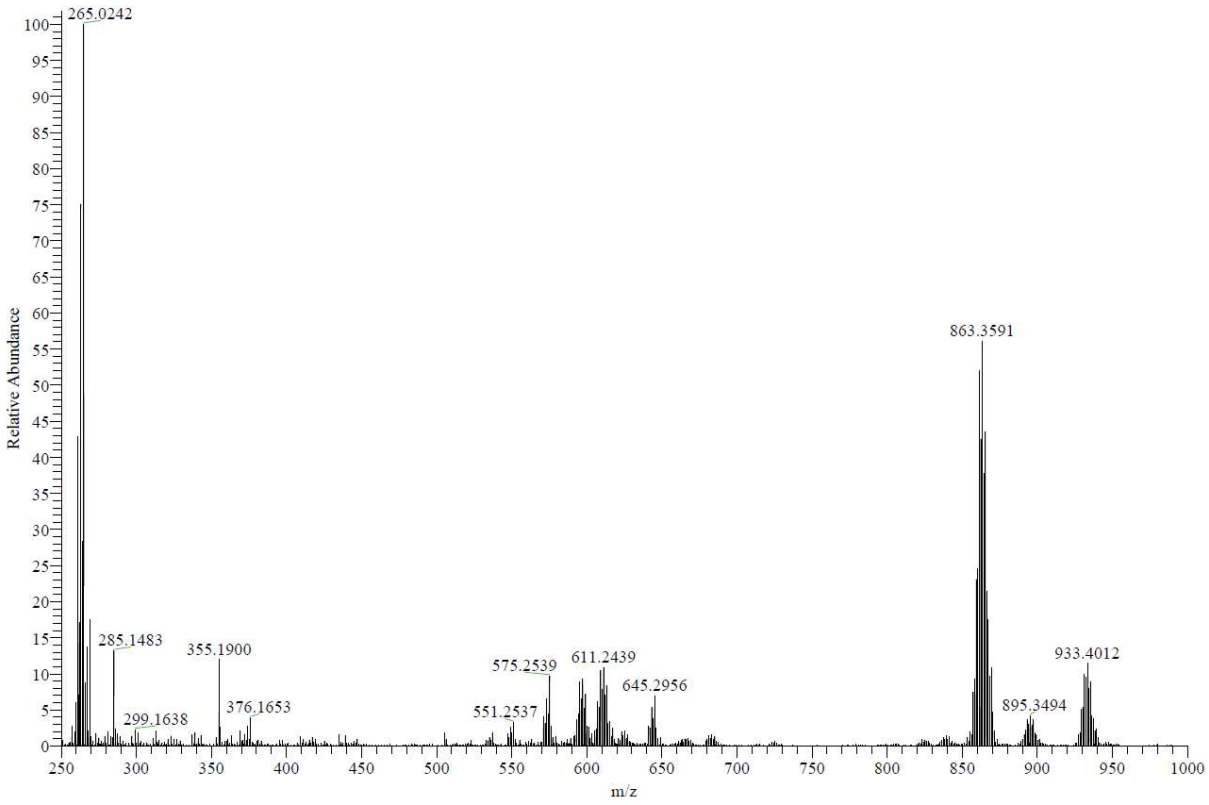

Figure S5.3.74. *HRMS (APCI) spectrum of* ***6c^{Hex}****.*

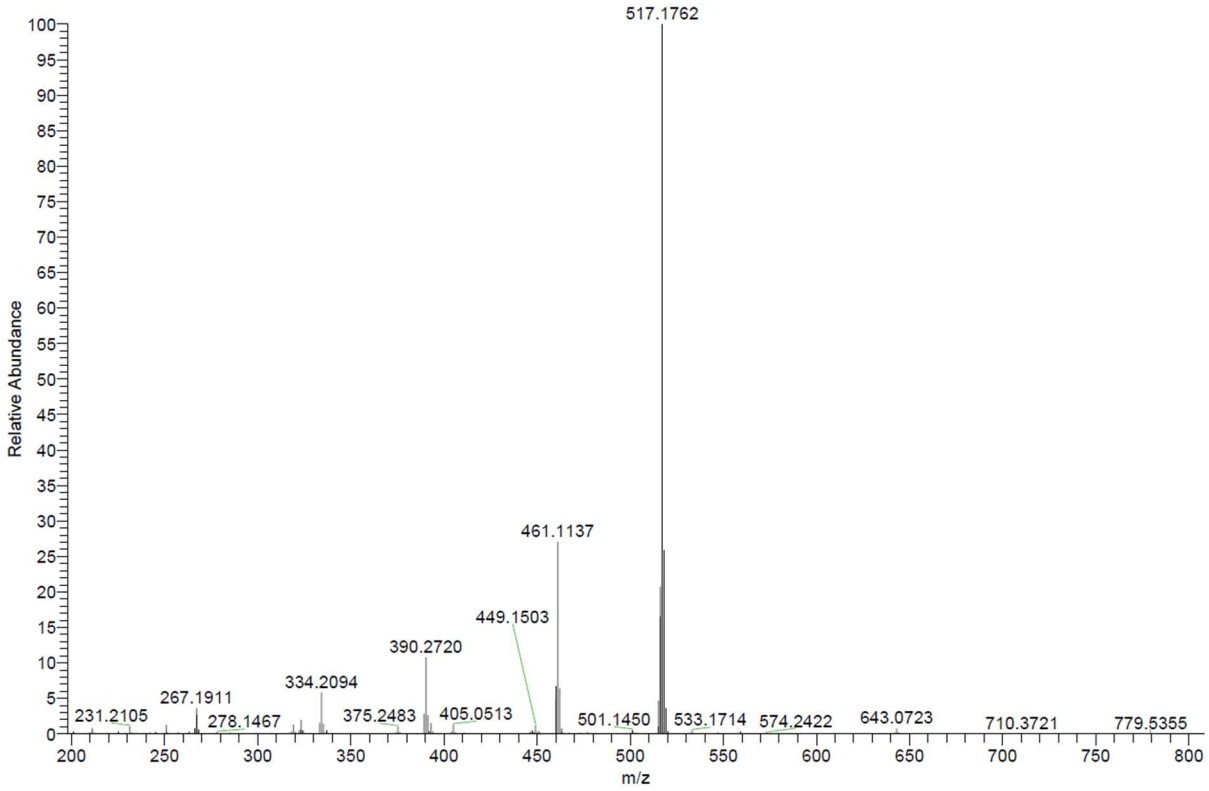

Figure S5.3.75. *ASAP spectrum of* ***4****.*

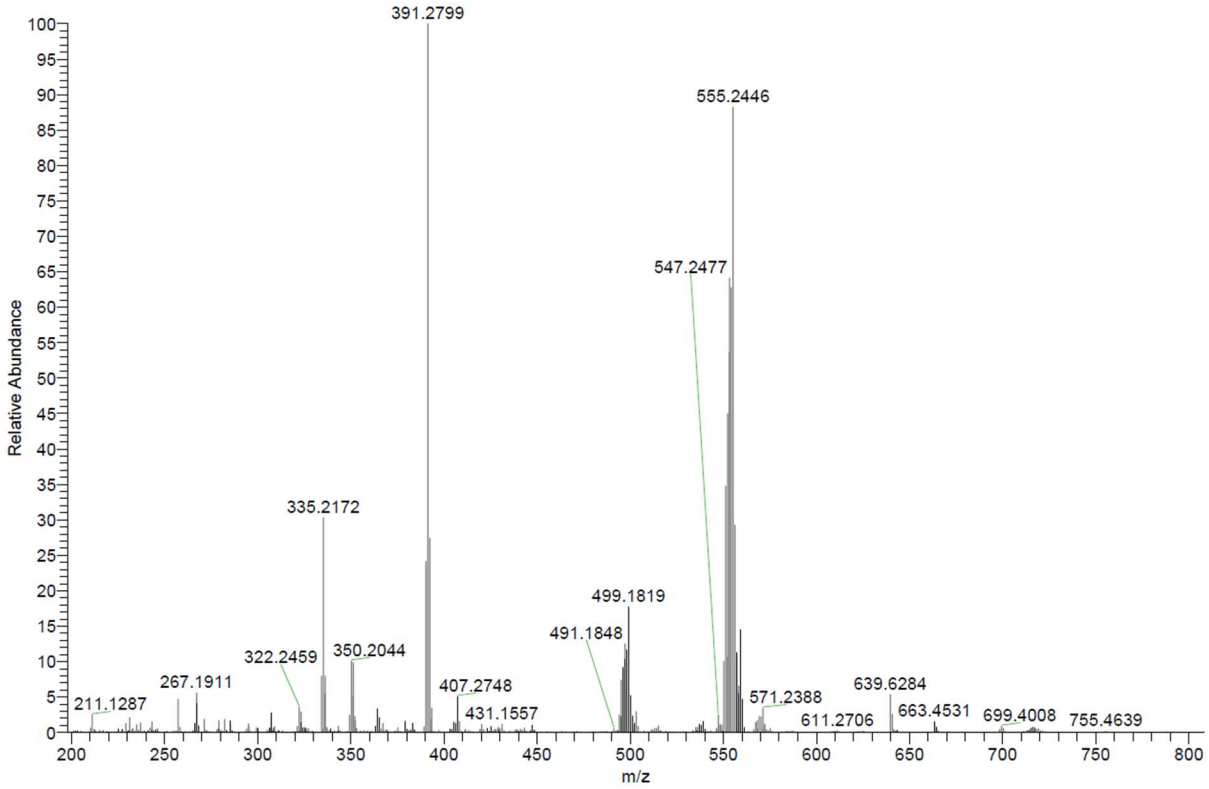

Figure S5.3.76. *APCI spectrum of* ***5****.*

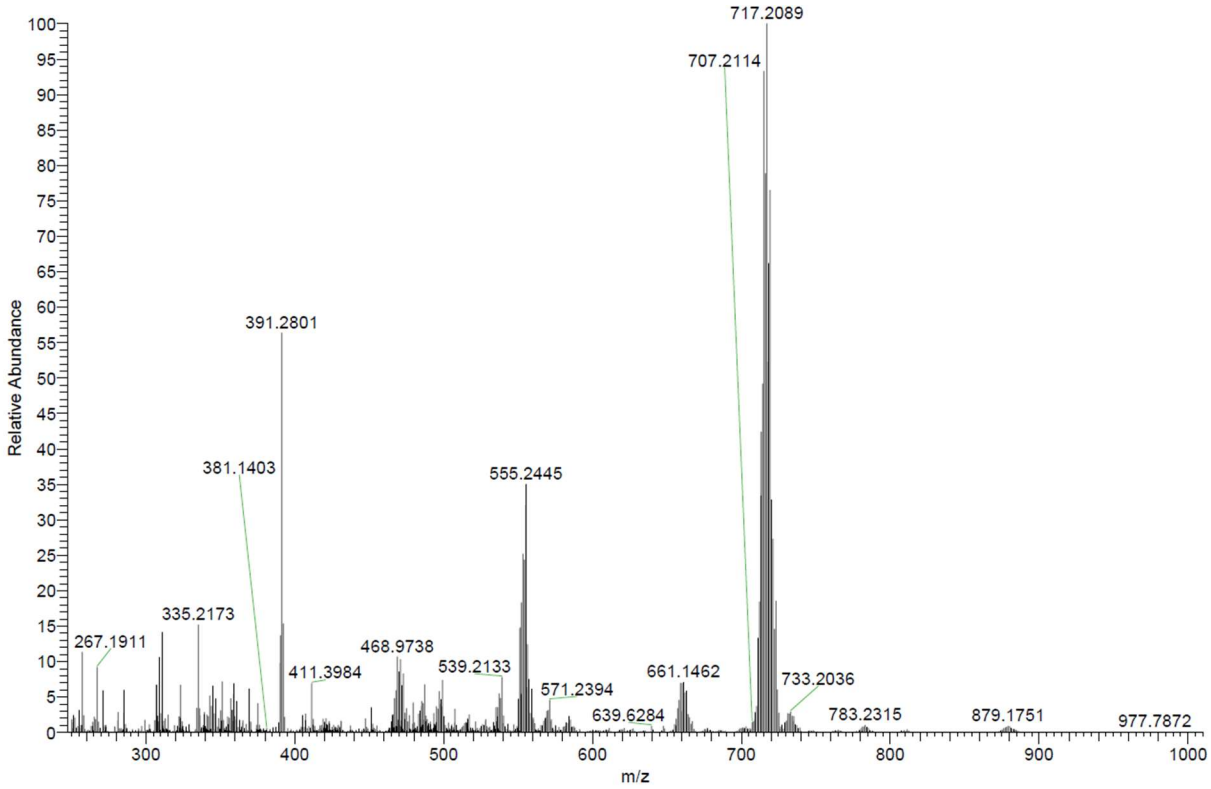

Figure S5.3.77. *ASAP spectrum of* ***9****.*

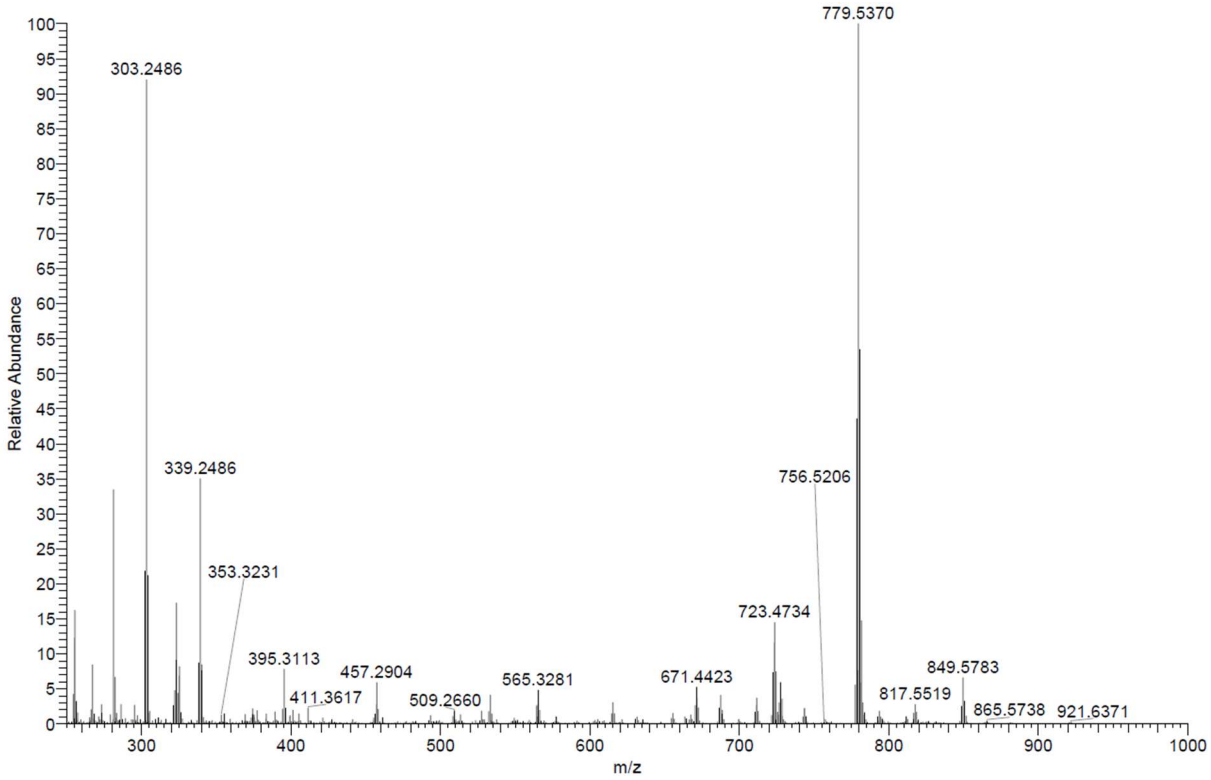

Figure S5.3.78. *APCI spectrum of* ***BB2F****.*

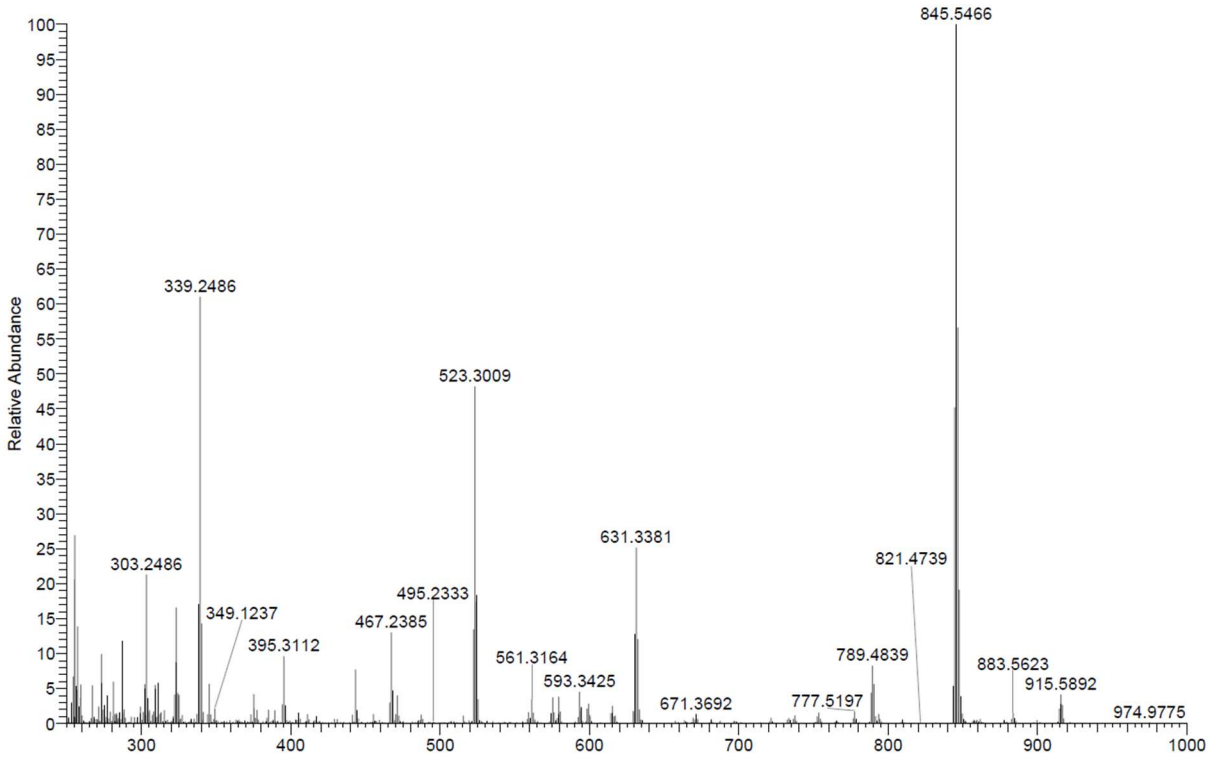

Figure S5.3.79. *APCI spectrum of* ***BB3F****.*

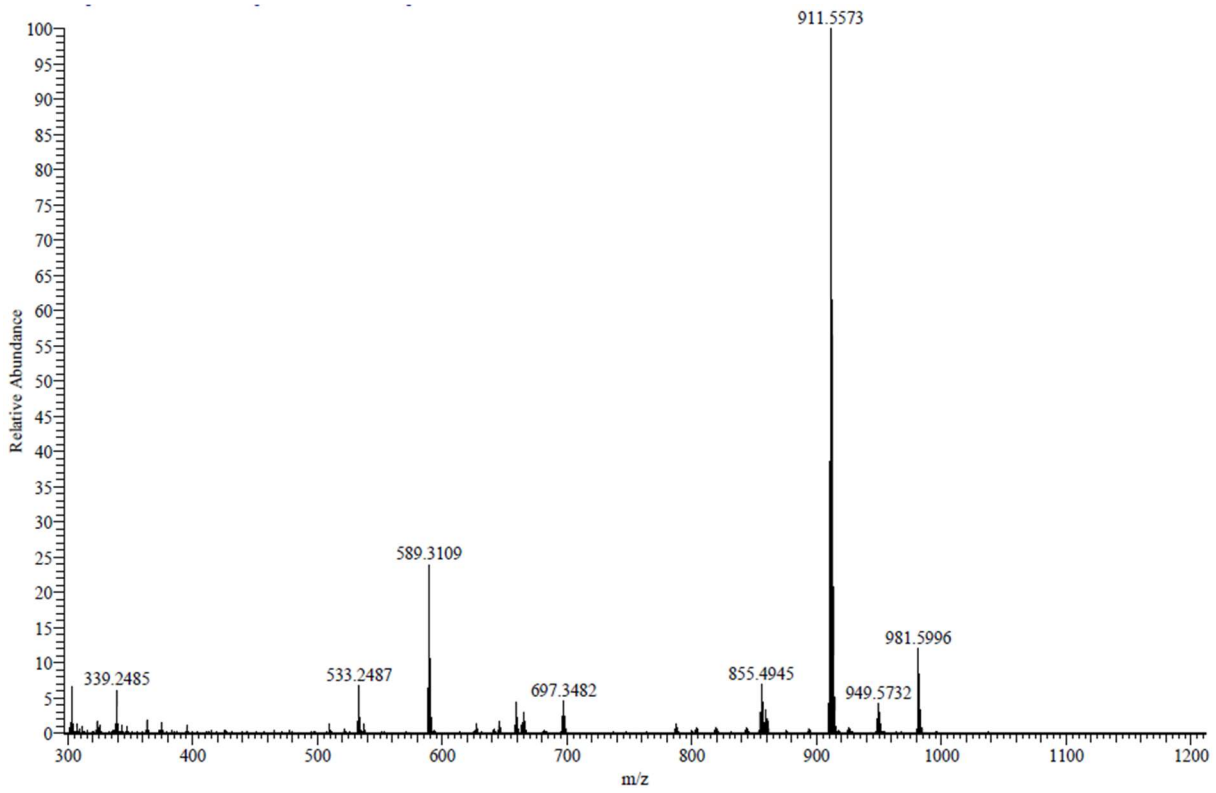

Figure S5.3.80. *APCI spectrum of* ***BB4F****.*

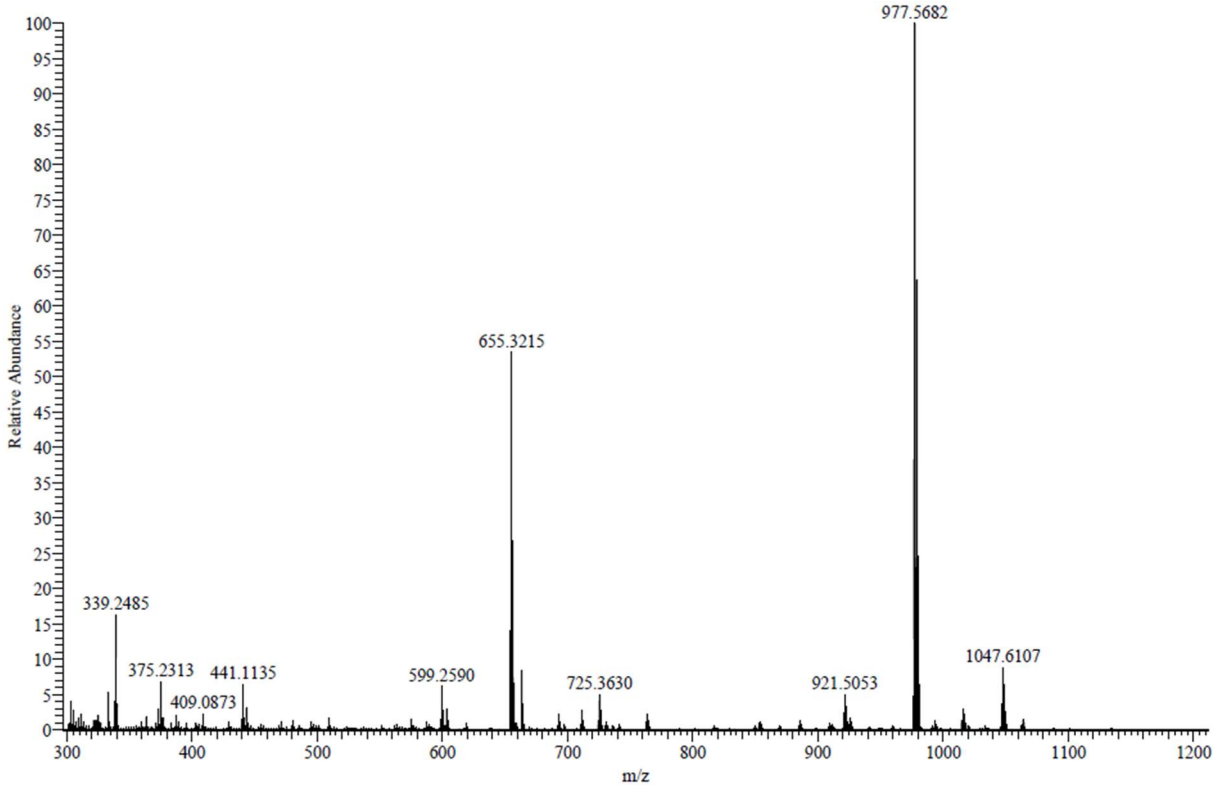

Figure S5.3.81. *APCI spectrum of* ***BB5F****.*

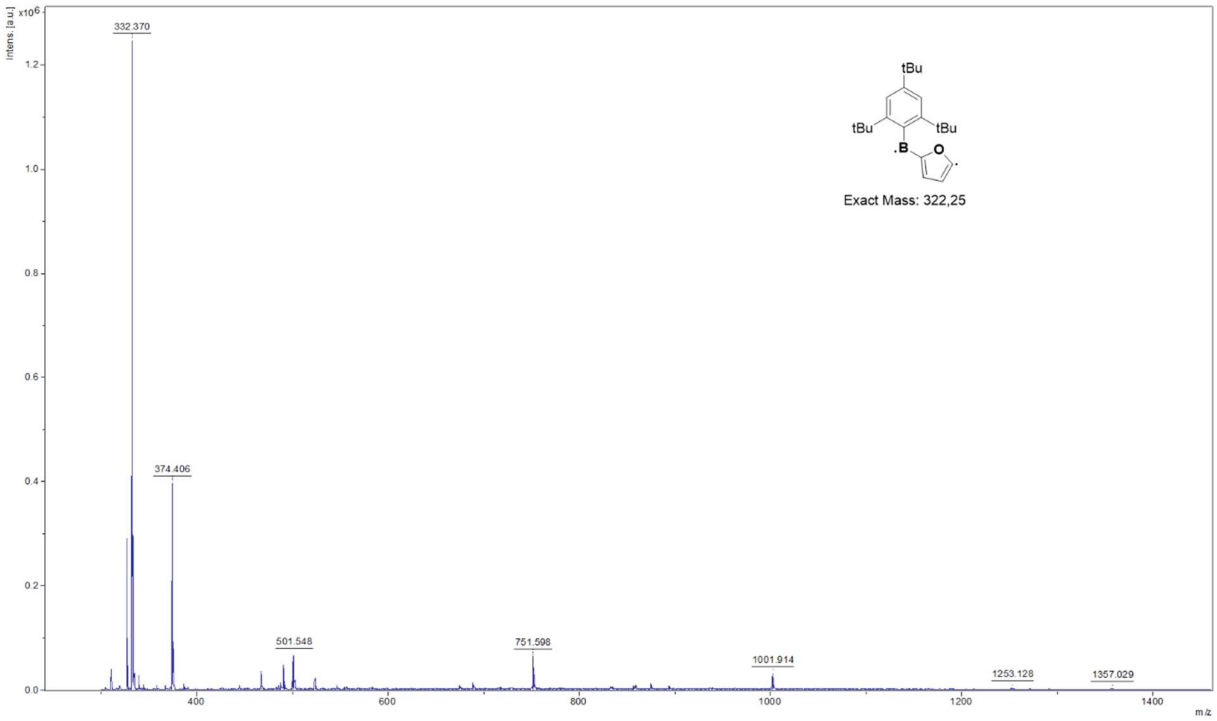

Figure S5.3.82. *MALDI mass spectrum of* ***PB1F*** *(matrix: DCTB).*

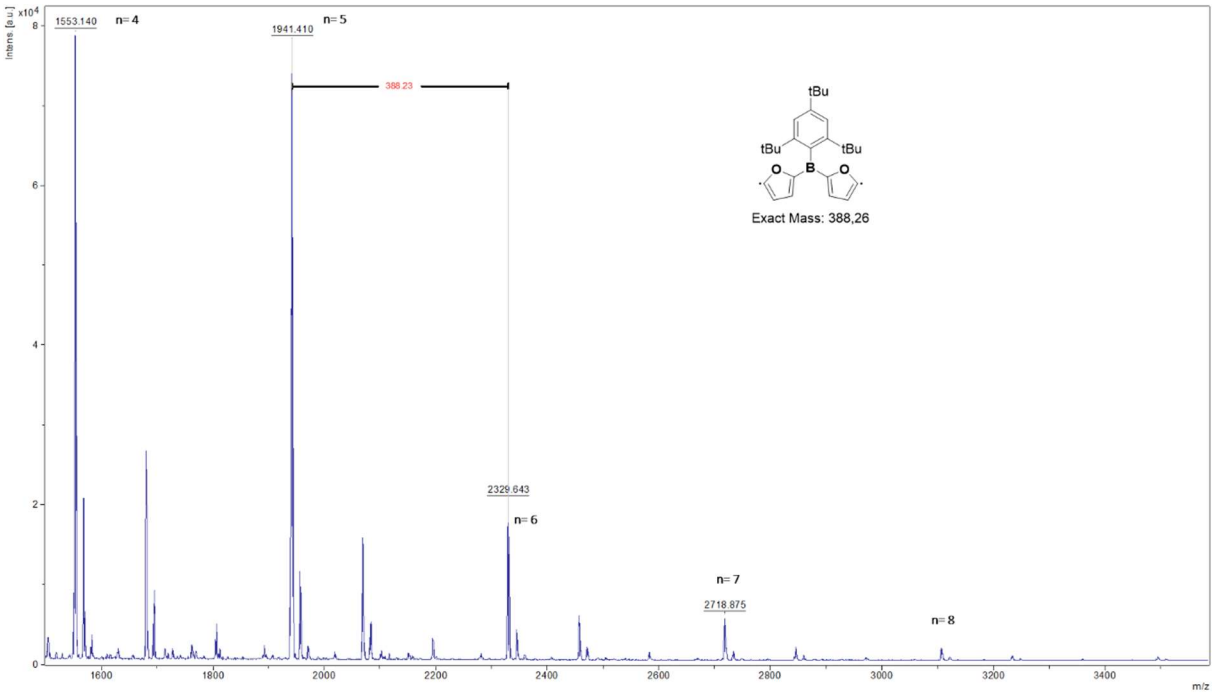

Figure S5.3.83. *MALDI mass spectrum of* ***PB2F*** *(matrix: DCTB).*

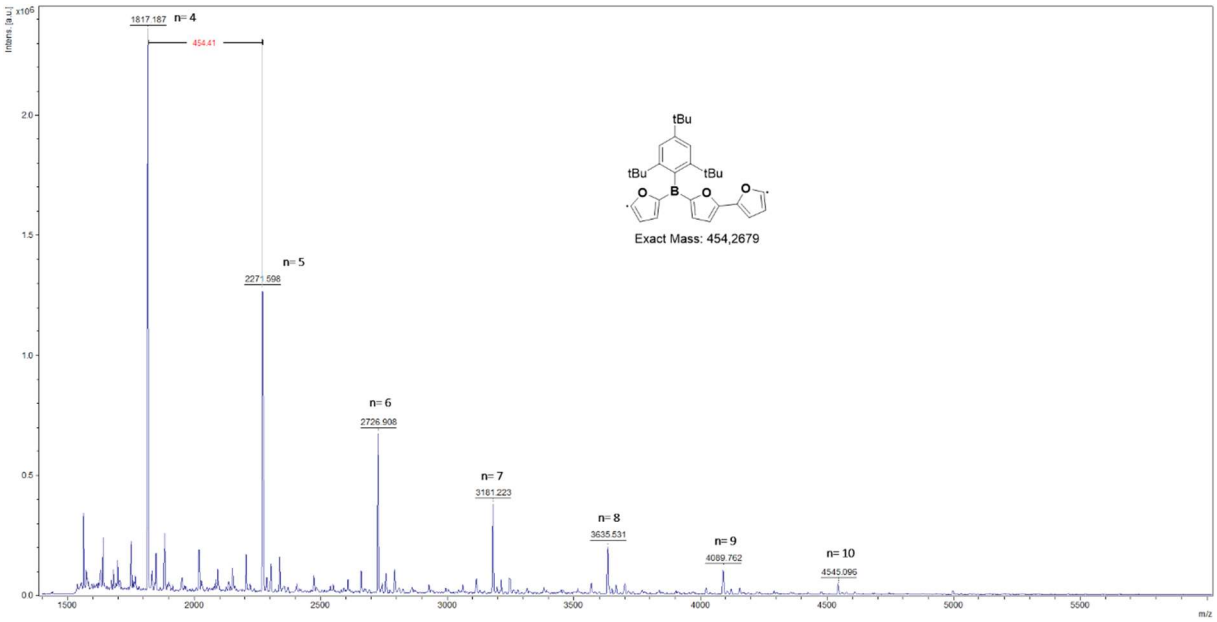

Figure S5.3.84. *MALDI mass spectrum of* ***PB3F*** *(matrix: DCTB).*

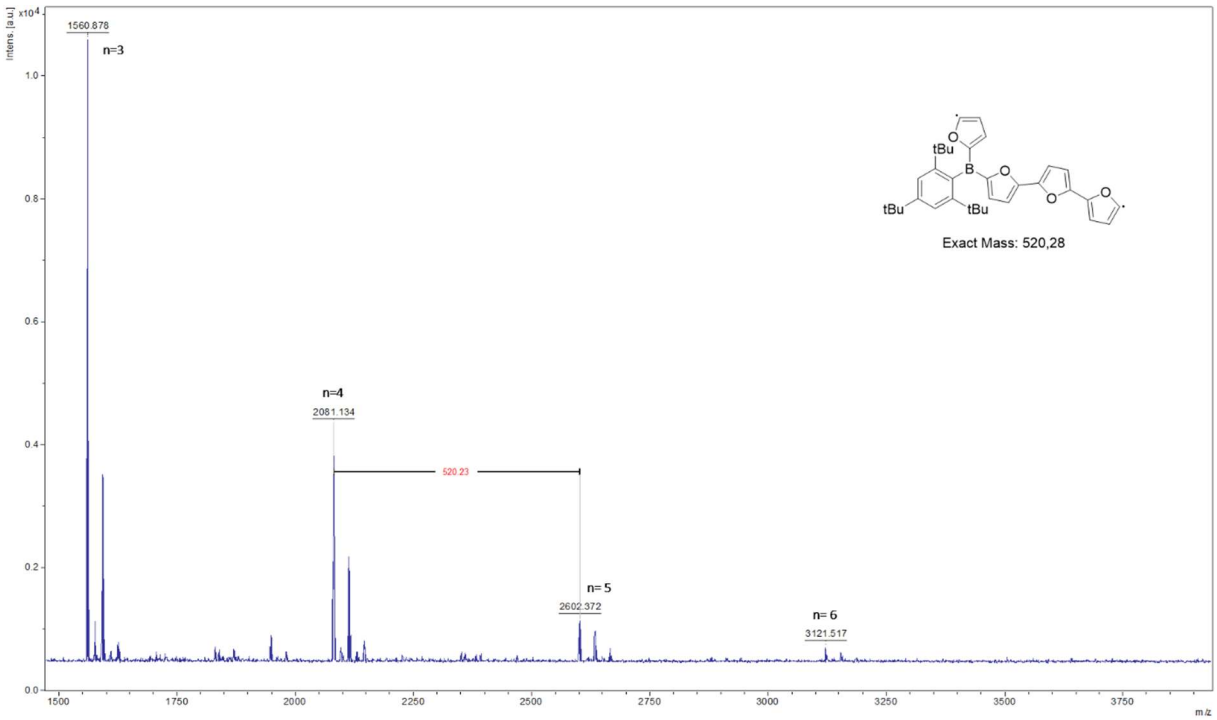

Figure S5.3.85. *MALDI mass spectrum of* ***PB4F*** *(matrix: DCTB).*

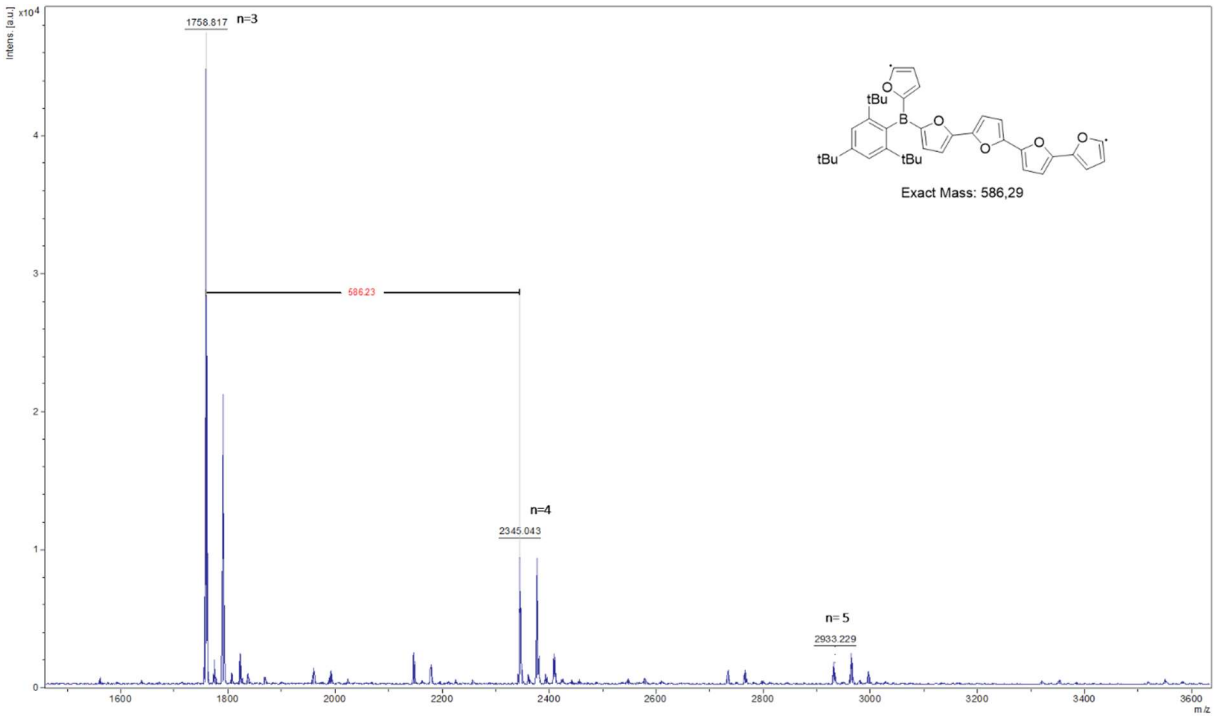

Figure S5.3.86. *MALDI mass spectrum of* ***PB5F*** *(matrix: DCTB).*

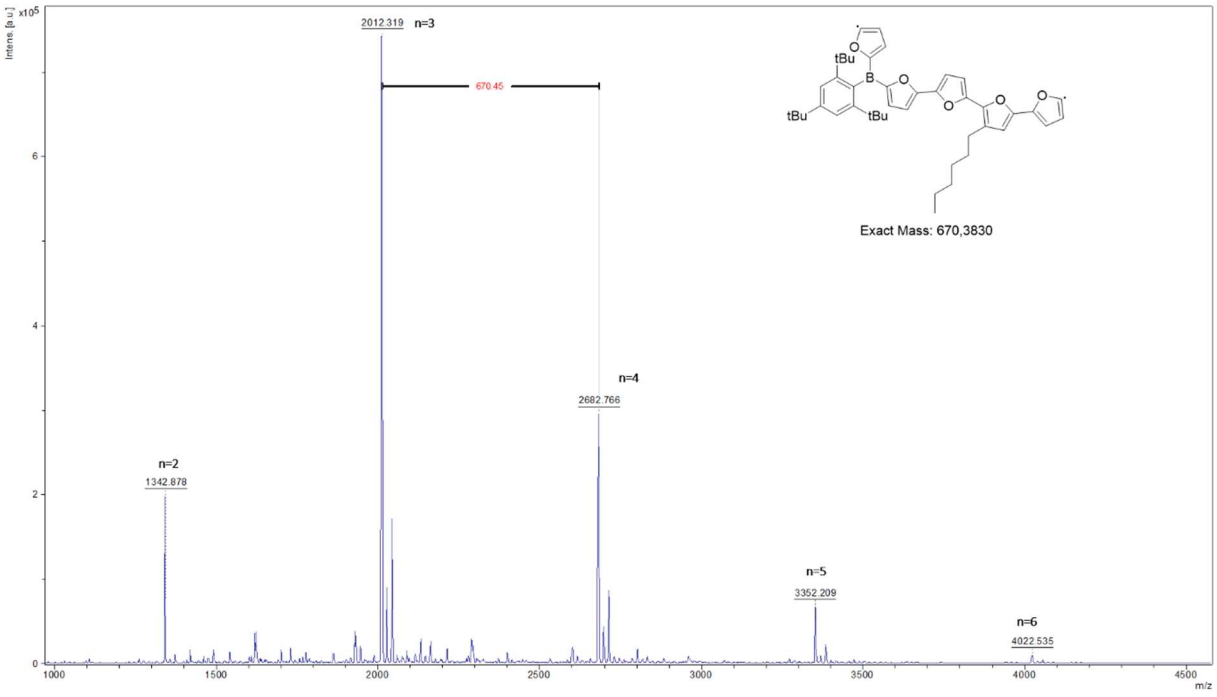

Figure S5.3.87. *MALDI mass spectrum of* ***PB5F^{Hex}*** *(matrix: DCTB).*

Electrochemical Studies

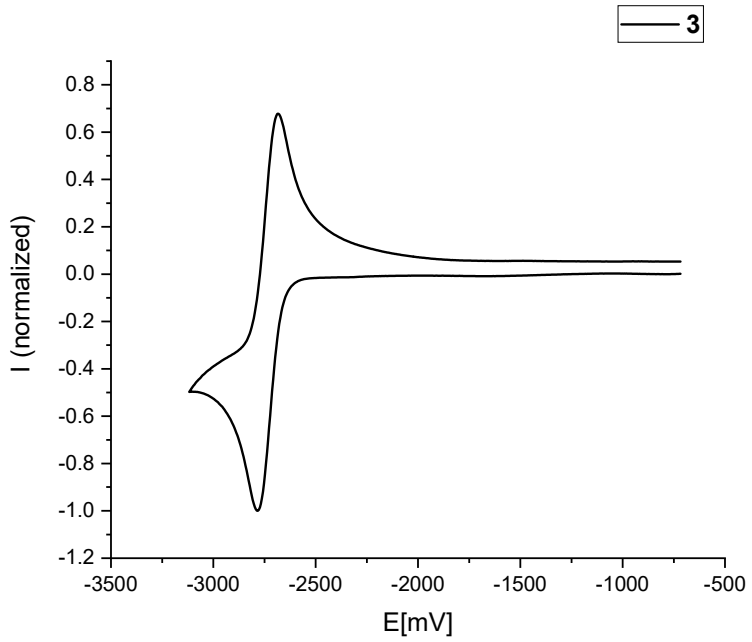

Figure S5.3.88. *Cyclic voltammogram of monomer* ***3*** *(in THF).*

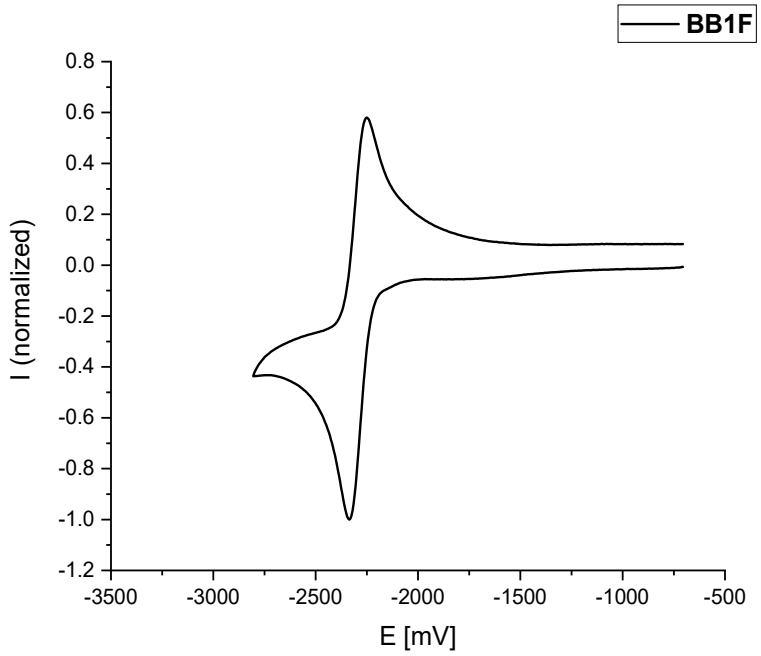

Figure S5.3.89. *Cyclic voltammogram of first reduction of* ***BB1F*** *(in THF).*

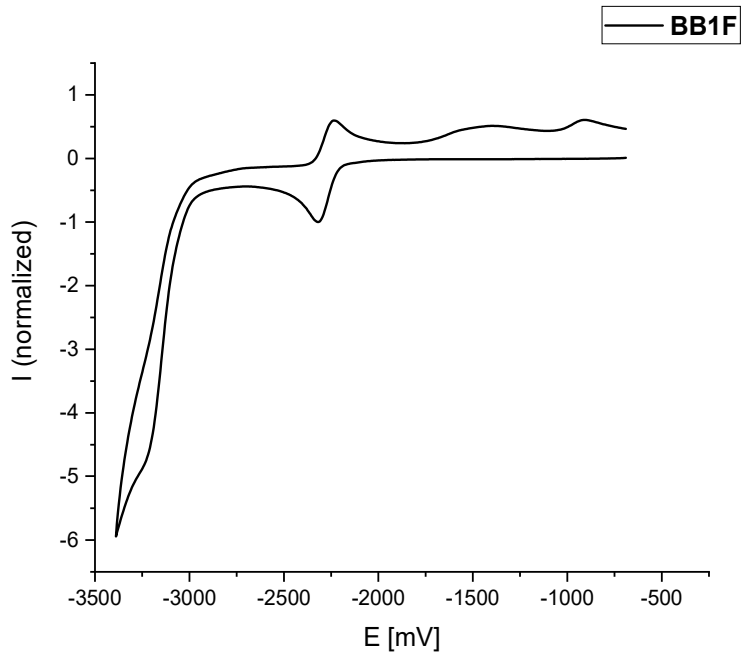

Figure S5.3.90. *Cyclic voltammogram of the possible second reduction wave of* ***BB1F****, which is partially obscured by the solvent window (in THF).*

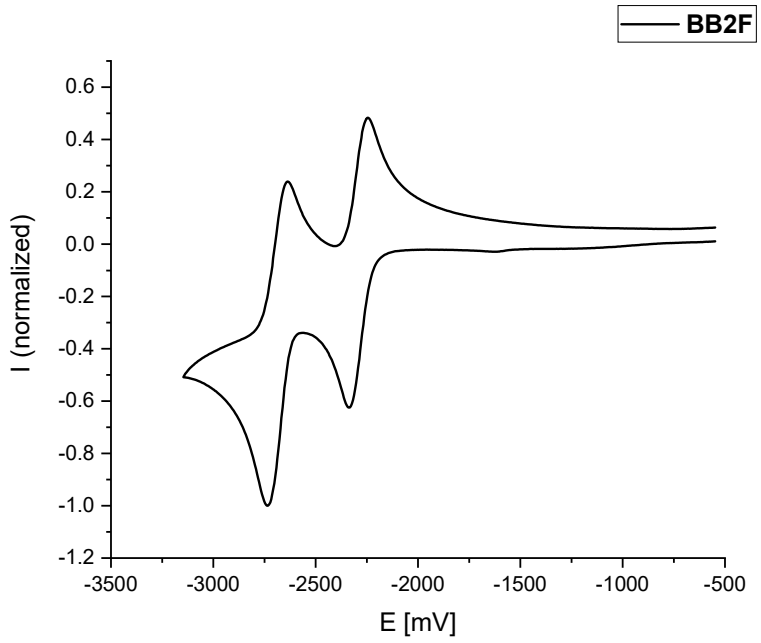

Figure S5.3.91. *Cyclic voltammogram of* ***BB2F*** *(in THF).*

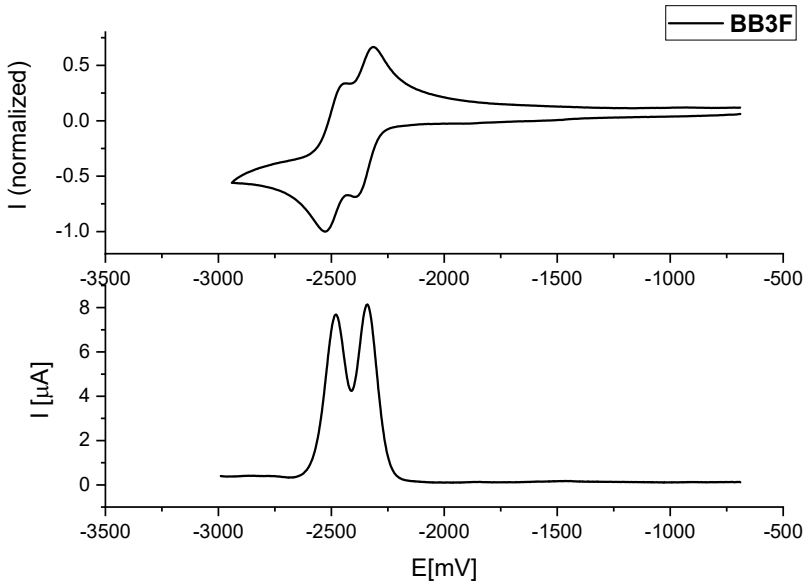

Figure S5.3.92. *Cyclic voltammogram and square wave voltammogram of* ***BB3F*** *(in THF).*

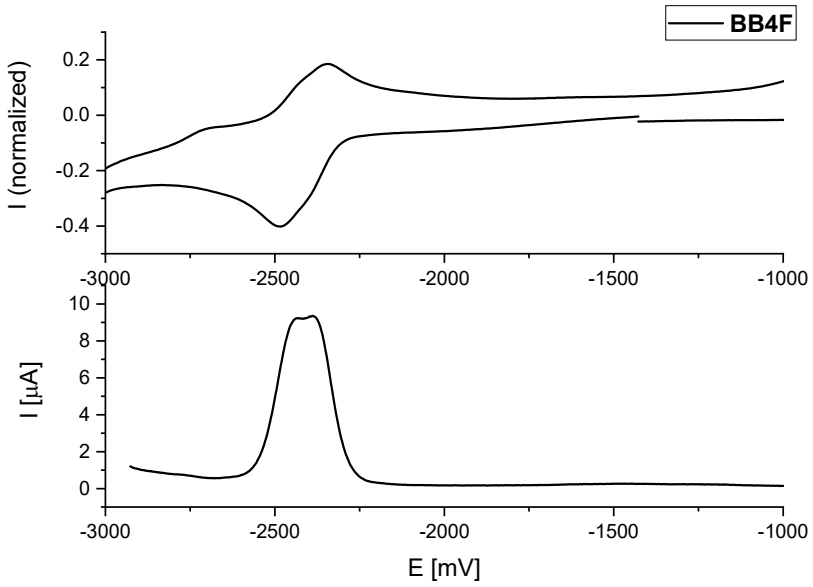

Figure S5.3.93. *Cyclic voltammogram and square wave voltammogram in the cathodic region of* ***BB4F*** *(in THF).*

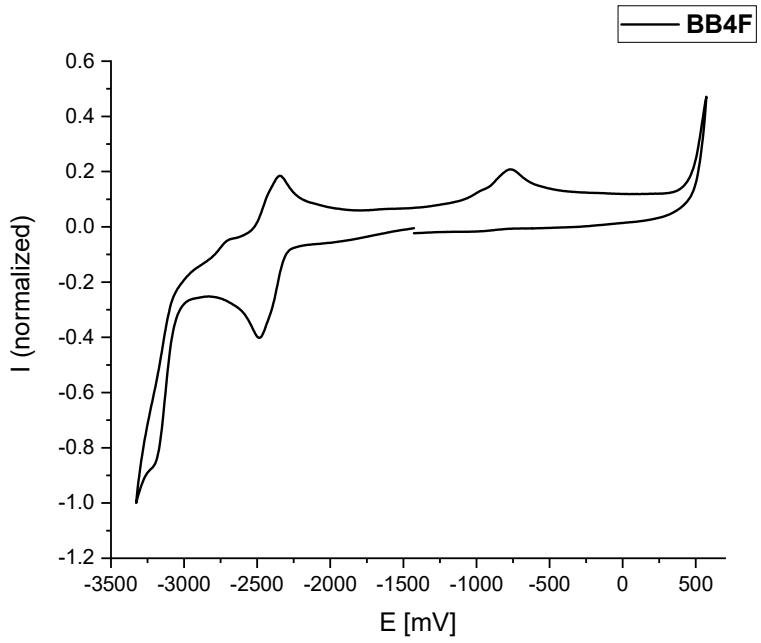

Figure S5.3.94. *Full cyclic voltammogram of* ***BB4F*** *(in THF).*

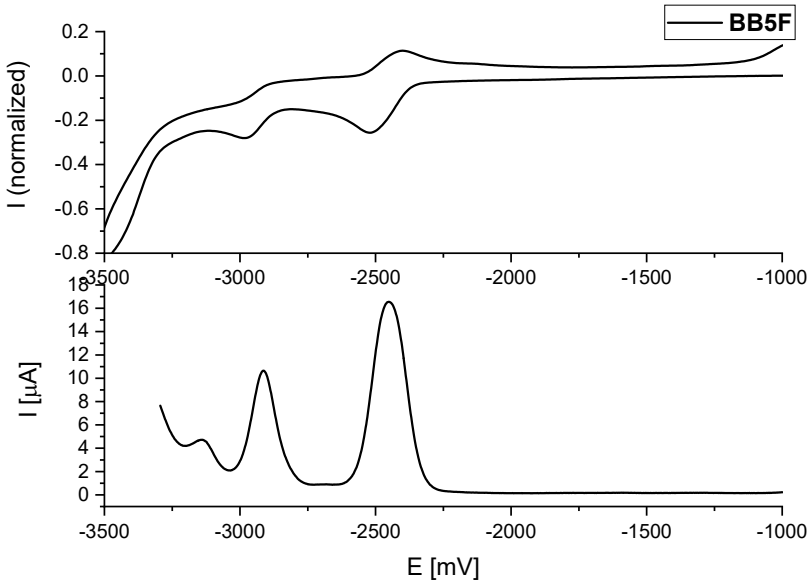

Figure S5.3.95. *Cyclic voltammogram and square wave voltammogram in the cathodic region of* ***BB5F*** *(in THF).*

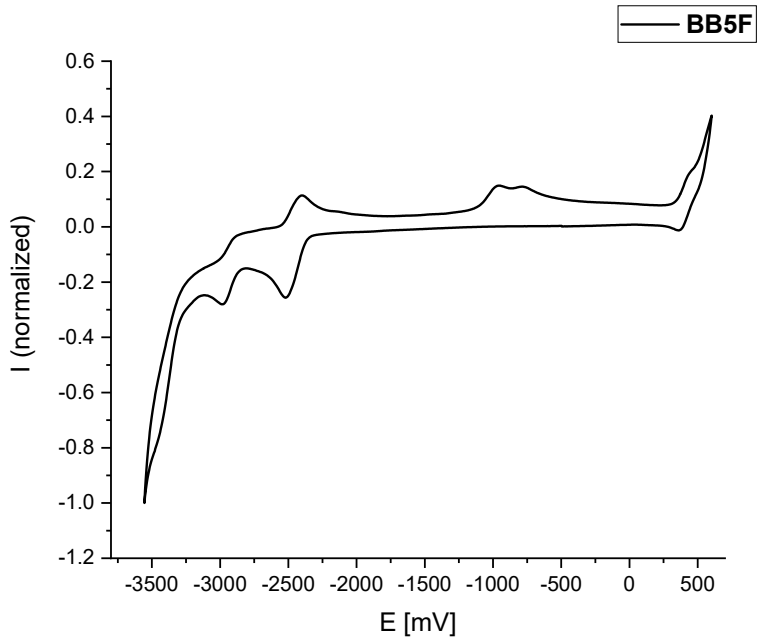

Figure S5.3.96. *Full cyclic voltammogram of* ***BB5F*** *(in THF).*

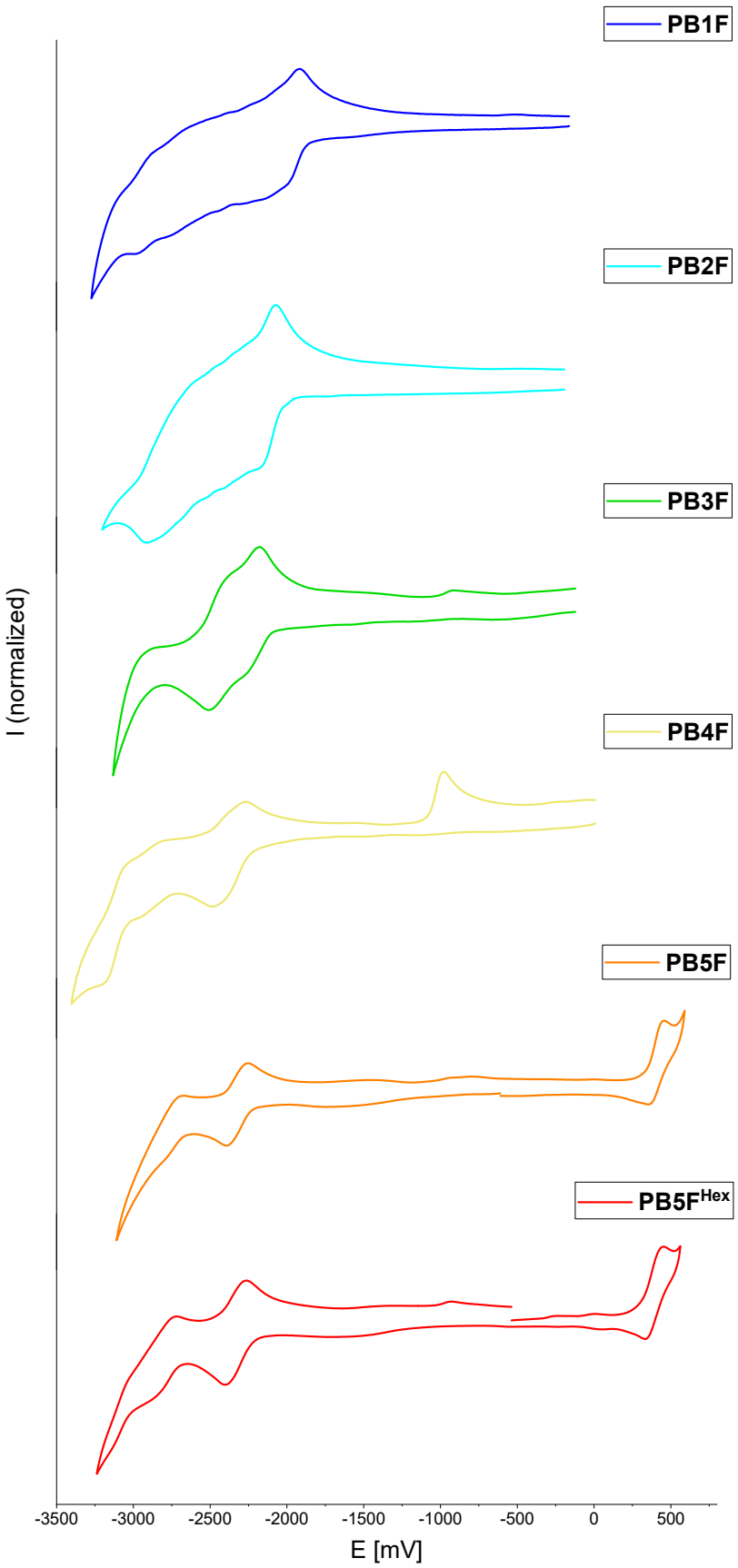

Figure S5.3.97. *Cyclic voltammograms of polymers* ***PB1F*** *–* ***PB5F^{Hex}*** *(in THF).*

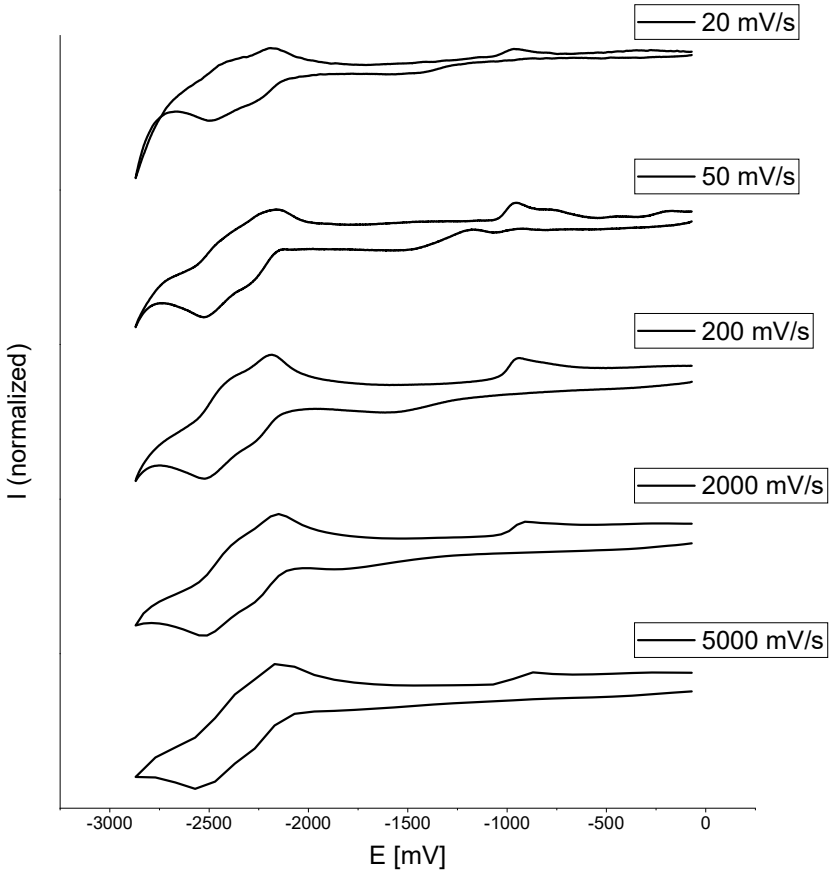

Figure S5.3.98. *Cyclic voltammograms of* ***PB3F*** *at different scan rates (in THF).*

TGA curves

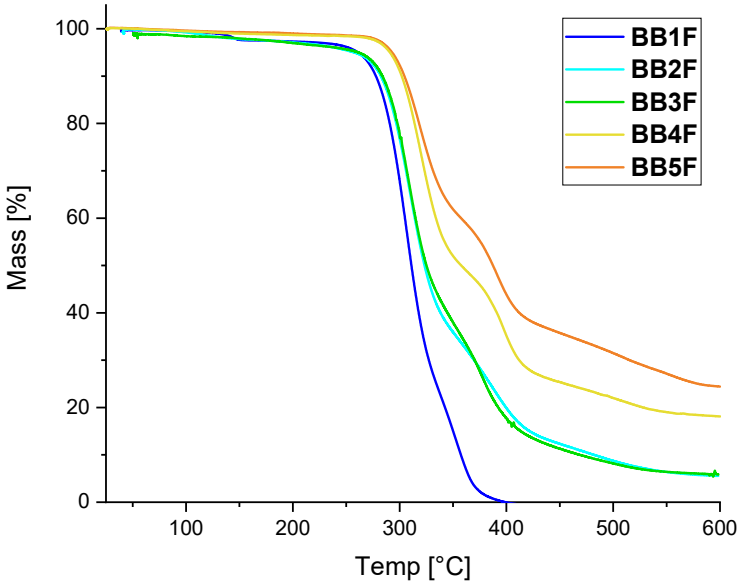

Figure S5.3.99. *TGA curves of* ***BB1F*** *–* ***BB5F****.*

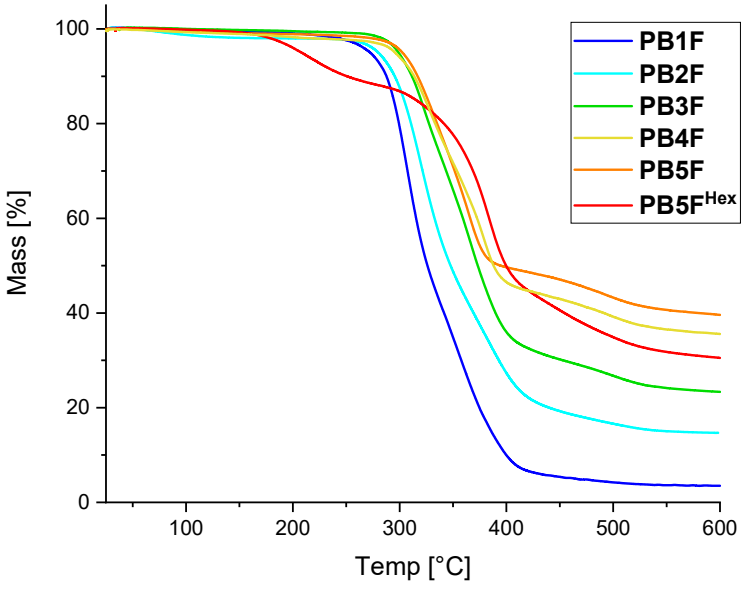

Figure S5.3.100. *TGA curves of* ***PB1F*** *–* ***PB5F^{Hex}****.*

GPC traces

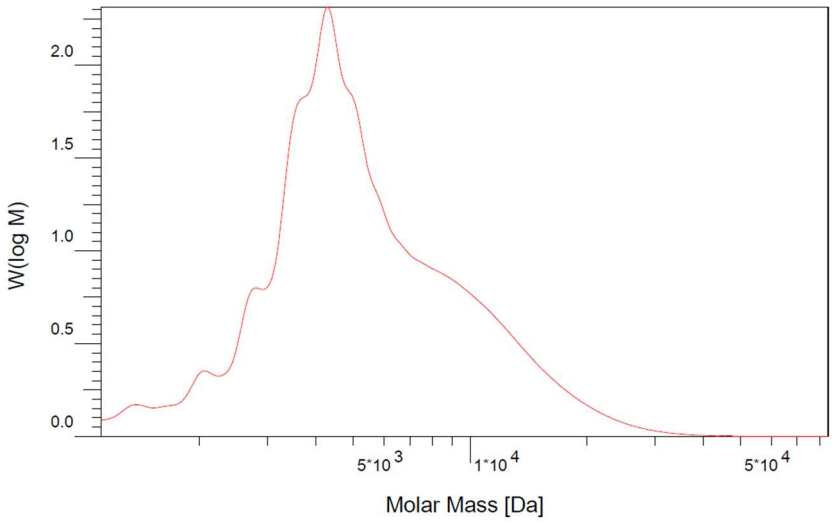

I1: VWD 1, Signal A

Mn :	4.5014e3	g/mol
Mw :	6.3352e3	g/mol
Mz :	9.3029e3	g/mol
Mv :	0.000000	g/mol
D :	1.4074e0	
[n]:	0.000000	ml/g
Vp :	2.5730e1	ml
Mp :	4.2904e3	g/mol
FI :	9.6352e2	ml*V
< 1115	0.00	
w% :	100.00	
> 84094	0.00	

Figure S5.3.101. *GPC trace of* ***PB1F*** *(in THF, vs polystyrene standard).*

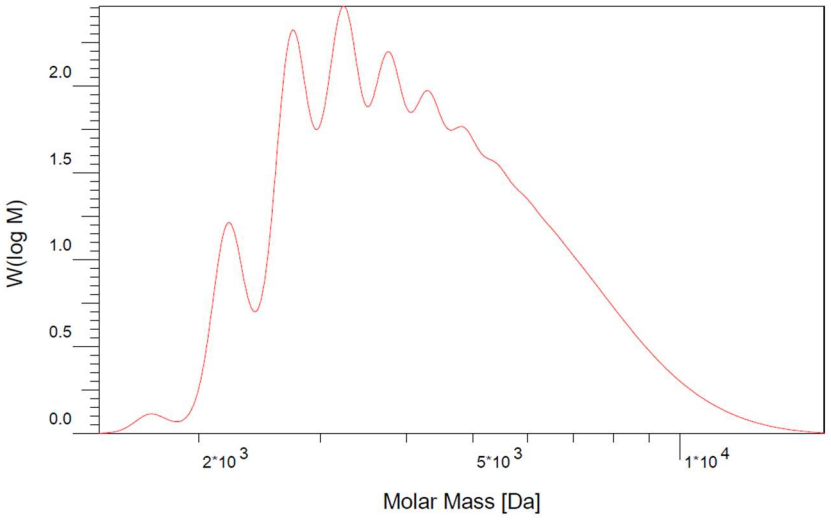

I1: VWD 1, Signal A

Mn :	3.8320e3	g/mol
Mw :	4.5210e3	g/mol
Mz :	5.4124e3	g/mol
Mv :	0.000000	g/mol
D :	1.1798e0	
[n]:	0.000000	ml/g
Vp :	2.6473e1	ml
Mp :	3.2402e3	g/mol
FI :	8.2942e2	ml*V
< 1432	0.00	
w% :	100.00	
> 16176	0.00	

Figure S5.3.102. *GPC trace of* ***PB2F*** *(in THF, vs polystyrene standard).*

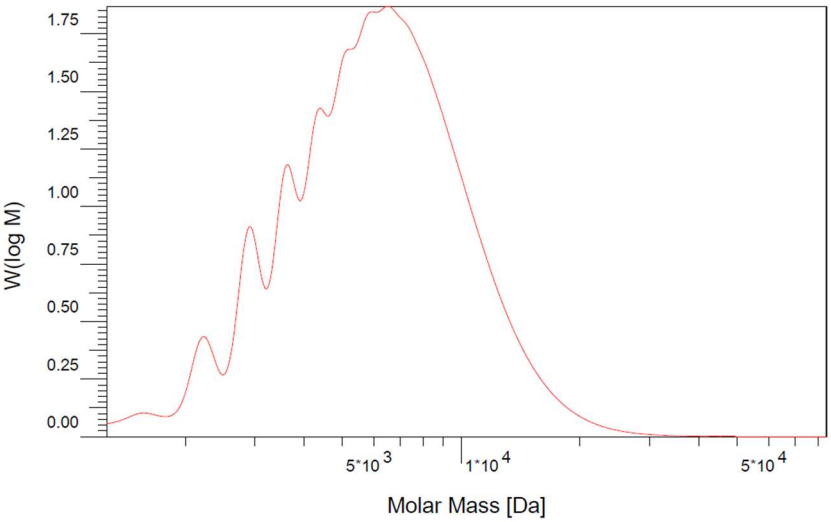

I1: VWD 1, Signal A

Mn :	5.2051e3	g/mol
Mw :	6.7644e3	g/mol
Mz :	8.6991e3	g/mol
Mv :	0.000000	g/mol
D :	1.2996e0	
[n]:	0.000000	ml/g
Vp :	2.4615e1	ml
Mp :	6.5460e3	g/mol
FI :	5.5425e2	ml*V
< 1263	0.00	
w% :	100.00	
> 84094	0.00	

Figure S5.3.103. *GPC trace of* ***PB3F*** *(in THF, vs polystyrene standard).*

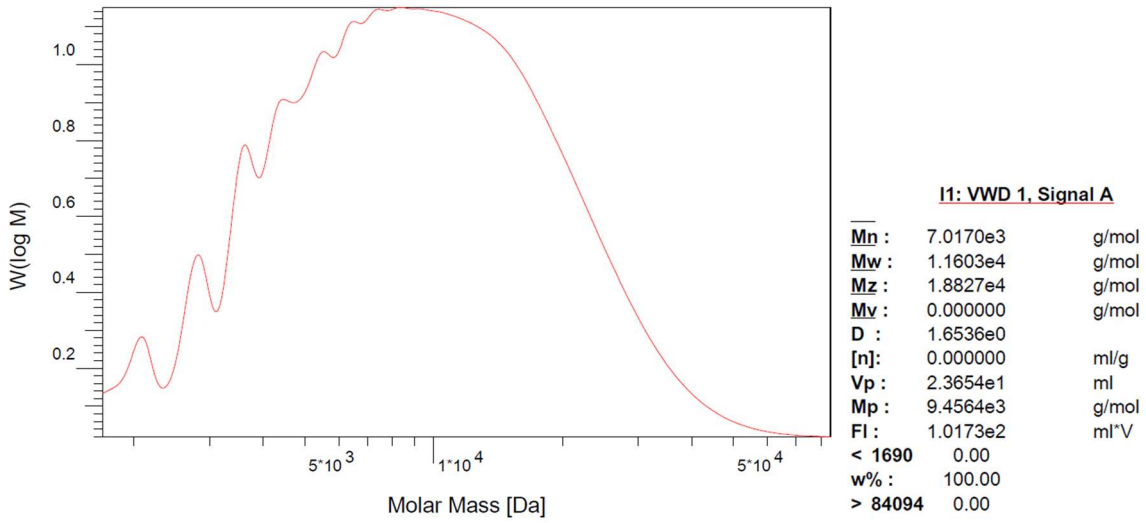

Figure S5.3.104. *GPC trace of* ***PB4F*** *(in THF, vs polystyrene standard).*

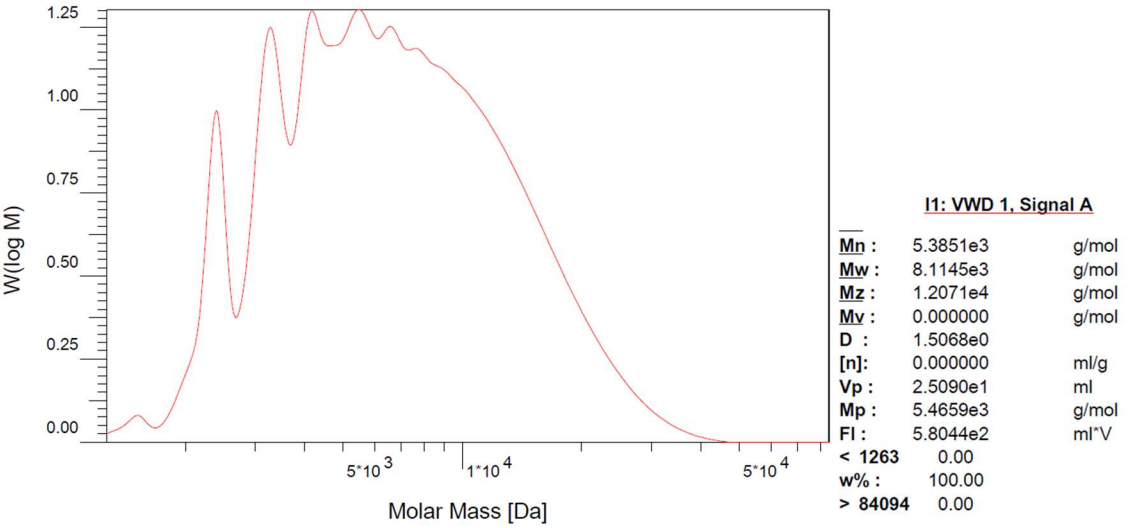

Figure S5.3.105. *GPC trace of* ***PB5F*** *(in THF, vs polystyrene standard).*

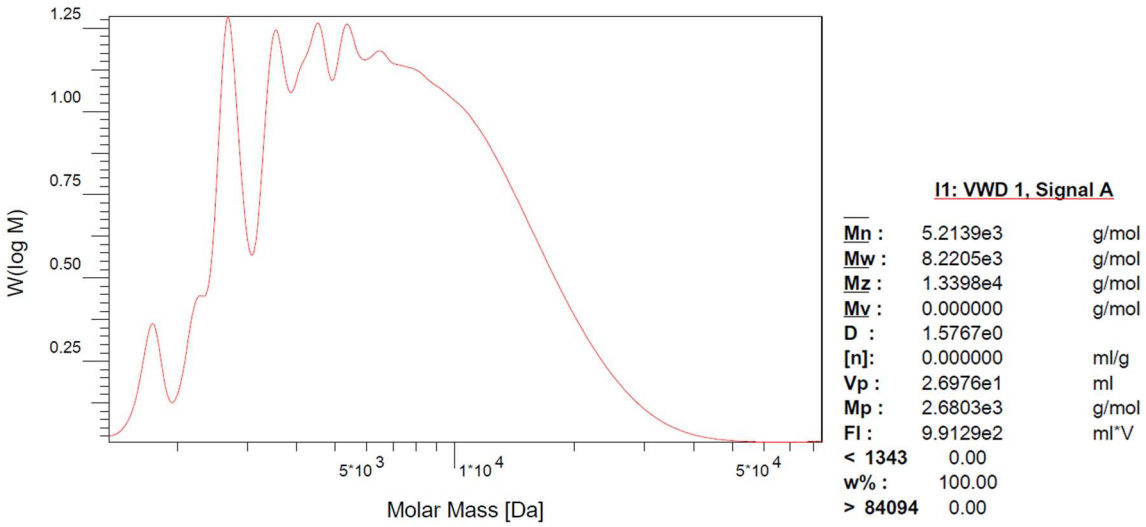

Figure S5.3.106. *GPC trace of* ***PB5F^{Hex}*** *(in THF, vs polystyrene standard).*

X-Ray crystallography

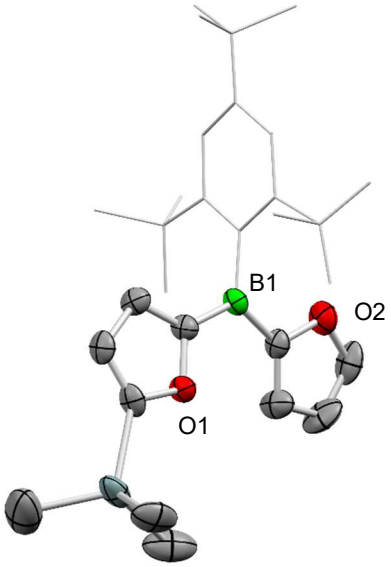

Figure S5.3.107. *X-Ray structure of* ***5*** *(disorders omitted for clarity).*

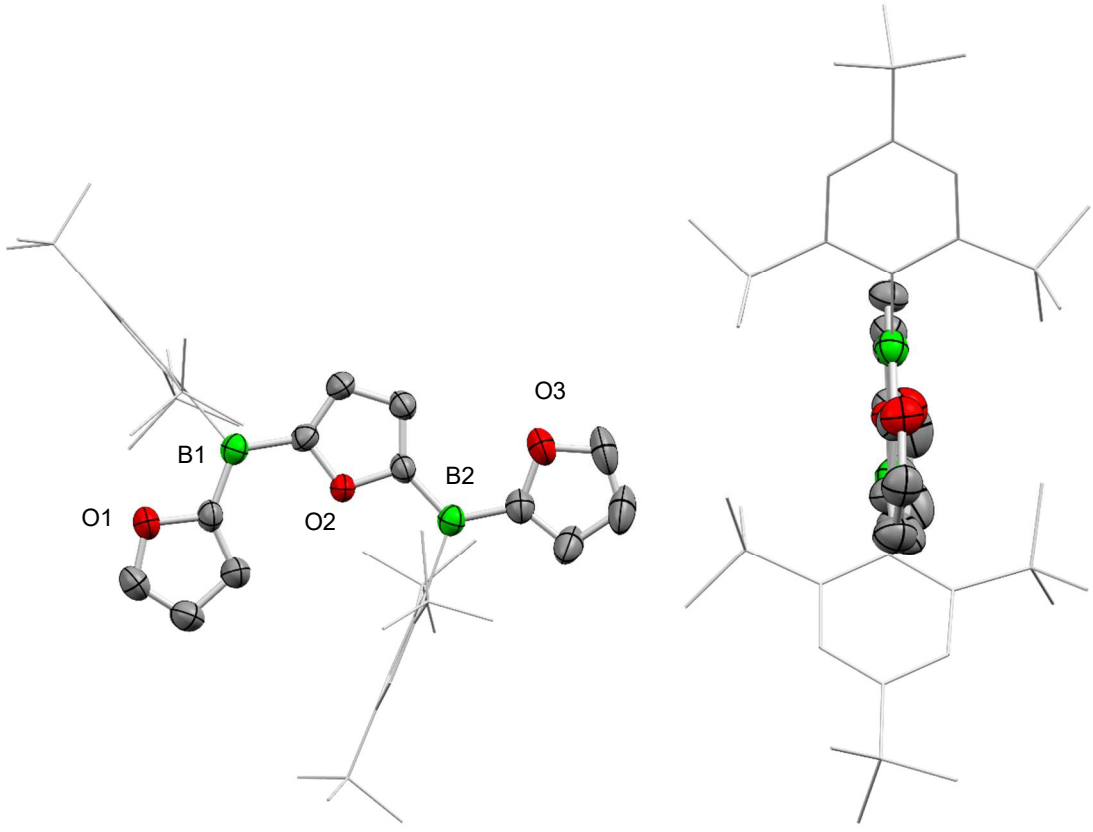

Figure S5.3.108. *X-Ray structure of* ***BB1F*** *(disorders omitted for clarity).*

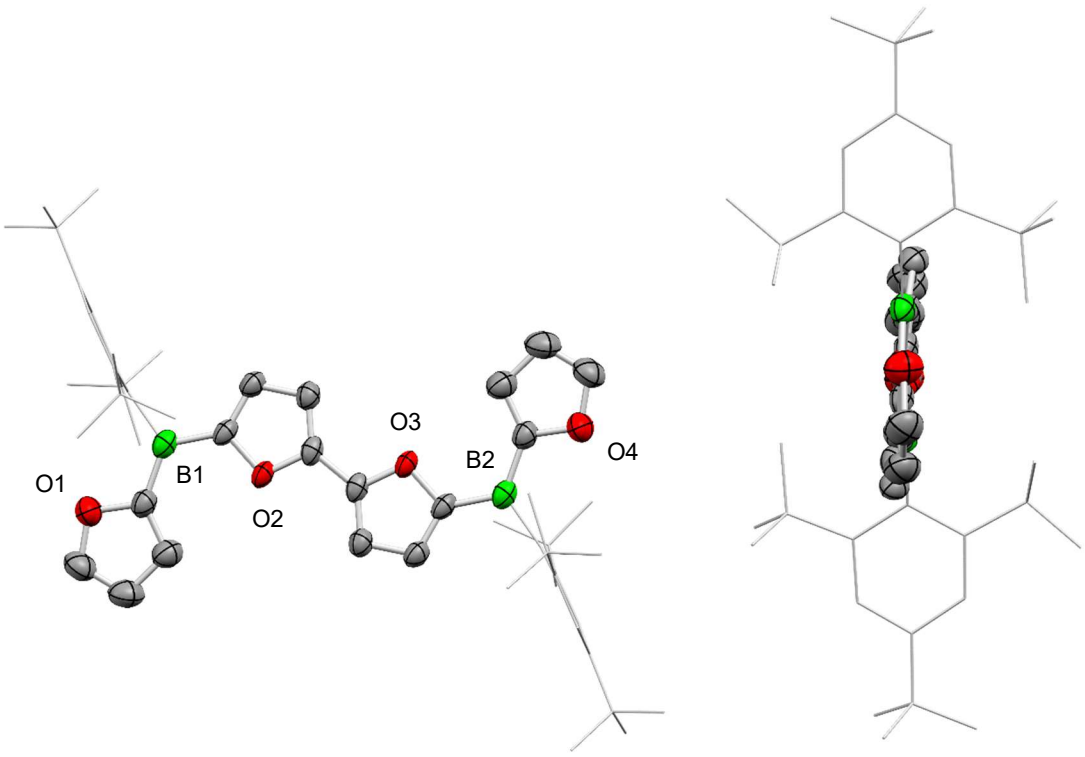

Figure S5.3.109. *X-Ray structure of* ***BB2F*** *(disorders and solvents omitted for clarity).*

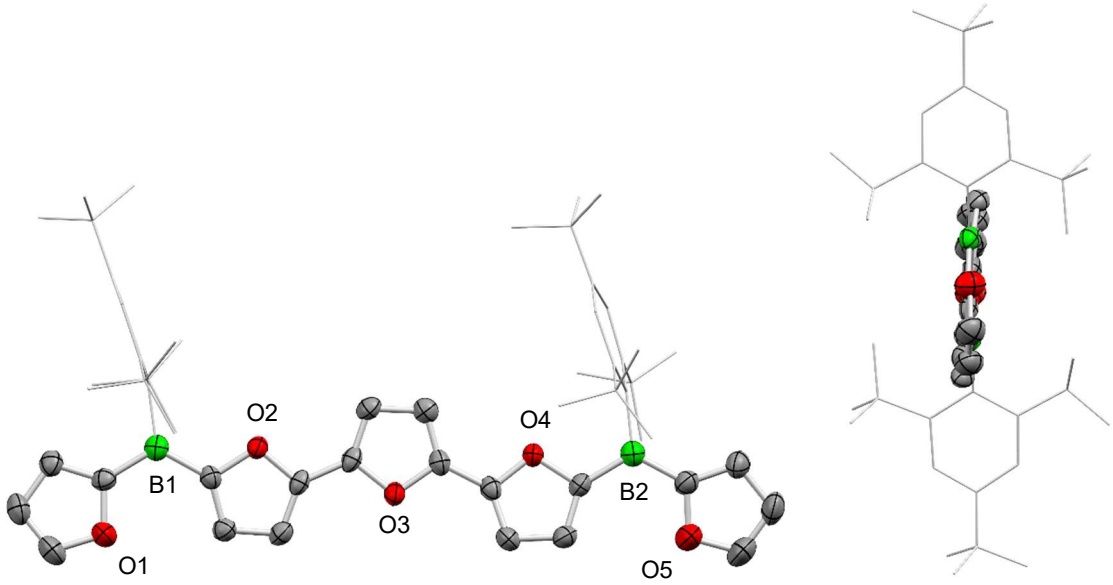

Figure S5.3.110. *X-Ray structure of* ***BB3F*** *(disorders and solvents omitted for clarity).*

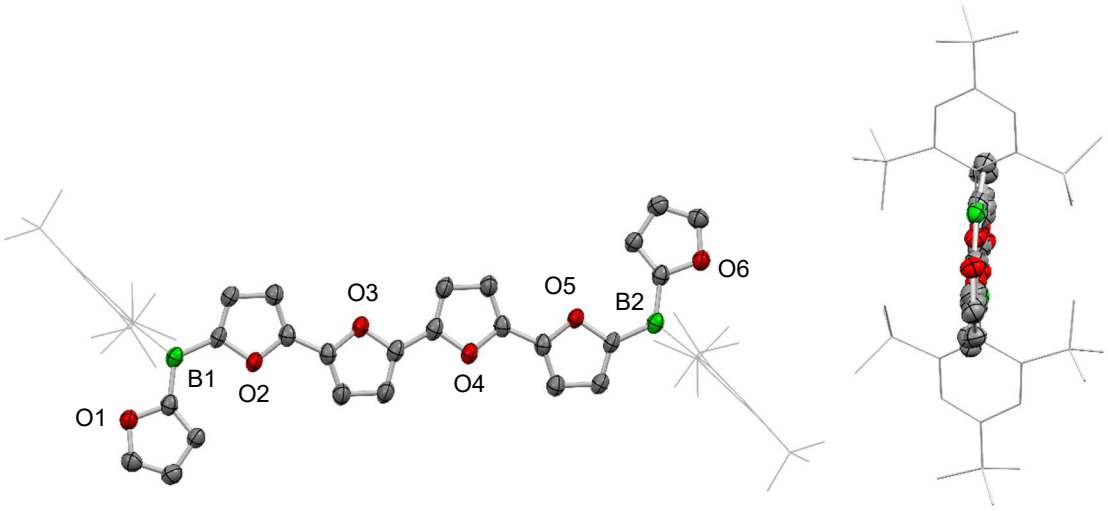

Figure S5.3.111. *X-Ray structure of* ***BB4F*** *(disorders and solvents omitted for clarity).*

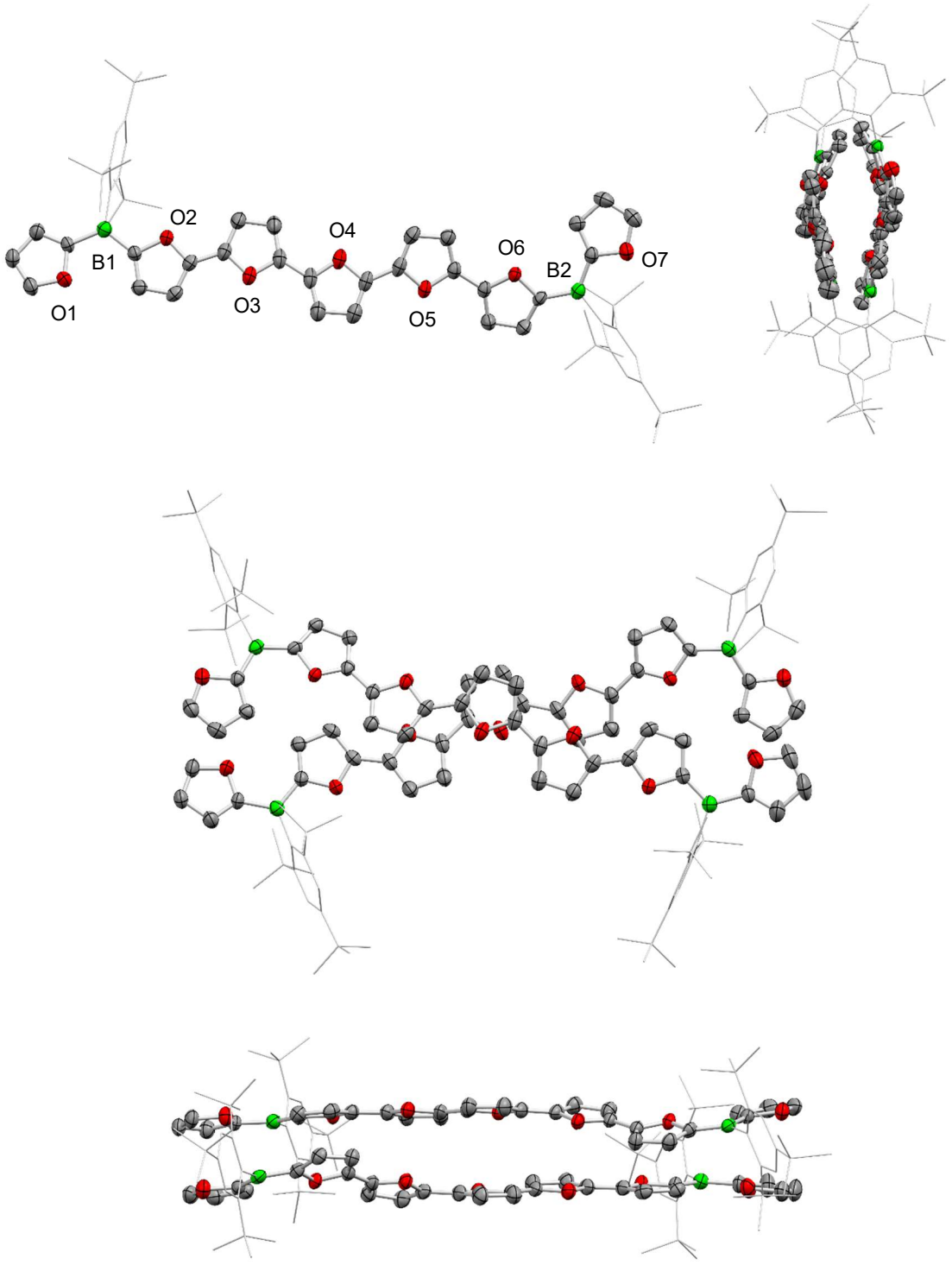

Figure S5.3.112. *X-Ray structure of* ***BB5F*** *and of complete unit cell (disorders and solvents omitted for clarity).*

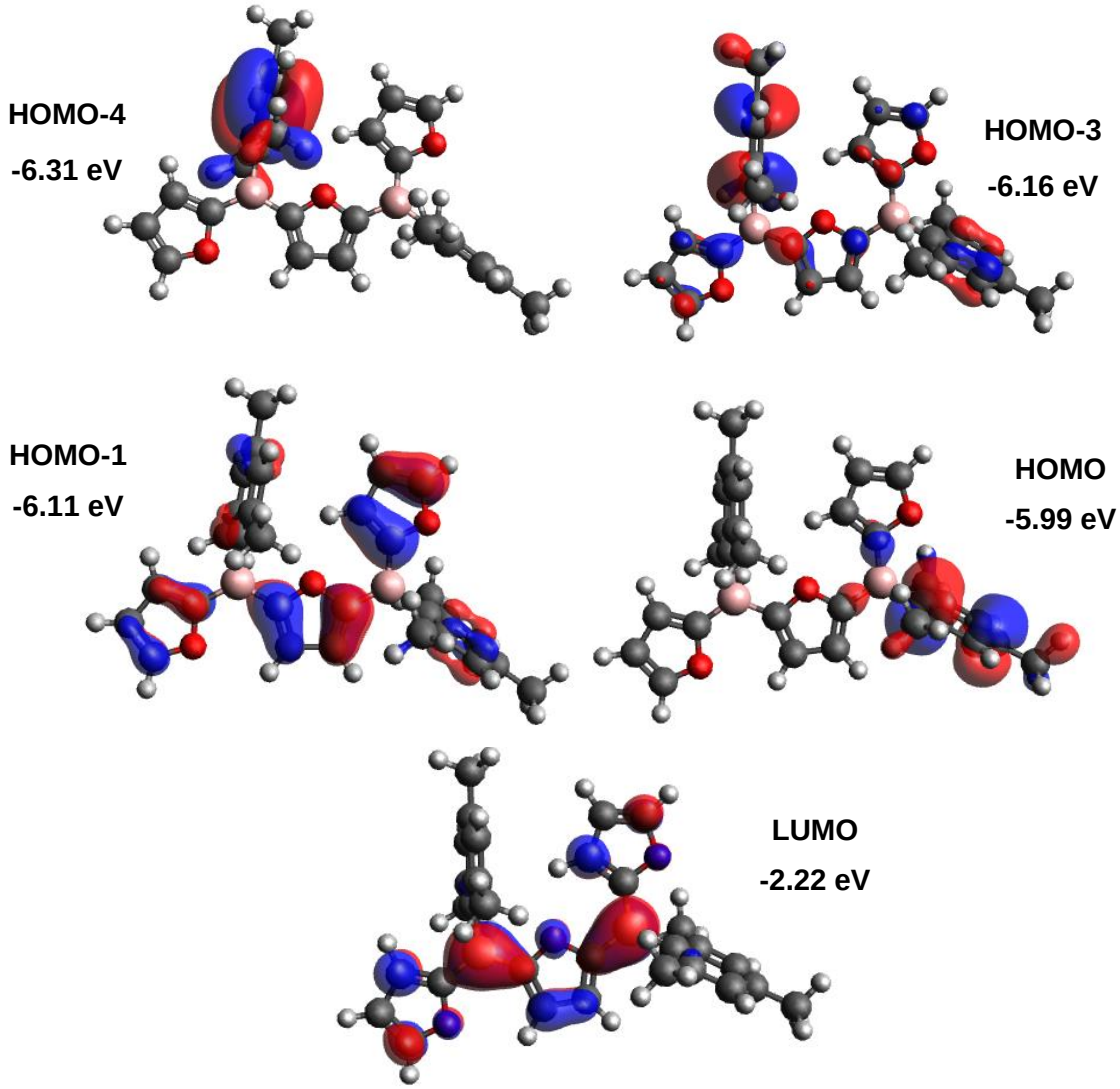

Figure S5.3.113. *Calculated frontier orbitals of* ***BB1F^{Mes}*** *(isovalue 0.03 a.u.).*

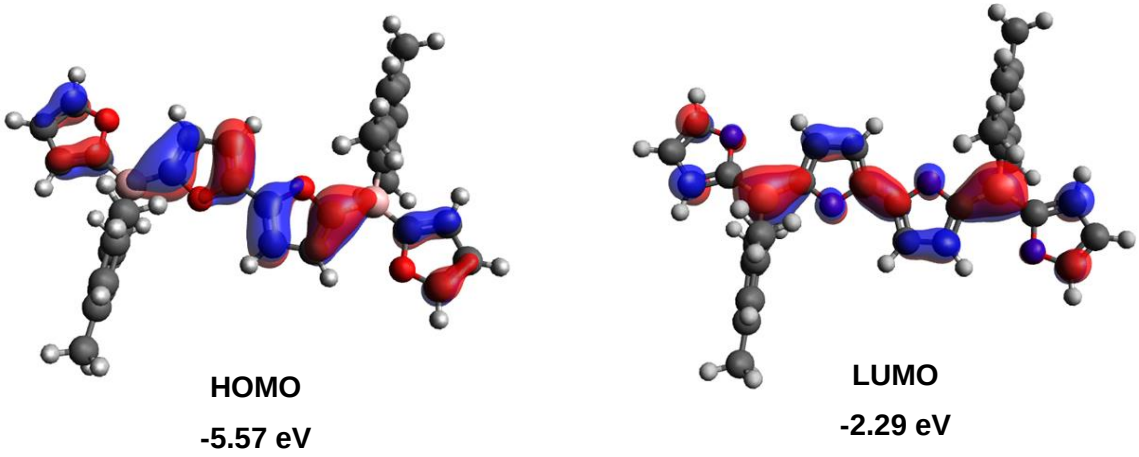

Figure S5.3.114. *Calculated frontier orbitals of* ***BB2F^{Mes}*** *(isovalue 0.03 a.u.).*

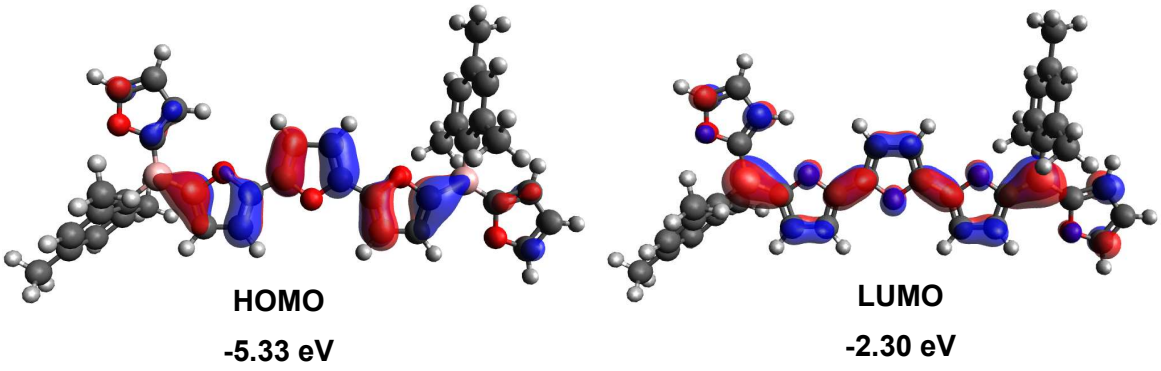

Figure S5.3.115. *Calculated frontier orbitals of* ***BB3F^{Mes}*** *(isovalue 0.03 a.u.).*

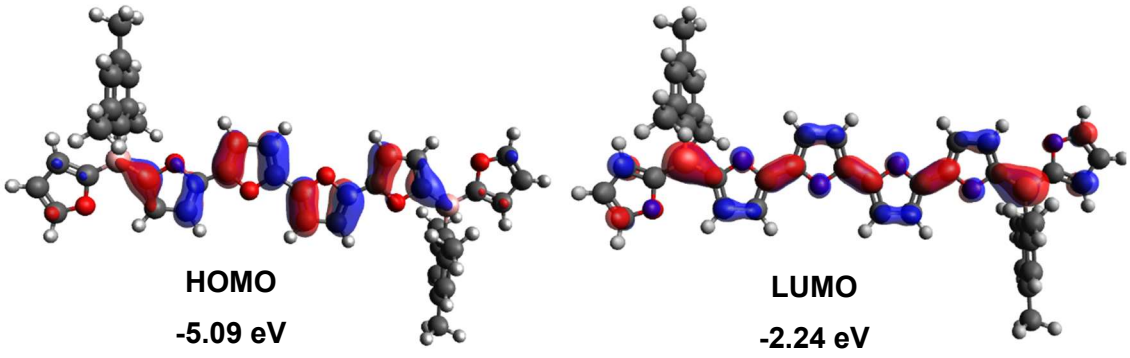

Figure S5.3.116. *Calculated frontier orbitals of* ***BB4F^{Mes}*** *(isovalue 0.03 a.u.).*

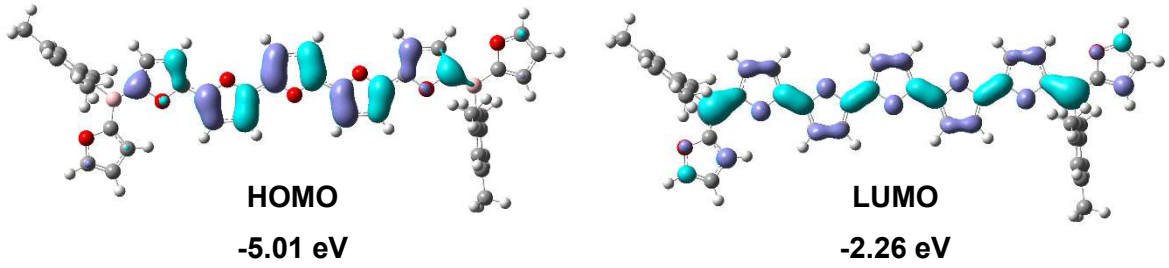

Figure S5.3.117. *Calculated frontier orbitals of* ***BB5F^{Mes}*** *(isovalue 0.03 a.u.).*

Cartesian coordinates [Å] and total energies [a.u.] of optimized stationary points

BB1F^{Mes}:

Total energy (B3LY*P*-D3(BJ)/def2-SV(P)): -1426.890130

C	-3.242559	7.141331	-4.171712
C	-2.094080	7.872132	-4.081178
O	-2.204507	8.924711	-4.948747
C	-3.371995	8.857072	-5.560659
C	-4.077390	7.783170	-5.136645
B	-0.819726	7.724818	-3.241360

C	0.376956	8.733885	-3.341860
C	1.194753	8.739938	-4.472472
C	2.266256	9.610238	-4.541719
C	2.540322	10.499189	-3.513500
C	1.718875	10.493018	-2.402330
C	0.646623	9.618398	-2.303413
C	0.907573	7.804290	-5.611156
C	3.683040	11.463838	-3.624820
C	-0.212450	9.636028	-1.070108
C	-0.711805	6.518298	-2.273535
O	-1.752510	5.684841	-2.148687
C	-1.460792	4.689256	-1.289948
C	-0.186195	4.878200	-0.843141
C	0.297869	6.060376	-1.479468
B	-2.582116	3.655181	-1.063265
C	-3.915226	3.881636	-1.865567
C	-4.158570	3.186111	-3.045690
C	-5.272362	3.495233	-3.810541
C	-6.159880	4.483389	-3.422238
C	-5.908036	5.170135	-2.246189
C	-4.795192	4.887653	-1.473925
C	-3.201356	2.124298	-3.506915
C	-7.373032	4.796497	-4.246224
C	-4.502319	5.705440	-0.250008
C	-2.414677	2.468252	-0.109530
O	-1.246954	2.249158	0.561837
C	-1.384063	1.173432	1.320792
C	-2.621723	0.646217	1.189219
C	-3.291486	1.496225	0.253352
H	-0.532299	0.881743	1.908715
H	-3.008310	-0.225282	1.687035
H	-4.299259	1.406973	-0.112898
H	0.328848	4.242144	-0.146453
H	1.263852	6.521667	-1.371420
H	-5.443901	2.961206	-4.734372
H	-6.582014	5.956019	-1.935444
H	-3.242696	1.250802	-2.855567
H	-3.434461	1.807023	-4.522224
H	-2.174748	2.494104	-3.493096
H	-5.382833	6.261778	0.068427
H	-4.176668	5.075091	0.578195
H	-3.703272	6.417871	-0.460293
H	-8.241200	4.242481	-3.882242
H	-7.612681	5.858605	-4.196956
H	-7.215623	4.523240	-5.289069
H	2.901009	9.600325	-5.416827
H	1.914017	11.183466	-1.593786
H	-3.467118	6.252131	-3.611991

H	-5.057474	7.480287	-5.460154
H	-3.589718	9.629664	-6.276485
H	-0.117739	10.587938	-0.549159
H	-1.263554	9.486854	-1.318515
H	0.076457	8.840839	-0.381836
H	-0.027349	8.078906	-6.099022
H	1.707437	7.834806	-6.349803
H	0.807310	6.776257	-5.259137
H	3.403752	12.321636	-4.240684
H	3.975363	11.836257	-2.643733
H	4.548571	10.990591	-4.088628

BB2F^{Mes}:

Total energy (B3LY*P*-D3(BJ)/def2-SV(P)): -1663.367040

C	-1.438237	-2.892049	-4.781548
C	-0.755434	-1.682495	-4.530488
C	-1.420360	-0.457206	-4.760687
C	-2.732652	-0.459512	-5.248344
C	-3.418931	-1.652980	-5.509185
C	-2.754995	-2.859977	-5.261672
B	0.725741	-1.692580	-3.992465
C	1.862629	-1.937006	-4.994186
O	3.187729	-1.990434	-4.595332
C	3.949143	-2.202532	-5.680373
C	3.175784	-2.293237	-6.811864
C	1.833441	-2.122024	-6.366396
C	-0.722453	0.851573	-4.466030
C	-4.823866	-1.632044	-6.062496
C	-0.762005	-4.220058	-4.520291
C	1.016625	-1.446237	-2.508897
C	2.169738	-1.390479	-1.734020
C	1.787363	-1.115373	-0.398882
C	0.405141	-1.013975	-0.421756
O	-0.058858	-1.210864	-1.668929
C	-0.554447	-0.745959	0.610957
O	-0.089007	-0.541853	1.856432
C	-1.163105	-0.297434	2.695577
C	-2.317334	-0.359893	1.922874
C	-1.936855	-0.646654	0.589605
B	-0.867640	-0.026776	4.174027
C	-1.997920	0.274757	5.167635
C	-1.956030	0.589853	6.515566
C	-3.295387	0.787568	6.959012
C	-4.079954	0.580751	5.850702
O	-3.327797	0.277049	4.781123
C	0.615622	-0.036305	4.706308
C	1.454143	1.080564	4.495811
C	2.768956	1.063584	4.978035
C	3.287428	-0.043093	5.661993

C	2.451021	-1.150295	5.850342
C	1.128591	-1.161680	5.387702
C	0.940262	2.283666	3.737281
C	0.262369	-2.383087	5.604598
C	4.696917	-0.031928	6.203781
H	-5.427593	-0.828391	-5.604076
H	-4.821626	-1.452250	-7.155402
H	-5.342029	-2.591065	-5.888713
H	-3.278096	-3.805625	-5.443966
H	-3.236379	0.497679	-5.426283
H	-1.463926	-5.061973	-4.645461
H	0.088715	-4.383515	-5.207146
H	-0.355066	-4.269438	-3.493092
H	0.265781	0.905426	-4.959134
H	-1.318265	1.715061	-4.807562
H	-0.547759	0.969795	-3.380377
H	5.023316	-2.268522	-5.509734
H	3.528822	-2.460472	-7.828828
H	3.177399	-1.537222	-2.117962
H	2.418477	-1.000752	0.480488
H	-3.324457	-0.209623	2.306907
H	-2.569248	-0.768515	-0.287863
H	-3.639251	1.047486	7.959524
H	-5.156774	0.616481	5.687918
H	2.840775	-2.032982	6.370129
H	1.662852	3.117185	3.760762
H	-0.014678	2.651040	4.155949
H	0.751012	2.030656	2.677544
H	3.408608	1.937875	4.811742
H	4.727308	0.378810	7.232047
H	5.364184	0.592745	5.584217
H	5.122385	-1.049954	6.247110
H	-0.588466	-2.162387	6.275013
H	0.837620	-3.212362	6.050381
H	-0.168800	-2.744936	4.652589
H	-1.042194	0.665751	7.104397
H	0.926150	-2.128273	-6.969880

BB3F^{Mes}:

Total energy (B3LY*P*-D3(BJ)/def2-SV(P)): -1891.927200

O	3.539583	0.043401	-4.517146
C	2.657262	0.698758	-3.672718
C	1.583607	-0.152088	-3.454942
C	1.822711	-1.349910	-4.184302
C	3.034049	-1.161673	-4.807460
B	3.024902	2.107088	-3.194462
C	4.364114	2.800290	-3.652387
C	5.586116	2.465611	-3.026494
C	6.766332	3.107627	-3.418023

C	6.776513	4.073925	-4.432963
C	5.561892	4.389304	-5.051811
C	4.360930	3.770940	-4.676258
C	5.617842	1.411822	-1.942710
C	8.067701	4.730082	-4.860377
C	3.070168	4.144488	-5.371835
C	2.112774	2.883699	-2.235675
C	2.272087	4.133751	-1.654558
C	1.146102	4.383909	-0.831265
C	0.343311	3.260821	-0.948363
O	0.910785	2.364849	-1.781623
C	-0.916510	2.917268	-0.357453
C	-1.728610	1.803535	-0.448662
C	-2.853957	2.057021	0.383653
C	-2.657413	3.309923	0.930046
O	-1.481867	3.831949	0.480251
C	-3.435346	4.103633	1.834689
O	-4.591755	3.578070	2.276556
C	-5.196105	4.488496	3.129836
C	-4.367373	5.601893	3.201923
C	-3.240121	5.364219	2.378859
B	-6.537512	4.100580	3.756526
C	-7.283039	5.060522	4.693807
C	-8.509689	4.935874	5.324075
C	-8.737838	6.126047	6.073363
C	-7.632104	6.911032	5.855504
O	-6.760726	6.295712	5.040065
C	-7.194423	2.703144	3.441625
C	-7.078664	1.632553	4.354495
C	-7.670747	0.398009	4.056880
C	-8.387555	0.192224	2.872043
C	-8.487953	1.259632	1.970831
C	-7.900992	2.503247	2.235389
C	-6.306008	1.809365	5.643207
C	-8.010894	3.624250	1.226451
C	-9.055218	-1.131431	2.585686
H	-3.710428	1.412193	0.570774
H	-1.527415	0.915949	-1.045357
H	0.931931	5.260495	-0.223238
H	3.129221	4.785092	-1.821904
H	0.724154	0.083780	-2.830225
H	1.190535	-2.235233	-4.244665
H	3.632577	-1.788511	-5.467857
H	7.706242	2.845216	-2.918528
H	5.547430	5.138648	-5.851551
H	6.618514	1.330164	-1.485228
H	4.893736	1.634743	-1.137277
H	5.349532	0.419590	-2.350281

H	2.381176	4.676494	-4.689840
H	3.254659	4.798242	-6.241257
H	2.531685	3.247999	-5.731595
H	8.676430	4.047787	-5.485024
H	7.881577	5.642237	-5.453372
H	8.687941	5.009354	-3.989422
H	-2.388195	6.015367	2.193458
H	-4.577331	6.487939	3.797965
H	-9.162069	4.067178	5.239740
H	-9.600170	6.374849	6.690916
H	-7.344511	7.900787	6.208941
H	-7.565752	-0.428095	4.769622
H	-9.036050	1.118641	1.032043
H	-5.283765	2.186301	5.451688
H	-6.794767	2.542699	6.310847
H	-6.216269	0.857672	6.194072
H	-8.669348	3.349408	0.384944
H	-8.414323	4.545741	1.685374
H	-7.018882	3.880793	0.810501
H	-8.534343	-1.965221	3.088449
H	-10.103386	-1.137436	2.943796
H	-9.081219	-1.346457	1.502796

BB4F^{Mes}:

O	0.609902	1.805492	-1.455305
C	0.458297	2.375538	-0.202187
C	0.704755	1.388253	0.736784
C	1.014781	0.187158	0.035529
C	0.939383	0.513379	-1.296387
B	0.068756	3.850037	-0.026728
C	-0.047873	4.425597	1.436007
C	-1.311944	4.560735	2.050127
C	-1.402083	5.071843	3.351288
C	-0.264960	5.466186	4.066846
C	0.981736	5.341274	3.441006
C	1.106223	4.826203	2.144326
C	-2.565494	4.170370	1.299948
C	-0.375339	5.984924	5.480624
C	2.471571	4.713482	1.502505
C	-0.214459	4.744793	-1.234680
C	-0.200942	4.565053	-2.613016
C	-0.565735	5.790924	-3.219802
C	-0.788599	6.673373	-2.172884
O	-0.581004	6.060739	-0.993735
C	-1.180322	8.050784	-2.134348
C	-1.399886	8.927901	-1.091271
C	-1.770964	10.168048	-1.681316
C	-1.753776	9.968883	-3.048498
O	-1.395490	8.683355	-3.324171

C	-2.028899	10.825210	-4.162015
C	-2.011421	10.625775	-5.529160
C	-2.381471	11.866048	-6.119541
C	-2.600799	12.743485	-5.076679
O	-2.386538	12.110991	-3.886663
C	-2.990995	14.121348	-5.039001
C	-3.214376	15.004665	-3.992939
C	-3.575975	16.230878	-4.601025
C	-3.560118	16.050461	-5.979243
O	-3.195496	14.733764	-6.218811
B	-3.838135	16.945277	-7.188415
C	-3.718499	16.368491	-8.650431
C	-4.871143	15.976464	-9.364201
C	-4.743593	15.459560	-10.660824
C	-3.495396	15.324831	-11.279587
C	-2.358426	15.711600	-10.557999
C	-2.451493	16.223815	-9.258441
C	-6.239619	16.100024	-8.731001
C	-3.374887	14.802172	-12.691141
C	-1.199389	16.606359	-8.501866
C	-4.224209	18.420878	-7.014637
C	-4.464090	19.408850	-7.954582
C	-4.772679	20.611044	-7.254579
C	-4.703116	20.284738	-5.922364
O	-4.378414	18.991577	-5.762124
H	1.091726	-0.060731	-2.209842
H	1.260529	-0.788754	0.452804
H	0.659816	1.535996	1.815648
H	0.051487	3.629786	-3.109157
H	-0.660059	6.019835	-4.279522
H	-2.388876	5.168659	3.818501
H	1.884104	5.657859	3.976799
H	-2.497758	3.140234	0.903736
H	-3.458751	4.226525	1.945155
H	-2.731430	4.837706	0.433799
H	3.253432	5.171000	2.132307
H	2.750444	3.657832	1.329075
H	2.495396	5.214538	0.516903
H	-0.258650	5.166561	6.217999
H	0.406803	6.733009	5.699688
H	-1.358587	6.452168	5.665277
H	-2.021639	11.099150	-1.177269
H	-1.300635	8.690273	-0.033781
H	-2.480151	12.103641	-7.177096
H	-1.761099	9.694433	-6.032941
H	-3.827660	17.166829	-4.105797
H	-3.122349	14.776170	-2.932926
H	-5.645383	15.149890	-11.201358

H	-1.369873	15.607377	-11.020173
H	-4.856866	20.859451	-5.009522
H	-5.013745	21.587703	-7.672834
H	-4.415752	19.260819	-9.033257
H	-7.019594	15.639920	-9.361261
H	-6.271167	15.607878	-7.741159
H	-6.515608	17.158189	-8.568582
H	-1.262915	17.636805	-8.105792
H	-1.041987	15.937897	-7.635037
H	-0.303257	16.544892	-9.142591
H	-2.484373	14.159409	-12.810760
H	-4.262745	14.214676	-12.982468
H	-3.275400	15.631536	-13.418546

BB5F^{Mes}:

C	-0.424360	5.735761	-0.341845
C	-1.126720	6.279199	0.755687
C	-2.245346	5.585736	1.266811
C	-2.634785	4.371562	0.686981
C	-1.936903	3.814138	-0.391647
C	-0.834102	4.515536	-0.894099
B	-0.659144	7.639213	1.400560
C	-1.040119	8.984896	0.774358
C	-0.792562	10.311366	1.095339
C	-1.422915	11.122261	0.110870
C	-2.020501	10.240920	-0.759302
O	-1.805146	8.974879	-0.381281
C	-3.029644	6.156622	2.427457
C	-2.345822	2.483800	-0.977432
C	0.755725	6.477436	-0.928391
C	0.204594	7.568141	2.665667
C	0.691524	6.473378	3.365959
C	1.451771	6.952972	4.461475
C	1.393608	8.334957	4.377846
O	0.654388	8.708384	3.313205
C	1.960601	9.370347	5.190039
C	1.919501	10.748536	5.124449
C	2.687814	11.228230	6.221910
C	3.150388	10.110775	6.889552
O	2.709113	8.983624	6.264284
C	3.965390	9.938823	8.053546
C	4.424318	8.824162	8.726623
C	5.197703	9.305504	9.820463
C	5.162461	10.683817	9.746009
O	4.413710	11.068801	8.672736
C	5.739329	11.720704	10.546712
C	5.704608	13.099762	10.467470
C	6.478081	13.583321	11.559206
C	6.935879	12.470294	12.235228

O	6.486693	11.337816	11.619798
C	7.751717	12.316292	13.402436
C	8.209211	11.199274	14.086414
C	8.973666	11.701506	15.166898
C	8.953140	13.089837	15.101511
O	8.188561	13.439862	13.998537
B	9.557188	14.219263	15.937363
C	10.425793	13.924646	17.167986
C	11.076661	14.781698	18.039284
C	11.748404	13.986502	19.012297
C	11.466914	12.685038	18.676091
O	10.685105	12.629998	17.585736
C	9.303248	15.724726	15.544812
C	10.098738	16.347492	14.558579
C	9.865090	17.686385	14.220774
C	8.850267	18.433141	14.832709
C	8.059129	17.799625	15.798878
C	8.271539	16.463484	16.163048
C	11.187175	15.564305	13.859690
C	7.388670	15.810251	17.202815
C	8.634716	19.885607	14.480357
H	11.770885	16.202041	13.174373
H	7.586707	20.190832	14.646102
H	7.972635	15.489751	18.085300
H	0.435166	7.436705	-1.375928
H	-3.436529	2.327226	-0.904266
H	-3.355790	7.192925	2.220760
H	1.509120	6.718686	-0.155728
H	1.255271	5.887513	-1.715490
H	-2.420030	6.193344	3.349133
H	-3.930057	5.555907	2.641902
H	-1.859354	1.643994	-0.443370
H	-2.058682	2.403570	-2.040644
H	11.890209	15.112057	14.583806
H	10.758919	14.734026	13.267681
H	9.270168	20.547100	15.101198
H	8.888533	20.088832	13.425014
H	6.898478	14.904186	16.799742
H	6.596729	16.495223	17.551124
H	11.750368	11.728577	19.114350
H	12.358335	14.324195	19.849501
H	11.058111	15.868823	17.965725
H	9.496657	11.129047	15.930764
H	8.007016	10.162523	13.824675
H	6.683726	14.617010	11.830796
H	5.182099	13.680720	9.710286
H	5.720554	8.722198	10.575623
H	4.222222	7.789645	8.456742

H	2.884481	12.261984	6.498259
H	1.396012	11.334578	4.371545
H	1.980839	6.381591	5.221426
H	0.504278	5.435303	3.092437
H	10.490516	18.159786	13.455068
H	7.250545	18.360825	16.281007
H	-0.213591	10.641688	1.955718
H	-1.436597	12.209859	0.046871
H	-2.613336	10.379384	-1.662987
H	-3.510264	3.847500	1.087187
H	-0.279428	4.102242	-1.744376

5.4 Mechanistic Investigations on the Catalytic Si/B Exchange Condensation to Form Di(het)aryl-bromoboranes

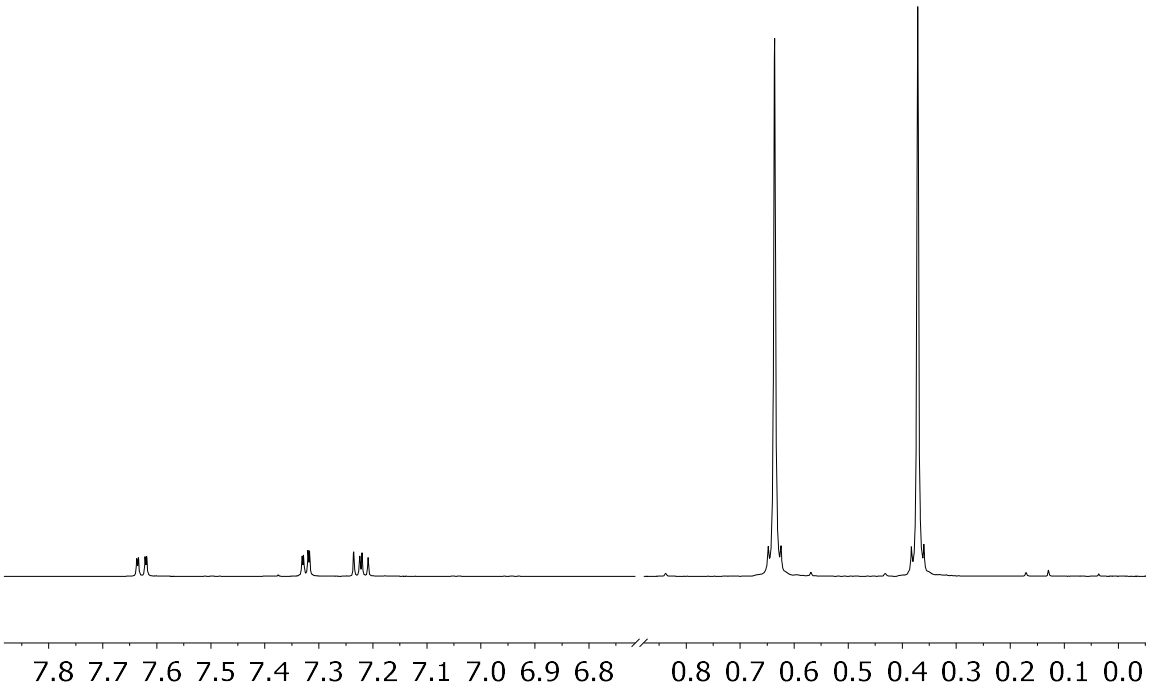

Figure S5.4.1: *In situ ^{1}H NMR of stoichiometric reaction between **7a** and **9** after 24h (in CD_2Cl_2).*

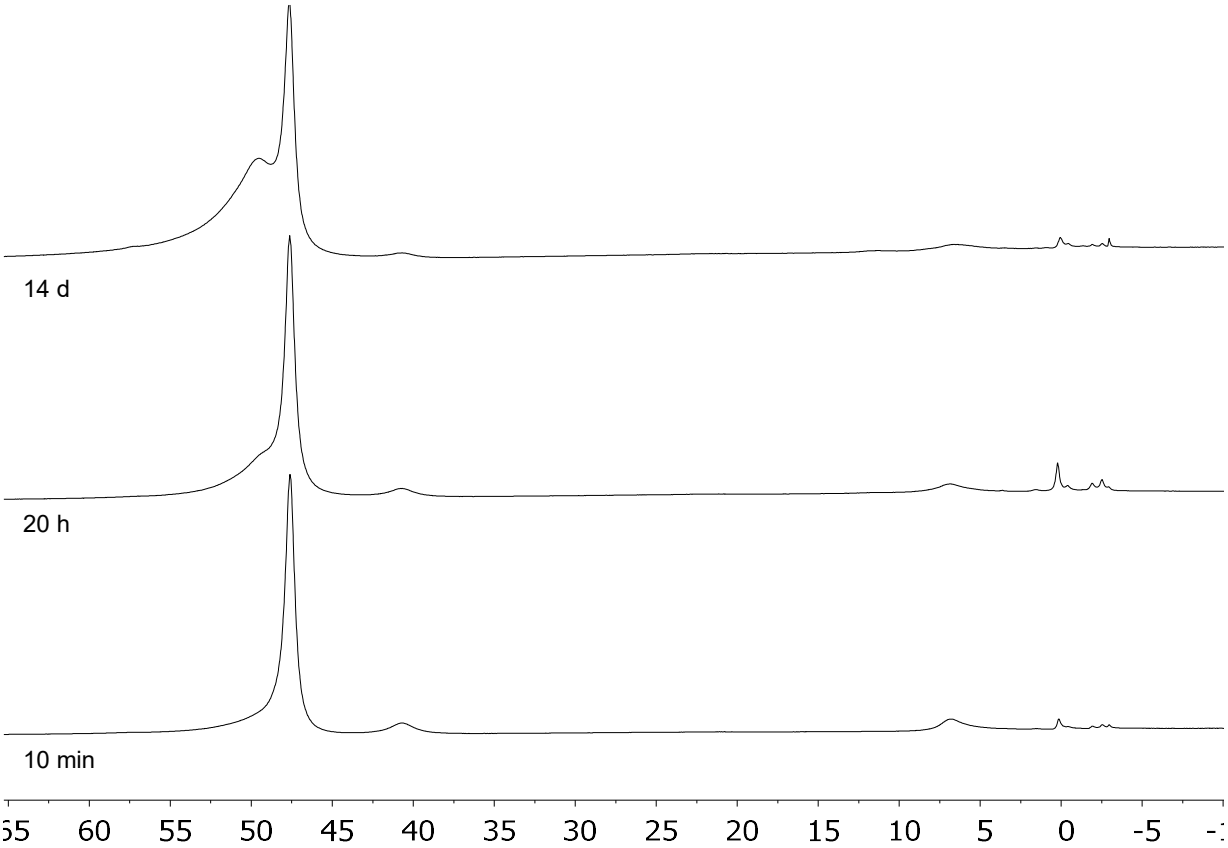

Figure S5.4.2: *In situ $^{11}B\{^{1}H\}$ NMR of stoichiometric reaction between **6a** and **9** (in CD_2Cl_2).*

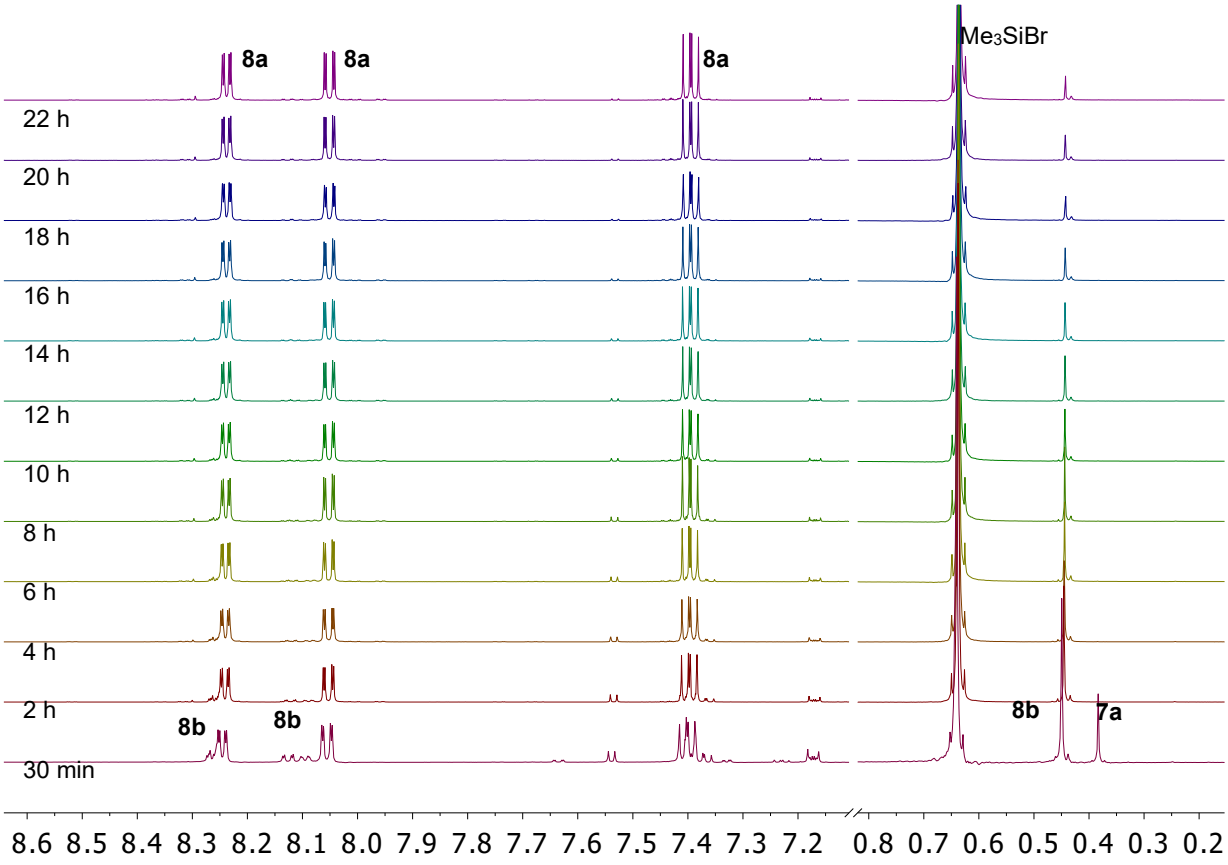

Figure S5.4.3: *In situ ^{1}H NMR spectra of the catalytic reaction between* ***6a*** *and* ***7a*** *(in CD_2Cl_2).*

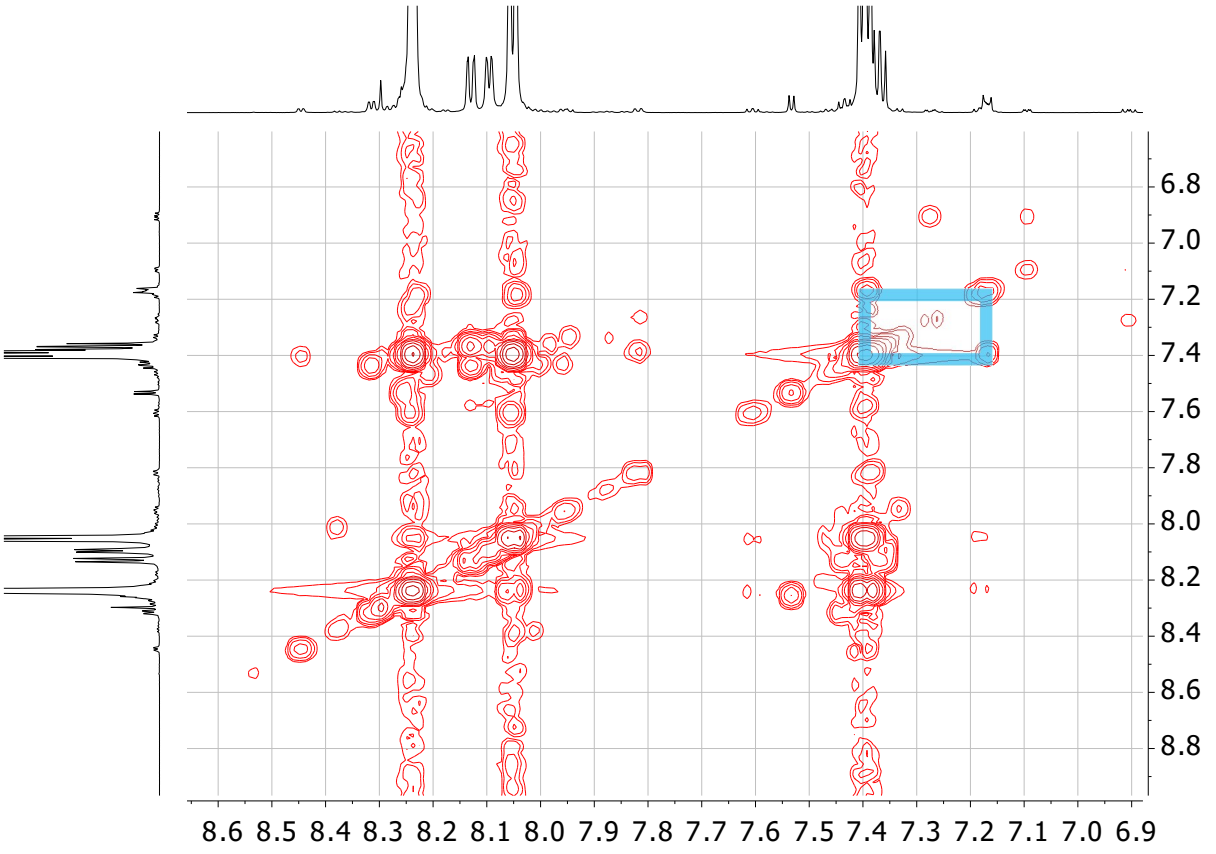

Figure S5.4.4: *COSY ^{1}H NMR aromatic region of catalytic reaction of* ***6a*** *and* ***7a*** *(in CD_2Cl_2).*

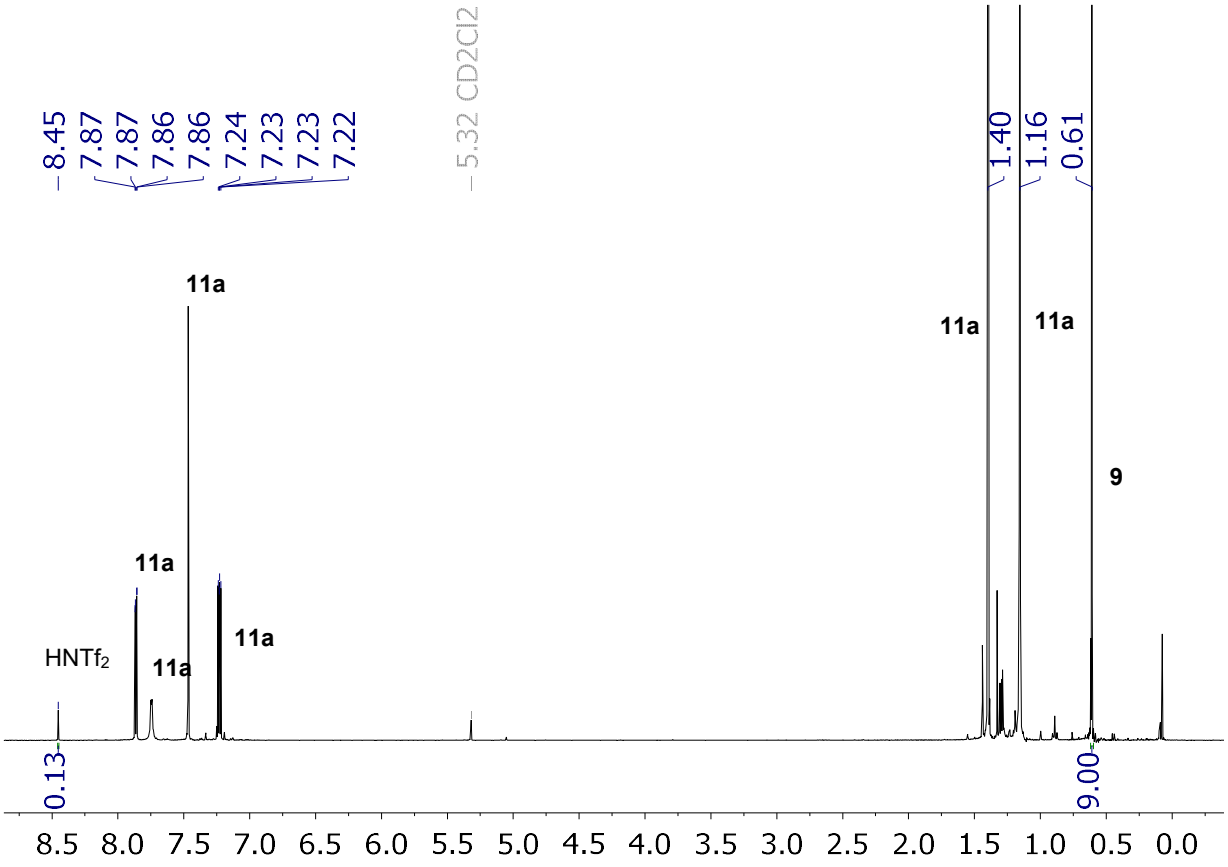

Figure S5.4.5: *In situ ^{1}H NMR of reaction between* ***11b*** *and $HNTf_2$ after 12 min.*

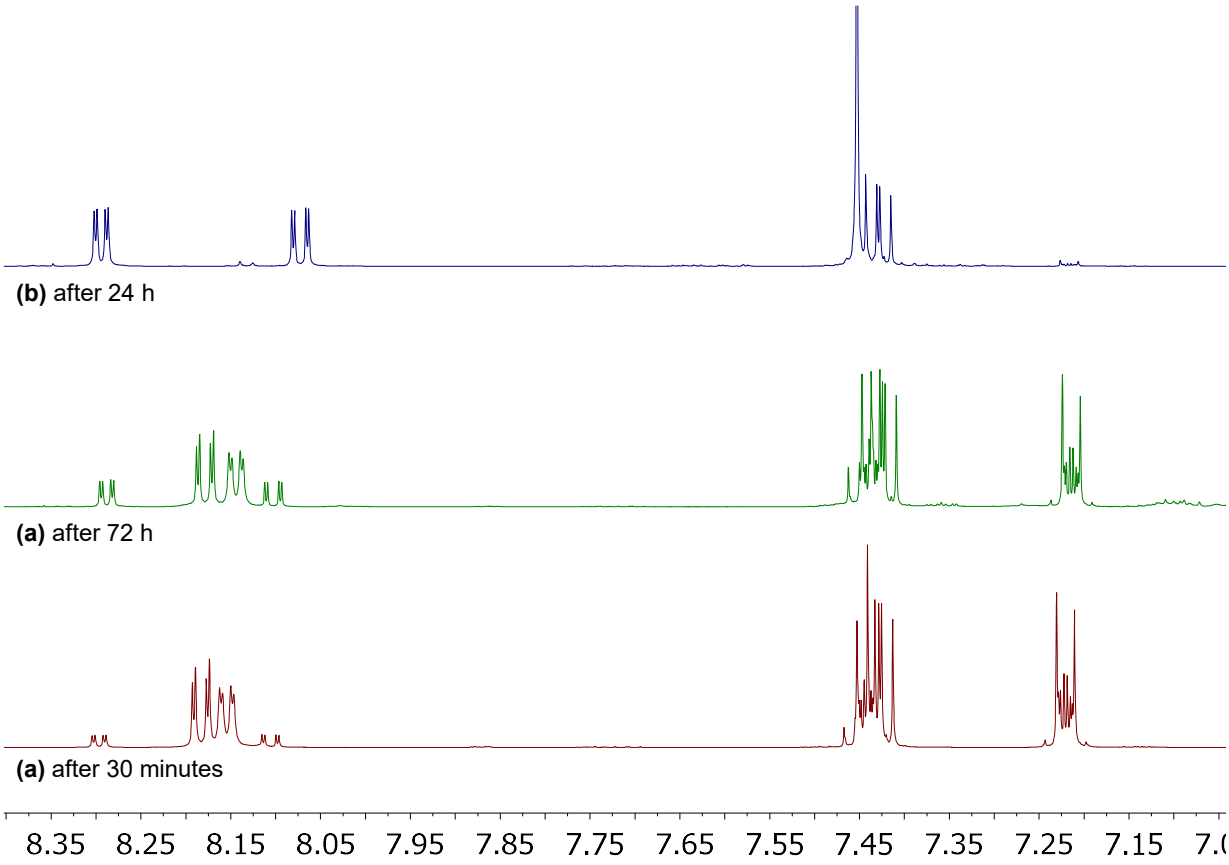

Figure S5.4.6: *In situ ^{1}H NMR spectra of the reactions between* ***6a****, thiophene and trimethyl(phenyl)silane* ***7j*** *(in CD_2Cl_2).*

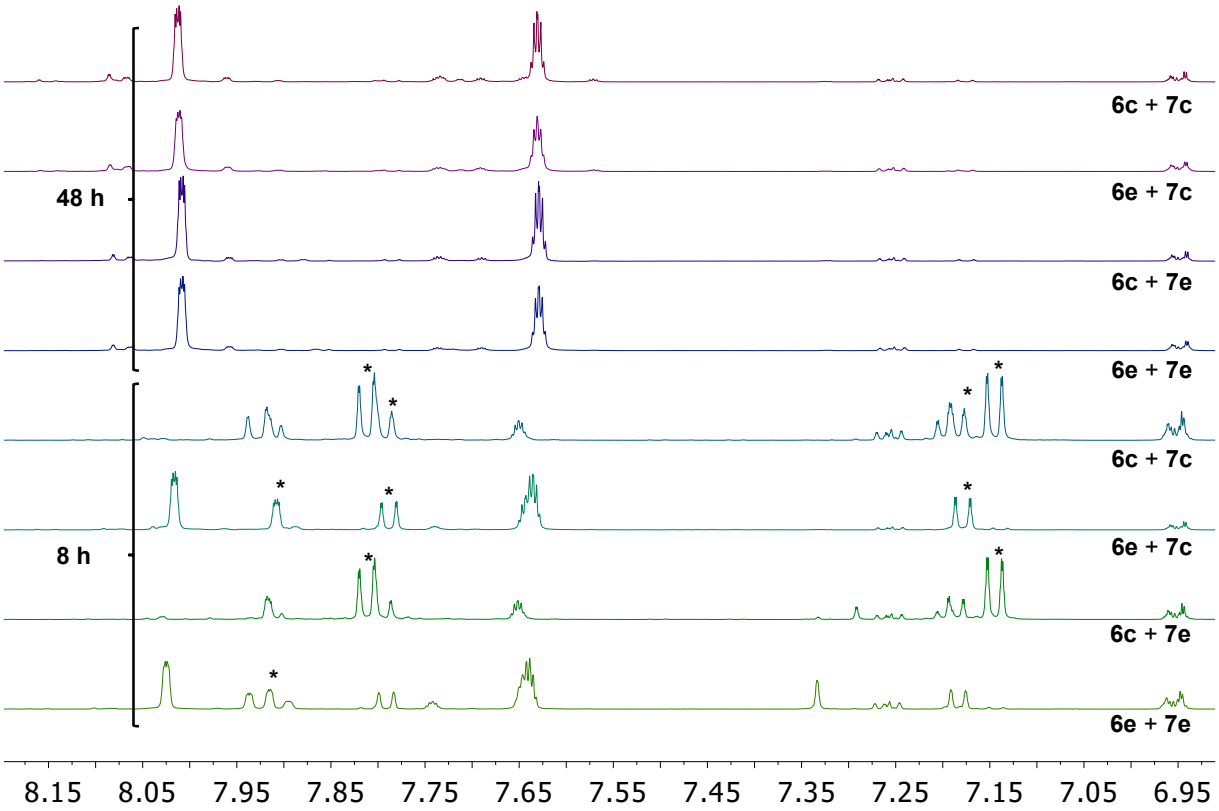

Figure S5.4.7: *In situ ^{1}H NMR aromatic region of reactions between* ***6c,e*** *and* ***7c,e*** *after 3 h and 48 h reaction time (in CD_2Cl_2). Substrate signals are marked with an asterisk.*

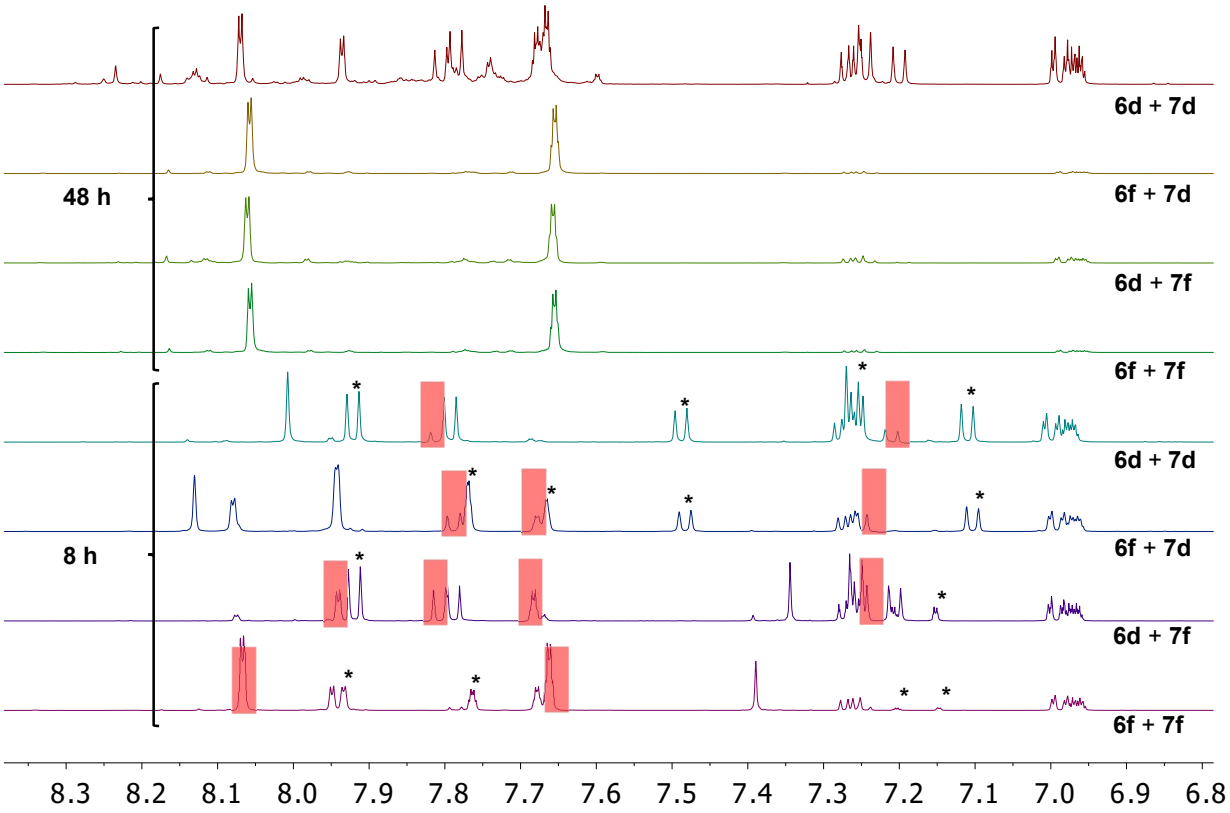

Figure S5.4.8: *In situ ^{1}H NMR aromatic region of reactions between* ***6d,f*** *and* ***7d,f*** *after 3 h and 48 h reaction time (in CD_2Cl_2). Substrate signals are marked with an asterisk, Si/B exchange product signals are marked red.*

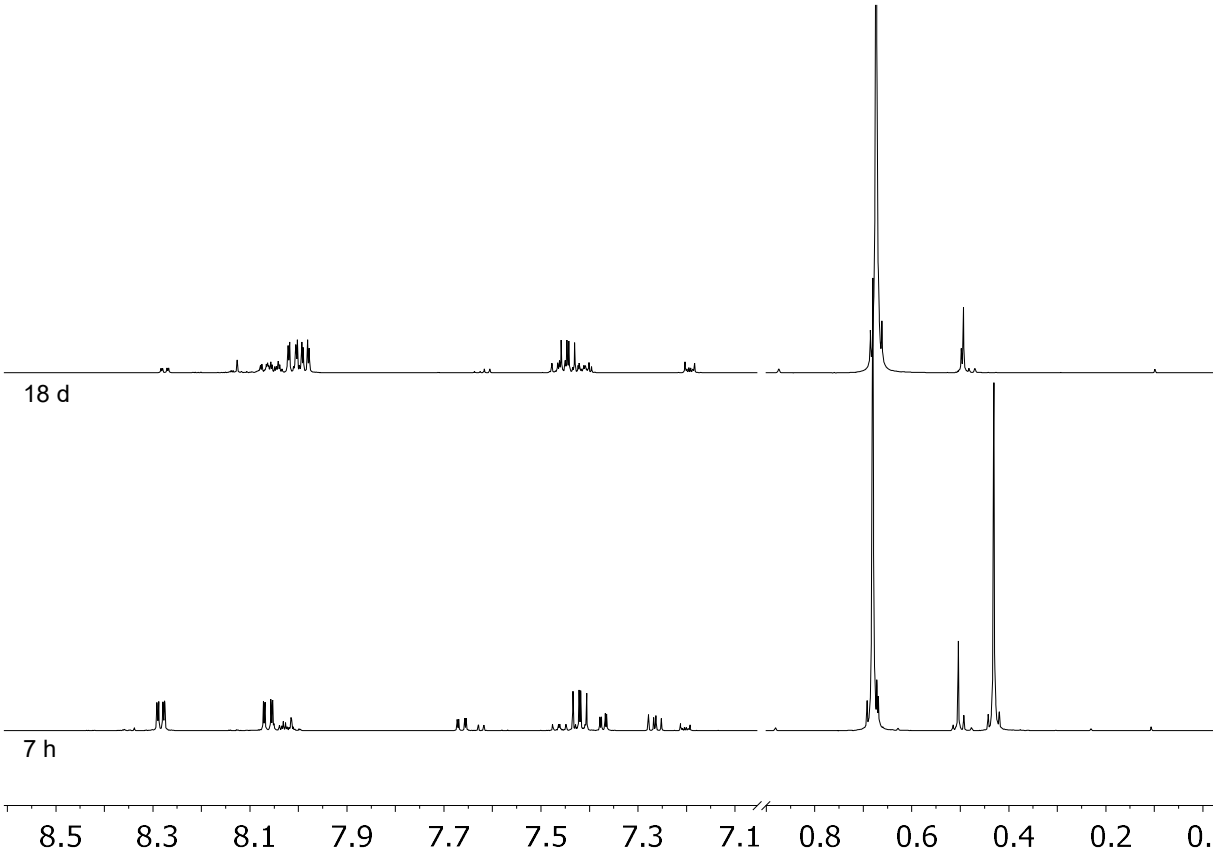

Figure S5.4.9: *In situ ^{1}H NMR of the formation of* ***12a*** *at different reaction times.*

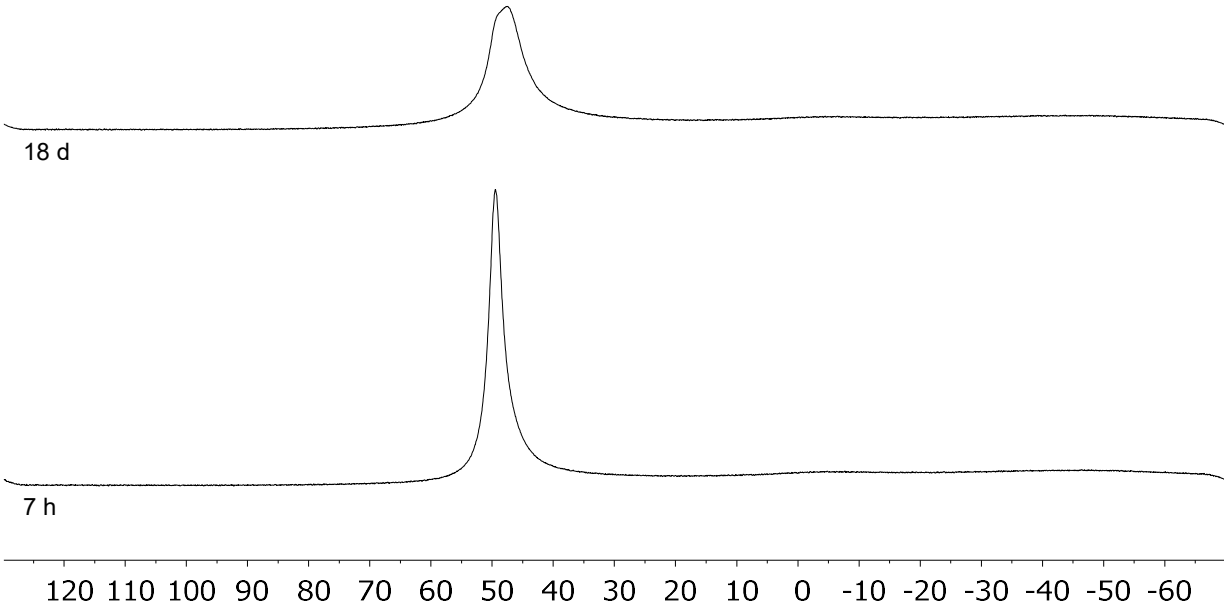

Figure S5.4.10: *In situ $^{11}B\{^{1}H\}$ NMR of the formation of* ***12a*** *at different reaction times.*

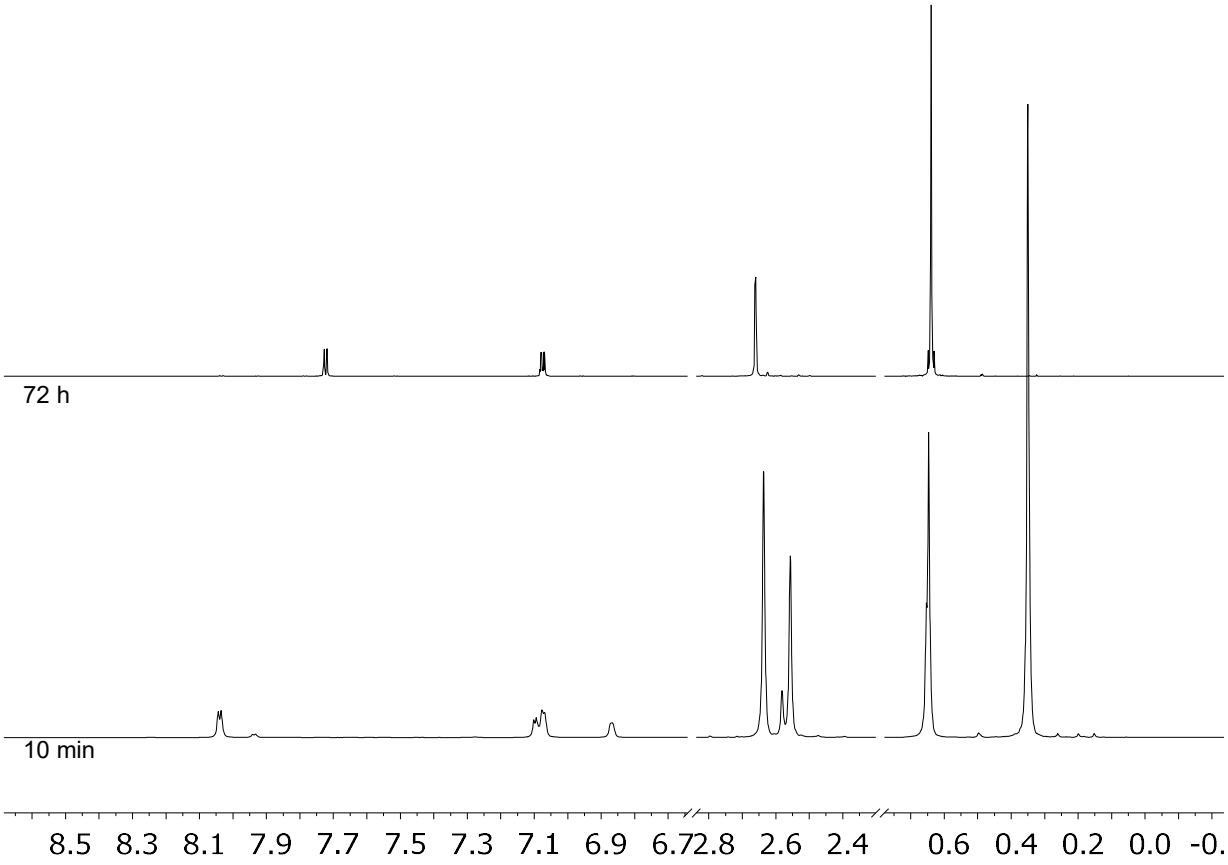

Figure S5.4.11: *In situ ^{1}H NMR of the formation of* ***12g*** *at different reaction times.*

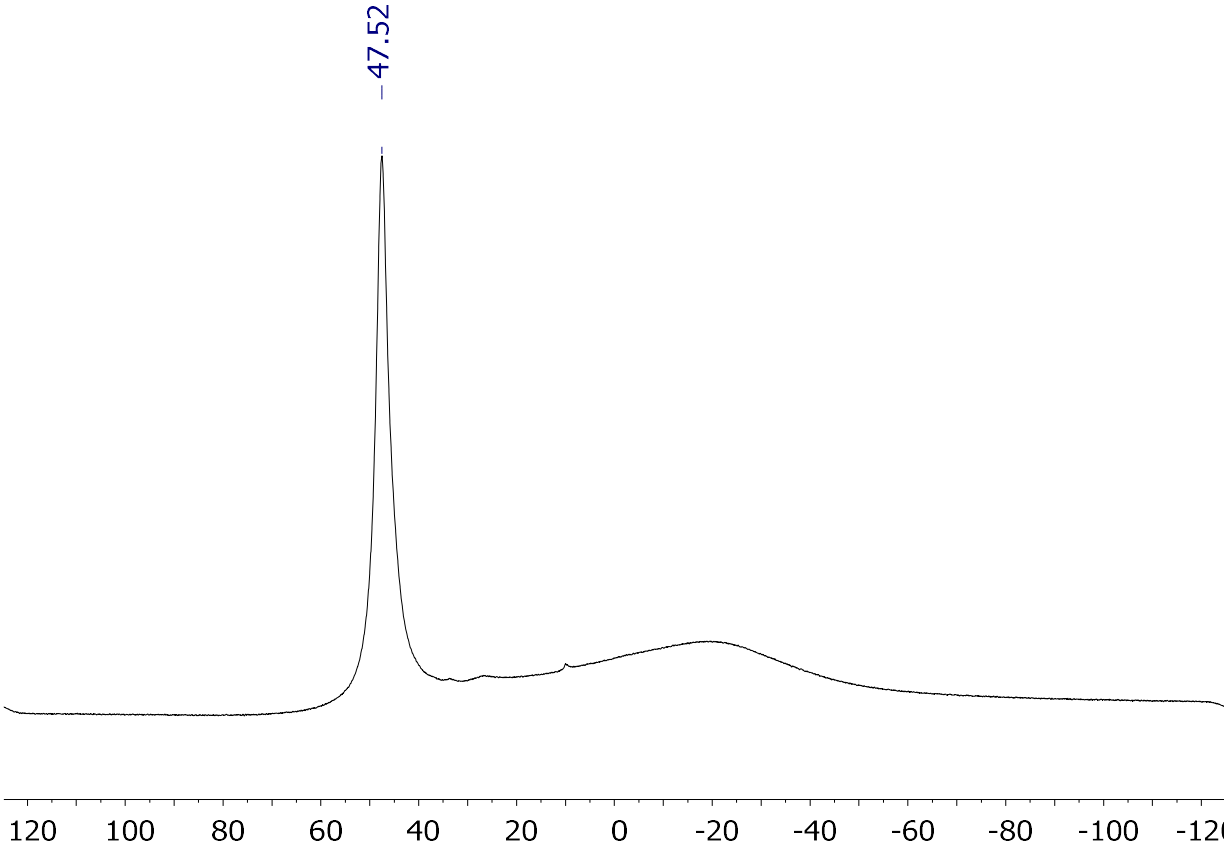

Figure S5.4.12: *In situ $^{11}B\{^{1}H\}$ NMR of the formation of* ***12g*** *after 72 h.*

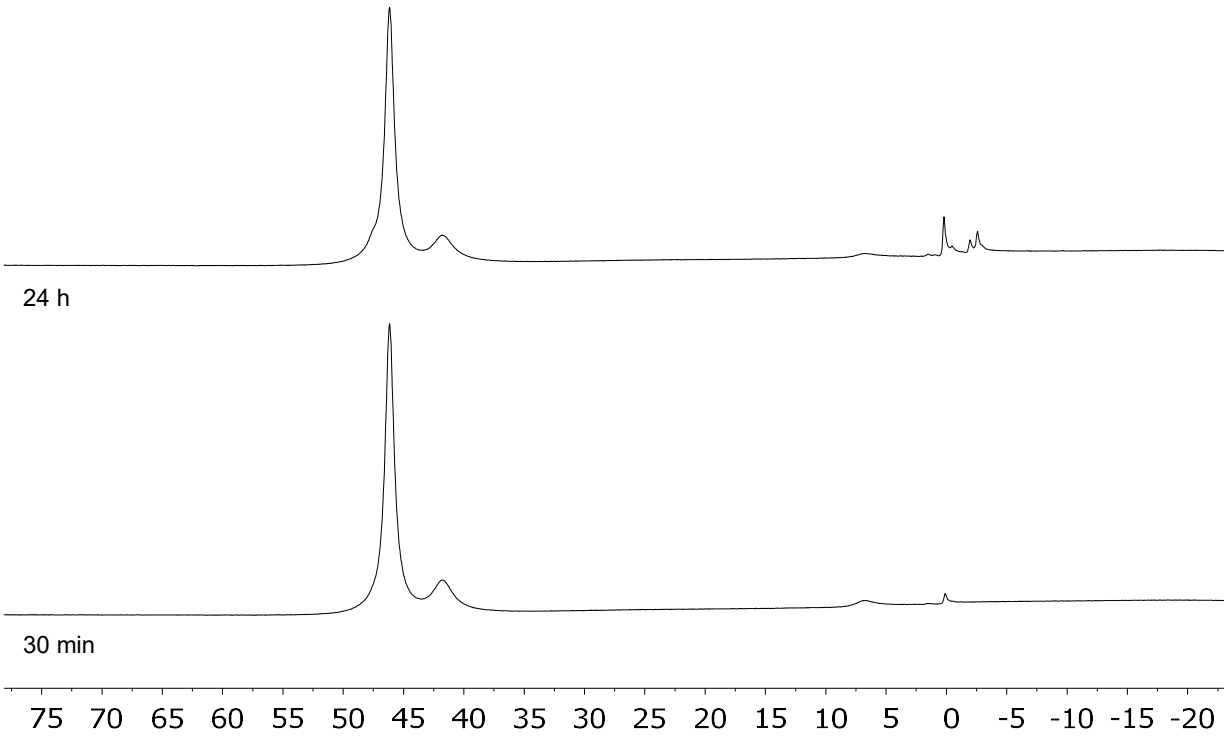

Figure S5.4.13: *In situ $^{11}B\{^1H\}$ NMR of stoichiometric reaction between **6g** and **9** (in CD_2Cl_2).*

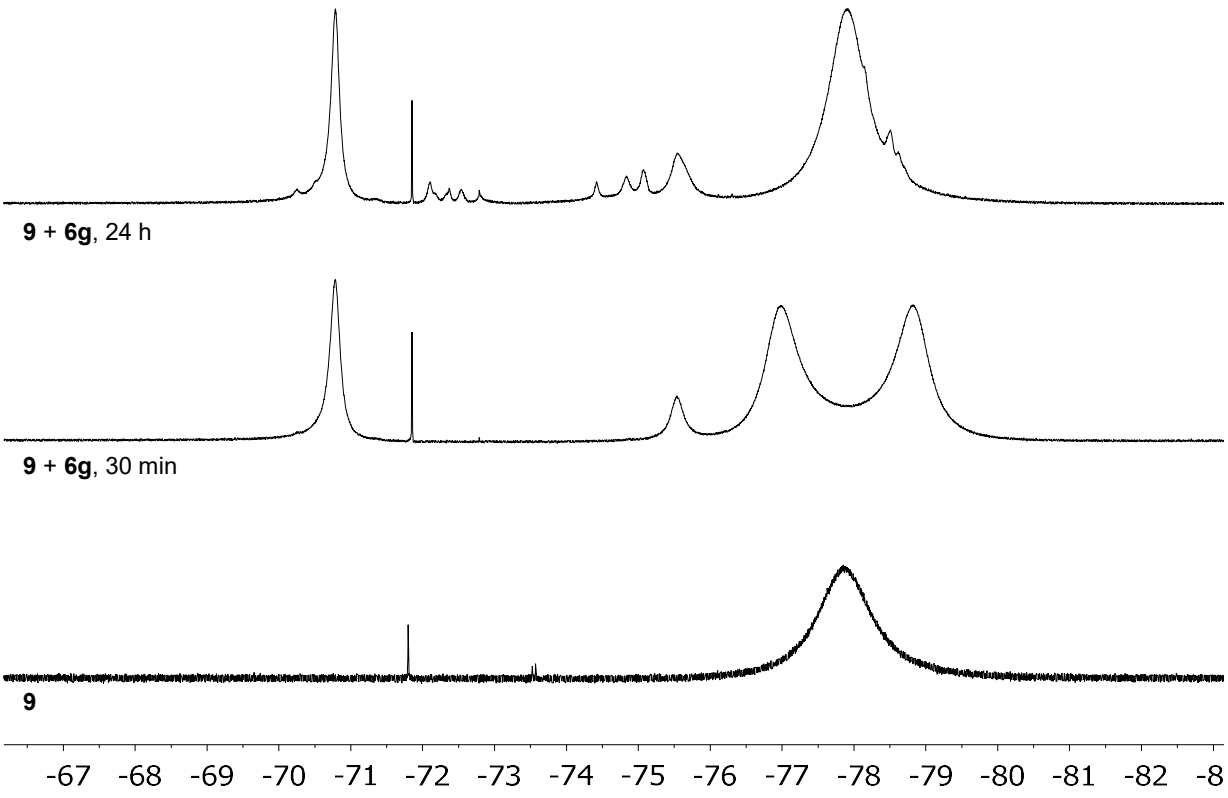

Figure S5.4.14: *In situ $^{19}F\{^1H\}$ NMR of stoichiometric reaction between **6g** and **9** (in CD_2Cl_2).*

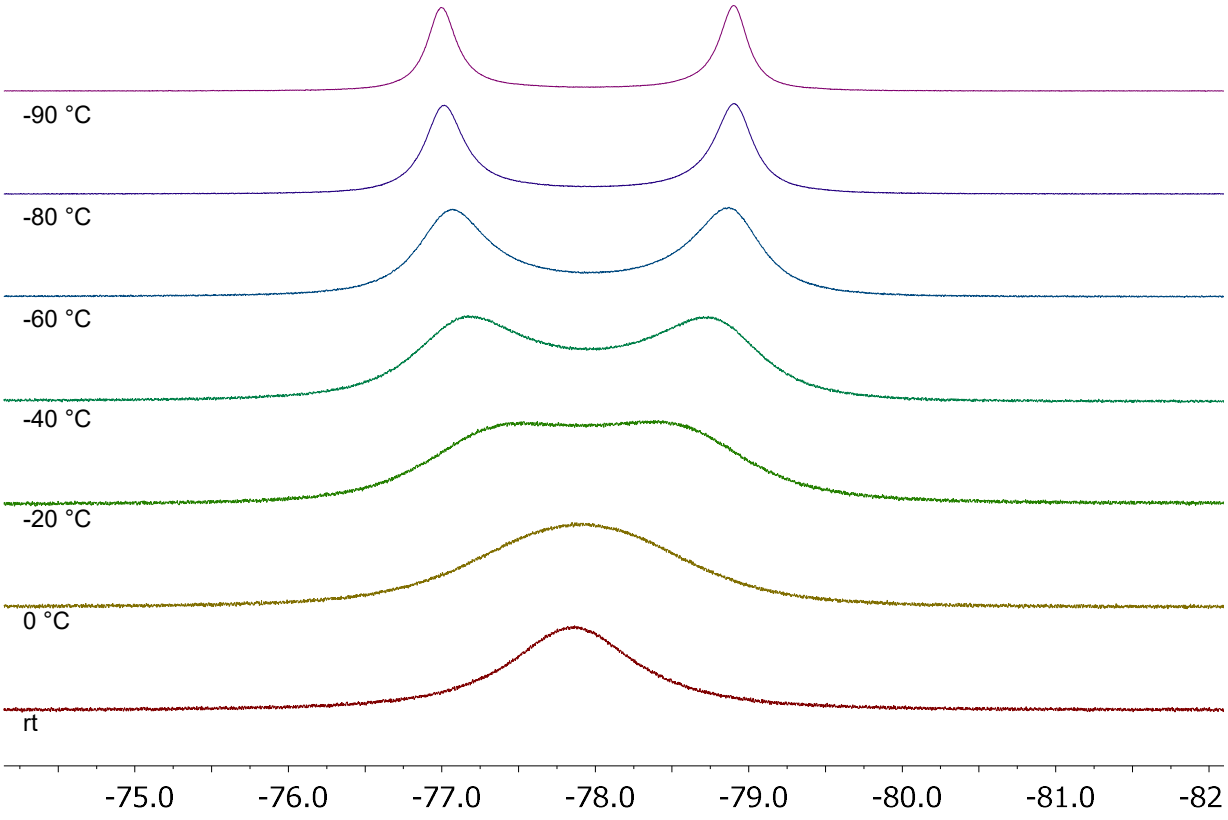

Figure S5.4.15: *VT ^{1}H NMR of catalyst **9** (in CD_2Cl_2).*

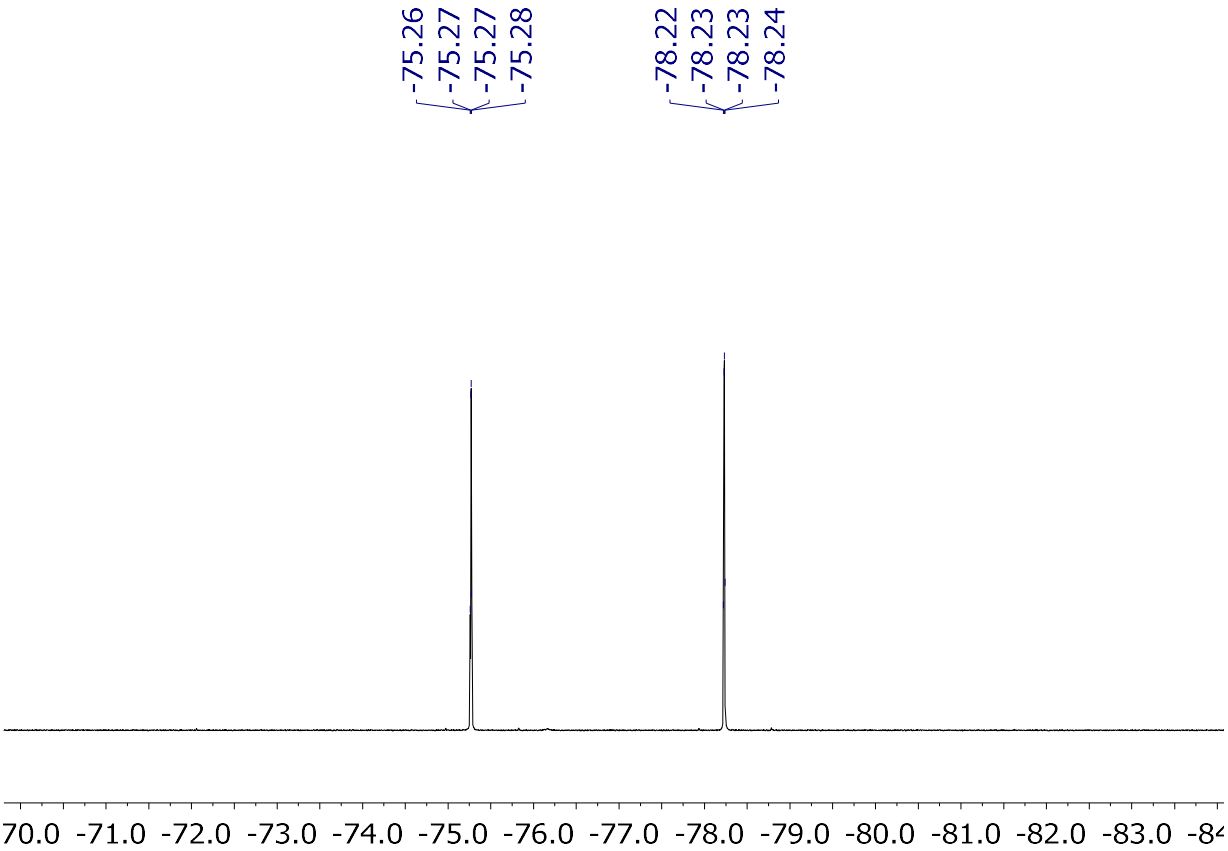

Figure S5.4.16: *$^{19}F\{^{1}H\}$ NMR of **14** (in $CDCl_3$).*

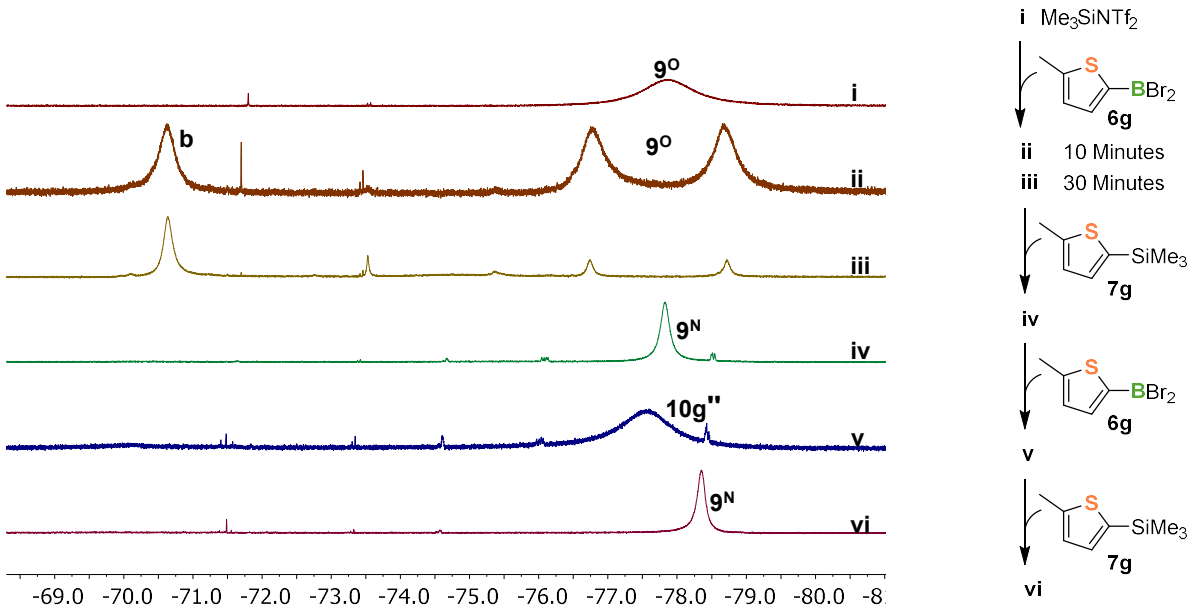

Figure S5.4.17: *In situ 19F{1H} NMR spectra of catalytic reaction between* ***6g****,* ***7g*** *and* ***9*** *(in CD_2Cl_2).*

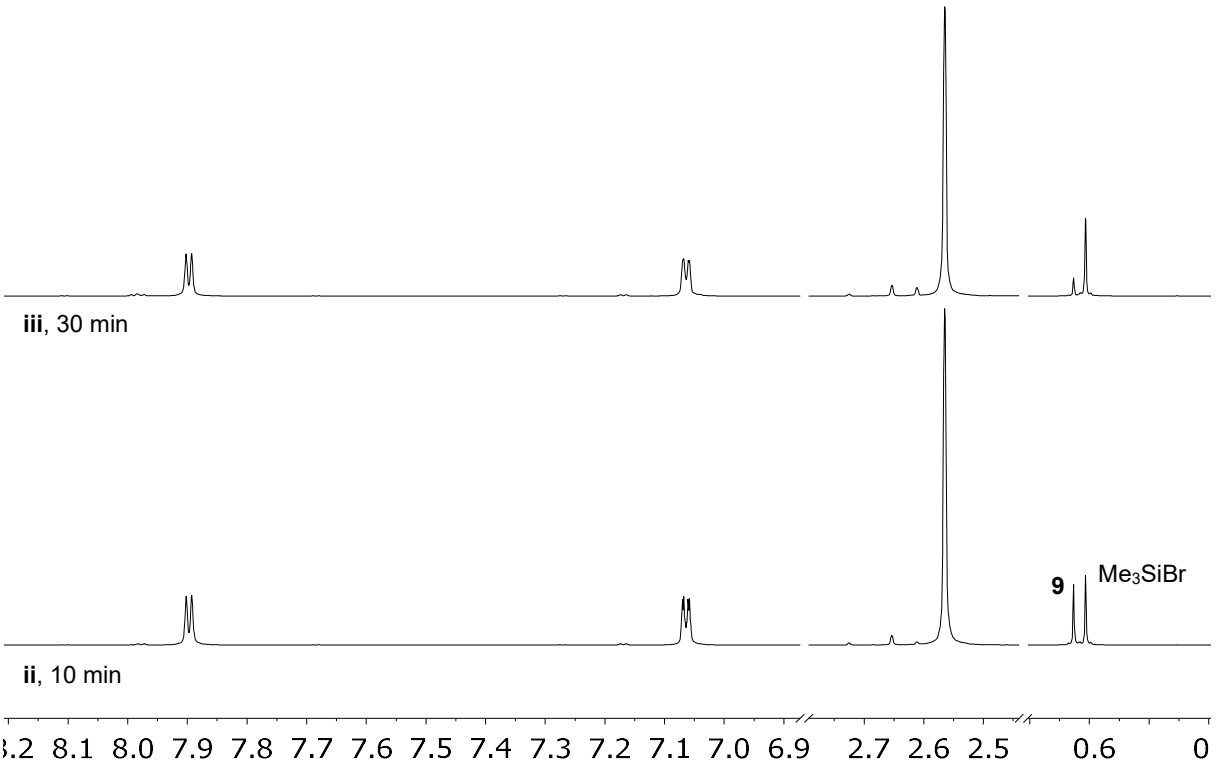

Figure S5.4.18: *In situ ^1H NMR of reaction mixture of* ***7g*** *with catalytic amounts of* ***9*** *(steps ii and iii, in CD_2Cl_2).*

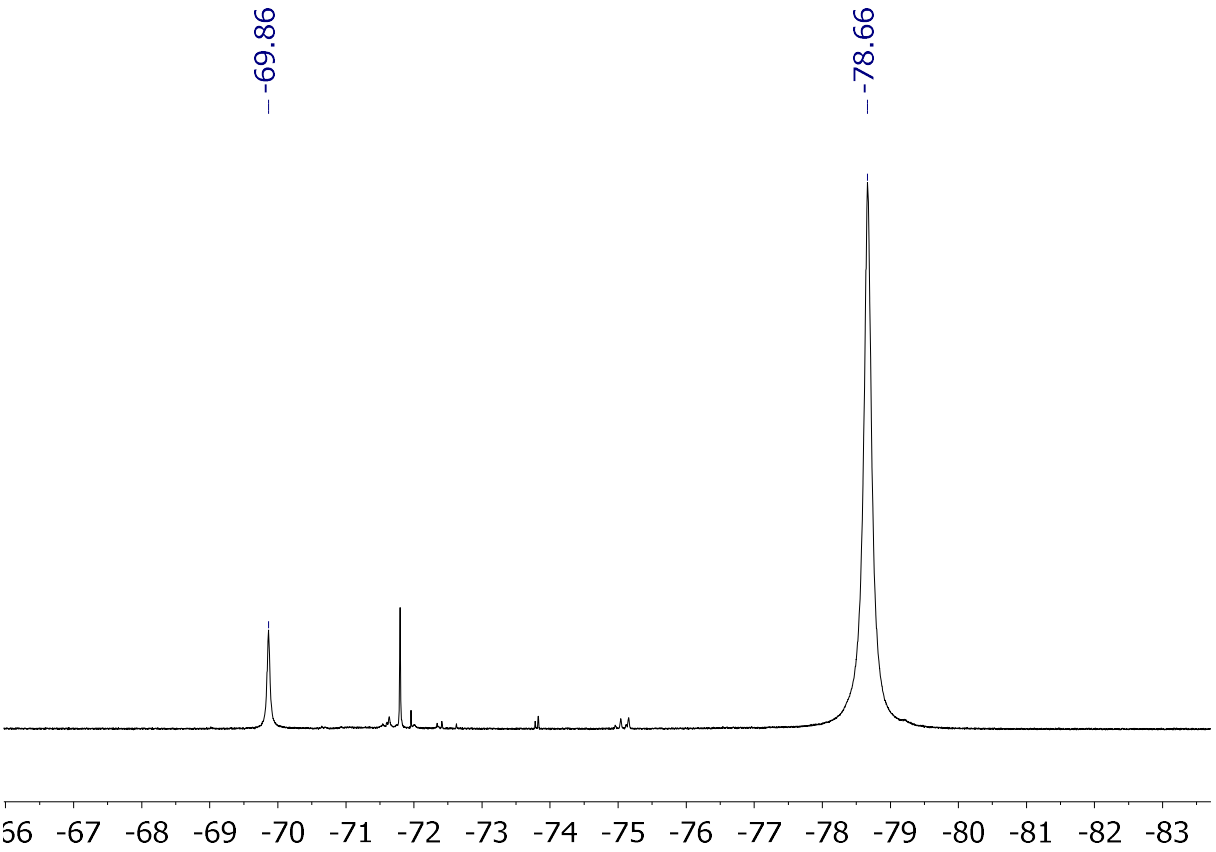

Figure S5.4.19: *In situ $^{19}F\{^{1}H\}$ NMR spectrum at -90 °C after first catalysis of* ***6g***, ***7g*** *and* ***9*** *(step iv, in CD_2Cl_2).*

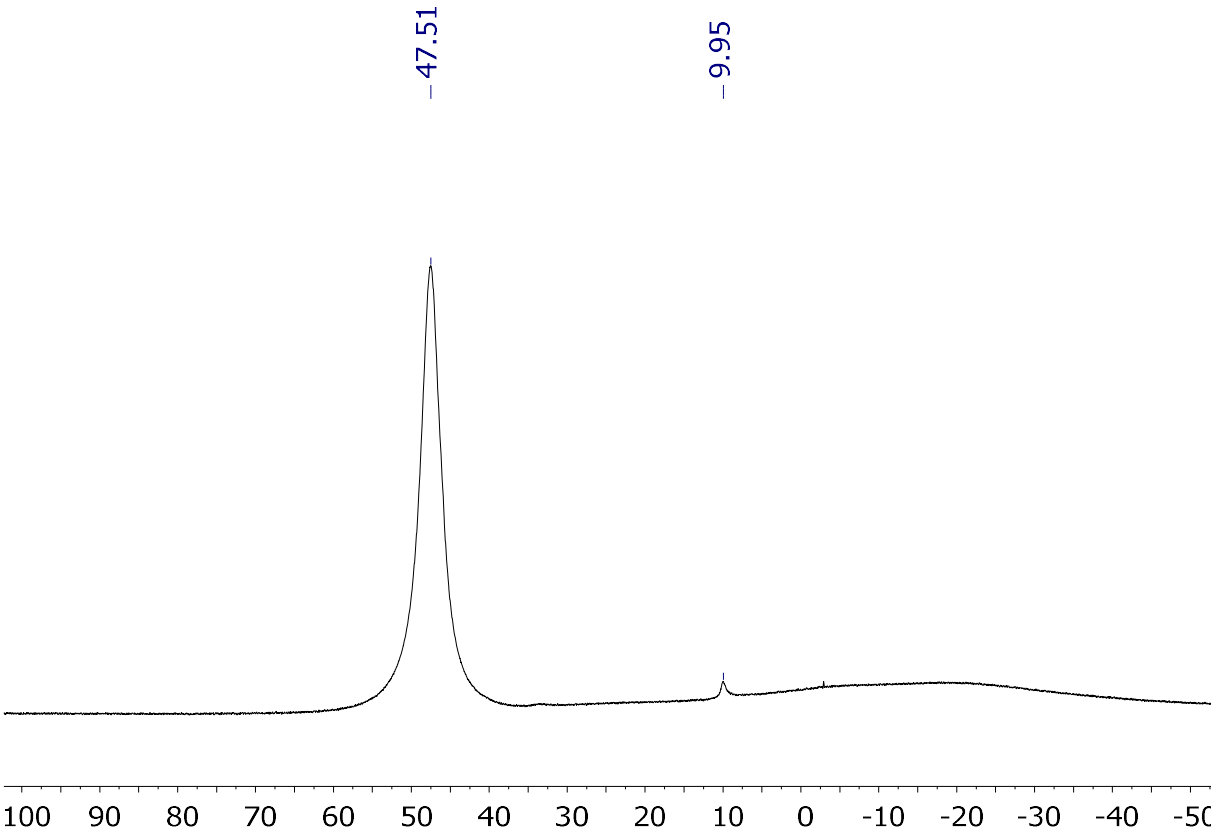

Figure S5.4.20: *In situ $^{11}B\{^{1}H\}$ NMR spectrum after first catalysis of* ***6g***, ***7g*** *and* ***9*** *(step v, in CD_2Cl_2).*

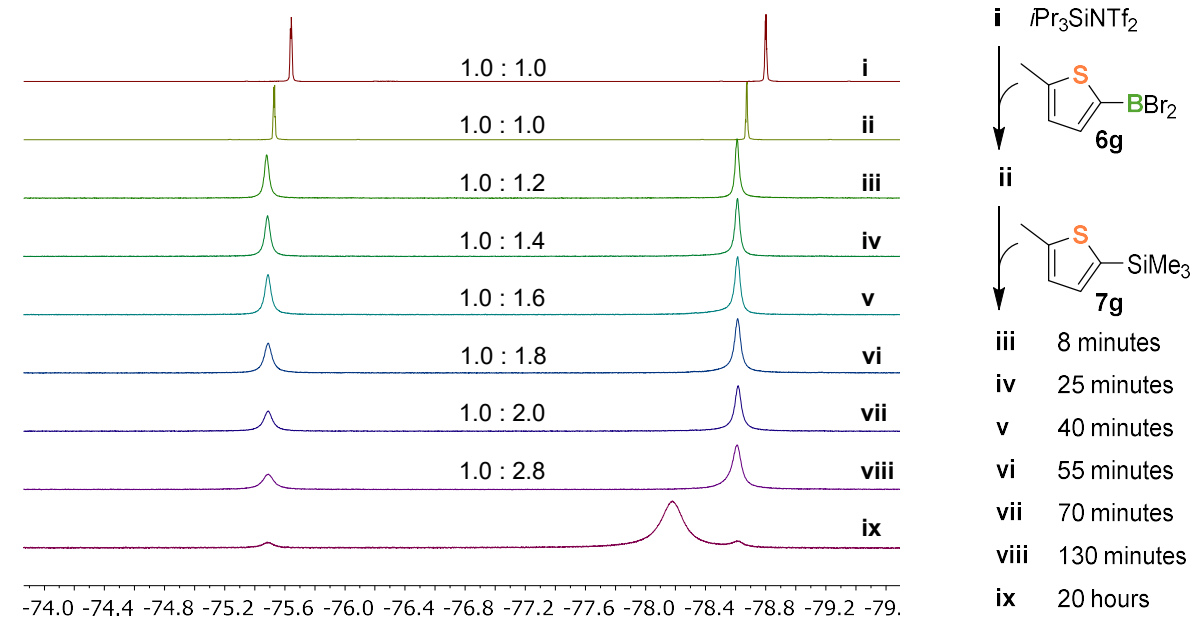

Figure S5.4.21: *In situ 19F{^{1}H} NMR spectra of catalytic reaction between* ***6g***, ***7g*** *and* ***14*** *(in CD_2Cl_2).*

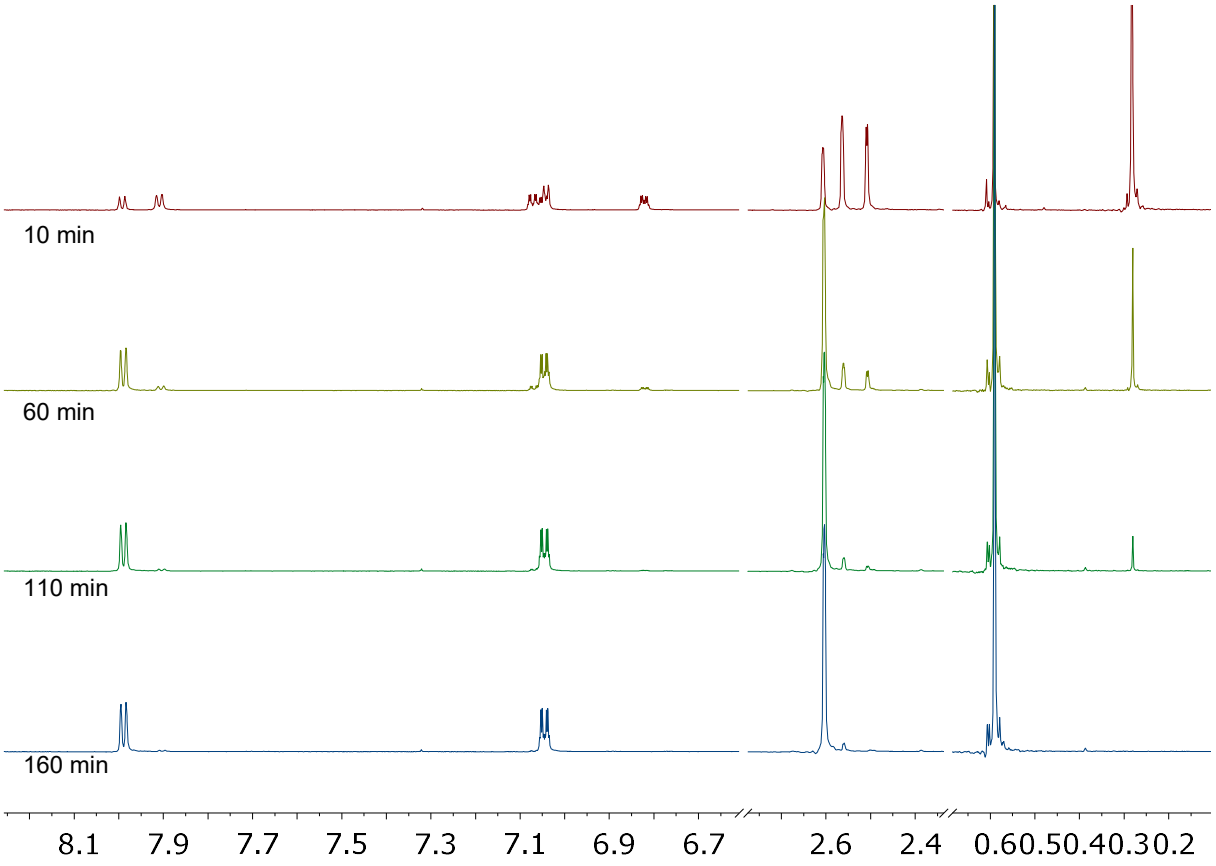

Figure S5.4.22: *^{1}H NMR spectra of VTNA reaction 1 at different reaction times (in CD_2Cl_2).*

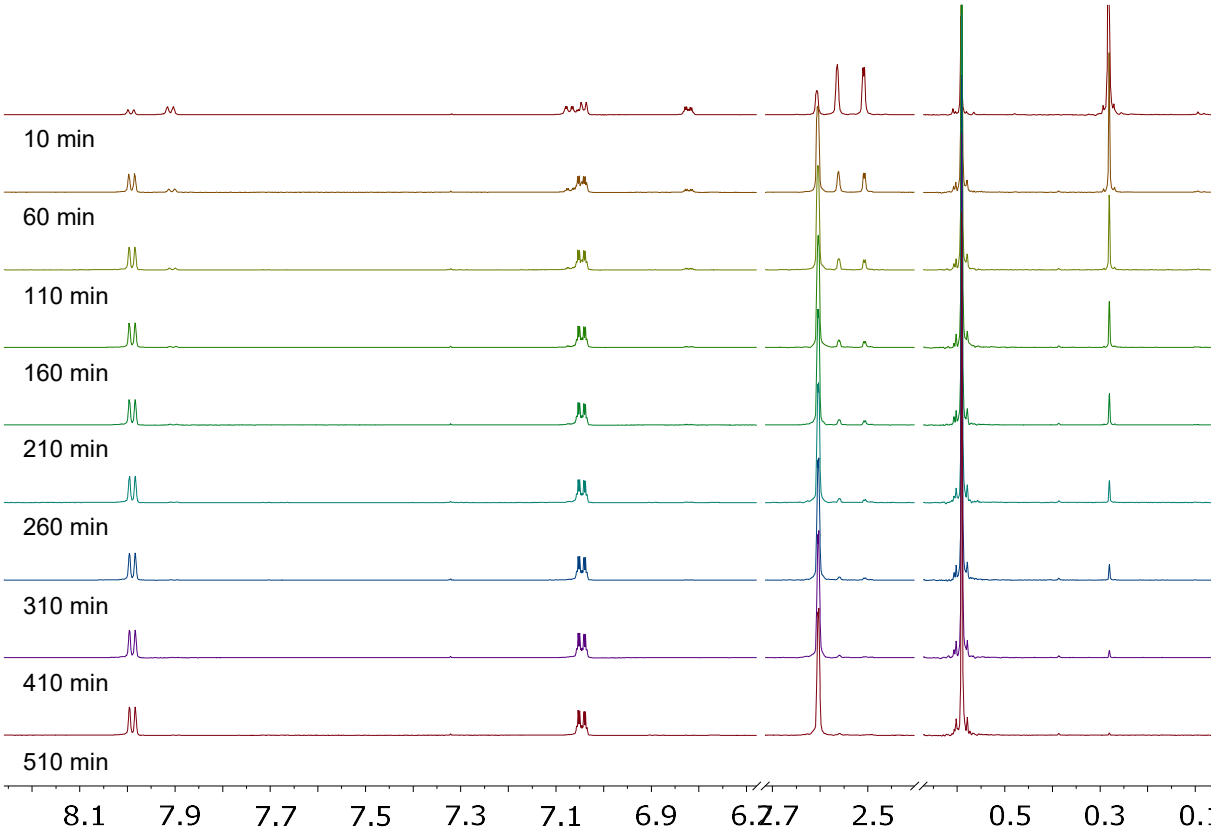

Figure S5.4.23: *^{1}H NMR spectra of VTNA reaction 2 at different reaction times (in CD_2Cl_2).*

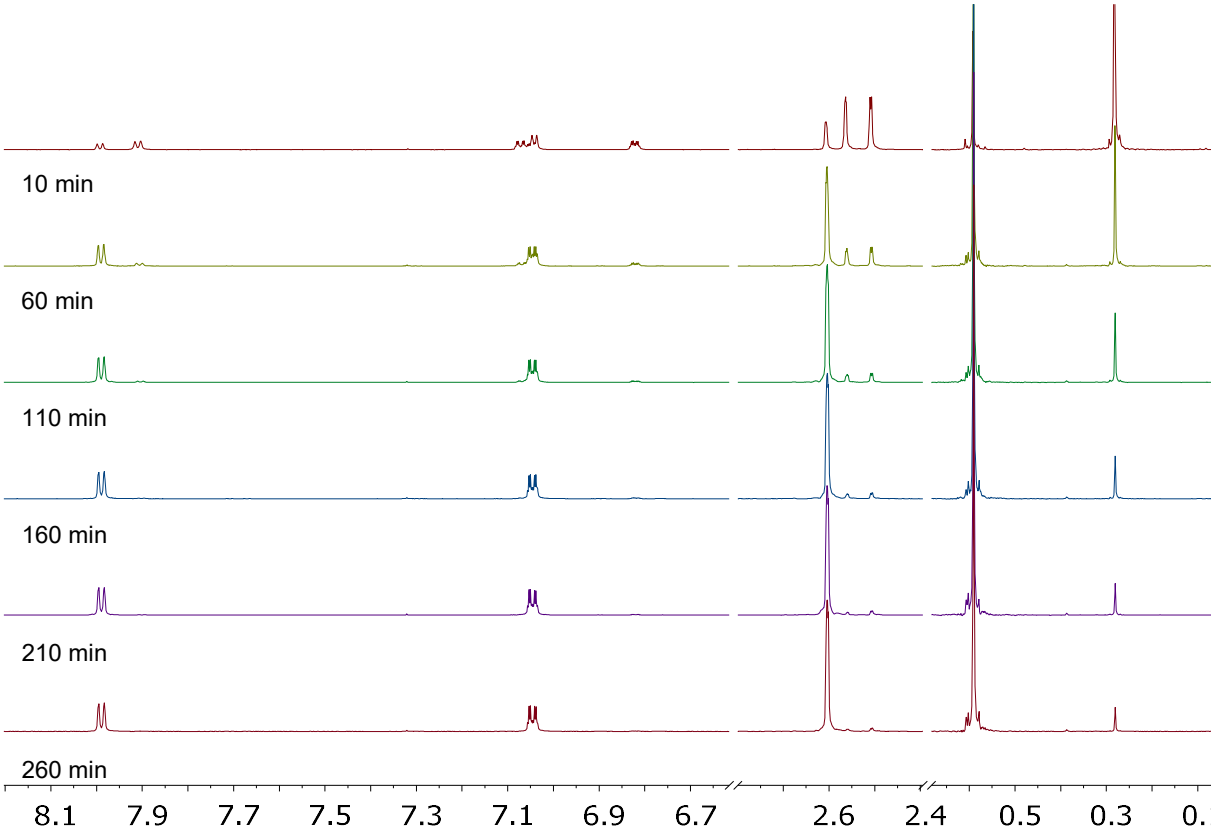

Figure S5.4.24: *^{1}H NMR spectra of VTNA reaction 3 at different reaction times (in CD_2Cl_2).*

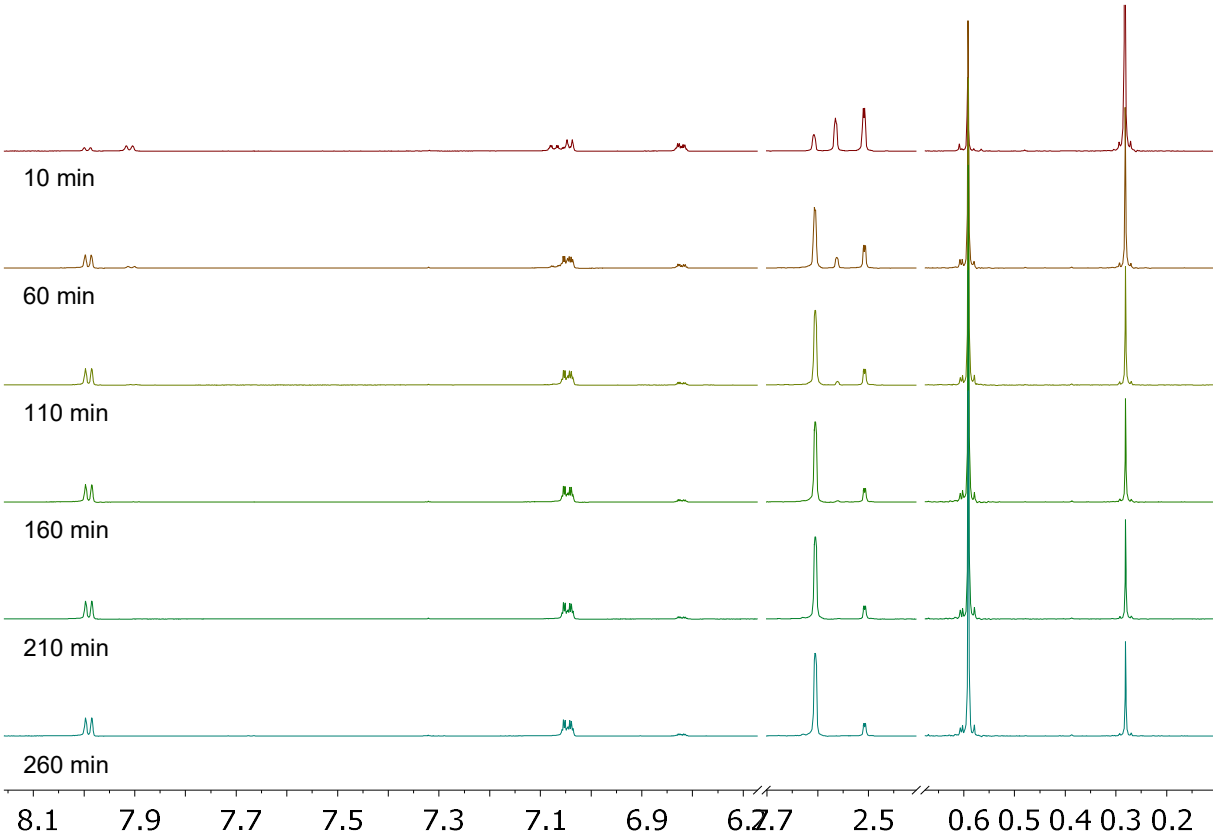

Figure S5.4.25: *^{1}H NMR spectra of VTNA reaction 4 at different reaction times (in CD_2Cl_2).*

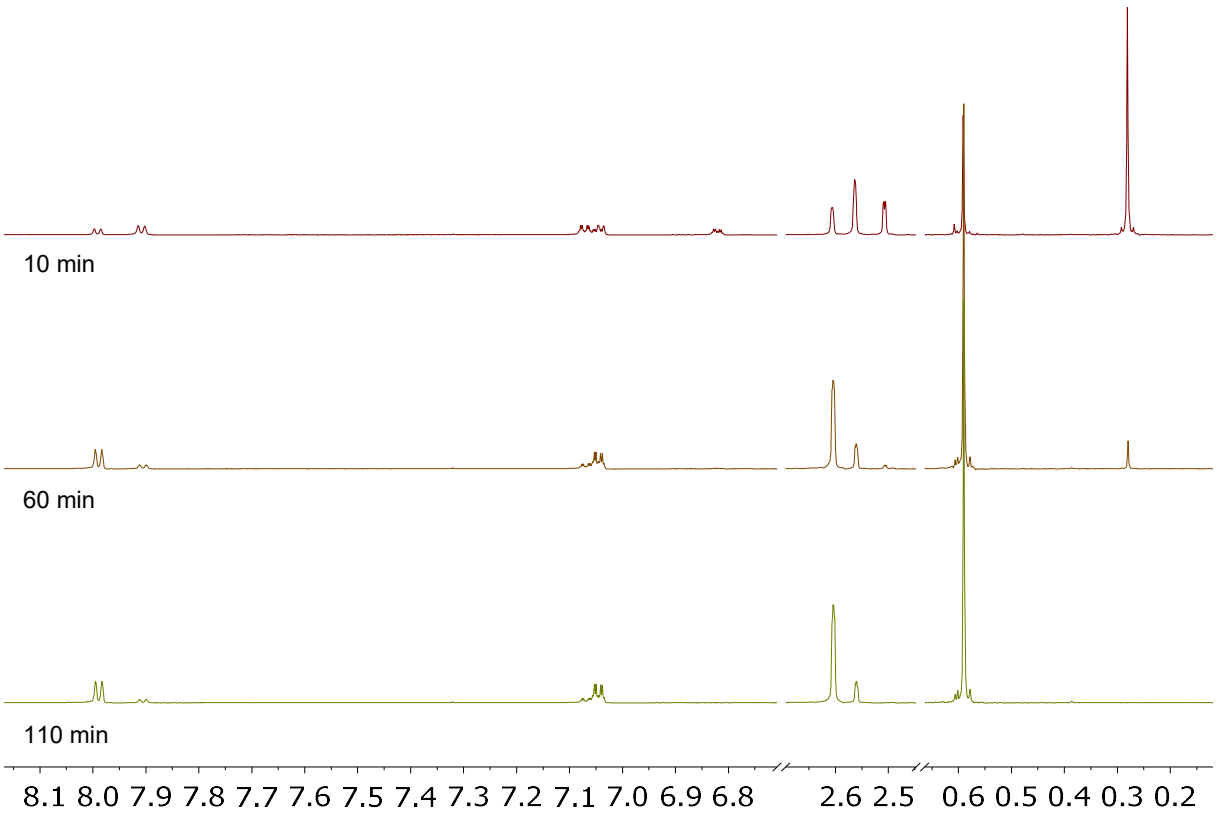

Figure S5.4.26: *^{1}H NMR spectra of VTNA reaction 5 at different reaction times (in CD_2Cl_2).*

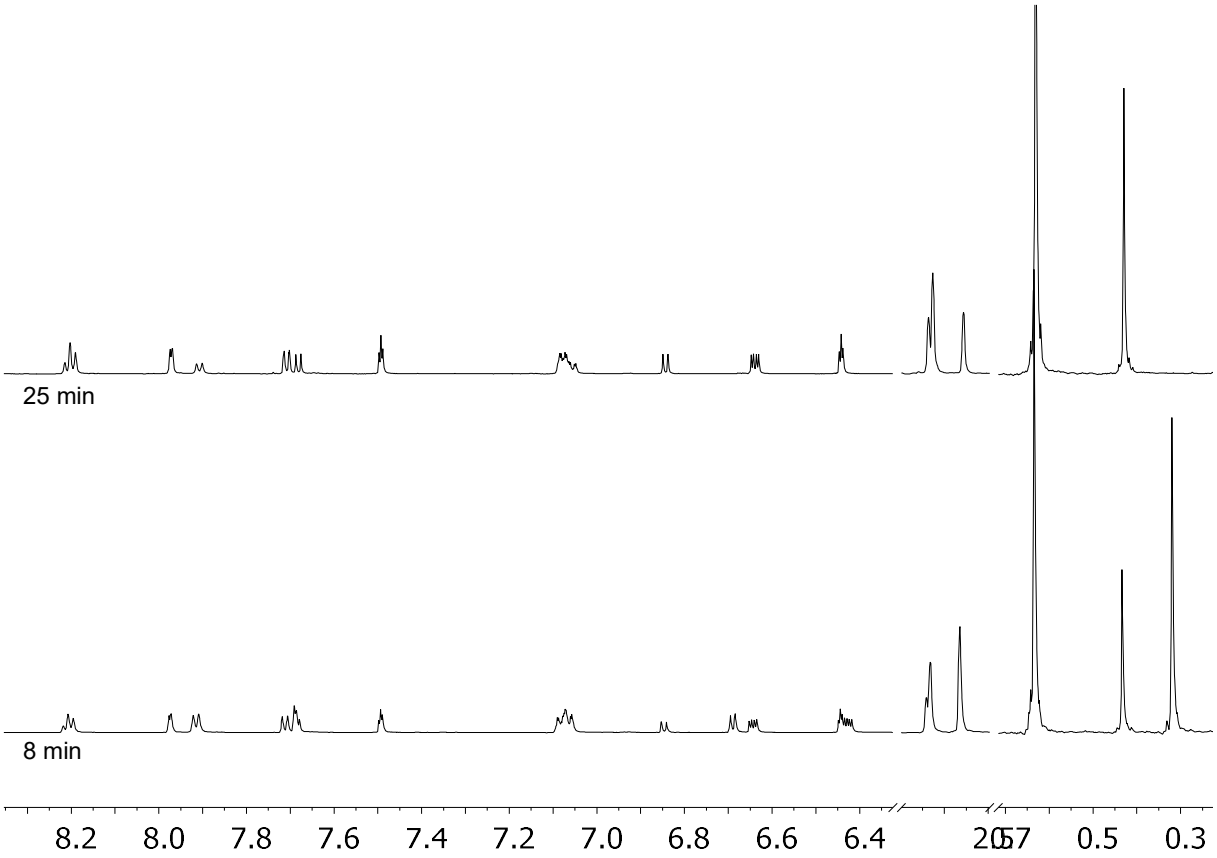

Figure S5.4.27: *In situ ^{1}H NMR of the catalytic reaction between* ***6g*** *and* ***7i*** *(in CD_2Cl_2).*

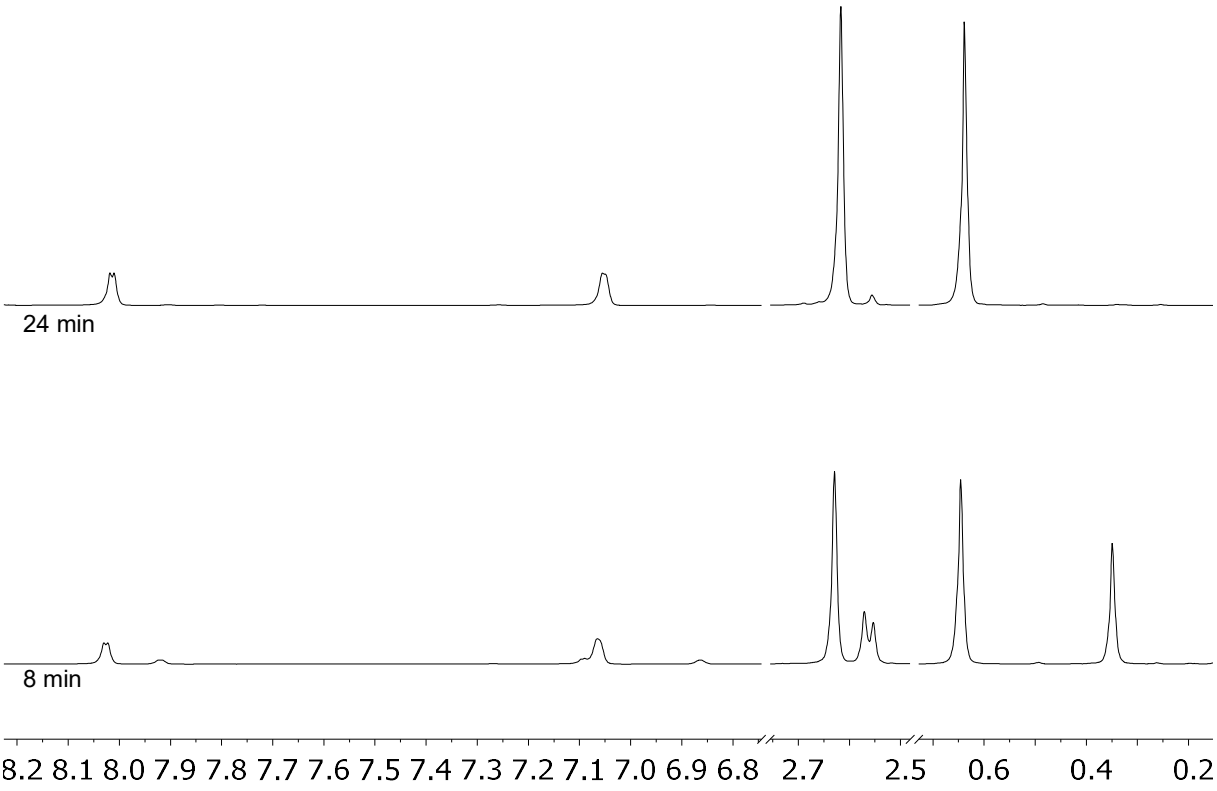

Figure S5.4.28: *In situ ^{1}H NMR of the catalytic reaction between* ***6g*** *and* ***7g*** *(in CD_2Cl_2).*

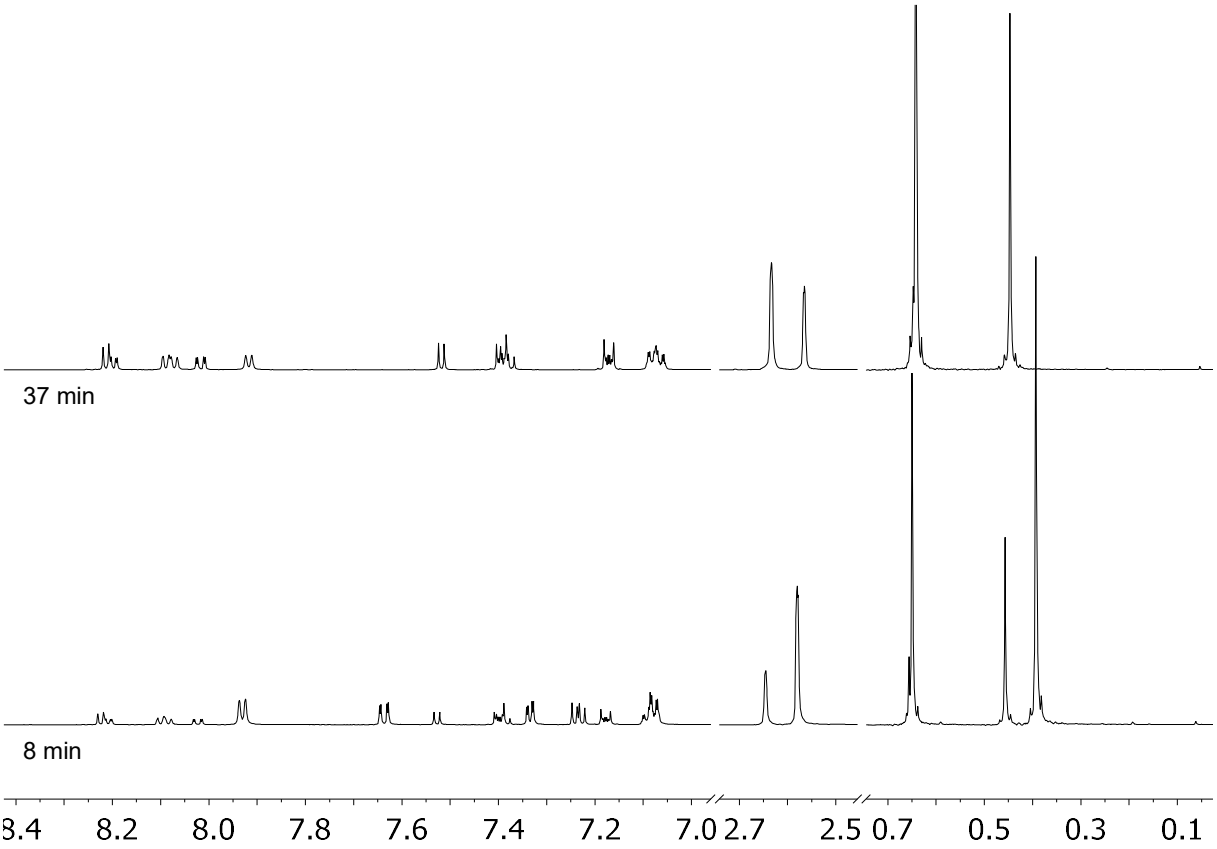

Figure S5.4.29: *In situ ^{1}H NMR of the catalytic reaction between* ***6g*** *and* ***7a*** *(in CD_2Cl_2).*

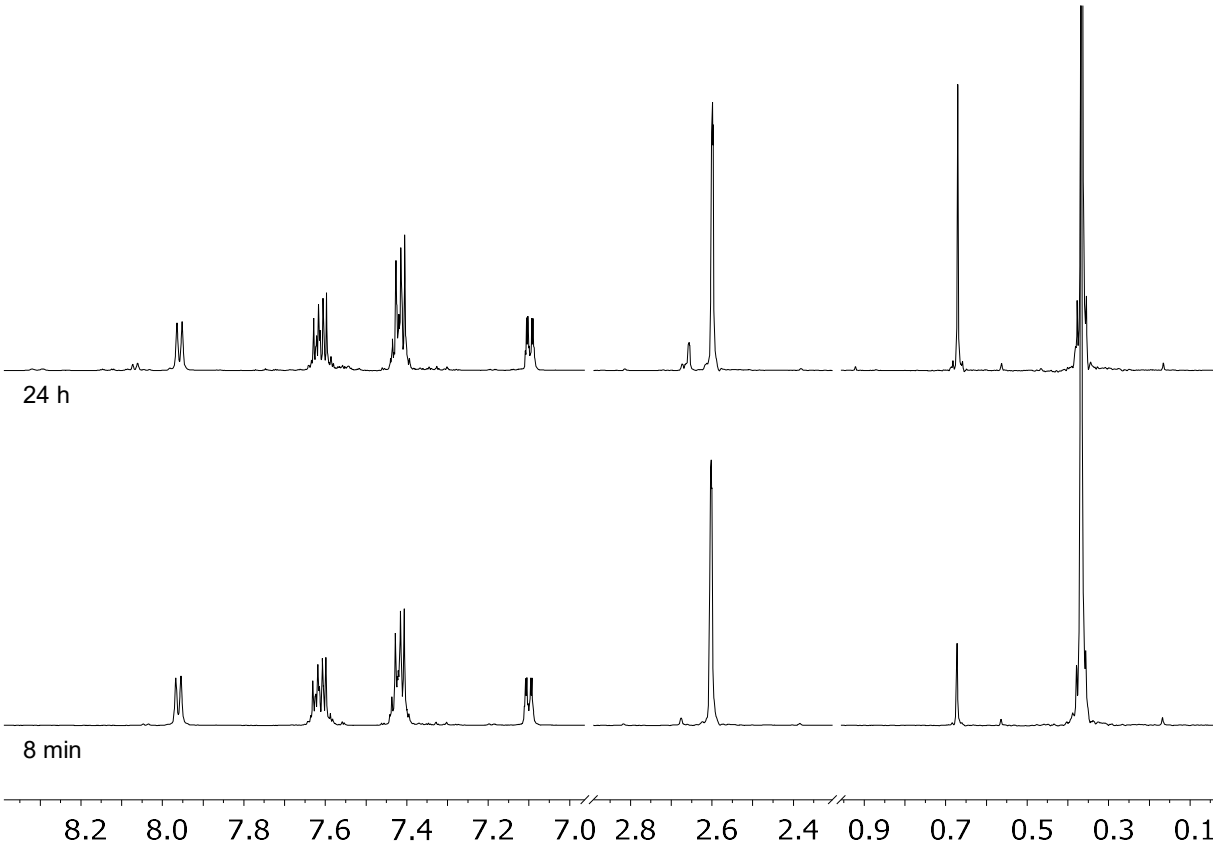

Figure S5.4.30: *In situ ^{1}H NMR of the catalytic reaction between* ***6g*** *and* ***7j*** *(in CD_2Cl_2).*

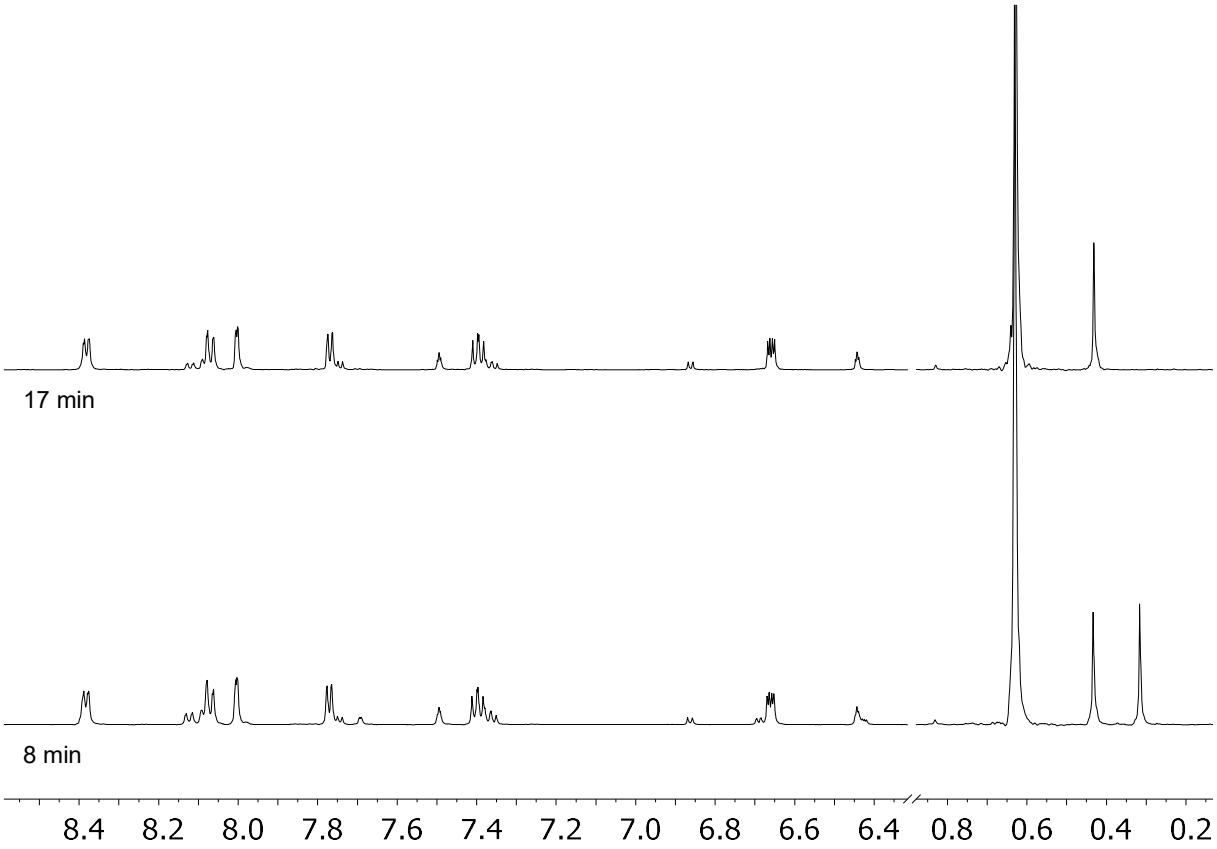

Figure S5.4.31: *In situ ^{1}H NMR of the catalytic reaction between* ***6a*** *and* ***7i*** *(in CD_2Cl_2).*

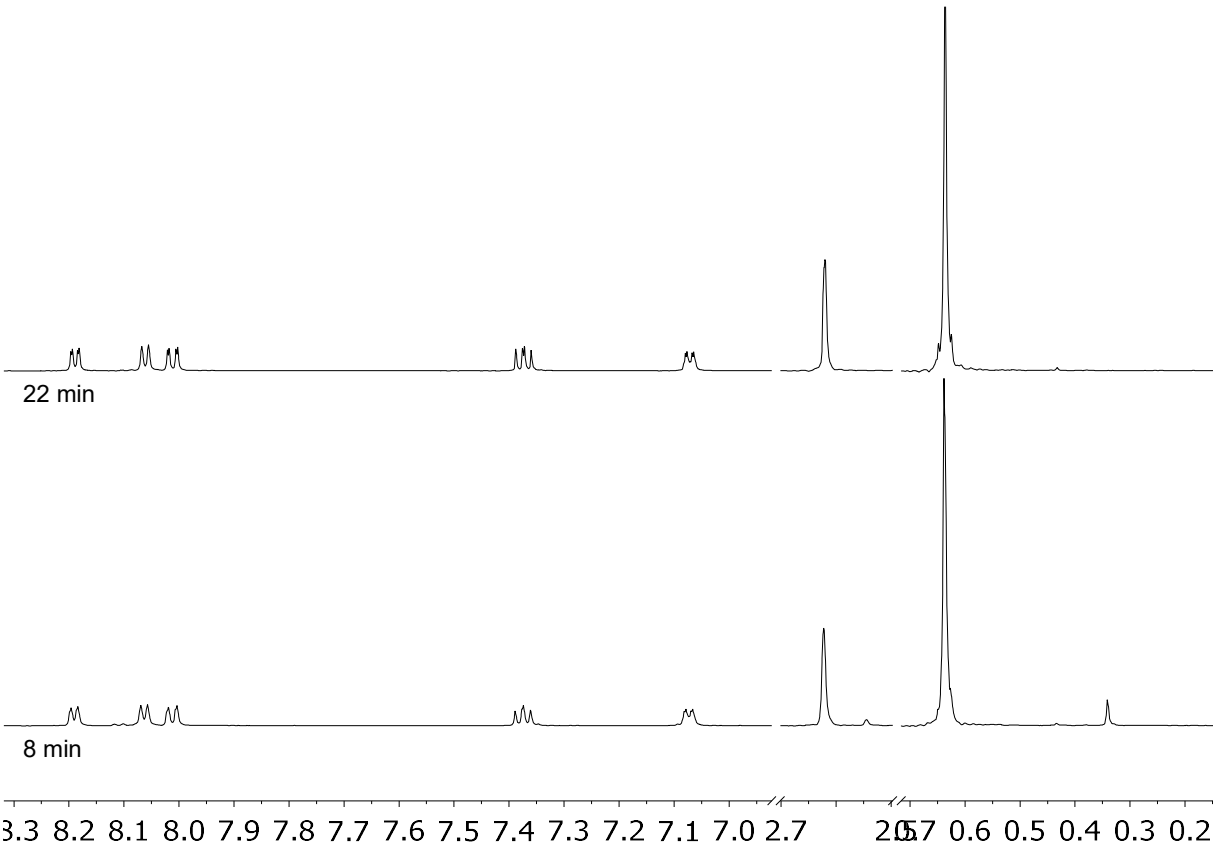

Figure S5.4.32: *In situ ^{1}H NMR of the catalytic reaction between* ***6a*** *and* ***7g*** *(in CD_2Cl_2).*

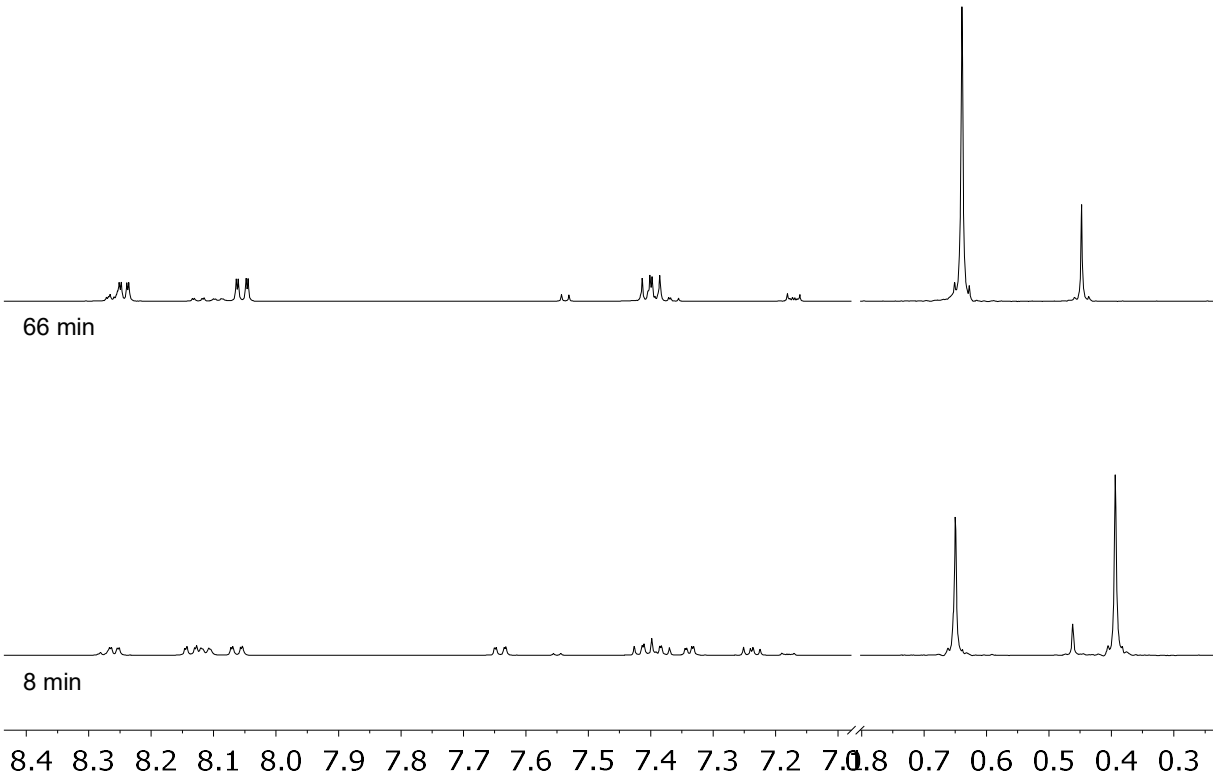

Figure S5.4.33: *In situ ^{1}H NMR of the catalytic reaction between* ***6a*** *and* ***7a*** *(in CD_2Cl_2).*

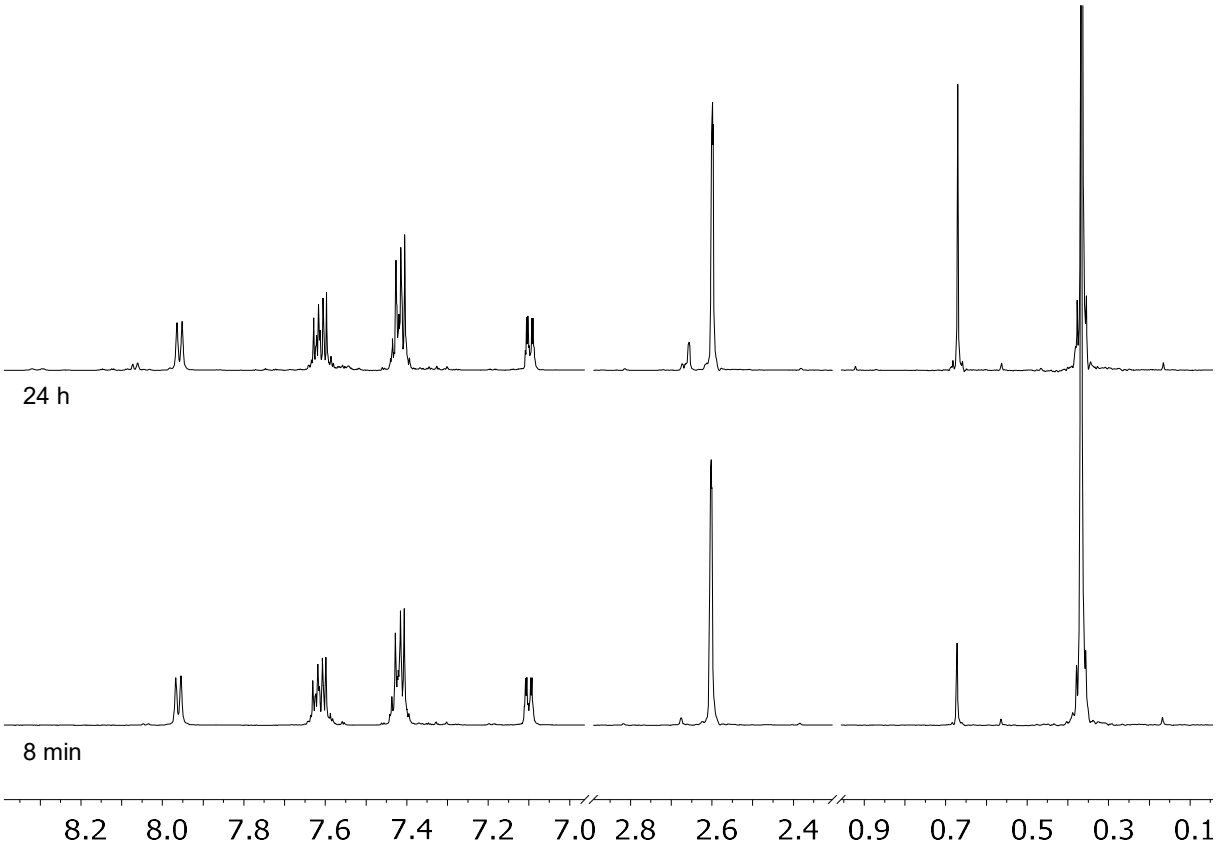

Figure S5.4.34: *In situ ^{1}H NMR of the catalytic reaction between* ***6a*** *and* ***7j*** *(in CD_2Cl_2).*

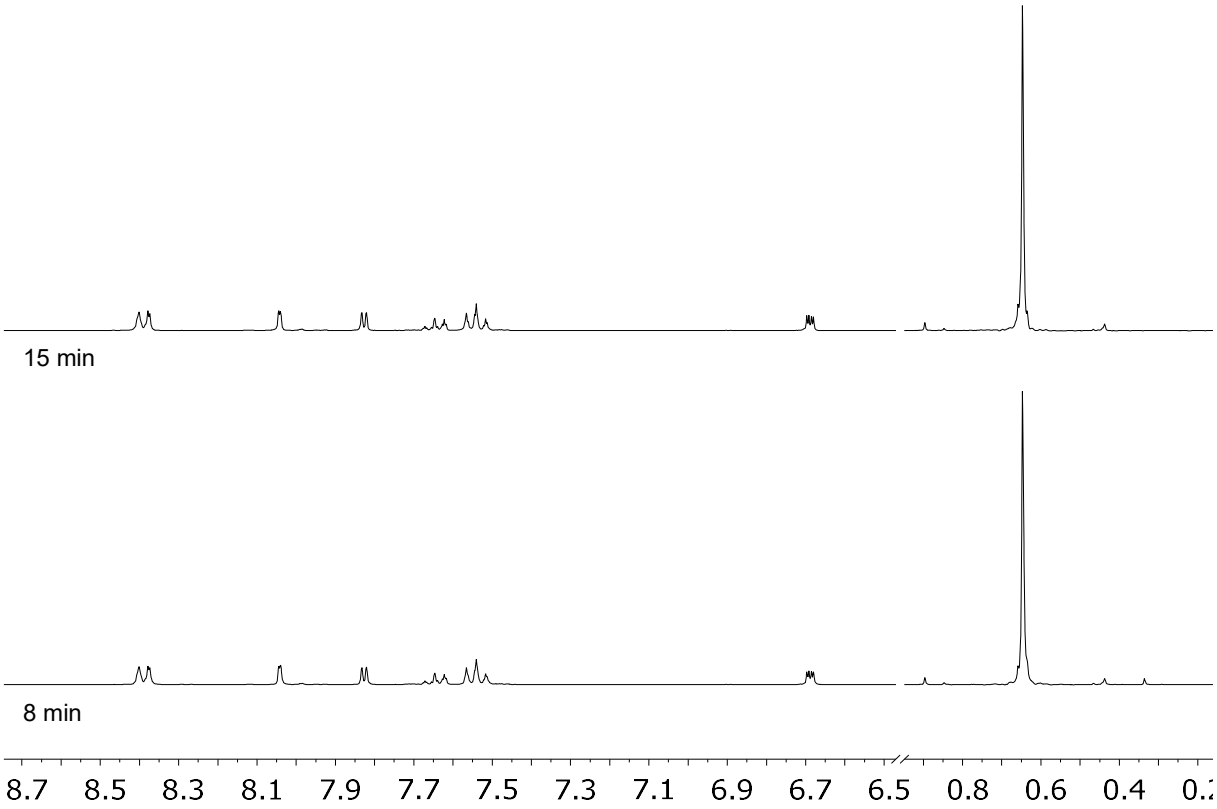

Figure S5.4.35: *In situ ^{1}H NMR of the catalytic reaction between* ***6j*** *and* ***7i*** *(in CD_2Cl_2).*

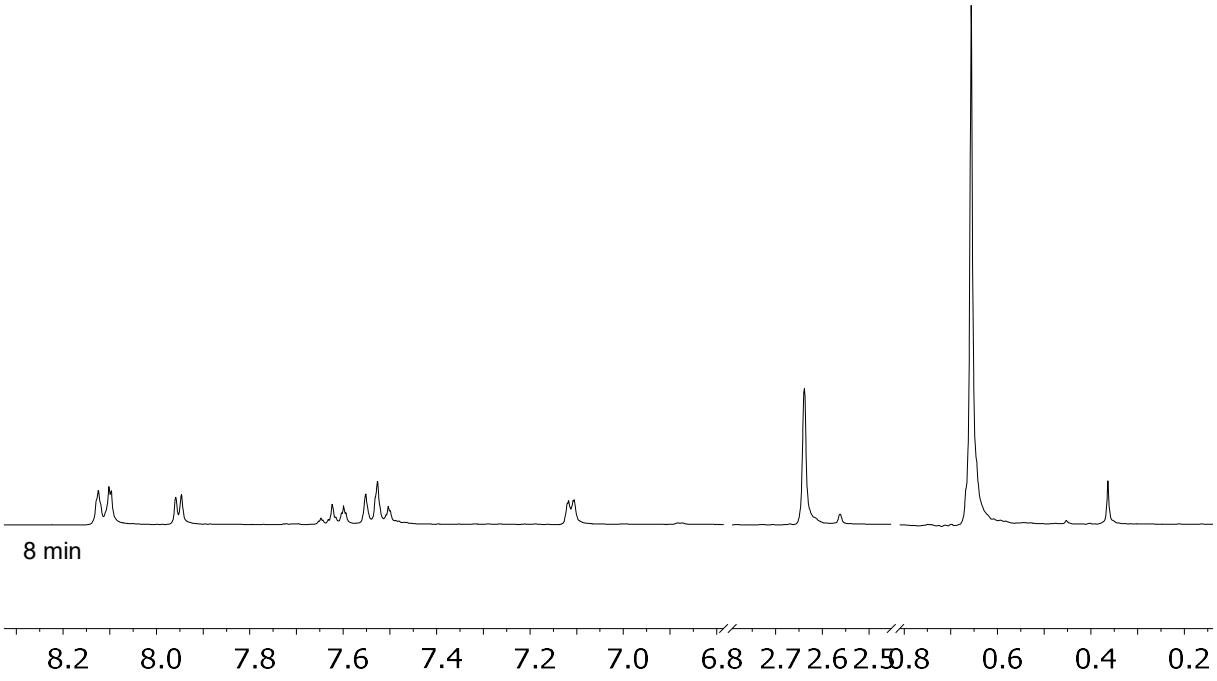

Figure S5.4.36: *In situ ^{1}H NMR of the catalytic reaction between* ***6j*** *and* ***7g*** *(in CD_2Cl_2).*

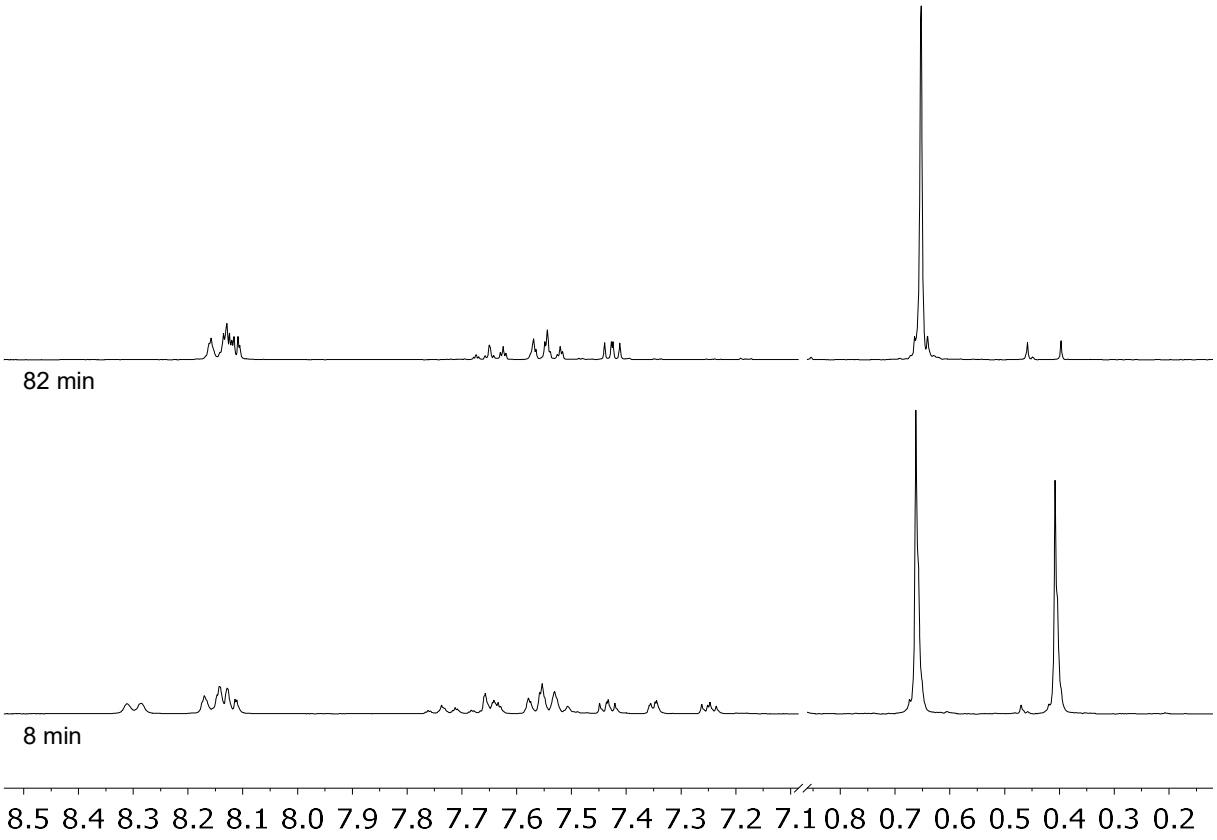

Figure S5.4.37: *In situ ^{1}H NMR of the catalytic reaction between* ***6j*** *and* ***7a*** *(in CD_2Cl_2).*

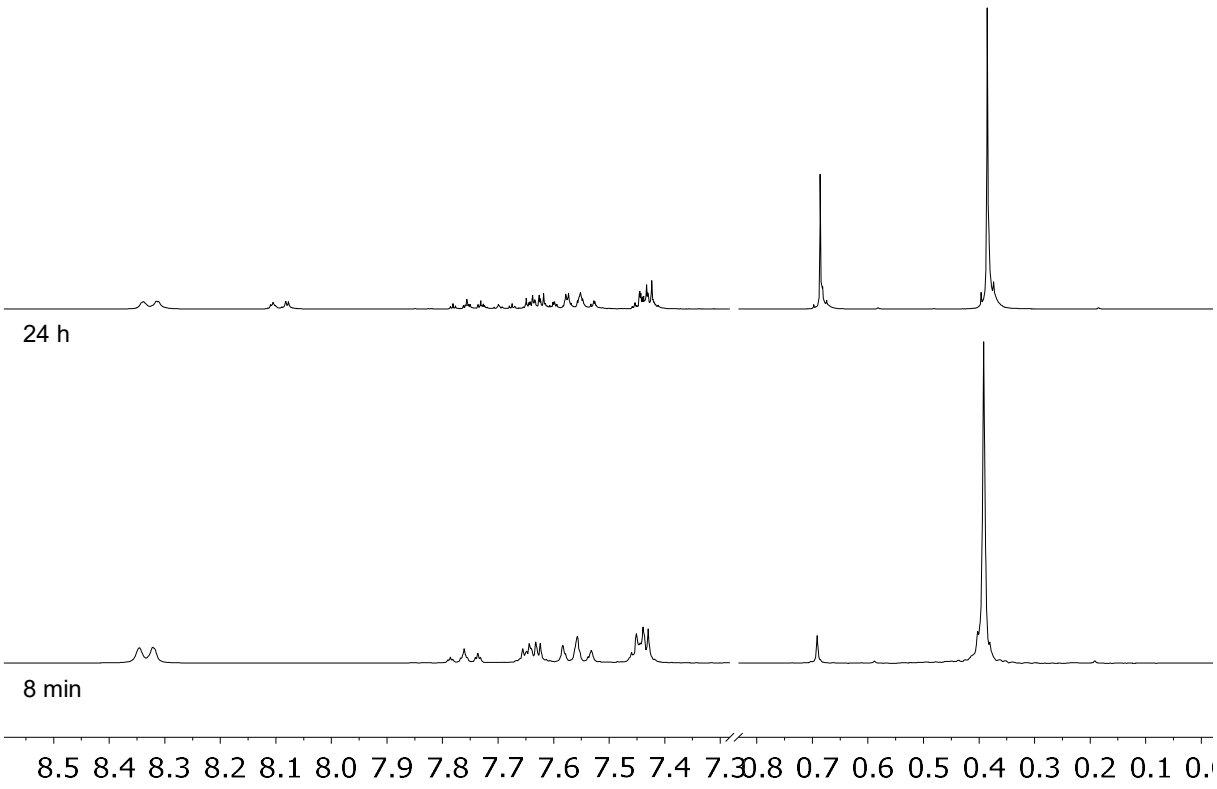

Figure S5.4.38: *In situ ^{1}H NMR of the catalytic reaction between* ***6j*** *and* ***7j*** *(in CD_2Cl_2).*

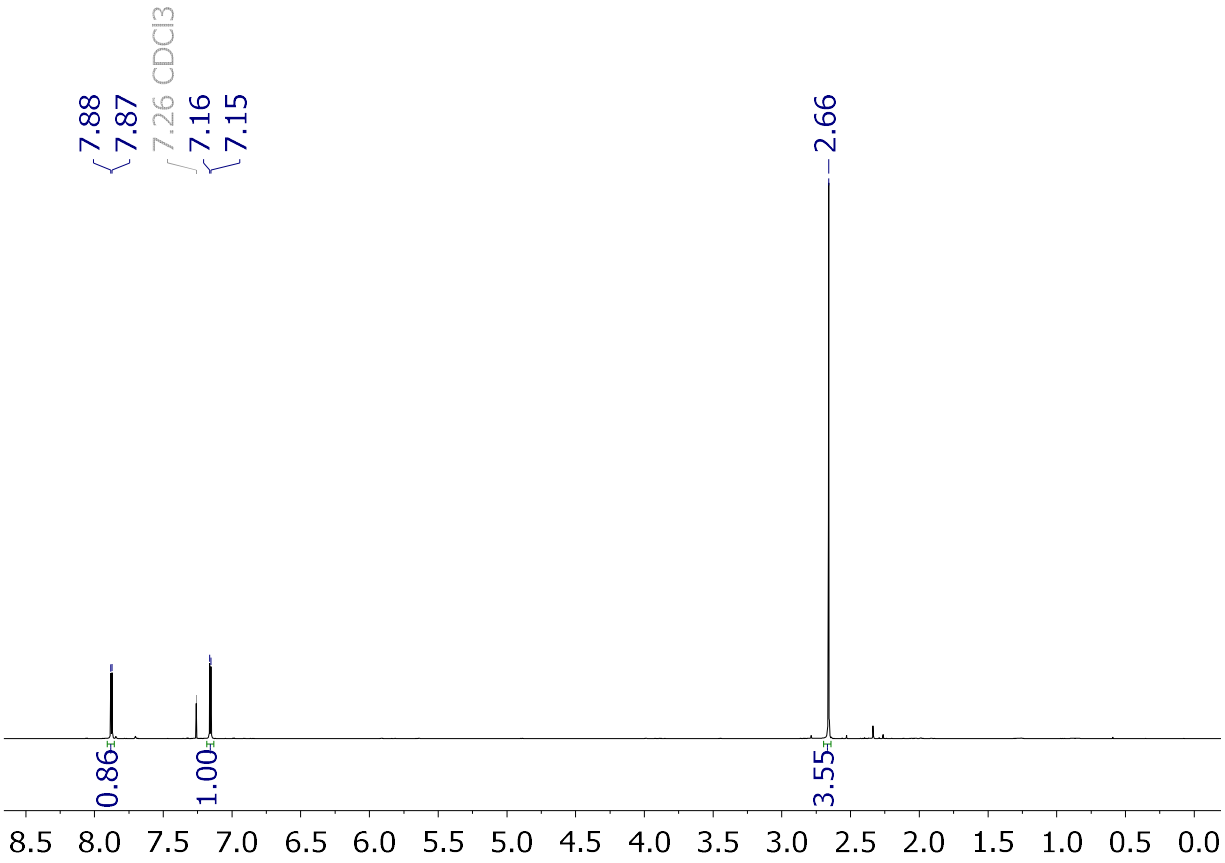

Figure S5.4.39: *^{1}H NMR spectrum of* ***6c*** *(in $CDCl_3$).*

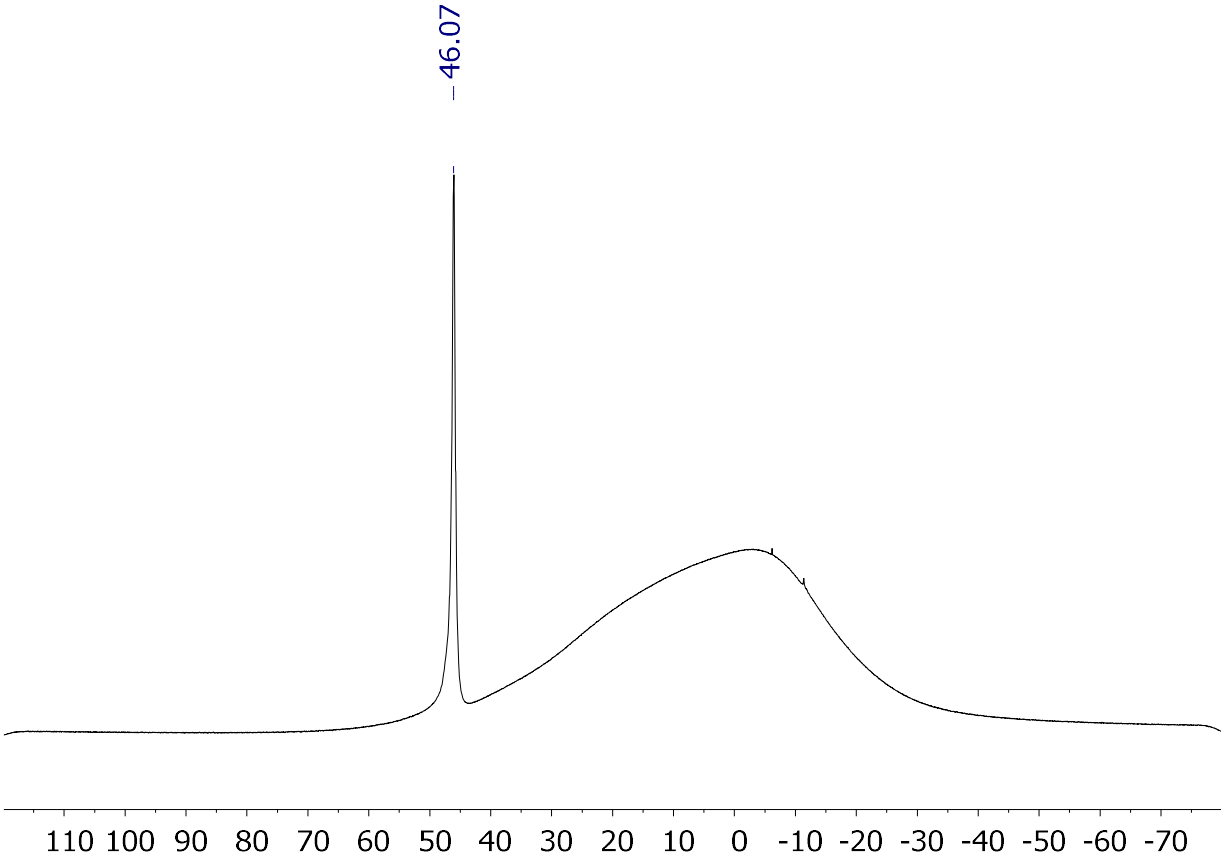

Figure S5.4.40: *$^{11}B\{^{1}H\}$ NMR spectrum of* ***6c*** *(in $CDCl_3$).*

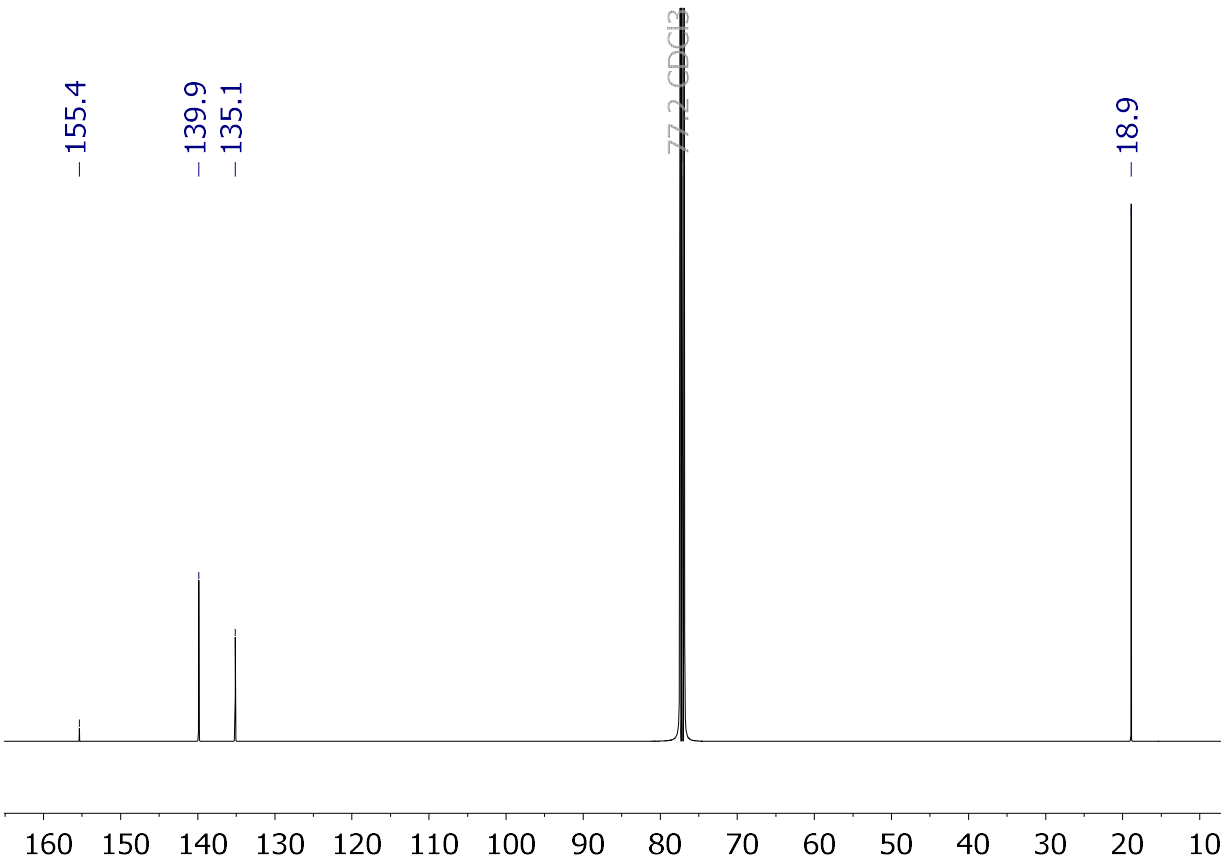

Figure S5.4.41: *$^{13}C\{^{1}H\}$ NMR spectrum of* ***6c*** *(in $CDCl_3$).*

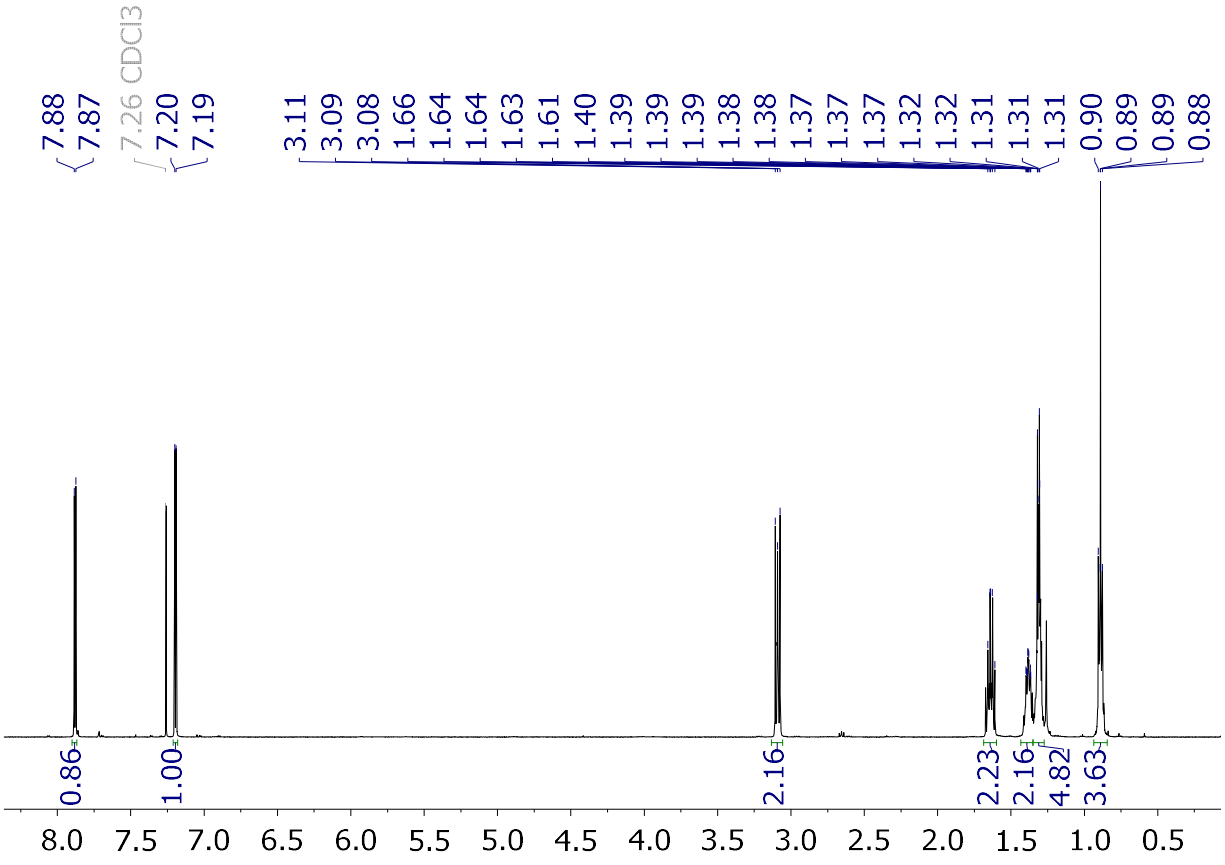

Figure S5.4.42: *^{1}H NMR spectrum of* ***6d*** *(in $CDCl_3$).*

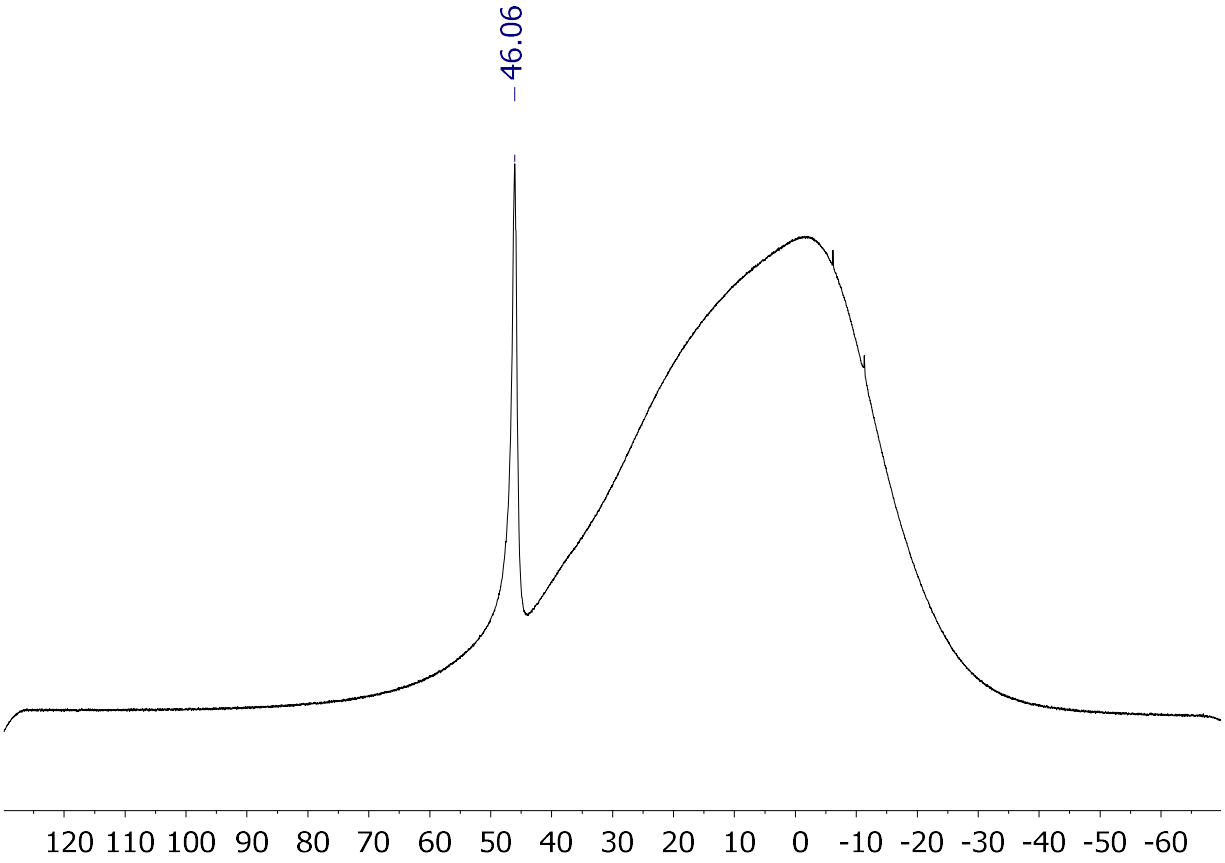

Figure S5.4.43: *$^{11}B\{^1H\}$ NMR spectrum of* ***6d*** *(in $CDCl_3$).*

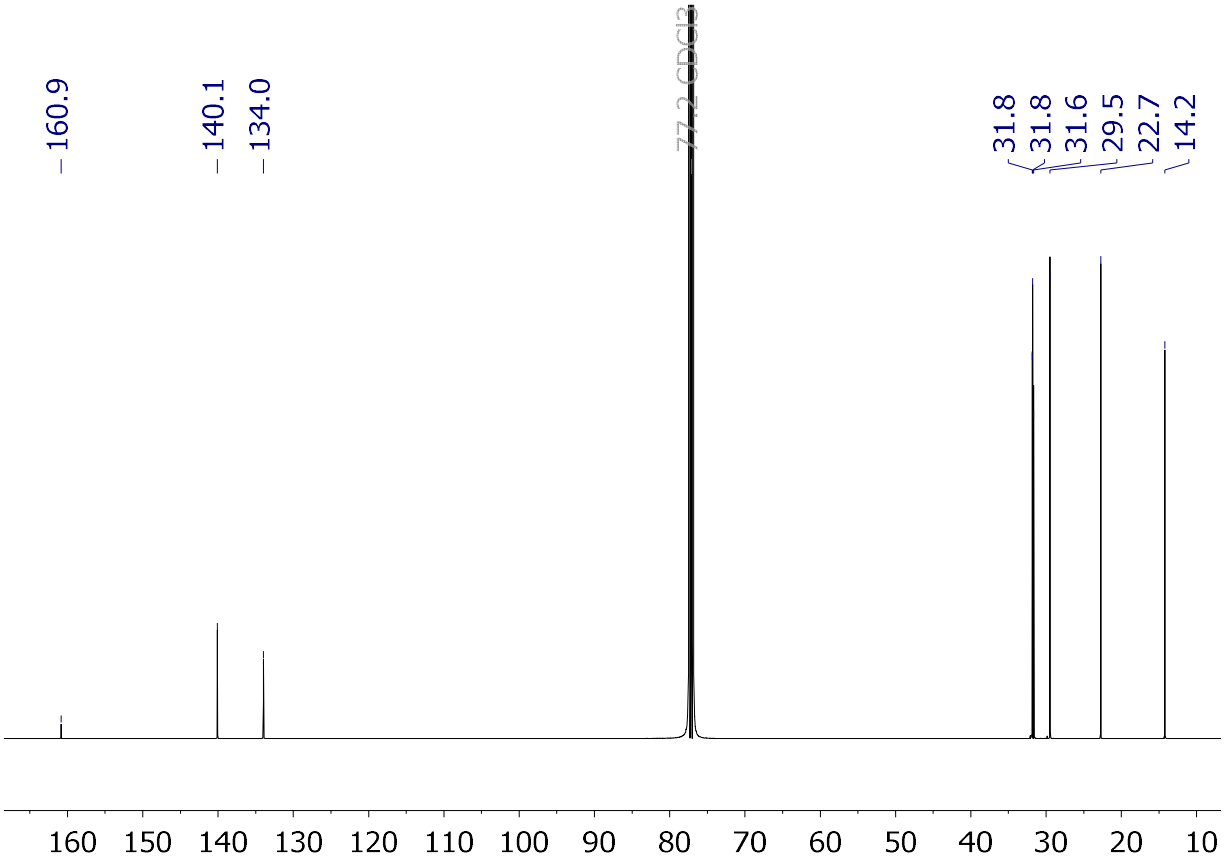

Figure S5.4.44: *$^{13}C\{^1H\}$ NMR spectrum of* ***6d*** *(in $CDCl_3$).*

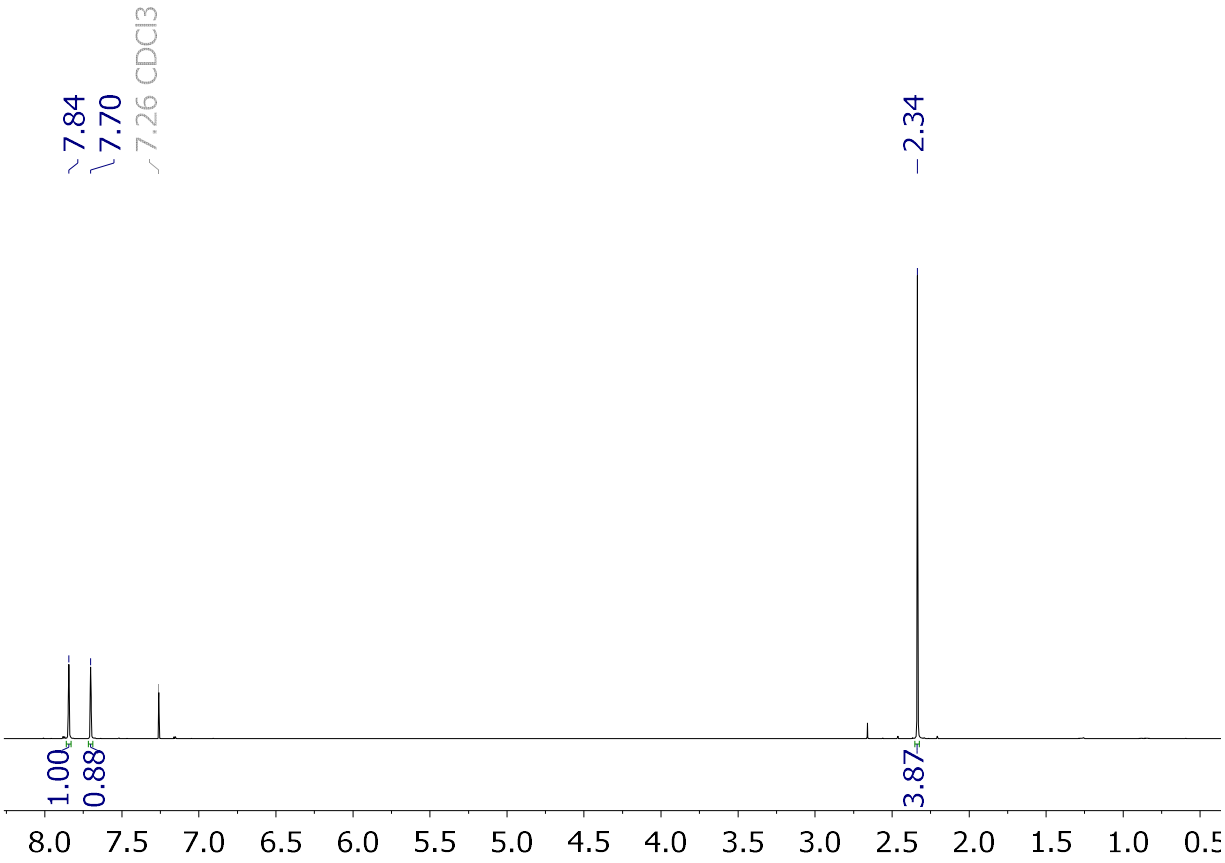

Figure S5.4.45: *^{1}H NMR spectrum of* ***6e*** *(in $CDCl_3$).*

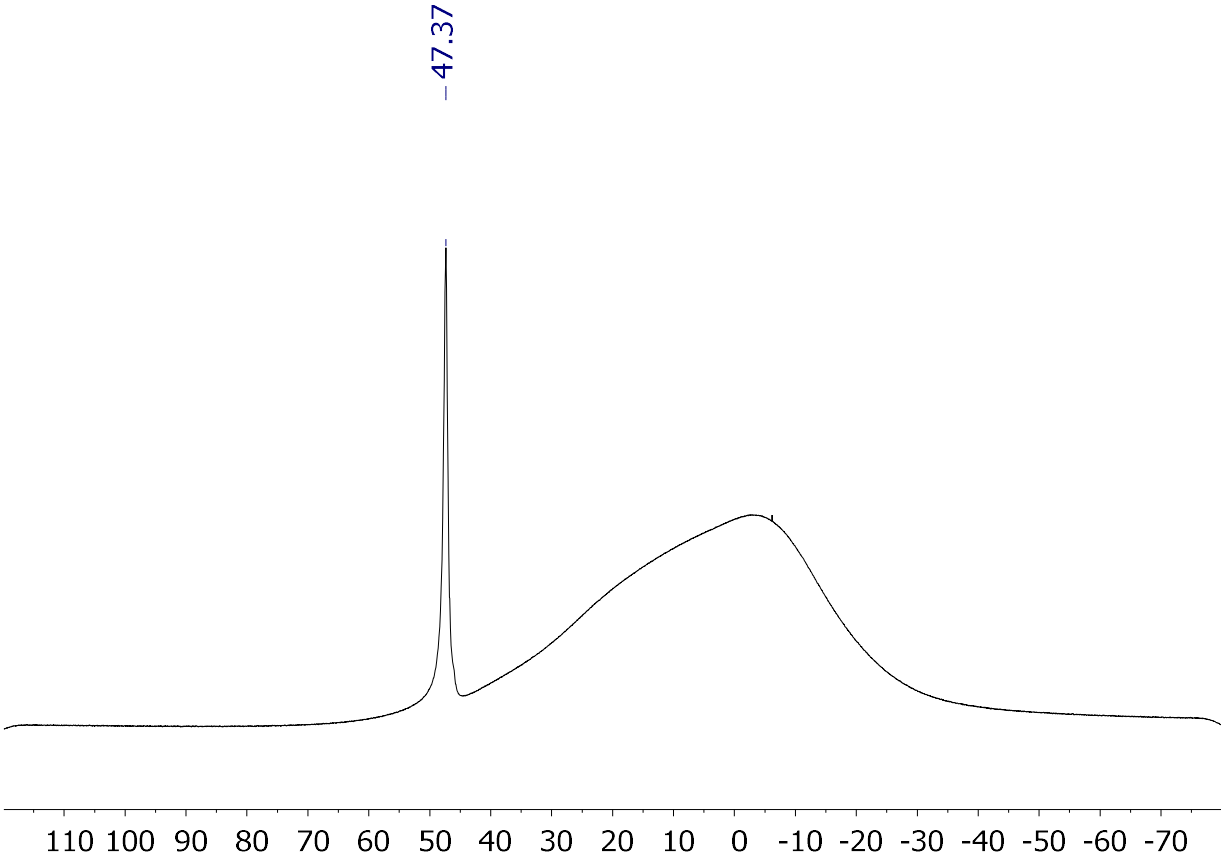

Figure S5.4.46: *$^{11}B\{^{1}H\}$ NMR spectrum of* ***6e*** *(in $CDCl_3$).*

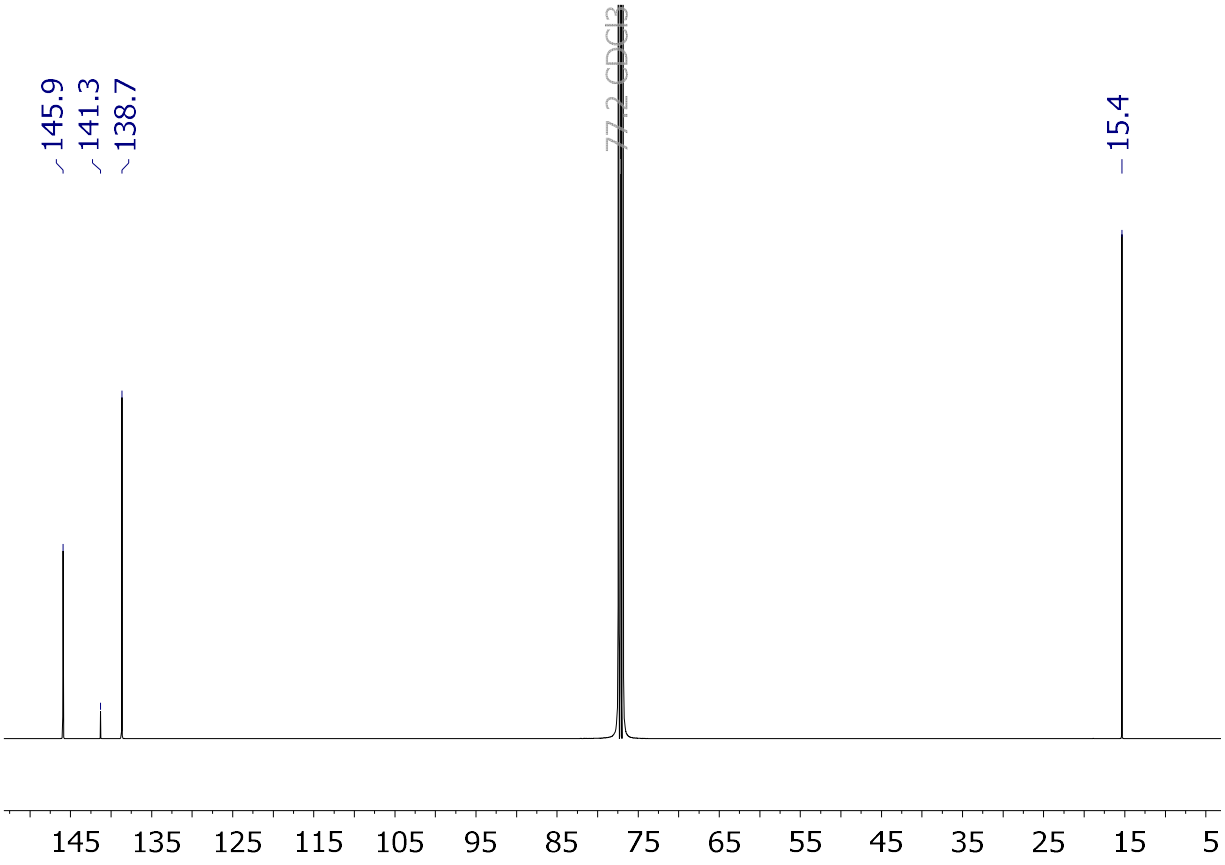

Figure S5.4.47: *$^{13}C\{^{1}H\}$ NMR spectrum of* ***6e*** *(in $CDCl_3$).*

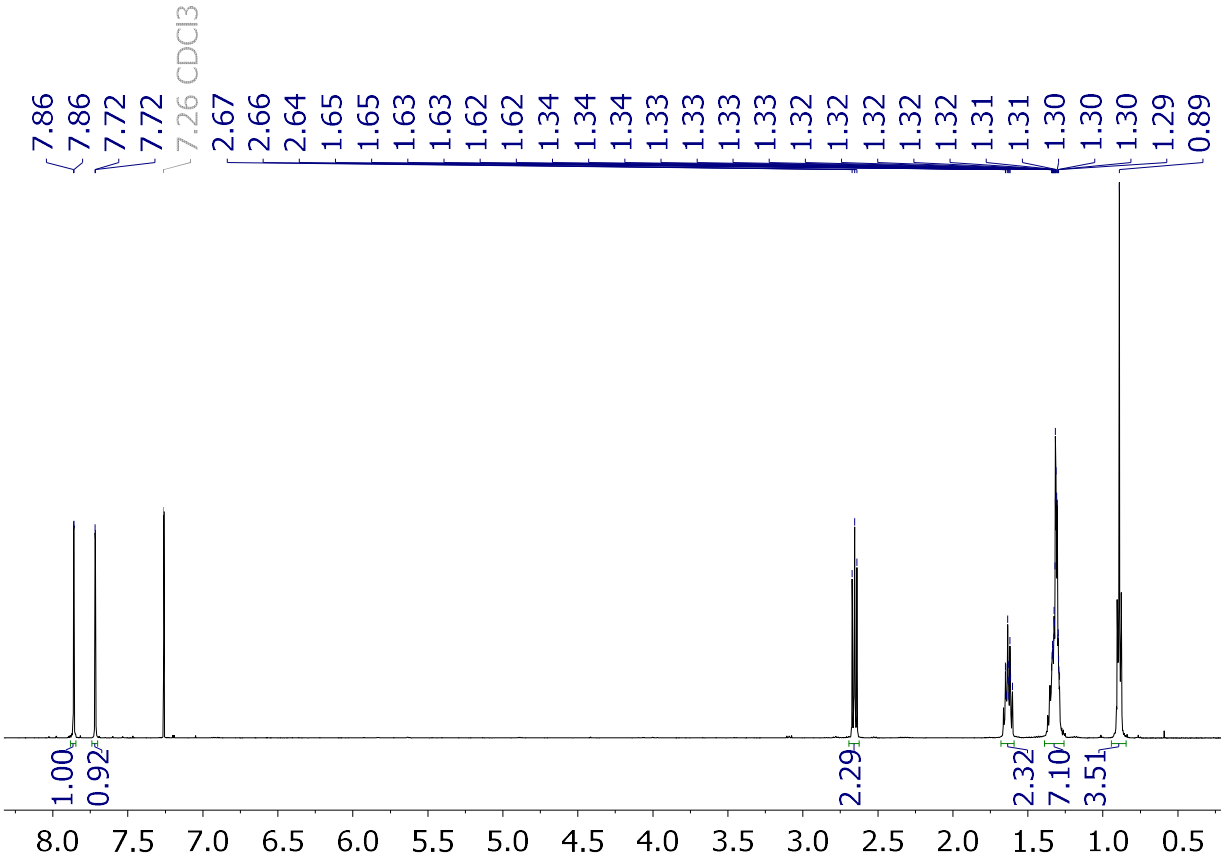

Figure S5.4.48: *^{1}H NMR spectrum of* ***6f*** *(in $CDCl_3$).*

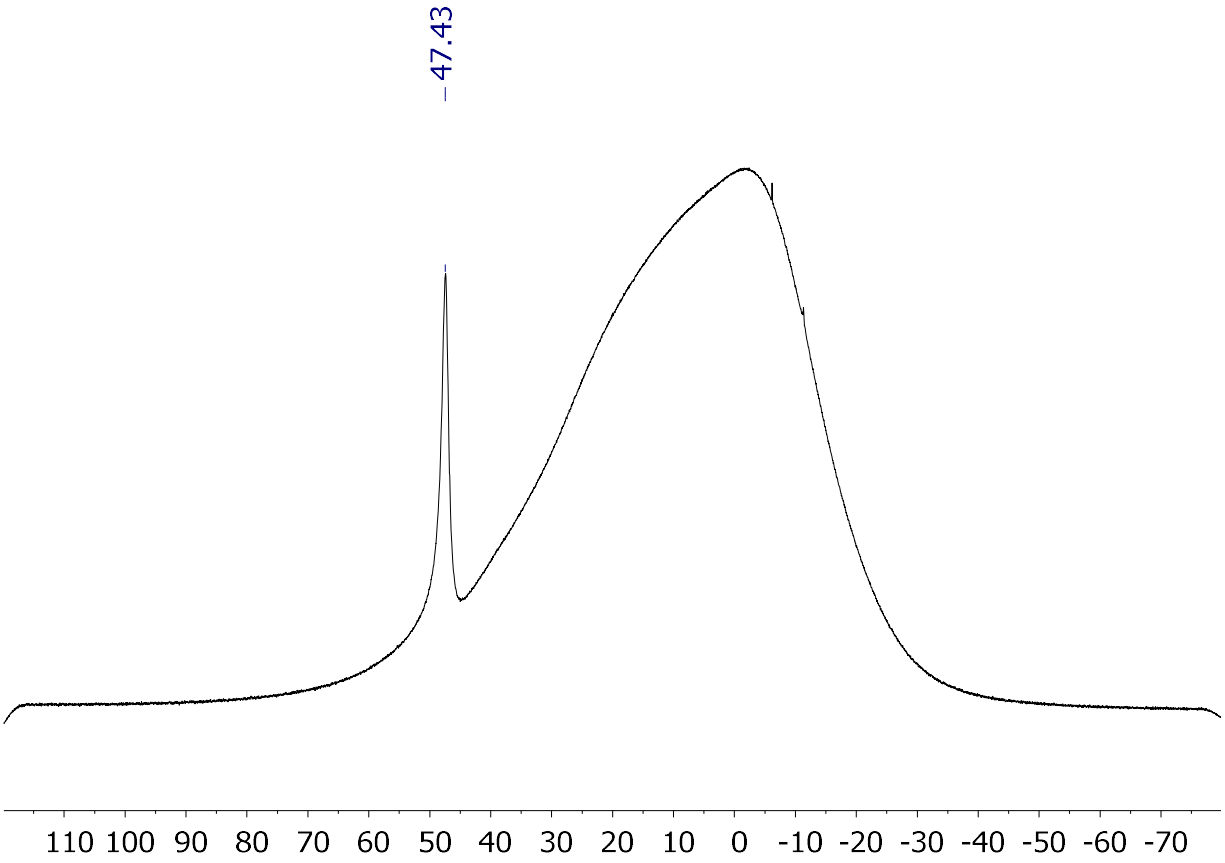

Figure S5.4.49: *$^{11}B\{^1H\}$ NMR spectrum of **6f** (in $CDCl_3$).*

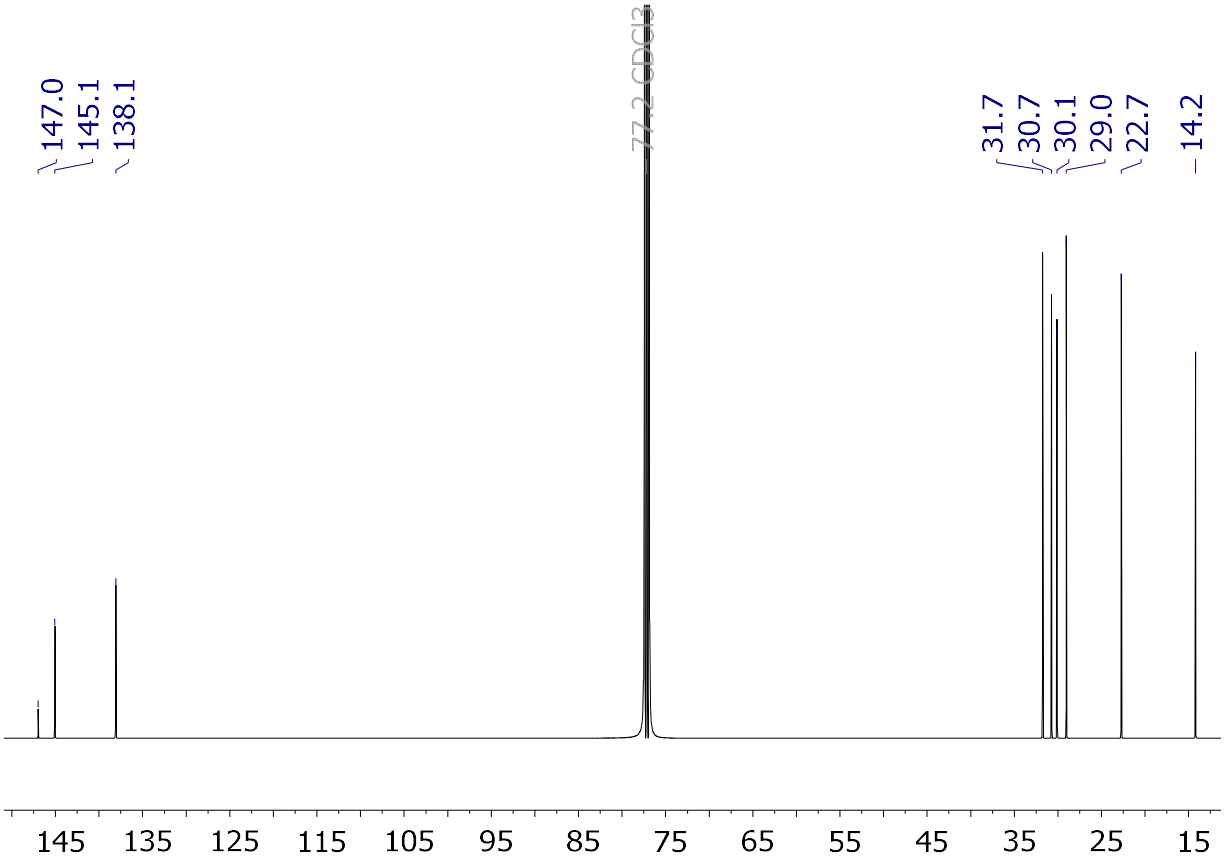

Figure S5.4.50: *$^{13}C\{^1H\}$ NMR spectrum of **6f** (in $CDCl_3$).*

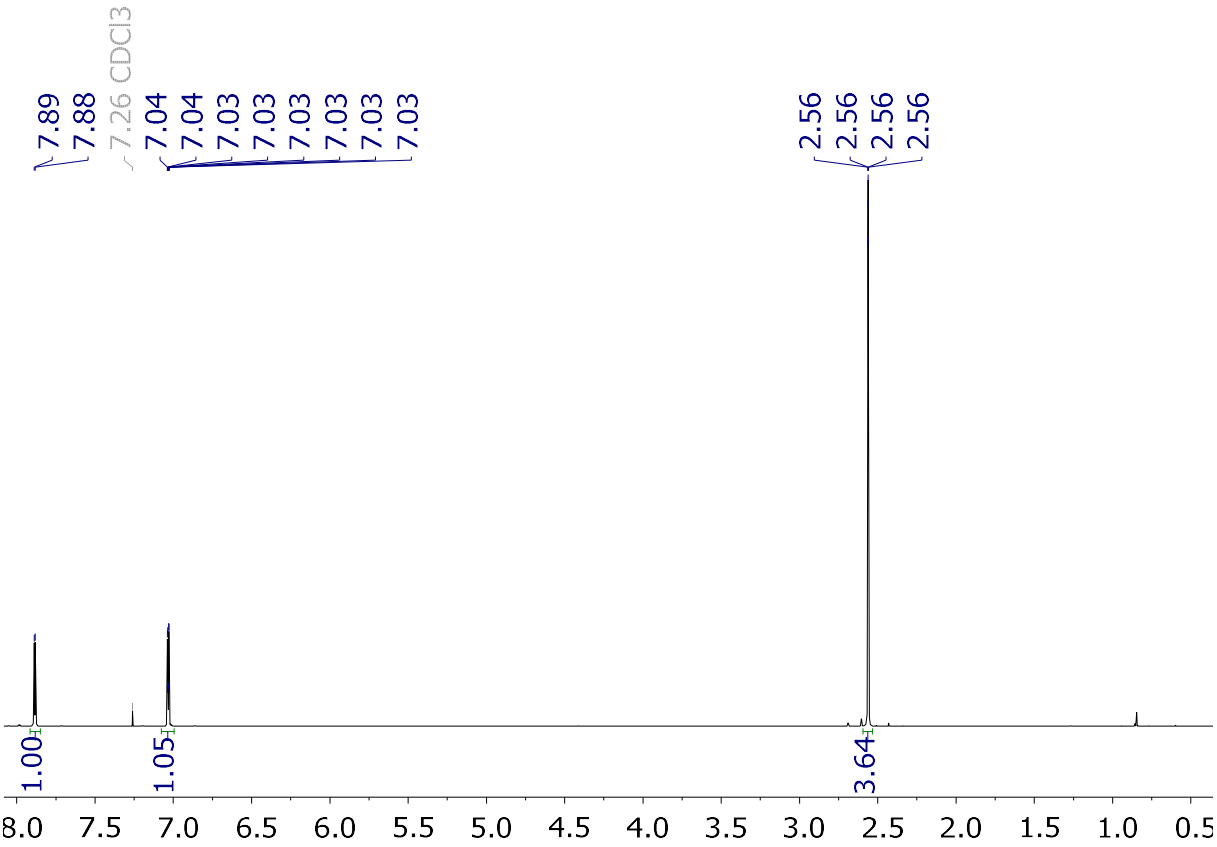

Figure S5.4.51: *^{1}H NMR spectrum of **11b** (in $CDCl_3$).*

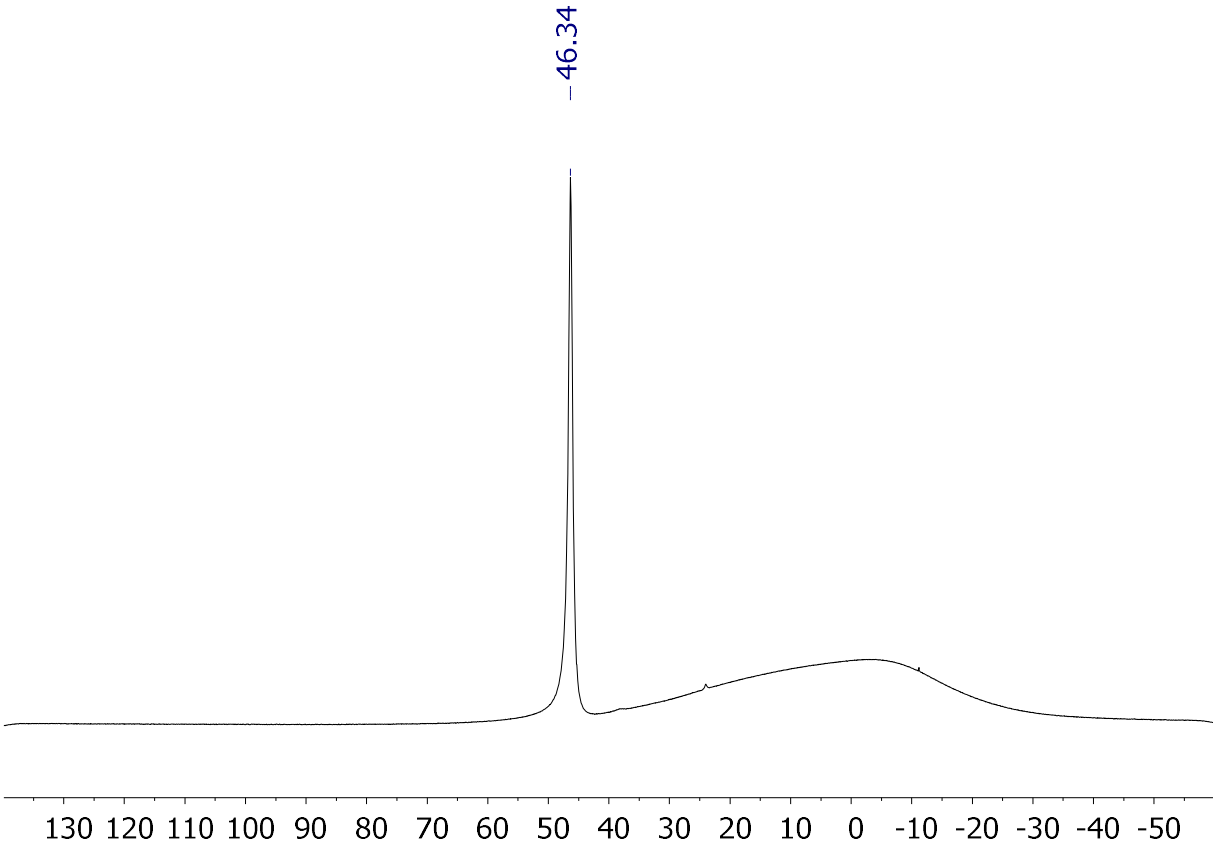

Figure S5.4.52: *$^{11}B\{^{1}H\}$ NMR spectrum of **11b** (in $CDCl_3$).*

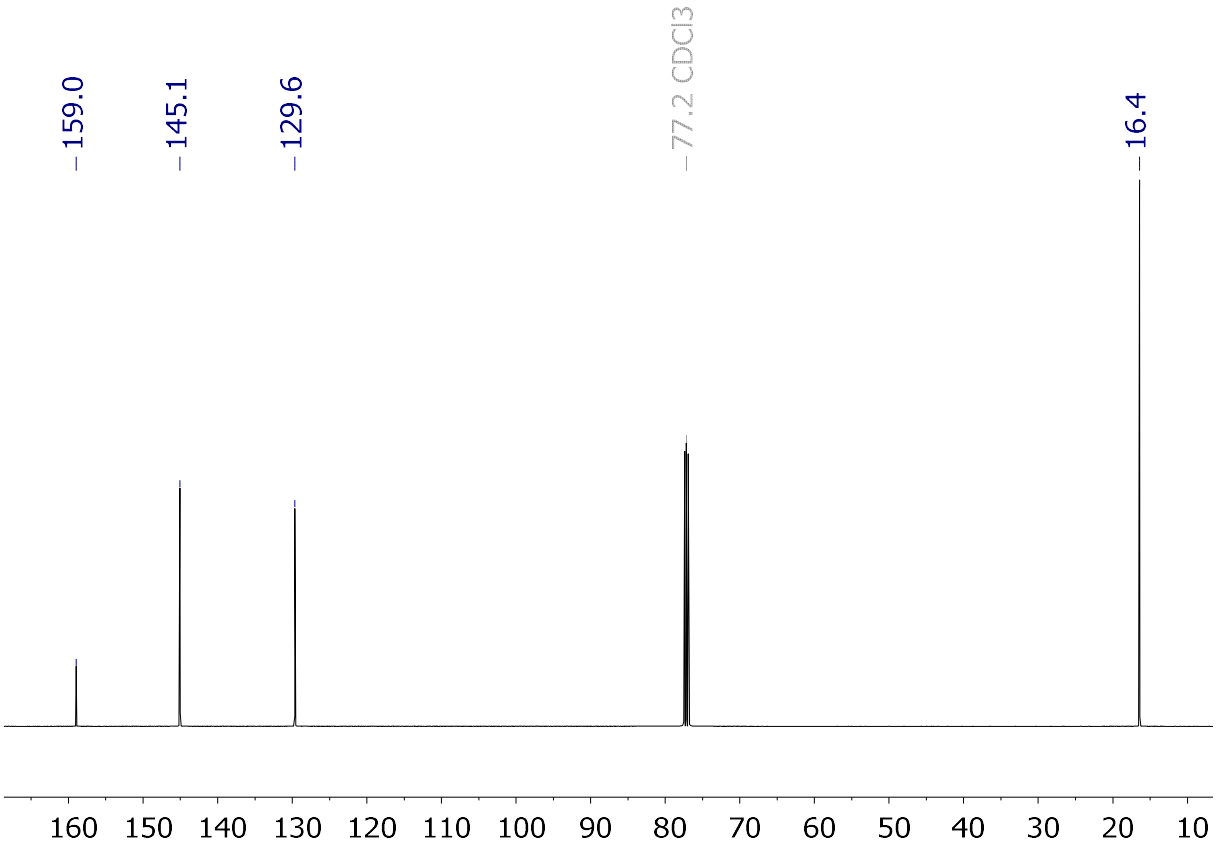

Figure S5.4.53: *$^{13}C\{^{1}H\}$ NMR spectrum of* ***11b*** *(in $CDCl_3$).*

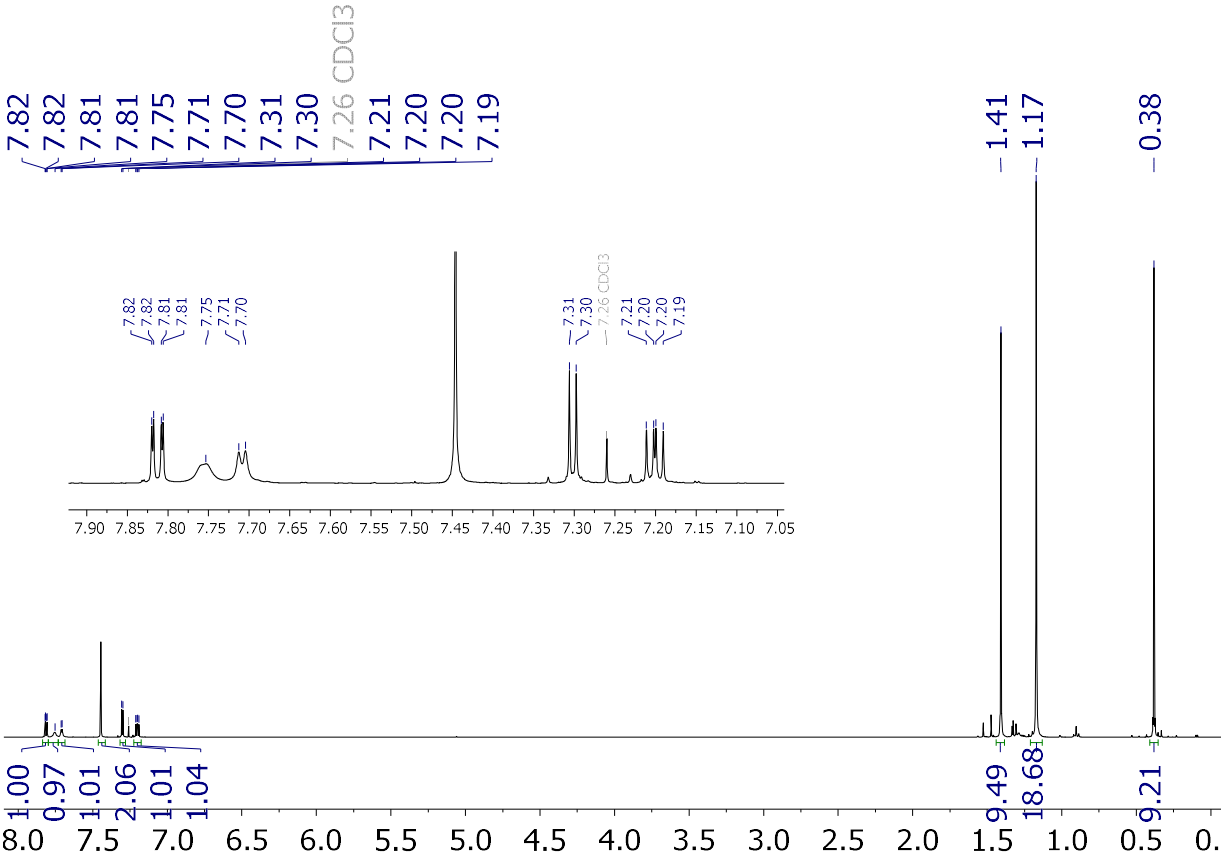

Figure S5.4.54: *^{1}H NMR spectrum of* ***11b*** *(in $CDCl_3$).*

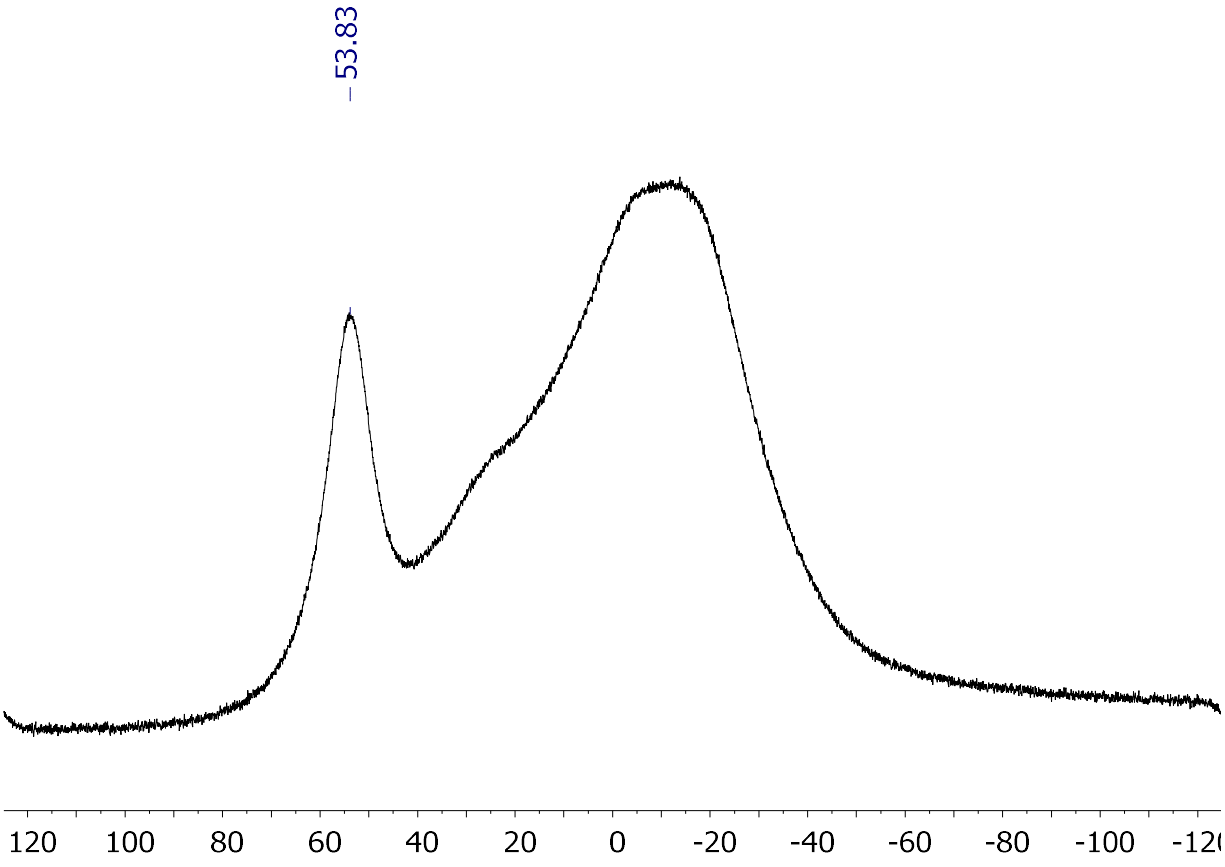

Figure S5.4.55: *$^{11}B\{^1H\}$ NMR spectrum of* ***11b*** *(in $CDCl_3$).*

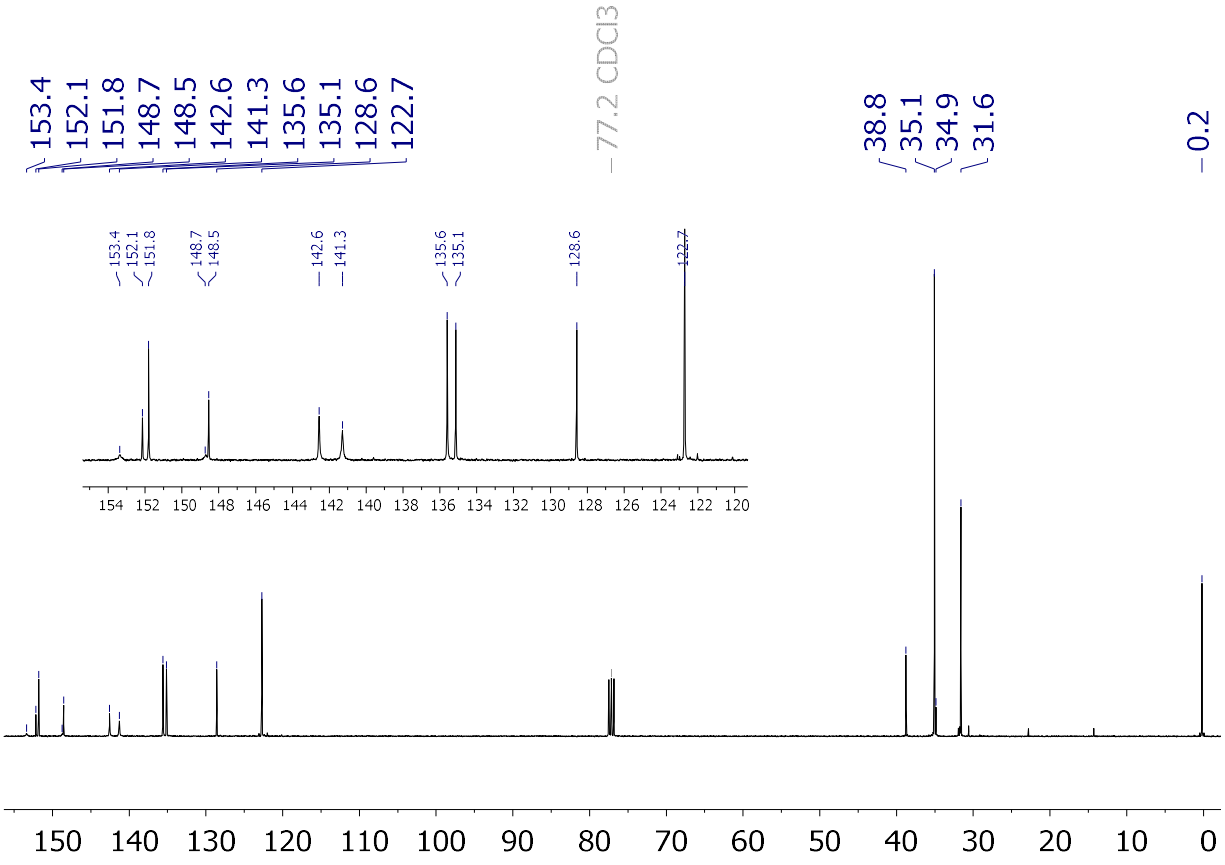

Figure S5.4.56: *$^{13}C\{^1H\}$ NMR spectrum of* ***11b*** *(in $CDCl_3$).*

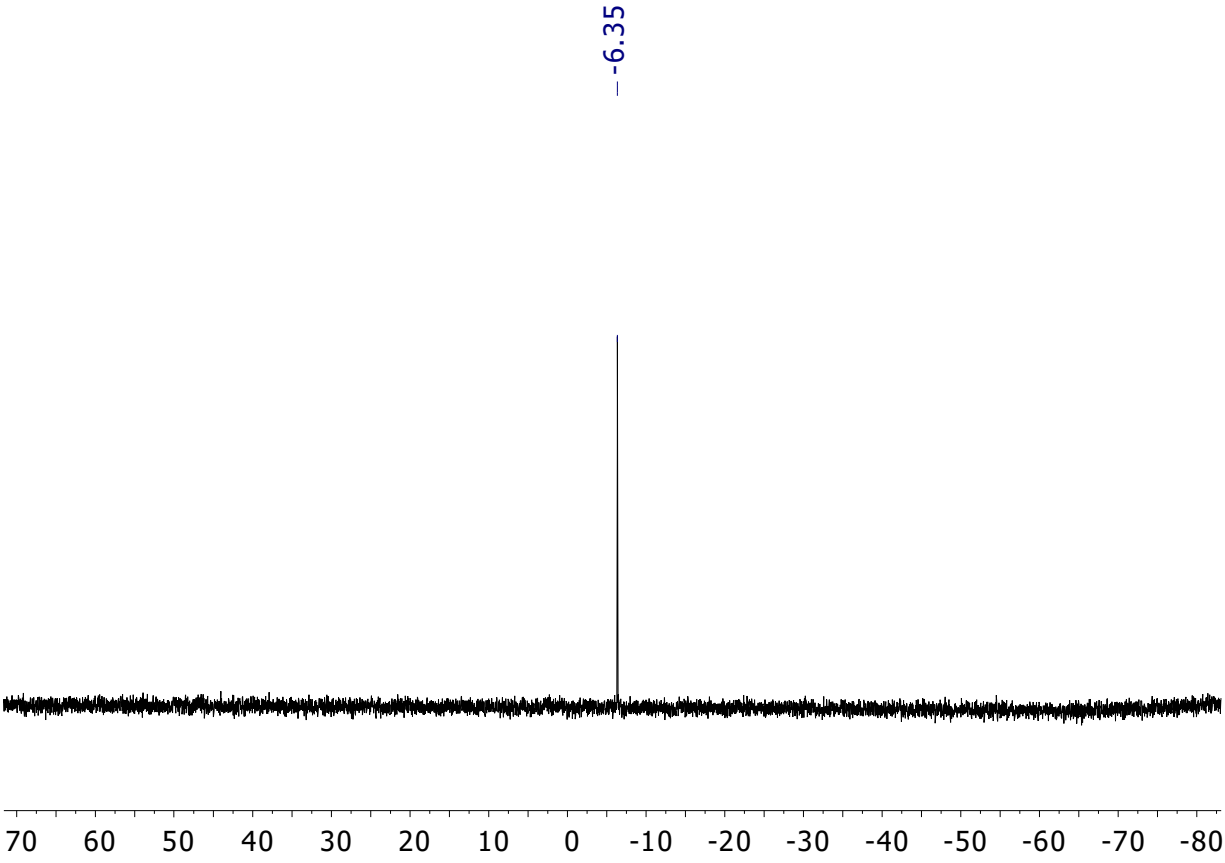

Figure S5.4.57: *^{29}Si NMR spectrum of **11b** (in $CDCl_3$).*

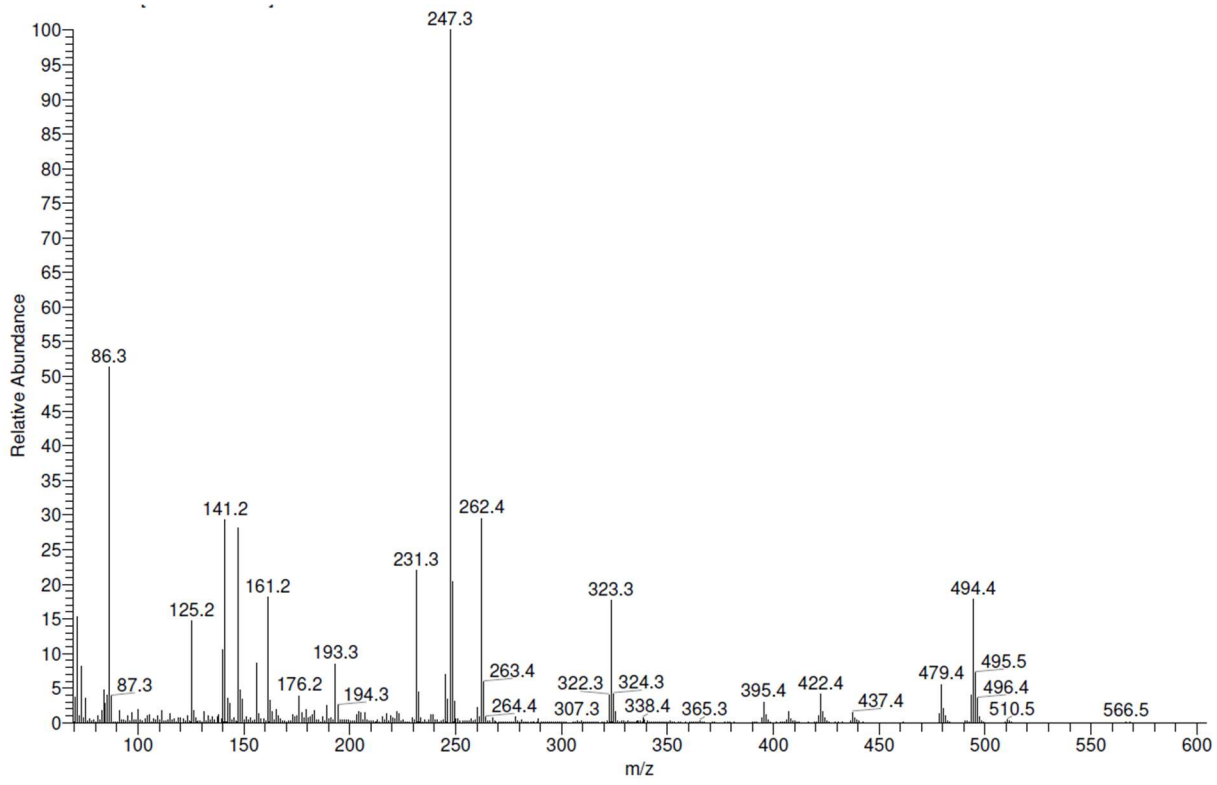

Figure S5.4.58: *Mass spectrum of **11b** (EI).*

UCLR UL2DATA SAVE ULIST FILE: ac-ahn-lf-125

1:	494.26599	41403.00000	0.00000	0.00000
2:	494.26654	40484.00000	0.00000	0.00000
3:	494.26761	47083.00000	0.00000	0.00000
4:	0.00000	0.00000	0.00000	0.00000
5:	0.00000	0.00000	0.00000	0.00000
6:	0.00000	0.00000	0.00000	0.00000
7:	0.00000	0.00000	0.00000	0.00000
8:	0.00000	0.00000	0.00000	0.00000
9:	0.00000	0.00000	0.00000	0.00000
10:	0.00000	0.00000	0.00000	0.00000
11:	0.00000	0.00000	0.00000	0.00000
12:	0.00000	0.00000	0.00000	0.00000
13:	0.00000	0.00000	0.00000	0.00000
14:	0.00000	0.00000	0.00000	0.00000
15:	0.00000	0.00000	0.00000	0.00000
16:	0.00000	0.00000	0.00000	0.00000
17:	0.00000	0.00000	0.00000	0.00000
18:	0.00000	0.00000	0.00000	0.00000
19:	0.00000	0.00000	0.00000	0.00000
20:	0.00000	0.00000	0.00000	9112017.00000
LINK	NONE	NONE	NONE	NONE
SIZE	3.00000	3.00000	0.00000	20.00000
MEAN	494.26671	42990.00000	0.00000	455600.85000
SUM	1482.80014	128970.00000	0.00000	9112017.00000
S.D.	0.00082	3574.30091	0.00000	2037508.94241
MAX	494.26761	47083.00000	0.00000	9112017.00000
MIN	494.26599	40484.00000	0.00000	0.00000

ULIST:

Figure S5.4.59: *HRMS information of* ***11b*** *(EI).*

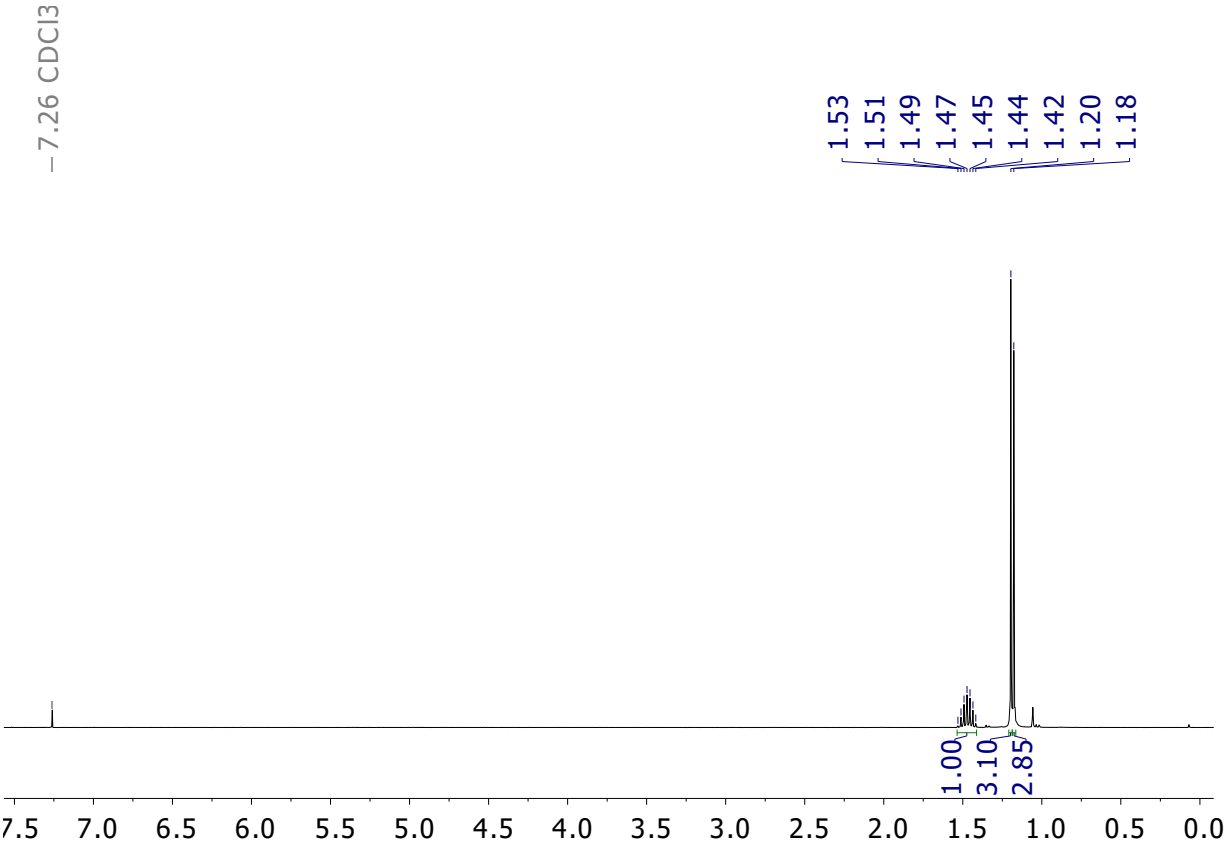

Figure S5.4.60: *^{1}H NMR of* ***14*** *(in $CDCl_3$).*

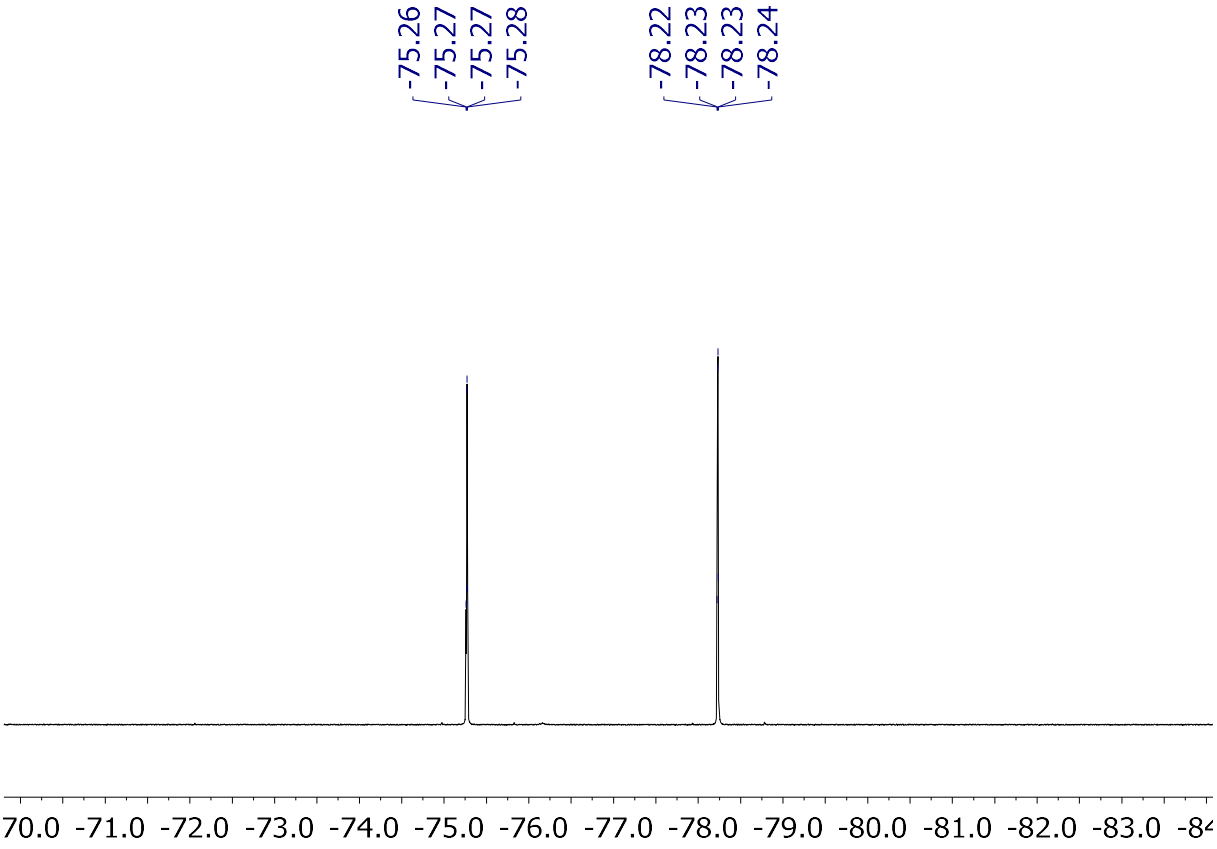

Figure S5.4.61: *$^{19}F\{^{1}H\}$ NMR of **14** (in $CDCl_3$).*

9^{N}_$CHCl_3$:

Total energy (B3LYP/6-31++G**): -2236.854714

N	0.169339	0.470173	-0.343240
Si	1.081277	2.042269	0.338215
C	2.915244	1.696417	0.455467
h	3.383560	1.561057	-0.518199
h	3.336958	2.598389	0.915826
h	3.174811	0.853263	1.094339
C	0.385865	2.340111	2.046977
h	0.946490	3.165047	2.499528
h	-0.669018	2.610410	2.034050
h	0.520061	1.462591	2.684750
C	0.788360	3.401846	-0.909508
h	-0.250911	3.726962	-0.944632
h	1.409731	4.260058	-0.632491
h	1.093817	3.083337	-1.909953

S	0.997107	-0.868922	-0.999767
S	-1.512350	0.643549	-0.638912
O	2.270290	-0.415171	-1.523325
O	0.099291	-1.697065	-1.779336
O	-1.847452	1.943655	-0.081495
O	-1.884027	0.286712	-1.990557
C	1.409380	-1.911722	0.546448
C	-2.368409	-0.606078	0.524983
F	1.894229	-1.151495	1.526688
F	0.314929	-2.530738	0.974154
F	2.320501	-2.809911	0.188719
F	-2.289535	-1.837633	0.046338
F	-1.809339	-0.550454	1.731214
F	-3.643266	-0.238282	0.607867

9^{N}_CH_2Cl_2:

Total energy (B3LYP/6-31++G**): -2236.856251

N	0.166041	0.471223	-0.350486
Si	1.074854	2.047076	0.339126
C	2.907218	1.698753	0.466533
h	3.381547	1.566106	-0.504532
h	3.325771	2.599535	0.931850
h	3.161438	0.854236	1.105811
C	0.367586	2.340770	2.043190
h	0.926237	3.165209	2.498941
h	-0.687107	2.611528	2.024450
h	0.498573	1.462497	2.680458
C	0.785399	3.404143	-0.911530
h	-0.254948	3.724908	-0.954082
h	1.401263	4.264582	-0.629420
h	1.099628	3.085765	-1.909236
S	0.999413	-0.866032	-1.001095
S	-1.514955	0.635744	-0.643979
O	2.271044	-0.409309	-1.526531

O	0.106679	-1.700103	-1.781644
O	-1.856391	1.939272	-0.098688
O	-1.889768	0.265375	-1.991883
C	1.414246	-1.904466	0.548718
C	-2.362335	-0.609959	0.530721
F	1.868333	-1.136818	1.536479
F	0.327135	-2.548227	0.957978
F	2.349322	-2.781456	0.200043
F	-2.289062	-1.841747	0.050023
F	-1.790879	-0.555740	1.730351
F	-3.635868	-0.240983	0.625876

9^{O}_$CHCl_3$:

Total energy (B3LYP/6-31++G**): -2236.862070

N	0.870334	0.744555	0.551982
S	-0.451897	0.720937	-0.277604
S	1.845400	-0.546185	0.826847
O	-0.427237	0.597623	-1.726107
O	2.550825	-0.312744	2.073816
O	1.186375	-1.823535	0.569114
C	-1.123714	2.435447	0.169966
C	3.152980	-0.350791	-0.529524
F	-1.262563	2.553024	1.480477
F	-0.287630	3.355430	-0.288348
F	-2.307296	2.565723	-0.423347
F	2.585622	-0.453171	-1.730612
F	3.752387	0.832659	-0.424729
F	4.057789	-1.319521	-0.385323
O	-1.525271	-0.177419	0.387749
Si	-2.576561	-1.570289	-0.060464
C	-1.717243	-2.498508	-1.425668
h	-1.621757	-1.894254	-2.329791
h	-0.721997	-2.821602	-1.113415
h	-2.303184	-3.389645	-1.672822

C	-4.181689	-0.773414	-0.568160
h	-4.053959	-0.143612	-1.451444
h	-4.917035	-1.546158	-0.811634
h	-4.591684	-0.161042	0.239036
C	-2.660352	-2.491773	1.553089
h	-3.061924	-1.863850	2.352135
h	-3.315822	-3.361496	1.444172
h	-1.671358	-2.846682	1.850637

9^{O}_CH_2Cl_2:

Total energy (B3LYP/6-31++G**): -2236.863818

N	0.826317	0.803086	0.519174
S	-0.486821	0.782878	-0.311968
S	1.778762	-0.510702	0.817193
O	-0.472200	0.695787	-1.762202
O	2.442406	-0.312316	2.087033
O	1.090622	-1.762383	0.507104
C	-1.205490	2.462694	0.180497
C	3.117520	-0.306978	-0.505553
F	-1.345955	2.548343	1.493228
F	-0.399249	3.418038	-0.258683
F	-2.396359	2.576036	-0.406852
F	2.571017	-0.371621	-1.719885
F	3.733721	0.862529	-0.361068
F	4.001989	-1.294291	-0.367417
O	-1.571459	-0.141150	0.323715
Si	-2.396950	-1.676830	-0.053645
C	-1.575229	-2.449495	-1.535900
h	-1.617788	-1.799652	-2.412616
h	-0.529048	-2.680283	-1.324758
h	-2.087362	-3.385923	-1.782030
C	-4.155489	-1.136489	-0.377076
h	-4.218980	-0.491292	-1.257353
h	-4.791920	-2.009057	-0.557000

h	-4.569406	-0.592726	0.476095
C	-2.188984	-2.647967	1.521138
h	-2.595976	-2.108596	2.380335
h	-2.711933	-3.607064	1.447512
h	-1.130950	-2.847585	1.705293

14^{O}_$CHCl_3$:

Total energy (B3LYP/6-31++G**): -2472.780413

N	1.756131	0.601949	0.584999
S	0.516355	0.946968	-0.299505
S	2.445529	-0.880814	0.719763
O	0.559427	0.809874	-1.746975
O	3.042488	-0.978542	2.040153
O	1.602361	-1.953755	0.201198
C	0.355154	2.786915	0.127068
C	3.905049	-0.728830	-0.478021
F	0.196287	2.951922	1.430851
F	1.443789	3.419112	-0.286288
F	-0.709742	3.256105	-0.519129
F	3.463426	-0.515207	-1.716523
F	4.696162	0.277808	-0.112860
F	4.597669	-1.867951	-0.447265
O	-0.785516	0.401050	0.323654
Si	-2.306841	-0.546231	0.084626
C	-1.795158	-2.199806	-0.683897
h	-0.922011	-2.498128	-0.090461
C	-3.456535	0.621332	-0.869462
h	-3.404949	1.556151	-0.295097
C	-2.815197	-0.726150	1.900404
h	-3.745269	-1.311193	1.871467
C	-3.131944	0.622916	2.575938
h	-3.463391	0.458717	3.606325
h	-2.246475	1.263813	2.616560
h	-3.923305	1.173799	2.061603

C	-1.785388	-1.521897	2.727504
h	-1.595895	-2.516887	2.317896
h	-0.828410	-0.995216	2.781220
h	-2.146134	-1.651432	3.752947
C	-2.890603	-3.270861	-0.476089
h	-3.798613	-3.036772	-1.039960
h	-2.529422	-4.240339	-0.833697
h	-3.169642	-3.393852	0.573206
C	-1.356147	-2.161689	-2.160502
h	-0.597743	-1.402223	-2.358244
h	-0.932268	-3.131236	-2.441577
h	-2.203924	-1.973188	-2.824046
C	-3.047946	0.946909	-2.319502
h	-3.176221	0.081838	-2.973962
h	-3.683176	1.748286	-2.710962
h	-2.010789	1.276835	-2.406912
C	-4.921253	0.131133	-0.817805
h	-5.579917	0.879740	-1.269590
h	-5.054609	-0.797676	-1.380232
h	-5.273706	-0.040889	0.202521

14^{O}_CH_2Cl_2:

Total energy (B3LYP/6-31++G**): -2472.782041

N	1.767928	0.655622	0.559964
S	0.517406	0.984754	-0.300164
S	2.427148	-0.847952	0.745731
O	0.517694	0.850078	-1.747971
O	3.035327	-0.913133	2.057512
O	1.536871	-1.901124	0.267857
C	0.330150	2.818989	0.124952
C	3.862120	-0.766583	-0.487117
F	0.208835	2.992744	1.432159
F	1.386505	3.477430	-0.328833
F	-0.769519	3.262895	-0.487026

F	3.395717	-0.576625	-1.720958
F	4.686114	0.228947	-0.170305
F	4.525106	-1.922049	-0.439322
O	-0.783889	0.434151	0.348108
Si	-2.256216	-0.556017	0.085275
C	-1.710640	-2.194071	-0.693516
h	-0.826652	-2.472134	-0.107308
C	-3.446600	0.574191	-0.868318
h	-3.449177	1.500587	-0.277848
C	-2.789815	-0.768297	1.892695
h	-3.698208	-1.385983	1.845963
C	-3.164835	0.563393	2.572729
h	-3.501640	0.382814	3.598723
h	-2.304413	1.236446	2.627412
h	-3.970315	1.088565	2.052890
C	-1.745076	-1.531833	2.731474
h	-1.501376	-2.510805	2.312335
h	-0.813096	-0.966253	2.813609
h	-2.120193	-1.692697	3.747385
C	-2.776631	-3.294240	-0.485686
h	-3.695590	-3.083052	-1.041546
h	-2.393823	-4.252237	-0.851757
h	-3.045018	-3.432370	0.564700
C	-1.278386	-2.139244	-2.171881
h	-0.539880	-1.361156	-2.370281
h	-0.830764	-3.096413	-2.458077
h	-2.132710	-1.970301	-2.833098
C	-3.030918	0.945560	-2.305263
h	-3.105340	0.087459	-2.977133
h	-3.696827	1.722489	-2.695592
h	-2.009217	1.323978	-2.368976
C	-4.886299	0.013509	-0.849056
h	-5.575589	0.732407	-1.303800
h	-4.964685	-0.913876	-1.424410

h	-5.248088	-0.189518	0.162580

14^{N}_$CHCl_3$:

Total energy (B3LYP/6-31++G**): -2472.759079

N	0.107873	-0.024790	-0.328316
Si	-1.809108	-0.033656	0.122285
C	-2.467747	1.768115	0.235726
h	-2.166691	2.293837	-0.669060
C	-2.101583	-0.790911	1.857166
h	-2.878257	-0.101445	2.218838
C	-2.700740	-0.861444	-1.351555
h	-3.745824	-0.784979	-1.015100
S	0.906452	1.285460	-1.081518
S	0.801893	-1.593704	-0.504339
O	-0.094423	2.249131	-1.492722
O	1.936622	0.809560	-1.980034
O	-0.070833	-2.441441	0.291728
O	1.132092	-1.919356	-1.873694
C	1.862987	2.141898	0.351283
C	2.457126	-1.590822	0.460045
F	1.262141	1.955340	1.527300
F	3.099366	1.663503	0.414156
F	1.905634	3.442631	0.080454
F	3.441528	-1.094740	-0.268563
F	2.332412	-0.895454	1.590563
F	2.714104	-2.862795	0.751384
C	-1.982986	2.590929	1.443348
h	-0.905810	2.745512	1.448960
h	-2.450853	3.580839	1.423774
h	-2.258013	2.126145	2.394793
C	-4.016516	1.720176	0.248191
h	-4.414398	1.149989	1.094285
h	-4.404872	2.739443	0.343638
h	-4.436249	1.299886	-0.667386

C	-2.572688	-0.027837	-2.645084
h	-1.553515	-0.063671	-3.039724
h	-3.230881	-0.438399	-3.417805
h	-2.836778	1.022654	-2.510245
C	-2.452310	-2.348650	-1.668684
h	-1.479357	-2.503765	-2.138130
h	-2.502326	-2.988975	-0.789395
h	-3.208723	-2.693074	-2.382246
C	-2.723388	-2.198445	1.905812
h	-3.614843	-2.281510	1.278359
h	-2.013182	-2.963169	1.591917
h	-3.028543	-2.427474	2.932969
C	-0.927595	-0.674615	2.847780
h	-0.471419	0.317516	2.852168
h	-1.281802	-0.877881	3.864071
h	-0.150497	-1.404755	2.621226

14^{N}_CH_2Cl_2:

Total energy (B3LYP/6-31++G**): -2472.760327

N	0.107873	-0.024790	-0.328316
Si	-1.809108	-0.033656	0.122285
C	-2.467747	1.768115	0.235726
h	-2.166691	2.293837	-0.669060
C	-2.101583	-0.790911	1.857166
h	-2.878257	-0.101445	2.218838
C	-2.700740	-0.861444	-1.351555
h	-3.745824	-0.784979	-1.015100
S	0.906452	1.285460	-1.081518
S	0.801893	-1.593704	-0.504339
O	-0.094423	2.249131	-1.492722
O	1.936622	0.809560	-1.980034
O	-0.070833	-2.441441	0.291728
O	1.132092	-1.919356	-1.873694
C	1.862987	2.141898	0.351283

C	2.457126	-1.590822	0.460045
F	1.262141	1.955340	1.527300
F	3.099366	1.663503	0.414156
F	1.905634	3.442631	0.080454
F	3.441528	-1.094740	-0.268563
F	2.332412	-0.895454	1.590563
F	2.714104	-2.862795	0.751384
C	-1.982986	2.590929	1.443348
h	-0.905810	2.745512	1.448960
h	-2.450853	3.580839	1.423774
h	-2.258013	2.126145	2.394793
C	-4.016516	1.720176	0.248191
h	-4.414398	1.149989	1.094285
h	-4.404872	2.739443	0.343638
h	-4.436249	1.299886	-0.667386
C	-2.572688	-0.027837	-2.645084
h	-1.553515	-0.063671	-3.039724
h	-3.230881	-0.438399	-3.417805
h	-2.836778	1.022654	-2.510245
C	-2.452310	-2.348650	-1.668684
h	-1.479357	-2.503765	-2.138130
h	-2.502326	-2.988975	-0.789395
h	-3.208723	-2.693074	-2.382246
C	-2.723388	-2.198445	1.905812
h	-3.614843	-2.281510	1.278359
h	-2.013182	-2.963169	1.591917
h	-3.028543	-2.427474	2.932969
C	-0.927595	-0.674615	2.847780
h	-0.471419	0.317516	2.852168
h	-1.281802	-0.877881	3.864071
h	-0.150497	-1.404755	2.621226

5.5 Selective C–H Activation of Heterocyclic Systems by Intermolecular Electrophilic Borylation

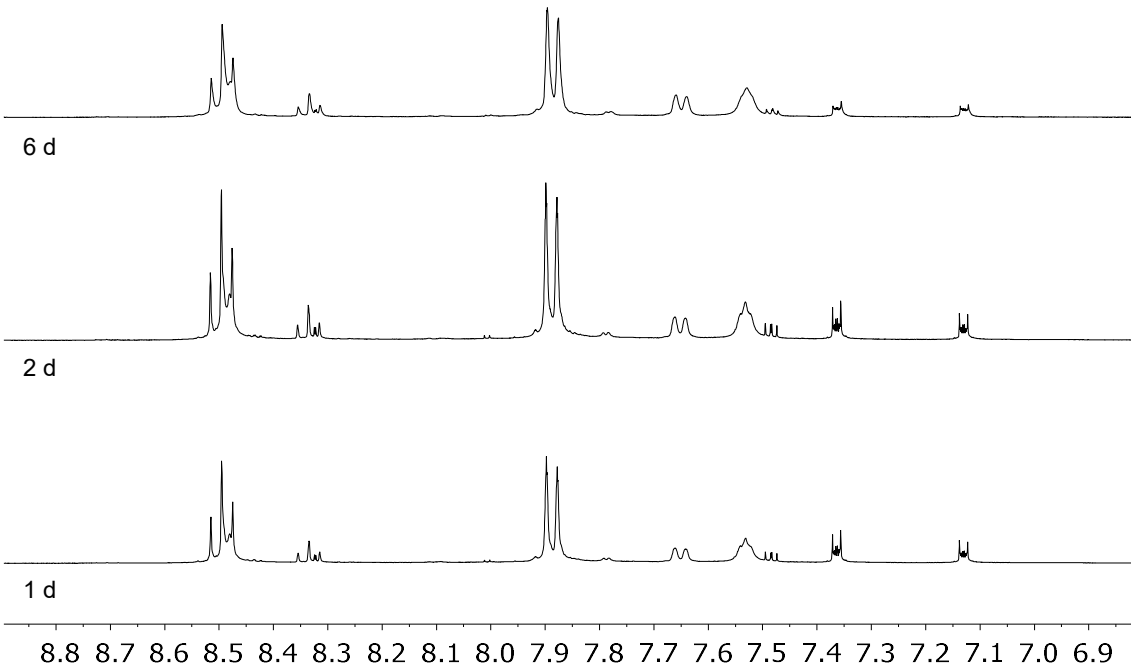

Figure S5.5.1: *In situ ^{1}H NMR aromatic region of the reaction of* ***18^{Cl}****, Thiophene, $AlCl_3$ and 2,6-Lut (in CD_2Cl_2).*

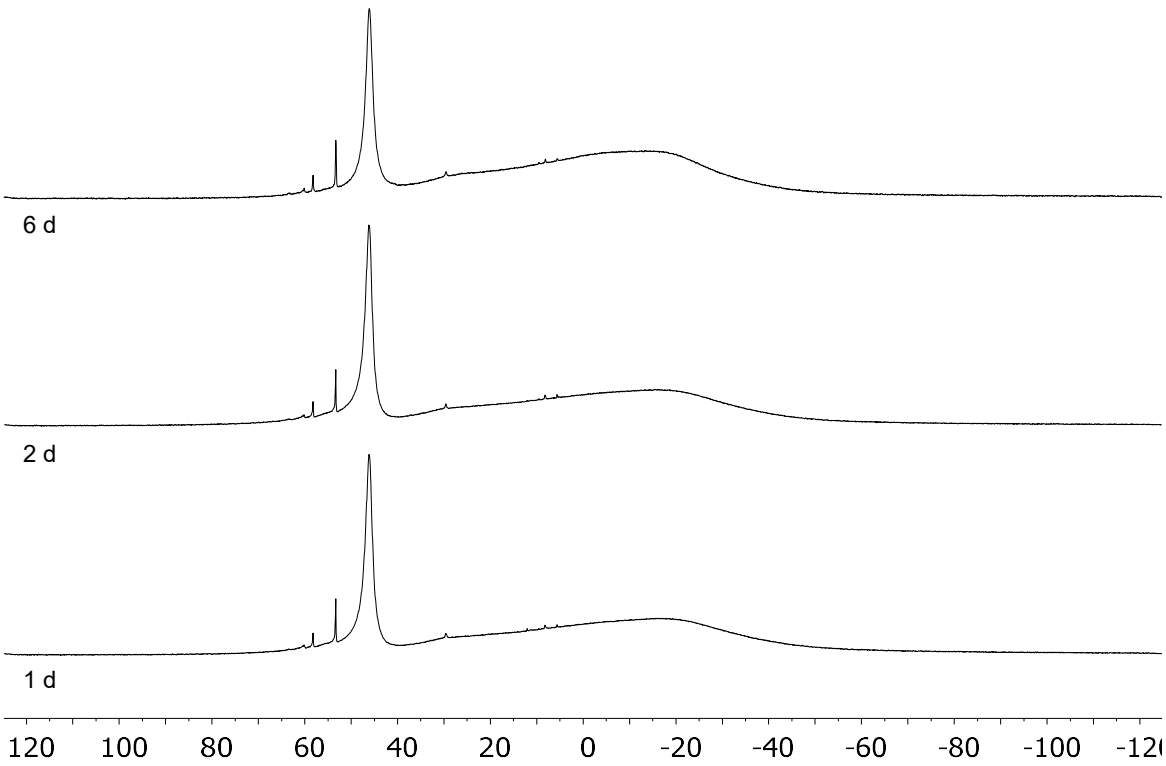

Figure S5.5.2: *In situ $^{11}B\{^{1}H\}$ NMR of the reaction of* ***18^{Cl}****, Thiophene, $AlCl_3$ and 2,6-Lut (in CD_2Cl_2).*

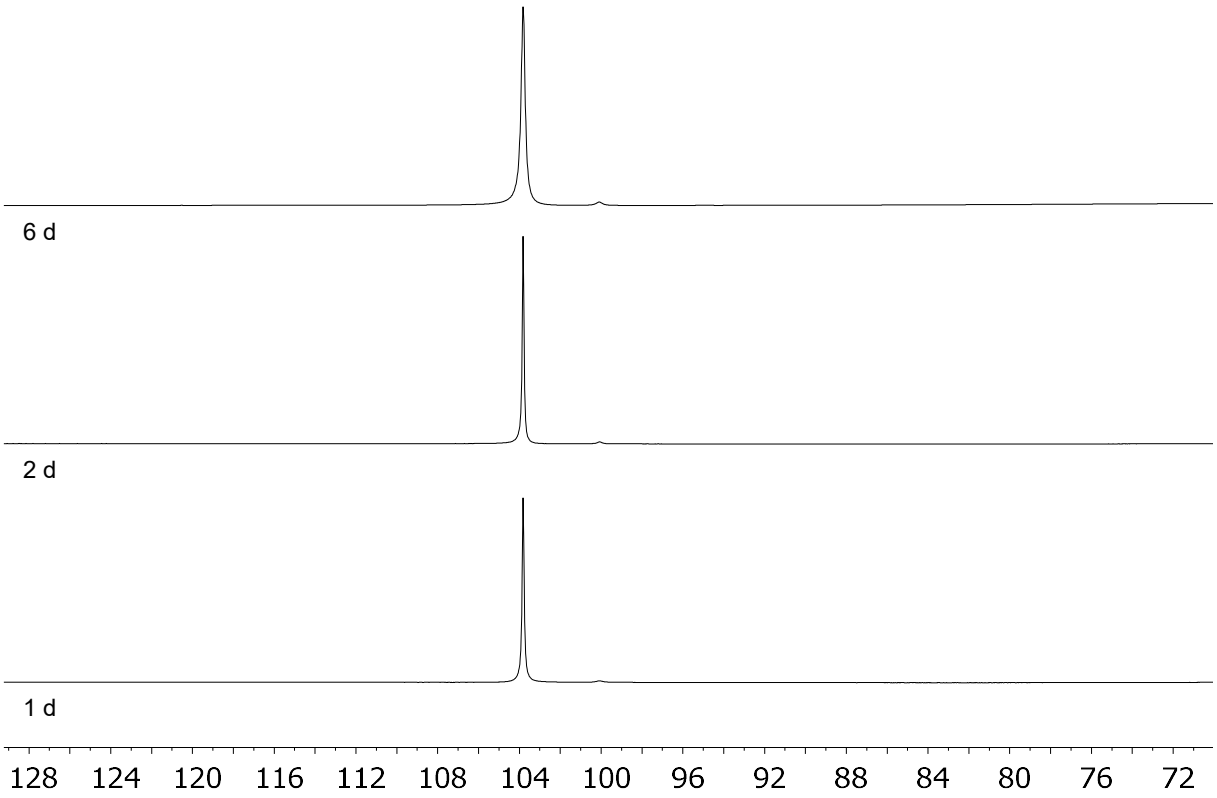

Figure S5.5.3: *In situ ^{27}Al NMR of the reaction of* ***18^{Cl}****, Thiophene, $AlCl_3$ and 2,6-Lut (in CD_2Cl_2).*

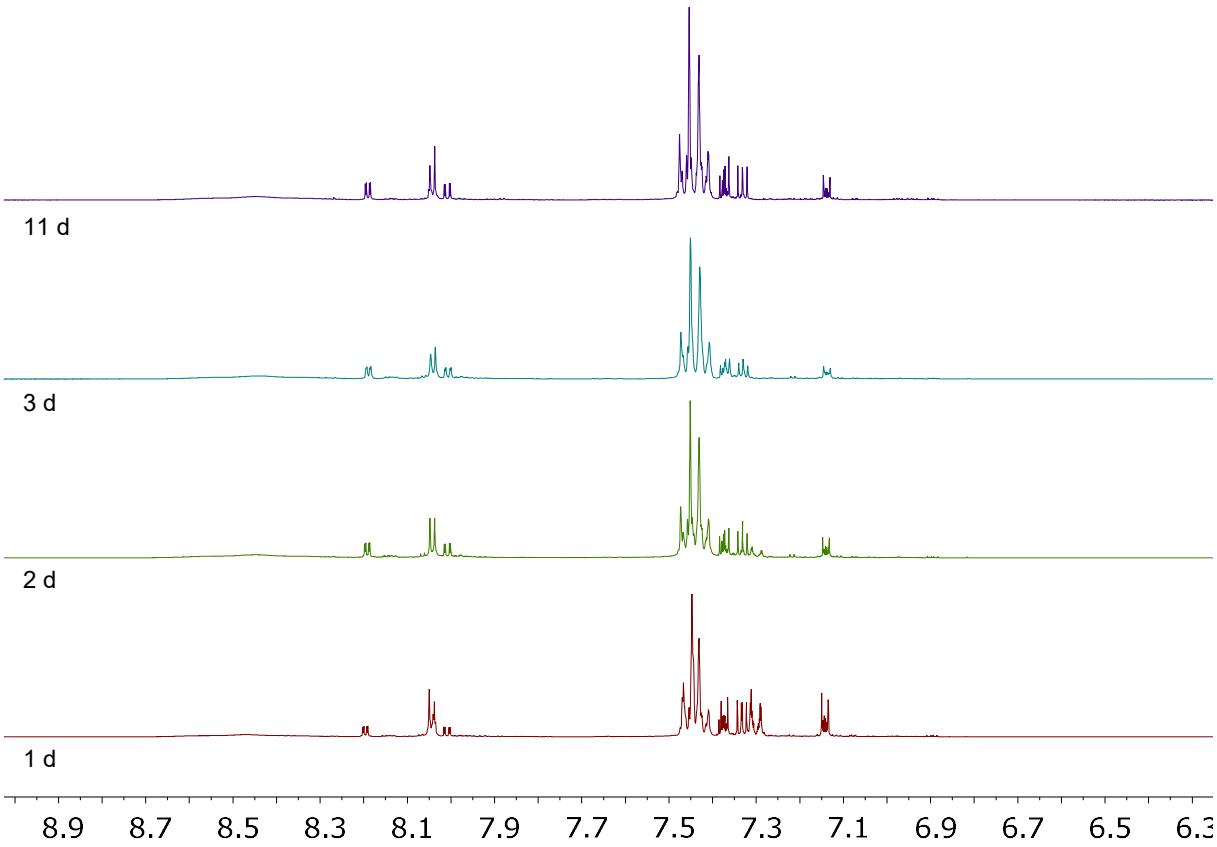

Figure S5.5.4: *In situ ^{1}H NMR aromatic region of the reaction of* ***18^{Cl}****, Thiophene, $AlCl_3$ and Me_2NTol (in CD_2Cl_2).*

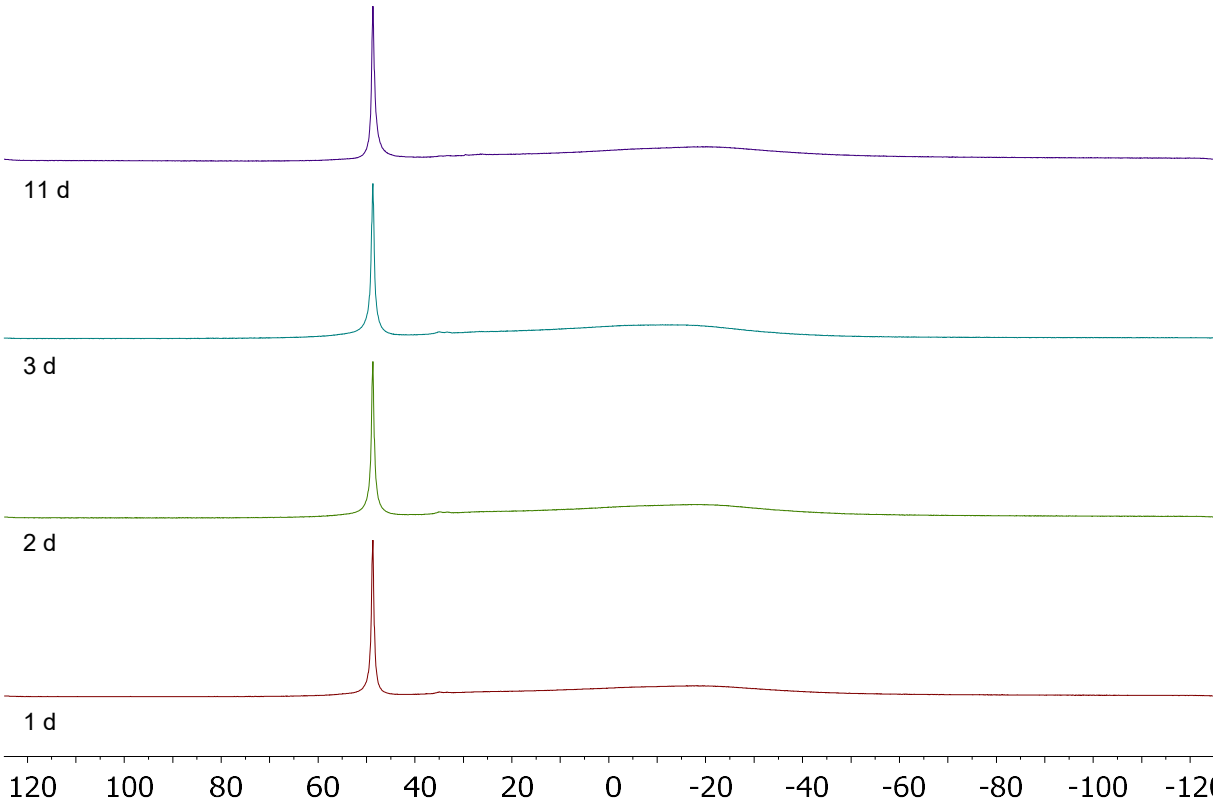

Figure S5.5.5: *In situ $^{11}B\{^{1}H\}$ NMR of the reaction of* ***18^{Cl}****, Thiophene, $AlCl_3$ and Me_2NTol (in CD_2Cl_2).*

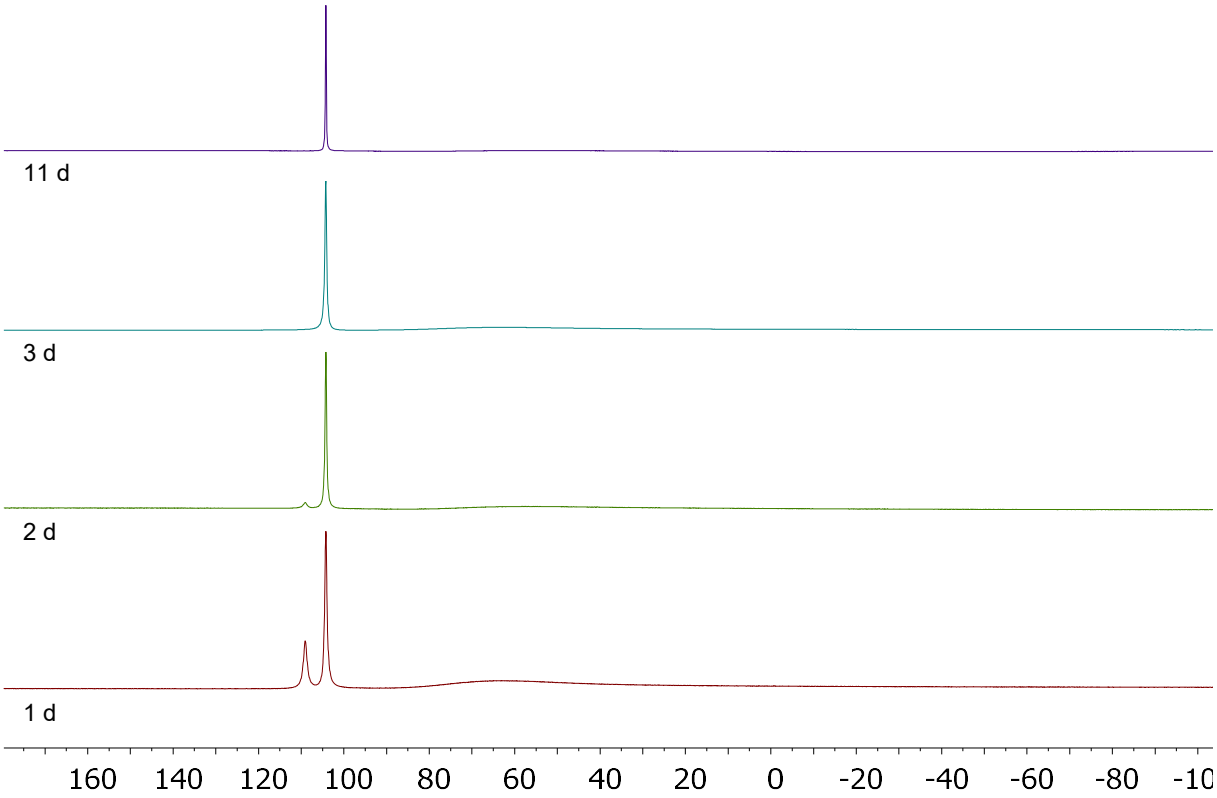

Figure S5.5.6*: In situ ^{27}Al NMR of the reaction of* ***18^{Cl}****, Thiophene, $AlCl_3$ and Me_2NTol (in CD_2Cl_2).*

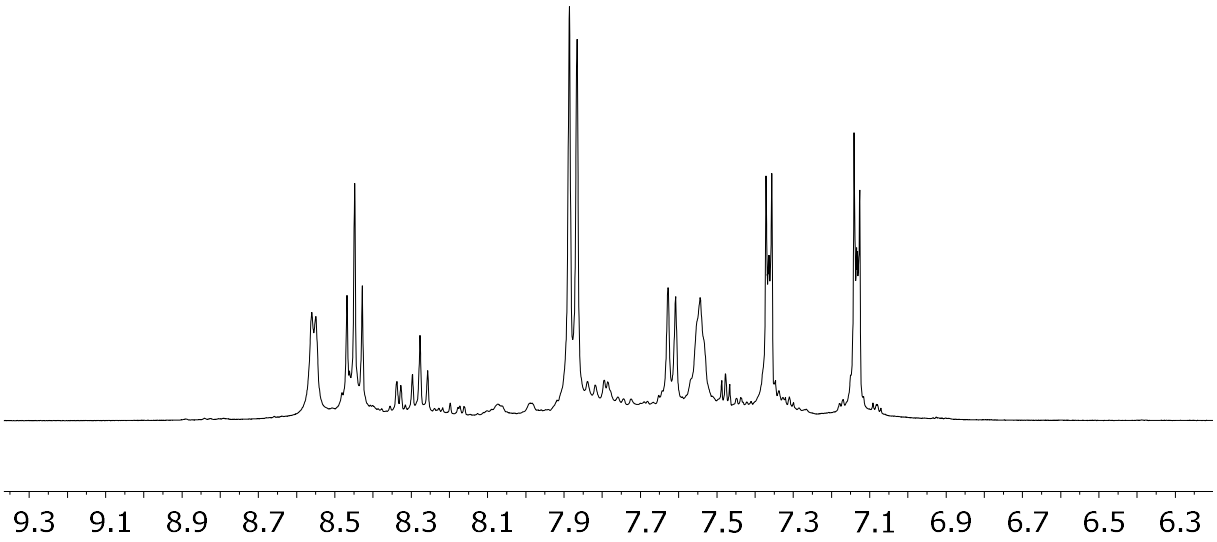

Figure S5.5.7: *In situ ^{1}H NMR aromatic region of the reaction of* ***18^{Br}****, Thiophene, Me_3SiNTf_2 and 2,6-Lut after 24 h reaction time (in CD_2Cl_2).*

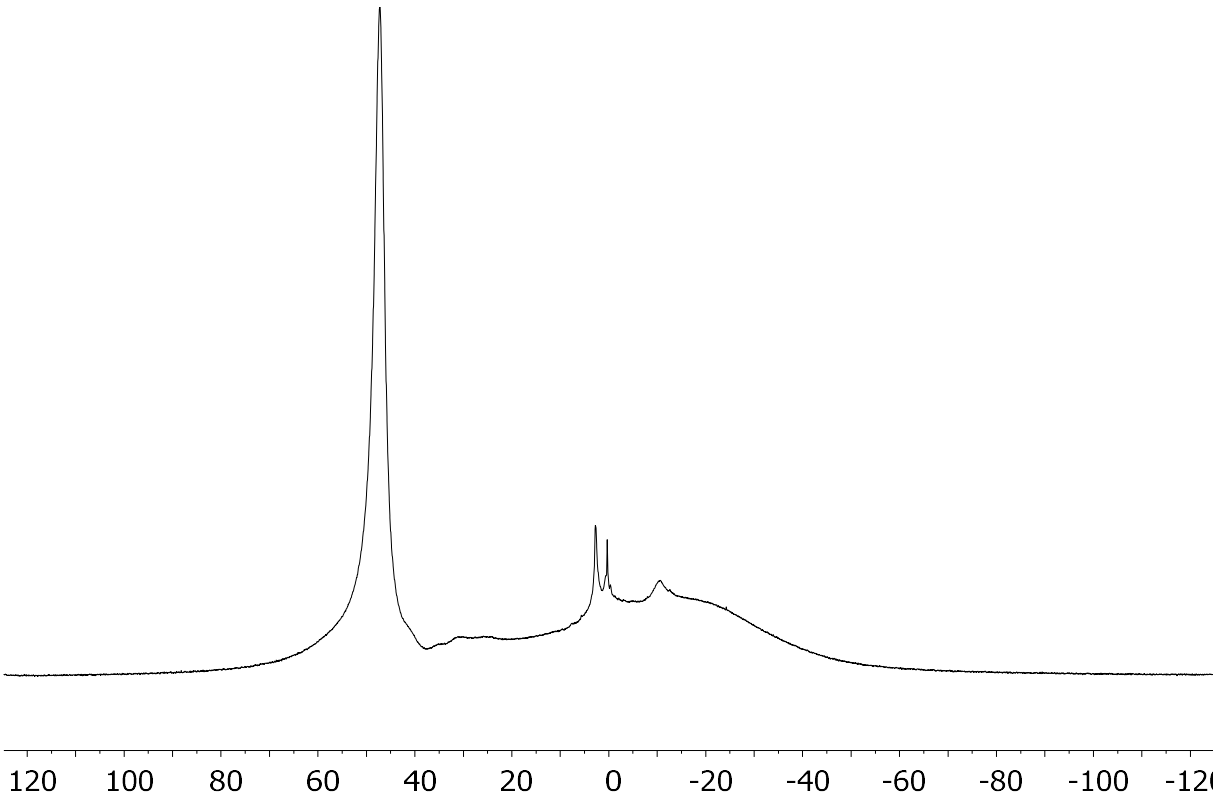

Figure S5.5.8: *In situ $^{11}B\{^{1}H\}$ NMR of the reaction of* ***18^{Br}****, Thiophene, Me_3SiNTf_2 and 2,6-Lut after 24 h reaction time (in CD_2Cl_2).*

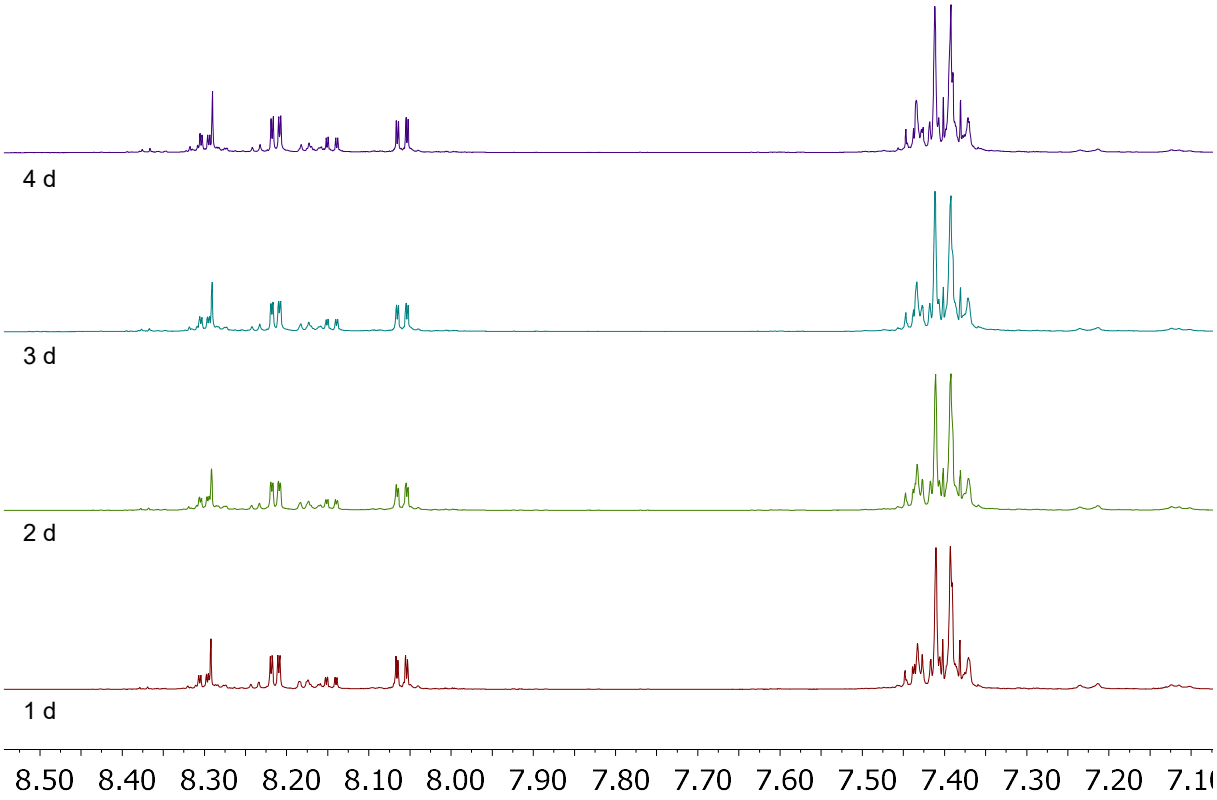

Figure S5.5.9: *In situ ^{1}H NMR aromatic region of the reaction of* ***18^{Br}****, Thiophene, Me_3SiNTf_2 and Me_2NTol (in CD_2Cl_2).*

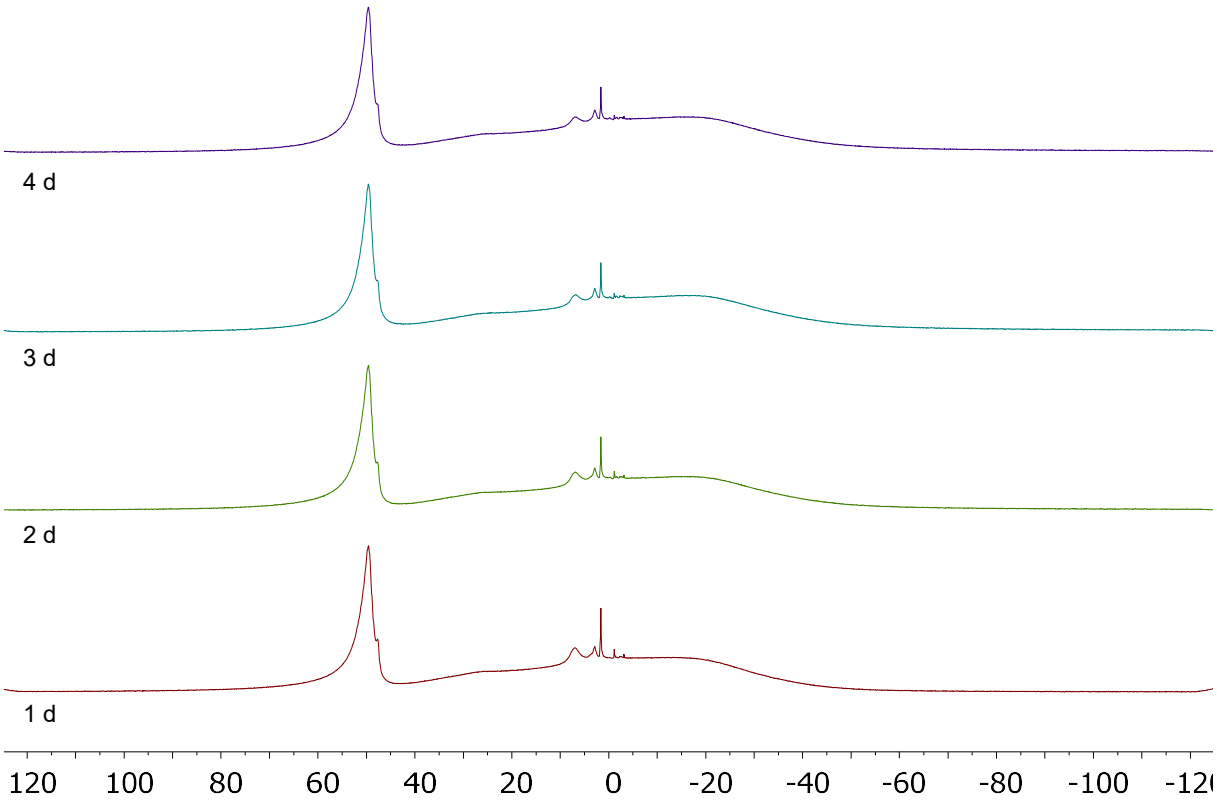

Figure S5.5.10: *In situ $^{11}B\{^{1}H\}$ NMR of the reaction of* ***18^{Br}****, Thiophene, Me_3SiNTf_2 and Me_2NTol (in CD_2Cl_2).*

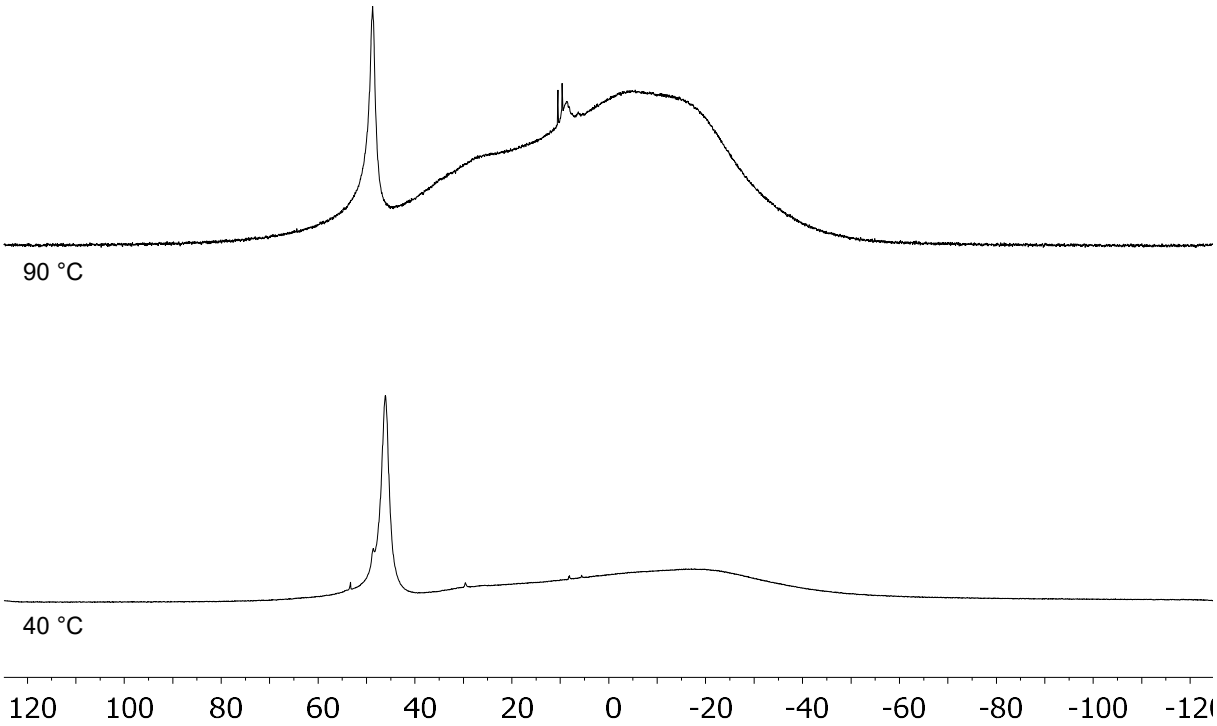

Figure S5.5.11: *In situ $^{11}B\{^1H\}$ NMR of the reaction of **18^{Cl}**, Thiophene, $AlCl_3$ and Me_2NTol at 40 °C and 90 °C after 24 h reaction time (in CD_2Cl_2).*

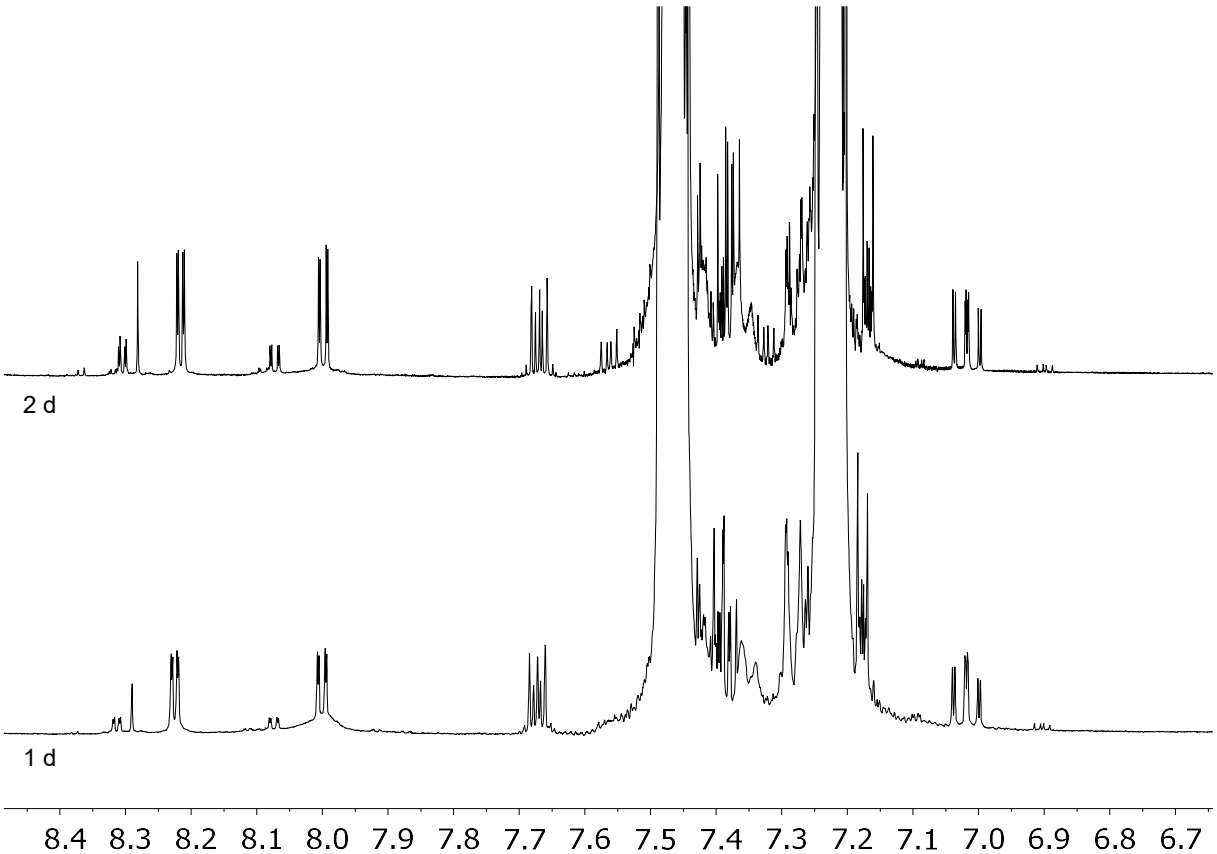

Figure S5.5.12: *In situ ^1H NMR aromatic region of the reaction of **18^{Cl}**, Thiophene, $AlCl_3$ and Me_2NTol at 90 °C (in CD_2Cl_2).*

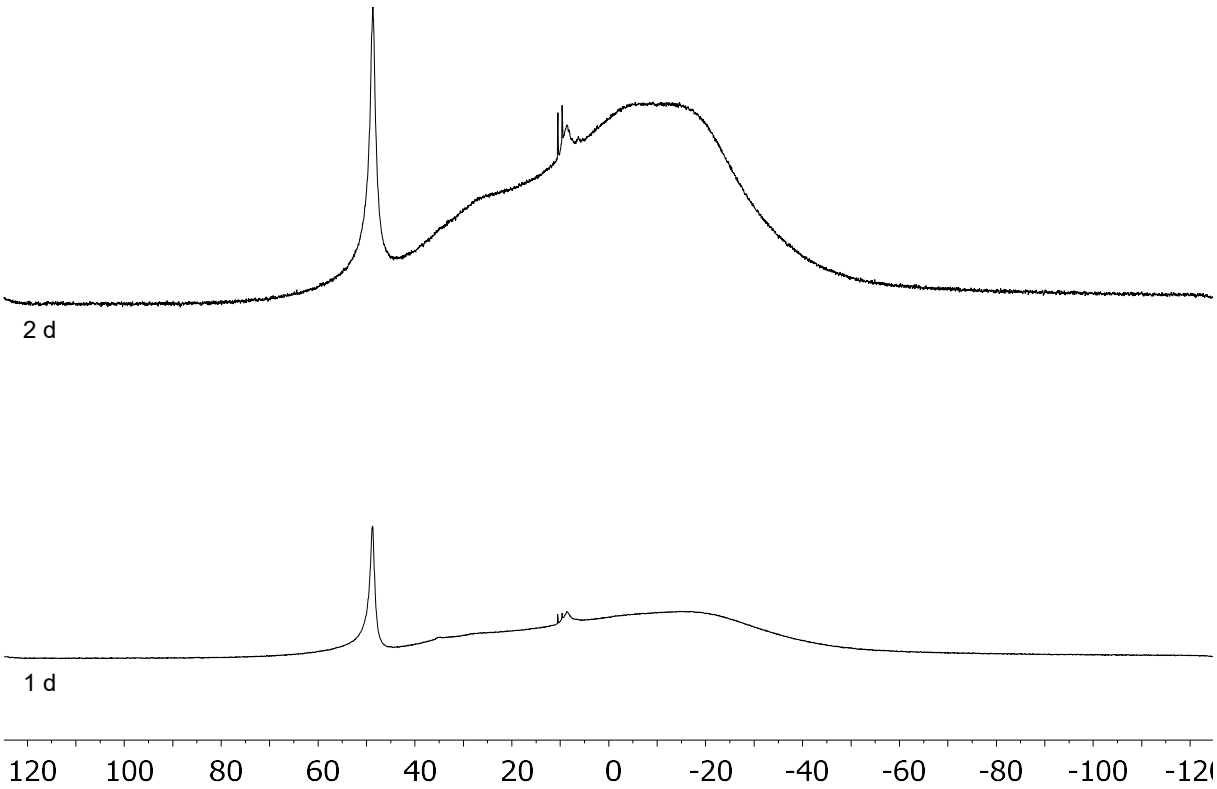

Figure S5.5.13: *In situ $^{11}B\{^1H\}$ NMR of the reaction of* ***18^{Cl}****, Thiophene, $AlCl_3$ and Me_2NTol at 90 °C (in CD_2Cl_2).*

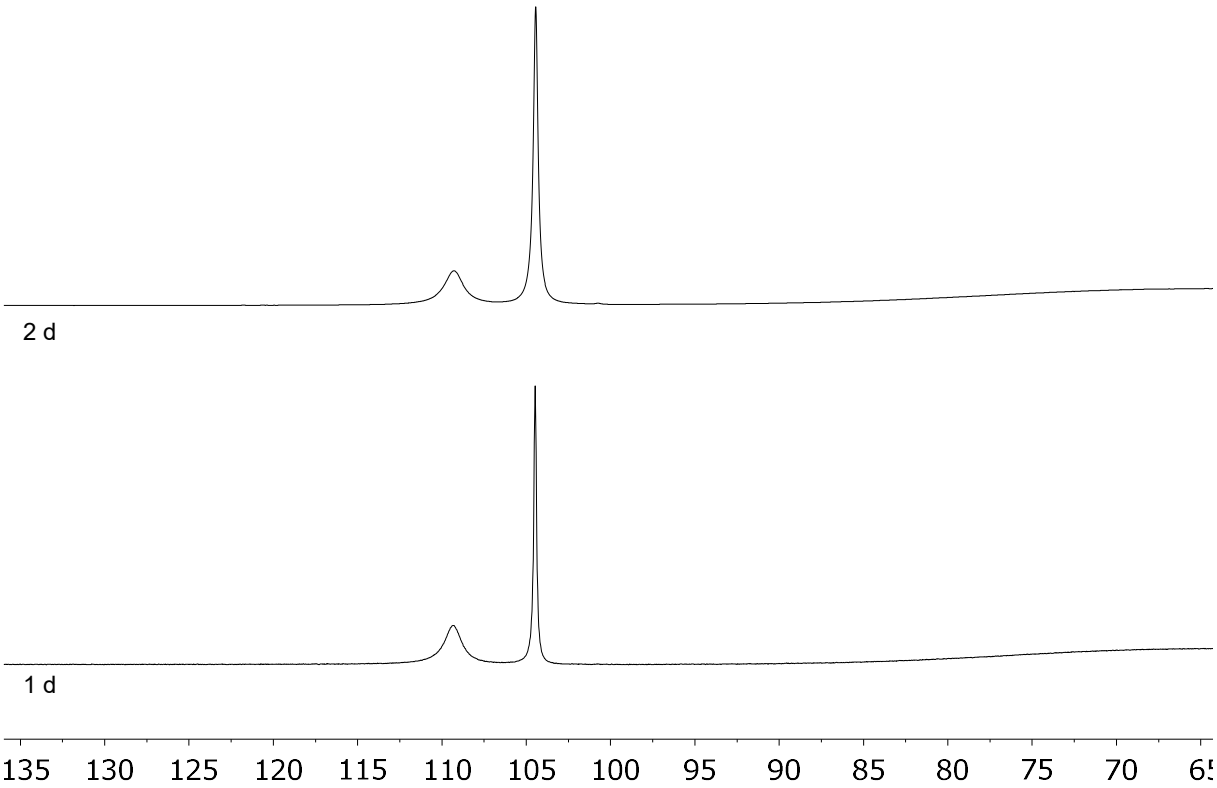

Figure S5.5.14: *In situ ^{27}Al NMR of the reaction of* ***18^{Cl}****, Thiophene, $AlCl_3$ and Me_2NTol at 90 °C (in CD_2Cl_2).*

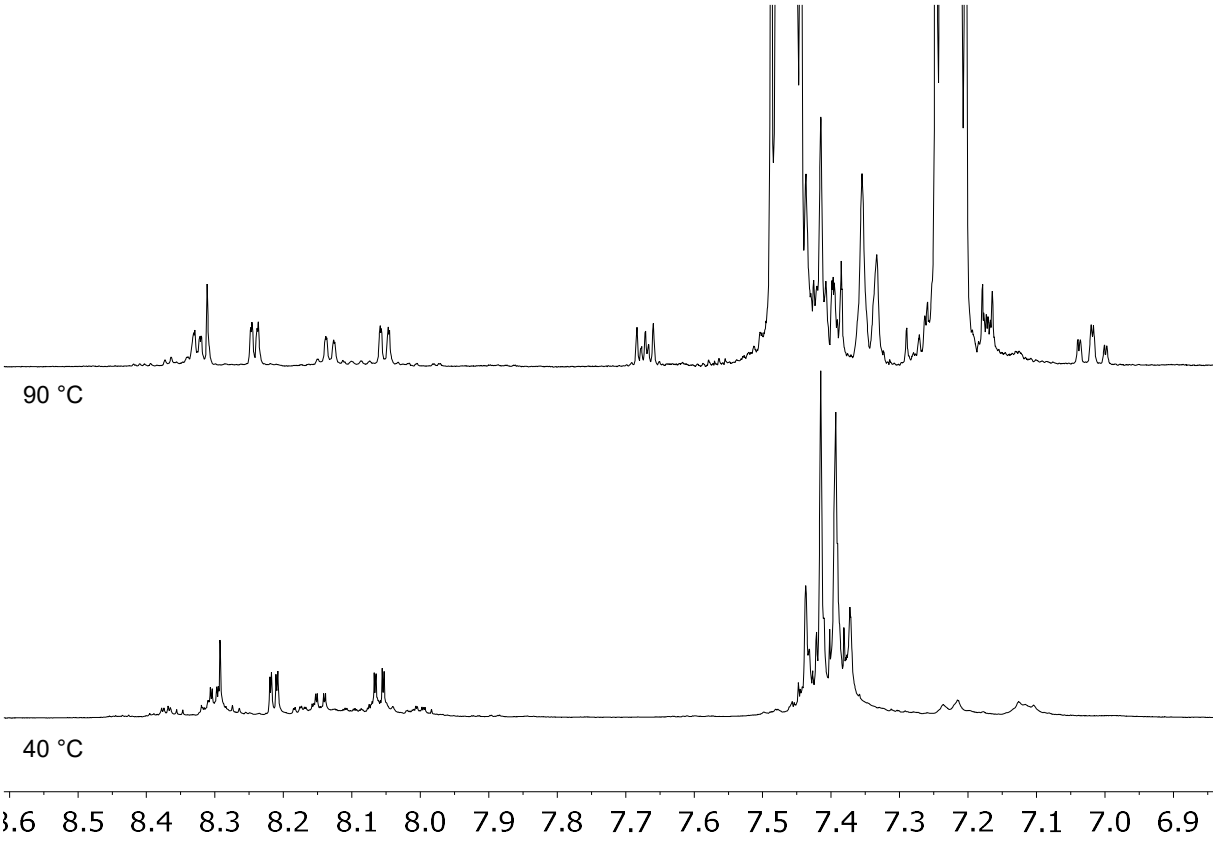

Figure S5.5.15: *In situ ^{1}H NMR of the reaction of **18^{Br}**, Thiophene, Me_3SiNTf_2 and Me_2NTol at 40 °C and 90 °C after 6 days reaction time (in CD_2Cl_2).*

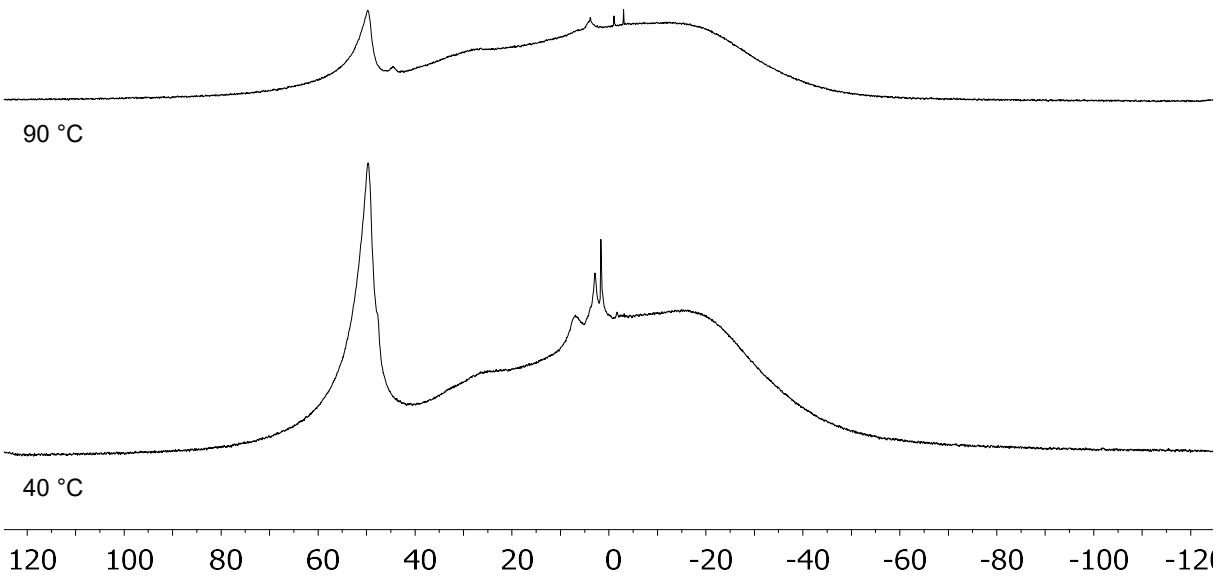

Figure S5.5.16: *In situ $^{11}B\{^{1}H\}$ NMR of the reaction of **18^{Br}**, Thiophene, Me_3SiNTf_2 and Me_2NTol at 40 °C and 90 °C after 6 days reaction time (in CD_2Cl_2).*

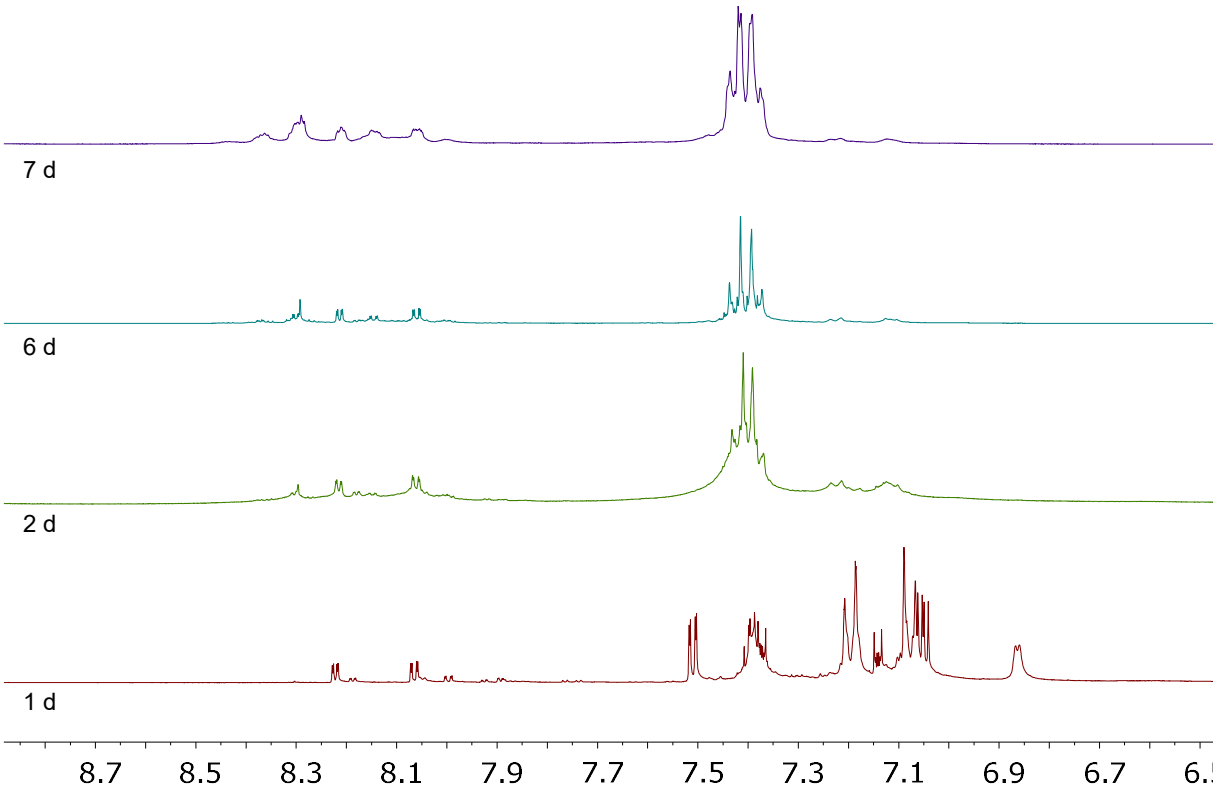

Figure S5.5.17: *In situ ^{1}H NMR aromatic region of the reaction of* ***18^{Br}****, Thiophene, Me_3SiNTf_2 and Me_2NTol at 40 °C (in CD_2Cl_2).*

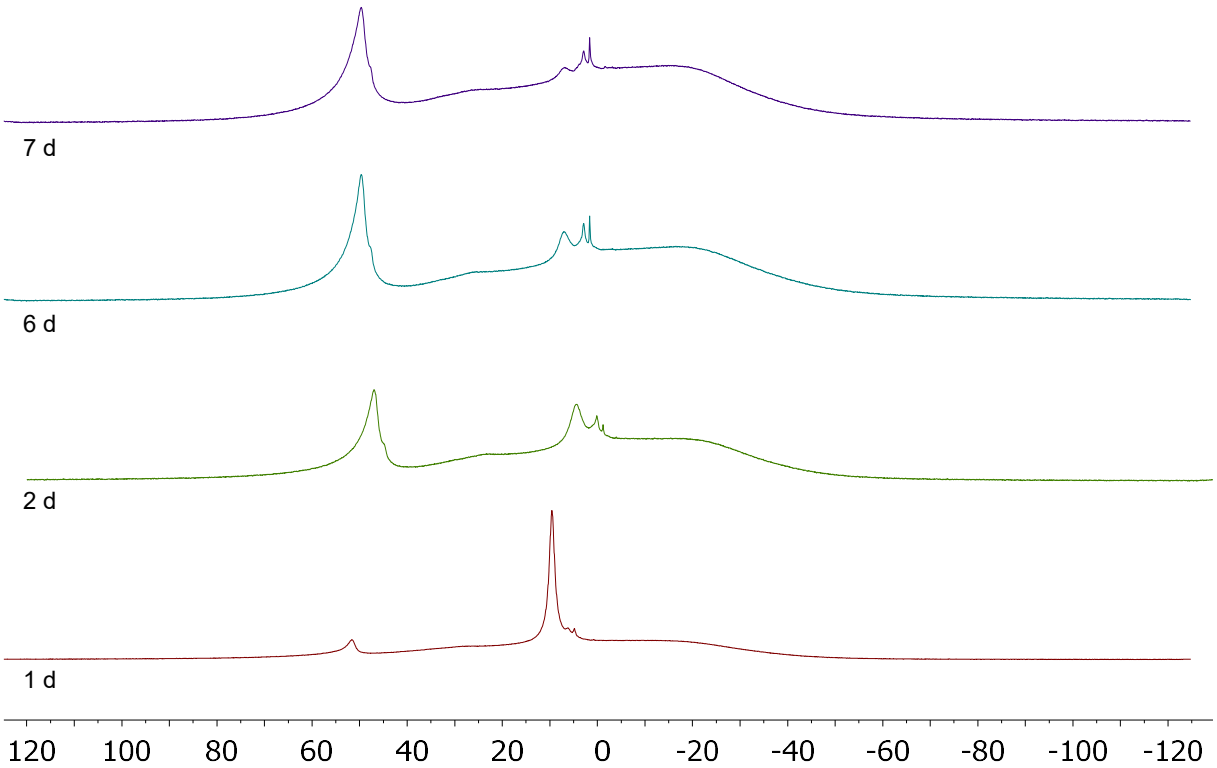

Figure S5.5.18: *In situ $^{11}B\{^{1}H\}$ NMR of the reaction of* ***18^{Br}****, Thiophene, Me_3SiNTf_2 and Me_2NTol at 40 °C (in CD_2Cl_2).*

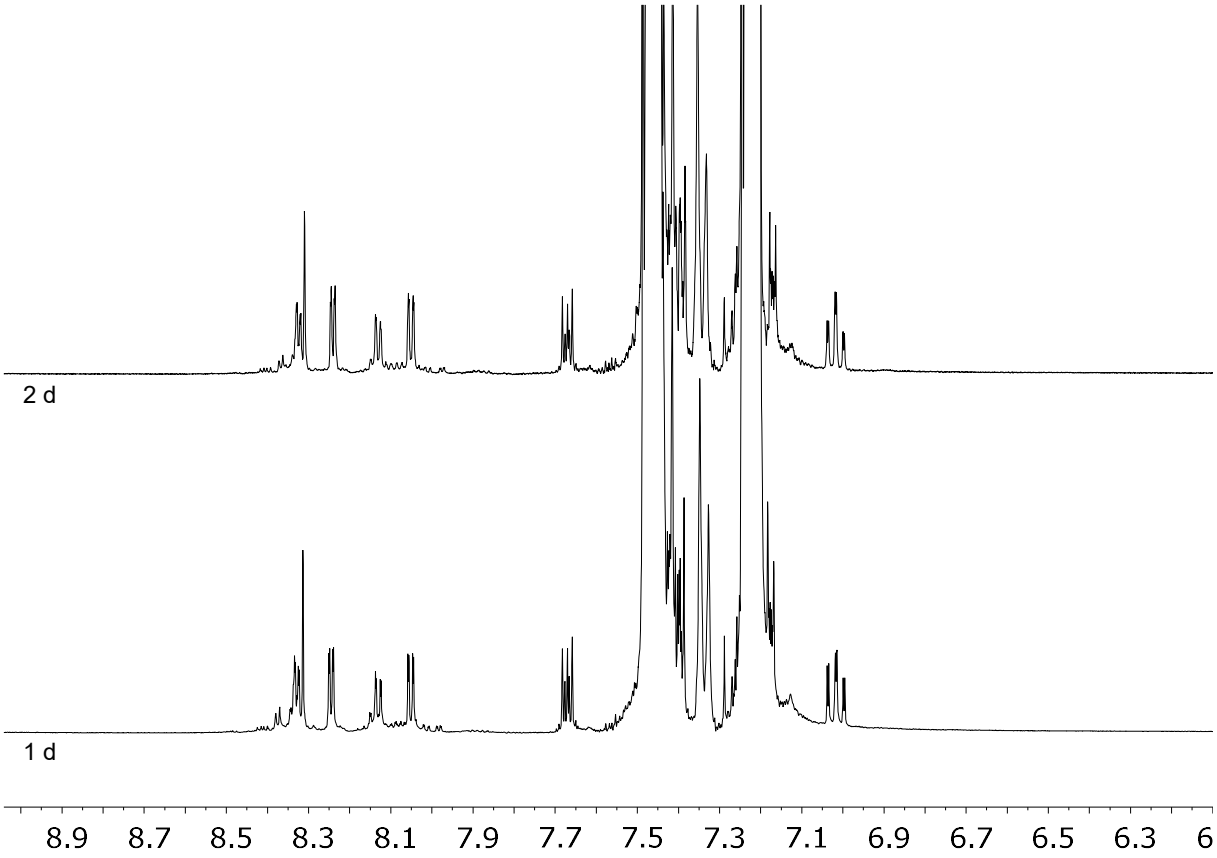

*Figure S5.5.19: In situ ^{1}H NMR aromatic region of the reaction of **18^{Br}**, Thiophene, Me_3SiNTf_2 and Me_2NTol at 90 °C (in CD_2Cl_2).*

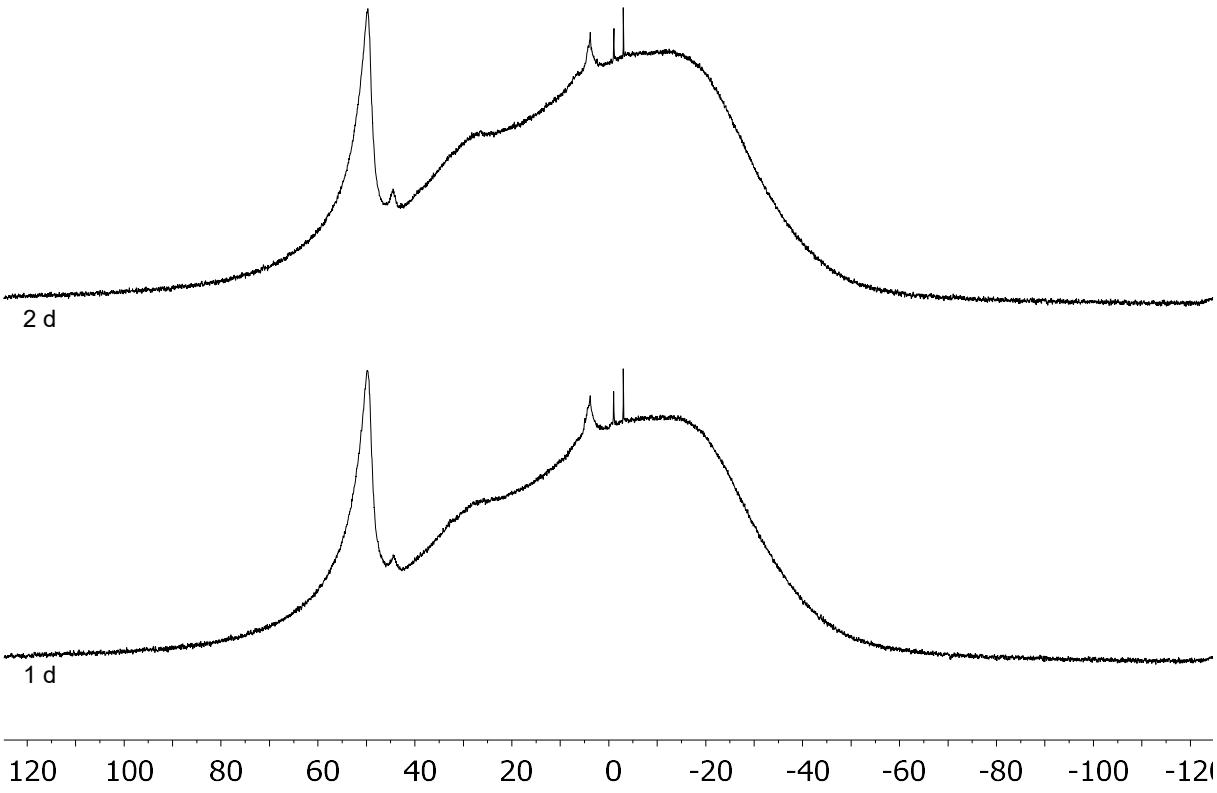

*Figure S5.5.20: In situ $^{11}B\{^{1}H\}$ NMR of the reaction of **18^{Br}**, Thiophene, Me_3SiNTf_2 and Me_2NTol at 90 °C (in CD_2Cl_2).*

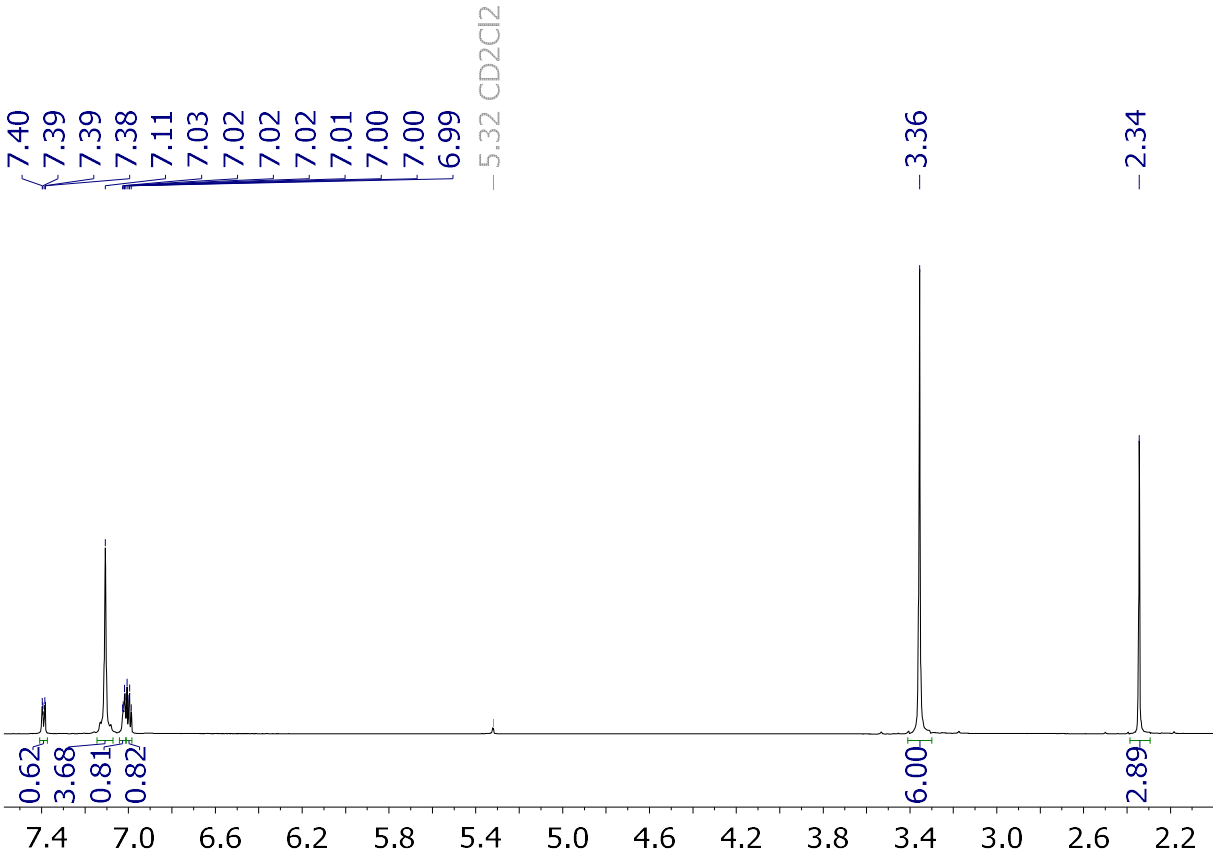

***Figure S5.5.21**: ^{1}H NMR spectrum of **24^{Cl}**.*

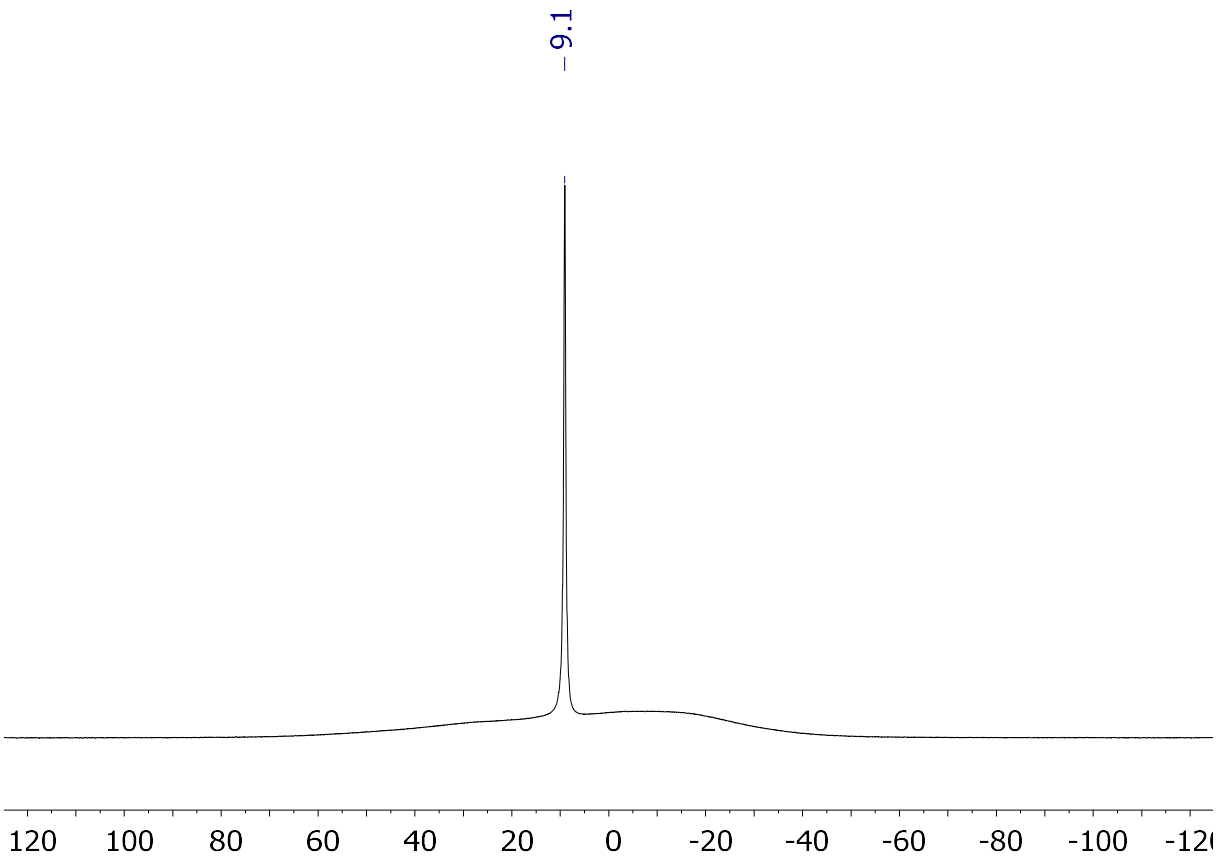

***Figure S5.5.22:** $^{11}B\{^{1}H\}$ NMR spectrum of **24^{Cl}**.*

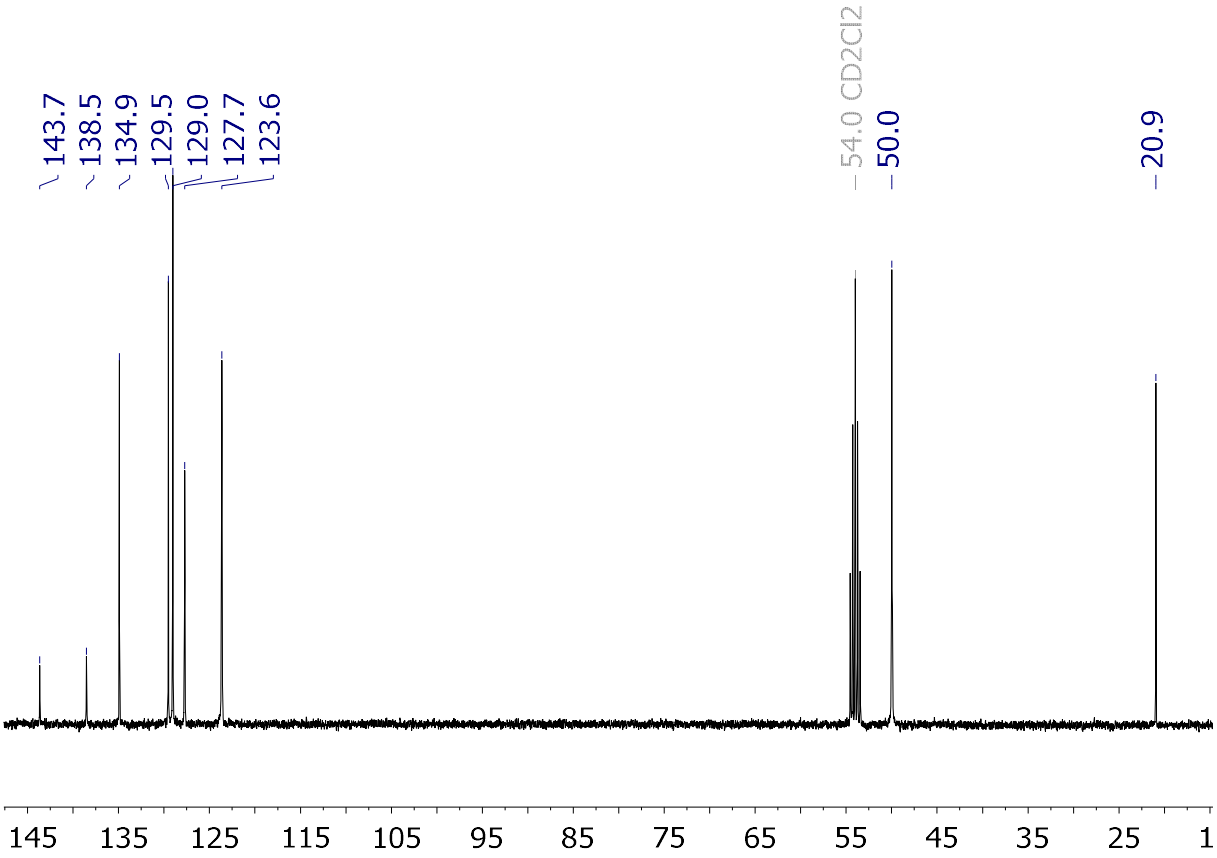

Figure S5.5.23: *$^{13}C\{^{1}H\}$ NMR spectrum of* ***24^{Cl}****.*

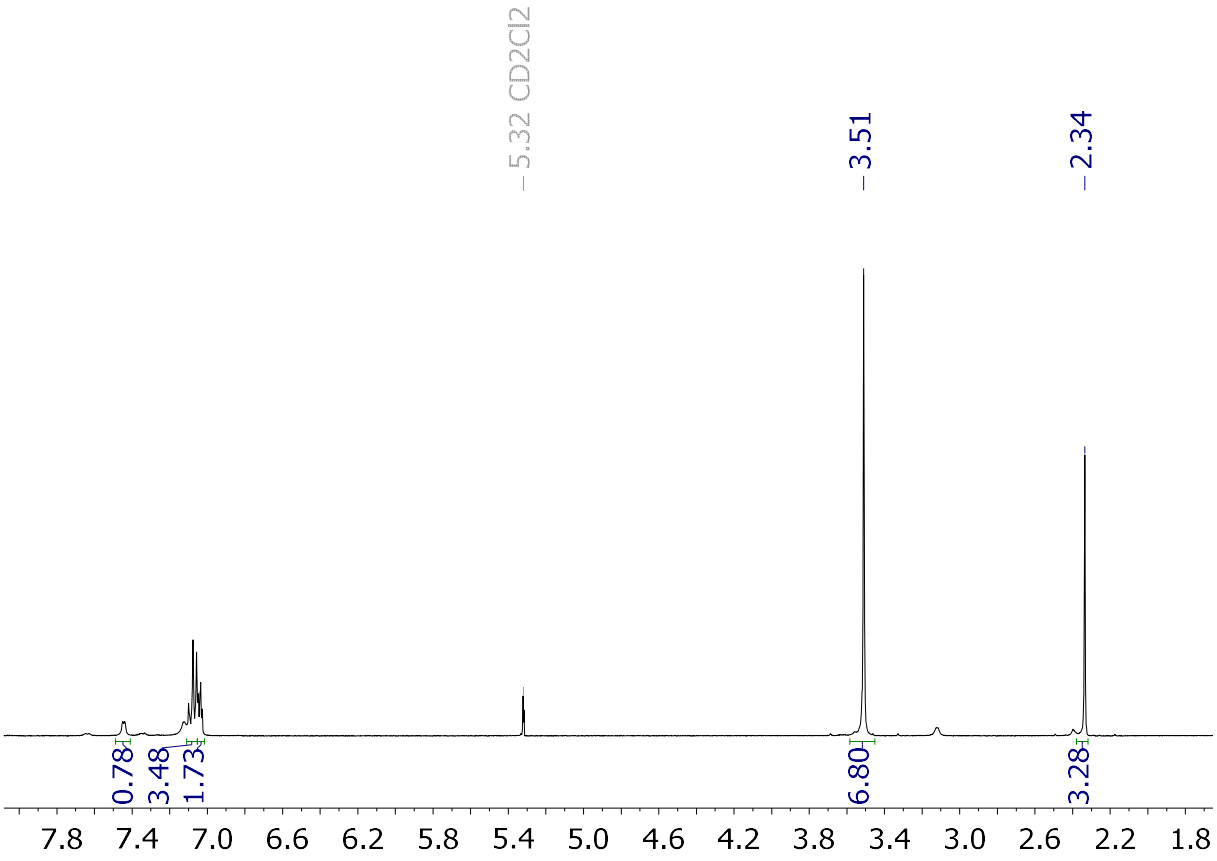

Figure S5.5.24: *^{1}H NMR spectrum of* ***24^{Br}****.*

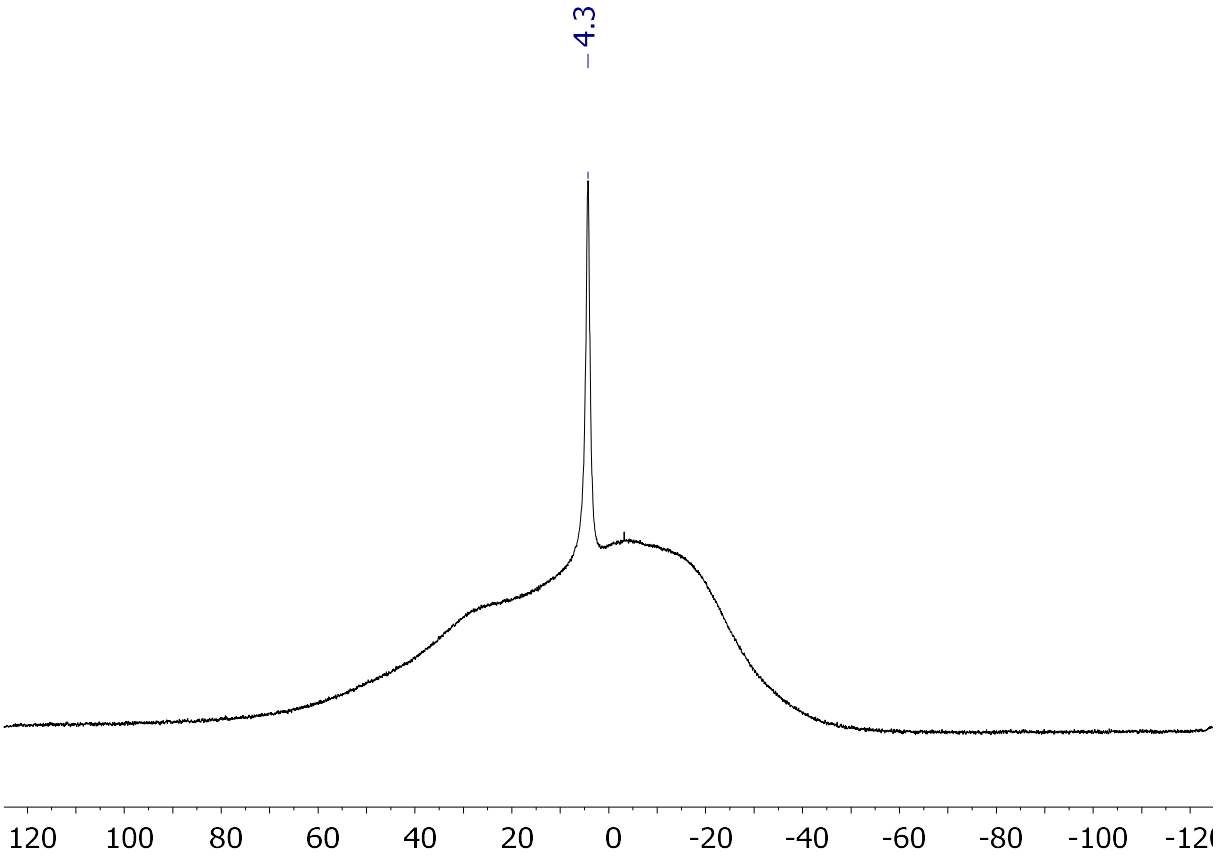

Figure S5.5.25: *$^{11}B\{^{1}H\}$ NMR spectrum of* ***24^{Br}****.*

5.6 A Conjugated Boron-doped Tetraoxaporphyrinogen

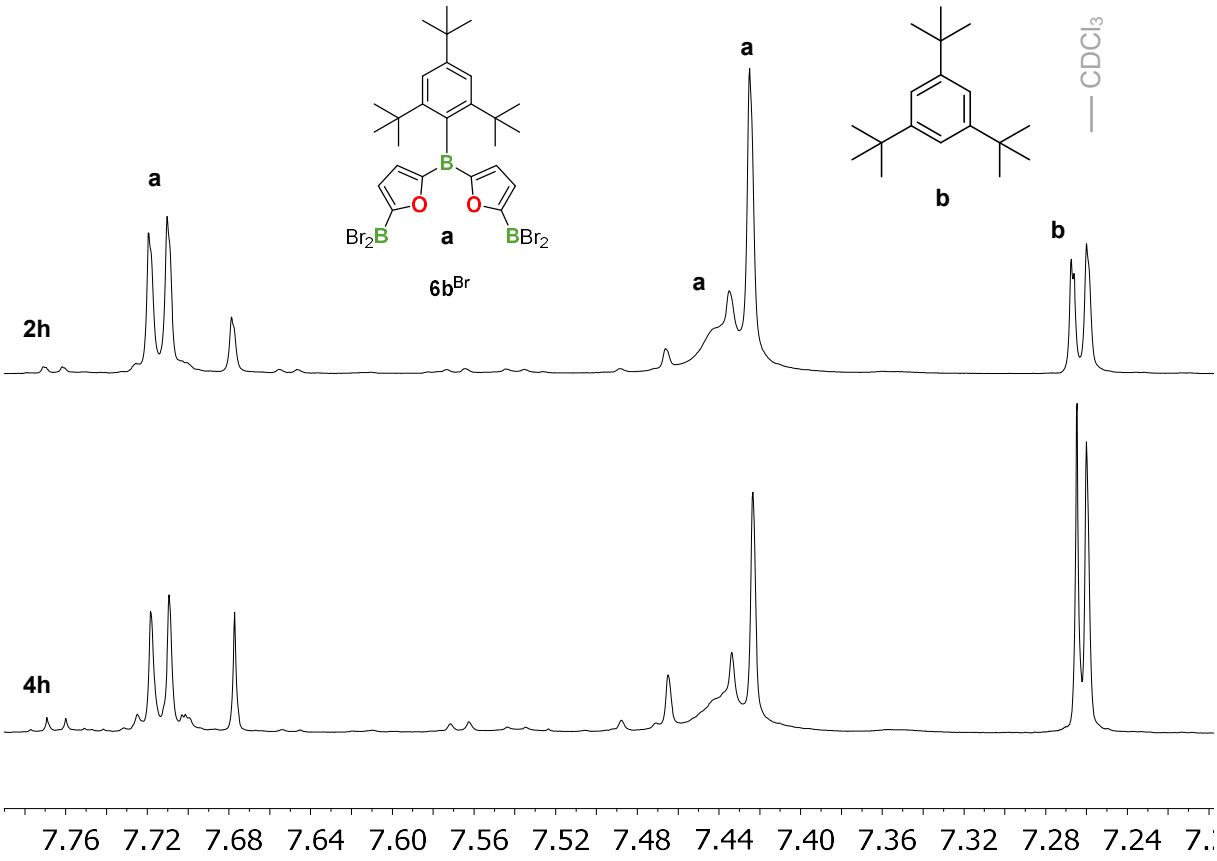

Figure S5.6.1: *In situ ^{1}H NMR of* ***6b^{Br}*** *(in $CDCl_3$).*

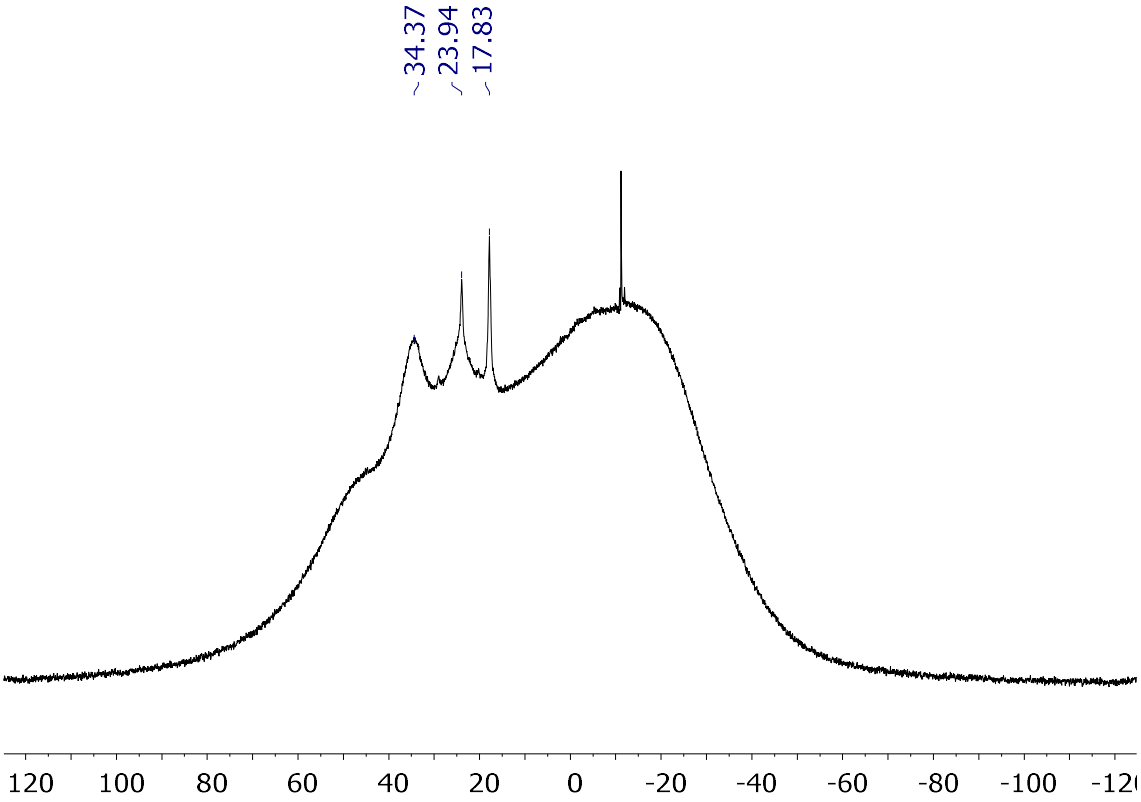

Figure S5.6.2: *In situ $^{11}B\{^{1}H\}$ NMR spectrum of a mixture of* ***6b^{ORF}***, ***6b^{ORFBr}*** *and $B(OCH_2CF_3)$ (in $CDCl_3$).*

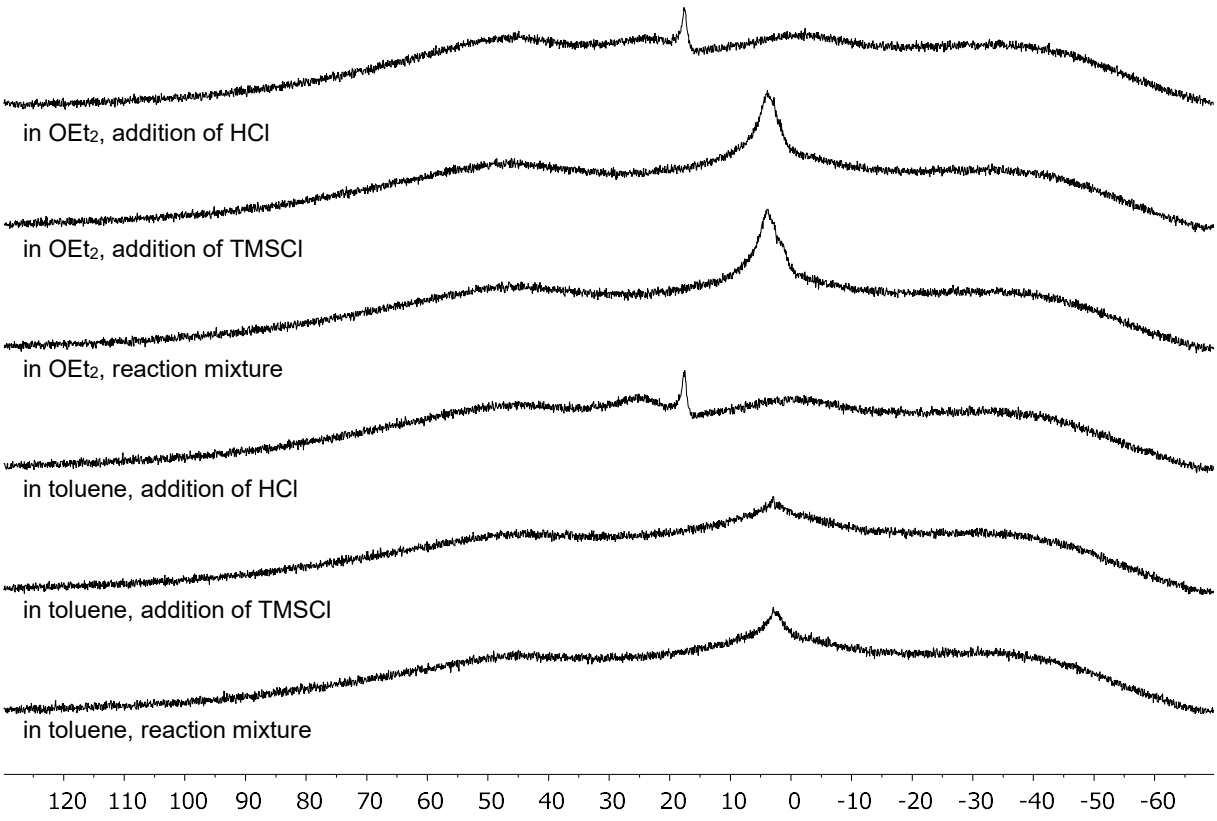

Figure S5.6.3: *In situ $^{11}B\{^1H\}$ NMR of reactions of* ***6b^{ORF}*** *and Mes*Li in OEt_2 and toluene (in $CDCl_3$).*

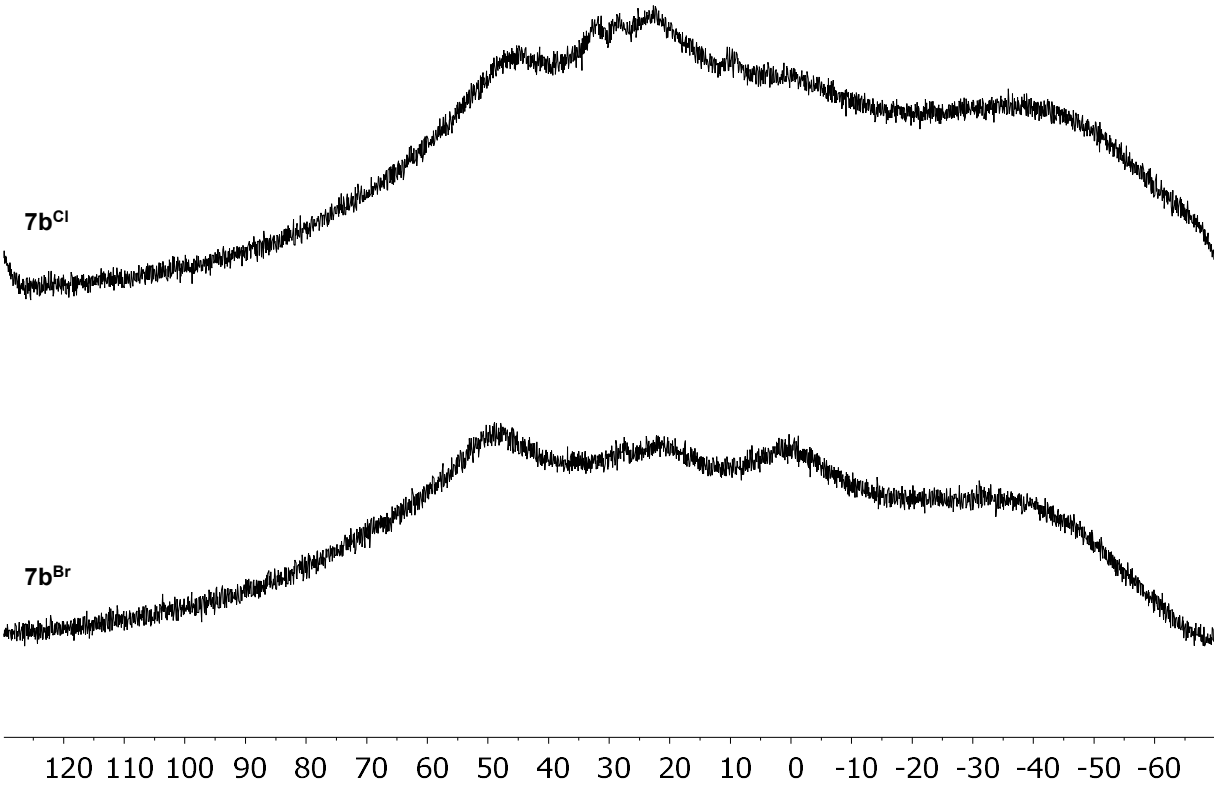

Figure S5.6.4: *In situ $^{11}B\{^1H\}$ NMR of reactions to* ***7b^{Br}*** *and* ***7b^{Cl}*** *(in $CDCl_3$).*

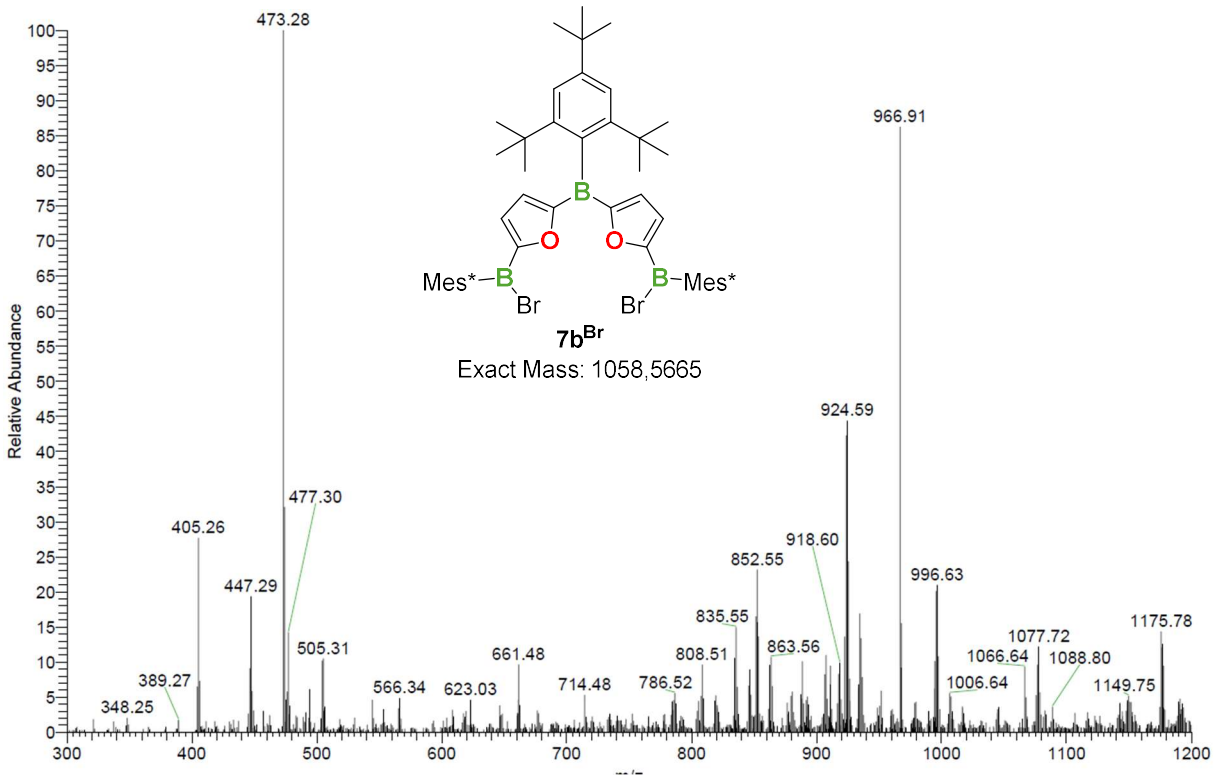

Figure S5.6.5: *Mass spectrum of the reaction of* ***6b^{Br}*** *and Mes*Li (LIFDI).*

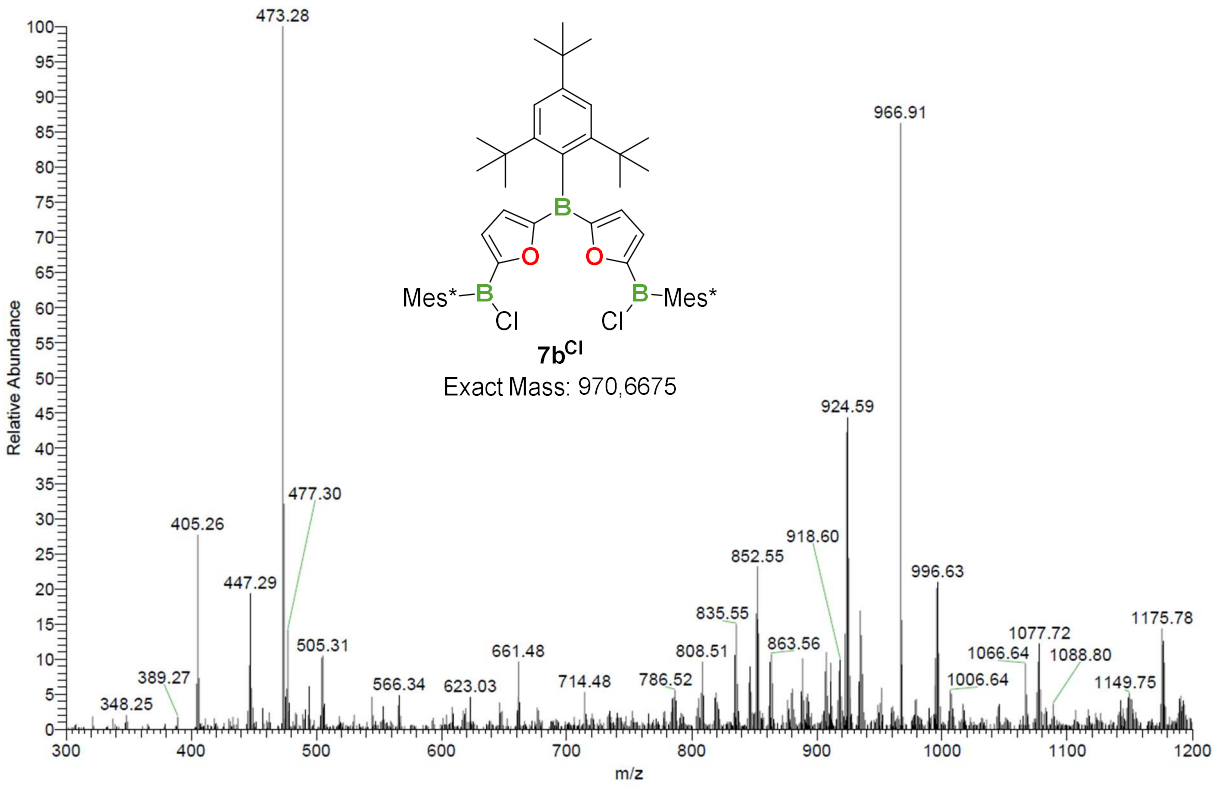

Figure S5.6.6: *Mass spectrum of the reaction of* ***6b^{Cl}*** *and Mes*Li (LIFDI).*

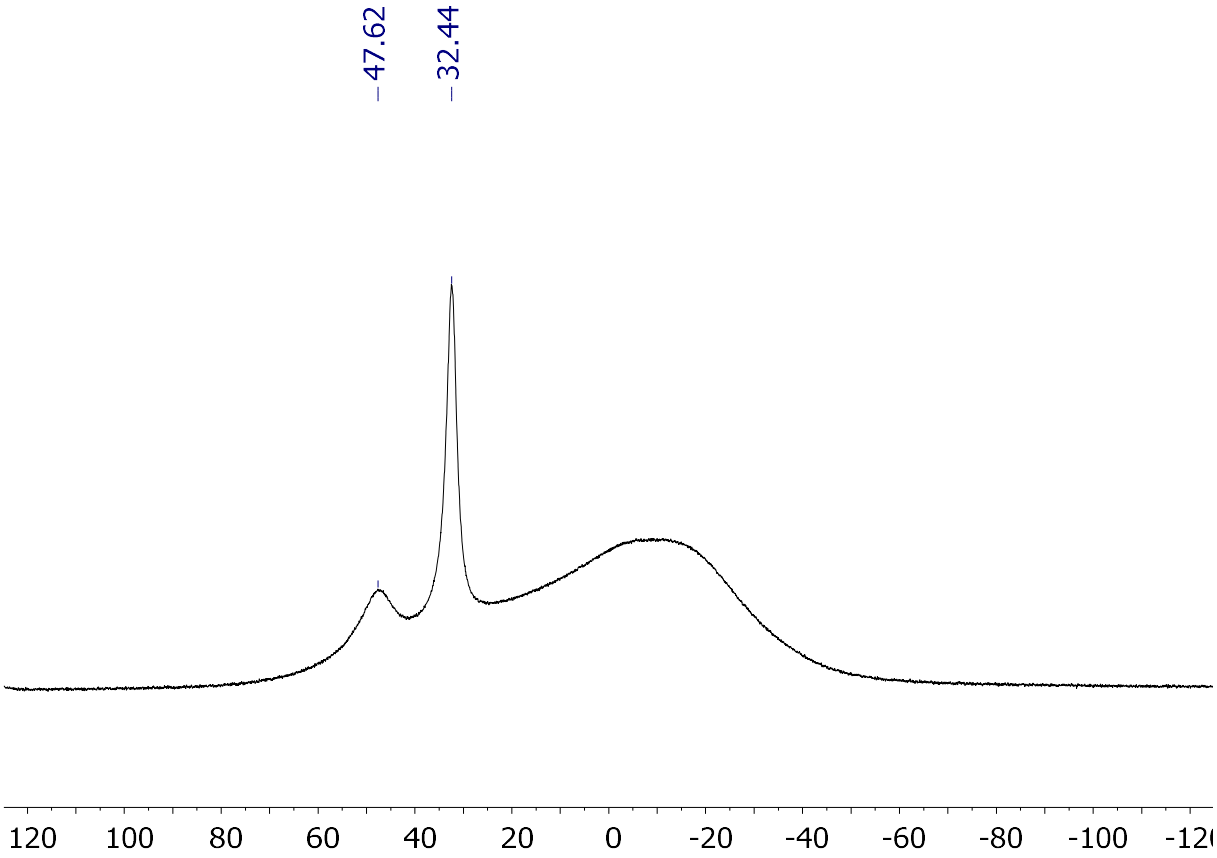

Figure S5.6.7: *In situ $^{11}B\{^1H\}$ NMR spectrum of the reaction of* ***4b^{Li}*** *with Mes*B(OMe)$_2$ (in $CDCl_3$).*

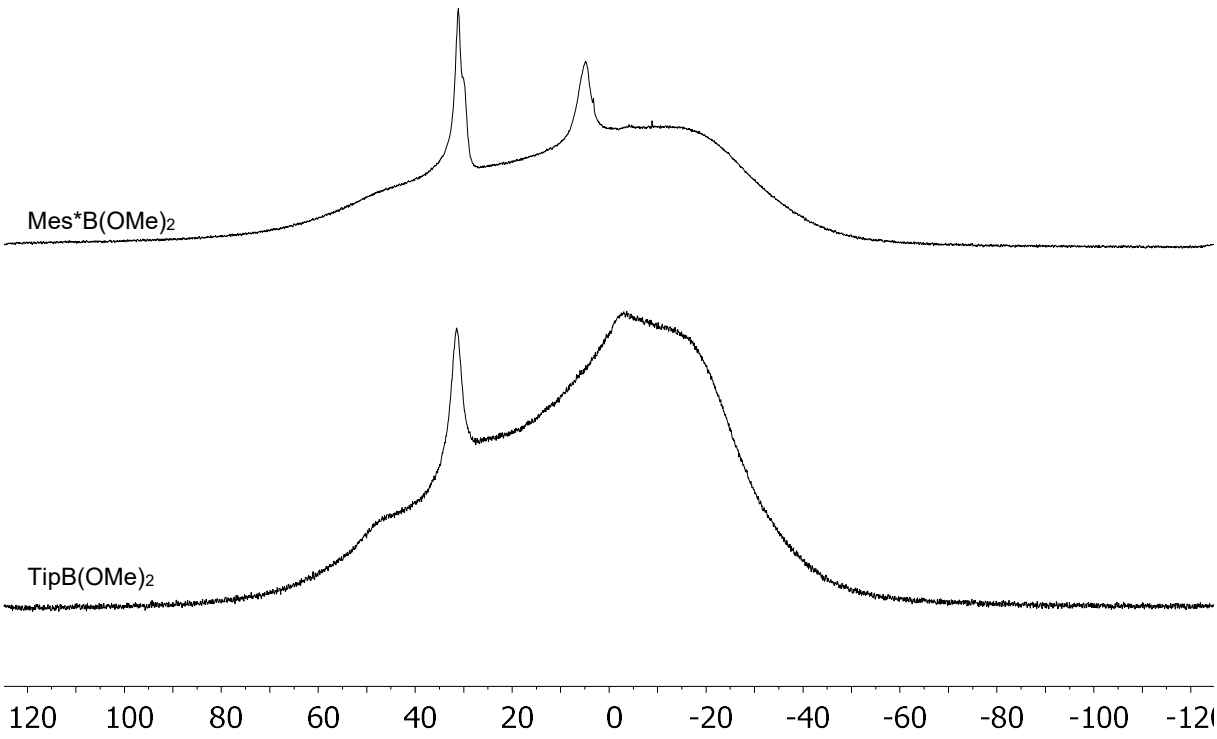

Figure S5.6.8: *In situ $^{11}B\{^1H\}$ NMR of the reaction of* ***4b^{Li}*** *with TipB(OMe)$_2$ and MesB(OMe)$_2$ (in $CDCl_3$).*

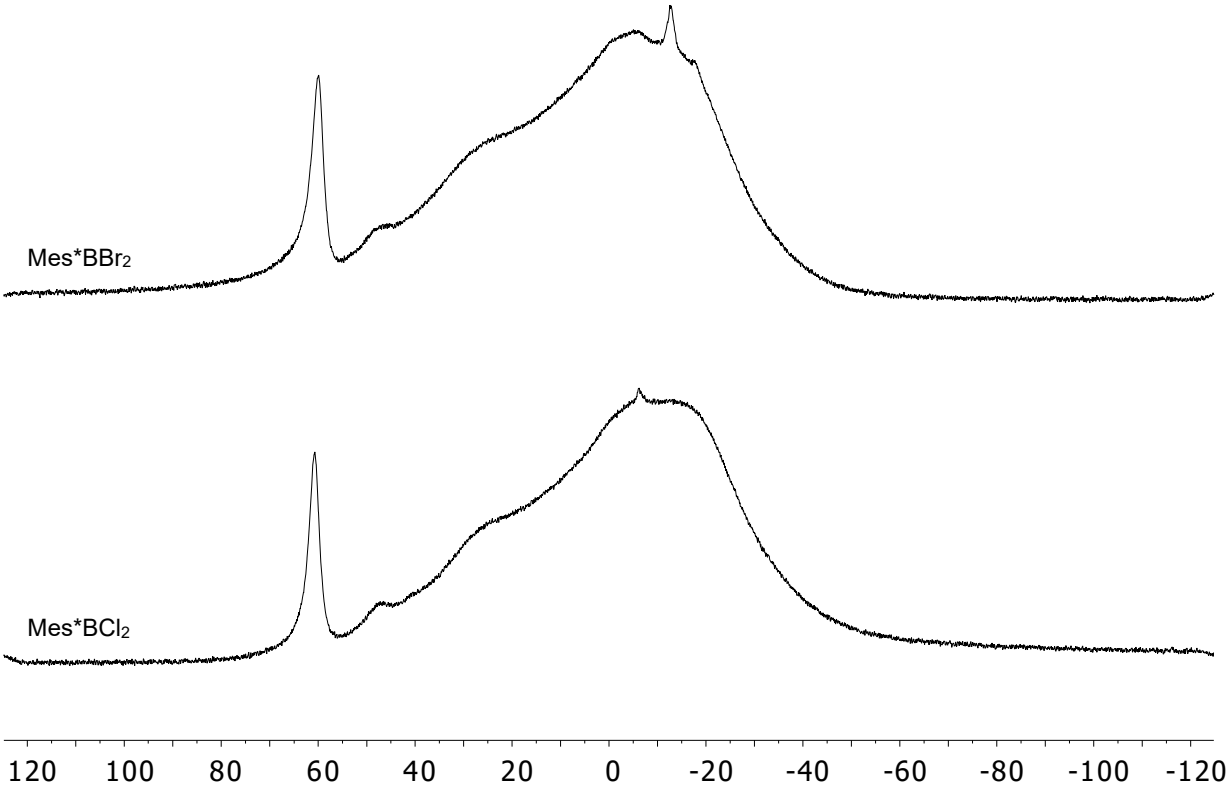

Figure S5.6.9: *In situ $^{11}B\{^1H\}$ NMR of the reaction of* ***4b^{Li}*** *with Mes*BBr_2 *and Mes*BCl_2 *(in* $CDCl_3$*).*

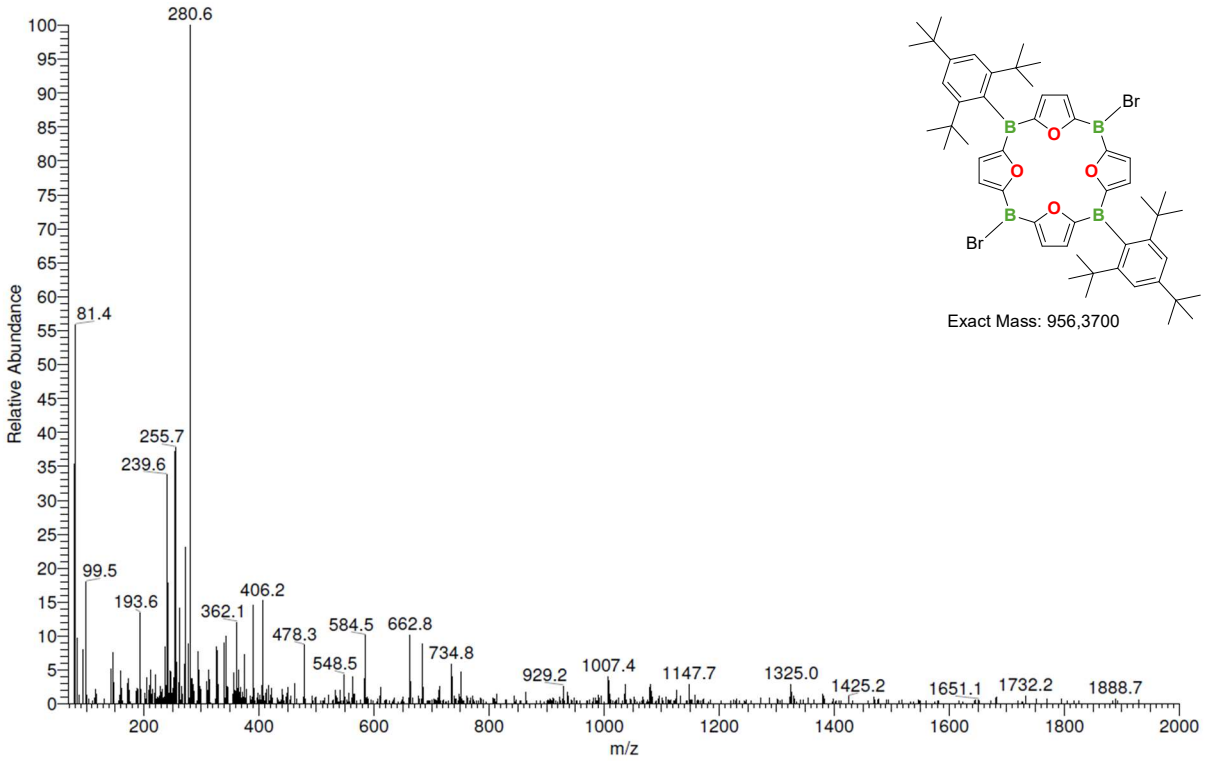

Figure S5.6.10: *Mass spectrum of the reaction of* ***6b^{Cl}*** *and Mes*Li (SIMS).*

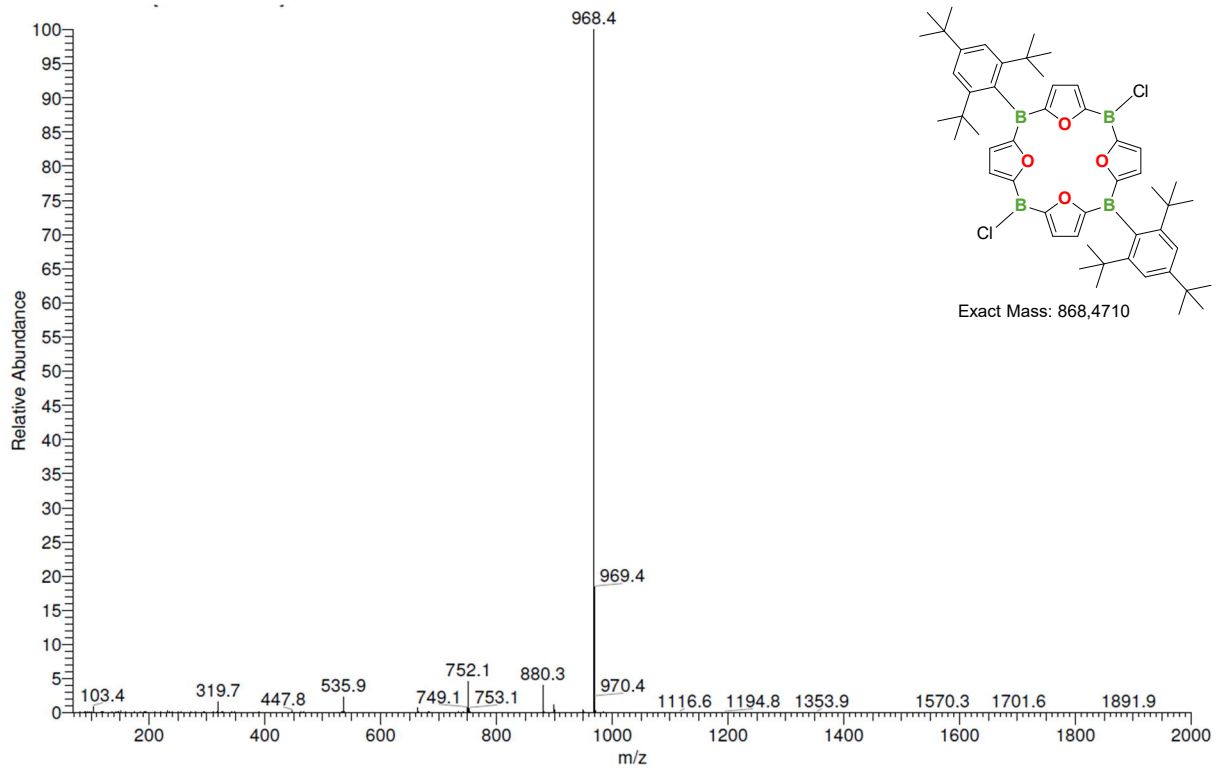

Figure S5.6.11: *Mass spectrum of the reaction of* ***6b^{Cl}*** *and Mes*Li (SIMS).*

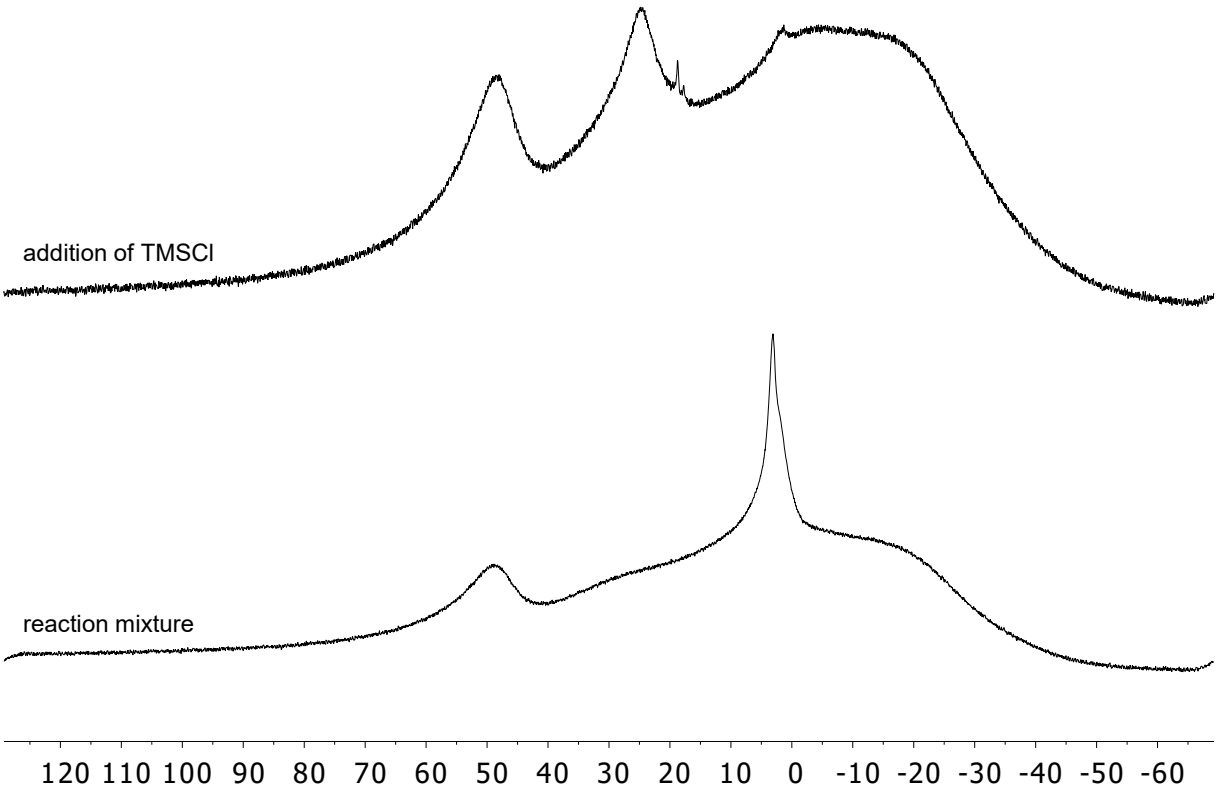

Figure S5.6.12: *In situ $^{11}B\{^{1}H\}$ NMR of the reaction of* ***6b^{OMe}*** *and* ***4b^{Li}*** *(in $CDCl_3$).*

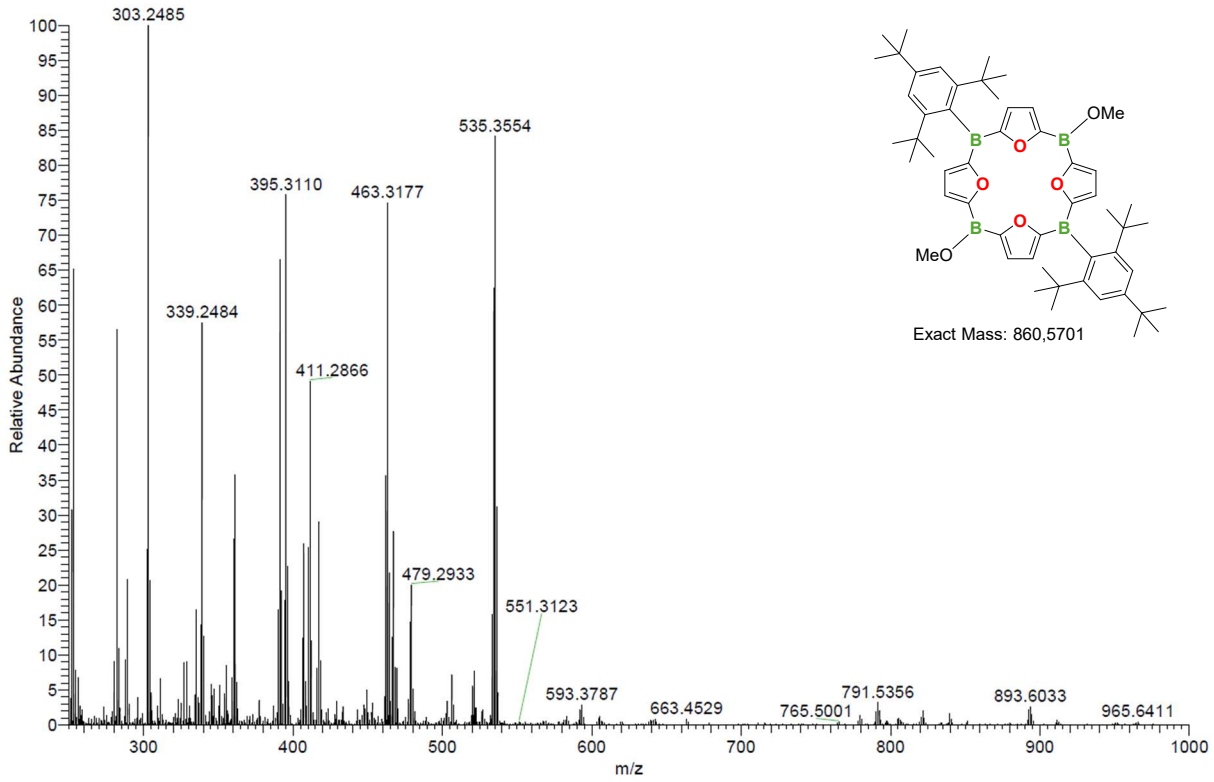

Figure S5.6.13: *Mass spectrum of the reaction of* ***6b^{OMe}*** *and* ***4b^{Li}*** *(APCI).*

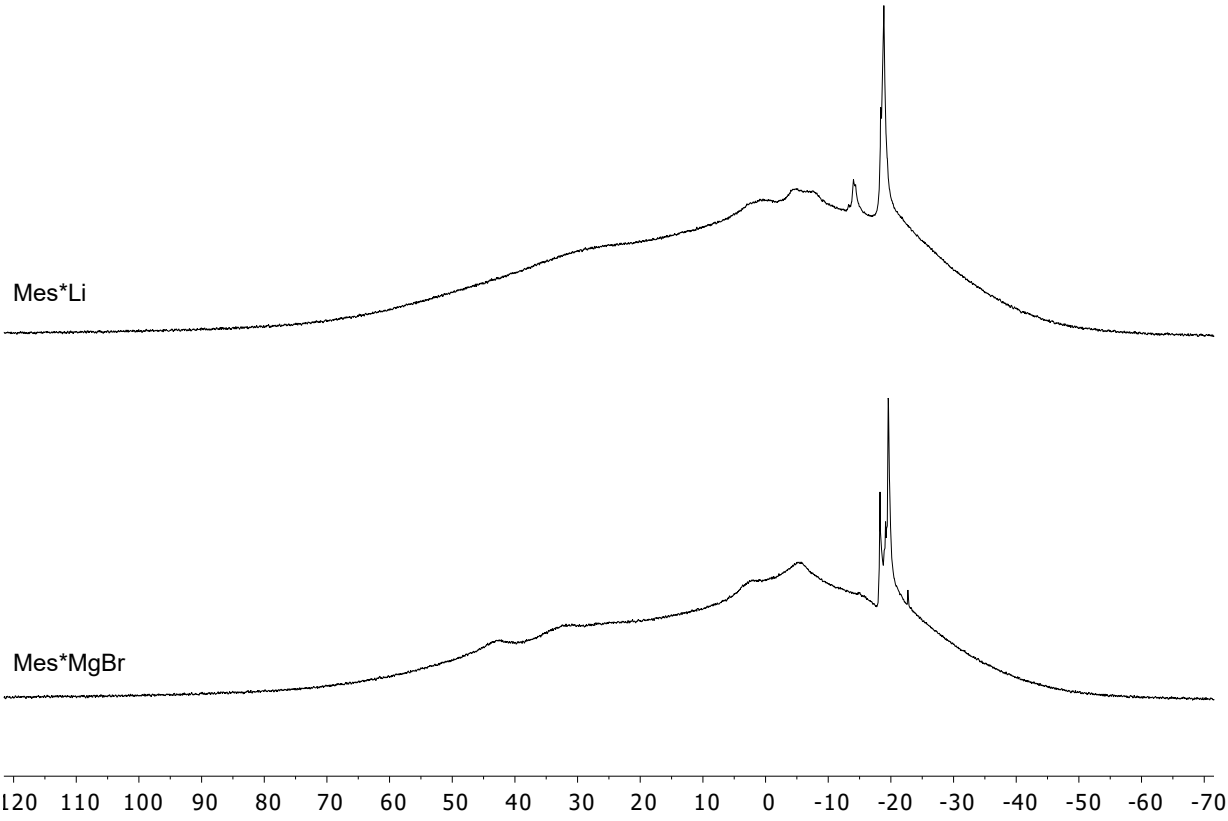

Figure S5.6.14: *In situ $^{11}B\{^{1}H\}$ NMR of the reaction of* ***16*** *and Mes*Li or Mes*MgBr (in $CDCl_3$).*

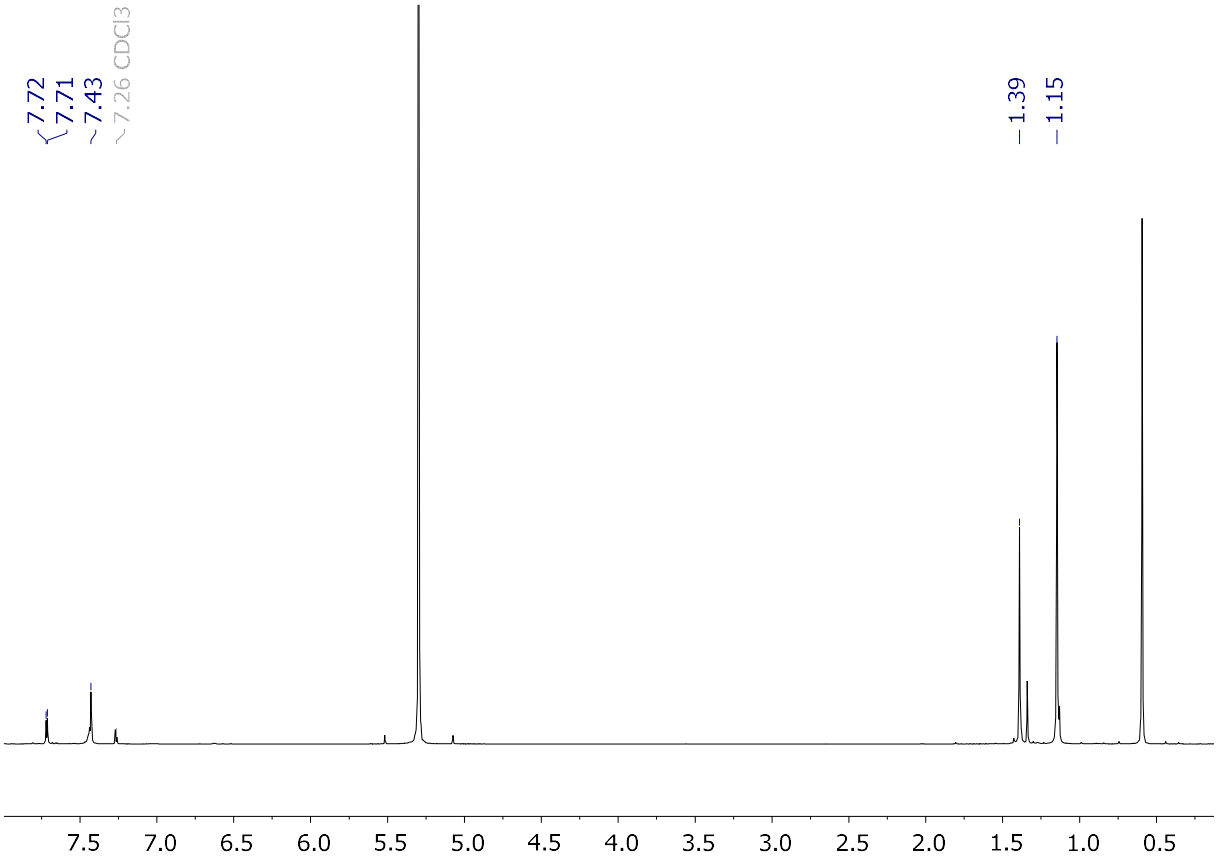

Figure S5.6.15: *In situ ^{1}H NMR spectrum of* ***6b^{Br}*** *(in $CDCl_3$).*

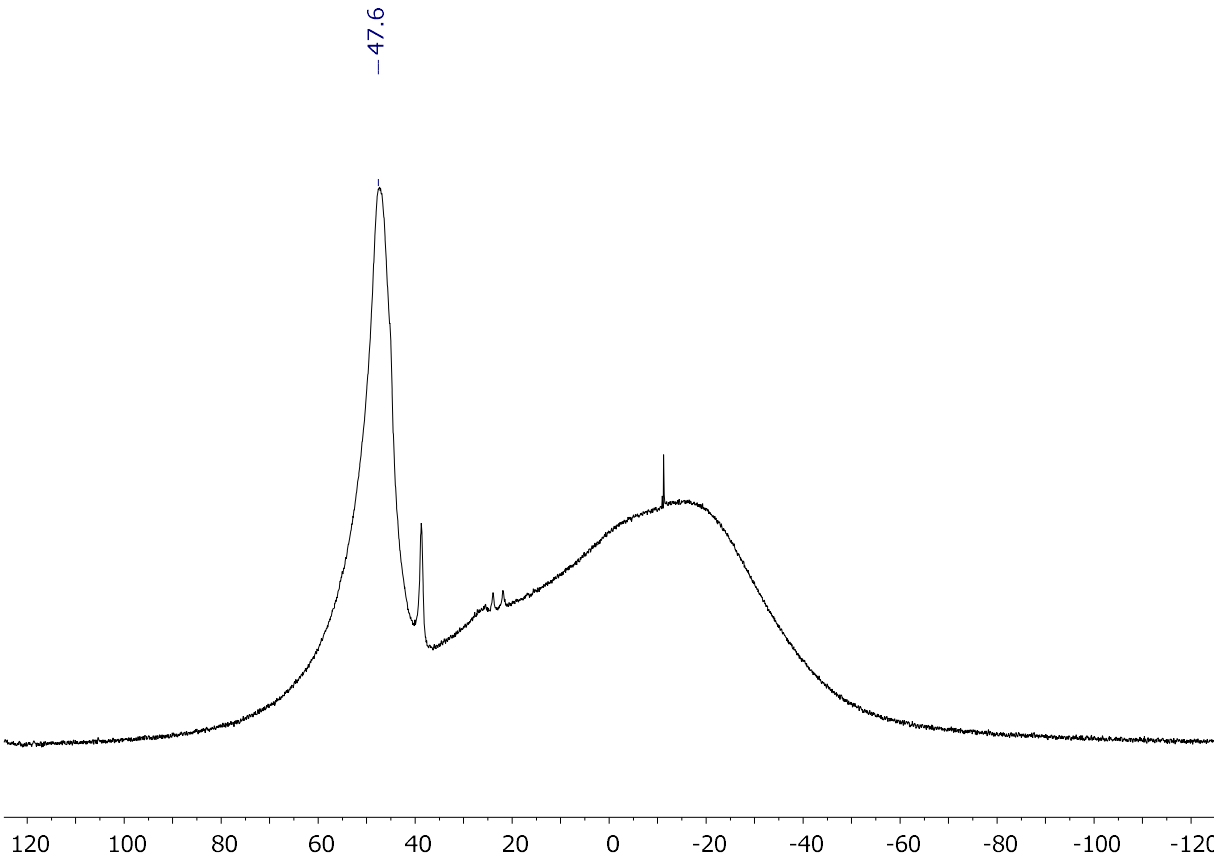

Figure S5.6.16: *In situ $^{11}B\{^{1}H\}$ NMR spectrum of* ***6b^{Br}*** *(in $CDCl_3$).*

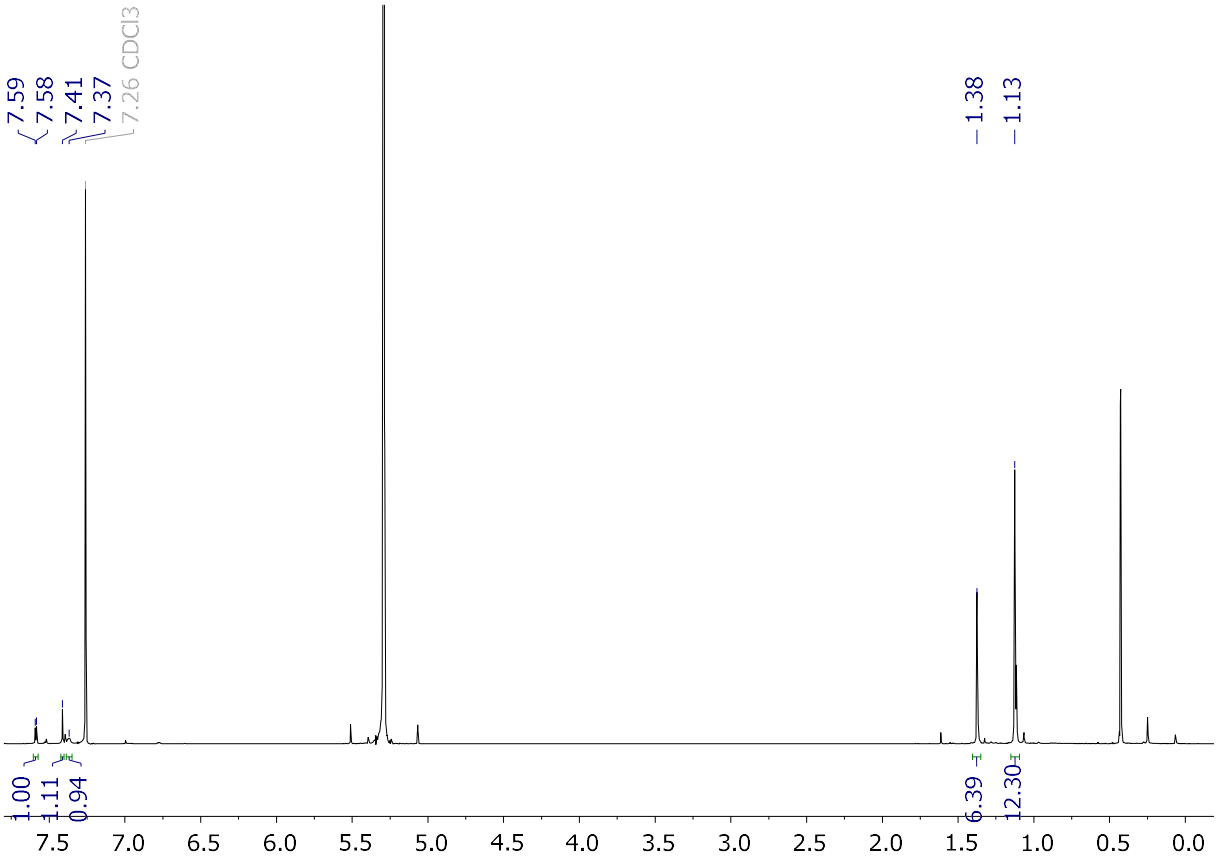

Figure S5.6.17: *In situ ^{1}H NMR spectrum of* ***6b^{Cl}*** *(in $CDCl_3$).*

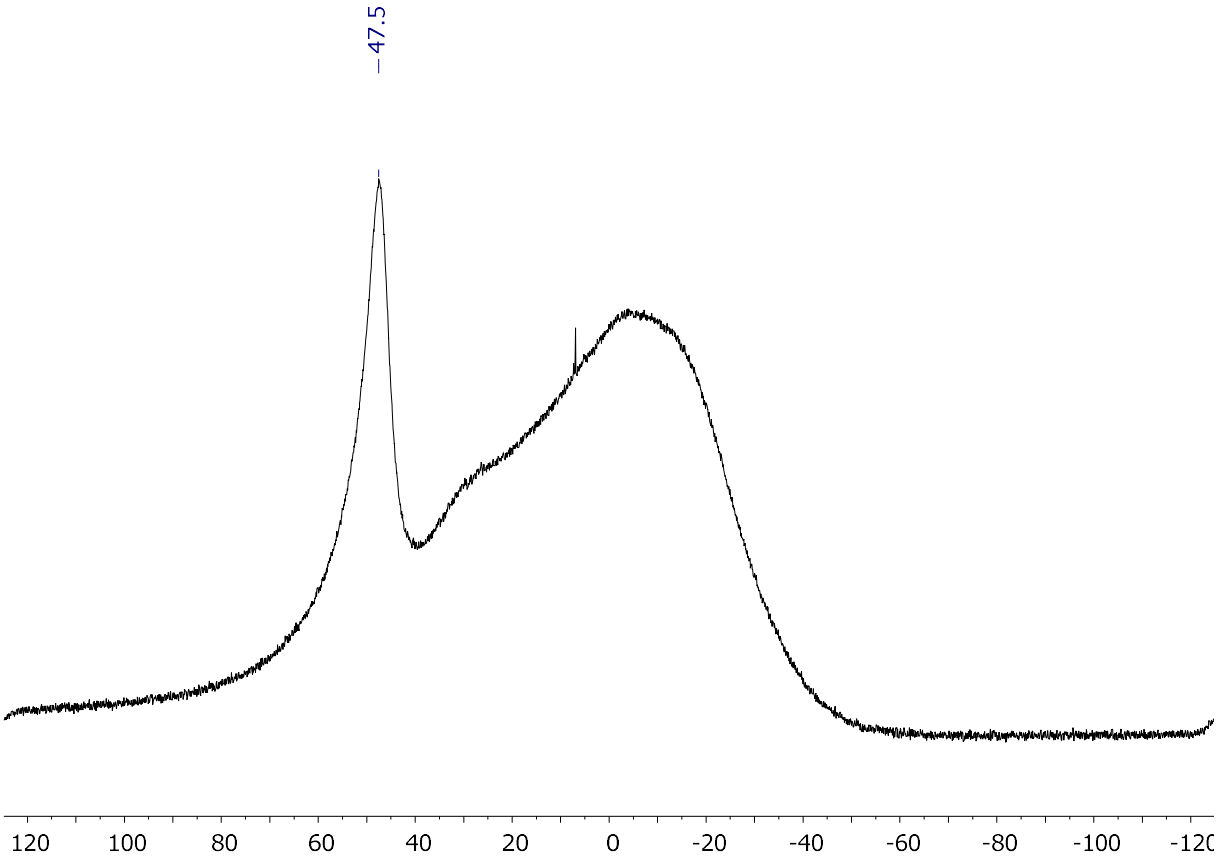

Figure S5.6.18: *In situ $^{11}B\{^{1}H\}$ NMR spectrum of* ***6b^{Cl}*** *(in $CDCl_3$).*

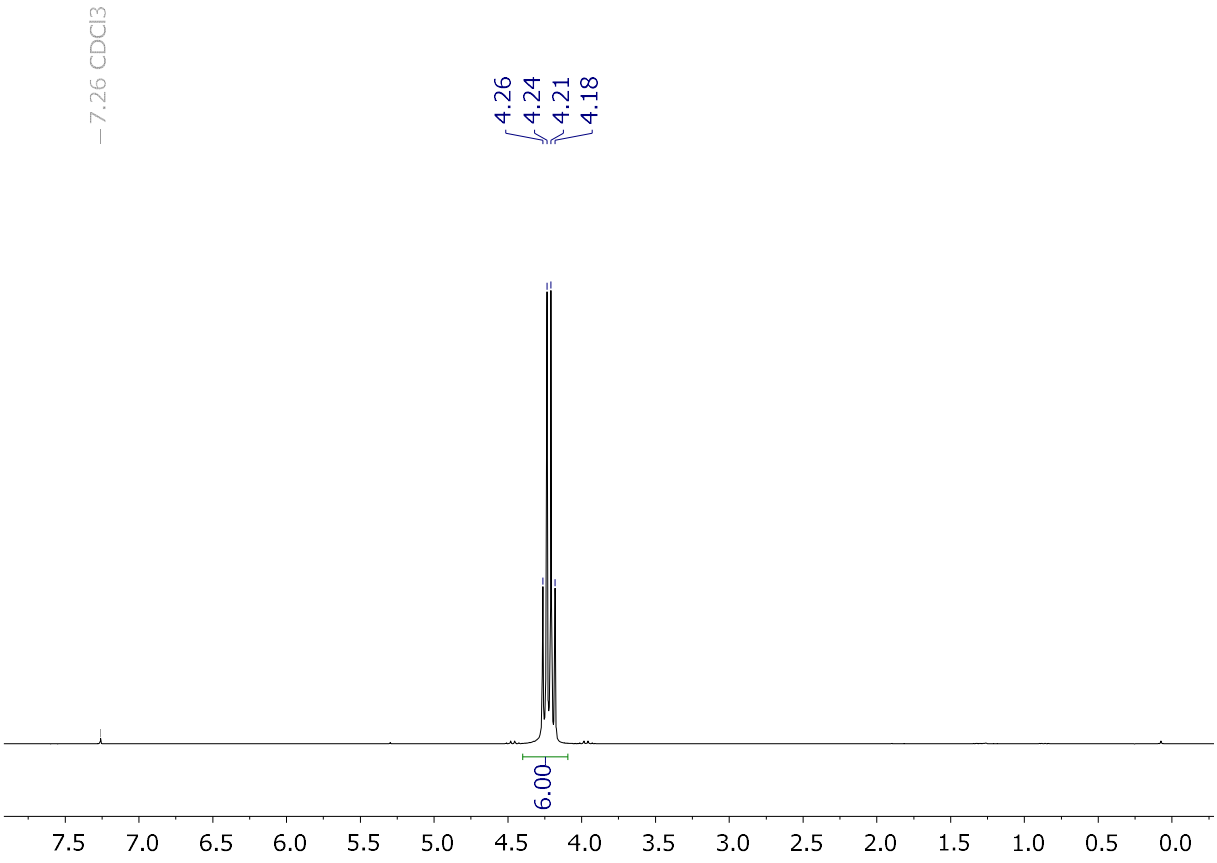

Figure S5.6.19: *^{1}H NMR spectrum of $B(OCH_2CF_3)_3$ (in $CDCl_3$).*

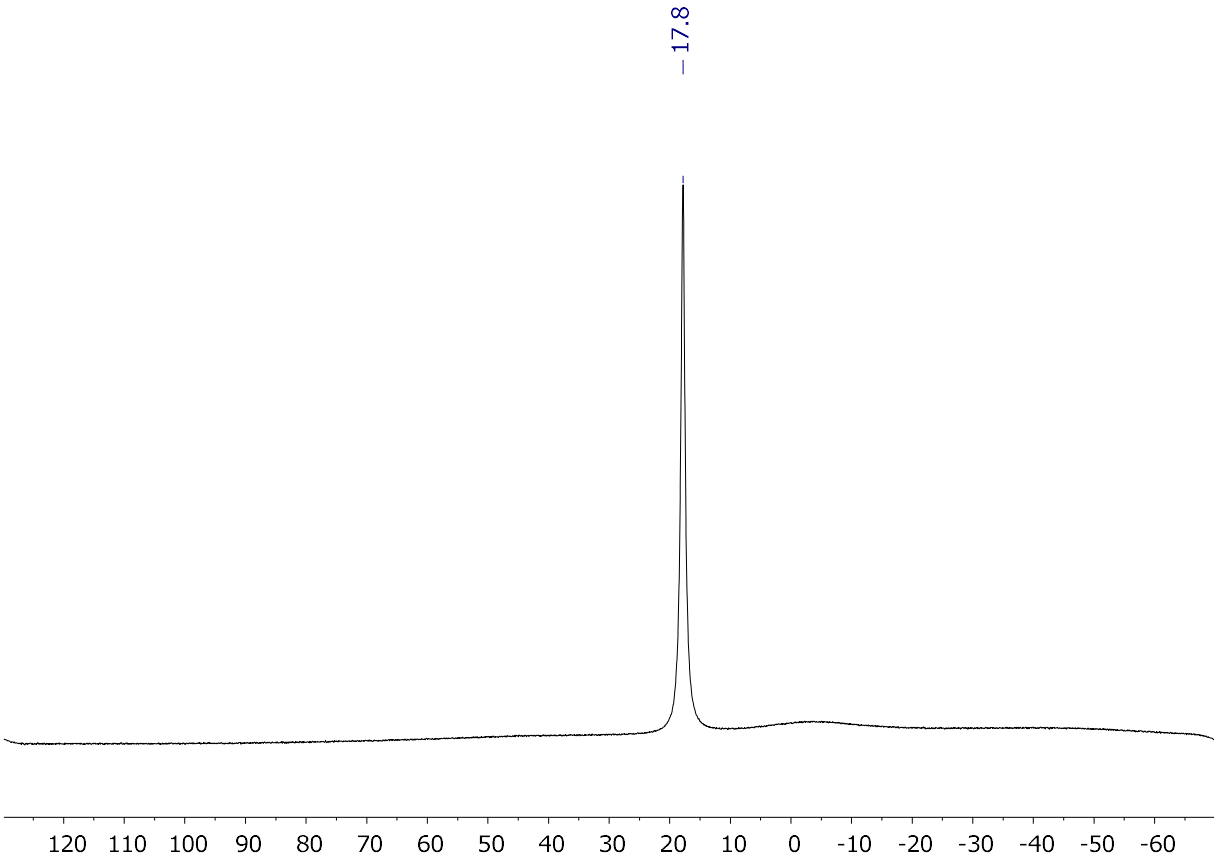

Figure S5.6.20: *$^{11}B\{^{1}H\}$ NMR spectrum of $B(OCH_2CF_3)_3$ (in $CDCl_3$).*

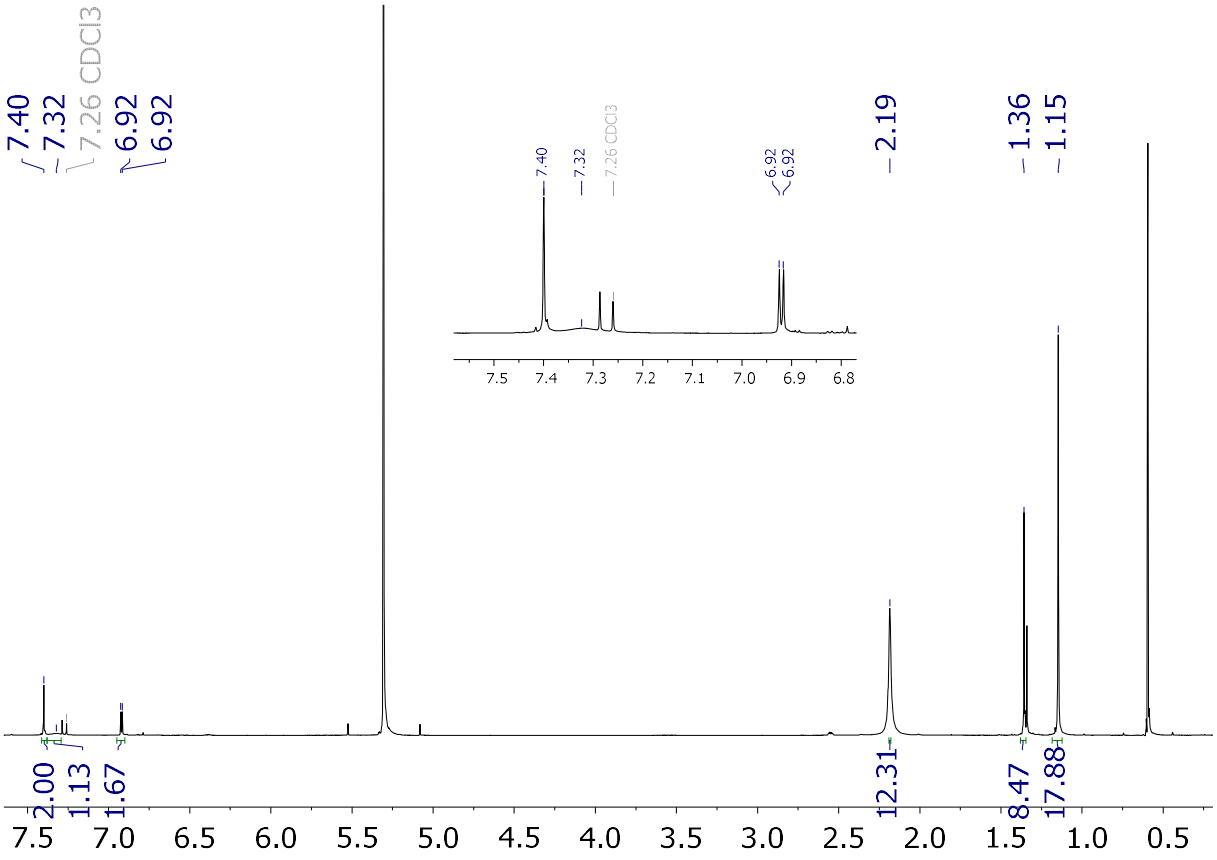

Figure S5.6.21: *In situ ^{1}H NMR spectrum of* ***8b^{Br}*** *(in $CDCl_3$).*

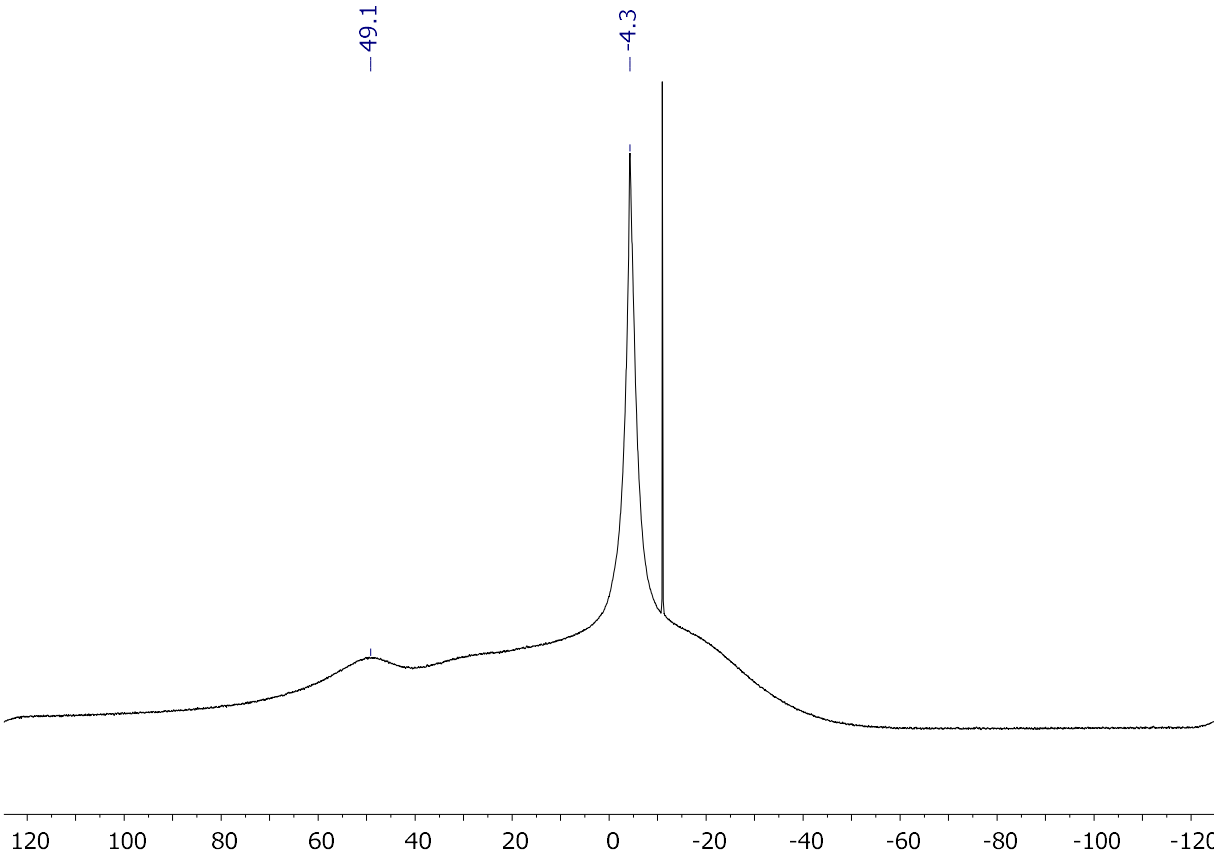

Figure S5.6.22: *In situ $^{11}B\{^{1}H\}$ NMR spectrum of* ***8^{Br}*** *(in $CDCl_3$).*

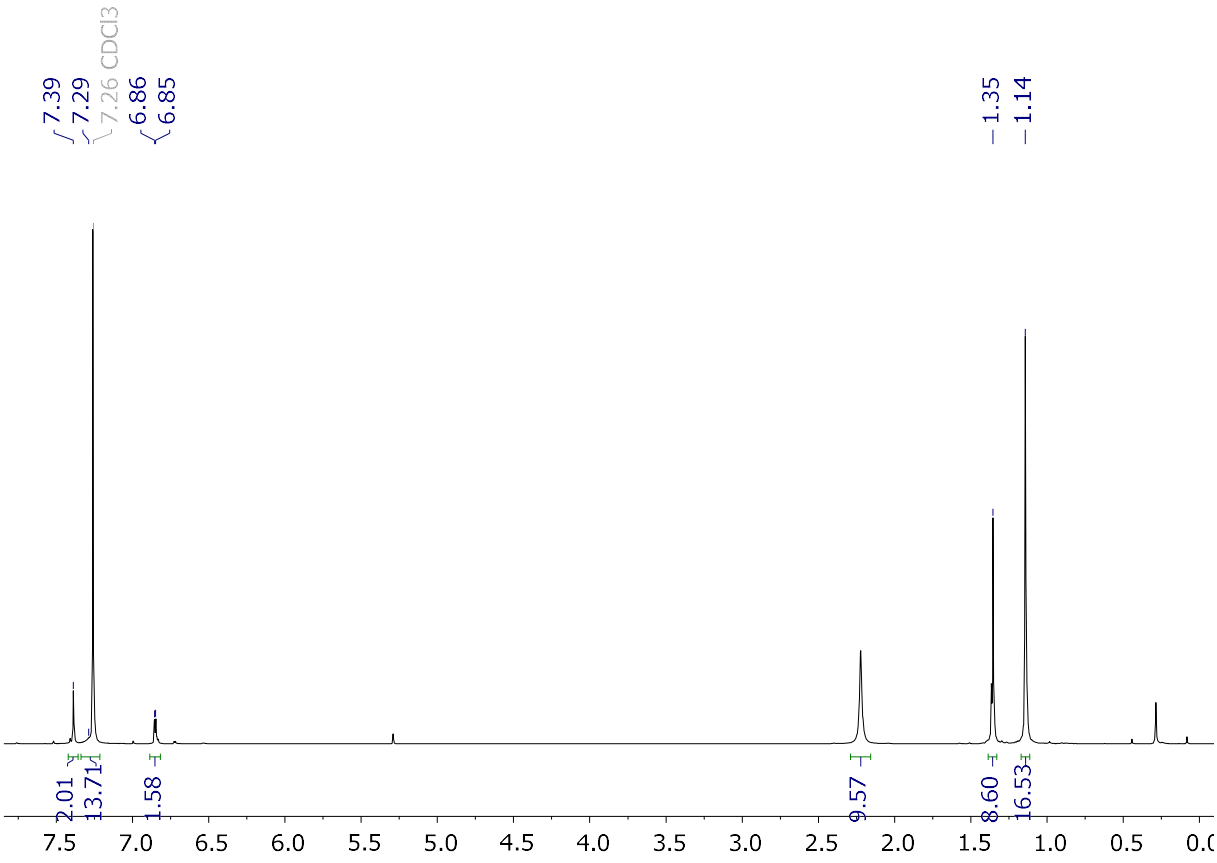

Figure S5.6.23: *^{1}H NMR spectrum of **8b^{Cl}** (in $CDCl_3$).*

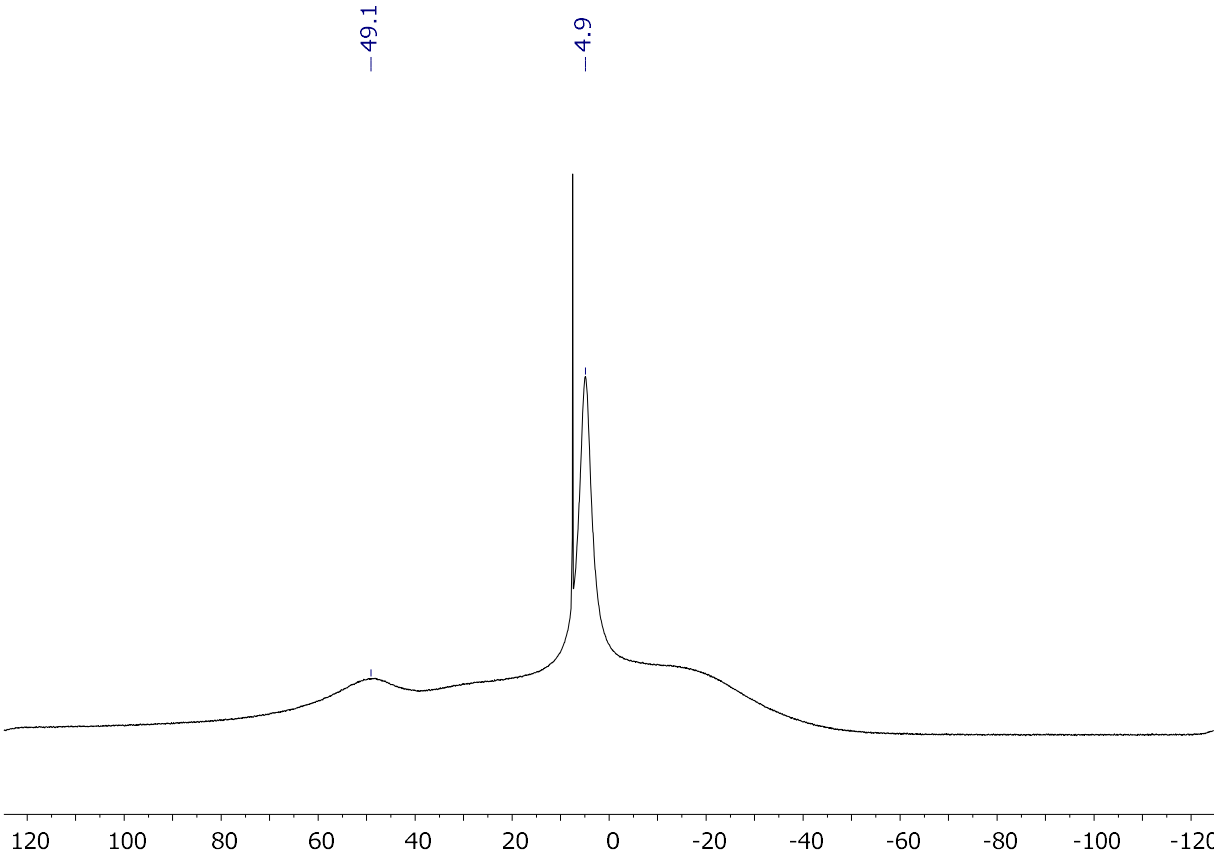

Figure S5.6.24: *$^{11}B\{^{1}H\}$ NMR spectrum of **8^{Cl}** (in $CDCl_3$).*

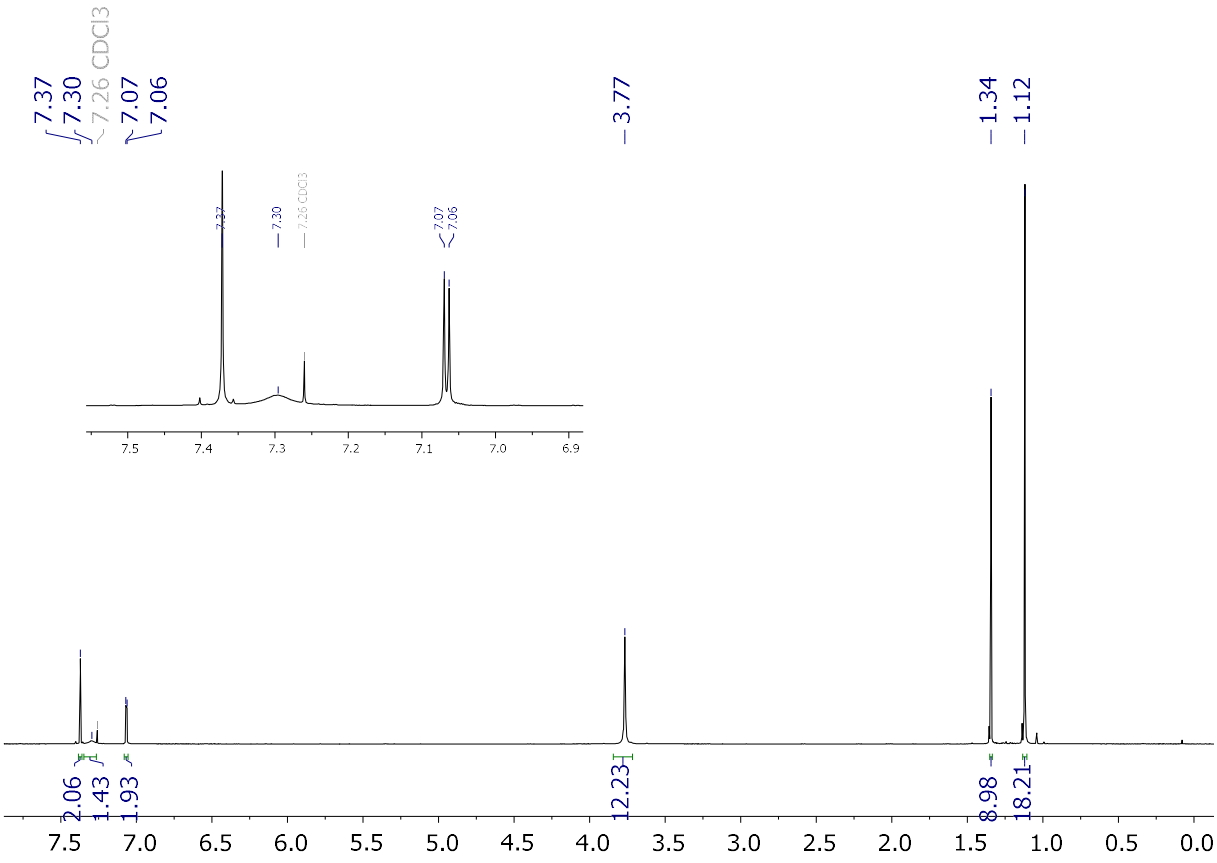

Figure S5.6.25: *^{1}H NMR spectrum of* ***6b^{OMe}*** *(in $CDCl_3$).*

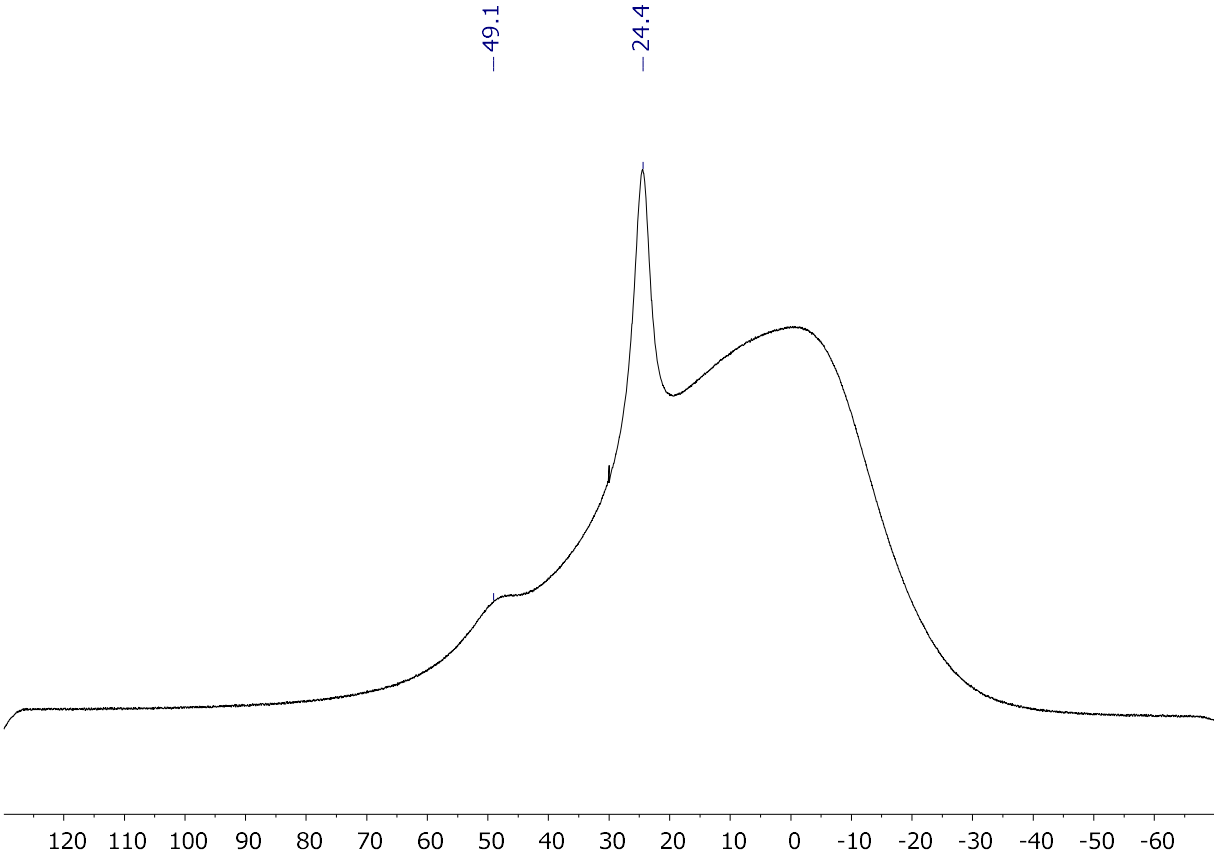

Figure S5.6.26: *$^{11}B\{^{1}H\}$ NMR spectrum of* ***6b^{OMe}*** *(in $CDCl_3$).*

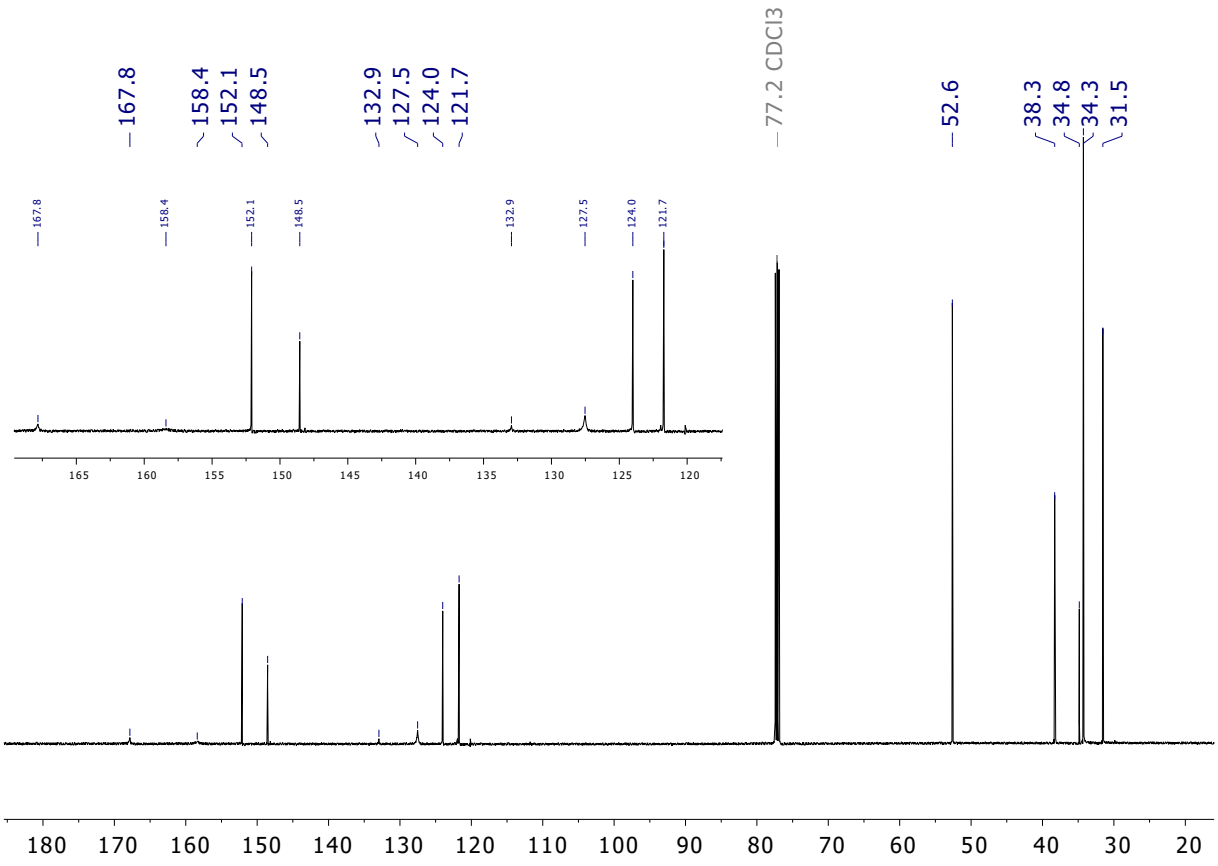

Figure S5.6.27: *$^{13}C\{^{1}H\}$ NMR spectrum of* ***6b^{OMe}*** *(in $CDCl_3$).*

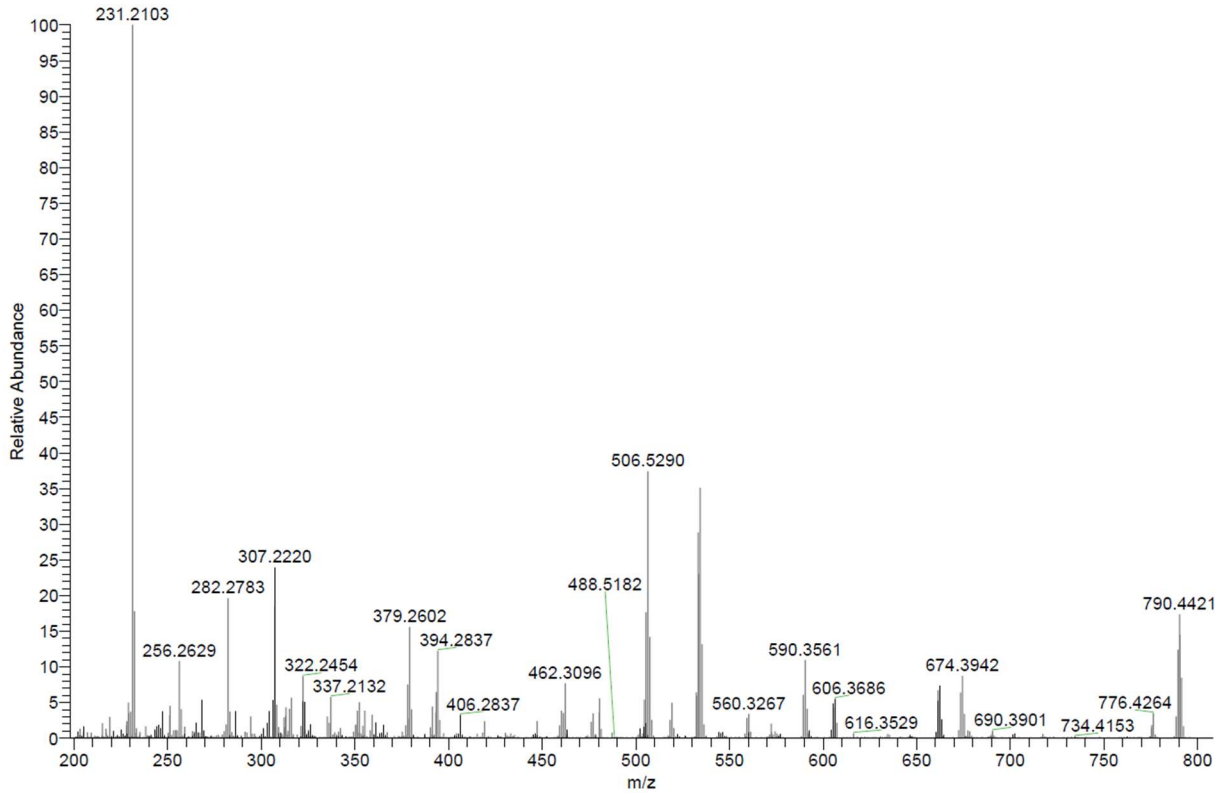

Figure S5.6.28: *Mass spectrum of* ***6b^{OMe}*** *(LIFDI).*

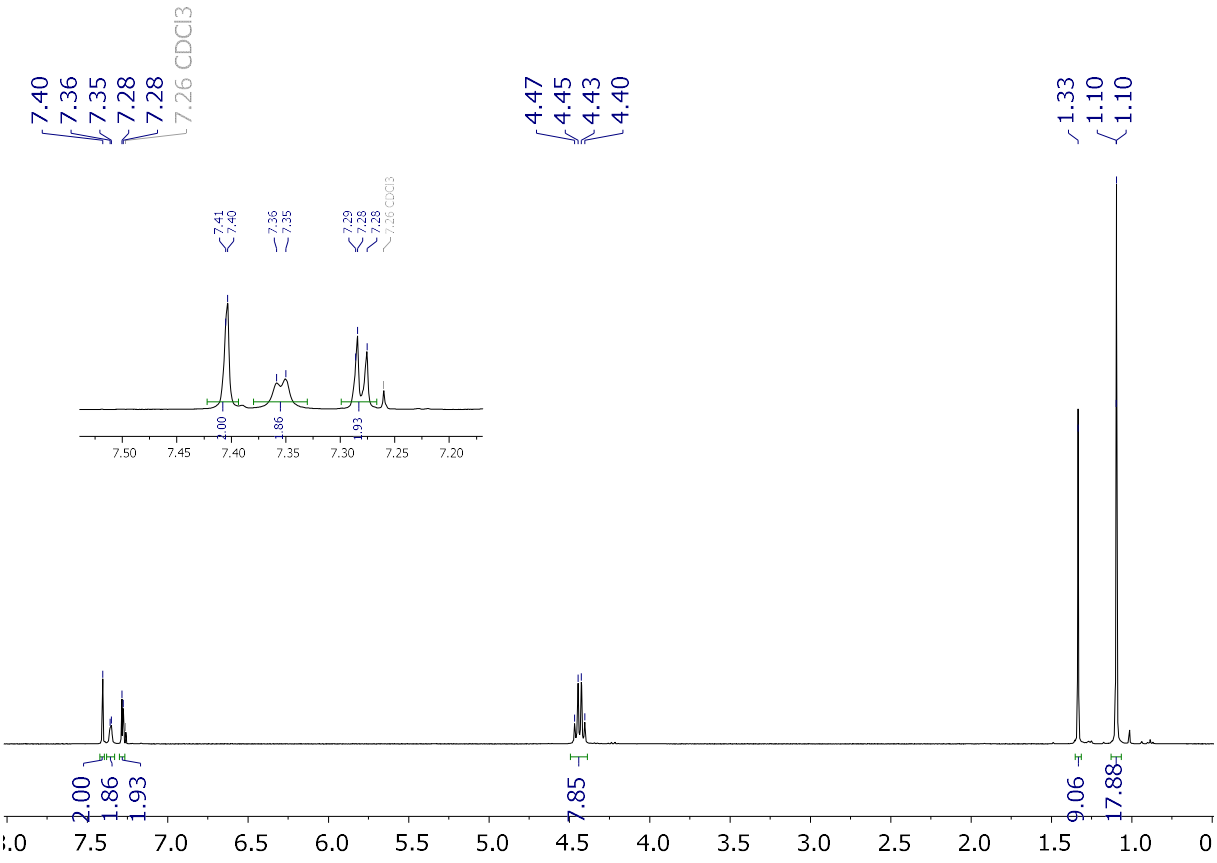

Figure S5.6.29: *^{1}H NMR spectrum of* ***6b^{ORF}*** *(in $CDCl_3$).*

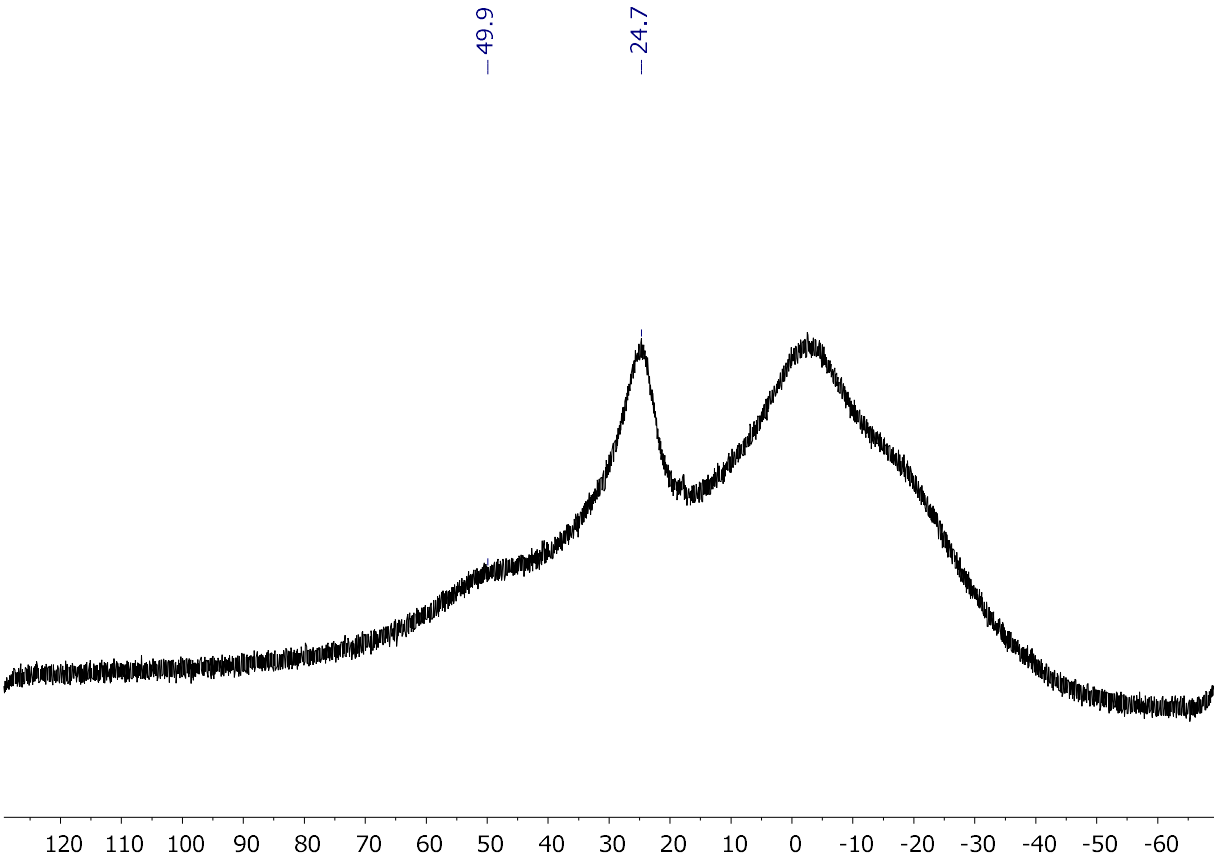

Figure S5.6.30: *^{11}B{^{1}H} NMR spectrum of* ***6b^{ORF}*** *(in $CDCl_3$).*

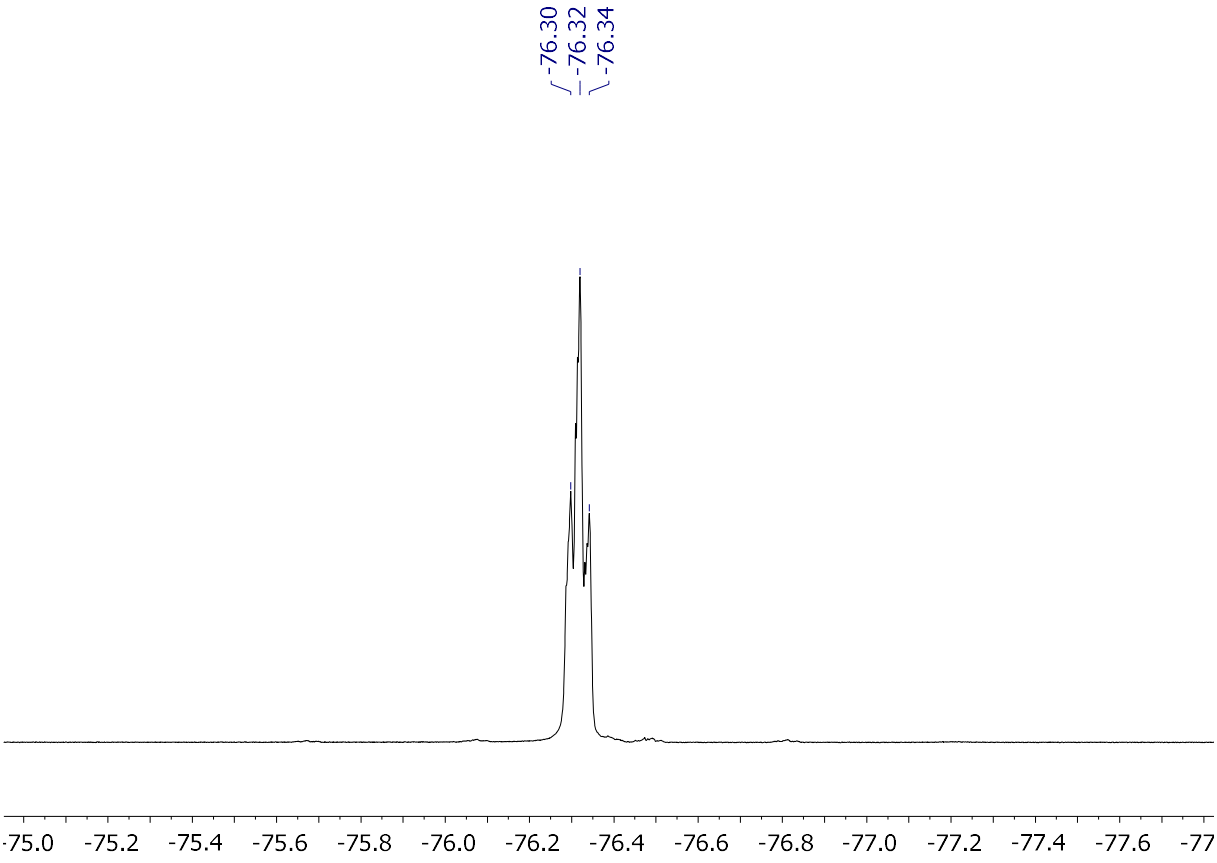

Figure S5.6.31: *^{19}F NMR spectrum of **6b^{ORF}** (in $CDCl_3$).*

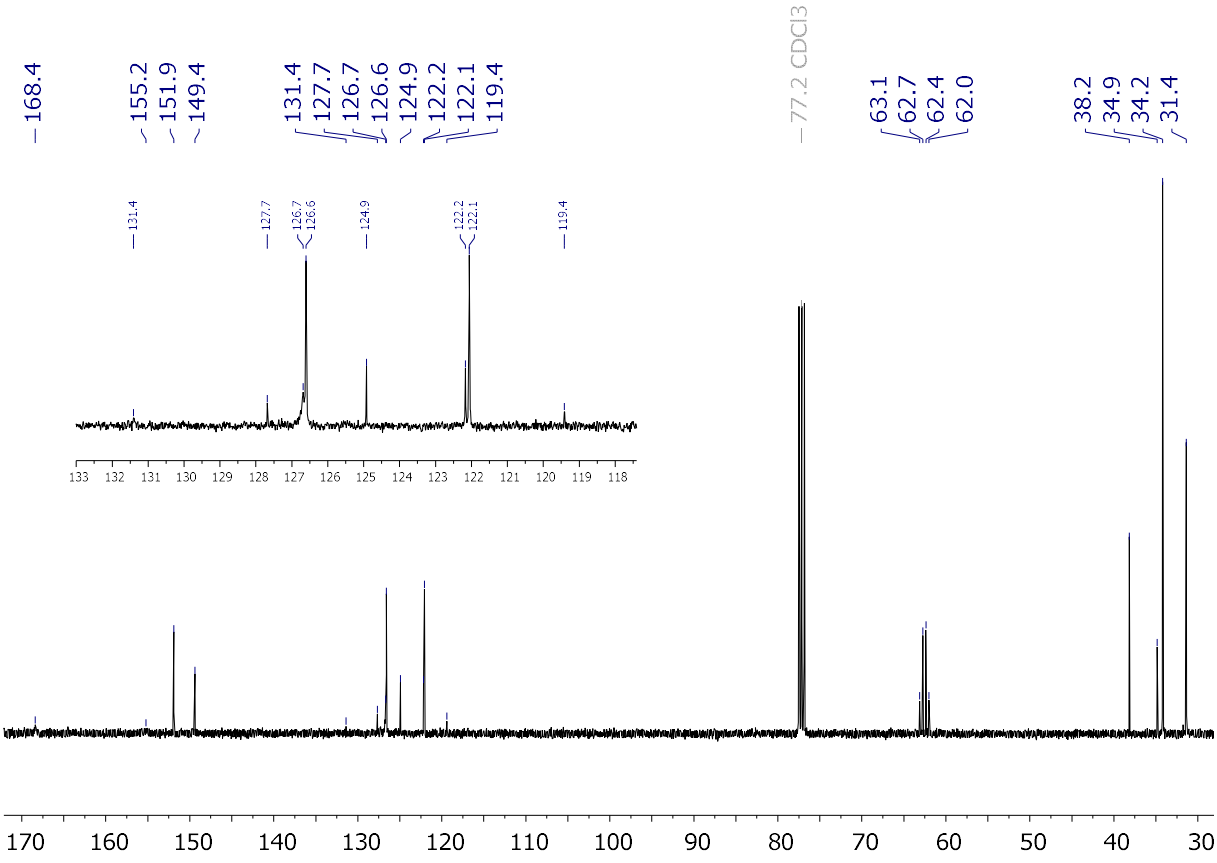

Figure S5.6.32: *$^{13}C\{^1H\}$ NMR spectrum of **6b^{OMe}** (in $CDCl_3$).*

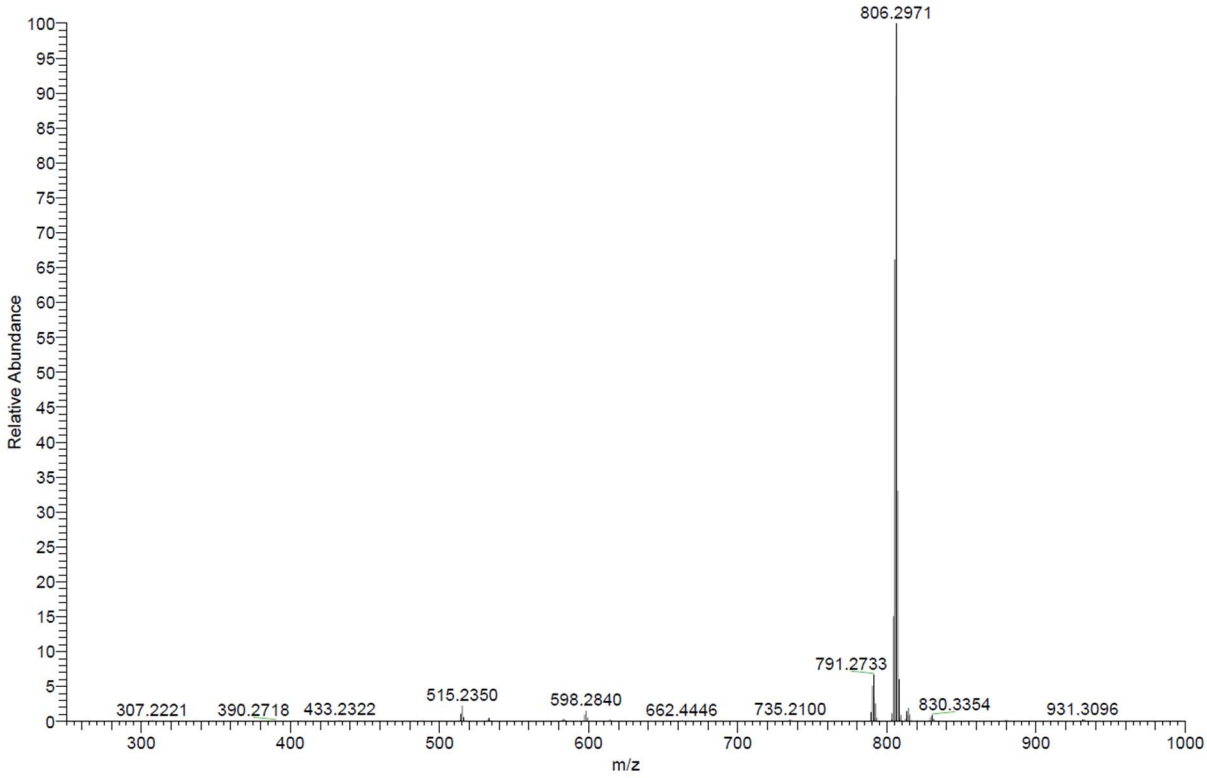

Figure S5.6.33: *Mass spectrum of* ***6b^{ORF}*** *(LIFDI).*

Cartesian coordinates [Å] and total energies [a.u.] of optimized stationary points

3b:

Total energy (B3LYP/6-311++G**): -2413.858220

C	-1.891047	2.661797	0.000403
C	-1.847126	4.047412	-0.000726
C	-0.493865	4.421386	-0.000531
C	0.255306	3.254989	0.000719
C	2.661880	1.890449	0.002042
C	4.047618	1.846810	0.002792
C	4.421643	0.493628	0.002586
C	3.255053	-0.255456	0.001701
C	1.890946	-2.662241	-0.000058
C	1.847014	-4.047844	-0.001495
C	0.493745	-4.421843	-0.001510
C	-0.255437	-3.255461	-0.000046
C	-2.661921	-1.890745	0.001910
C	-4.047660	-1.847207	0.003357

C	-4.421752	-0.494045	0.003381
C	-3.255213	0.255098	0.002039
H	-2.712599	4.691133	-0.001515
H	-0.081686	5.418136	-0.001116
H	4.691233	2.712322	0.003299
H	5.418394	0.081470	0.002906
H	2.712532	-4.691474	-0.002401
H	0.081532	-5.418553	-0.002414
H	-4.691259	-2.712758	0.004101
H	-5.418484	-0.081894	0.004137
B	-3.159221	1.790715	0.000948
B	3.159084	-1.791071	0.000634
C	-4.539698	2.573252	-0.000061
C	-5.161470	2.932689	-1.214884
C	-5.166076	2.928465	1.213765
C	-6.375318	3.625540	-1.196960
C	-6.379877	3.621246	1.193780
C	-7.004477	3.977898	-0.002145
H	-6.839017	3.897946	-2.141230
H	-6.847210	3.890268	2.137275
C	4.539586	-2.573598	-0.000069
C	5.166721	-2.926746	1.213853
C	5.166111	-2.925407	-1.214764
C	6.384465	-3.612694	1.194199
C	6.383786	-3.611377	-1.196512
C	7.010187	-3.967971	-0.001489
H	6.856177	-3.873430	2.137797
H	6.854972	-3.871090	-2.140660
C	-4.536505	2.571841	2.543776
H	-4.400982	1.490628	2.646709
H	-3.548321	3.029366	2.655855
H	-5.156147	2.910264	3.376763
C	-4.526767	2.580953	-2.543874
H	-3.537877	3.038230	-2.650141

H	-4.391652	1.499900	-2.650605
H	-5.142773	2.923180	-3.378021
C	-8.332326	4.697225	-0.003242
H	-8.444652	5.326082	-0.889798
H	-9.165599	3.985477	0.000087
H	-8.442959	5.332102	0.879326
C	4.538230	-2.567575	2.543716
H	4.411165	-1.485464	2.648797
H	3.546327	-3.017436	2.653330
H	5.153841	-2.912801	3.376893
C	4.536840	-2.564765	-2.543884
H	3.544756	-3.014252	-2.653291
H	4.410014	-1.482482	-2.647800
H	5.151805	-2.909336	-3.377813
C	8.309378	-4.737876	-0.002413
H	8.906237	-4.514510	0.885246
H	8.126525	-5.818298	-0.009664
H	8.911414	-4.503669	-0.883804
C	-2.573849	-4.539417	-0.000009
C	-2.932841	-5.161800	-1.214675
C	-2.928453	-5.165820	1.213931
C	-3.625687	-6.375670	-1.196485
C	-3.621364	-6.379577	1.194220
C	-3.978112	-7.004466	-0.001556
H	-3.898378	-6.839472	-2.140631
H	-3.890675	-6.846474	2.137811
C	2.573785	4.539025	0.000790
C	2.923781	5.167707	1.214813
C	2.928409	5.164188	-1.213802
C	3.610466	6.385024	1.195359
C	3.614987	6.381516	-1.195348
C	3.969104	7.009080	-0.000224
H	3.869367	6.857599	2.139029
H	3.877462	6.851334	-2.139423

C	-2.570626	-4.536555	2.543834
H	-1.488056	-4.415731	2.652166
H	-3.014941	-3.541820	2.650190
H	-2.921877	-5.148741	3.377023
C	-2.579815	-4.528177	-2.543753
H	-3.024380	-3.533089	-2.645172
H	-1.497626	-4.407087	-2.655641
H	-2.934174	-5.137561	-3.377667
C	-4.697906	-8.332135	-0.002346
H	-3.986353	-9.165515	0.000567
H	-5.332347	-8.442610	0.880509
H	-5.327270	-8.444299	-0.888587
C	2.559972	4.541568	2.544558
H	1.476631	4.426185	2.651043
H	2.999179	3.544728	2.652480
H	2.912889	5.152583	3.377914
C	2.569750	4.534086	-2.543028
H	3.009191	3.536935	-2.646185
H	1.486811	4.418504	-2.653438
H	2.926054	5.142525	-3.376806
C	4.740108	8.307591	-0.000802
H	4.514029	8.906274	0.884938
H	5.820436	8.123890	-0.003816
H	4.509567	8.908174	-0.884154
B	-1.790950	-3.159085	0.000736
B	1.790763	3.158781	0.001314
O	-2.185543	-0.604099	0.001237
O	0.604231	-2.186249	0.000824
O	2.185445	0.603823	0.001455
O	-0.604349	2.185769	0.001286

3a:

Total energy (B3LYP/6-311++G**): -3705.780446

C 3.144100 1.397500 -0.039000
356

C	4.335100	0.871000	-0.535600
C	4.388300	-0.538200	-0.540200
C	3.240900	-1.156600	-0.046500
C	1.402400	-3.140700	0.066900
C	0.877700	-4.335100	0.557000
C	-0.531600	-4.388600	0.568600
C	-1.151900	-3.237900	0.085100
C	-3.135200	-1.398900	-0.016200
C	-4.327000	-0.874500	-0.513000
C	-4.380700	0.534500	-0.522400
C	-3.232700	1.154700	-0.032800
C	-1.394700	3.139000	0.057500
C	-0.868300	4.333900	0.544500
C	0.540900	4.386300	0.549700
C	1.159300	3.235100	0.065000
H	5.132100	1.503600	-0.907400
H	5.230400	-1.106200	-0.916900
H	1.511700	-5.134900	0.918900
H	-1.097900	-5.233700	0.941900
H	-5.123700	-1.509100	-0.881900
H	-5.223200	1.101200	-0.899600
H	-1.501100	5.134000	0.909200
H	1.109000	5.230900	0.920100
B	2.674600	2.881500	0.015900
B	-2.667100	-2.883000	0.036900
C	3.745900	4.039300	0.021400
C	4.019300	4.773300	-1.154500
C	4.452000	4.358100	1.201800
C	4.980100	5.786900	-1.132200
C	5.394400	5.390400	1.190300
C	5.675700	6.116900	0.032900
H	5.189800	6.332200	-2.048700
H	5.924300	5.628700	2.108800
C	-3.743600	-4.036200	0.030700

C	-4.454100	-4.366800	1.206200
C	-4.016800	-4.754900	-1.153300
C	-5.402200	-5.392100	1.179300
C	-4.984500	-5.763300	-1.146100
C	-5.689500	-6.099100	0.010100
H	-5.930500	-5.643900	2.095100
H	-5.189300	-6.301800	-2.067500
C	4.188500	3.609400	2.491500
H	3.150100	3.725900	2.819700
H	4.369700	2.536700	2.376200
H	4.830600	3.973400	3.296300
C	3.303200	4.458000	-2.451400
H	3.509800	3.436300	-2.787600
H	2.218300	4.546000	-2.341100
H	3.615200	5.136100	-3.248400
C	6.681700	7.243000	0.043800
H	7.248900	7.280400	-0.890000
H	6.185300	8.212800	0.162000
H	7.391200	7.135600	0.867600
C	-4.182700	-3.640600	2.506600
H	-3.147500	-3.776700	2.836500
H	-4.346900	-2.563800	2.405500
H	-4.833100	-4.005200	3.304100
C	-3.290500	-4.433600	-2.442500
H	-3.487400	-3.407300	-2.770400
H	-2.206800	-4.530400	-2.327600
H	-3.603800	-5.101500	-3.247500
C	-6.750100	-7.173800	-0.007000
H	-6.762800	-7.737400	0.929500
H	-7.747500	-6.739600	-0.138800
H	-6.589600	-7.879200	-0.825500
C	-4.036800	3.740600	-0.021800
C	-4.363700	4.416000	-1.217200
C	-4.766200	4.040500	1.150100

C	-5.399200	5.354600	-1.224000
C	-5.785200	4.994600	1.108100
C	-6.123400	5.660100	-0.071600
H	-5.643000	5.861800	-2.153400
H	-6.328800	5.223600	2.020700
C	4.042700	-3.744600	-0.024600
C	4.769500	-4.047000	1.147100
C	4.372600	-4.416800	-1.222300
C	5.786300	-5.005400	1.105700
C	5.405200	-5.357700	-1.228800
C	6.121100	-5.673000	-0.072500
H	6.332300	-5.231900	2.017400
H	5.655700	-5.856700	-2.161100
C	-4.438900	3.359500	2.462300
H	-4.506400	2.270700	2.375400
H	-3.421100	3.592200	2.793500
H	-5.122700	3.676400	3.252800
C	-3.621900	4.120800	-2.503100
H	-2.546200	4.284800	-2.393500
H	-3.756400	3.080000	-2.815500
H	-3.977300	4.756200	-3.316600
C	-7.255300	6.658900	-0.102800
H	-8.222600	6.153900	-0.203400
H	-7.292000	7.249700	0.816100
H	-7.156300	7.347500	-0.945000
C	4.450300	-3.359000	2.457700
H	4.532000	-2.271300	2.368800
H	3.429700	-3.578200	2.789000
H	5.129900	-3.682900	3.249000
C	3.638200	-4.111200	-2.510500
H	2.562100	-4.278300	-2.406900
H	3.772800	-3.067000	-2.812800
H	3.998200	-4.739300	-3.327900
C	7.205900	-6.723500	-0.094100

H	7.902200	-6.594600	0.737700
H	6.780200	-7.730000	-0.013500
H	7.778300	-6.687200	-1.024600
B	-2.878300	2.670200	0.003100
B	2.886100	-2.671800	0.000200
S	-0.075800	2.113300	-0.429500
S	-2.114000	-0.078100	0.474500
S	0.081200	-2.115800	-0.414600
S	2.122900	0.078700	0.457000

Julius-Maximilians-
UNIVERSITÄT
WÜRZBURG

Fakultät für
CHEMIE UND
PHARMAZIE

Erklärung zur Autorenschaft

Difuryl(supermesityl)borane: a versatile building block for extended π-conjugated materials,
N. A. Riensch, L. Fritze, T. Schindler, M. Kremer, H. Helten, Dalton transactions 2018, 47, 10399 – 10403.

Detaillierte Darstellung der Anteile an der Veröffentlichung (in %)
Angabe Autoren/innen (ggf. Haupt- / Ko- / korrespondierende/r Autor/in) mit Vorname Nachname (Initialen)

Hauptautor: Nicolas Riensch (NR), Hauptautor: Lars Fritze (LF), Tobias Schindler (TS), Marius Kremer (MK), korrespondierender Autor: Holger Helten (HH)

Autor	NR	LF	TS	MK	HH							∑ in Prozent
Idee/-entwicklung/Konzept	2,1%	2,1%			12,5%							16,7%
Synthesen	16,2%	16,2%										32,3%
Analysen	11,5%	11,5%	1%	1%								25,0%
Rechnungen					1%							1%
												0%
												0%
Verfassen der Veröffentlichung	3,3%	3,3%			10,1%							16,7%
Korrektur der Veröffentlichung	1,4%	1,4%			1,4%							4,2%
Koordination der Veröffentlichung					4,2%							4,2%
Summe	34,5%	34,5%	1%	1%	29,2%							100%

Julius-Maximilians-
UNIVERSITÄT
WÜRZBURG

Fakultät für
CHEMIE UND
PHARMAZIE

Erklärung zur Autorenschaft

Catalytic Si/B Exchange Condensation: A Green B–C Coupling Method That Provides Access to Monodisperse (Het)arylborane 'Trimers',
L. Fritze, N. A. Riensch, H. Helten, Synthesis 2019, 51, 399 – 406.

Detaillierte Darstellung der Anteile an der Veröffentlichung (in %)
Angabe Autoren/innen (ggf. Haupt- / Ko- / korrespondierende/r Autor/in) mit Vorname Nachname (Initialen)

Hauptautor: Lars Fritze (LF), Hauptautor: Nicolas Riensch (NR), korrespondierender Autor: Holger Helten (HH)

Autor	LF	NR	HH									∑ in Prozent
Idee/-entwicklung/Konzept	2,1%	2,1%	12,5%									16,7%
Synthesen	16,7%	16,7%										33,3%
Analysen	12,5%	12,5%										25,0%
												0%
												0%
												0%
Verfassen der Veröffentlichung	3,3%	3,3%	10,1%									16,7%
Korrektur der Veröffentlichung	1,4%	1,4%	1,4%									4,2%
Koordination der Veröffentlichung			4,2%									4,2%
Summe	36%	36%	28%									100%